International Journal on Advances in Telecommunications

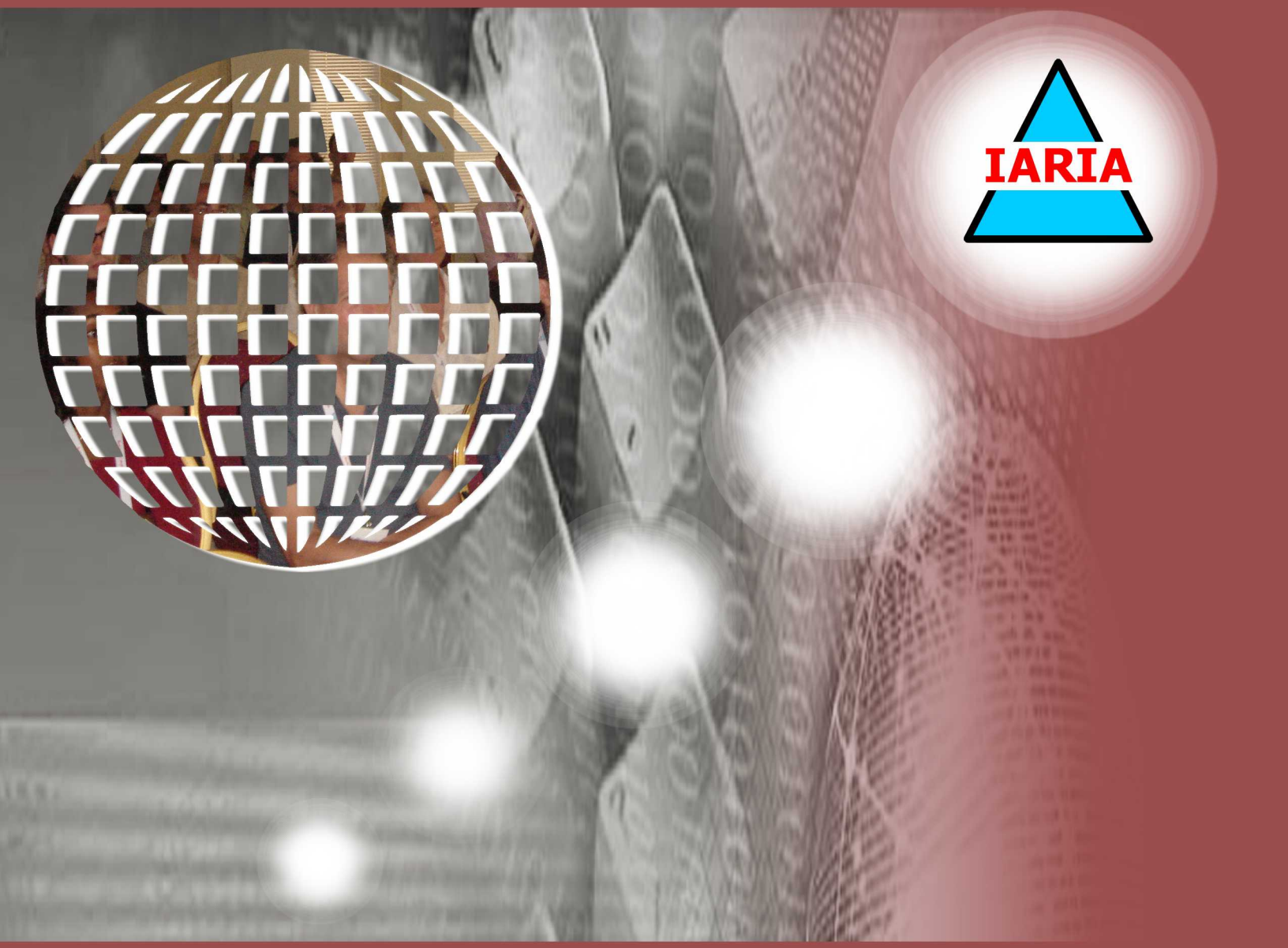

2010 vol. 3 nr. 3&4

The *International Journal on Advances in Telecommunications* is published by IARIA.
ISSN: 1942-2601
journals site: http://www.iariajournals.org
contact: petre@iaria.org

Sponsored by IARIA
www.iaria.org

International Journal on Advances in Telecommunications
Volume 3, Number 3 & 4, 2010

- Bilal Al Momani, Cisco Systems, Ireland
- Tulin Atmaca, IT/Telecom&Management SudParis, France
- Claus Bauer, Dolby Systems, USA
- Claude Chaudet, ENST, France
- Gerard Damm, Alcatel-Lucent, France
- Michael Grottke, Universitat Erlangen-Nurnberg, Germany
- Yuri Ivanov, Movidia Ltd. – Dublin, Ireland
- Ousmane Kone, UPPA - University of Bordeaux, France
- Wen-hsing Lai, National Kaohsiung First University of Science and Technology, Taiwan
- Pascal Lorenz, University of Haute Alsace, France
- Jan Lucenius, Helsinki University of Technology, Finland
- Dario Maggiorini, University of Milano, Italy
- Pubudu Pathirana, Deakin University, Australia
- Mei-Ling Shyu, University of Miami, USA

Communication Theory, QoS and Reliability

- Eugen Borcoci, University "Politehnica" of Bucharest (UPB), Romania
- Piotr Cholda, AGH University of Science and Technology - Krakow, Poland
- Michel Diaz, LAAS, France
- Ivan Gojmerac, Telecommunications Research Center Vienna (FTW), Austria
- Patrick Gratz, University of Luxembourg, Luxembourg
- Axel Kupper, Ludwig Maximilians University Munich, Germany
- Michael Menth, University of Wuerzburg, Germany
- Gianluca Reali, University of Perugia, Italy
- Joel Rodriques, University of Beira Interior, Portugal
- Zary Segall, University of Maryland, USA

Wireless and Mobile Communications

- Tommi Aihkisalo, VTT Technical Research Center of Finland - Oulu, Finland
- Zhiquan Bai, Shandong University - Jinan, P. R. China
- David Boyle, University of Limerick, Ireland
- Bezalel Gavish, Southern Methodist University - Dallas, USA
- Xiang Gui, Massey University-Palmerston North, New Zealand
- David Lozano, Telefonica Investigacion y Desarrollo (R&D), Spain
- D. Manivannan (Mani), University of Kentucky - Lexington, USA
- Himanshukumar Soni, G H Patel College of Engineering & Technology, India
- Radu Stoleru, Texas A&M University, USA
- Jose Villalon, University of Castilla La Mancha, Spain
- Natalija Vlajic, York University, Canada
- Xinbing Wang, Shanghai Jiaotong University, China
- Ossama Younis, Telcordia Technologies, USA

Systems and Network Communications

- Fernando Boronat, Integrated Management Coastal Research Institute, Spain
- Anne-Marie Bosneag, Ericsson Ireland Research Centre, Ireland
- Huaqun Guo, Institute for Infocomm Research, A*STAR, Singapore
- Jong-Hyouk Lee, INRIA, France
- Elizabeth I. Leonard, Naval Research Laboratory – Washington DC, USA
- Sjouke Mauw, University of Luxembourg, Luxembourg
- Reijo Savola, VTT, Finland

Multimedia

- Dumitru Dan Burdescu, University of Craiova, Romania
- Noel Crespi, Institut TELECOM SudParis-Evry, France
- Mislav Grgic, University of Zagreb, Croatia
- Christos Grecos, University of Central Lancashire, UK
- Atsushi Koike, Seikei University, Japan
- Polychronis Koutsakis, McMaster University, Canada
- Chung-Sheng Li, IBM Thomas J. Watson Research Center, USA
- Artur R. Lugmayr, Tampere University of Technology, Finland
- Parag S. Mogre, Technische Universitat Darmstadt, Germany
- Chong Wah Ngo, University of Hong Kong, Hong Kong
- Justin Zhan, Carnegie Mellon University, USA
- Yu Zheng, Microsoft Research Asia - Beijing, China

Space Communications

- Emmanuel Chaput, IRIT-CNRS, France
- Alban Duverdier, CNES (French Space Agency) Paris, France
- Istvan Frigyes, Budapest University of Technology and Economics, Hungary
- Michael Hadjitheodosiou ITT AES & University of Maryland, USA
- Mark A Johnson, The Aerospace Corporation, USA
- Massimiliano Laddomada, Texas A&M University-Texarkana, USA
- Haibin Liu, Aerospace Engineering Consultation Center-Beijing, China
- Elena-Simona Lohan, Tampere University of Technology, Finland
- Gerard Parr, University of Ulster-Coleraine, UK
- Cathryn Peoples, University of Ulster-Coleraine, UK
- Michael Sauer, Corning Incorporated/Corning R&D division, USA

International Journal on Advances in Telecommunications
Volume 3, Numbers 3 & 4, 2010

CONTENTS

CARMA: A Distance Estimation Method for Internet Nodes and its Usage in P2P Networks

Gennadiy Poryev
National Technical University of Ukraine "KPI"
Kiev, Ukraine
core@barvinok.net

Hermann Schloss
Logica Deutschland GmbH & Co. KG
Hennef, Germany
hermann.schloss@logica.com

Rainer Oechsle
Trier University of Applied Sciences
Trier, Germany
oechsle@fh-trier.de

***Abstract*—Topological distance estimation is the key to the efficiency in distributed systems and peer-to-peer networks. Contrary to many existing or proposed methods, which usually require the exchange of messages between the nodes, we have developed a metric, which is computed purely within a node, and which is based on the preloaded and precomputed topological structure of the Internet. Many distributed systems and applications may benefit from this metric, since it estimates the topological distance between any arbitrary pair of nodes in the Internet. As a proof of concept we have first shown the correlation between our metric and a few established distance indicators, such as hop count or round trip time of a message. Then, we employed this metric as an "edge weight" representing the connection quality between two network nodes and we used it for the construction of a multicast overlay network based on a Minimum Spanning Tree approximation. According to the evaluation results, this metric corresponds fairly well to the actual measured distances. By using this metric, our approach minimizes communication costs and avoids extraneous communication needed for latency measurements.**

***Keywords*-Internet, Topology, Distance Estimation Method**

I. Introduction

Since the beginning of the 21st century the usage, scale and diversity of *peer-to-peer* (P2P) networks widened significantly, and the application scope of P2P systems has been notably extended. Being previously considered as a means for file sharing or instant messaging, today's P2P networks serve as a basic infrastructure for a wide range of innovative application scenarios such as VoIP, multimedia on-demand, software delivery, massive multiuser environments or online games.

The initial driving motivation behind P2P systems was to relieve load stress from centralized server farms. However, the intrinsic asymmetry of end-user broadband data links have caused *Internet Service Providers* (ISP) to increase maintenance and upgrade cost of the "last mile" hardware in order to keep quality of service steady. Some ISPs had also introduced controversial measures to detect and forcibly shape end-user bandwidth for traffic recognized as P2P, affecting file sharing networks in particular.

For this reason, researches in the area of P2P systems are aiming to optimize P2P traffic and consider the inherently clustered nature of the Internet as a potential leverage mechanism. The general idea is to maximize network throughput inside the particular network clusters while minimizing the traffic usage between such clusters. The scope of the cluster is not defined clearly, and there is usually more than one clustering layer.

In this paper, we propose a locally computed approach for topological distance estimation that does not rely on third-party non-guaranteed external infrastructures and consider its usage in P2P networks.

The rest of this paper is organized as follows. In Section II we first take a look at related work dealing with traffic optimization in P2P networks and consider then several application-level multicast approaches, based on a *Minimum Spanning Tree* (MST) or on its approximation. Afterwards in Section III, we describe the computation of the *Combined Affinity Reconnaissance Metric Architecture* (CARMA) metric [1]. In Section IV we consider two application scenarios, which benefit from the utilization of the CARMA metric: a) the selection of peers – network nodes that may serve the requested content – and b) the construction of the ***CAR**MA-based **M**ulticast **In**frastructure* (*CARMIn*), based on the MST approximation method. Then in Section V we discuss the experimental validation of the CARMA metric and explain the flavor distribution, anomalies and statistical characteristics. As the evaluation results show (Section V), our CARMIn multicast tree achieves a good MST approximation with respect to a communication cost metric and avoids – due to utilization of CARMA – extraneous communication needed for latency measurements. In Section VI we provide a brief overview of our contribution and discuss our future plans.

II. Related Work

Usenet [2] was introduced 30 years ago as one of the first P2P networks. However, only at the end of the 1990s P2P applications have achieved a breakthrough and become very popular because of the widespread use of file sharing platforms like *Napster* [3]. Nowadays, there is a wide variety of P2P file sharing networks. Among them are *Gnutella*

[4], *eDonkey2000* (ED2K) [5] and *BitTorrent* [6]. In [7] a multicast P2P overlay is described that is used for content distribution in large-scale enterprise networks. The proposed approach reduces the completion time compared to BitTorrent without wasting additional resources.

Various surveys suppose that 30% to 50% of today's end-user-generated traffic is caused by P2P applications. In [8] the authors claim that most P2P systems use application-level routing based on the overlay topology and completely neglect the topology of the underlying transport network. Because of this, P2P systems cause a lot of extraneous traffic. In order to avoid this traffic, the authors propose the ISP-aided neighbor selection by considering the node proximity in the underlying network at the application-level.

The authors of [9] have recently described the design, deployment and evaluation of an approach, minimizing the expensive cross-ISP traffic. The authors show that the application of their approach significantly reduces the latency delays. The *P4P* architecture [10] also aims towards the minimization of the network traffic. In order to achieve their objective, the authors take into account the conditions of the underlying network layer during the overlay construction.

According to [11] the consideration of a node's topological locality is the key to efficient communication in P2P systems. It improves performance and increases availability, since the probability of transmission failures increases with the distance and depends also on bandwidth conditions.

Modern network modeling environments that deal with network topology rarely take locality into account. Most of them use either the network latency metric measured in time units between request and response (ping), or the hop count metric measured as the number of nodes between source and destination hosts [12]. We deem the ping method as generally unreliable as it heavily depends on link speeds and bandwidth conditions. For example, a zero-loaded end-user ADSL link can produce slower pings than an almost fully loaded Gbps link. As shown in [13] standard routing trace methods may also be unreliable and affected by bandwidth conditions or indicating non-existent links due to traffic switch-overs.

A number of researches have proposed schemes that involve building the external (in relation to the P2P overlay) infrastructures dedicated to keeping track of the condition of intra-network and inter-network links, remembering explicitly measured routing paths and delivering path prediction on their basis. Such schemes, for instance, include P4P [10] and *iPlane* [14]. Other proposals, such as [15] are concerned with an active intervention into the P2P exchange protocols to augment traffic usage patterns in accordance with ISP policies.

Contrary to the methods employing external infrastructures for distance estimation, we propose an approach based on the preloaded and precomputed topological structure of the Internet and running locally on client machines. By using our distance estimation method, clients are able to create a multicast overlay at the application-level without relying on a central instance or external infrastructures.

While the problems of scalable data localization have been exhaustively addressed, the problem of reducing *multicast costs* in very large, global scale environments still remains inadequately considered. In [16] the authors state that multicast has become an important communication primitive in P2P networks. The authors note that the consideration of communication cost caused by multicast overlays is a critical issue in P2P networks due to dynamic and rapidly changing network topology conditions.

In [17] the authors argue that nowadays the network infrastructure itself becomes a precious resource. They state that the construction methods of multicast trees considerably influence the network load and that current available strategies often waste too many network resources. In order to adjust the multicast tree infrastructure to the physical network conditions the authors propose the use of transmission delays between peers as a performance metric. On the basis of this metric, the authors construct a network friendly multicast tree. However this metric cannot be applied in advance without transmitting a message between two peers.

To address this issue of reducing multicast costs in our work, we propose the construction of an application-level multicast infrastructure, based on an MST approximation. The MST problem is one of the most popular and important problems in the research area of graph theory, distributed computing and networks. In opposition to the theoretical models where we usually have a global knowledge of all nodes and the corresponding distances for the MST construction, in a realistic network (e.g., the Internet) a node neither knows all other nodes involved in the same application scenario nor exact distances between these nodes.

The ALMI (Application Level Multicast) project [18] uses a central instance for MST computation. In [19] the authors propose a MST-based multicast cluster for P2P video streaming and show that the utilization of the MST approach reduces the network traffic. However, since here all network nodes are considered for MST construction, high management and maintenance costs can be expected in large scale networks. In our CARMIn approach we avoid the additional communication by using the CARMA metric and address the question of a distributed approximation of an MST that is, constructing a suboptimal spanning tree whose communication cost is near-optimal.

Similar to our approach, [20] have considered the problem of the construction of suboptimal spanning trees. In [21] the authors propose the construction of a *Nearest Neighbor Tree* (NNT) instead of an MST. To ensure both acceptable multicast costs and latency delays JXTA [22] nodes always connect to the nearest node (in terms of latency) achieving an MST approximation, too. However, the quote in [23] "There is no satisfactory approximation algorithm known for the

MST problem" encouraged us to address this problem in our work.

In [24] the authors propose a *binning* scheme by adjusting adjacent nodes to certain bins depending on their *Round Trip Time* (RTT) distance to certain landmark severs. To be more exact, a node measures its round-trip time to each of these landmarks and orders these landmarks in ascending order. Nodes having the same order of landmarks are considered closer than nodes having different order. This approach significantly reduces the amount of communication necessary for the capturing of node distances. However, the communication with the landmark servers for the RTT measurements is required.

Several MST or NNT-based approaches readjust their infrastructures when nodes are joining or leaving the infrastructure. However under churn (i.e., peers arriving and departing at a high rate) this readjustment makes them useless for large scale application scenarios. Thus in our CARMIn approach only direct neighbors are involved into joining and leaving of peers in this way avoiding the readjustment. Similar to our approach in [25], the authors propose the Orchard algorithm for building and maintaining application-level multicast trees taking into account the problem of churn.

III. CARMA METRIC

The Internet is in no way a uniform structure. There are large backbone networks involved in international and intercontinental links, national-tier ISPs, end-user-servicing ISPs, hosting companies and end-users. Network latency and quality of service are accordingly very different depending on the link speed from tens of Gbps to less than 56 Kbps for dial-up modems. On the scale of a country, the Internet structure used to be organized rather sporadically – individual ISPs established arbitrary links among themselves and to foreign upstream ISPs. This had lead to peering conflicts and situations in which a message to a neighboring house traveled halfway the continent.

To alleviate this problem, *Internet Exchange Points* (commonly abbreviated as IX or IXP) were introduced. Usually, a number of national telecom operators create the dedicated facility to which all national ISPs then connect. Thus, consumer traffic within the scope of an IX does not travel expensive international or satellite links. This helps balance mutual peering and to ensure lower maintenance costs per ISP, allowing lower prices for end-users. Developed countries are used to having more than one nationwide IX. From the customer point of view, it is generally assumed that traffic within a single IX scope flows faster and is cheaper than between different IXes. The presence of an IX can also provide for a lower hop count in the packet path. Figure 1 depicts an Internet segment consisting of some networks, which are grouped by *Autonomous Systems* (AS) [26]. Some of these ASes are connected to a single IX.

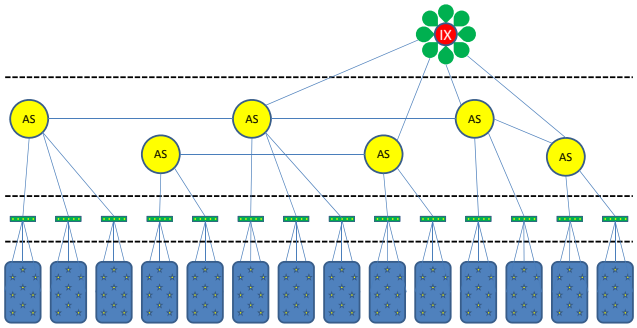

Figure 1. Example of an Internet segment covered by an IX

In network-based applications, we often need global knowledge of all network nodes and distances between these nodes. This information is usually managed by a central instance or may be inferred from external infrastructures. By having this knowledge, nodes in a network are able to construct complex infrastructures and achieve efficient communication at the application as well as at the network layer.

Without relying on a central instance or external infrastructures, clients usually apply either ping or hop count methods to estimate node distances. The problem hereby is that even if the ping or hop count methods would provide reasonable and reliable results, there is no way to apply these methods to a pair of foreign IP addresses. That is, it is easy to measure the ping or hop distance from the node a to the node b or to the node c. But there is no way to measure the ping distance between the nodes b and c from the node a. That means, if clients are interested in this kind of information, they have to explicitly request this information from corresponding nodes, which causes a significant communication overhead.

To sum up, the construction of complex structures requires either additional communication between nodes (in decentralized P2P systems), or is not scalable due to the existence of a *Single Point of Failure* (in P2P systems with a central instance) managing relevant information, which is a big drawback in global scale networks.

In order to sidestep these drawbacks, in our work we employ decentralized P2P systems and propose the combined affinity metric, which is calculated locally on each node. This metric is calculated given the remote IP address of the peer and all information then can be implicitly inferred from it. The "combined" adjective in the CARMA acronym means that despite our work's prevailing focus on only the first layer of the proposed metric, its design does, however, contain several additional components that can be included in a metric calculation in the future, as follows:

1) average response time to keep-alive requests;
2) average hop count to the destination, including the possibility of its change during communication [13];

3) bandwidth and average consumption at the moment of decision, including preset constraints;
4) "gratitude" and "greed" values calculated as the amount of traffic the remote party had provided and consumed respectively.

Generally speaking, we consider CARMA as three-layered, with the first layer being the locality awareness expressed in flavors (see their explanations below), a second layer that utilizes additional traffic but does not involve actual P2P communication (see Section V-A), and a third layer that requires active communication to remote parties over a compatible protocol.

CARMA works by initially preloading structural information from publicly accessible services called *Regional Internet Registries* (RIRs) and converting it into an internal graph-like data structure. Unlike solutions based on the PlanetLab infrastructure or those using RouteViews, the RIR services and databases are mandatorily public, essential for the functioning of the Internet and therefore much more reliable. The pieces of information important to CARMA include the *delegated-latest-** databases of registered IPv4 ranges, *Autonomous System Numbers* (ASNs) and various WHOIS databases of registered subranges and *Autonomous System Sets* (ASSETs).

Since the RIR database expansion rate is relatively slow and the IPv4 address space is nearing its exhaustion, CARMA only needs to update its locally cached data from those databases once every few days. Once loaded, CARMA builds a model to approximate the Internet topology with some simplifications, resulting in 4 structural layers as follows: a) IPv4 ranges are divided into b) subranges but at the same time they also belong to c) Autonomous Systems (ASes), which are joined into sets called d) AS-SETs or ASSETs. It is assumed that lower layer entities are explicitly connected through their common upper-layer entity, and AS-SETs are arbitrarily connected to each other. It is understood that such assumptions in the model are more optimistic than what happens in reality, as there may be ASes that spread worldwide, for example. However, exceptions like this are not numerous and pertain only to the departments of the few telecom operators specializing in providing transoceanic and transcontinental links. Therefore, Internet end-users are unlikely to be encountered in the ranges assigned to such ASes.

Let's take a closer look at IPv4 ranges and subranges, ASes, and ASSETs (with examples from the RIPE registry, which is responsible for Europe):

IPv4 range – a subset of an IPv4 address space defined by the first address of the range and a host count. Note that the host count is not necessarily a power of 2 as implied by the *Classless Inter-Domain Routing* (CIDR) rules now commonly used for Internet routing. There are records that specify an arbitrary number of nodes, but for practical reasons such definitions are subsequently augmented by CARMA to contain a power of 2 number of nodes. IPv4 ranges are defined in the *delegated*-file (see Listing 1).

```
ripencc|EU|ipv4|143.65.0.0|65536|19900326|assigned
ripencc|EU|ipv4|143.93.0.0|65536|19940413|assigned
ripencc|NO|ipv4|143.97.0.0|65536|20070104|assigned
ripencc|EU|ipv4|143.99.0.0|65536|19900907|assigned
```

Listing 1. Excerpt from a database file with IP ranges

```
ripencc|EU|asn|2857|1|19931227|allocated
ripencc|EU|asn|2858|1|19940112|allocated
ripencc|SE|asn|2859|1|19940127|allocated
ripencc|EU|asn|2860|1|19940118|allocated

route:          143.93.192.0/18
descr:          FH-RPL-NET
origin:         AS2857
mnt-by:         AS2857-MNT
changed:        weiss@uni-mainz.de 20001220
source:         RIPE
```

Listing 2. Excerpt from database files with AS definitions and relations

AS – a registered Autonomous System. Every AS has a numerical identifier known as *Autonomous System Number* ASN. AS definitions are also listed in the *delegated*-file along with the ISO country code and the date of allocation. However, this file does not specify a relationship between IPv4 ranges and ASes. For this relationship CARMA uses the *ripe.db.route.gz* file (see Listing 2). The latter file contains definition blocks, each block specifies an IPv4 range (this time in proper CIDR notation), and related ASes. This information is used to establish relationships between ranges and ASes listed in the *delegated*-files. Note that a relationship between an IPv4 range and an AS is not unambiguous: The same range can be announced under different ASes; some ASes or ranges listed in the *delegated*-file may not be linked at all, and some relationships specified in *ripe.db.route.gz* may contain ASes and IPv4 ranges, which are unspecified in the *delegated*-file. The incidence of such inconsistencies is low, however.

IPv4 subrange – a subset of the IPv4 address space defined by the addresses of the first and last address of the subrange. These definitions are listed in the *ripe.db.inetnum.gz*-file (see Listing 3). The subranges differ from ranges in that they are not explicitly related to an AS. Subranges are generally smaller in terms of address space. A vast majority of them are derived from splitting up ranges. It is therefore possible to establish a relationship between one or more subranges and a single range, although not all ranges are split into subranges. When parsing information from this file, one should take care to check for sanity of the subranges specified. For instance, a subrange may specify an entire IPv4 address space, or a subrange may even have a netmask length such as 3 bits and may thus be much larger than an IPv4 range. Such cases are dictated by the internal workings of the WHOIS server software but are obviously invalid for

```
inetnum:        143.93.32.0 - 143.93.63.255
netname:        FH-RPL-NET
descr:          Fachhochschule Trier
descr:          Rechenzentrum
descr:          Schneidershof
descr:          D-54293 Trier
country:        DE
admin-c:        KM624-RIPE
tech-c:         RB373-RIPE
status:         ASSIGNED PI
mnt-by:         TRANSKOM-MNT
changed:        hostmaster@transkom.net 20050207
source:         RIPE
```

Listing 3. Excerpt from a database file with IPv4 subranges

```
as-set:         AS-DECIX-CONNECTED
descr:          ASN of DE-CIX members
descr:          DE-CIX, the German Internet Exchange
admin-c:        AN6695-RIPE
tech-c:         WT6695-RIPE
tech-c:         DM6695-RIPE
tech-c:         SJ6695-RIPE
notify:         notify@de-cix.net
mnt-by:         DECIX-MNT
source:         RIPE
changed:        auto-upd@de-cix.net 20091011
members:        AS42
...
members:        AS2828
members:        AS2857
members:        AS2914
...
members:        AS65333
```

Listing 4. Excerpt from a database file with ASSET definitions

CARMA and therefore filtered out of the model.

AS set or *ASSET* – a topological junction point that may declare an arbitrary number of ASes and other ASSETs and facilitate connectivity among them. It is assumed that the information flow between two ASes belonging to the same ASSET does not take a route via other ASSETs. Unlike ASes, ASSETs have alphanumeric identifiers. In terms of CARMA, an IX point is an ASSET with a significant number of member ASes (usually hundreds), although, technically, every ASSET can be considered as a kind of IX as there is usually no explicit requirement in terms of member count. The definitions for ASSETs can be found in the *ripe.db.as-set.gz* file (see Listing 4).

When all database files are processed, the resulting incomplete graph reflects the Internet topology as close as it could be done without having access to *Border Gateway Protocol* (BGP) information. It is not necessary to devise any graph-walking algorithm to calculate the affinity value subsequently called *flavor*, because the purpose of CARMA is to estimate the affinity of two given nodes, not calculating an exact hop count. The proposed flavors of the remote node in relation to the originator node are given below in the order of corresponding tests undertaken by CARMA:

1) *Subrange* identifies the presence of the remote node's IP address in the same IPv4 subrange specified in the *ripe.db.inetnum.gz* database file dealing with administrative IP subranges. However, if such a presence is found, CARMA does not immediately return this flavor, because subranges may overlap with different netmask lengths, which in turn may happen to be shorter than that of the corresponding range (see below). This flavor identifies the presence of the remote node most likely within the scope of operation of a single router or the same network operations center. For example, this could be for end-users connected to the same point of presence of a telecom operator, or nodes within a university network, which usually have single upstream ISP.
2) *Range* identifies the presence of the remote node's IP address in the same IPv4 range specified in the *delegated*-file or the *ripe.db.route.gz* WHOIS excerpts dealing with ASNs and IPv4 delegations. If the subrange lookup yielded any results, the ranges found are examined and compared in terms of netmask length. In this case, the range flavor is only returned if the shortest range netmask is shorter than or equal to that of a subrange, otherwise the subrange flavor is returned. This ensures that the subrange flavor is never returned for allocations larger than the corresponding range, even if they overlap. This flavor means that both nodes most likely reside within the scope of the same department or the same small organization, and that the traffic between these nodes is unlikely to travel outside of the single business network of their ISP.
3) *AS* identifies the presence of the remote node's IP address within the address space allocated to the same AS as defined in the *ripe.db.route.gz* file. Although this fact does not guarantee such an immediate connectivity as the previous flavors, packets are unlikely to travel networks outside this AS, since an AS is the basic Internet routing entity [26]. This flavor suggests that the traffic between two nodes is handled by the ISP internally, and that incoming traffic from outside of the Internet destined to one node undergoes the same routing rules as traffic to the other node.
4) *ASSET/IX* states that both nodes belong to different ASes announced by the same ASSET, which may happen to be an IX if the number of member links is large enough (not every ASSET is an IX, but all IXes are ASSETs). The immediate advantage of this knowledge is not obvious, but in developing countries the difference in quality of service may largely depend on this flavor to the extent that network speed and latency differ by some *orders of magnitude* for nodes within and outside of the same IX. In such national Internet configurations ISPs often implement mandatory traffic shaping policies to limit the packet flow to and from outside of the IX.
5) *ASSET-link* indicates that the node addresses belong to different ASes, which belong to different ASSETs,

and at least one ASSET includes the other ASSET.

6) *Backbone* indicates that the node addresses belong to different ASes, which belong to different ASSETs, and both ASSETs are declared within the scope of a third ASSET.
7) *Distant* identifies that all previous CARMA affinity tests had failed to yield a positive match, and the relative locality of the originator and target node cannot be reliably estimated. Therefore they are assumed to be located topologically far away.

By using these flavors any arbitrary pair of IP addresses can be assigned to an affinity cluster, which in the most cases corresponds to the real topological distance between these nodes.

IV. CARMA-based Application Scenarios

In this section we take a look at two application scenarios, which benefit from the CARMA distance estimation method. The first scenario considers a preselection of peers in a P2P file sharing application. The second scenario discusses the construction of a multicast infrastructure in P2P networks based on an MST approximation.

A. CARMA-based Peer Selection

Regardless of the differences in their protocols and implementations, there is something common in all file sharing networks. That is, after the request for a published entity is processed by either the indexing server or other nodes, a response is obtained in the form of a list of peers. Whether this is done using Distributed Hash Tables (DHT) such as *Kademlia* [27], indexing servers or message flooding [4], the result will contain at least a list of IP addresses and ports.

¿From this point on, it is completely up to the client software to decide which nodes should be queried and in what order. From our previous experiences of analyzing the ED2K and BitTorrent network traffic from a single node, we found out that the client software usually performs queries in the order, which was initially reported by the network or index servers.

By their design ED2K clients will query every known source and will attempt to place themselves in the download queue of every source they managed to successfully negotiate with. The other (receiving) side will organize the download queue initially according to the FIFO principle. Modern clients (eMule [28] and its numerous clones) also feature a reward system, which advances inbound clients in the queue according to the amount of related traffic they had provided to the node. This is supposed to discourage leeching but also has obvious drawbacks in delaying new nodes that do not have any part of the content yet.

Although eMule provides a few tuning methods such as queue rotation, speed and chunk management based on the popularity of the file, none of them takes into account anything related to connectivity (client bandwidth, network latency etc.), let alone the geographical location or topological affinity.

In the popular BitTorrent network, the number of peers for highly-demanded content can easily reach tens of thousands, whereas for most end-user nodes it is quite impractical to initiate more than a hundred connections simultaneously, even when having high-speed links.

The BitTorrent protocol is simpler than ED2K. It does not feature any reward system, and due to the per-content swarm isolation BitTorrent is generally faster. Also, a tracker may not report all peers to the client initially. However, this is usually circumvented later by the peer exchange and DHT mechanisms.

Recently there have been some advances in the locality awareness for BitTorrent networks. Popular nationwide trackers (rutracker.org, for instance) have introduced so-called “retrackers” – dedicated secondary servers. These servers are optionally connected to a primary database, but mainly supposed to only return a peer list local to a specific network scope. This scope usually consists of an IP address pool allocated to customers of a particular ISP, or, more frequently, contains the private unroutable IP ranges of a local intranet. This provides for a significant speed burst for affected ISP clients, but it is a very simple method that only allows for a two-tier locality awareness.

We believe that it is essential to not leave the peer selection process to pure luck. In our previous research in the area of file-sharing networks [29] we figured out a method, which could be used to improve the performance of these networks. The key to the performance improvement is the consideration of CARMA distance estimation flavors for the arrangement of the peer query order. That is, choosing the peers with the lowest flavors would reduce the network latency and increase the exchange speed. In Section V-A we evaluate the quality of the CARMA metric and its impact to peer selection in file sharing applications.

B. CARMIn - *CARMA-based Multicast Infrastructure*

In this section we propose a multicast infrastructure based on an MST approximation. For a large scale number of network nodes the construction of an MST as a communication tree T will lead to unacceptable high network maintenance costs in the case of joining, leaving or failing of nodes. Hence, we have to find a tradeoff between the minimization of multicast costs and latency delays on the one hand and acceptable network maintenance costs on the other hand.

One problem of constructing an MST in real networks is the fact that we do not know exact distances between the nodes (latency delays) as we do in a graph theoretical setting. Measurements of the round trip latency between nodes for the purpose of distance acquisition by sending extraneous ping messages induce an inacceptable high communication overhead in large scale networks and hence have to be avoided. As mentioned before, CARMA flavors indicate the

Algorithm 1: Join Operation

Input: node n, spanning tree $T = (V, E_T, w)$ and bootstrapping set $BS \subseteq V$;
Output: $T' = (V', E'_T, w)$ including n;
begin
  if $V \neq \emptyset$ **then**
    Arrange $v \in BS$ such that
    $\forall\ v_i \in BS : w(v_i, n) \leq w(v_{i+1}, n)$ holds;
    $E'_T = E_T \bigcup \{n, v_1\}$, where v_1 is the first node in BS;
  $V' = V \bigcup \{n\}$;

Algorithm 2: Leave Operation

Input: node n, spanning tree $T = (V, E_T, w)$ and neighbor set $N \subseteq V$;
Output: spanning tree $T' = (V', E'_T, w)$ without n;
begin
  if $degree(n) > 1$ **then**
    Identify $v \in N$ such that the condition
    $\forall\ v_i \in N : w(v, n) \leq w(v_i, n)$ holds;
    Advise all $v_i \in (N \setminus \{v\})$ to connect to v_i;
  $E'_T = E_T$;
  forall the $v_i \in V$ *with* $\{v_i, n\} \in E_T$ **do**
    $E'_T = E'_T \setminus \{v_i, n\}$;
  $V' = V \setminus \{n\}$;

node locality by telling whether a remote peer belongs to the same subnet, the same AS, the same IX, and so on. Therefore, in our approach we utilize the CARMA flavors as a distance substitute for a spanning tree approximation.

Another problem that we have to address, is the lack of global knowledge needed for a spanning tree construction. Most of the existing P2P networks designed for provision of application-level multicast use a bootstrapping process, which returns a list of nodes identified by their IP addresses that are presumed to be online. That is, the initial knowledge of a node is limited to these nodes delivered from the bootstrapping process. In our work we assumed this list to contain between $\log N$ and $\sqrt{N}$ entries, where N is the number of network nodes.

In our CARMIn approach we rely on the NNT principle, where a new node connects to the nearest (in terms of topological distance) known network node.

In our approach we model the Internet as an undirected and connected graph $G = (V, E, w)$. Hereby V stands for the set of vertices $v_i,\ 1 \leq i \leq |V|$, representing network nodes, E is the set of edges $e_{i,j} = \{v_i, v_j\}$ representing the logical connections between nodes, and $w : E \rightarrow \mathbb{N}$ is a weight function assigning a weight to an edge. Generally, the weight function w returns latency time (in milliseconds) of the edge e. However, in this special case it represents a CARMA flavor. On the basis of this graph, we have to create a near-optimal approximation of an MST $T = (V, E_T, w)$ where $E_T \subseteq E$. T is per definition a *connected* graph without *cycles*. In the following we describe the key operations of our approach.

On *joining* (Algorithm 1), the new node first arranges nodes from the bootstrapping set BS depending on their CARMA flavor, and then connects to an arbitrary node with a flavor identifying best network conditions to this node.

Figure 2(a) shows a CARMIn multicast overlay with five nodes. Hereby the nodes b and c belong to the same subrange, the nodes c and e to the same AS, the nodes a and c to the same ASSET, and the nodes c and d belong to the same ASSET link.

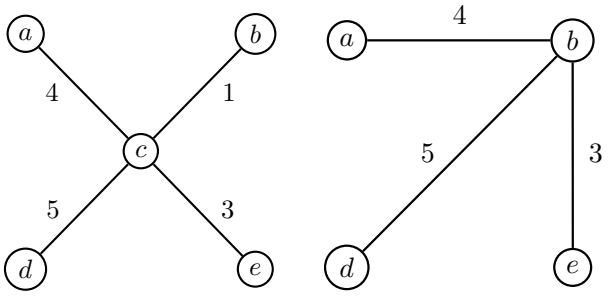

(a) Before leaving of node c (b) After leaving of node c

Figure 2. CARMIn multicast overlay

On *leaving* (Algorithm 2), the leaving node identifies the node v with the lowest CARMA flavor from all of its neighbors N and then advises all remaining neighbors $N \setminus \{v\}$ to create a connection with v.

Figure 2(b) represents the above depicted CARMIn overlay after the leaving of node c. As proposed, all remaining nodes create connections with the *nearest neighbor* of c which is node b.

These definitions of *join* and *leave* operations ensure that our approximation is *connected* and *cycle-free* (key characteristics of a tree) at any stage of the overlay network construction. However, if a hub node – maintaining a significant number of connections – fails, these characteristics may be violated.

In order to guarantee that our MST approximation always satisfies these characteristics independent of node failures, we introduce a *backup* routine. According to this routine, each node notifies its direct neighbors about its connections and the corresponding connection quality. That is, a network node always knows all of its direct neighbors and all their neighbors including the corresponding CARMA flavors (2-hop neighborhood).

If the node n_f fails, nodes in its neighborhood N will be aware of n_f's nearest node v_i, and thus are able to create

connections to v_i in analogy to the regular *leave* operation.

The special feature of the proposed CARMIn approach is the fact, that only the local knowledge of 2-hop neighborhood (no global knowledge) is required for maintaining a multicast infrastructure. Although CARMIn can be used with any other distance estimation or measurement method, it benefits from the utilization of CARMA, since in this way, no additional communication is required for distance estimation. Therefore, CARMIn may be considered as a potential application of the CARMA metric in practice.

We evaluate the quality and cost of our CARMIn MST approximation in Section V-B by comparing it with other multicast approaches.

V. Evaluation Results

In this section we evaluate the quality of the CARMA-based peer selection and of the CARMA-based MST approximation by taking a closer look at the quality of the CARMA distance estimation, and by comparing our CARMA-based multicast approach with other multicast infrastructures.

A. Evaluation of the CARMA-based Peer Selection

The extensive test-runs of CARMA were conducted from a site residing in the customer's address pool of the ISP UkrTelecom for two IPv4 address pools obtained from two of the most popular public trackers of BitTorrent swarms in the Ukraine, namely RuTracker [30] and TorrentsNetUA [31]. These trackers differ significantly in one key aspect, which is important to highlight and validate the CARMA advantages, namely the different percentages of nodes within the same national IX as the vantage point from which the experiments were conducted. From observing the outcome of the "country resolution" feature (which is done by simply querying WHOIS servers for the "country" field) in the popular BitTorrent client μTorrent, we estimate that RuTracker has roughly one-fifth Ukrainian users while TorrentsNetUA harbors about 95% active users from within the Ukrainian exchange point (UA-IX) at any given time. If CARMA is able to confirm such a prevalence, it would be a good sign, prompting the validity of its mathematical model.

Due to established technological and business practices of member ISPs participating in UA-IX, the bandwidth and price for the traffic inside and outside of UA-IX may differ significantly, up to some orders of magnitude. In spite of this, CARMA has large optimization potential. If CARMA-based peer selection rules were to be implemented in, for example, popular BitTorrent clients operating under UA-IX or a similar national Internet setup, far fewer nodes would have to connect outside of their exchange points and many more nodes would be able to choose their peers among those with a more likely higher bandwidth availability.

We decided to use a modified ICMP *traceroute* method in our software. It is assumed that the first IPv4 address from a given address pair is the address of the node where the software runs. The software performs a series of special ICMP *traceroute* requests towards the second address. The modified ICMP *traceroute* method differs from the standard version of the *traceroute* tool as follows:

- *ICMP protocol* – much like the Windows version of traceroute ICMP is used rather than UDP, which is common in its GNU counterpart. This is mostly because the primary runtime environments for CARMA are Microsoft Windows x86 and x64, where easy to use ICMP ping functions are part of the programmer-friendly IP Helper API.
- *No DNS queries* – IP addresses of intermediate nodes are not resolved into their host names, neither their IP addresses are indicated, because our evaluation method is only interested in the number of nodes.
- *Speedy and Smart Verification* – unlike the traceroute command-line tool, the reply timeout is set to one second. If the last responded node is not the intended target, or the reply timeout occurs anywhere on the path, the whole query is restarted. This restart can only happen three times. If the target node is not reached on the second and third attempt, the hop count is assumed to be the largest number of intermediate nodes found in all three passes. This effectively eliminates the influence of accidental network lags, which may cause premature ping timeouts of more than one second.

This modified ICMP *traceroute* method was tested from an asymmetric end-user ADSL connection within the UA-IX, characterized by an average response time of around 50 milliseconds from the nodes of its immediate IX neighborhood and of less than 300 milliseconds from the nodes abroad. The tests indicated that an average measurement session for an address pair lasts anywhere from less than half a second, if the target node responds to ICMP requests, to no more than 5 seconds, if it does not respond because of timeout, and no more than 3 seconds, if it does not respond because of reported network or host unreachability. Nevertheless, the sampling of each of the thousand address pairs requires about 1 hour to complete.

The ICMP measurement module was integrated into the CARMA batch-processing software such that for every processed address-pair the real hop count can be measured and written together with the computed CARMA flavor value, unless an ICMP loophole is detected (which was the case for about 2 address pairs per thousand). We consider the gathered statistics later in the course of this section as well.

To obtain a broad spectrum of CARMA affinity flavors as well as hop counts, both trackers were used to gather sampling swarms. However, the volumes of swarms differ significantly: RuTracker was able to produce a swarm of 3610 peers while TorrentsNetUA struggled to achieve 900. The reason for this was that RuTracker features the mandatory enabling of the DHT and *peer exchange (PEX)*

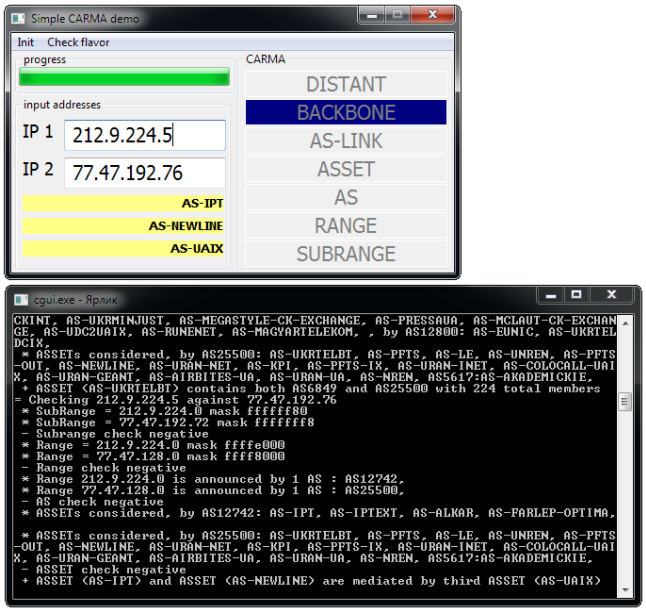

Figure 3. Screenshot of CARMA concept demonstration tool

mechanisms. Both are features of the BitTorrent protocol [6] allowing a list of new peers from already connected peers to be gotten. DHT and PEX essentially provide a large peer list within a few seconds, instead of the usually limited number of bootstrap peers provided otherwise by tracker alone.

The sampling swarm from RuTracker consisted of 3610 peer nodes of which a small, but notable percentage was believed to belong to the UA-IX address space. TorrentsNetUA provided a sampling swarm of 891 peer nodes of which the vast majority was expected to belong to the UA-IX. Each peer was processed by the CARMA software against the address of its own host machine (also within the UA-IX, see Figure 3), and then the apparent network distance from the host machine to the peer node was measured in terms of a hop count. Figure 3 shows a screenshot of the CARMA concept demonstration tool with a pair of IPv4 addresses as input and their computed flavor with a portion of the calculation logic logfile.

The experiment took about 5 hours to complete. Due to its extended duration, the test-runs were performed in the time period between 01:00 and 06:00 UTC, during which the average Internet traffic volumes generated by the end-users in Russian and Ukrainian segments are at their lowest. This was done to ensure the most favorable conditions for our modified ICMP *traceroute* tool, including the low occurrence of traffic switchovers. We also have observed that nighttime does not cause the numbers of the peers participating in the BitTorrents swarms to drop. This is because the majority of active BitTorrent users either operate so-called seedboxes (dedicated servers customized for BitTorrent) or keep their computers turned on during the night to gain the advantages

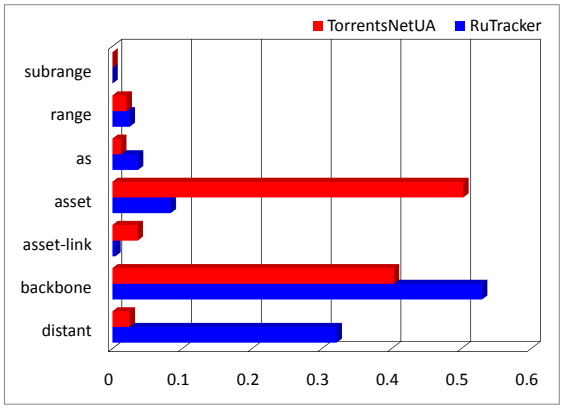

Figure 4. Normalized flavor breakup for the sampling swarms

of the lower nighttime traffic prices.

The preliminary analysis of the obtained data revealed several key insights into the functioning of CARMA. The visible abundance of ASSET-flavored peers is due to the fact that RuTracker historically harbors a large Ukrainian user base. CARMA was able to identify almost 19% of participating users in all tested swarms as Ukrainian, as most of the end-users of Ukrainian ISPs are topologically "under" two major IX points, namely UA-IX and DataGroup-IX [32]. This would trigger the ASSET flavor for most of them if tested by CARMA against a Ukrainian address.

Figure 4 represents the normalized percentage breakup of the sampling swarms obtained from the TorrentsNetUA (upper bar) and RuTracker (lower bar) trackers. First, the TorrentsNetUA flavor breakup in Figure 4 shows that the quantity of distant nodes is 2.5% of the whole swarm space, which is consistent with our predictions. It should be noted however, that in rare occasions this flavor could denote an IPv4 address space registered within the Ukraine and actually operating under UA-IX, if, for some reason, the stored information of its linkage is wrong. Conversely, not all backbone-flavored nodes belong to UA-IX either, as, for example, many Russian IPv4 addresses were flavored as backbone because of an intermediate link between the Ukrainian and Russian major IX points by TeliaSonera AB.

Secondly, the notable low percentage of ASSET-link flavored nodes in both cases may indicate the similarly low likelihood of encountering an arbitrary cross-AS link not mediated by the higher-level ASSET, or a general trend towards building hierarchical routing policies within the national Internet exchange setups, which is consistent with the conclusions drawn in [32].

Also surprising is the fact that none of the nodes had fallen into the subrange flavor. This may have happened due to either the small sample size, or because the subrange announced for the host machine address matched the same range, in which case CARMA chooses the latter.

Meanwhile, our primary goal for this validation was to ensure that the affinity flavor predicted by CARMA corresponds to the topological distance in the network. It is well understood that the nature of these two parameters (flavor and hop count) is completely different and that the numerical representation of the resulting CARMA flavor has no physical meaning unlike the hop count. Still they have to correspond with enough accuracy to prove the effectiveness of CARMA as a traffic-less, purely computational distance estimation metric. To prove the point, we decided to employ two well-known methods of mathematical statistics, such as the chi-square criterion and one-way analysis of variance (abbreviated one-way ANOVA). Strictly speaking, the latter is formally not suitable for analyzing data of digital or otherwise discrete nature, as it was designed for normally distributed data. But we decided to use it anyway due to the significantly large sample size.

However, before calculating the statistical criteria, the results must undergo a sanity test. To give an impression of the nature of the results, the significant portion of them is shown on Figure 5 depicting the accordance between CARMA flavors and hop counts for the RuTracker sampling swarm. The horizontal axes correspond to CARMA flavors (symbolic names) and traceroute hop counts (numeric), while the vertical axis corresponds to the number of occurrences. It is apparent from Figure 5 that within each flavor the hop count distribution is more or less gradual and dome-like (increasing and decreasing slowly along the hop count axis). But at the farthest corner of the graph we see one distinct verge reaching about 100 occurrences for a small hop count with backbone and distant flavors. Figure 6 reveals anomalous occurrences in the hop count flavor distribution: underlined values are those flagged by CARMA as topologically very far while having traceroute hop counts extremely low (2 and 3).

To determine the causes of such anomalies, we conducted manual traceroute runs on the addresses, which yielded specific combinations, such as backbone:3, distant:2 and distant:3. Traceroute unexpectedly stopped at the second and third hop and no subsequent nodes replied at all. Since this behavior was observed only from our vantage point (many LookingGlass servers traced the route to these nodes without any problem), future versions of the CARMA batch processing software [1] should include mechanisms to filter out bogus results caused by temporary malfunctions of ISP routers.

The parameters relevant to the chi-square criterion were automatically calculated by the CARMA batch processing software for both passes, see Table I. As the probability levels for both samples are far below 0.001, we conclude that the correspondence between the predicted CARMA flavor and the actual hop count does exist and is certain. We now proceed to apply the one-way ANOVA method to determine the influence level. We define the influence level

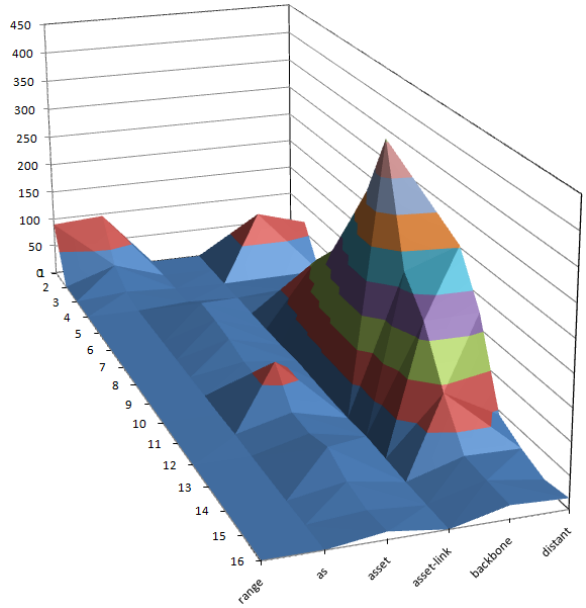

Figure 5. Flavors and hop counts of the RuTracker swarm

	range	as	asset	asset-link	backbone	distant
1	0	0	0	0	0	0
2	90	96	0	0	0	4
3	0	29	0	0	94	69
4	0	7	2	0	1	2
5	0	0	5	1	6	6
6	0	0	30	0	27	19

Figure 6. Anomalous occurrences in the hop count flavor distribution

as the ratio of the Sum of Squares (SS) between groups and the total SS, see Table II. As can be seen from the table, the correspondences between the chosen parameters (hence, influence levels) are 31.425% and 8.684% for RuTracker and TorrentsNetUA, respectively. The lower influence level for the sample obtained from TorrentsNetUA swarm could be explained by its topologically constrained nature, in the sense that distant flavored nodes were much less frequent.

	RuTracker	TorrentsNetUA
Degrees of freedom (d)	120	75
chi-square (χ^2)	3722.86	413.20
Probability (p)	$p < 0.001$	$p < 0.001$

Table I
STATISTICAL PARAMETERS RELEVANT TO THE CHI-SQUARE CRITERION

	RuTracker	TorrentsNetUA
Range variance	0	0.941
AS variance	1.029	2.083
ASSET variance	9.949	1.585
ASSET-Link variance	6.466	4.933
Backbone variance	8.576	3.802
Distant variance	10.937	0.177
SS between groups	14785.941	215.419
SS among groups	32265.495	2265.020
SS total	47051.436	2480.439
Level of influence	31.425%	8.684%

Table II
STATISTICAL PARAMETERS RELEVANT TO VARIANCE ANALYSIS

However, both levels of influence are quite optimistic.

In order to get an impression of the value of the CARMA distance estimation method returning a distance flavor and the corresponding hop count, we compared it with the results of the ping method returning the round trip time of a message in milliseconds. Therefore, we first measured the CARMA distance (flavor and hop count) between the University of Applied Sciences in Trier (Germany) and 17 other universities. Then we sorted these results in ascending order. Afterwards we measured the ping distance to these IP addresses. As the results in Table III show, for 4 of 17 positions (less than 25%) the ping order differs from the CARMA order. Based on these results we claim that CARMA provides a feasible approximation for node distances in the Internet. Moreover, as the results show, 4 of 17 IP addresses were not accessible by the ping method. This behavior indicates a significant drawback of the ping and traceroute methods already described in Section II: Some ISPs are filtering those requests. Therefore ping or traceroute requests cannot guarantee that a valid result will be returned. This fact may be considered as a definite advantage of CARMA compared to ping and traceroute, since CARMA always returns a result.

It is understood that the results obtained in this set of the experiments are rather preliminary and are somewhat lacking the concrete proof of explicit performance improvement in case CARMA is implemented in BitTorrent client software. The purpose of this paper, however, is to evaluate the feasibility of the CARMA model in P2P applications in general by comparing it with traditional network distance metrics.

B. Quality and Cost of the CARMIn MST Approximation

The problem of minimizing communication costs can be reduced to the problem of finding a *Minimum Communication Cost Spanning Tree* (MCT) [33][34] known to be NP-hard. This problem is formalized in [35] as follows: having a set of peers $V = \{v_1, \ldots, v_n\}$ there is a matrix $R_{n\times n} = (r_{i,j})$ of communication requirements where $r_{i,j}$ represents the expected communication from v_i to v_j. The distances between peers are stored in a distance matrix

Destination	Flavor	Hops	Ping [ms]
143.93.54.111	1	3	4
136.199.199.105	2	9	7
131.246.120.51	3	11	8
82.165.77.114	3	13	12
143.169.9.245	3	15	-
193.1.101.61	3	16	39
193.232.113.151	3	17	47
141.20.5.188	3	17	**26**
163.1.13.189	3	20	**24**
130.92.253.230	3	22	-
131.180.77.26	5	12	**17**
217.21.43.11	5	18	51
169.229.131.81	5	26	**166**
131.130.70.8	6	14	-
217.173.193.11	6	15	-
77.47.133.2	6	16	53
128.112.132.86	6	20	106

Table III
CARMA VS. PING COMPARISON

$W_{n\times n} = (w_{i,j})$, where $w_{i,j}$ represents the latency time for sending a message from v_i to v_j. [35] denotes the distance $dist(v_i, v_j, G)$ between two arbitrary nodes v_i and v_j in a network graph G as the minimum sum of the edge weights from W along any path connecting v_i and v_j in G. For every two peers v_i and v_j a spanning tree $T = (V, E_T, w)$ ($E_T \subseteq E$) contains a unique path of length $dist(v_i, v_j, T)$. The communication cost over the network tree is defined as:

$$C(T) = \sum_{i,j} r_{i,j} \cdot dist(v_i, v_j, T)$$

The algorithm proposed in [35] guarantees a $O(\log^2 |V|)$ approximation of the considered problem.

However, in a P2P system we cannot exactly specify the expected amount of communication $r_{i,j}$ between two arbitrary nodes v_i and v_j. By assuming that $r_{i,j} = 1$, $\forall\ 1 \leq i,\ j \leq |V|$, [36] proposes the reduction of multicast costs by using an MST approximation. Hereby the multicast cost $C(E_T)$ is denoted as the cost for propagating a message to all recipients in the group, which is the sum of all edge weights in the tree representing latency delays along any path taken by the message:

$$C(E_T) = \sum_{e \in E_T} w(e)$$

We use the $C(E_T)$ metric as the quality function for the comparison of different approaches.

In order to provide meaningful results, we compare our CARMIn approach with some of the existing P2P approaches supporting application-level multicast such as ALMI, JXTA, and HiOPS [36]. To extend the range of our evaluation, we have also considered a *RANDOM* infrastructure, where a new node builds up connections to a randomly selected node from the bootstrapping set. Figure 7 shows MST approximations by using the above mentioned approaches in networks with 100 nodes.

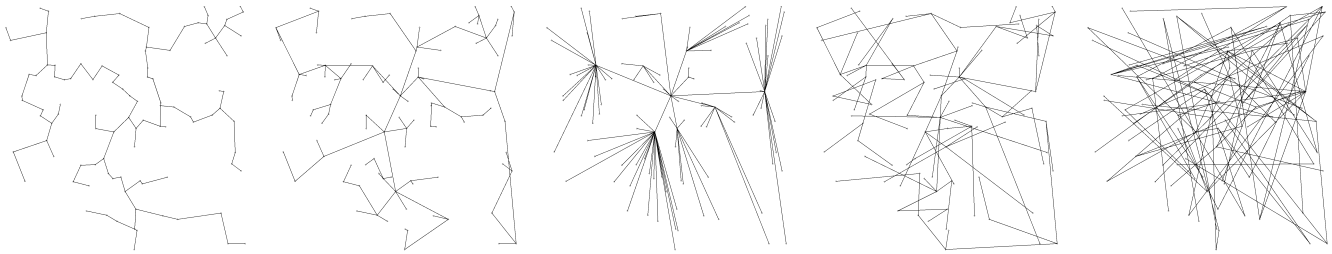

(a) ALMI (b) JXTA (c) HiOPS (d) CARMA (e) RANDOM

Figure 7. MST approximations in networks with 100 nodes

To compare these networks with respect to the communication cost $C(E_T)$, we set up a simple simulation environment. Using this environment, we can create an arbitrary number of network nodes, interconnect them according to a given algorithm and then compute the communication cost metric $C(E_T)$. We have performed several evaluation runs where we randomly created 10, 500, 1000, 1500, 2000, 2500, 3000, 3500, 4000, 4500, and 5000 nodes interconnecting them with ALMI, JXTA, HiOPS, CARMIn and RANDOM infrastructures. After each run, we computed the communication cost $C(E_T)$ in milliseconds needed for the propagation of a multicast message to all existing nodes.

As Figure 8 shows, the JXTA and ALMI approaches relying on global knowledge do provide low $C(E_T)$ values. But as mentioned before, these do not scale in terms of a large number of users. As expected, the RANDOM infrastructure incurs the highest communication cost. The scalable CARMIn approach provides nearly the same $C(E_T)$ values as does the HiOPS overlay, but relies only on local knowledge as does the RANDOM infrastructure, by this means providing a good trade-off between construction and communication costs. The binning approach [24] would show almost the same behavior in terms of the communications cost as the CARMIn approach. However, CARMIn does not require any additional communication for ordering the nodes in the bootstrapping set, whereas nodes following the binning approach have to contact the landmark servers.

We denote the metric describing the knowledge i.e., the number of nodes, which should be known by a new node to join the multicast infrastructure, as $K(V)$. In order to construct an MST, ALMI requires global knowledge of all involved nodes $K(V) = |V|$. A new JXTA node requires the same amount of knowledge $K(V) = |V|$ in order to identify the nearest node. In HiOPS and CARMIn the amount of knowledge is variable and depends on the initial settings. For our comparison in [1] we have used bootstrapping lists for CAMRA and HiOPS with up to $K(V) = \sqrt{|V|}$ nodes. Only the RANDOM infrastructure does not require any global knowledge. Here it is enough to know only one node. Figure 9 represents the respective amounts of knowledge.

We denote the metric describing the running time complexity i.e., the construction cost of any multicast tree as

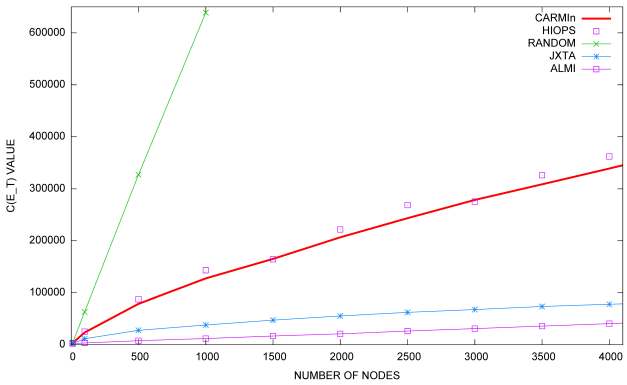

Figure 8. Communication cost $C(E_T)$

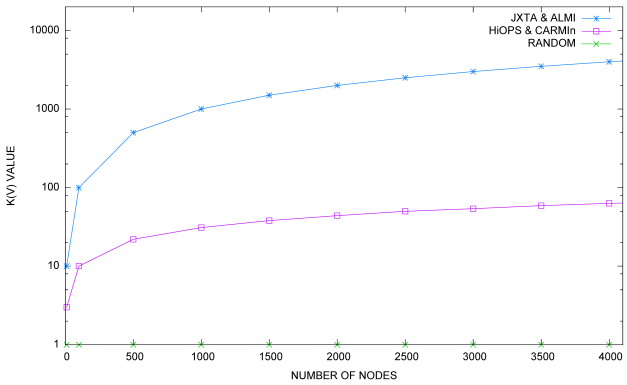

Figure 9. Amount of knowledge K(V)

$O(T)$. The running time complexity for the MST construction is dominated by sorting of edges i.e., node distances [37]. The sorting complexity is given by

$$\begin{aligned} O(T) &= O(\log|E||E|) = O(\log|V|^2|E|) \\ &= O(2\log|V||E|) = O(\log|V||E|). \end{aligned}$$

Because of this sorting complexity the same construction cost is needed for construction of the JXTA-NNT. As discussed in [1], in HiOPS only rendezvous nodes ($|V_R| = \sqrt{|V|}$) are involved in the MST construction. Assuming that the implication $|V_R| = \sqrt{|V|} \Rightarrow |E_R| = \sqrt{|E|}$

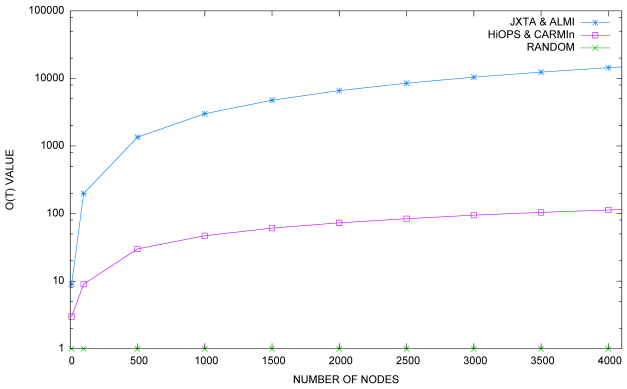

Figure 10. Construction cost O(T)

holds, the construction cost of the HiOPS infrastructure equates to $O(T) = O(\log \sqrt{|V|}\sqrt{|E|})$. According to the CARMIn approach, the nodes from the bootstrapping list ($\sqrt{V}$) have to be sorted depending on their CARMA distance. Thus, the construction cost here corresponds to $O(T) = O(\log \sqrt{|V|}\sqrt{|E|})$ due to sorting complexity too. The construction of the RANDOM infrastructure does not require any nameable construction cost ($O(T) = O(1)$). Figure 10 compares the considered multicast approaches with respect to required construction costs. As shown by this figure, the construction cost of ALMI and JXTA infrastructures is simply too high.

As the evaluation results show, a clear performance improvement of CARMIn over the RANDOM approach is observed. With respect to other algorithms computing an optimal MST (ALMI) or relying on global knowledge (JXTA), the simplicity of the CARMIn approach (lower construction cost, local knowledge) is the advantage, but the multicast cost deteriorates. Moreover CARMIn does provide a more scalable solution than HiOPS, since due to the utilization of CARMA it does not require any additional communication. Therefore, in large-scale application scenarios, which cannot rely on global knowledge and do not have exact information about node distances, we would prefer our CARMIn approach to all other considered approaches.

VI. Conclusion and Future Work

By design, CARMA is meant to be dynamically changing as the communication goes on, reflecting and adapting to the changes in bandwidth conditions. The life-cycle of a CARMA-capable node in a P2P network starts with the downloading of the most recent IP and AS allocation databases from all regional Internet registries and compiling them into an easily indexable internal format. This may take tens of minutes to complete, depending on the CPU speed and bandwidth. Although the RIR databases are updated daily, their growth rate is rather low. Therefore, the startup sequence to refresh the data may be called less frequently than once a day.

In this paper we also have partially addressed the second layer of CARMA, leaving active measurements of bandwidth as well as the integration of CARMA into P2P client software for future publications. Under the assumption that the traceroute hop count represents, to a certain degree, a real topological distance, an experimental validation indicated that the correspondence between predicted flavors and actual topological distances exists and is significant.

The most obvious and straightforward leveraging mechanism for CARMA is peer list reordering. As mentioned in Section IV-A, a P2P client starts to actively request the downloading of a file upon receiving a list of peers who had earlier indicated the possession of the desired content. In all of the P2P clients that we analyzed, either no precedence is given to any peer from the list or it has nothing to do with topological affinity. In fact, in many practical scenarios, even not all peers from the list are queried until the downloading is stopped. However, if the peer list is very large and diverse enough in terms of topological distance and bandwidth conditions, the corresponding precedence mechanism can ensure a significant burst of performance by choosing peers that are likely (according to their CARMA flavor) to provide higher transfer speeds and lower latency.

Therefore, in our future work we would like to address the complete second and third layers of CARMA, calculated by direct measurements involving additional traffic. These layers may be expressed as weighted scores by which all peer priorities are then fine-tuned within the boundaries of their respective first-layer flavors. It should be noted that an implementation of the second CARMA layer will require modifications to the existing software, and that the third CARMA layer will require extensions to existing protocols in order to have any impact on the performance. In this case, the life-cycle of a CARMA-capable node is extended to include the following steps after the initial startup and peer list ordering based on the first-layer flavors:

1) an additional check is performed using the second layer of CARMA in such a way that the original order is not substituted, but rather fine-tuned;
2) at this point, the actual communication to remote parties is initiated; if connections are setup using a CARMA-enabled protocol, the third layer is utilized by the parties providing bandwidth conditions and related information to each other; using this information, peer lists may once again be reordered placing less-loaded nodes at higher positions.

If a peer exchange mechanism is enabled, newly reported nodes must go through all layers of CARMA in order to be placed in the peer list.

We plan to demonstrate the effectiveness of the CARMA approach by performing extensive experiments using the set of BitTorrent client software with plugin support that allow peer ordering to be manipulated. If this proves to be

effective, we plan to integrate CARMA into real-life P2P networks. We are currently developing a software library, implementing CARMA under the LGPL license to assist software engineers wishing to optimize the performance of their P2P applications.

REFERENCES

[1] G. Poryev, H. Schloss, and R. Oechsle, "CARMA Based MST Approximation for Multicast Provision in P2P Networks," in *Proceedings of the 2010 Sixth International Conference on Networking and Services (ICNS '10)*. Washington, DC, USA: IEEE Computer Society, 2010, pp. 123–128.

[2] S. Daniel, J. Ellis, and T. Truscott, "USENET - A General Access UNIX at Network," 1980.

[3] Napster-Homepage, Access date: January 2011. [Online]. Available: www.napster.com

[4] M. Jovanovic, F. Annexstein, and K. Berman, "Scalability Issues in Large Peer-to-Peer Networks - a Case Study of Gnutella," 2001. [Online]. Available: citeseer.ist.psu.edu/jovanovic01scalability.html

[5] eDonkey2000 Homepage, Access date: January 2011. [Online]. Available: http://tinyurl.com/ed2klink

[6] B. Cohen, "Incentives Build Robustness in BitTorrent," in *the First Workshop on the Economics of Peer-to-Peer Systems*, 2003.

[7] R. Bustos, A. Aguilar, K. Makki, and R. K. Ege, "Multicast-P2P Content Distribution in Large-Scale Enterprise Networks," in *IEEE Symposium on Computers and Communications (ISCC 2008)*, 2008, pp. 487–494.

[8] A. Feldmann and V. Aggarwal, "ISP-Aided Neighbor Selection in P2P Systems," in *IETF P2P Infrastructure Workshop (P2Pi)*, Berlin, Germany, May 2008.

[9] D. R. Choffnes and F. E. Bustamante, "Taming the Torrent: a Practical Approach to Reducing Cross-isp Traffic in Peer-to-Peer Systems," *SIGCOMM Comput. Commun. Rev.*, vol. 38, no. 4, pp. 363–374, 2008.

[10] H. Xie, A. Krishnamurthy, A. Silberschatz, and R. Y. Yang, "P4P: Explicit Communications for Cooperative Control Between P2P and Network Providers," DCIA P2P MARKET CONFERENCE, 2008.

[11] J. Kubiatowicz, "Extracting Guarantees from Chaos," *Commun. ACM*, vol. 46, no. 2, pp. 33–38, 2003.

[12] G. Lucas, A. Ghose, and J. Chuang, "On Characterizing Affinity and its Impact on Network Performance," in *Proceedings of the ACM SIGCOMM workshop on Models, methods and tools for reproducible network research (MoMeTools '03)*. New York, NY, USA: ACM, 2003, pp. 65–75.

[13] B. Augustin, X. Cuvellier, B. Orgogozo, F. Viger, T. Friedman, M. Latapy, C. Magnien, and R. Teixeira, "Avoiding Traceroute Anomalies with Paris Traceroute," in *Proceedings of the 6th ACM SIGCOMM conference on Internet measurement (IMC '06)*. New York, NY, USA: ACM, 2006, pp. 153–158.

[14] H. Madhyastha, T. Isdal, M. Piatek, and C. Dixon, "iPlane: An Information Plane for Distributed Services," in *Proceedings of the 7th USENIX Symposium on Operating Systems Design and Implementation*. USENIX, 2006, pp. 367–380.

[15] T. Karagiannis, P. Rodriguez, and K. Papagiannaki, "Should Internet Service Providers Fear Peer-Assisted Content Distribution?" in *Proceedings of the 5th ACM SIGCOMM conference on Internet measurement (IMC '05)*. New York, NY, USA: ACM, 2005, pp. 63–76.

[16] T. Jiang and A. Zhong, "A Multicast Routing Algorithm for P2P Networks," in *GCC 2003*, 2003, pp. 452–455.

[17] T. Peng, Q. Zheng, and Y. Jin, "Transmission Latency based Network Friendly Tree for Peer-to-Peer Streaming," *j-jucs*, vol. 15, no. 9, pp. 2011–2025, 2009, http://www.jucs.org/jucs_15_9/transmission_latency_based_network.

[18] D. Pendarakis, S. Shi, D. Verma, and M. Waldvogel, "ALMI: an Application Level Multicast Infrastructure," in *Proceedings of the 3rd conference on USENIX Symposium on Internet Technologies and Systems (USITS'01)*. Berkeley, CA, USA: USENIX Association, 2001, pp. 5–5.

[19] K. Radab and A. U. Haque, "A Minimum Spanning Tree Algorithm for Efficient P2P Video Streaming System," in *The 12th International Conference on Advanced Communication Technology (ICACT 2010), 2010*, 2010, pp. 93 – 97.

[20] D. Peleg and V. Rubinovich, "A Near-Tight Lower Bound on the Time Complexity of Distributed Minimum-Weight Spanning Tree Construction," *SIAM J. Comput.*, vol. 30, no. 5, pp. 1427–1442, 2000.

[21] M. Khan and G. Pandurangan, "A Fast Distributed Approximation Algorithm for Minimum Spanning Trees," *Distributed Computing*, vol. 20, no. 6, pp. 391–402, April 2008. [Online]. Available: http://dx.doi.org/10.1007/s00446-007-0047-8

[22] JXTA-Homepage, Access date: January 2011. [Online]. Available: https://jxta.dev.java.net

[23] E. Michael, "Distributed Approximation: a Survey," *SIGACT News*, vol. 35, no. 4, pp. 40–57, 2004.

[24] S. Ratnasamy, M. Handley, R. Karp, and S. Shenker, "Topologically-aware Overlay Construction and Server Selection," in *Proceedings of Twenty-First Annual Joint Conference of the IEEE Computer and Communications Societies (INFOCOM 2002)*, vol. 3, 2002, pp. 1190– 1199 vol.

[25] J. J. D. Mol, D. H. J. Epema, and H. J. Sips, "The Orchard Algorithm: P2P Multicasting without Free-Riding," in *Proceedings of the Sixth IEEE International Conference on Peer-to-Peer Computing*. Washington, DC, USA: IEEE Computer Society, 2006, pp. 275–282. [Online]. Available: http://portal.acm.org/citation.cfm?id=1157740.1158270

[26] J. Hawkinson and T. Bates, "Guidelines for Creation, Selection, and Registration of an Autonomous System (AS)," RFC 1930 (Best Current Practice), Internet Engineering Task Force, mar 1996. [Online]. Available: http://www.ietf.org/rfc/rfc1930.txt

[27] P. Maymounkov and D. Mazieres, "Kademlia: A Peer-to-Peer Information System Based on the XOR Metric," 2002, http://www.cs.rice.edu/Conferences/IPTPS02/109.pdf.

[28] eMule Homepage, Access date: January 2011. [Online]. Available: http://www.emule-project.net

[29] G. Poryev, T. Rudyk, and O. Sulima, "Traffic Regulation and Reputation Handling in the BitTorrent Peer-to-Peer Networks," National Technical University of Ukraine "KPI", Tech. Rep., 2008.

[30] RuTracker-Homepage, Access date: January 2011. [Online]. Available: http://rutracker.org

[31] TorrentsNetUA-Homepage, Access date: January 2011. [Online]. Available: http://torrents.net.ua

[32] V. Furashev, V. Zubok, and D. Lande, "Parameters of the Ukrainian Internet segment as a complex network," *in Proceedings of the Open Informatics and Computer Technologies*, vol. 40, pp. 235–242, 2008.

[33] P. Crescenzi and V. Kann, "A compendium of NP Optimization Problems." [Online]. Available: http://www.nada.kth.se/~viggo/wwwcompendium/node77.html#4555

[34] M. R. Garey and D. S. Johnson, *Computers and Intractability: A Guide to the Theory of NP-Completeness*. W. H. Freeman, 1979.

[35] D. Peleg and E. Reshef, "Deterministic Polylog Approximation for Minimum Communication Spanning Trees," in *Proceedings of the 25th International Colloquium on Automata, Languages and Programming (ICALP '98)*. London, UK: Springer-Verlag, 1998, pp. 670–681.

[36] H. Schloss, R. Oechsle, J. Botev, M. Esch, A. Hoehfeld, and I. Scholtes, "HiOPS Overlay - Efficient Provision of Multicast in Peer-to-Peer Systems," in *16th IEEE International Conference on Networks (ICON 2008)*, New Delhi, India, 2008, pp. 1–6.

[37] J. B. Kruskal, "On the Shortest Spanning Subtree of a Graph and the Traveling Salesman Problem," *Proc. Am. Math. Soc.*, vol. 7, pp. 48–50, 1956.

Improving IPTV QoE taking the suitable MPEG-2/MPEG-4 Quantizer based on Jitter, Delay and lost packets measurements

Alejandro Canovas[1], Miguel Garcia[1], Jaime Lloret[1], Marcelo Atenas[1] and Rafael Rizo[2]
[1]Universidad Politécnica de Valencia, Camino Vera s/n, 46022, Valencia, Spain
[2]France Telecom R&D, ORANGE LABS, Barcelona, Spain,
alcasol@posgrado.upv.es, migarpi@posgrado.upv.es, jlloret@dcom.upv.es, marat1@posgrado.upv.es, rafael.rizo@orange-ftgroup.com

***Abstract* — The main issue in Digital Terrestrial Television and in IPTV networks is the Quality of Experience received by the end users. For this reason, mechanisms to automatically measure the video quality of the images received by the user are needed. In this paper, we analyze video quantization in order to determine an optimal quantizer_scale factor value for its transmission. Then, it is used as an automatic measure to improve the video quality received by the end user. The paper shows the measurements taken for Objective and subjective Video Quality, Video Quality Metric and the bandwidth consumed for several types of video quality. We use the jitter, delay and lost packets measurements in order to take the appropriate quantizer. Finally, we show the visual comparison between a high quantizer_scale factor and a reference video. Our work shows that an optimal quantizer_scale factor can be used to save bandwidth in an IPTV network or to improve the Video Quality for the same bandwidth consumption. Finally, we present some discussions of the measurements gathered and some comments of other authors.**

Keywords – MPEG-2/MPEG-4 Quantizer, Video Quality, IPTV.

I. INTRODUCTION

MPEG-2 and MPEG-4 encoding are standards that are widely used by the digital television industry [1]. Although, nowadays, MPEG-2 is the most used, MPEG-4 is gaining ground because it provides good quality image with lower bandwidth consumption [2]. The application fields where MPEG-4 can be applied are Digital Television, interactive graphical applications and interactive multimedia, while providing high audiovisual data compression to store or stream video and, at the same time, audio and video quality. MPEG-4 reduces the data rate in half, with the same image quality than MPEG-2. This will increase the offer and the plurality of channels and, at the same time, the scalability of network services. MPEG-4 compression is based on visual-objects coding [3] and uses further coding tools, like System Decoder Model, Sync Layer, Flexible Multiplex, etc. [4], to achieve higher compression factors than MPEG-2, thus it needs less bandwidth for its transmission, but MPEG-2 is the most used codec in Digital Terrestrial Television and in IPTV networks, because it has lower complexity and hardware requirements at the end user.

MPEG-2 compression format is quite used for video storage in hardware devices (DVD, SVCD, etc) and to transmit real time video in several Digital Video Broadcasting (DVB) standards [5]:

- DVB-T: This system transmits compressed digital audio, video and other data in a MPEG-2 transport stream, using COFDM modulation.
- DVB-S: This system increases the data transmission capacity and digital television via a satellite UH11 using the MPEG-2 format, and QPSK modulation.
- DVB-C: This system transmits MPEG-2 or MPEG-4 family digital audio/video stream, using several QAM modulations with channel coding.

DVB system has been used as a basis to standardize the Internet Protocol Television (IPTV). It includes MPEG-2 DVB services [6] encoded with MPEG-2 technology and encapsulated in MPEG-2 Transport Stream (MPEG-2 TS) [7]. But, MPEG-4 can be also added in this transport stream. Moreover, it covers Live Media Broadcast services (i.e TV or radio styles), Media Broadcast with Trick Modes and Content on Demand services (CoD). The goal of DVB-IP is to specify technologies on the interface between an IP based network and a DVB-IP Set-top-Box, which uses a protocol stack for DVB IP services. A diagram of the protocol stack is given in Figure 1.

Once DVB services are encoded, the video content is packaged and encapsulated. This involves inserting and organizing video data into individual packets. The encapsulation of the video content is done using MPEG-2 TS, where all MPEG-2 TS will be encapsulated in Real time Transport Protocol (RTP) according to RFC 1889 [8] in conjunction with RFC 2250 [9], and RFC 768 [10] as the transport layer protocol.

Initially, MPEG-4 doesn't define a transport layer [11]. There are only two adjustments on the MPEG-2 TS to transport MPEG-4 streams. The first one is defined in RFC 3016, which is based in RTP packets [12]. The second one is DMIF, or Delivery Multimedia Integration Framework, which is an interface between the application and the transport. It allows the MPEG-4 application developer to stop worrying about MPEG-4 transport. A single application can run on different transport layers.

The message fields used in the transport stream of the MPEG-2 based DVB content over IP are the following ones: a standard IP header, an UDP header, a RTP header and an integer number of 188 bytes MPEG-2 TS packets, see Figure 2. The maximum size of IP datagram (65535 octets for IPv4) is limited. In the case of an Ethernet-based network, with a Maximum Transfer Unit (MTU) of 1492 or 1500 bytes, the number of MPEG-2 TS packets is 7.

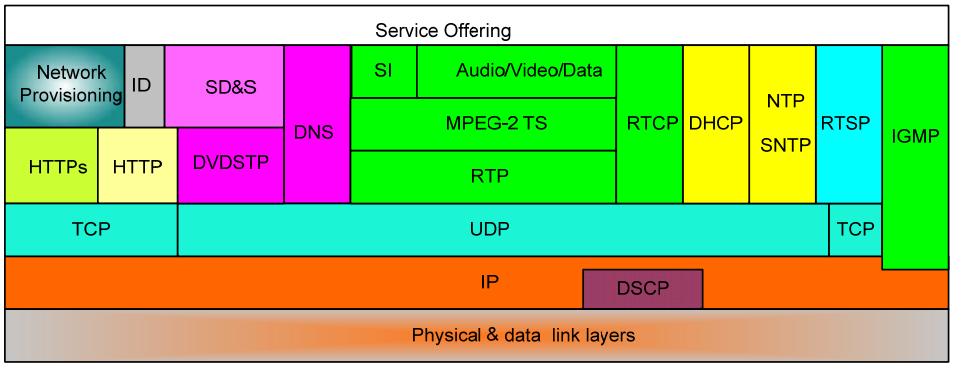

Figure 1. Protocol stack for DVB-IP services

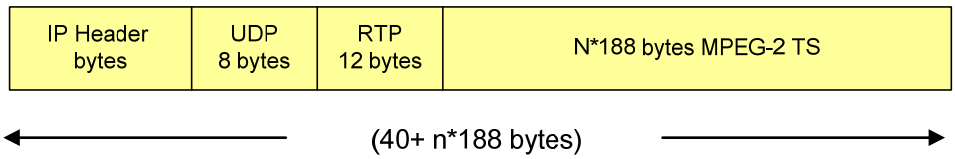

Figure 2. Message to transport MPEG-2 based DVB content

The main challenge in current IPTV systems is to provide high Quality of Experience (QoE) to the user, but using noninvasive methods while the network is being monitored.

In the paper with reference [13] we analyze MPEG-2/MPEG-4 quantization in MPEG-2 TS packets, as a noninvasive method to evaluate the video quality function. It is useful because it allows us to measure the QoE perceived by the IPTV customer. Several quantizer scales are used to evaluate, which of them are better according to the bandwidth, objective video quality, etc. In this paper, we have extended [13] by adding many more tests and adding more variables for our comparison. Moreover, we now have another conclusion: QS=4 is better taking into account the Bandwidth, Jitter, Delay, Lost Packets, VQM, MOS and subjective analysis, while in [13] the best one was QS=2.

The remainder of this paper is organized as follows. Section II explains some work related with video MPEG-2 and MPEG-4 encoding and user video-quality perception. Section III explains the general concept of quantization. The system architecture used to perform our test is presented in Section IV. Section V shows the measurements obtained when different quantization scales are used in order to find the optimal quantizer_scale factor. Objective and subjective video quality for IPTV is shown in Section VI. Section VII shows the jitter, delay and lost packets test. Section VIII provides some discussions of the measurements gathered and the ones taken from other authors. Finally, Section IX draws the conclusion and indicates further research.

II. RELATED WORK

There are several works published where the authors improve the efficiency of the MPEG-2 and MPEG-4 algorithms by modifying some of their parameters.

In [14], Zhenzhong Chen and King Ngi Ngan review the recent advances in rate control techniques for video coding. The video quantization is used to reduce the bit rate of the compressed video signal. It lets meet the size or bandwidth limitation properly. The rate control algorithms recommended for the video coding standards are briefly described and analyzed. Moreover, the recent advances, such as new concepts in rate-distortion modeling and quality constrained control, are presented. With these techniques, the rate control performance can be improved.

An example is given in [15], where O. Verscheure et al. analyze how the user-perceived quality is related to the average encoding bitrate for a variable bitrate (VBR) MPEG-2 video. They show why simple distortion metrics may lead to inconsistent interpretations. Furthermore, for a given coder setup, they analyze the effect of packet loss on the user-level quality. Finally, they demonstrate that, when jointly studying the impact of coding bit rate and packet loss, the reachable quality is upperbound and exhibits one optimal coding rate for a given packet loss ratio.

The authors in [16] describe a complete practical two-pass MPEG-2 encoding system that can be tuned to produce a variable bit rate (VBR) stream in a second pass. In a first pass, the video sequence is encoded with constant bit rate (CBR), while statistics concerning coding complexity are gathered. Next, the first-pass data is processed to prepare the control parameters for the second pass, which performs the actual VBR compression. They conclude their paper saying that the second-pass VBR sequences visually appear to have a higher overall quality than the ones coded with CBR. For VBR to visually outperform CBR, a mix of “easy” scenes and “difficult” scenes is always required.

Sung-Hoon Hong et al. propose a rate control scheme using a rate-distortion (R-D) estimation model, which produces a consistent picture quality between consecutive frames, in [17]. Their rate control scheme ensures that the video buffers do not underflow and overflow by satisfying the buffer constraint. Their simulation results show that their control scheme achieves 0.52-1.84 dB peak signal-to-noise

ratio (PSNR) gain over MPEG-2 Test Model 5 (TM5) rate control and maintains very consistent quality within a frame as well as between frames.

Another paper where the authors try to improve the efficiency of the encoders is shown in [18]. The authors optimize the operational control of MPEG-2, H.263, MPEG-4, and H.264/AVC encoders respect to their rate-distortion efficiency using Lagrangian optimization techniques. The performance of the H.264/AVC compliant encoder in all experiments clearly demonstrates the potential importance of this standard in future applications of video streaming as well as interactive video coding.

In [19] Zhihai He and Sanjit K. Mitra present an adaptive estimation scheme to estimate linear relationship between the coding bit rate and the percentage of zeros among the quantized transform coefficients. Based on the linear source model and the adaptive estimation scheme, a unified rate control algorithm is proposed for various standard video coding systems (MPEG-2, H.263, and MPEG-4). This algorithm is outperformed with other algorithms providing more accurate and robust rate control with very low computational complexity and implementation cost.

If a system makes a change in the quantizer, this may be more efficient in the transcoding process. In [20], the authors present a rate control scheme for MPEG-2 to H.264 transcoder. They construct an analytic model to set a reasonable initial quantization parameter (QP) for the first frame at the beginning of transcoding. The QP for each frame and each macroblock are adjusted by QPs extracted from the incoming MPEG-2 pictures to avoid consuming bits without video quality gain. They demonstrate by the experiment results that their algorithm improves overall quality for transcoded video while retaining smooth quality.

Finally, an efficient conversion scheme in order to apply the already existent DCT-domain transcoding schemes to MPEG-2/H.264 transcoding is proposed in [21]. Their scheme consists of two conversion steps: the quantization conversion and the DCT conversion. The quantization conversion changes the MPEG-2 quantization step size (Qstep) to the new H.264/AVC Qstep. Additionally, it can improve PSNR performance by reducing the reconstruction errors caused in the pixel-domain transcoder. Their experimental results show that the proposed scheme reduces computational complexity by 5-11% and improves video quality by 0.1- 0.5 dB compared with other solutions.

In this work we analyze the quantizer scale factor (QS) based on the measurements taken of the jitter, delay and lost packets. This study allows us to improve the quality of experience (QoE) in IPTV networks.

III. QUANTIZATION

Quantization is basically a process for reducing the precision of the Discrete Cosine Transform (DCT) coefficients in an encoder. This is very important, since lower precision implies a lower bit rate in the compressed data stream. The quantization process involves the division of the integer DCT coefficients by integer quantization values. The result is an integer and fraction, and the fractional part must be rounded according to the rules defined by MPEG [22]. The result is the quantized value that is transmitted to the decoder.

For reconstruction, the decoder must first dequantize the quantized DCT coefficients in order to reproduce the DCT coefficients computed by the encoder. Essentially, the Inverse Quantization (IQ) scales every element by a unique quantized weight. Since some precision was lost quantizing, the reconstructed DCT coefficients are necessarily approximations to the values before quantization.

After entropy decoding, the two-dimensional array of coefficients, QF[v][u], is inverse quantized to produce the reconstructed DCT coefficients, F[v][u]. In MPEG, IQ consists of three stages: Inverse Quantization Arithmetic, Saturation, and Mismatch Control. The inverse quantization arithmetic produces F''[v][u] coefficients [22]. For DCT coefficients matrix expression 1 is used:

$$F''(v,u) = \sum_{v=0}^{7} \sum_{u=0}^{7} \left[\left(2^n \times Q_F(v,u)\right) \times k\right] \times a + \left[\left(2 \times Q_F(v,u) + \left(\frac{d|Q_F(v,u)|}{d(u,v)} \times (1-k)\right)\right) \times W(w,v,u) \times Q_S/32\right] \times (1-a) \quad (1)$$

Where, 2^n represents the multiplier intra DC, the intra_dc_mult factor, for $n \in \{0, 1, 2, 3\}$. It is derived from the data element intra_dc_ precision (in case of MPEG-2, it is estimated according to Table 7-4 of the ITU-T Recommendation H.262 [22], in case of MPEG-4, it is estimated according to [3]). The *a* variable depends of the intrablocks (see expression 2), when the three conditions are complied it doesn't get a null value, otherwise, only operates with the second one. The second part of expression 1 depends of the value of *k* (seen in expression 3), the luminance and chrominance.

$$a = \begin{cases} 1 & v = 0, \quad u = 0, \quad k = 1 \\ 0 & others \end{cases} \quad (2)$$

$$k = \begin{cases} 1 & \text{intrablocks} \\ 0 & \text{non} - \text{intrablocks} \end{cases} \quad (3)$$

The quantizer_scale factor (QS) is an integer and is encoded with a 5-bit fixed-length code. Thus, it has values in the range {1,....,31}. 0 value is not allowed. Each weighting coefficient, W[w][v][u]; w = 0 ... 3; v =0...7; u = 0... 7, is represented on an 8-bit integer. The operator /' represents the integer division with truncation of the result towards zero.

One of the main uses of QS is for bit rate adaptation. The higher the QS value, the lower the bit rate, but a lower bit rate means a less picture quality, therefore the QS value must be chosen so as to minimize perceived distortion in the reconstructed picture.

In an encoder, the QS can be changed at the start of coding of each macroblock. Each time it is changed, the new value must be coded in the bitstream and there is coding overhead in doing this. In the case of IPTV this is done using MPEG-2 TS packets. Therefore, the QS can be retrieved very simply in the IQ block of the MPEG decoder, without adding extra devices, in an IPTV receiver (Set-Top-Box).

IV. SYSTEM ARCHITECTURE

The system is divided into two main parts: the server level and the user level. Both are linked by a communication network based on TCP / IP.

At the user level, the system is based almost in the preprocessing and transmission of uncompressed images in PNG format with a resolution of 1920x1080. The videos were generated from 14315 uncompressed PNG images [23] and encoded and quantized using ffmpeg software [24]. We made 8 video sequences with the following characteristics:

- MPEG-2 and MPEG-4 coding
- 720x576 of resolution
- 25 fps
- 120 seconds long
- QS {1, 2, 4, 6, 8, 10, 16, 31}, see [13].

Figure 3 shows the steps from the preprocessing of encoding of the uncompressed PNG images until they are transported to the end user. In the preprocessing stage, after the PNG images are encoded, we obtain a standard definition television (SDTV) MPEG1 video with a resolution of 720x576 dpi. This video will be the reference video used for the different tests. This video is later compressed in MPEG-2 and MPEG-4 format. Then, they are quantized to different QS for each format. In the transport stage, the videos are packaged in MPEG-2 TS and transmitted by the server in broadcasting to the network. We used VLC Media Player [25] as IPTV video server to send the SDTV MPEG-2 Transport Streams for both compressions types.

The IPTV network (shown in Figure 3) has been simulated using a PC placed in a Fast Ethernet network. The final user has a commercial set-top box to watch the video from the TV. It can also be observed directly from PC.

At the user level, we have also installed the VLC Media player. There, we can see the captured video and measure it subjectively. On the other hand, we installed the Clearsight Analyzer Software [26] in user's PC. It lets us capture and analyze the MPEG-2 TS packets. We measured the video quality at the receiver, and estimated the Mean Opinion Score (MOS). There is also installed a sniffer at the user level, which allows us to obtain the QoS parameter values of the video transmission (jitter, delay and lost packets). These measures will serve to evaluate the QS.

Our network architecture uses IPv4 because nowadays the most of commercial set-top boxes only use IPv4, but it can be implemented in an IPv6 network with IPv6 set top boxes easily.

V. QS ANALISYS

In order to analyze the optimal QS, we encoded several videos with the different QS values shown in the previous section. The Video Quality (VQ) results, obtained by the IPTV analyzer software of each video transmitted through our test bench, is shown in Figures 4 and 5. The VQ is measured in MOS values. In order to obtain the MOS, we compare the captured video with the video reference. MOS is an ITU (International Telecommunication Union) standardized term [27], used as a methodology for the subjective assessment of the quality of television pictures. MOS scores are rated on a scale from 1 to 5, where 5 is the best possible score, and indicates the degree of the user's satisfaction. In Figure 4 and 5, the best scores are obtained for QS {1, 2}, which provide a medium-high VQ value (4 at the MOS scale), while the rest of QSs have VQ values below 4. So, we can say that optimal QS, is 1 or 2 according our needs. If we want the best video quality without considerer the file size we will choose 1, but if we take into account the size of the video, we will select QS equal 2. However the tests were conducted using fixed QS in the video encoder. But in practice, a commercial MPEG encoder often uses variable QS, which assigns different values to intraframe or interframe, even to macro-blocks contained in each of them. For that reason, an average QS of 4 could be the highest value used by a video encoder. It seems that, according to the values of Figure 4 and 5, QS values upper than 4 will give fair or poor VQ. To check the results, we used an objective video quality method [28]; which is used traditionally to determine the video quality in presence of impairments. This will be discussed at the next section. Furthermore, in order to analyze, which is the best QS for video streaming, we used new testing measures as jitter, delay and packet lost, which will be explained in next sections.

Another important aspect in the QS analysis is the used instantaneous bandwidth. In Figures 6 and 7, the bandwidth used by MPEG-2 and MPEG-4 videos, and their respective QS, is shown. The appearance of traffic peaks on all graphs, with the same behavior, indicates that the tests have been conducted with the same sequence of images. Analyzing MOS and BW results we see that Q1 and Q2 have practically the same quality and features. According to [29], a MOS between 3.1 and 4.0 is acceptable. These videos are high quality, but the bandwidth needed for transmission is very high. Quantification values higher than Q8 are below the acceptable MOS. This reflects will serve for further analysis.

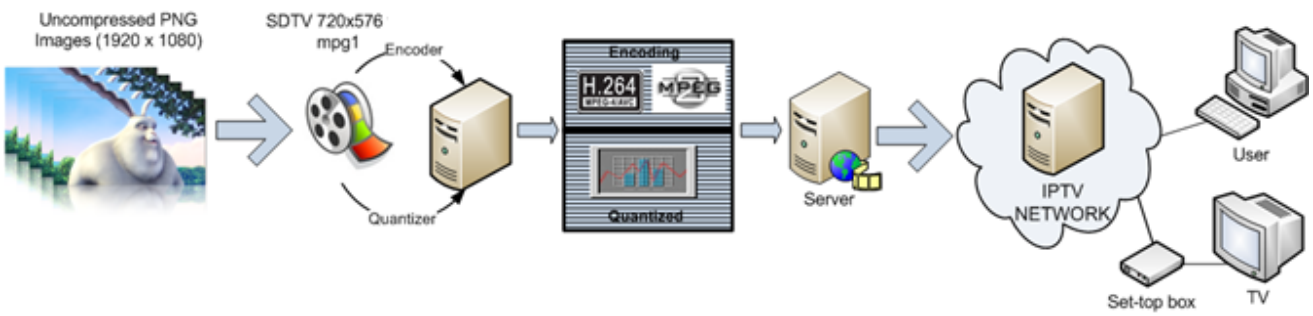

Figure 3. Encoding process and location of IPTV devices

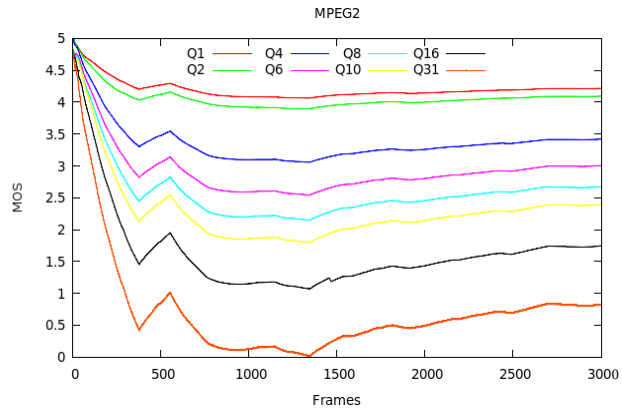

Figure 4. Video Quality in MOS value using the MPEG-2 codec quantizer

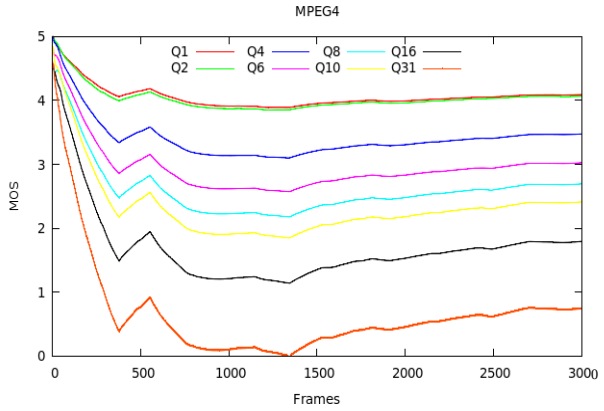

Figure 5. Video Quality in MOS value using the MPEG-4 codec quantizer

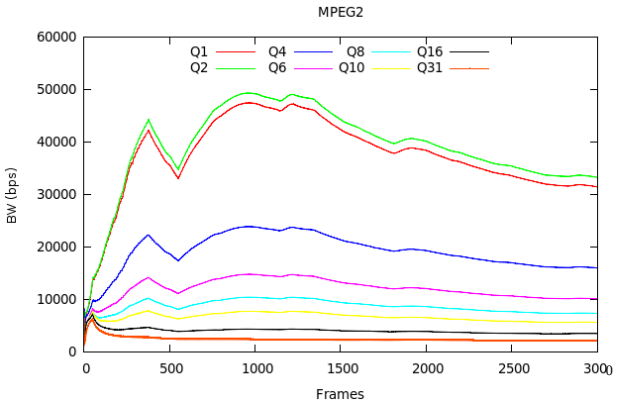

Figure 6. Bandwidth used by MPEG-2 video with different QS

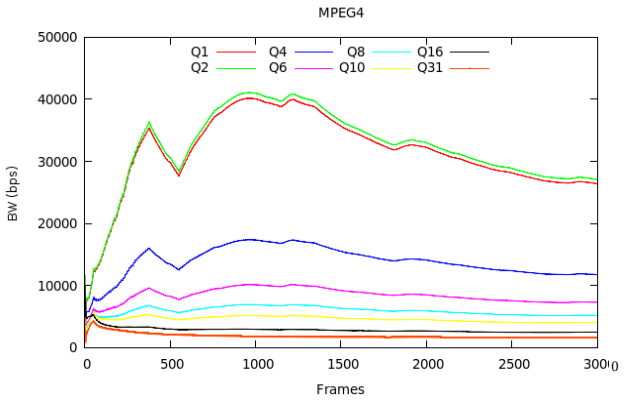

Figure 7. Bandwidth used by MPEG-4 video with different QS

VI. OBJECTIVE AND SUBJECTIVE VIDEO QUALITY

The goal of the objective video quality assessment is to design quality metrics in order to predict the perceived video quality automatically. The subjective video quality is a tool for the evaluation of videos from the point of view of the observer.

A video signal, whose quality is being evaluated, can be thought of as a sum of the reference signal and an impairment signal. We may assume that the loss of quality is directly related to the strength of the impairment signal. Therefore, a natural way to assess the quality of an image is to quantify the error between the distorted signal and the reference signal, which is fully available in Full Reference (FR) quality assessment [28]. But this is a problem because these videos of reference require a large amount of storage and, in many cases, it is impossible to obtain it. Reduced-reference (RR) [30] quality assessment does not assume the complete availability of the reference signal, only a partial reference information that is available through an ancillary data channel. Partial reference information could be Packet Loss Rate (PLR), is the probability that a packet is dropped at any router, or I/B/P Frames Statistics Losses (FSL), while in our case is QS.

In our case we will quantify the error between the distorted signal and the reference signal using Video Quality Metric VQM [31]. VQM uses the zero value as the best possible value; this means that there is no error between the reference video and the impairment video. The results of MPEG-2 and MPEG-4 are shown in Figures 8 and 9 respectively. In both Figures, the best value is QS1 and the worst QS31, although the difference is lower in MPEG-4. This verify that the larger the QS, the lower image quality (as we mentioned in the previous sections). We can see that when there are errors, the MPEG-4 video is seen with higher quality image than the MPEG-2 video because lower values of VQ are obtained. Again, QS2 was the optimal value.

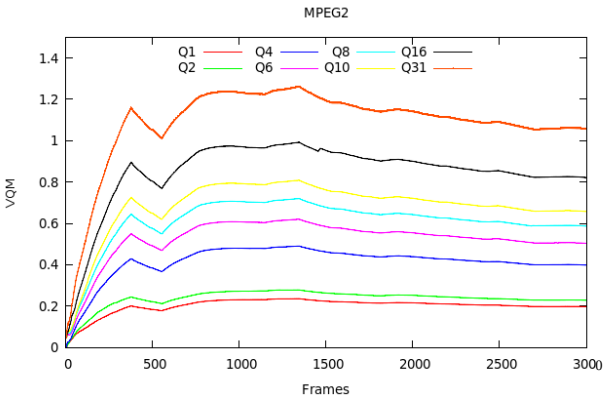

Figure 8. Objective video quality for MPEG-2

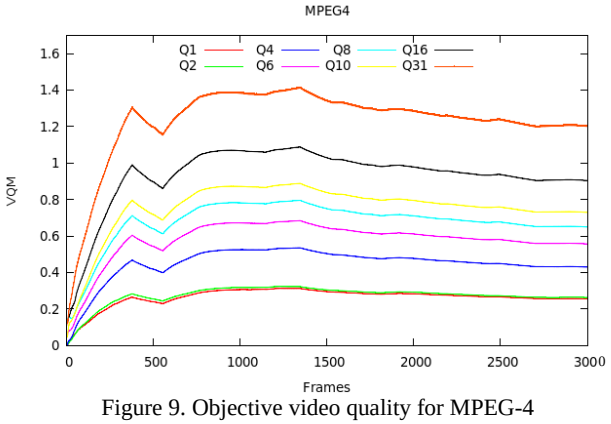

Figure 9. Objective video quality for MPEG-4

Figure 10. Visual comparison between a video with lost packets (at the bottom), QS31 video (in the middle), and the reference video (at the top)

Figure 10 shows a visual comparison between a video with lost packets (at the bottom), QS31 video (in the middle) and the reference video (at the top). In the video with loss packets we can see that when losses occur in the network, there is a lack of information in the video and pixels appears empty or with adjacent information. In the QS31 video, we can see that it has color degradation, figure pixelation, and it loses clarity. These issues are given due to the high value of QS. This information allows us to compare the video received with the reference. Videos with QS31 and QS16 do not exceed the minimum requirements of subjective assessment because the end user does not get a good picture quality.

VII. JITTER, DELAY AND LOSS PACKETS TEST

The latest set of tests conducted in this work has been to measure the jitter, delay and lost packets. The aim is to find how these parameters affect the QS. Finally, we will gather all the measurements and select an optimal value of QS. In order to perform this experiment, we added changes in the network parameters by applying different values of jitter, delay and lost packets in the video transmission in a controlled manner. It has been done by using the software NetDisturb [32]. Based on our previous experiments [13] we will only analyze QS1, QS4, QS6, QS8 and Q10. We will cause 0.1% ,1% and 3% of loss packets in the network during the a IPTV channel transmission because higher values than these ones, give very low video quality results as it is shown in Figure 10 (bottom). The results can be seen in the following test bench.

In Figure 11, the average delay when there is a loss of 0.1% for several values of quantizer (Q) in the MPEG-2 encoding can be observed. When the value of Q increases, the instant average delay is higher. The behavior of the delay is the same regardless of the Q value. If we have a low Q the file size to be transmitted is greater, so the number of packets to transmit will be bigger. For example, when Q=1 we have an average delay lower than 2 milliseconds, but the number of packets transmitted is approximately 70000. But when Q=6, the delay is lower than 5 milliseconds and the transmitted packets are approximately 24000.

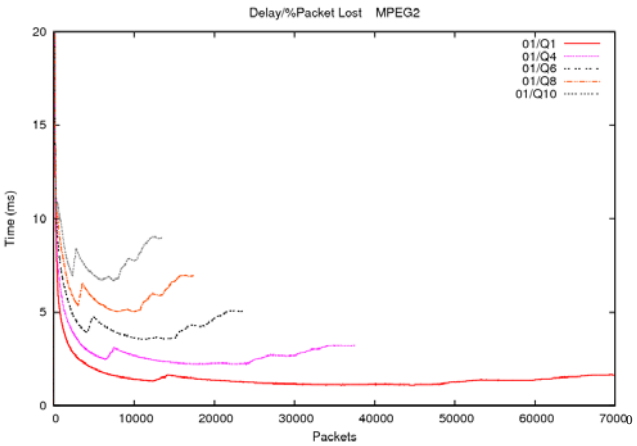

Figure 11. Delay when the loss rate is 0.1% for different Q of MPEG-2 videos.

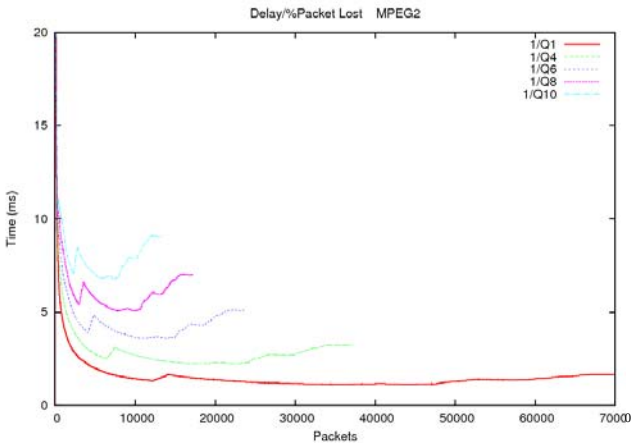

Figure 12. Delay when the loss rate is 1% for different Q of MPEG-2 videos.

In Figure 12, we can see that we obtained similar results, but in this case the losses introduced in the network were 1%. We can say that in a network with 0.1% and 1% losses, in the case of MPEG2 encoding, the behavior of the delay is very similar.

Finally, in Figure 13, we show the delay for a network with a loss of 3%. In this case, the delay follows the same behavior such as the previous figures but the average values are slightly smaller when there is a low Q. In this case, the delay increases for higher Q compared to Figures 11 and 12. This phenomenon can be seen when we have Q=1 (the delay decreases compared to the delays with a loss of 1% and 0.1%) and Q=10 (the delay increases)

We have also evaluated the delay compared to a loss rate for different Q of MPEG4 video encoding (see Figures 14, 15 and 16). With a loss rate of 0.1%, with Q=1, the observed delay is lower than 2 milliseconds, while with Q=4 this delay increases almost up to 4 milliseconds. Moreover, as we see in Figure 14, increasing the value of Q, the delay is also increased. This behavior is also obtained in the figures related to MPEG-2.For a network loss rate of 1%, the behavior of the delay is the one obtained in Figure 15. In this figure we see that for a Q=1 the delay is lower than 2 milliseconds and in the case of Q=4 this delay is lower than 4 milliseconds. With a loss rate of 3% in MPEG-4 videos, we obtained the delay shown in Figure 16. In this case, we see that the delay is slightly higher compared to loss rates of 0.1% -1%. This difference in delay is very small but exists.

As a general conclusion related to the delay measurements, we can say that, regardless of the codec used, there are Q values, which contribute with lower delays, but the number of transmitted packets is higher when we use small QS. Besides, this delay is referenced to belay between packets. For this reason when we have more packets, the intermediate devices will need more resources to give the same service. In all cases, the delay is lower than 20 milliseconds, an acceptable delay in the transmission of IPTV channels.

In the Figures 17, 18, 19, 20, 21 and 22, we can observe the instantaneous average jitter using MPEG-2 and MPEG-4 encoded videos for different loss rates. In Figure 17, we analyze the jitter for a loss rate of 0.1%. In this case, we observe that the measurements obtained have an exponential behavior. It can be seen that the video with Q=4 has the smallest jitter, something that can be taken into account for the IPTV transmission.

When we have a loss rate of 1%, the behavior of the jitter follows the graph shown Figure 18. In this case, the jitter has an exponential behavior. We have also observed that when Q increases, the jitter is reduced. For an efficient IPTV transmission, it is the better to have a small jitter, but we can't choose the highest Q value because the video quality is very poor.

Figure 19 shows the jitter measurements obtained for a rate loss of 3%. In this case, we see that the behavior is not the same as that obtained in the previous figures. This is because packet losses are already quite high and the jitter doesn't follow any specific distribution. We observed that the Q=4 value has the smallest jitter values (around 1500 packets), then this jitter value increases. We must indicate that the jitter values obtained in this figure are very small and therefore they will not affect to the transmission of IPTV channels.

In the MPEG4 encoding, the jitter obtained for different Q and a loss rate of 0.1% is seen in Figure 20. In this case, the behavior of this parameter is also exponential. In figure 20 we observe that the values of Q=1 and Q=6 are the ones that provide lowest jitter. In this figure, we can see that the value of Q=10 has the worst jitter value introduced into the network. Figure 21 shows the obtained jitter for various Q values when the loss rate increases to 1%. In this case, the Q value that introduces more jitter to the IPTV transmission is the Q=8, having the other cases much lower jitter values.

Finally, the jitter obtained for a loss rate of 3% is represented in the Figure 22. In this case, we see that the behavior doesn't follow any pattern. The Q value, which introduces lowest jitter is when we encode the video with Q=8. Otherwise, when there is higher jitter, the Q=1 is the quantizer, which provides higher jitter values to the IPTV transmission.

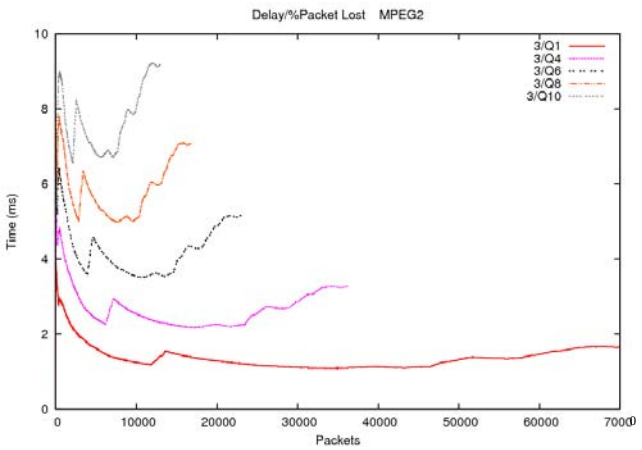

Figure 13. Delay when the loss rate is 3% for different Q of MPEG-2 videos.

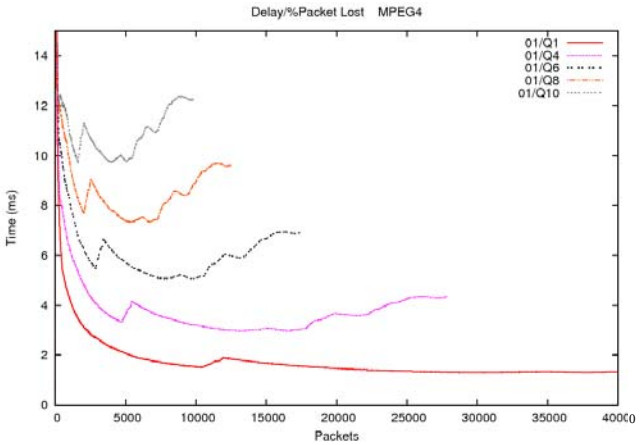

Figure 14. Delay when the loss rate is 0.1% for different Q of MPEG-4 videos

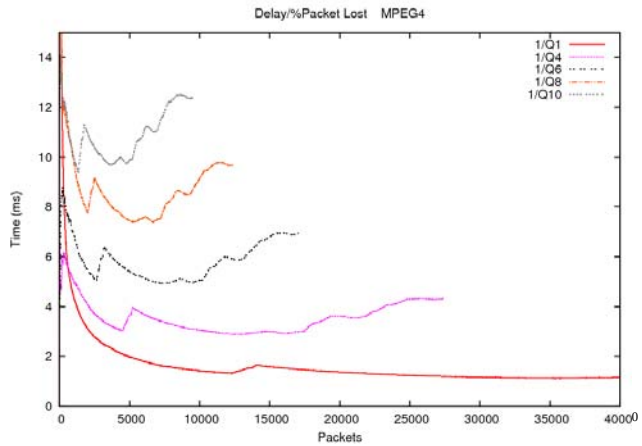

Figure 15. Delay when the loss rate is 1% for different Q of MPEG-4 videos

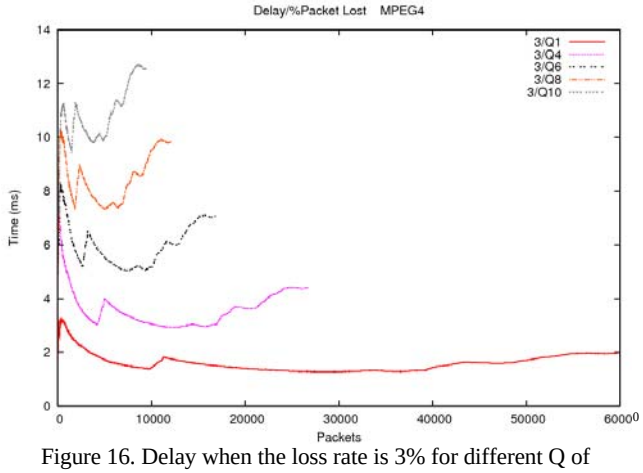

Figure 16. Delay when the loss rate is 3% for different Q of MPEG-4 videos

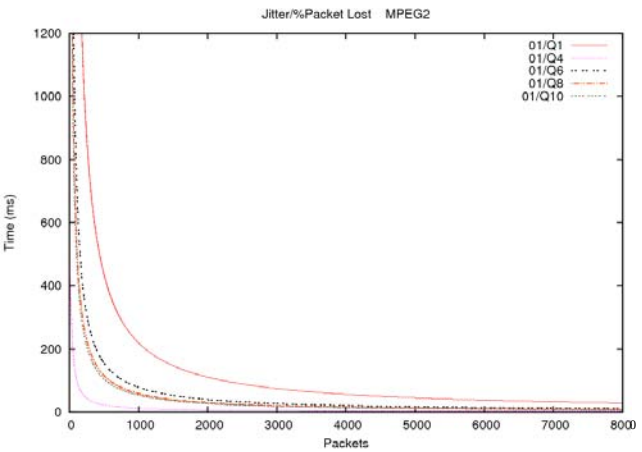

Figure 17. Jitter when the loss rate is 0.1% for different Q of MPEG-2 videos.

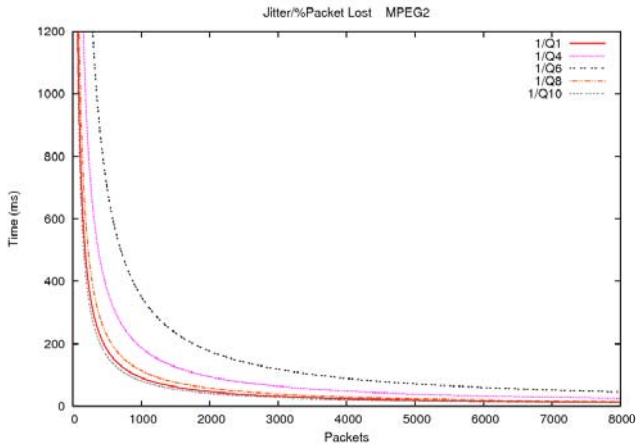

Figure 18. Jitter when the loss rate is 1% for different Q of MPEG-2 videos.

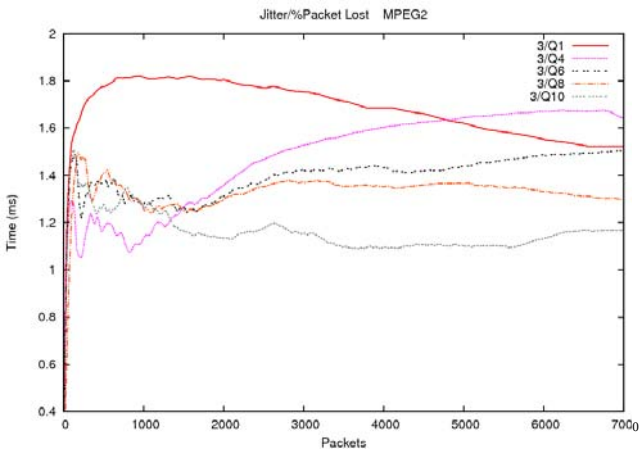

Figure 19. Jitter when the loss rate is 3% for different Q of MPEG-2 videos.

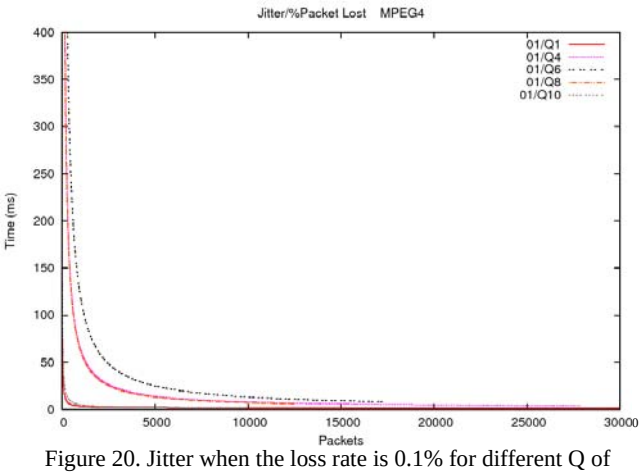

Figure 20. Jitter when the loss rate is 0.1% for different Q of MPEG-4 videos

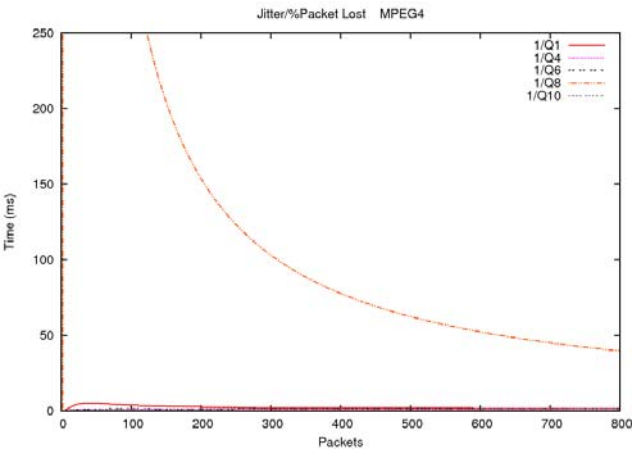

Figure 21. Jitter when the loss rate is 1% for different Q of MPEG-4 videos

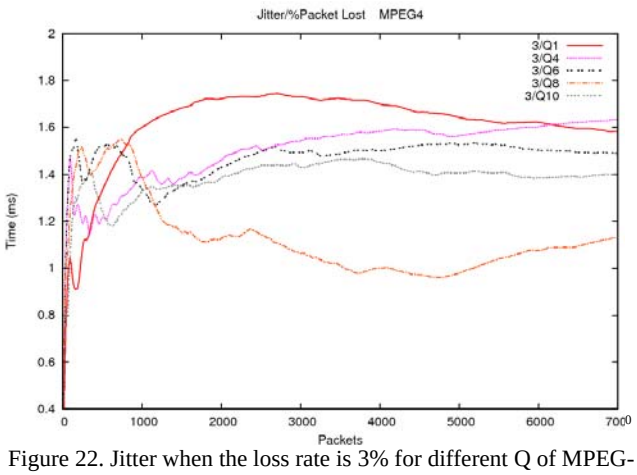

Figure 22. Jitter when the loss rate is 3% for different Q of MPEG-4 videos

VIII. DISCUSSION

Authors of reference [33] recommend a maximum loss of 5 consecutive IP packets every 30 minutes in SDTV. They say that between 0.5% and 1.5% of packet loss is acceptable. We have taken this into account when we made our test. For this reason we don't presented loss packet values higher than 3%.

Authors of reference [34] recommend that delay bounds for the various grades of perceived performance in terms of human interaction can be defined as: Good (0ms-150ms), Acceptable (150ms-300ms), Poor (> 300ms). Moreover, the authors of reference [29] suggest the following jitter values to be reasonably reliable to determine the grade of perceived performance: Good (0ms-20ms), Acceptable (20ms-50ms), Poor (> 50ms).

The jitter values of our test bench ranges between 200 ms and 2 ms and, for delay values between 2 and 30 ms. Therefore, we see that there are videos that don't satisfy this consideration, like the ones p given by QS31.

We made a subjective analysis of the video quality. It is shown in Figure 23. In the first line of the figure we see an image of the reference video (first in the left), an image of the QS4 video (second) and the difference between them (third). In the second line we see an image of the reference video (first in the left), an image of the QS6 video and the difference between them.

With this information and the information taken from the previous sections, we can deduce that the optimum values of QS are both QS4 and QS6 for MPEG-2 and MPEG-4 videos. Taking into account the extreme values of QS31 and QS1, we built the comparative shown in table I. In that table the average values for the different measures taken respect to the optimal values of QS31 and QS1is shown.

IX. CONCLUSION

In this paper, we have analyzed the QS as visual quality parameter. QS can be calculated at the decoder by extracting the information encoded in MPEG-2 TS packets, and, then, it could be used in VQ in order to create a reduced reference model to be used in the estimation of the QoE of the user .

Figure 23. Subjective Video Quality for QS4 (first line) and QS6 (second line).

TABLE I. AVERAGE VALUES WITH SEVERAL QS FOR MPEG2 AND MPEG4 CODECS

		Jitter_01% (ms)	Jitter_1% (ms)	Jitter_3% (ms)	Delay_0.1% (ms)	Delay_1% (ms)	Delay_3% (ms)	BW (bps)	MOS
QS1	**2**	74.98	10.41	1.4	1.86	1.57	1.37	37355.7	4.20
	4	23.98	10.41	1.48	1.75	1.57	1.6	31452.7	4.06
QS4	**2**	3.95	41.87	1.65	2.98	3.01	2.68	19000.93	3.36
	4	18.96	1.58	1.6	3.88	3.56	3.61	13898.6	3.40
QS6	**2**	25.99	48.57	1.37	4.65	6.42	13.17	12029.7	2.92
	4	50.23	1.39	1.42	6.31	5.87	5.99	8406.34	2.94
QS31	**2**	91.84	143.69	1.29	21.84	22.11	20.92	2377.25	0.7
	4	204.39	136.53	1.39	26.73	26.98	26.99	1833.02	0.64

We reached the conclusion that QS4 and QS6 are the optimum values when we include changes in the network and the network conditions are not optimum. Moreover, QS4 provide better video quality. IPTV service providers will require less bandwidth when QS4 and QS6 MPEG-4 videos are stream to the network. Therefore, we have shown that an optimal quantizer_scale factor can be used to save bandwidth in an IPTV network or to improve the Video Quality for the same bandwidth consumption.

In [13] we have demonstrated that the best QS value was equal to 2. However, in this paper we have added the bandwidth, jitter, delay and packet loss measurements in order to test the IPTV channel performance and the VQM and MOS. Now, we have demonstrated that the best QS values have been QS4 and QS6 when these parameters are included between the parameters taken into account. Moreover, in [13] we used a DVD video as a reference and then we codded it to MPEG-2 and MPEG-4, in this paper we have coded the raw video to MPEG-2 and MPEG-2 directly.

Reduced reference models are the next challenges for perceptual visual quality measurement techniques in multimedia services over digital television networks. Our future work will be focused on adding these results to the VQ algorithms in order to produce an efficient QoE to the user.

ACKNOWLEDGEMENTS

This research has been fully supported by France Telecom, Orange Labs, Spain.

REFERENCES

[1] The MPEG handbook: MPEG-1, MPEG-2, MPEG-4. John Watkinson. Focal Press, UK, 2001

[2] R. Koenen, “Overview of the MPEG-4 standard”, ISO/IEC JTC1/SC29/WG11 N1730, Luglio 1997.

[3] Coding of Audio-Visual Objects, Part-2 Visual, Amendment 4: Streaming Video Profile, ISO/IEC 14 496-2/FPDAM4, July 2000.

[4] Hill, Alberto Daniel. "MPEG-4 sobre CATV". Other thesis, Universidad Católica de Uruguay Dámaso Antonio Larranga, Facultad de Ingienería y Tecnologías. 2003.

[5] ETSI TR 102 033 V1.1.1. “Digital Video Broadcasting (DVB); Architectural framework for the delivery of DVB-services over IP-based networks”. April 2002. Available at http://www.etsi.org/deliver/etsi_tr/102000_102099/102033/01.01.01_60/tr_102033v010101p.pdf [July 2010]

[6] U. Reimers, “Digital Video Broadcasting (DVB): the International Standard for Digital Television”. Springer-Verlag New York, Inc. 1998.

[7] ISO/IEC 13818-1. “Information technology - Generic coding of moving pictures and associated audio information: Systems”. 2007.

[8] H. Schulzrinne, S. Casner, R. Frederick and V. Jacobson. “RFC1889 - RTP: A Transport Protocol for Real-Time Applications”. January 1996. Available at http://www.rfc-editor.org/rfc/rfc1889.txt [July 2010]

[9] D. Hoffman, G. Fernando, V. Goyal and M. Civanlar. “RFC2250 - RTP Payload Format for MPEG1/MPEG2 Video”. January 1998. Available at http://www.rfc-editor.org/rfc/rfc2250.txt [July 2010]

[10] J. Postel. “RFC768 - User Datagram Protocol”. August 1980. Available at http://www.rfc-editor.org/rfc/rfc768.txt [July 2010]

[11] ISO/IEC 11172-3, "Coding of Moving Pictures and Associated Audio for Digital Storage Media at up to about 1.5 Mbit/s, Part 3: Audio" (1992).

[12] Y. Kikuchi, T. Nomura, S. Fukunaga, Y. Matsui, H. Kimata. RFC 3016. RTP Payload Format for MPEG-4 Audio/Visual Streams.November 2000. Available at http://www.rfc-editor.org/rfc/rfc3016.txt

[13] Marcelo Atenas, Miguel Garcia, Alejandro Canovas, Jaime Lloret, A MPEG-2/MPEG-4 Quantizer to Improve the Video Quality in IPTV services, The Sixth International Conference on Networking and Services (ICNS 2010), Cancun (Mexico), March 7-13, 2010.

[14] Z. Chen and K. N. Ngan, “Recent advances in rate control for video coding”. Signal Processing: Image Communication, Vol. 22, Issue 1, Pages 19-38, January 2007.

[15] O. Verscheure, P. Frossard, and M. Hamdi, 1998. “MPEG-2 video services over packet networks: Joint effect of encoding rate and data loss on user-oriented QoS”. 8th Int. Workshop on Network and Operating Systems Support for Digital Audio and Video, Cambridge, UK., July 8-10, 1998.

[16] P. H. Westerink, R. Rajagopalan and C. A. Gonzales, "Two-pass MPEG-2 variable-bit-rate encoding". IBM Journal of Research and Development, Digital multimedia technology, vol. 4, number 4, pp. 471. 1999.

[17] S. H. Hong, S. J. Yoo, S. W. Lee, H. S. Kang, and S. Y. Hong. “Rate Control of MPEG Video for Consistent Picture Quality”. IEEE Transactions on Broadcasting, vol. 49, no. 1, pp. 1-13, March 2003.

[18] O. Werner, “Requantization for Transcoding of MPEG-2 Intraframes” IEEE Transactions on Image Processing, Vol. 8, No. 2, pp. 179-191, February 1999

[19] Z. He and S. K. Mitra. “A Linear Source Model and a Unified Rate Control Algorithm for DCT Video Coding”. IEEE Transactions on Circuits and Systems for Video Technology, vol. 12, no. 11, pp. 970-982. Nov. 2002.

[20] J. Yang, Q. Dai, W. Xu and R. Ding. “A rate control algorithm for MPEG-2 to H.264 real-time transcoding”. Proceedings of SPIE 2005, pp. 1995–2003, 2005.

[21] J. K. Lee and K. D. Chung. “Quantization/ DCT Conversion Scheme for DCT-domain MPEG-2 to H.264/AVC Transcoding”. IEICE Trans. Commun., vol. E87-B, no.7. pp. 1-9. July 2004

[22] ITU-T “Recommendation H.262, ISO/IEC 13818-2: Generic coding of moving pictures and associated audio information: Video”, February 2000. Available at http://webstore.iec.ch/preview/info_isoiec13818-2%7Bed2.0%7Den.pdf [July 2010]

[23] Big Buck Bunny uncompressed PNG files: Available at http://media.xiph.org/BBB/ [July 2010]

[24] ffmpeg software. Available at http://ffmpeg.org [July 2010]

[25] VLC Media Player. Available at http://www.videolan.org/vlc/ [July 2010]

[26] ClearSight Analyzer Software. Available at http://www.flukenetworks.com/fnet/en-us/StreamIt?Document=3780533&sot=true [July 2010]

[27] ITU-R “Recommendation BT.500: Methodology for the subjective assessment of the quality of television pictures”, June 2002. Available at http://www.itu.int/rec/R-REC-BT.500/en [July 2010]

[28] ITU-T, “Recommendation J.144: Objective perceptual video quality measurement techniques for digital cable television in the presence of a full reference”, March, 2004. Available at http://www.itu.int/rec/T-REC-J.144/en [July 2010]

[29] Prasad Calyam, Mukundan Sridharan, Weiping Mandrawa, Paul Schopis “Performance Measurement and Analysis of H.323 Traffic”, Passive and Active Measurement Workshop (PAM) Proceedings published by Springer in Lecture Notes in Computer Science, 2004.

[30] ITU-T, “Recommendation J.246: Perceptual audiovisual quality measurement techniques for multimedia services over digital cable television networks in the presence of a reduced bandwidth reference”, August, 2008. Available at http://www.itu.int/rec/T-REC-J.246/en [July 2010]

[31] Elecard Video Quality Estimator. Available at http://www.elecard.com/products/products-pc/professional/video-quest/ [July 2010]

[32] NetDisturb. Available at http://www.zti-telecom.com/brochuresN/NetDisturb%20Literature.pdf [July 2010]

[33] Tim Rahrer, Riccardo Fiandra, Steven Wright. Triple-play Services Quality of Experience (QoE) Requirements and Mechanisms. DSL Forum Working Text. WT-126. Feb.2006.

[34] ITU-T Rec. G.114 (05/2003) One-way transmission time. Available at http://www1.cs.columbia.edu/~andreaf/new/documents/other/T-REC-G.114-200305.pdf [July 2010]

International Journal on Advances in Telecommunications, vol 3 no 3 & 4, year 2010, http://www.iariajournals.org/telecommunications/

User Equipment Energy Efficiency versus LTE Network Performance

Kari Aho*, Tero Henttonen§, Jani Puttonen*, Lars Dalsgaard†, Tapani Ristaniemi‡
* Magister Solutions Ltd., Hannikaisenkatu 41, FIN-40100, Jyväskylä, Finland.
E-mail: {kari.aho, jani.puttonen}@magister.fi
† Nokia, P.O.BOX 45, FIN-00045 Nokia Group, Finland
E-mail: {lars.dalsgaard}@nokia.com
‡ University of Jyväskylä, P.O. Box 35, FIN-40014, Jyväskylä, Finland.
E-mail: {tapani.ristaniemi}@jyu.fi
§ Renesas Mobile Corporation, Porkkalankatu 24, FIN-00180 Helsinki, Finland
E-mail: {tero.henttonen}@renesasmobile.com

***Abstract*—The purpose of this article is to analyze the trade-off conditions between battery saving opportunities at the user terminal and Long Term Evolution network performance. To achieve the goal Voice over IP with discontinuous reception and a vast amount of different settings, including on duration, inactivity and discontinuous reception cycle timers, have been studied. An adaptive discontinuous reception with synchronizing the on duration time with the Voice over IP packet arrival has been proposed to minimize the delays caused by discontinuous reception. In addition, a channel quality indicator preamble time has been introduced to enable channel quality indicator update prior the on duration period. The quality of service and battery saving opportunities have been evaluated with a dynamic system simulator enabling detailed simulation of multiple users and cells with realistic assumptions. It can be concluded that high battery saving, i.e. increased talk-time opportunities, can be achieved without compromising the performance when discontinuous reception is properly adapted. Adaptive discontinuous reception and channel quality indicator preamble can effectively mitigate the capacity loss when more stricter DRX settings enabling higher energy efficiency at the terminal are applied.**

***Keywords*-DRX, VoIP, Battery savings, Energy Efficiency, Capacity, CQI, Preamble, Adaptivity**

I. Introduction

High peak data rates, low round trip times and high *Quality of Service (QoS)* enabled by current and upcoming wireless cellular technologies such as *Long Term Evolution (LTE)* [3][4] have driven the increase of wireless (data) subscribers to whole new levels. Despite of the fact that the growth is fueled by various innovative data services, the simple voice call service and especially *Circuit Switched (CS)* voice calls still remain as the main source of revenue for the cellular operators. However, the situation with CS voice is starting to change: Future systems, such as LTE, support only *Packet Switched (PS)* services meaning that voice calls would also have to be delivered via PS domain. Thus, this leads to situation where voice services are offered through Voice over IP (VoIP) protocols [5]. One of the benefits of sole PS system from the operator perspective is lower *Capital Expenditure (CAPEX)* and *Operating Expense (OPEX)* due to not having network elements for both CS (voice) and PS (data).

Generally, the requirement for successful penetration of IP based voice services, such as VoIP, is that the voice quality should be comparable to what is available using traditional CS voice [6]. There are numerous factors affecting VoIP QoS, which include, e.g., delay, packet loss and packet corruption. These performance indicators are challenges especially in the wireless domain due to more unreliable transmission media. Reliability in LTE networks is addressed through several radio resource management technologies such as *Hybrid ARQ (HARQ)*, *Link Adaptation (LA)*, *Channel Quality Indication (CQI)*, *Packet Scheduling (PS)* and short *Transmission Time Interval (TTI)* of 1 ms. The purpose of this article is to address LTE performance together with discontinuous reception and VoIP. Discontinuous reception cycles aim to improve the energy efficiency at the terminal by allowing possibilities to turn off the receiver circuitry during certain times. That kind of solutions are parallel as battery consumption at the terminal can very well become the limiting factor in providing satisfactory user experience along side of the network performance.

The rest of this article is organized as follows. Section II covers the motivation and related studies, which are followed by description of modeling and simulation assumptions related aspects in Section III. After those, simulation scenario is presented before simulation results and analysis. Conclusion is presented in Section V and finally in the Appendix reliability analysis of the used research tool and results is covered.

II. Motivation and Related Studies

Optimizing the VoIP over LTE performance in terms of QoS and the usage of radio resources has been studied in several articles [7][8][9]. From those it may be concluded that while the overall VoIP capacity may be control channel limited, the situation can be improved effectively by utilizing either packet bundling or semi-persistent packet scheduling. However, since the battery life of small hand-held devices might also very well become a limiting factor in providing satisfactory user experience, a prominent option to prolong the battery life is to use downlink *Discontinuous Reception (DRX)* cycles in conjunction with VoIP in LTE. DRX cycles, introduced by

Third Generation Partnership Project (3GPP) in [10] and [11], allow an idle *User Equipment (UE)* (i.e. UE that is currently not scheduled, i.e. neither transmitting nor receiving) to save battery by turning off the radio receiver for a predefined period (according to predefined, network-signaled parameters). This produces battery savings at the cost of somewhat reduced scheduling opportunities at the *Evolved Node-B (eNB)*.

Discontinuous reception has previously been studied both related to 3rd Generation systems as well as to LTE in several articles. In [12], the effects of DRX cycles and related timers to the queue lengths, packet waiting times, and the power saving factor were studied in Rel'99 wideband code division multiple access networks. The study showed quantitatively how to select appropriate DRX cycle values and the related inactivity timer for various traffic patterns. In [13] the scope is extended to consider DRX together with delay sensitive VoIP service over high speed downlink packet access, and the paper indicated that there are possibilities for high power savings but VoIP capacity can be compromised if improper parametrization is applied for DRX.

In [14] the DRX in LTE has been compared to DRX of 3rd Generation networks and it is concluded that LTE DRX is able to achieve more efficient battery usage through the use of short and long DRX cycles. In [15] an analysis of DRX with best-effort type of traffic over LTE networks was conducted. The paper showed with a single user simulations that a 95 % reduction of the UE power consumption with a moderate 10-20 % loss in throughput was achievable. In [16] the analysis is extended to a short DRX cycle and an inactivity timer. Both the short DRX cycle and inactivity timer aim to provide adaptibility to the variable traffic patterns. Both mechanisms improve the performance over a pure static DRX in terms of throughput and power consumption. However, short DRX with inactivity timer shows a gain of 0-3 times over DRX with just an inactivity timer. In [17] the DRX in LTE has been analyzed with video streaming and VoIP applications. It is concluded that DRX can save about 40-45 % of UE battery power without significantly impacting video quality; while for VoIP applications the saving can be approximately 60 %. However, the estimations are based on simple analytical calculations.

A part of the results in this article have earlier been published in conference articles [1] and [2]. In [1] we have studied DRX in a LTE network with high number of VoIP users. The focus was on the impact of DRX cycles and related timers on the system capacity as well as on battery saving opportunities. In [2] we proposed a CQI preamble for improving the VoIP performance with DRX. In this article, we have extended the work presented in [1] and [2] in several ways. We introduce an adaptive DRX, where the on duration time and VoIP packet arrival times are synchronized for buffering delay minimization. The CQI preamble scheme is analyzed with higher UE velocity where most of the CQI gains have been lost proving that most of the loss caused by DRX arise from the usage of out-dated CQI information. Finally, a statistical confidence analysis of the used simulation tool is presented at the end.

Our focus has been to study the combination of VoIP and DRX, since the performance degradation due to DRX is expected to be the highest with real-time delay sensitive traffic. Secondly, most of the previous work has focused on radio resource point of view of DRX and not on the battery saving opportunities. However, the DRX parameterization is clearly a trade-off between the capacity and battery savings. Finally, our analysis have been performed with a fully dynamic system simulator capturing the effects of dynamic nature of mobility.

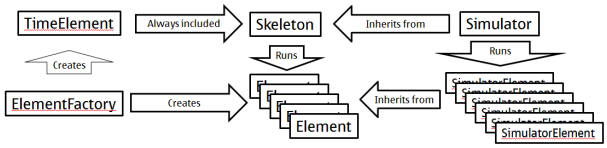

Fig. 1. Skeleton simulator

III. Modeling and Simulation Assumptions

The purpose of this section is to cover briefly the modeling issues related to dynamic system simulator used in these studies. Previously general modeling issues are presented briefly in [18] and VoIP specific issues, e.g., in [7]. In the following subsections the most critical aspects in terms of this paper are discussed.

A. Overview of the simulator

The general principle of all network simulators is quite much the same, where the simulation is configured through parameters, simulations are run with certain modeling assumptions and details and statistics are gathered e.g. by means of averages, cumulative distribution functions and time traces. For examples of other network simulators, see [19] and [20].

The simulator used for generating results is a fully dynamic system simulator, which means that the element of time passing is considered in details: channel conditions change, users move, traffic arrives at uplink and/or downlink buffer, scheduling happens and data is sent in downlink and/or uplink. The simulator works according to step-wise simulation principle: at each step, actions are executed in certain order before proceeding to the next step. The actions that are done depend on which features are turned on in the simulator (e.g. DRX can be turned off fully so that no UE uses it) and one simulation lasts for a certain number of predefined steps.

1) Simulator library: The simulator utilizes a library built for the purpose of enabling fast simulator development. The library is coded in C++, and contains many ready-made and tested implementations (i.e. sub-libraries) for e.g. propagation, channel, traffic and mobility models, as well as general purpose tools like scenario creation modules, parameter reader, random number distributions and simulation statistics collection utilities. At the heart of the library, there is also a so-called *skeleton simulator*: a built-in model of a simple simulator that dynamically loads simulator modules and executes them in the desired order. This is depicted in Fig. 1.

This kind of modularization of functionalities into stand-alone libraries enables code reuse in the future: For example,

several simulators may use the exact same modules that do the same basic functions of the simulators, which enables easier comparison between such simulators. For example, [21], which shows a comparison of real network VoIP capacity for HSPA and LTE, was done with two such simulators, which enabled an easy comparison of just the system differences without a massive campaign of verification simulations ensuring the modeling is compatible between the simulators. Also new simulators can be created with small effort by taking the skeleton and adding the needed modules on top of that.

2) Simulator structure: The most important part of simulator is the *Signal to Interference plus Noise Ratio (SINR)* calculation engine: It is abstracted so that the SINR is always calculated between two radio objects (typically eNB and UE, but UE-to-UE is also possible). Since these objects also contain the information about the antennas, relative position and any UE-specific information (such as UE-specific random number sequences for determining the current channel conditions), the interference calculation can be abstracted quite easily. Further, there is a class called *Physical Resource Blocks (PRB)* manager that acts as an initiator for the calculation between the radios: Newly scheduled PRBs are inserted to the PRB manager, which then (at the end of each step) handles the calculation of C and I for those PRBs that currently exist. At the end of each TTI, the existing PRBs are destroyed, keeping the interference calculation machinery generic (i.e. easily maintainable and modifiable if need be) and safely isolated from the actual scheduling decisions.

The rest of the simulator consists of inter-working between modules:

- UEs and eNBs are modeled as entities with a *connection* object joining them together, representing the active *Radio Resource Control (RRC)* connection.
- The tasks of the UE are to monitor the relevant downlink channels (i.e. *Physical Control Format Indicator Channel (PCFICH)*, *Physical Downlink Control Channel (PDCCH)*, *Physical Downlink Shared Channel (PDSCH)* and *Physical Broadcast Channel (P-BCH)*) and transmit data in uplink when triggered by protocol stack and when scheduled to transmit.
- The UE also maintains measurements of serving cell and neighbor cells, which may trigger measurement report according to eNB-configured RRC reporting configuration. The UE may also notice a connection failure (called *Radio Link Failure (RLF)*) and take appropriate actions after that (see [10] for further details).
- The tasks of the eNB are to transmit downlink data to UEs when necessary, handle the scheduling for uplink and downlink and decide on handovers for UEs.
- The connection object contains information relevant to both UE and eNB, like scheduling assignments, UL/DL data generation and protocol stacks handling the data. The connection also maintains the linking between eNB and UE, enabling an easy process when handover happens: The linked eNB is simply exchanged for another and appropriate actions done separately within the UE and source/target eNBs, but there is no need to create/destroy all objects related to traffic models and data buffers since these common parts are handled within the connection object that remains.
- In general, many algorithms (such as DRX, CQI or handover measurements) are further separated to their own modules as much as possible: Keeping the simulator as object-oriented makes it relatively easy to maintain and extend.

B. VoIP Traffic

VoIP traffic is used in the simulations to model an IP based voice call. The traffic model used is closely based on AMR codec, and a figure illustrating the anatomy of a VoIP call is shown in Fig. 2. For more detailed description, see below.

- *A VoIP call consists of both downlink and uplink traffic*. The duration of each VoIP call is randomly distributed according to truncated negative exponential distribution. The mean, minimum and maximum value of the distribution are given as parameters.
- *A VoIP call can be in two states: Active or DTX*. The states have different packet generation patterns and the duration of each state is distributed according to parametrized negative exponential distribution. The relative time a user spends in Active state determines the *Voice Activity Factor (VAF)* of the call: For example, a 50 % VAF means that on average, a user spends half of its time in Active state and half in DTX state.
- *Only downlink direction is considered* in these simulations, but the simulator supports simultaneous traffic in uplink and downlink (e.g. synchronized so that DTX in uplink occurs when downlink is in Active and vice versa).
- *During Active period*, fixed-size packets (i.e. AMR voice packets) are generated at constant intervals. In this study, VoIP packet is assumed to be 38 bytes and the interarrival time between packets is 20 ms [22].
- *During DTX period*, fixed-size *Silence Descriptor (SID)* packets, used for generating comfort noise, are transmitted at constant intervals. In this study, the SID packet size is assumed to be 14 bytes and the SID packets are generated at 160 ms intervals.
- *Robust Header Compression (ROHC)* is not modeled explicitly but ideal ROHC is assumed by taken it into account in packet sizes.
- *The characteristics of a VoIP call are fully parametrized*, and can be varied between the simulations. It is also possible to have a mix of different types VoIP calls in the same simulation.

The traffic model described above is the same as described in [22], but could also be further enhanced by considering e.g the effect of explicit ROHC or jitter in packet arrival (i.e. the

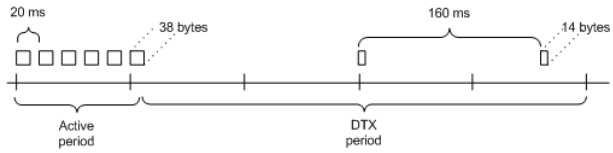

Fig. 2. Voice over IP traffic model

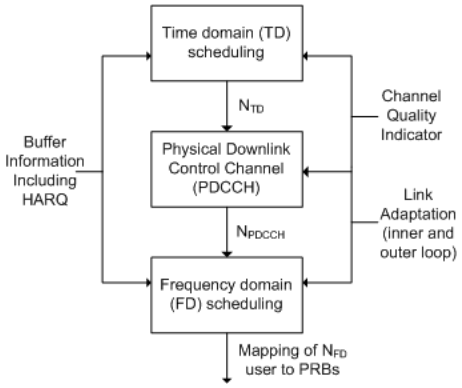

Fig. 3. De-coupled TD/FD-scheduler

packet arrival would not always be constant but could vary a little. However, in this paper, we concentrate on the basic model, to better account the basic interactions between DRX and VoIP.

C. Scheduling and Resource Allocation

In this study, we assume dynamic resource allocation for VoIP over LTE, i.e. we model a scheduler in the eNB that takes care of physical resource allocations for users. Each TTI, the eNB sends the scheduling allocations for users connected to the eNB in *Physical Downlink Control Channel (PDCCH)*, and UEs read the scheduling assignments and act accordingly (i.e. do nothing, transmit on uplink or receive in downlink). Since the scheduler is fully up to eNB implementation, there is no clear default behavior how the scheduling is done, but typically the scheduler assigns resources based based on each user's channel conditions: each user sends a *Channel Quality Indication (CQI)* report to eNB either at periodic intervals or when requested by the eNB.

Thus, the scheduler could vary the resource allocation of each user on a TTI basis. But this kind of fully dynamic scheduling of VoIP packets requires high amount of PDCCH resources, since each allocation for a UE consumes control channel resources each time it is signaled. Moreover, the scheduling assignments can be coded separately, i.e. they may consume different amount of resources depending on the selected coding scheme, so the limited availability of PDCCH resources also results in a varying amount UEs that can be scheduled per TTI. However, in general in this study we are assuming static amount of users (i.e., *Maximum Schedulable Users (MSU)*) that can scheduled per TTI, i.e., PDCCH is not explicitly modeled. Exclusion of explicit PDCCH modeling is done to better account the basic interactions between DRX and VoIP. The MSU value was chosen by estimating the average PDCCH capacity, though. Still, the impact of realistic PDCCH following modeling aspects from [23] and simulation principles from [24] are briefly addressed in this paper.

The scheduler used in these simulations has been a de-coupled *Time Domain (TD)-Frequency Domain (FD)* scheduler, presented in [18] and depicted in Fig. 3. This means that the scheduling is done in two stages: First, a TD-scheduler selects the candidates for the scheduling (up to MSU users). Next, a FD-scheduler chooses which resources (i.e. *Physical Resource Blocks (PRBs*) to assign to which candidate. After this, the scheduling allocations are sent to the users. Note, that if PDCCH is explicitly modeled, then MSU in TD scheduler is not limiting the amount of scheduling candidates, but the PDCCH resource check is done in between TD and FD schedulers.

Scheduling decisions done in TD-scheduler are based on *Head-of-Line (HoL)* packet delay, i.e., the user with the oldest packet in the buffer (i.e. the packet with the largest delay) is selected first in order to prioritize users who have the worst-delayed packets. In FD-scheduler, the candidates from TD-scheduler are treated in the order of delay: The first candidate is allocated the best PRBs based on CQI information sent by that user, and then the same is done for the next candidate and so on. The PRBs are assigned until it is deemed that the user gets enough PRBs to empty its data buffer [1] or there are no more PRBs available or the maximum limit of allocated PRBs for one user is reached. Finally, it should be noted that both HARQ retransmissions and control message (e.g. handover command in downlink, measurement report in uplink) transmissions are prioritized by TD- and FD-schedulers since these types of traffic are considered critical for the call.

D. Performance Evaluation Criteria

While the simulation enables a wide variety of possible statistics, here we present the simulation results through a comparison of *Quality of Service (QoS) criterion* and *Battery Saving Opportunities (BSO)*.

1) The QoS Criterion: The QoS criterion, also called *system capacity* later in this paper, is defined as a combination of user and cell *outage levels*: A user is in outage if too many of its packets are dropped or have large enough delay, and a cell is in outage if too many of its users are in outage. More precisely,

- A cell is in outage if more than 5 % of its users are in outage.
- A single user is in outage if 2 % or more of the packets (monitored over the whole call) are not received correctly within 50 ms (one-way) time.

Note 1: In addition to monitoring delay at the receiving end, packets can also be discarded at the transmitting side if the delay of the packets in the buffer reach the discard delay threshold.

Note 2: The 50 ms delay limit is called the radio network *Delay Budget*, and is based on ITU e-Model requirements for good quality voice [25] as well as to slightly stricter benchmarking requirements of *Next Generation Mobile Networks (NGMN)* and 3GPP evaluations [26] for VoIP.

Since it is very difficult (and not even realistic) to achieve exactly the same load in each cell even within one simulation, the overall system capacity is interpolated from a large set of

[1]With some additional limitations: In this paper one user may be assigned resources so that it is able to send up to a maximum of two packets during one TTI. This is called *packet bundling*

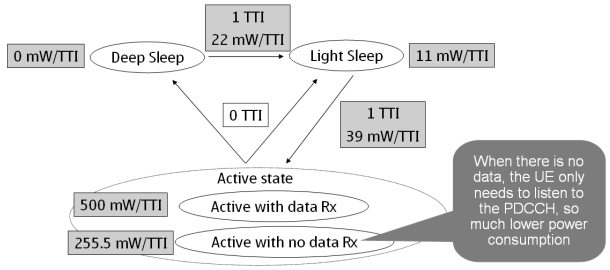

Fig. 4. Power Consumption Reference Model

simulated user amounts per cell (which lead different outage levels / cell). The target level for this interpolation is level where at most 5 % of users would be in outage, which is the absolute upper limit according to the QoS criterion described above.

2) Battery Saving Opportunity: The BSO is presented as the time a user spends in DRX state, i.e. the time during which the UE can be in reduced state of activity. The battery saving opportunities are calculated according to model presented in 3GPP contribution R2-071285 [27] and illustrated in Figure 4. Power consumption levels are calculated with and without DRX from which the relative power savings are finally calculated. In the power calculations one TTI is assumed to be the time used to receive one transmission. Time spent in active state, deep sleep and light sleep are collected for each call and the total 'Active with data Rx', illustrated in Figure 4, is calculated for each call in a following manner:

$$Rx_{active} = (N_{VoIPPackets} + N_{SIDPackets}) \times Tx_{mean}, \quad (1)$$

where Tx_{mean} is the average number of transmissions, $N_{VoIPPackets}$ and $N_{SIDPackets}$ represent the total number of VoIP/SID packets per call. $N_{VoIPPackets}$ and $N_{SIDPackets}$ are defined as follows:

$$N_{Packets} = (t_{call} \times \mu)/t_{IA}. \quad (2)$$

In Equation 2 μ represents the voice activity factor, t_{call} the total length of the call and t_{IA} interarrival time for packets (SID or VoIP).

E. Discontinuous Reception (DRX)

The discontinuous reception (DRX) feature was introduced to LTE as a network-configured feature (meaning it can be also turned off) that provides improved battery saving opportunities for the UE. DRX is specified at MAC level (see [11]), but is turned on by eNB by RRC (see [28]) signaling when eNB transmits the DRX parameters to the UE.

DRX consists of a cycle of alternating active period (called On Duration in MAC specification), during which UE functions just as without DRX, and an inactive period (also referred as DRX period), during which UE is not mandated to receive PDCCH (which means any scheduling assignment during that time would be lost so in practice eNB will not schedule the UE during that time) and can save power by turning off its receiver hardware. A set of timers, illustrated in Figure 5 and covered below, further control the operation of DRX cycle:

1) DRX Cycle Timer: specifies the periodic repetition of the on duration (active) time, which is followed by a possible period of inactivity time.

2) On Duration Timer (ODT): represents the minimum time in *Downlink (DL)* subframes that the UE is required to monitor the PDCCH at each DRX Cycle.

3) Inactivity Timer (IAT): specifies the number of consecutive subframes that UE shall stay active and monitor PDCCHs. Timer is (re-)started every time when the UE is scheduled and successfully decodes a PDCCH indicating new data transmission.

4) HARQ Round Trip Time (RTT): specifies the minimum amount of subframes before a DL HARQ re-transmission is expected by the UE. UE can enter to inactivity during RTT if not otherwise required to monitor the PDCCH.

5) Retransmission Timer (RTxT): specifies the maximum number of consecutive subframe(s) that UE waits for incoming retransmission after HARQ RTT. UE is not allowed to enter inactivity while retransmission timer is running in order to be able to receive the HARQ transmissions. However, when HARQ transmissions are prioritized, as the case is in this study, the retransmission timer does not have substantial impact. RTxT is stopped when retransmission is received.

F. CQI preamble concept

According to 3GPP specifications ([10], [11], [28]) UE only has to do measurements once during a DRX cycle, which means that the UE will typically do measurements (CQI or other) only during the active period. However, performing the measurements, processing and transmitting them and eNB receiving the measurements consumes time, so the active time may have passed before up-to-date CQI information is available in the e-Node B scheduler. Moreover, the lack of up-to-date information can lead to lowered performance. This procedure is illustrated in Fig. 6.

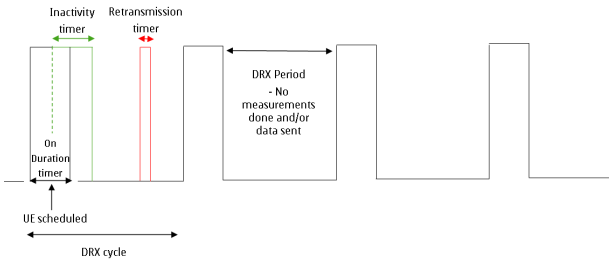

Fig. 5. Diagram of DRX operation

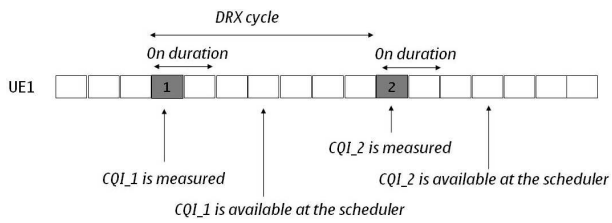

Fig. 6. Example of CQI measurement procedure with normal DRX. Assuming total CQI delay 3, on duration 2 and DRX cycle 7 TTIs

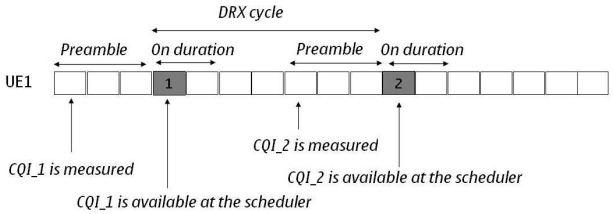

Fig. 7. Example of CQI measurement procedure with CQI preamble. Assuming total CQI delay 3, on duration 2 and DRX cycle 7 TTIs

To avoid possible performance loss, this paper considers a so-called CQI preamble scheme as a potential enhancement for the CQI measurement operation described above. With the CQI-preamble scheme, a CQI preamble time is applied before the actual on duration time takes place. During preamble time the UE turns its receiver circuitry on to perform and report the CQI measurements in addition to other possible *Radio Resource Management (RRM)* measurements. Naturally, when performing the measurements, the normal requirements, such as CQI measurement granularity and the CQI measurement period (i.e. minimum time since previous measurement), still apply. With the preamble scheme UEs could be scheduled with up-to-date CQI information for any potential DL data transmission as Fig. 7 illustrates. The downside of this operation is increased activity time, which leads to higher power consumption and shorter talk time from the UE/user point of view.

The current 3GPP specifications already allow this kind of improved operation. UE is allowed to do CQI measurements (and fall back to inactivity) before actual on duration. Though, according to [11] UE is not allowed to send the CQI report on PUCCH before the active time / on duration begins. Thus, from the UE side, CQI Tx part of the preamble scheme would be achieved through slightly prolonged on duration to allow the transmission. Changes could, however, be needed for the e-Node B scheduling: eNB should consider the time when the last CQI report has been received from a UE that has its on duration started / ongoing. Once CQI report is received during preamble time or within CQI requirements (e.g., period) UE becomes schedulable, not before. Also, changes could also possibly be needed in eNB implementation for evaluating and indicating the length of CQI preamble time for DRX purposes. CQI preamble time consists of the time before CQI is measured, transmitted, received and processed. In this paper preamble length is estimated to be as long as the total sum of CQI delay (defined through parameters) and the time that it takes to measure the CQI (1 TTI). Moreover, UEs are assumed to be active throughout the preamble time to better understand the ’worst-case’ scenario.

G. Adaptive DRX

As described above, DRX operates in predefined cycles of active and inactive states. Moreover, different UEs can (and should) be allocated with slightly different offset from which their cycle timers start so that even amount of candidate set for scheduling remains balanced in the downlink. That is handled by eNB, which signals the DRX configurations

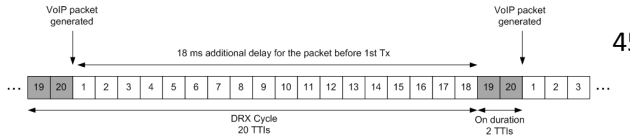

Fig. 8. Example of possible problems without adaptive DRX

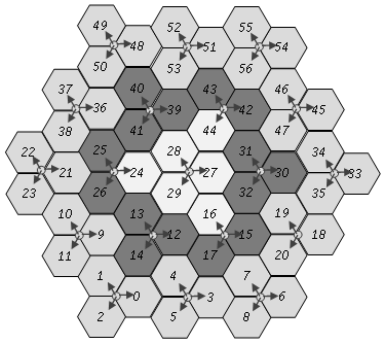

Fig. 9. Simulation scenario

to each UE. However, if the offset setting and timers are configured ’blindly’, i.e. without considering the expected packet arrival times, possible problems could occur especially for delay critical services such as VoIP. Fig. 8 illustrates this through simple example: Blind offset setting can lead to situation where a single VoIP packet can have additional delay of 18 ms, which, in the context of the typical 50 ms delay budget, means that almost 40 % of the delay budget is already consumed before the first transmission, thus reducing the time for possible retransmissions.

To mitigate the negative effects of offset setting this paper shows that DRX offset could be adapted to the data flow timing. In terms of the example presented in Fig. 8 it would mean that instead of having the DRX cycle starting 2 TTIs before the packet generation (blind setting) the DRX would be adapted to start during the time when packets are generated. This could be achieved in real networks, e.g., by monitoring the data flow some time before configuring the DRX. Even though there can be some jitter for the packets in real networks, on average the adapted offset would not cause as high additional delays as the blind offset would in the worst case.

IV. Simulation Scenario and Results Analysis

Simulations were run in a hexagonal macro cellular scenario with three tiers, see Fig. 9. Scenario consists of 7 active base stations with *Inter Site Distance (ISD)* of 500 m. Each base station has 3 sectors resulting into layout containing 21 active cells. Statistics are collected from 6 middle cells. Third, i.e., the outer tier is simulated as interfering tier, which adapts to the load of the statistic cells. Users are not allowed to move to the third tier but only within two inner tiers. The main simulation parameters are shortly listed in Table I.

In the following subsections the performance of VoIP over LTE downlink is analyzed with respect to system capacity and power saving opportunity criteria covered in Section III-D. The analysis for the trade-off between increased talk-time opportunities and LTE performance is based on vast amount

TABLE I
SIMULATION PARAMETERS.

Simulation time	1 million steps
Time resolution	1 step, i.e., 0.0714 ms
e-Node B Max. Tx power	46 dBm
Transmission Time Interval (TTI)	1 ms
Pathloss model	Modified Okumura-Hata [29]
Channel profile	Typical Urban (TU)
UE velocity	[3, 30] kmph
Handover	Hard, 3 dB threshold
MSU	[8, PDCCH]
CQI resolution	2 PRBs per CQI (fullband)
CQI delay	2 ms
CQI measurement period	5 ms
VoIP packet size	38 bytes [22]
VoIP packet interarrival time	20 ms
SID packet size	14 bytes
SID packet interarrival time	160 ms
VoIP call length	Negative exponential distribution, truncated, mean 20 s, min 5 s, max 60 s
Activity / Silence period length	Negative exponential distribution, mean 2.0 s
Layer 3 packet discard threshold	50 ms
Max. VoIP packet delay	50 ms
HARQ transmissions (max.)	7
HARQ RTT	8 TTIs
Retransmission Timer	10 TTIs
On duration timer	[1, 2, 3, 4] TTIs
Inactivity timer	[2, 10, 20] TTIs
DRX cycle timer	[10, 20, 40] TTIs

of different DRX adjustments and enhancements, including on duration, inactivity and DRX cycle timers as well as CQI preamble scheme and adaptive DRX.

A. On Duration Timer Impact

Figure 10 shows the impact of on duration timers (fixed inactivity timer of 2 TTIs) to the LTE downlink performance in terms of maximum number of VoIP users that can be served per cell with acceptable QoS. The power saving opportunities for those cases are illustrated in Figure 11, respectively. As those Figures show, with DRX cycle timer 10 TTIs the on duration results in significant power saving opportunities with only minor impacts on DL capacity, providing that the timer value is higher than one TTI. Similar trend can be seen with 20 TTI cycle with the exception that the LTE performance numbers are lower than with 10 TTI but at the same time the power saving opportunities are higher ($\tilde{7}$5-90 % versus $\tilde{5}$5-80 %). The reason behind the poor performance when the on duration is one TTI is that the scheduling opportunities are very scarce and with high probability there will be many users competing of that scheduling slot. Competition results into missed scheduling opportunities, which again leads to highly increased queuing delays for VoIP packets due to DRX cycles. Increased queuing delays lead to increased amount of discarded packets already at the transmitting end and thus

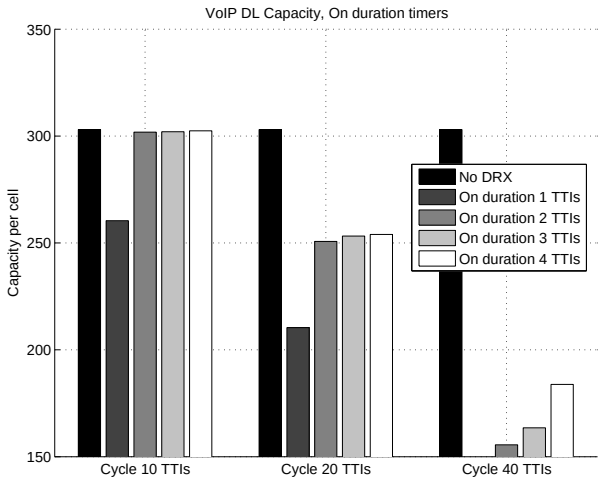

Fig. 10. VoIP DL capacity, ODTs, IAT 2 TTIs

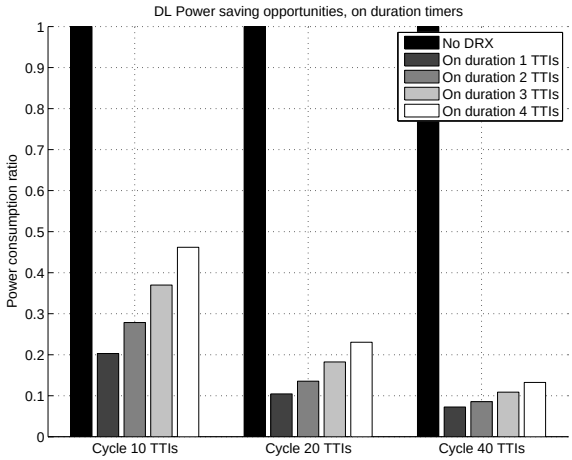

Fig. 11. DL power saving opportunities, ODTs, IAT 2 TTIs

to poor performance also from the system level perspective. Similar phenomena is seen and emphasized when the cycle length is very long. However, long cycles could possibly be taken into use when the cell is not fully loaded, assuming that DRX adapts to the different system loads.

B. Inactivity Timer Impact

The trade-off between VoIP DL capacity and DL power saving opportunities when inactivity timer is also varied on top of on duration and DRX cycle timers is shown in Figure 12 and 13. When compared to on duration timer results presented above the longer inactivity timer does not provide much higher capacity improvements, especially with cycles 10 and 20 TTIs. Power saving opportunities are also much lower when longer inactivity timer is used. With cycle 40 TTIs the inactivity timer can provide benefits as the cycle is so long that users will have multiple packets to be transmitted once they become active from DRX. Thus, longer inactivity timer allows users to deplete their packet buffers and possibly transmit new packets arriving their buffers while the inactivity timer is running. However, this combined effect of prolonged inactivity and on

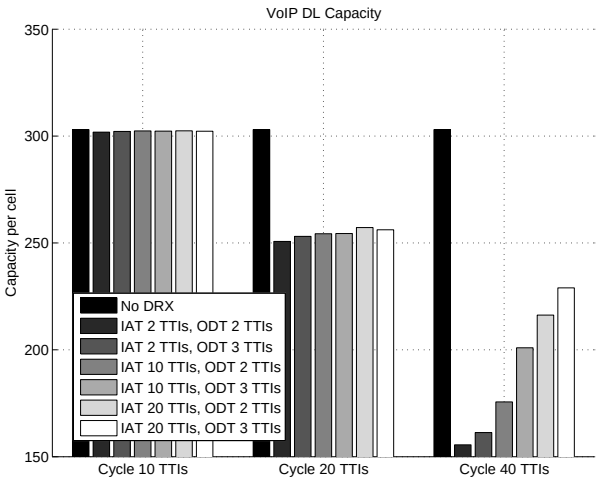

Fig. 12. VoIP DL capacity with different IATs and ODTs

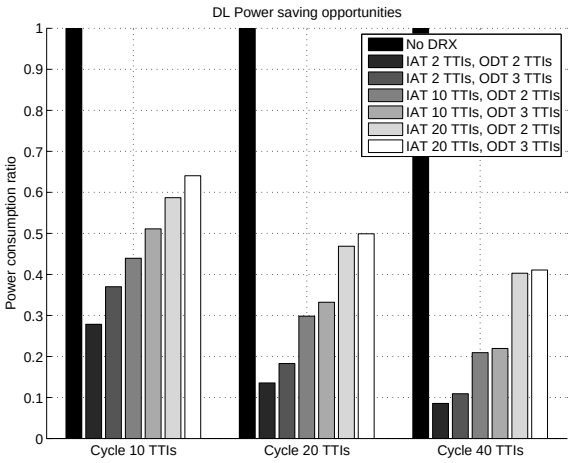

Fig. 13. DL power saving opportunities with different IATs and ODTs

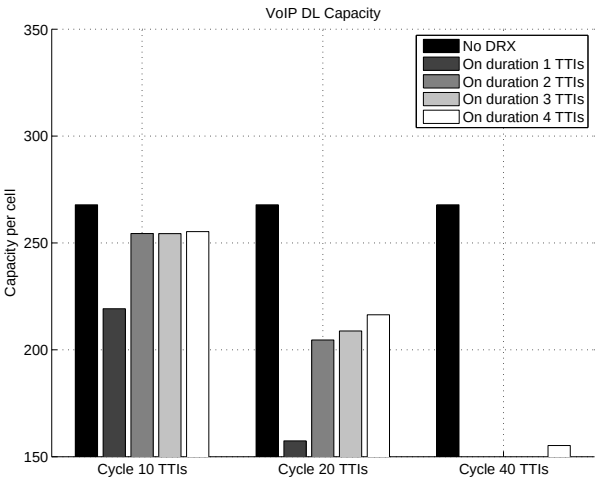

Fig. 14. VoIP DL capacity, realistic PDCCH

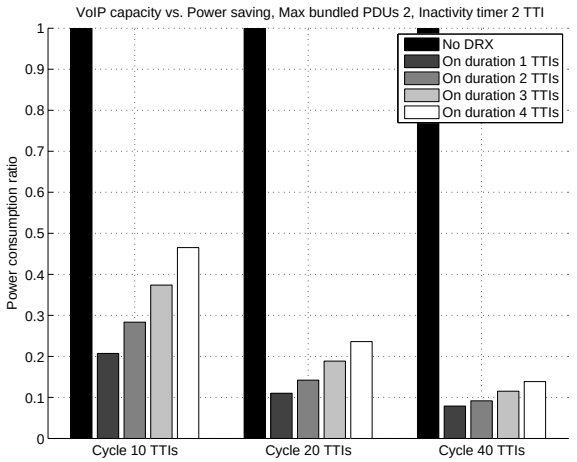

Fig. 15. DL power saving opportunities, realistic PDCCH

duration timer together with long cycle cannot reach significantly difference in power savings to justify the compromise in the system capacity. More optimal trade-off point can be achieved with timer settings described above.

C. DRX Performance with Realistic PDCCH

To further verify the trends presented above the performance of DRX is studied with realistic PDCCH modeling. This means that PDCCH resources can be exhausted even with a few users and PDCCH transmission can be erroneous leading to varying amount of users that can be scheduled per TTI. Previously presented results assumed fixed number of users that can be scheduled per TTI (MSU).

The performance of DRX with different activity timers and realistic PDCCH is illustrated in Figure 14 and 15. As the capacity Figure shows the absolute capacity numbers are on lower level, which indicates that the averaged number of schedulable users per TTI is actually a bit lower than the one that was assumed in this study as a basis (MSU 8). Apart from the absolute numbers the performance follows the same trends presented without detailed PDCCH modeling.

D. Performance with CQI Preamble

DRX and CQI preamble scheme (see Section III-F) performance in terms of VoIP capacity and power saving opportunities are illustrated in Figs. 16 and 17, respectively. In those figures three types of DRX scenarios are presented in addition to 'no DRX' case:

- *Ideal CQI*, which equals to the case where CQI is updated regardless of the DRX and power savings are unaffected. In reality this would not be possible but it is considered as a reference to benchmark the performance.
- *Normal DRX*, which equals to the case where normal DRX settings are used and thus CQI is updated only when UE is active.
- *Preamble 3*, which equals to the proposed scheme where UE wakes up before the actual on duration time to perform the measurements and to send them to e-Node B. Preamble length of 3 TTIs is assumed for this study.

When normal DRX operation is compared to the case with ideal CQI feedback (or no DRX case) it can be seen that the VoIP capacity is rather sensitive to the up-to-date CQI information availability. With cycle length of 20 TTIs the difference between those is around 15 % and with cycle of

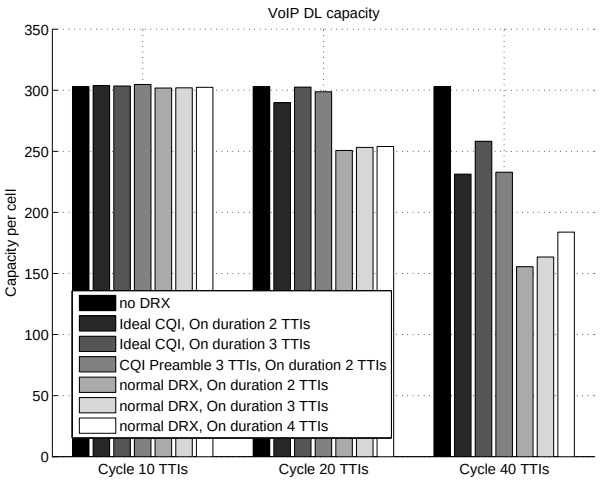

Fig. 16. VoIP DL capacity with and without DRX preamble, 3 kmph

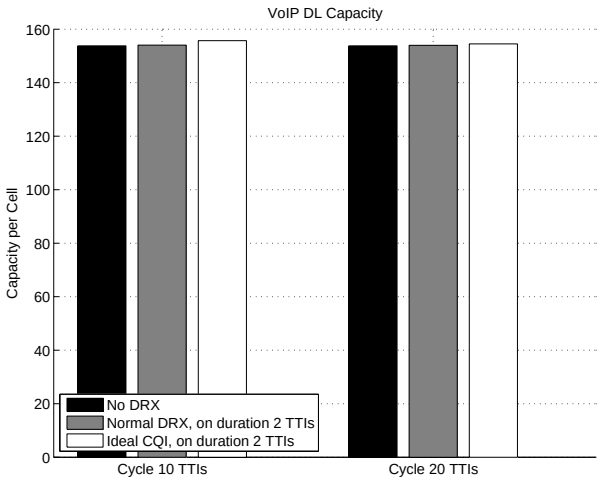

Fig. 18. VoIP DL capacity with and without ideal CQI, 30 kmph

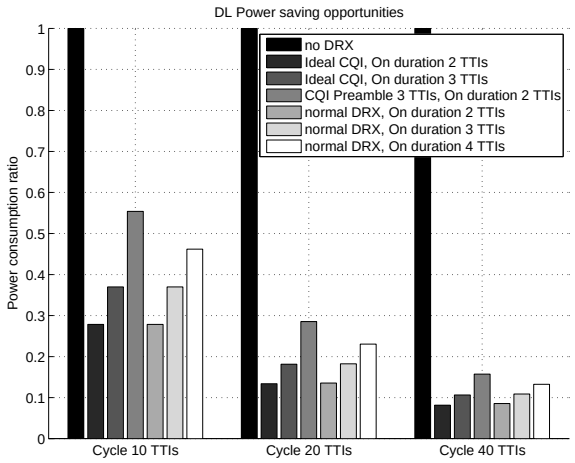

Fig. 17. DL power saving opportunities with and without DRX preamble, 3 kmph

40 TTIs even more. Moreover, as it can be seen from Fig. 16, mere increase of on duration time might not be adequate as UE can be scheduled at any point during that time, likely with outdated CQI information. This implies that some mechanism to guarantee newer CQI information for scheduling should be considered, CQI preamble scheme for instance.

When CQI preamble scheme is benchmarked against normal DRX cycle of 10 TTIs with different activity timer values it can be seen from Fig. 16 that preambles do not provide extra value as the capacity is not compromised with so short cycle. However, even though (normal) DRX cycle of 10 TTIs implies roughly 30-45 % power consumption versus 'no DRX' the higher cycles imply possibilities for even higher power savings, as Fig. 17 shows. Thus, more focus should be paid on longer cycles, which could guarantee longer UE talk times.

With CQI preamble scheme and longer cycles of 20 or even 40 TTIs the deterioration in terms of VoIP capacity with DRX can be mitigated quite well. The gain from preamble scheme over normal DRX becomes higher when the DRX cycle length is longer, which is quite intuitive as then the CQI information available in the scheduler is older (without preambles). Preamble scheme can even outperform 'ideal CQI' case in some situations due to preamble scheme forcing the periodic CQI measurements being synchronized with data transmissions. With 'ideal CQI' the periodic reporting happens every 5 ms regardless of the data flow / DRX.

In terms of downlink power saving opportunities the performance of CQI preamble scheme is expectedly lower than with normal DRX operation, as Fig. 17 implies. However, as the performance in terms of system capacity is much more robust against potential losses, the loss in battery savings with preambles can be considered as acceptable to guarantee more satisfactory service provision. Moreover, this paper evaluated only the scheme where UE stays active for the whole duration of preamble time but in principle after the UE has performed the measurements the UE could fall back to inactivity before actual on duration. By turning receiver circuitry off during those periods higher battery savings could be expected.

Finally, the findings and conclusions from CQI impact with DRX are confirmed in Fig. 18 where VoIP performance with all users moving with higher velocity is illustrated. As [30] indicates and this study confirms with higher UE velocity the frequency selectivity gain of CQI is lost to most extent and thus no additional gain could be achieved even with 'ideal CQI'.

E. Performance with Adaptive DRX

Finally, the purpose of this section is to cover how adaptive DRX presented in Section III-G affects to the performance. Figs. 19 and 20 illustrate the performance in capacity and power consumption ratio, respectively. As the capacity figure shows, adaptive DRX can provide noticeable gains, especially with longer cycles than 10 TTIs where practically no losses are seen if on duration is long enough. In terms of battery savings the adaptive DRX leads to slight increase in battery consumption. This due to the fact that blind offset setting could further induce the packet bundling and reduce the amount of retransmissions due to increased delays and thus reduce the time needed to keep receiver circuitry active.

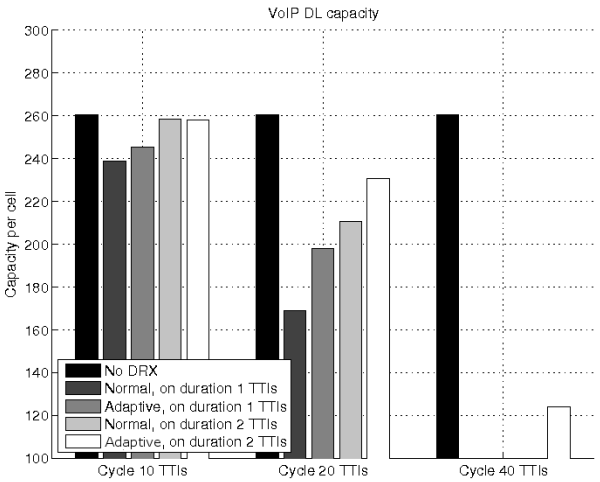

Fig. 19. VoIP DL capacity, adaptive DRX

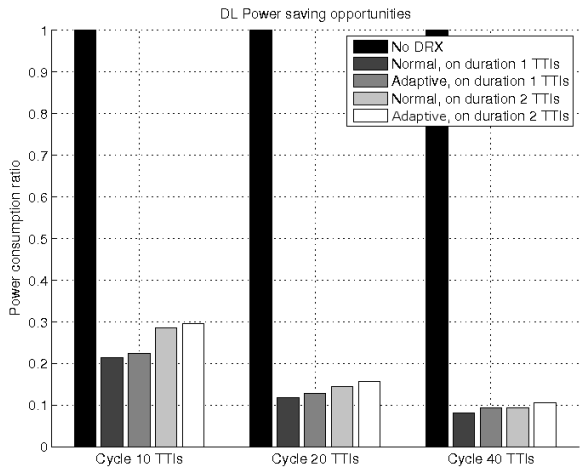

Fig. 20. DL power saving opportunities, adaptive DRX

V. Conclusion

The purpose of this article was to evaluate the trade-off conditions between energy efficiency at the user terminal and LTE performance. That goal is achieved by studying VoIP over LTE with various DRX related timers, which limit the scheduling freedom of users while increasing battery saving opportunities at the terminal. Increased power saving opportunities lead to increased talk-times for the terminals and thus more satisfactory user experience. The study was conducted with dynamic system simulator modeling LTE network with high level of detail.

This article indicates that for dynamic and PDCCH controlled scheduling, short DRX cycle timers together with appropriate on-duration timer is an attractive choice for LTE energy efficiency: Substantial power saving opportunities are achievable with minor trade-off in terms of maximum VoIP over LTE DL capacity. Regardless, this article also points out that in lower load situations different (more stricter) DRX adjustments could be used as then the capacity might not be compromised and the power savings would be higher. This article also shows that prolonging inactivity timer together with on duration and DRX cycle timers does not justify the slightly increased performance (capacity) as the trade-off in battery saving opportunities is too high.

TABLE II
Confidence intervals for interpolated VoIP capacity

	Capacity [UEs/cell]
MEAN	260.305
STANDARD DEVIATION	3.85448
CONFIDENCE INTERVAL, 90 %	$\pm$ 0.44 %
CONFIDENCE INTERVAL, 95 %	$\pm$ 0.52 %
CONFIDENCE INTERVAL, 99 %	$\pm$ 0.69 %

VoIP performance in terms of capacity may, however, be reduced by some extent if sub-optimal DRX settings are chosen. One main reason for reduced performance, especially with long cycles, is linked to outdated CQI information. CQI preamble scheme, introduced in this paper, mitigates the reduced performance quite well in terms of VoIP capacity when dynamic user scheduling is assumed. Moreover, the improvements can be achieved with acceptable trade-off in terms of battery saving opportunities.

Finally, this study introduces concept where DRX (offset) would adapt the data flow. The result show significant improvement in terms of capacity in situations where blind DRX configuration show losses. Moreover, adaptive DRX brings only minor impact to the power consumption ratio.

VI. Acknowledgments

This study is a collaborative work between Magister Solutions Ltd., University of Jyväskylä, Nokia, Nokia Wireless Modem Research (nowadays a part of Renesas Mobile Corporation) and Nokia Siemens Networks. The authors would like to thank all of their co-workers and colleagues for their comments and support. Finally, special thanks go to Hannu-Heikki Puupponen from University of Jyväskylä for his contributions on providing confidence analysis results.

Appendix

Research tool used in this study was presented briefly above. This appendix is aimed to deepen the presentation by providing statistical confidence analysis for the used system level tool.

Statistical analysis is based on evaluating the performance with a few selected test cases, namely VoIP simulations with different random number generator seeds. Based on the seed all random generators are initialized, these include e.g. starting position and direction of the movement for the UEs. Even though, all of the simulation results depend on random processes, the results are reproducible with certain level of accuracy, which is defined in this appendix.

An interval estimation can be used to define a confidence interval, which means that the sample ϕ, is within a defined interval with a certain probability. This probability can be expressed as follows

$$P(a \leq \phi \leq b) = 1 - \alpha \quad (3)$$

where the interval $[a, b]$ is a $(1-\alpha)\times 100\%$ confidence interval of ϕ. A probability that the ϕ is not within the interval is

α. When the number of samples n is ≤ 30 the standardized normal distribution, $N(0,1)$, can be used to define confidential interval, which is

$$(\overline{x} - z_{\alpha/2} \times s/\sqrt{n}, \overline{x} + z_{\alpha/2} \times s/\sqrt{n}). \quad (4)$$

In Eq. 4 the $\overline{x}$ is the average value, $z_{\alpha/2}$ is the critical value taken from the standardized normal distribution $N(0,1)$, s is the standard deviation and n is the number of samples i.e. in this case the number of simulation runs.

The simulation environment used for confidence analysis is the same macro cellular layout used for DRX studies. Main parameters are as well similar to the simulations presented above with the exception that dynamic scheduling MSU is assumed to be 6. This is done so that simulations take PDCCH restrictions better into account.

Confidence intervals are calculated for radio system capacity i.e. at the point where 5 % VoIP users are in outage. Capacity is interpolated from different cell loads i.e. from another one where the system outage level is below 5 % and another where it is above that. Thus, the required simulation amounts for confidence analysis equal two times $n = 31$.

The results for dynamic LTE system level tool are shown in Table II. As that table shows the difference even with the highest confidence interval are very minor. Thus, this gives the confidence that the results produced with the tool for this study are also well within the required level of reliability and reproducibility.

REFERENCES

[1] K. Aho, T. Henttonen, J. Puttonen, and T. Ristaniemi, "Trade-Off between Increased Talk-Time and LTE Performance," in *Proceedings of International Conference on Networks (ICN)*, April 2010.

[2] K. Aho, T. Henttonen, J. Puttonen, and L. Dalsgaard, "Channel Quality Indicator Preamble for Discontinuous Reception," in *Proceedings of IEEE Vehicular Technology Conference (VTC'S10)*, May 2010.

[3] H. Ekström and A. Furuskär and J. Karlsson and M. Meyer and S. Parkvall and J. Torsner and M. Wahlqvist, "Technical Solutions for the 3G Long Term Evolution," *IEEE Communications Magazine*, vol. 44, pp. 38–45, March 2006.

[4] A. Toskala, H. Holma, K. Pajukoski, and E. Tiirola, "UTRAN Long Term Evolution in 3GPP," in *Proceedings of IEEE International Symposium on Personal, Indoor and Mobile Radio Communications (PIMRC)*, September 2006.

[5] F. Persson, "Voice over IP Realized for the 3GPP Long Term Evolution," in *Proceedings of IEEE Vehicular Technology Conference (VTC'F07)*, September 2007.

[6] *Requirements for Evolved UTRA (E-UTRA) and Evolved UTRAN (E-UTRAN)*, 3GPP TR 35.913, Rev. v9.0.0, December 2009.

[7] J. Puttonen, T. Henttonen, N. Kolehmainen, K. Aschan, M. Moisio, and P. Kela, "Voice-over-IP Performance in UTRA Long Term Evolution Downlink," in *Proceedings of IEEE Vehicular Technology Conference (VTC'S08)*, May 2008.

[8] Y. Fan, P. Lunden, M. Kuusela, and M. Valkama, "Performance of VoIP on EUTRA Downlink with Limited Channel Feedback," in *Proceedings of International Symposium on Wireless Communication Systems (ISWCS'08)*, October 2008.

[9] D. Jiang, H. Wang, E. Malkamki, and E. Tuomaala, "Principle and Performance of Semi-Persistent Scheduling for VoIP in LTE System," in *Proceedings of International Conference on Wireless Communications, Networking and Mobile Computing (WiCom'07)*, September 2007, pp. 2861–2864.

[10] *Evolved Universal Terrestrial Radio Access (E-UTRA) and Evolved Universal Terrestrial Radio Access Network (E-UTRAN); Overall description; Stage 2*, 3GPP TS 36.300, Rev. v9.3.0, March 2010.

[11] *Evolved Universal Terrestrial Radio Access (E-UTRA) Medium Access Control (MAC) protocol specification*, 3GPP TS 36.321, Rev. v9.2.0, March 2010.

[12] S.-R. Yang and Y.-B. Lin, "Modeling UMTS Discontinuous Reception Mechanism," in *IEEE Transactions on Wireless Communications*, vol. 4, January 2005, pp. 312–319.

[13] K. Aho and I. Repo and T. Nihtilä and T. Ristaniemi, "Analysis of VoIP over HSDPA Performance with Discontinuous Reception Cycles," in *Proceedings of International Conference on Information Technology (ITNG)*, April 2009.

[14] L. Zhou, H. Xu, H. Tian, Y. Gao, L. Du, and L. Chen, "Performance Analysis of Power Saving Mechanism with Adjustable DRX Cycles in 3GPP LTE," in *Proceedings of IEEE Vehicular Technology Conference (VTC'F08)*, September 2008.

[15] T. Kolding, J. Wigard, and L. Dalsgaard, "Balancing Power Saving and Single User Experience with Discontinuous Reception in LTE," in *Proceedings of IEEE International Symposium on Wireless Communication Systems 2008 (ISWCS'08)*, October 2008.

[16] J. Wigard, T. Kolding, L. Dalsgaard, and C. Coletti, "On the User Performance of LTE UE Power Savings Schemes with Discontinuous Reception in LTE," in *Proceedings of IEEE International Conference on Communications (ICC'09)*, June 2009.

[17] C. Bontu and E. Illidge, "DRX Mechanism for Power Saving in LTE," *IEEE Communications Magazine*, vol. 47, pp. 48–55, June 2009.

[18] P. Kela, J. Puttonen, N. Kolehmainen, T. Ristaniemi, T. Henttonen, and M. Moisio, "Dynamic Packet Scheduling Performance in UTRA Long Term Evolution Downlink," in *Proceedings of International Symposium on Wireless Pervasive Computing (ISWPC)*, May 2008.

[19] D. Bültmann and M. Mühleisen and K. Klagges, "openWNS - open Wireless Network Simulator," in *Proceedings of the European Wireless*, May 2009.

[20] J. C. Ikuno, M. Wrulich, and M. Rupp, "System Level Simulation of LTE Networks," in *Proceedings of the IEEE Vehicular Technology Conference (VTC'S10)*, May 2010.

[21] K. Aho, I. Repo, J. Puttonen, T. Henttonen, M. Moisio, J. Kurjenniemi, and K. Chang, "Benchmarking of VoIP over HSDPA and LTE Performance with Realistic Network Data," in *Proceedings of the IEEE International Symposium on Wireless Pervasive Computing (ISWPC)*, May 2010.

[22] R. Cuny and A. Lakaniemi, "VoIP in 3G Networks: An End-to-End Quality of Service Analysis," in *Proceedings of IEEE Vehicular Technology Conference (VTC'S03)*, Jeju Island, Korea, April 2003.

[23] D. Lopez, C. U. Castellanos, I. Z. Kovacs, F. Frederiksen, and K. I. Pedersen, "Performance of Downlink UTRAN LTE Under Control Channel Constraints," in *Proceedings of IEEE Vehicular Technology Conference (VTC'S08)*, May 2008.

[24] J. Puttonen, H.-H. Puupponen, K. Aho, T. Henttonen, and M. Moisio, "Impact of Control Channel Limitations on the LTE VoIP Capacity," in *Proceedings of the International Conference on Networks (ICN'10)*, April 2010.

[25] *One-way transmission time*, ITU recommendation G.114, 2003.

[26] "LTE Physical Layer Framework for Performance Verification," 3GPP TSG RAN WG1 LTE contribution R1-070674, February 2007.

[27] "DRX Parameters in LTE," 3GPP TSG RAN WG2 LTE contribution R2-071285, March 2007.

[28] *Evolved Universal Terrestrial Radio Access (E-UTRA) Radio Resource Control (RRC) protocol specification*, 3GPP TS 36.331, Rev. v9.1.0, December 2009.

[29] *Selection procedures for the choice of radio technologies of the UMTS*, Universal Mobile Telecommunications System (UMTS 30.03) TR 101.112, Rev. v3.1.0, November 1997.

[30] N. Kolehmainen, J. Puttonen, P. Kela, T. Ristaniemi, T. Henttonen, and M. Moisio, "Channel Quality Indication Reporting Schemes for UTRAN Long Term Evolution Downlink," in *Proceedings of IEEE Vehicular Technology Conference (VTC'S08)*, May 2008.

Kari Aho received his M.Sc., L.Sc. and Ph.D. degrees in information technology in the field of mobile telecommunications from the University of Jyväskylä in 2006, 2009 and 2010, respectively. His Master's, Licentiate and Ph.D. thesis focused on various third generation cellular network performance enhancements, which were addressed mainly through VoIP and MBMS services. Currently he is working as project manager at Magister Solutions in the area of future HSPA evolution. Current research interests are VoIP performance, uplink transmit diversity and downlink multipoint transmission and reception issues.

Tero Henttonen received his M.Sc. degree in applied mathematics from the University of Helsinki in 2001. His master's thesis focused on compressed mode effects in WCDMA. He is currently working as Principal Researcher at Renesas Mobile Corporation, with research areas related to 3GPP Long Term Evolution; especially on mobility performance and heterogeneous networks. Current research interests include mobility in LTE-A and in heterogeneous networks.

Jani Puttonen received his M.Sc. and Ph.D. degree in information technology in the field of telecommunications from the University of Jyväskylä in 2003 and 2006, respectively. His Ph.D. thesis focused on IP level mobility management in heterogeneous networks. He is currently working as a Senior Research Scientist at Magister Solutions with research areas related to 3GPP Long Term Evolution; especially RAN features and performance. Current research interests are Minimization of Drive Tests and Self Organizing/Optimizing Networks.

Lars Dalsgaard received his M.Sc. degree in Telecommunications from Aalborg University in 1995. His master's thesis focused on applying OFDM multicarrier transmission within GSM. He is currently working as a senior specialist at Nokia Devices within work areas related to 3GPP Long Term Evolution with special focus on UE performance, power consumption and mobility. Current interests include mobility and Carrier aggregation within LTE-A, mobility in general including 3GPP inter-system and heterogeneous network.

Tapani Ristaniemi was born in Kauhava, Finland, in 1971. He received the M.Sc. in mathematics in 1995, Ph.Lic. in applied mathematics in 1997, and Ph.D. in telecommunications in 2000 from the University of Jyväskylä, Jyväskylä, Finland. During 2001-2003 he was a professor of telecommunications at the Department of Mathematical Information Technology, University of Jyväskylä, and 2003-2006 a professor of wireless data communications, Institute of Communications Engineering, Tampere University of Technology, Finland. In 2006 he joined the University of Jyväskylä, where he holds a professorship of computer science. His research interests include signal processing for communications, biosignal processing and system engineering for wireless communications.

Universal Ground Control Station for Heterogeneous Sensors

Axel Bürkle, Florian Segor, Matthias Kollmann, Rainer Schönbein
Fraunhofer Institute of Optronics, System Technologies and Image Exploitation IOSB
Karlsruhe, Germany
{axel.buerkle, florian.segor, matthias.kollmann, rainer.schoenbein}@iosb.fraunhofer.de

***Abstract*—Today, a wide range of sensors and mobile systems – both aerial and ground-based – are available for surveillance and reconnaissance tasks. For example, they provide first responders with current information about the situation at the operation site. In many cases those systems have their own dedicated control and exploitation station. The joint control of heterogeneous sensors and platforms, as well as the exploitation and fusion of heterogeneous data is a challenge. The surveillance system AMFIS presented in this paper is an integration platform that can be used to interconnect system components and algorithms. The specific tasks that can be performed using AMFIS include surveillance of scenes and paths, detection, localization and identification of people and vehicles as well as collection of evidence. The major advantages of this ground control station are its capability to display and fuse data from multiple sensor sources and the high flexibility of the software framework to build a variety of surveillance applications.**

Keywords - ground control station; sensors; unmanned aerial vehicles; security; surveillance; disaster management

I. INTRODUCTION

This paper presents a generic surveillance system and its control station called AMFIS. AMFIS is a component based modular construction kit currently under development as a research prototype. It has already served as the basis for developing specific products in the military and homeland security market. Applications have been demonstrated in exercises for the European Union under the PASR program (Preparatory Action for Security Research), German Armed Forces, and the defense industry. The tasks that have to be supported by such products are complex and involve among other tasks, control of sensors, mobile platforms and coordination with a control center.

The surveillance system AMFIS [1] is an adaptable modular system for managing mobile as well as stationary sensors. The main task of this ground control station is to work as an ergonomic user interface and a data integration hub between multiple sensors mounted on light UAVs (unmanned aerial vehicles) or UGVs (unmanned ground vehicles), stationary platforms (network cameras), ad hoc networked sensors, and a superordinated control center.

The AMFIS system is mobile and portable, allowing it to be deployed and operated anywhere with relative ease. It can supplement existing stationary surveillance systems or act as a surveillance system on its own if no preexisting infrastructure is available. The sensor carriers in this multi-sensor system can be combined in a number of different setups in order to meet a variety of specific requirements. At present, the system supports optical sensors (infra-red and visible) and alarms (PIR, acoustic, visual motion detection). There are plans to add support for chemical sensors in the future.

AMFIS has established standardized interfaces and protocols to integrate and control different kinds of sensors. This "plug and sense" approach allows the seamless integration of new sensors with a minimal effort. If necessary, all sensor data is automatically converted by dedicated services to a format usable by the ground control station.

After a short survey of related work an overview of the application scenarios is presented, followed by a detailed description of the apparatus in Section IV. Sections V and VI outline selected services and introduce a commercial flight platform modified to reach a higher level of autonomy and extending the ground control station presented in Section IV. Finally, in Section VII some first practical results are shown.

II. STATE OF THE ART

To the best of our knowledge, the combination of heterogeneous sensors and sensor platforms (ground, air, water) in an open homogeneous system allowing the fusion of various sensor data to generate a complex situation picture is quite a unique project. The integration of different sensors into one system has already been realized in previous systems but mainly in order to create specialized individual solutions tailored to individual customer requirements. Many projects deal with the development of supervision systems, new sensor platforms or control of sensors. The combination of these innovative supervision and reconnaissance attempts to one modular system has not yet been done.

Systems similar to AMFIS are the ground stations of the French company Aerodrones [2] and the American company AII [3], both developed as stand-alone control stations for multiple airborne drones. Another example is the product of the US company Defense Technologies [4], which focuses on military standardized interfaces to control different sensor platforms on the ground, in the air and in the water.

In contrast to AMFIS, Aerodrones and AII deal exclusively with airborne sensor platforms. Defense Technologies does not commit itself in the kind of used sensor platforms and is therefore more similar to AMFIS.

AII and Defense Technologies are concentrating on military solutions while AMFIS is mainly intended for civil applications.

III. APPLICATION SCENARIOS

The security feeling of our society has significantly changed during the past years. Besides the risks arising from natural disasters, there are dangers in connection with criminal or terroristic activities, traffic accidents or accidents in industrial environments.

Even though a lot of effort is put into protecting threatened or vulnerable infrastructure, most threats cannot be foreseen in their temporal and local occurrence, so that stationary in situ security and supervision systems are not present. Such ad hoc scenarios require quick situation-related action.

Possible scenarios that deal with these specifications are the supervision of big events or convoys for security reasons, natural and man-made disasters such as earthquakes or major fire control but also intrusion of unauthorized persons into sites and buildings, e.g., to take hostages or place explosives.

Especially in the civil domain, in case of big incidents there is a need for a better data basis to support the rescue forces in decision making. The search for buried people after a building collapses or the clarification and location of fires at big factories or chemical plants are possible scenarios addressed by our system. Only in the minority of cases the rescue forces can rely on an already available sensor infrastructure at the incident site. If there were sensors available, there is a significant chance they will be destroyed or at least partially corrupted. A transportable sensor system to be used remotely at the site of the event is proposed to close this gap.

The micro UAVs used in AMFIS can deliver a highly up-to-date situation picture from the air during a conflagration in a chemical factory or a similar scenario. Ground robots can enter the building in parallel to the fire-fighting work and penetrate areas, which are not yet accessible for the fire fighter and search for injured people or unknown sources of fire without endangering human life. Additionally, the mobile sensor platforms can be complemented by stationary systems. These can be temperature sensors for the fire aftercare or the measuring of the fire development and expansion or vibration and motion sensors to use in a collapsed building. These sensors can be used to prevent or at least to warn of any further structural changes in a collapsed building by detecting vibration and movement in the debris. The UAVs or ground robots can also act as platforms to deploy sensors at points of interest.

Besides the system's capability of ad hoc deployment during disasters or accidents, AMFIS can also be used as a versatile protection and supervision system. Premises or vulnerable infrastructures can be monitored with all types of sensors and actuators. Equipping the perimeter with motion detectors and cameras is a typical setup. In addition, mobile ground robots can patrol the area and respond to events. Other tasks that can arise are the detection of danger potential, the supervision of scenes and ways or the localization, tracking and identification of people and vehicles.

When several sensor systems and platforms are used in a complex scenario at the same time, conventional control systems designed as single use- and controlling-systems quickly reach their limits. First of all, every subsystem needs its own console and a specially trained operator due to the fact that each system has its own interface. Secondly the fusion and synchronized filing of sensor and status data from different systems is not an easy task.

The control of the individual sensors and platforms from the situation center is hardly practicable on account of the complexity, delay in the data transfer and distance to the place of action (often several kilometers).

As a connection between the sensors and the situation center an authority directly on the site of the event is necessary, which processes the reconnaissance missions independently. That includes steering sensor platforms, controlling sensors as well as filtering and densification of sensor data so that only information relevant for decisions like situation reports, alarms and critical video sequences are transmitted in an appropriate way to the situation center.

An analysis of the demands in complex scenarios incorporating micro UAVs has shown that at least two operators are necessary on the ground control station to deal with the requirements and problems arising from such a scenario. One operator is exclusively responsible for the control and supervision of the mobile sensor platforms. The second operator looks after the evaluation of the sensor data streams and the communication with the situation center.

According to a recent Frost & Sulivan report [5] micro UAVs are already used in vast and diverse civil applications. Some of the tasks that can be supported with UAVs in general include but are not limited to: enhancing agricultural practices, police surveillance, pollution control, environment monitoring, fighting fires, inspecting dams, pipelines or electric lines, video surveillance, motion picture film work, cross border and harbor patrol, light cargo transportation, natural disaster inspection, search and rescue, and mine detection.

Figure 1. A team of micro UAVs

Obviously some of these tasks are not suitable for single micro UAVs due to their limited operating range and payload. With groups or swarms of micro UAVs (Figure 1) it is possible to realize scenarios that are inefficient or even not

feasible with a single micro drone. Some situations where cooperating MAVs (micro aerial vehicles) add value include:

- A wider area has to be searched. A team of MAVs can increase coverage and reduce the time required.
- A UAV loses connection to the ground control station because it moved too far or the signals are blocked by an obstacle. In a group of UAVs, one of them can be "parked" in reach of the ground control station and act as relay station.
- Several intruders enter the site. They later split up, each taking different directions. A single drone would have to decide, which person to follow, while a swarm of UAVs can form subgroups and track each intruder individually.
- The duration of surveillance exceeds battery life time. In a team, assignments can be planned accordingly and another UAV can take over the task of an out-of-battery drone.
- A threat has to be monitored with different sensor types. For example, an intruder who is tracked visually suddenly places an object. Besides the visual sensor some CBRNE (chemical, biological, radiological, nuclear, and explosive) detection devices are needed. Since the payload of a single quadrocopter is very limited, a swarm could carry different sensors.
- Multi-sensor capability can also be used to visually control the action of different drones. For example an infrared sensor equipped UAV could be employed by the operator located at the ground control station to navigate a chemical sensor equipped micro UAV through a dark building.

These use cases illustrate that there is a need for the coordinated use of micro UAVs. The combination with other sensor platforms, such as UGVs (unmanned ground vehicles) or stationary sensors, adds further value to the system.

IV. System Overview

In order to be adaptable to a wide range of different requirements and applications, AMFIS was developed as a mobile and generic system, which delivers an extensive situation picture in complex surroundings - even with the lack of stationary security technology. In order to achieve maximum flexibility, the system is implemented open and mostly generalized so that different stationary and mobile sensors and sensor platforms can be integrated easily with minimal effort (Figure 2), establishing interoperability with existing assets in a coalition such as UAVs.

The system is modular and can be scaled arbitrarily or be adapted by choosing the modules suitable to the specific requirements. Because of the open interfaces, the accumulated data can be delivered on a real-time basis to foreign systems (e.g., command and control systems or exploitation stations, cf. Figure 3).

The AMFIS system can be divided into a mobile ground control station, which can control and coordinate different UAVs, land vehicles or vessels (sensor platforms), as well as stationary autonomous ad hoc sensor networks and video cameras. Depending on the used sensors and sensor platforms, the system is extended with suitable broadcasting systems for the transmission of the control signals and the sensor data (e.g., video recordings.)

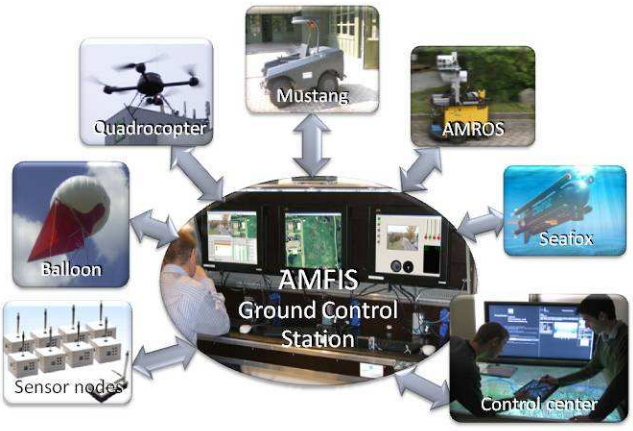

Figure 2. The AMFIS ground control station serves as integration platform for various sensors and vehicles

By the universal approach, the system is able to link with a wide range of sensors and can be equipped with electric-optical or infrared cameras, with movement dispatch riders, acoustic, chemical or radiation sensors depending on the operational aim. If supported or even provided by the manufacturer, these sensors can be mounted on mobile sensor platforms or be installed in fixed positions. The only requirement such sensors have to fulfill in a mobile scenario is that they work properly without the need for any pre-existing infrastructure.

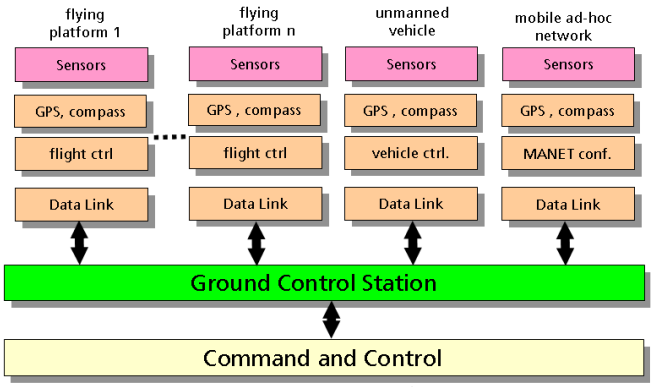

Figure 3. AMFIS interfaces

The AMFIS system is scalable and can be extended to any number of workstations. Due to this fact several sensor platforms can be coordinated and controlled at the same time. The most different sensor platforms can be handled in a similar manner by a standardized pilot's working station that in turn minimizes the training expenditure of the staff and raises the operational safety. The user interface is

automatically adapted according to the sensor or sensor platform at hand by using standardized descriptions.

Data fusion is one of the most important tasks of a multi sensor system. Without merging the data from different sensors the use of such a system is very limited. Linking data of sensors that complement each other can generate an entire situation picture.

All information gathered during the operation is immediately available to the crew of the ground control station, in which a GIS-supported, dynamic situation picture plays a central role. At the same time all received data is archived and stored into databases, e.g., a CSD (Coalition Shared Data) [6] or SSD (SOBCAH Shared Data) [7]. This serves the perpetuation of evidence and allows an additional subsequent analysis of the events.

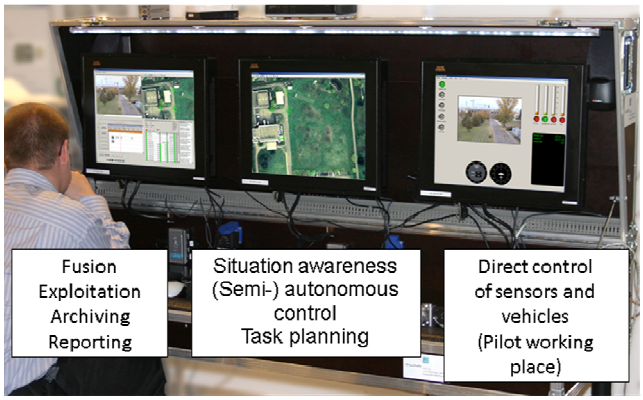

Figure 4. The AMFIS ground control station and its user interface

The open interface concept supports the integration of AMFIS in existing security systems so that data can be exchanged on a real-time basis with other guidance, supervision or evaluation systems. Mission planning, manual and automatic vehicle guidance, sensor control, local and temporal linking (coalescence) of sensor data, the coordination of the people on duty, reporting and the communication with the leading headquarters in the situation center belongs to the other tasks of a reconnaissance system.

Combination of sensor events and appropriate actions are implemented by predefined rules with an easy to use production system for situation specific adaptations.

A. *User Interface*

The user interface of the AMFIS ground control station at Fraunhofer IOSB consists of three workstations (Figure 4). Basically, the system is designed such that each display can be used to interact with each function allocated by AMFIS. The standard setup consists of two workstations with one operator each, and one situation awareness display in between that supports both operators. The duties of the two operators can be divided into sensor and vehicle control, called pilot working place, and data fusion, archiving, exploitation and coordination tasks.

The user interface of the latter working place primarily provides a function for the visualization of sensor data streams. Therefore the operator gains access to the accumulated data. His task is to obtain and keep an overview of the situation and to inform the higher authorities about important discoveries. He provides the associated data so that external systems or personnel can utilize that information. It is incumbent on him to mark important data amounts and to add additional information when necessary. Furthermore, he is the link to the pilot and coordinates and supports the pilot in his work. The analyst as well as the pilot relies on the central geographical information system-supported situation representation that provides an overview of the whole local situation. The geographical relation is established here and the situation and position of the sensors and sensor platforms can be visualized. This includes for example, the footprints of cameras or the position and heading of UAVs or UGVs.

The pilot's workstation is designed to control many different sensor platforms. It is not clear from the start, which sensor platforms will be used in the future and it is also not clear, which situation information will be provided by the different systems, or which information is needed to control the future platforms in a proper way. For this purpose the pilot workstation provides a completely adaptable user interface, which allows selectively activating or deactivating the required displays. For example, an artificial horizon is completely useless in order to control a stationary swiveling camera but very helpful for controlling an airborne drone. The surface can be adapted to the particular circumstances and is configurable for a wide range of standard applications. No matter what sensor platform the user is currently controlling or supervising, the task is the same. He does not have to switch between different proprietary control stations. The user interface is identical except for individual volitional or necessary adaptations.

B. *System and Software Architecture*

The physical sensors and sensor carriers are mapped logically to the so-called sensor web. This is a tree structure describing the real-world entities: The root node, the sensor web itself, connects to different sensor networks, each representing a number of similar sensor carriers, for example a team of UAVs. Each of those sensor networks is made up of one or more sensor nodes, equal to a physical sensor carrier (e.g., a single UAV), which in turn contain numerous sensors (e.g., camera, GPS receiver, etc.). The sensor web is permanently stored in a database, from which an XML file is generated at runtime by the central message hub of the AMFIS ground control station, the Connector.

The standard communications protocol within AMFIS is based on XML messages transported via TCP socket. To ease the use of this protocol, implementations exist in various runtime environments (e.g., .NET, Java), encapsulating the XML-handling and offering the user an object-oriented view of the messages. When a client application connects to the Connector, it first receives the aforementioned XML-version of the sensor web followed by a steady stream of XML messages, each containing metadata (e.g., sensor values, commands, etc.) originating from or destined to one of the sensors in the sensor web.

A client application can be anything from a GUI application to a low-level service:

- The various GUI applications of the user interface, most importantly the analyst's interface, the situation overview and the pilot's interface. Those applications offer a visual representation of received metadata to the user, for example by displaying the current geographical locations of the various sensor carriers in the map, and transmit commands to the sensor carriers, for example a user-generated waypoint for a UAV.
- A number of services running in background, notably the video server, offering time shifting and archiving for both video and metadata (more on video management within AMFIS see below), the rules engine, the flight path planning tool and the multi-agent system, all supporting the user by automating certain processes (see Section V).
- Drivers for various sensor carriers, for example a dedicated control software for UAVs, which translates high-level flight commands like waypoints into the proprietary RS232-based control protocol of the respective drone, and in turn generates metadata XML status messages containing the current position, heading, remaining flight time etc.
- Interfaces to third-party applications or networks, for example superior command centers.

The current implementation of the communication protocol is strictly multicast-based: Every message sent to the Connector is relayed to every connected client application, leaving it to the respective application to decide what to do with it. For future versions, a subscription-based model is planned.

The protocol relies on lower-level protocols such as TCP to ensure delivery of the messages. Since most of the messages contain live status data, they are transferred in a fire-and-forget manner, thus eliminating possible race conditions within the Connector.

While all metadata – be it sensor values, commands or user-generated textual comments – is transmitted via XML, the extensive amount of video data accumulated by the various cameras has to be processed and stored by other means. A central application within AMFIS is the video server, which receives and records all available network video streams along with incoming XML messages. Since the analyst's interface heavily relies on the capability to go back in time and review critical situations, the video server serves the dual purpose of both recording the video streams for later archival as well as providing time shifting-enabled streams to other clients. If required the video server can store (and later play back) the accumulated data using a standard MySQL database.

In order to interface with third-party systems, it can become necessary to transcode available data into another format. Upon request, the video server can spawn a so-called transcoder process, multiplexing video and metadata into a single stream to be transmitted to a remote command center. To receive incoming commands from a command center, an XMPP client (Extensible Messaging and Presence Protocol, formerly Jabber [8][9]) has been implemented, which seamlessly integrates into the AMFIS ground control station.

Figure 5 shows a logical representation of the AMFIS system.

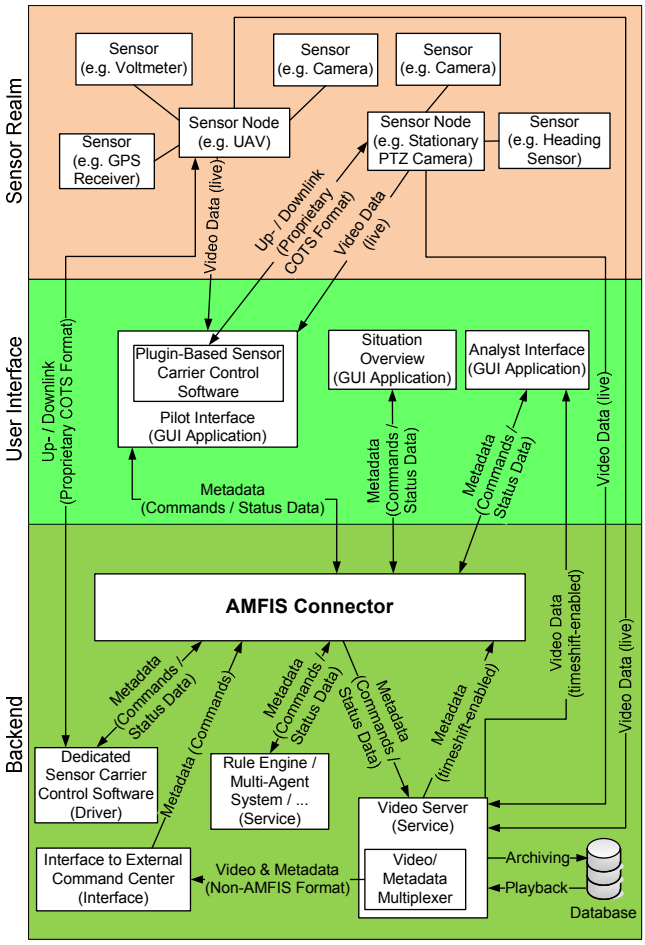

Figure 5. AMFIS system overview

V. AMFIS SERVICES

In addition to being an integration platform, AMFIS offers a number of support services related to surveillance and reconnaissance tasks. Those services facilitate resource planning, sensor and vehicle coordination, sensor data exploitation, and training. Three of these services, i.e., rule-based event response, photo flight and simulation, are described in the following paragraphs.

A. *Rule-Based Event Response*

This service is a support system for the automatic combination and selection of sensor data sources in a surveillance task. Autonomous reactions, e.g., responding to an intrusion alert triggered by a motion detector, are very important during a surveillance scenario. Therefore a solution was developed, which grants users an easy, powerful and versatile platform for defining reactions.

The implementation is universal so that the support system can be adapted to several scenarios at different

individual sites. This is accomplished by the use of rule sets, which are created site and task specific. These rules contain work flows which are pushed if a certain predefined event occurs. Thus, for example, a watchman can be automatically informed or a UAV can be sent off for reconnaissance of a defined area without any user interaction.

The support component in AMFIS is implemented with the Drools rules engine [10] using production rules for representing procedural task knowledge. The engine uses the Rete algorithm, which repeatedly assesses the current situation and selects the rules to execute. Drools is open source and contains a well developed rule language.

The rule language is based on the when-then schema (Figure 6). Additionally, Boolean logic, methods of compiled Java source code and their return values can be used.

```
rule "rule"
    when
            sensor triggers alarm
            <additional preconditions>
    then
            camera turns to sensor position
            drone flies to sensor position
end
```

Figure 6. Layout of a rule

The integration of the rule-based event response application into the AMFIS system is depicted in Figure 7.

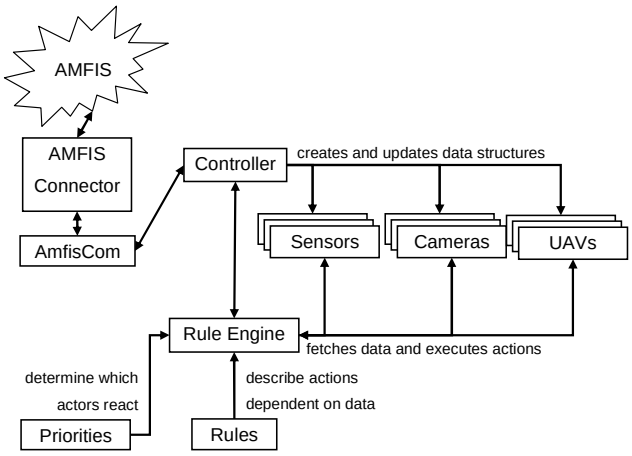

Figure 7. Integration of a rule engine

The rule engine uses AmfisCom, a communication library for interfacing the AMFIS Connector (cf. Section IV.B) to establish a connection to the Connector Service, the message hub of AMFIS, and receives data. Data structures containing e.g., positions and IDs of sensors, cameras and UAVs are created and updated with the received data. When there is an alarm message it can be assigned to its corresponding sensor through the unique ID. After this initialization phase the rule interpretation starts. When a rule becomes applicable messages are sent to the corresponding assets (cameras, UAVs, etc) to change their positions accordingly. Furthermore, every camera has a priority list of targets. Before the message is sent, this list is evaluated. Only if the new target has at least the same priority as the current target, the camera pans to the new target.

Additionally, a tool providing a graphical user interface has been developed. It facilitates the definition of rules and the creation of priority lists for cameras. The rules can be assembled by clicking and saved as XML file. These files are editable by the user at any time. Furthermore, the rule engine can import these files and convert the content into the specific rule language.

B. *Photo flight*

The photo flight service assists the operator in obtaining an up-to-date situation picture of a site. One or more UAVs with camera payloads fly to defined waypoints and capture high resolution still images. These images are later combined to a mosaic. The photo flight service manages the available assets (i.e., UAVs and payloads) and automatically calculates flight paths based on a user-defined area of interest.

In the flight path planning tool, the user can define any polygonal shape on the map. He then selects one or more UAVs from a list of available drones, which is distributed by the AMFIS Connector. The Connector provides the necessary information about all drones and their current payloads. For each selected UAV the user is requested to enter some variable parameters like desired photo flight height or safety height. The safety height parameter is an additional safety feature that defines individual cruising heights in order to prevent collisions between UAVs.

After that, the operator can start the photo flight or add/remove additional drones to/from the list. Once all necessary information has been entered correctly and the "Calculate" button is clicked, the planning algorithm starts and shows the resulting flight path on the map (Figure 8).

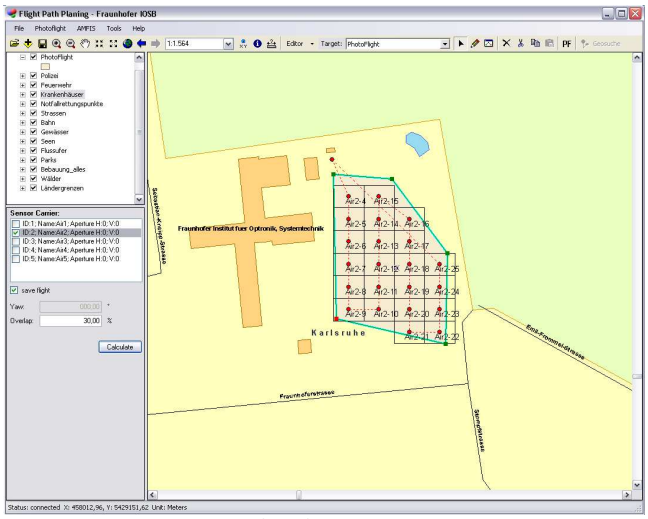

Figure 8. GUI of the flight path planning service

Additionally, the flight path planning service offers the possibility to export the calculated waypoints in an AMFIS specific file format or upload the points directly to the respective UAV using the Connector.

C. Simulation

In order to assess different cooperation strategies for teams of UAVs and other assets, a simulation tool has been developed. The tool is also useful when it comes to training and briefing of the operators. Modeling and visualization of scenarios was done using a computer game engine with corresponding editing tools. An interface between AMFIS and the engine has been implemented. It allows full control of the virtual entities as well as feedback from the virtual world. The simulation tool is fully integrated into the AMFIS ground control station allowing seamless combination of virtual and real assets. Virtual vehicles can be monitored and controlled analogous to real assets through the AMFIS situation map, whereas real UAVs can be displayed in the virtual world next to simulated components.

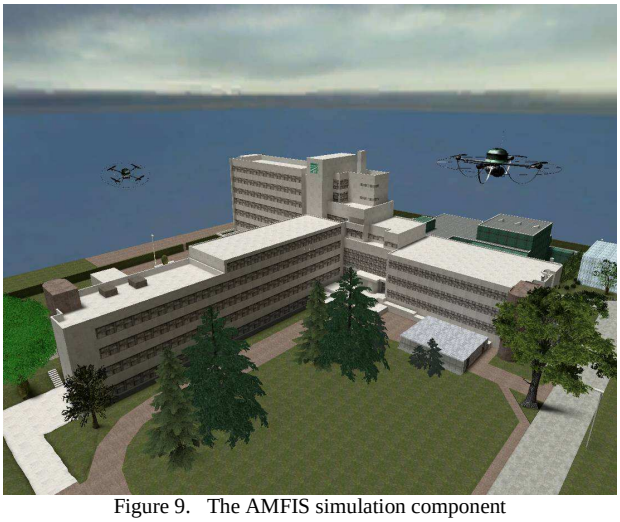

Figure 9. The AMFIS simulation component

An example scenario that simulates an intrusion has been realized (Figure 9). Besides the UAVs and the actors in the scenario, sensors have also been modeled. Different kinds of sensors such as motion detectors, cameras, ultra sonic or LIDAR (light detection and ranging) sensors can be modeled with their specific characteristics. The simulation tool can determine if an object lies within the range of a sensor. This helps evaluate and optimize the use of different sensing techniques.

The intelligence of team members is implemented in software agents as described in Section VI.C. They interface with the simulation engine using the same control command interface as the actual quadrocopters. This subsequently can allow the simulation to be transferred to the real world without changes to the agents.

VI. AUTONOMOUS SENSOR PLATTFORMS

AMFIS as an open and generic system supports the simultaneous operation of a large number of sensors and sensor platforms. While the handling of single platforms is already well understood, control and coordination of several mobile platforms can be a challenging task.

For this purpose one of the research focuses lies on the improvement of the application of multiple miniature UAVs. Our approach is to increase the level of autonomy of each drone. Therefore a vast amount of effort has been put into the selection of the flight platform. Such a platform preferably comes with a range of sensors and an advanced internal control system with autonomous flight features, which minimizes the regulation need from outside. When it comes to flying autonomously, the system has to be highly reliable and possess sophisticated safety features in case of malfunction or unexpected events.

Figure 10. Sensor platform AirRobot 100-B

Other essential prerequisites are the possibility to add new sensors and payloads and the ability to interface with the UAV's control system in order to allow autonomous flight. A platform that fulfils these requirements is the quadrocopter AR100-B by AirRobot. It can be both controlled from the ground control station through a command uplink and by its payload through a serial interface.

A. UAV Control Hardware

To support the pilot at his work at the ground control station and to give him the possibility to supervise multiple flying sensor platforms at the same time, several steps are necessary. The first step is to enhance the hardware in order to reach a higher level of autonomy. Therefore, a payload was developed, which carries a processing unit that can take over control and thereby steer the quadrocopter.

Due to space, weight and power constraints of the payload, this module has to be small, lightweight and energy-efficient. On the other hand, a camera as a sensor system should not be omitted. An elegant solution is the use of a "smart" camera, i.e., a camera that not only captures images but also processes them. Processing power and functionalities of modern smart cameras are comparable to those of a PC. Even though smart cameras became more compact in recent years, they are still too heavy to be carried by a quadrocopter such as the AR100-B. In most applications, smart cameras remain stationary whereby their weight is of minor importance. However, a few models are available as board cameras, i.e., without casing and the usual plugs and sockets (Figure 11). Thus, their size and weight are reduced to a minimum. The camera that was chosen has a freely programmable DSP, a real-time operating system and several interfaces (Ethernet, I²C, RS232). With its weight of only 60g (without the lens), its compact size and a power consumption of 2.4W, it is suitable to replace the standard video camera payload.

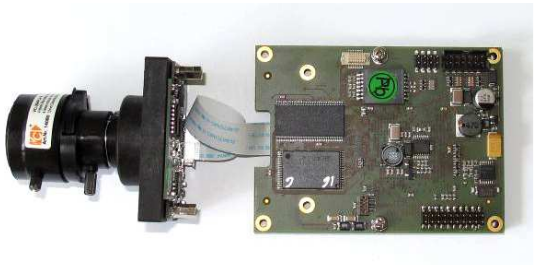

Figure 11. A programmable camera module controls the UAV

The camera can directly communicate with the drone's controller though a serial interface. The camera receives and processes status information from the UAV such as position, altitude or battery power, and is able to control it by sending basic control commands or GPS-based waypoints.

A drawback of the board camera is its lack of an analogue video output thus rendering the quadrocopter's built-in video downlink useless. Image data is only available through the camera's Ethernet interface. To enable communication between the smart camera and the ground control station, a tiny WiFi module was integrated into the payload. The WiFi communication link allows streaming of live video images, still shots and status information from the UAV to the ground control station. Furthermore, programs can be rapidly uploaded to the camera during operation.

Currently, the above enhanced UAVs are able to perform basic maneuvers, such as take-off, fly to position, and landing, all autonomously. Furthermore, a software module was implemented, that calculates the footprint of the camera, i.e., the geographic co-ordinates of the current field of view. In the future we will also use the camera's image processing capabilities to generate control information. As a safety feature, it is always possible for the operator to override autonomous control and take over control manually.

B. Communication Infrastructure

For a single UAV communication usually consists of two dedicated channels, an uplink channel for control commands and a downlink channel for video and status information. In present UAVs, each of these channels has its own communication technique in a special frequency band. In complex scenarios that require multiple UAVs there has to be twice as many RF channels as UAVs used. These channels are all point-to-point connections, which, if at all, see the other UAVs only as interferer. There is no channel between two UAVs; all communication goes via the base station.

Besides this direct control of UAVs, there is a more abstract way, which can use the benefits of an intelligent payload. The group of UAVs receives complex tasks, which they will fulfill autonomously. This kind of control however brings the standard system with up- and downlink to its limits because it poses demands, which cannot be fulfilled with the standard communication:

- No interference between communication of multiple UAVs (ideally: use of multihopping)
- Adding UAVs to the swarm must not require a new RF channel
- Opening of data channels to transmit the results to the base-station
- Opening of control channels to transmit any kind of commands to the UAV
- Sending broadcast messages to all UAVs
- Opening direct communication channels between UAVs

In addition to the new demands, the standard requirements for UAVs still must maintain the following:

- Monitor the status of every UAV in the air
- Manual control of every UAV as fallback function

To fulfill these needs the (video-) downlink is replaced by a module capable of using networking communications. In our prototype we use a WiFi module because of its high data rates and good range, though other technologies might be feasible too. The UAV's uplink channel is retained as fallback control option in case of an emergency.

With the WiFi network, we implemented a communication solution that meets the demands listed above. This solution differentiates between UAV and base-station, i.e., the ground control station. There is only one base-station within the network. A base-station monitors the status of every UAV assigned to it. It also acts as gateway to other system components.

Our communication setup uses four types of channels (cf. Figure 12):

- Broadcast channel
  a channel, which offers random access to every subscriber in the network
- Control channel
  a dedicated channel between a UAV and the base-station to transmit status information from the UAV and to receive commands from the base-station
- Data channel
  a dedicated channel between UAV and the base-station to send results of task i.e., images
- Co-op channel
  this channel is opened between two UAVs if one of them needs assistance to finish a task

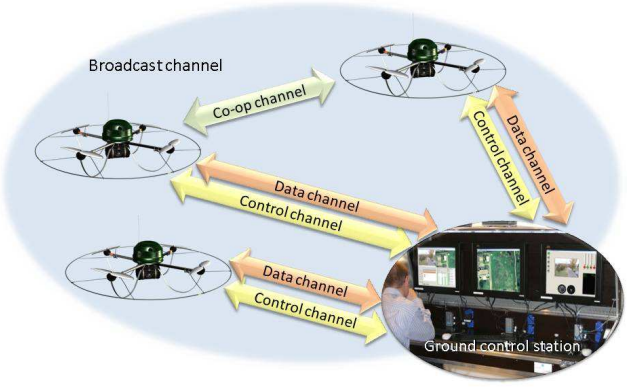

Figure 12. Communication channels between UAVs and the ground control station

1) Broadcast channel

The broadcast channel is mainly used for initializing the other channels. If a UAV is not assigned to a base-station it will look for a base-station on this channel. Also if a UAV needs assistance to finish a job, e.g., when its battery runs low or it needs a UAV with another sensor, the UAV calls for assistance on this channel. Through the broadcast channel it is possible to reach all UAVs with a single message. If a UAV, for example, detects an obstacle it can inform all other UAVs in the group. Another main feature of this channel is communicating new tasks. When this task is transmitted to the whole group instead of a single UAV, the decision regarding which UAV best fits the needs for this task can be done by the group.

2) Control channel

The control channel is a dedicated channel between a UAV and a base-station. Over this channel a UAV sends its status as well as an "Alive" Message. These data make it possible to monitor the UAVs in the base-station. The second feature of this channel is a command uplink to the UAV. It can be used to transmit tasks as well as to configure the UAV. Reconfiguring can be done by changing internal parameters of the UAV or by uploading new software modules.

3) Data channel

The data channel sends results (usually video images) to the base-station. The format of the data has to be predefined.

4) Co-op channel

The co-op channel is opened between two UAVs, if necessary. If the UAV has a task, which cannot be done on its own, it seeks a wingman over the broadcast channel. If there is an idle UAV, which can assist, a co-op channel is opened between the two drones. Over this channel the UAV has the possibility to send subtasks to the wingman. After completion, it receives the results over the co-op channel.

Replacing the standard downlink with a networking module is a big step towards autonomy of each UAV. With this adaptive communication solution it is possible to set up an expandable network of UAVs. The implemented channels provide communication links between all subscribers in the net.

C. UAV Control Software

The second step to reaching a higher level of autonomy is based on the development of a multi-agent system to implement team collaboration. An agent-based framework is implemented where the individual entities in a team of UAVs are represented by software agents. The agents implement the properties and logic of their physical counterparts. Their behavior defines the reaction to influences in the environment, such as alarms generated by sensors in the AMFIS network.

An agent is "…any entity that can be viewed as perceiving its environment through sensors and acting upon its environment through effectors" [11]. Incorporating that "An agent is a computer system, situated in some environment that is capable of flexible autonomous action in order to meet its design objectives" [12], a multi-agent system appears to perfectly meet the challenges of realizing an intelligent swarm of autonomous UAVs.

Software agents are computational systems that inhabit some complex dynamic environment, which sense and act autonomously in this environment, and by doing so, realize a set of goals or tasks, for which they are designed [13]. Hence, they meet the major requirements for a suitable architectural framework: to support the integration and cooperation of autonomous, context-aware entities in a complex environment.

The agent-based approach allows a natural system modeling approach facilitating the integration of flight platforms, sensors, actuators and services. The core-agents of the multi-agent system presented in this paper are based on the following three agent classes:

- Action Listener: This agent has two basic tasks: connecting the agent system to the AMFIS ground control station and managing the different Teamleader Agents (see below). The Action Listener receives messages from the AMFIS Connector and sends corresponding commands or data to the relevant Teamleader Agents. Through the Action Listener, the operator can directly task a UAV, bypassing the agents' logic.
- Teamleader Agent: A team leader agent controls a group of agents consisting of at least one other agent. It co-ordinates higher tasks and assigns sub-tasks to team members, for examples areas they have to monitor. A team leader is always aware of the positions and capabilities of all team members. A team leader itself can be controlled by a superordinate team leader.
- Universal Agent: This agent represents a single UAV. Every drone must be assigned to a team leader. The Universal Agent manages all basic behaviors and data of the UAV it represents. Basic behaviors are for example the direct flight to a waypoint and receiving and handling messages from the team leader.

UAVs in a team can be equipped with different payloads, for example cameras or gas sensors. Therefore, specific agents exist, such as Video Agents and Sensor Agents, which inherit the basic behaviors from the Universal Agent. Additionally, they also have their own specific behaviors. By this separation in universal and specific agents, adaptations of the general behavior or the specific behavior can be made very efficiently, i.e., only one agent has to be modified. For example, if we want to change the behavior to fly to a waypoint we only have to do that in the Universal Agent, not in the specific payload agent.

The communication between the agents of one team is direct. It is not possible to directly communicate with a Universal Agent of another team. Communication to a Universal Agent of another team has to go through the corresponding Teamleaders. A communication between two

agents in different teams is usually not necessary, because every team has its own task.

The use of this multi-agent system is not limited to UAVs. As well, it can be applied to coordinate a heterogeneous fleet of ground and air assets.

VII. RESULTS

Figure 13 shows a high-resolution situation picture generated with AMFIS using its photo flight tool presented in Section V.B. The picture is geo-referenced and can be overlaid onto the existing GIS-based, dynamic situation map.

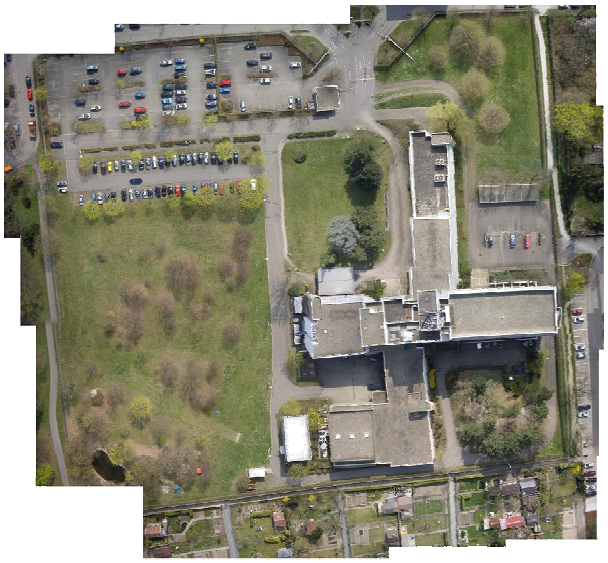

Figure 13. Situation picture generated with the AMFIS photo flight tool (ca. 9500 x 9000 pixel)

CONCLUSION

The presented surveillance and reconnaissance system AMFIS with its extensions is constantly under development. Due to its generic nature, it forms a rather universal integration platform for new sensors, platforms, interfaces, supporting application programs and customized solutions. The knowledge gained from the participation in various exercises is constantly used to optimize the ergonomics of the work stations and to improve the algorithms for data fusion. The advancement of sensor technology and robotics, increasing processing power, progress in information and network technology provide continuous input for the permanent development and optimization of the AMFIS system.

Presently, the human is still the most important link in the supervision chain. The operator must evaluate the data, which is delivered by the sensors and derive decisions to meet the existing dangers. Lastly, it is a person that is accountable and bears the responsibility for the resultant action, not the supporting machine.

The above introduced duties of the situation analysis and situation response are so versatile and complicated that further research is inevitable to fully automate them. Up to now, humans are still indispensable in their varied roles as head of operations, pilot, analyst, watchman etc. The AMFIS system with its ability to integrate different sensors, sensor platforms and data sources can support and assist people with those tasks.

With the use of the mobile AMFIS system in industry, as well as at authorities and organizations like fire brigade, search and rescue services, and police, the geographical and information data bases can be improved decisively. With the gathered reconnaissance information fused or linked to information extracted from different sources, the task forces deploying the AMFIS system can be better protected and coordinated and decision making in critical situations can be optimized.

ACKNOWLEDGMENT

The authors would like to thank their colleagues and students who have contributed to the work presented in this paper, especially Sandro Leuchter, Thomas Partmann, Sven Müller, Steffen Burger, Frederic Schumacher, and Torsten Großkurth.

REFERENCES

[1] F. Segor, A. Bürkle, T. Partmann, R. Schönbein, “Mobile Ground Control Station for Local Surveillance,“ In: ICONS 2010, The Fifth International Conference on Systems, 11-16 April 2010, Menuires, The Three Valleys, France.

[2] AERODRONES, France, http://www.aerodrones.com, 2011.

[3] AAI Corporation, USA, http://www.aaicorp.com, 2011.

[4] Defense Technologies, Inc., USA, http://www.dtiweb.net, 2011.

[5] Frost & Sullivan, “Advances in platform technologies for unmanned aerial vehicles,” Technical Insights Report D1B0, San Antonio, TX, 2009.

[6] B. Essendorfer and W. Müller, “Interoperable sharing of data with the Coalition Shared Data (CSD) server,” North Atlantic Treaty Organization (NATO)/Research and Technology Organization (RTO): C3I in crisis, emergency and consequence management, 2009.

[7] B. Essendorfer, E. Monari, and H. Wanning, “An integrated system for border surveillance,” In: R. Ege (ed.), ICONS 2009: The Fourth International Conference on Systems, 1-6 March 2009, Gosier, Guadeloupe/France.

[8] RFC 3920: “Extensible Messaging and Presence Protocol (XMPP): Core,” The Internet Engineering Task Force (IETF), 2004.

[9] RFC 3921: “Extensible Messaging and Presence Protocol (XMPP): Instant Messaging and Presence,“ The Internet Engineering Task Force (IETF), 2004.

[10] M. Proctor, M. Neale, M. Frandsen, S. Griffith Jr., E. Tirelli, F. Meyer, and K. Verlaenen, “Drools Documentation (V. 4.0.4),” 2008, http://downloads.jboss.com/drools/docs/4.0.4.17825.GA/html_single/index.html

[11] S. J. Russell and P. Norvig, “Artificial Intelligence: A Modern Approach,” Prentice Hall, ISBN 9780137903955, 2003.

[12] N. R. Jennings, K. Sycara, and M. Wooldridge, “A roadmap of agent research and development,” Journal of Autonomous Agents and Multi-Agent Systems, 1(1), pp. 7–38, ISSN 1387-2532, 1998.

[13] P. Maes, “Agents that reduce work and information overload,” Communications of the ACM 37, 7 (July 1994), pp. 30-40, ISSN 0001-0782, 1994.

Secure Video for Android Devices

Raimund K. Ege
Department of Computer Science
Northern Illinois University
DeKalb, IL 60115, USA
ege@niu.edu

***Abstract*—Android is rapidly gaining market share among smart phones with high-speed next-generation Internet connectivity. A whole new generation of users is consuming rich content that requires high throughput. Applications like FaceBook and YouTube have reached mobile devices. Multimedia data, i.e. video, is becoming easily accessible: large multi-media files are being routinely downloaded. Peer to-peer content delivery is one way to ensure the volume that can be efficiently delivered. However, the openness of delivery demands adaptive and robust management of intellectual property rights. In this paper we describe a framework and its implementation to address the central issues in content delivery: a scalable peer-to-peer-based content delivery model, paired with a secure access control model that enables data providers to reap a return from making their original content available. Our prototype implementation for the Android platform for mobile phones is described in detail.**

Keywords-broadband video sharing; peer-to-peer content delivery; access control; Android video client

I. INTRODUCTION

The Apple iPhone, and now increasingly Android-based smart phones, have ushered in a new era in omni-present broadband media consumption. Services such as iTunes, YouTube, Joost and Hulu are popularizing delivery of audio and video content to anybody with a broadband Internet connection. High bandwidth internet connectivity is no longer limited to reaching PCs and laptops: a new generation of devices, such as netbooks and smart phones, is within reach of 3G/4G telecommunication networks.

In this paper we describe a new "app" for Android phones that delivers video in a secure and managed way. Figure 1 shows a screenshot of the Android home screen featuring our new Oghma secure multi-media delivery "app."

Delivering multimedia services has many challenges: the ever increasing size of the data requires elaborate delivery networks to handle peek network traffic. Another challenge is to secure and protect the property rights of the media owners. A common approach to large-scale distribution is a peer-to-peer model, where clients that download data immediately become intermediates in a delivery chain to further clients. The dynamism of peer-to-peer communities means that principals who offer services will meet requests from unrelated or unknown peers. Peers need to collaborate and obtain services within an environment that is unfamiliar or even hostile.

Figure 1. Oghma on Android Home Screen

Therefore, peers have to manage the risks involved in the collaboration when prior experience and knowledge about each other are incomplete. One way

to address this uncertainty is to develop and establish trust among peers. Trust can be built by either a trusted third party [2] or by community-based feedback from past experiences [3] in a self-regulating system. Conventional approaches rely on well-defined access control models [4] [5] that qualify peers and determine authorization based on predefined permissions. In such a complex and collaborative world, a peer can benefit and protect itself only if it can respond to new peers and enforce access control by assigning proper privileges to new peers.

The general goal of our work is to address the trust in peers which are allowed to participate in the content delivery process, to minimize the risk and to maximize the reward garnered from releasing data in to the network. In our prior work [9][15] we focused on modeling the nature of risk and reward when releasing content to the Internet. We integrated trust evaluation for usage control with an analysis of risk and reward. Underlying our framework is a formal computational model of trust and access control. In the work reported here we focus on the implementation aspects of the framework.

Our paper is organized as follows: the next section will elaborate on how the data provider and its peers can quantify gain from participating in the content delivery. It also explains our risk/reward model that enables a data source to initially decide on whether to share the content and keep some leverage after its release. Section III describes our prototype architecture that is based on a bittorrent-style of peer-to-peer content delivery. A central tracker manages peers and maintains a database of trust information. Peers can serve both as source and as consumer of data. Section IV introduces our prototype client for the Android platform. Section V elaborates on details of the Java implementation of the tracker, source and peer processes. Data is exchanged using the Stream Control Transmission Protocol (SCTP) which improves over the current standard-bearers Transmission Control Protocol (TCP) and User Datagram Protocol (UDP) for multi-stream session-oriented delivery of large multi-media files over fast networks. Data is secured using a PKI-style exchange of public keys and data encryption.

The paper concludes with our perspective on how modern content delivery approaches will usher in a new generation of Internet applications.

An earlier version of this paper appeared in the Proceedings of the Fifth International Conference on Systems (ICONS 2010) [1].

II. UNITS OF RISK AND REWARD

We assume that the data made available at the source has value. Releasing the data to the Internet carries potential for reaping some of the value, but also carries the risk that the data will be consumed without rewarding the original source. There is also a cost associated with releasing the data, i.e. storage and transmission cost. For example, consider a typical "viral" video found on YouTube.com: the video is uploaded onto YouTube.com for free, stored and transmitted by YouTube.com and viewed by a large audience. The only entity that is getting rewarded is YouTube.com, which will accompany the video presentation with paid advertising. The person that took the video and transferred it to YouTube.com has no reward: the only benefit that the original source of the video gets is notoriety.

In order to provide a model or framework to asses risk and reward, we need to quantize aspects of the information interchange between the original source, the transmitting medium and the final consumer of the data. In a traditional fee for service model the reward *"R"* to the source is the fee *"F"* paid by the consumer minus the cost *"D"* of delivery:

$$R = F - D$$

The cost of delivery *"D"* consist of the storage cost at the server, and the cost of feeding it into the Internet. In the case of YouTube, considerable cost is incurred for providing the necessary server network and their bandwidth to the Internet. YouTube recovers that cost by adding paid advertising on the source web page as well as adding paid advertising onto the video stream. YouTube's business model recognizes that these paid advertisings represent significant added value. As soon as we recognize that the value gained is not an insignificant amount, the focus of the formula shifts from providing value to the original data source to the reward that can be gained by the transmitter. If we quantify the advertising reward as *"A"* the formula now becomes:

$$R = F - (D - A)$$

Even in this simplest form, we recognize that *"A"* has the potential to outweigh *"D"* and therefore reduce the need for *"F"*. As YouTube recognizes, the reward lies in *"A"*, i.e. paid ads that accompanies the video.

In some of our prior work [8] we focused on mediation frameworks that capture the mutative nature of data delivery on the Internet. As data travels from a source to a client on lengthy path, each node in the path may act as mediator. A mediator transforms data from an input perspective to an output perspective. In the simplest scenario, the data that is fed into the delivery network by the source and is received by the ultimate client unchanged: i.e. each mediator just

passes its input data along as output data. However, that is not the necessary scenario anymore: the great variety of client devices already necessitate that the data is transformed to enhance the client's viewing experience. We apply this mediation approach to each peer on the path from source to client. Each peer may serve as a mediator that transforms the content stream in some fashion. Our implementation employs the stream control transmission protocol (SCTP) which allows multi-media to be delivered in multiple concurrent streams. All a peer needs to do is add an additional stream for a video overlay message to the content as it passes through.

The formula for reward can now be extended into the P2P content delivery domain, where a large number of peers serve as the transmission/storage medium. Assuming "*n*" number of peers that participate and potentially add value the formula for the reward per peer is now:

$$R_p = \sum_{i=1}^{n} (F_i - (D_i - A_i) - F_p$$

D_i and A_i are now the delivery cost and value incurred at each peer that participates in the P2P content delivery. F_i is the fee potentially paid by each peer. F_p is the fee paid to the data source provider. Whether or not the data originator will gain any reward depends on whether the client and the peers are willing to share their gain from the added value. In a scenario where clients and peers are authenticated and the release of the data is predicated by a contractual agreement, the source will reap the complete benefit.

In our model we quantify the certainty of whether the client and peers will remit their gain to the source with a value of trust *"T"*: *T* represents the trust in the client that consume that data, *T* represents the trust in each peer that participates in the content delivery. The trust is evaluated based on both actual observations and recommendations from referees. Observations are based on previous interactions with the peer. Recommendations may include signed trust-assertions from other principals, or a list of referees that can be contacted for recommendations. The trust value, calculated from observations and recommendations, is a value within the [0, 1] interval evaluated for each peer that requests to be part of the content delivery.

Our model enables an informed decision on whether to accept a new peer based on the potential additional reward gained correlated to the risk/trust encumbered by the new peer.

III. PROTOTYPE ARCHITECTURE

Peer-to-peer (P2P) delivery of multimedia aims to deliver multi-media content from a source to a large number of clients. For our framework, we assume that the content comes into existence at a source. A simple example of creating such multimedia might be a video clip taken with a camera and a microphone, or more likely video captured via a cell phone camera, and then transferred to the source. Likewise the client consumes the content, e.g. by displaying it on a computing device monitor, which again might be a smart phone screen watching a YouTube video. We further assume that there is just one original source, but that there are many clients that want to receive the data. The clients value their viewing experience, and our goal is to reward the source for making the video available.

In a P2P delivery approach, each client participates in the further delivery of the content. Each client makes part or all of the original content available to further clients. The clients become peers in a peer-to-peer delivery model. Such an approach is specifically geared towards being able to scale effortlessly to support millions of clients without prior notice, i.e. be able to handle a "mob-like" behavior of the clients.

The exact details of delivery may depend on the nature of the source data: for example, video data is made available at a preset quality using a variable-rate video encoder. The source data stream is divided into fixed length sequential frames: each frame is identified by its frame number. Clients request frames in sequence, receive the frame and reassemble the video stream which is then displayed using a suitable video decoder and display utility. The video stream is encoded in such a fashion that missing frames don't prevent a resulting video to be shown, but rather a video of lesser bit-rate encoding, i.e. quality, will result [7]. We explicitly allow the video stream to be quite malleable, i.e. the quality of delivery need not be constant and there is no harm if extra frames find their way into the stream. It is actually a key element of our approach that the stream can be enriched as part of the delivery process.

In our approach, multi-media sources are advertised and made available via a central tracking service: at first, this tracker only knows the network location of the source server. Clients that want to access the source do so via the tracker: they contact the tracker, which will respond with the location of the source. The tracker will also remember (or track) the clients as potential new sources of the data. Subsequent client requests to the tracker are answered with all known locations of sources: the original and the known clients. Clients that receive locations of sources from the tracker issue frame requests immediately to all

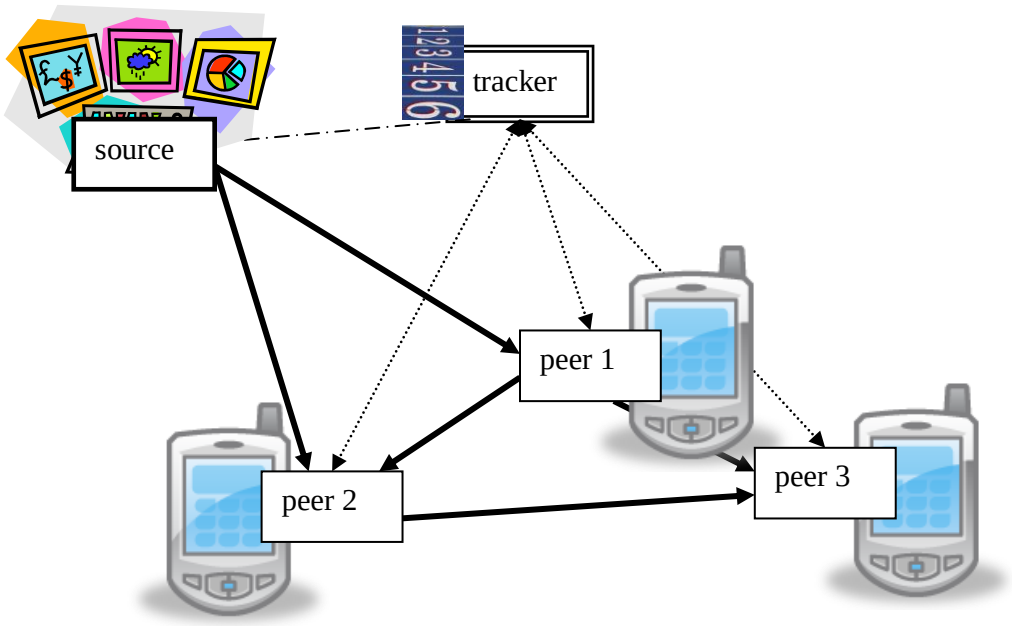

Figure 2. P2P Content Delivery Network

sources. As the sources deliver frames to a client, the client stores them. The client then assumes a server role and also answers requests for frames that they have received already, which will enable a cascading effect, which establishes a P2P network where each client is a peer. Every client constantly monitors the rate of response it gets from the sources and adjusts its connections to the sources from which the highest throughput rate can be achieved.

Figure 2 shows an example snapshot of a content delivery network with one source, one tracker, 2 intermediate peers and one client. The source is where the video data is produced, encoded and made available. The tracker knows the network location of the source. Clients connect to the tracker first and then maintain sessions for the duration of the download: the 2 peers and the single client maintain an active connection to the tracker. The tracker informs the peers and client which source to download from: peer 1 is fed directly from the source; peer 2 joined somewhat later and is now being served from the source and peer 1; the client joined last and is being served from peer 1 and peer 2. In this example, peer 1 and 2 started out as clients, but became peers once they had enough data to start serving as intermediaries on the delivery path from original source to ultimate client.

IV. ANDROID CLIENT

We chose the new and emerging Android platform to implement a proof-of-concept client for a mobile device. Android is part of the Open Handset Alliance [10]. Android is implemented in Java and therefore offers a flexible and standard set of communication and security features.

Figures 3, 4, 5 and 6 show four sample screen shots taken from the Android system. It shows our Oghma Secure P2P media client. Figure 3 shows the login screen to our Oghma mobile client. It uses OpenID[6] user credentials and allows to establish a connection to a tracker URL.

Once the tracker has authenticated the new client it will respond with a list of available video streams (Figure 4). After the user has made a selection, the screen shown in Figure 5 appears. Once a sufficient read-ahead buffer has been accumulated, the video stream starts playing on the Android device (Figure 6).

Figure 3. Oghma Login Screen

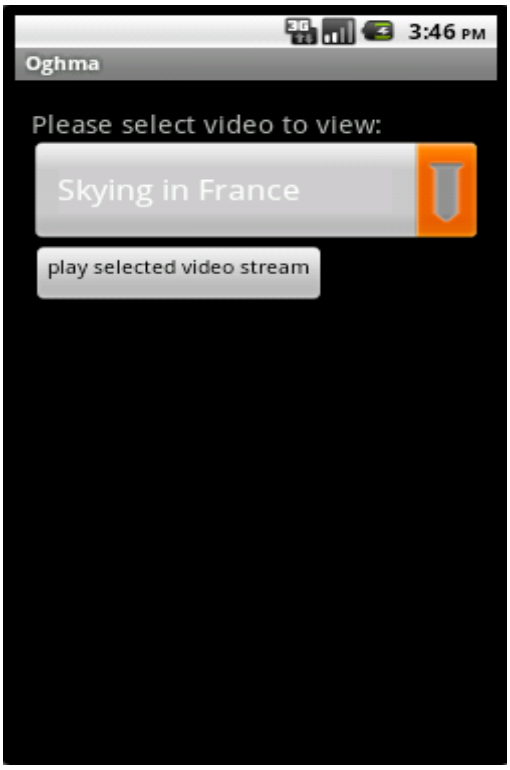

Figure 4. Oghma Stream Selection Screen

Figure 5. Video download is starting

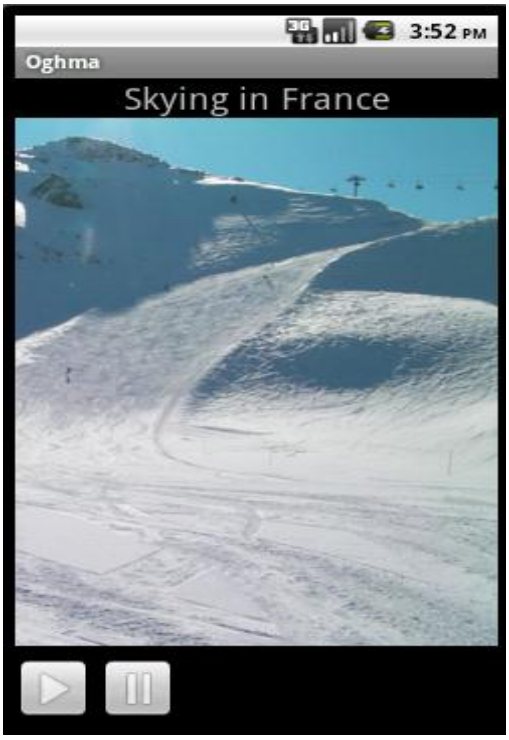

Figure 6. Oghma Video Delivery Screen

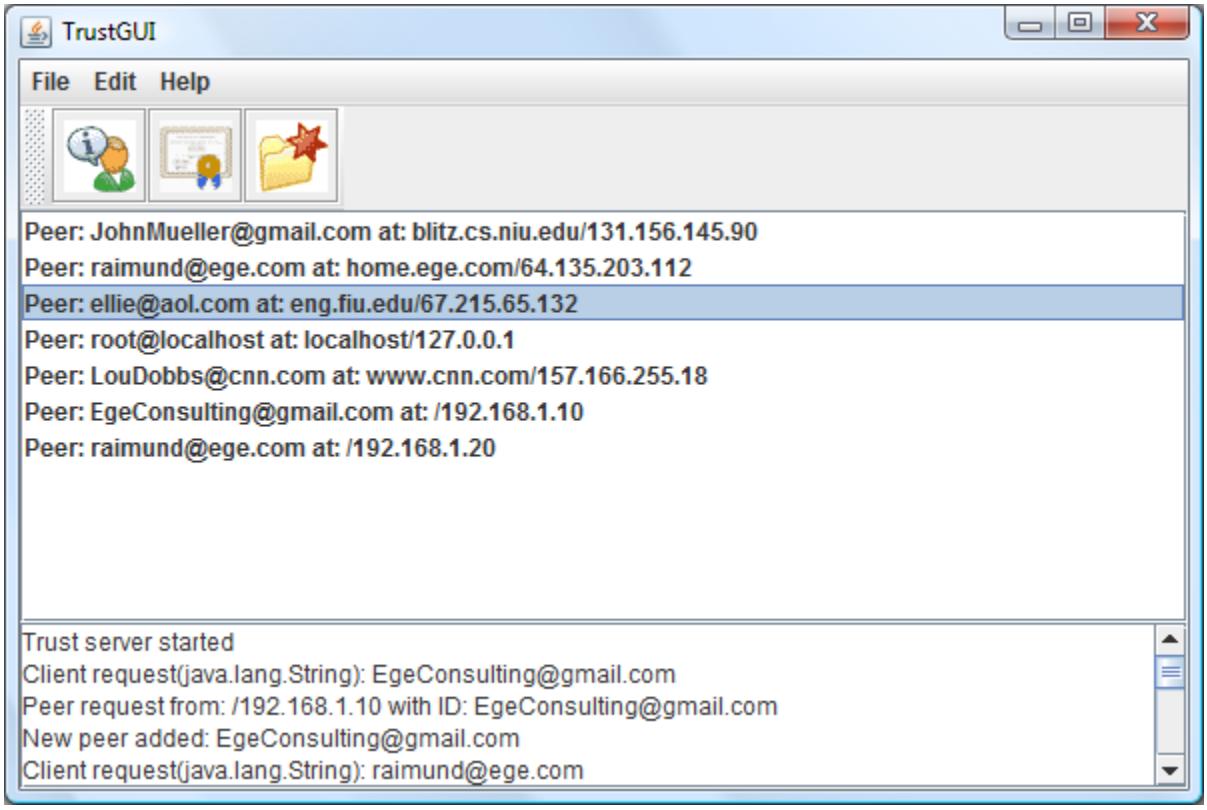

Figure 7. Tracker maintains peer database

V. IMPLEMENTATION DETAIL

Our implementation framework features 3 types of participants:

A. tracker, where all information on the current status of the content delivery network is maintained and all access decisions are made.

B. source, where the data is available for further dissemination. The original source is the first source. Peers that have downloaded and consumed the data can become new sources.

C. client, where the consumption of the data occurs.

A. Tracker

The core of the content delivery model is the tracker. The tracker knows the location of the original/first source. The tracker maintains a database of peer information: each peer is authenticated with an OpenID and carries historical data on past peer behavior.

Peers that wish to participate in the content delivery must first locate the tracker. A peer will start by establishing a connection to a tracker. Peers use their openID and password to login to the tracker. The peer will transmit its public key to the tracker, which will consider the request from a new peer and gather the necessary data on the trust in the new peer. If the peer is new and not yet listed in the tracker(s) database, then a new entry is created.

Figure 7 shows the tracker's graphical user interface: the center of the screen shows peers that have been accepted into the P2P content delivery network; the bottom of the screen shows a log of access requests from other peers. Figure 8 shows the security information, i.e. the public key, for the peer with openId "RaimundEge@gmail.com."

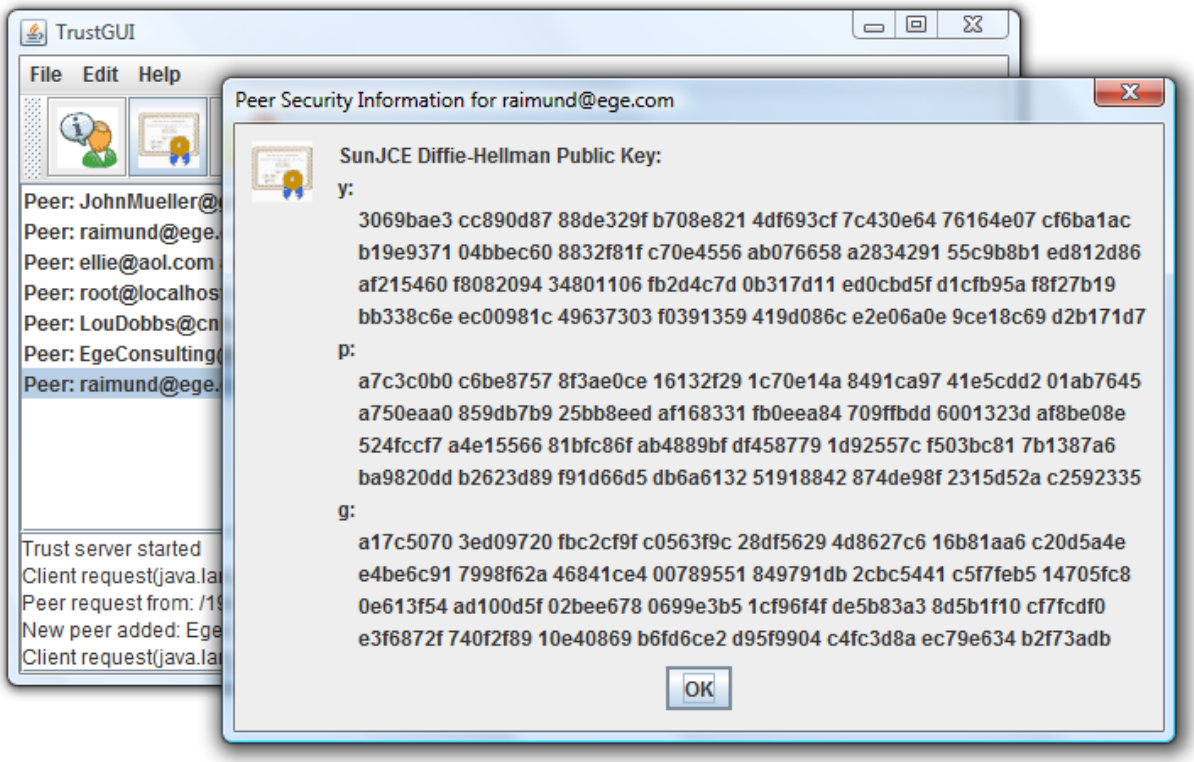

Figure 8. Security information

B. Source

At least one source must exist for the content delivery network to get started. The source first establishes contact with the tracker. It generates a PKI [11] public/private key par and transmits its public key to the tracker. It then stands ready for data requests from clients. If a request from a client is received, it requests the client's public key from the tracker and uses a Diffie-Hellman key agreement algorithm [12] to produce a session key. The session is then used by the source to encrypt all data that is sent to the client.

C. Client

The key to a smooth scaling of this ad-hoc p2p network is the algorithm used by the client to request frames from a source (either the original source or another client). A client consists of three processes:

1) a process to communicate with the tracker. The client initiates the negotiation with the tracker to enable the tracker's decision on whether the peer is admitted into the content delivery network. Upon success, the tracker informs the client which sources the client should use accompanied by their public keys. The client will update the tracker on its success in downloading the source data;
2) a process to request data from the given sources. Fragments or frames may be requested from multiple sources. Frames that are received are decrypted using a session key that is established via a key agreement using the public key of the data source.
3) a process to sequence the frames/fragments received from sources and to assemble them into a usable media stream.

Our prototype uses the Java implementation [13] of the SCTP [14] transport layer protocol. SCTP is serving in a similar role as the popular TCP and UDP protocols. It provides some of the same service features of both, ensuring reliable, in-sequence transport of messages with congestion control. We chose SCTP because of its ability to deliver multimedia in multiple streams. Once a client has established a SCTP association with a server, packages can be exchanged with high speed and low latency. Each association can support multiple streams, where the packages that are sent within one stream are guaranteed to arrive in sequence. Each

source can divide the original video stream into set of streams meant to be displayed in an overlay fashion. Streams can be arranged in a way that the more streams are fully received by a client, the better the viewing quality will be. When sending a packet over a SCTP channel we need to provide an instance of the MessageInfo class, which specifies which stream the packet belongs to. The first stream is used to deliver a basic low quality version of the video stream. The second and consecutive streams will carry frames that are overlaid onto the primary stream for the purpose of increasing the quality. In our framework we also use the additional streams to carry content that is "added value", such as advertising messages or identifying logos. The ultimate client that displays the content to a user will combine all streams into one viewing experience.

The second feature of SCTP we use is its new class "SctpMultiChannel" which can establish a one-to-many association for a single server to multiple clients. The SctpMultiChannel is able to recognize which client is sending a request and enables that the response is sent to that exact same client. This is much more efficient than a traditional "server socket" which for each incoming request spawns a subprocess with its own socket to serve the client. Figure 9 shows the Java source code where an incoming request is received. Each packet that is received on the channel carries a MessageInfo object which contains information on the actual client that is the actual other end point of this association. The Java code on line 06 retrieves the "association" identity from the incoming message "info" instance. The association is then used to send the response via the same SctpMultiChannel instance but only to the actual client that had requested the frames. The code on line 17 shows that a new outgoing message info instance is created for the same "association" that carried the incoming request. The message info instance is then used to send the response packet to the client. The code to receive SctpMultiChannel packets is logically similar to any UPD or TCP style of socket receive programming. Figure 10 shows a sample.

```
01 SocketAddress socketAddress = new InetSocketAddress(port);
02 channel =  SctpMultiChannel.open().bind(socketAddress);
03 MessageInfo info;
04 while ((info = channel.receive(bb, null, null)) != null) {
05   // determine requestor
06   Association association = info.association();
07   // determine which frame range
08   bb.flip();
09   int fromFrame = bb.getInt();
10   int toFrame = bb.getInt();
11   // send frames to requestor
12   for (int i=fromFrame; i<= toFrame; i++) {
13     bb.clear();
14     bb.putInt(i);
15     bb.put(framePool.getFrame(i));
16     bb.flip();
17     channel.send(bb,
                MessageInfo.createOutgoing(association, null,0));
18   }
19 }
```

Figure 9. Source receives request for frame

```
01 SocketAddress socketAddress =
             new InetSocketAddress(peer.address, peer.port);
02 SctpChannel channel = SctpChannel.open(socketAddress, 1, 1);
03 // send requested frame range to peer
04 ByteBuffer byteBuffer = ByteBuffer.allocate(128);
05 byteBuffer.putInt(fromFrame);
06 byteBuffer.putInt(toFrame);
07 byteBuffer.flip();
08 channel.send(byteBuffer, MessageInfo.createOutgoing(null, 0));
09 // here is where we read response
10 byteBuffer = ByteBuffer.allocate(64000);
11 while ((channel.receive(byteBuffer, null, null)) != null) {
12    byteBuffer.flip();
13    int frame = byteBuffer.getInt();
14    System.out.print("Message received: " + frame);
15    …
```

Figure 10. Client receives frame

The three major components of the framework are implemented as "SourceMain", "TrackerMain" and "ClientMain", which are composed from classes that implement the core behavior of maintaining communication sessions, accepting requests for frames and delivering them, and requesting and receiving frames. The major classes are FrameRequestor and FrameServer. The original source starts out as the sole instance of FrameServer. The first client starts out as the sole instance of FrameRequestor. As the client accumulates frames it then also instantiates a FrameServer that is able to receive requests from other clients. A client that contains both a FrameRequestor and FrameServer instance becomes a true peer in the P2P content delivery framework.

In summary, tracker, source and client together contribute to build a highly efficient delivery network.

VI. CONCLUSION

In this paper we have described a model and framework for a new generation of content delivery networks. We have described a prototype implementation that follows a bittorrent-style of P2P network, where a tracker disseminates information on which sources are available to download from, and includes a Java-based client for the Android platform for smart phones. Such P2P content delivery has great potential to enable large scale delivery of multimedia content.

Our framework is designed to enable content originators to assess the potential reward from distributing the content to the Internet. The reward is quantified as the value added at each peer in the content delivery network and gauged relative to the actual cost incurred in data delivery but also correlated to the risk that such open delivery poses.

Consider the scenario we described earlier in the paper: a typical "viral" video found on YouTube.com: the video is uploaded onto YouTube.com for free, stored and transmitted by YouTube.com and viewed by a large audience. The only entity that is getting a reward is YouTube.com, which will accompany the video presentation with paid advertising. The only

benefit that the original source of the video gets is notoriety.

Using our model, the original data owner can select other venues to make the video available via a peer-to-peer approach. The selection on who will participate can be based on how much each peer contributes in terms of reward but also risk. Peers will have an interest in being part of the delivery network, much like YouTube.com has recognized its value. Peers might even add their own value to the delivery and share the proceeds with the original source.

Whereas in the YouTube.com approach the reward is only reaped by one, and the original source has shouldered all the risk, i.e. lost all reward from the content, our model will enable a more equitable mechanism for sharing the cost and reward. Our model might just enable a new and truly openness of content delivery via the Internet.

REFERENCES

[1] Raimund K. Ege. Trusted P2P Media Delivery to Mobile Devices. Proceedings of the Fifth International Conference on Systems (ICONS 2010), pages 140-145, Menuires, France, April 2010.

[2] Y. Atif. Building trust in E-commerce. IEEE Internet Computing, 6(1):18–24, 2002.

[3] P. Resnick, K. Kuwabara, R. Zeckhauser, and E. Friedman. Reputation systems. Communications of the ACM, 43(12):45–48, 2000.

[4] E. Bertino, B. Catania, E. Ferrari, and P. Perlasca. A logical framework for reasoning about access control models. In SACMAT '01: Proceedings of the sixth ACM symposium on Access control models and technologies, pages 41–52, New York, NY, USA, 2001.

[5] S. Jajodia, P. Samarati, M. L. Sapino, and V. S. Subrahmanian. Flexible support for multiple access control policies. ACM Transaction Database System, 26(2):214–260, 2001.

[6] OpenID, http://www.openid.net. [accessed September 22, 2010]

[7] C. Wu, Baochun Li. R-Stream: Resilient peer-to-peer streaming with rateless codes. In Proceedings of the 13th ACM International Conference on Multimedia, pages 307-310, Singapore, 2005.

[8] R. K. Ege, L. Yang, Q. Kharma, and X. Ni. Three-layered mediator architecture based on dht. Proceedings of the 7th International Symposium on Parallel Architectures, Algorithms, and Networks (I-SPAN 2004), Hong Kong, SAR, China. IEEE Computer Society, pages 317–318, 2004.

[9] L. Yang, R. Ege, Integrating Trust Management into Usage Control in P2P Multimedia Delivery, Proceedings of Twentieth International Conference on Software Engineering and Knowledge Engineering (SEKE'08), pages 411-416, Redwood City, CA, 2008.

[10] Open Handset Alliance, http://www.openhandsetalliance.com/. [accessed November 19, 2010]

[11] Gutmann, P., 1999. The Design of a Cryptographic Security Architecture, *Proceedings of the 8th USENIX Security Symposium*, pages 153-168, Washington, D.C., 1999.

[12] Network Working Group, Diffie-Hellman Key Agreement Method, Request for Comments: 2631, RTFM Inc., June 1999.

[13] java.net – The Source for Java Technology Collaboration, The JDK 7 Project, http://jdk7.dev.java.net. [accessed September 22, 2010]

[14] R. Stewart (ed.), Stream Control Transmission Protocol, Request for Comments: 4960, IETF Network Working Group, September 2007, http://tools.ietf.org/html/rfc4960. [accessed September 22, 2010]

[15] Raimund K. Ege, Li Yang, Richard Whittaker. Extracting Value from P2P Content Delivery. Proceedings of the Fourth International Conference on Systems (ICONS 2009), pages 102-108 Cancun, Mexico, March 2009.

Evaluation of Spectrum Occupancy in an Urban Environment in a Cognitive Radio Context

Alexandru Marţian, Călin Vlădeanu, Ioana Marcu, Ion Marghescu
Department of Telecommunications
Faculty of Electronics, Telecommunications and Information Technology
Politehnica University of Bucharest
1-3 Iuliu Maniu, Bucharest 6, 061071, Romania
e-mail: martian@radio.pub.ro, calin@comm.pub.ro, imarcu@radio.pub.ro, marion@comm.pub.ro

Abstract — **Lack of frequency spectrum is becoming one of the major problems in the telecommunication field with the introduction of several new radio communication technologies. Cognitive Radio (CR) technology promises to be one possible solution to this problem, by allowing access of unlicensed users in licensed bands, based on an opportunistic approach and without interfering with the licensed (primary) user. In order to identify which frequency bands are more suitable for such purposes, it is necessary to evaluate the degree in which licensed bands are actually used. Although some measurement campaigns have already been carried out, most of them were done in the USA and only a few in other locations worldwide. This paper presents results of a measurement campaign conducted in Bucharest, Romania, covering the frequency range from 25 MHz up to 3.4 GHz. An overview of the various spectrum sensing methods available for evaluating the spectral occupancy is presented. The measurement results are confronted with the frequency allocation table published by the national authority for communications and an analysis of the obtained data is being made.**

Keywords - spectrum occupancy; spectrum sensing; cognitive radio; measurement campaign.

I. INTRODUCTION

Radio frequency spectrum is a resource of fundamental importance in wireless communication systems. During recent years a multitude of wireless applications and services were developed, and as a result, the need for new frequency bands increased. As most of the available spectrum has already been allocated, the lack of spectrum resources has become a serious problem.

In order to address this problem, one possible approach is to create user equipment devices that are able to dynamically detect free spectrum resources and use them in order to improve overall spectrum usage. A first step in this direction was the introduction of Software Defined Radio (SDR), devices where components that have been usually implemented in hardware (e.g. filters, amplifiers, modulators/demodulators, etc.) are instead implemented by means of software. Such an approach allows the equipment to be easily reconfigured in order to receive and transmit different radio protocols by selecting which part of the software is to be used.

J. Mitola III introduced in 1999 the cognitive radio (CR) term, which can be defined as a wireless communication system that allows spectrum sharing over a wide frequency range and that is able to handle multiple radio access technologies [2].

An application of CR that would greatly contribute to an increased spectral efficiency is to allow unlicensed users access to licensed bands. In order to avoid any harmful interference to the primary (licensed) system, CR equipment should include the following functionality:

- Frequency-agility and re-configuration of radios;
- Spectrum sensing, in order to be aware of the surrounding radio environment;
- Capability of discerning between secondary and primary systems and avoidance of interference to the primary system;
- Spectrum management, in order to achieve effective co-existence and radio resource sharing with primary systems.

The spectrum sensing functionality is a key element of any CR equipment, allowing it to detect accurately the spectrum holes.

Although there are several ways in which cognitive radio spectrum sensing can be performed, a first classification can be made according to how the information is shared between CR devices in the following two categories:

- Non-cooperative spectrum sensing: This form of spectrum sensing occurs when a CR acts on its own. The CR device configures itself according to the signals it can detect.
- Cooperative spectrum sensing: Within a cooperative CR spectrum sensing system, sensing is performed by a number of different radios within the CR network. Typically, a central station will receive information from a variety of radios in the network, process it and adjust the overall CR network accordingly.

The current work represents an extension of a paper presented at the AICT 2010 conference [1]. The paper presents the results of a measurement campaign regarding spectrum occupancy conducted in Bucharest, Romania. These results represent just a preliminary work as the collected data is just instantaneous. Further measurements including long time measurements and data collected from other rural locations have been done and the results have been published in [3].

The paper is organized as follows. At first, results obtained during several other measurement campaigns are commented. Section II contains a description of the equipment used for performing the measurements. An overview of the various conventional spectrum sensing methods is given in Section III. The methodology and results of the measurements are presented in Section IV. During Section V, the measurement results are being analyzed from the cognitive radio perspective. Finally, in Section VI, the conclusion is being drawn and aspects concerning the future work are presented.

A. Related Work

Several measurement campaigns concerning spectrum occupancy were conducted worldwide [4]-[11], most of them were carried out the in the USA [4]-[5] and only a few in other locations worldwide, including Singapore [6], Germany [7]-[9], New Zeeland [10] and Spain [11], in urban or suburban scenarios. Results of a measurement campaign conducted in Chicago, USA showed a mean occupancy as low as 17.4% in the frequency band 30 to 3000 MHz [4]. Studies were also targeted at narrower frequency bands, like the public safety ones, and the benefits of cooperative sensing were highlighted [5]. During spectrum measurements taken over 12 weekday periods for a wider frequency band up to 5850 MHz in Singapore a mean occupancy value of only 4.54% was obtained [6]. The difference between indoor and outdoor locations was discussed in [7] based on measurements performed in Aachen, Germany.

Spectrum power measurements during a large public event (the 2006 Football World Cup in Germany) are presented in [8] and [9]. The campaign was conducted in 2 different cities, Dortmund and Kaiserslautern, and the measurements were taken in the proximity of football stadiums during match days. The obtained results clearly indicated a strong interdependency between spectrum occupancy values and different stages of the football match. Data collected throughout the measurement campaign was analyzed in order to find suitable methods for evaluating the vacancy of spectrum bands due to time-dependent statistics, including average channel allocation, average run length and amount of runs.

The measurement campaign conducted in urban Barcelona goes as high as 7075 MHz, using 2 different discone antennas, a low-noise amplifier and a high performance spectrum analyzer [10]. Three different metrics were used for evaluating the spectrum occupancy: power spectral density, instantaneous evolution of the temporal spectrum occupancy and duty cycle as a function of frequency. For the entire frequency band between 75MHz and 7075MHz the measured spectrum occupancy was quite low 17.78%, but if for the frequency area below 1 GHz the spectrum usage was moderate, for the are above 2 GHz the spectrum remained mostly underutilized.

However, as frequency spectrum regulations differ considerably between regions and even countries, it is important to obtain results from as many different scenarios as possible, in order to analyze the possible situations that a CR user equipment might encounter.

II. Spectrum Sensing Methods

Several spectrum sensing methods can be used in order to decide if a certain frequency band is available for opportunistic access [12]-[15]. For each of the described methods, a short description of the principle used is given, and the strengths and weaknesses of the method are underlined.

A. Energy Detection

The energy detection method provides an optimal detection in cases where the primary user signal is unknown [13]. The received radio frequency energy or the received signal strength indicator is measured and compared to a precomputed threshold to determine whether the spectrum is occupied or not.

The energy can be measured in several ways. When using an analogue implementation, a pre-filter with fixed bandwidth is required. However, this solution is not suitable for simultaneous sensing of narrowband and wideband signals, situation that is very often expected considering modern communication systems. More flexibility can be obtained when using a digital implementation, because of FFT-based spectral estimates. In this case, various bandwidth types are supported, which will allow simultaneous sensing of multiple signals.

The advantages of the energy-detection methods are universal applicability, relative low computational complexity and reduced amount of prior signal knowledge required.

The most serious drawbacks of the energy detection method are that it is highly susceptible to changes in the background noise spectral density and to the presence of in-band interference. Another major disadvantage, specific to cognitive radio scenarios, is that the energy detection method cannot distinguish the primary systems from the secondary ones sharing the same channel. This becomes a critical challenge when multiple primary systems are present in the same area where cognitive radio equipment operates.

B. Matched Filtering

A filter matched to a received signal has an impulse response equal to a conjugated and time-reversed version of the received signal [15]. This matched filter represents an optimal detection method as it provides a maximum signal-to-noise ratio (SNR) output in the presence of additive white Gaussian noise (AWGN). The output of the matched filter is compared to a threshold in order to decide if the signal

corresponding to a primary system is present or not. The binary decision that has to be made is

$$\begin{aligned} &\bullet H_0, if \sum_{n=1}^{N} y[n]x[n]^* \le \lambda \\ &\bullet H_1, otherwise \end{aligned} \quad (1.1)$$

where λ represents the threshold, $y[n]$ represents the unknown signal and $x[n]^*$ represents a time-reversed version of the assumed signal.

In order to apply this matched filtering method, a priori knowledge is required about the signal that is to be detected, at both physical and medium access control layers. Fortunately, for most of the actual communication systems there is enough information available (e.g., pilot subcarrier synchronization sequence in OFDM systems, midamble sequence in GSM systems) in order to allow signal detection using this method.

Between the advantages offered by the matched filtering method can be mentioned optimality for AWGN channels, relative low computational complexity needed and the possibility to be applied to most licensed systems.

The most important disadvantages of this method are sensitivity to imperfect synchronization and poor performance in non-AWGN channels. A further drawback of the matched filtering method is that a CR equipment that operates in an area where multiple possible primary systems could be present will need a dedicated receiver for every kind of primary system. This will generate an increase of the complexity and will make the implementation of such equipment a significant challenge, even in case of programmable realization.

A variant of matched-filtering detection is tone detection. In this particular case, the presence of a tone of finite strength is detected, and this presence implies the presence of a particular signal associated with that tone's frequency. Matched filtering or Fourier analysis of a narrow frequency band around the expected tone frequency can be used in order to detect the presence of this tone.

C. Cyclostationary Feature Detection

Spectral correlation is a statistical property that is characteristic for cyclostationary signals [15]. One or several probabilistic parameters (e.g., mean, autocorrelation, probability density function, nth-order moment, or nth-order cumulant) of cyclostationary signals are periodic functions in time domain. An example of how the cyclostationary detection can be performed is the following. First, the cyclic autocorrelation function $R_x^{\alpha}(\tau)$ of the observed signal $x(t)$ is computed as

$$R_x^{\alpha}(\tau) = \lim_{T\to\infty} \frac{1}{T} \int_{-T/2}^{T/2} x(t+\tau/2)x^*(t-\tau/2)e^{-j2\pi\alpha t}dt \quad (1.2)$$

where α denotes a cyclic frequency. Further on, the spectral correlation function (SCF) $S_x^{\alpha}(f)$ is calculated as the discrete Fourier transformation of the cyclic autocorrelation function:

$$S_x^{\alpha}(f) = \int_{-\infty}^{\infty} R_x^{\alpha}(\tau)e^{-j2\pi f\tau}d\tau \quad (1.3)$$

It can be proved that

$$\begin{aligned} &S_x^{\alpha}(f) = \\ &= \lim_{T\to\infty}\lim_{Z\to\infty} \frac{1}{TZ} \int_{-Z/2}^{Z/2} X_T(t, f+\frac{\alpha}{2}\tau)X_T^*(t, f-\frac{\alpha}{2}\tau)dt \end{aligned} \quad (1.4)$$

where

$$X_T(t, f) = \int_{t-T/2}^{t+T/2} x(u)e^{-j2\pi fu}du \quad (1.5)$$

Finally, the detection is concluded by looking for the unique cyclic frequency corresponding to a maximum value in the SCF plane.

The most important advantage of the cyclostationary detection method consists in its insensitivity to noise and co-channel insensitivity. The reason for that is that noise has no spectral correlation, and the SCF can reflect only the spectral correlation properties of a single signal if the cyclic frequency is unique to that signal. A further advantage of the cyclostationary detection method is applicable to nearly all the modern communication signals. This method can work also with lower SNR than the energy detection method, as it exploits the information embedded in the received signal.

The main disadvantage of the cyclostationary detection method is that the cyclic frequency has to be be known by the secondary user. It also requires a more complex implementation and a longer observation time than in case of the energy detection method. This may cause the cyclostationary detector to be inefficient in case of spectrum holes of short time duration.

D. Wavelet Detection

The wavelet detection method is particularly suitable in case of wideband signals, as it presents advantages in terms of implementation and flexibility compared to the conventional approach of using multiple narrowband bandpass filters [15].

The entire frequency band of a wideband signal is modeled as a series of consecutive frequency sub-bands, in order to identify spectrum holes. The power spectral characteristic is smooth within each sub-band, but changes abruptly on the border of two neighboring sub-bands. By using a wavelet transform of the power spectral density of

the observed signal $x[n]$, the singularities of the power spectral density $S(f)$ can be located and the available frequency bands can be identified.

The main weakness of the wavelet detection method is related to the high sampling rates needed when building a wavelet detector for large bandwidth signals.

E. Delay-and-Multiply Detection

Another sensing technique is the delay-and-multiply signal detector, which multiplies the collected data block with a delayed and conjugated version of itself in order to generate an additive sine-wave component the presence of which can be detected by using Fourier methods [14]. The presence of the tone implies the presence of the signal, and the exact frequency of the tone provides a parameter estimate for the signal, usually equal to the symbol rate (chip rate for direct sequence spread spectrum signals).

The delay-and-multiply detector is a simple exploitation of cyclostationarity in that it employs a quadratic transformation to generate a spectral line. This is only possible for CS signals.

The strengths of the delay-and-multiply detector are that it can provide superior sensitivity relative to the energy detectors, is robust to uncertainties in the noise power and interference parameters, and is computationally less expensive than more thorough methods that exploit the cyclostationarity property. Its main weaknesses are that it is not applicable to a large number of signals and that optimum performance requires knowledge of the optimum delay, which in turn requires knowledge of the transmitter filtering applied to the signal to be detected. That is, the optimum delay for rectangular-pulse signals is half the symbol interval, but for signals that have been filtered with a square-root raised-cosine filter, the optimum delay is zero.

F. Swiss Army Knife Solutions

In order to improve the overall sensing performance it would be possible to implement a spectrum-sensing device that contains a highly specialized detector for each type of signal that has to be detected: a matched filter for DVB-T, a delay-and-multiply detector for DSSS, an energy detector for GSM, etc. This kind of sensing strategy is called a Swiss Army knife (SAK) solution because of the disparate nature, computational requirements, and achievable performance of the various signal-specific sensors [14]. A possible approach would be to make a choice between the various available detectors depending of the frequency band that is scanned, which could provide information about what type of licensed signals are expected in the respective frequency area.

III. MEASUREMENT EQUIPMENT

The measurement campaign has been carried out from the top of the main building of our Department, which proves to be an excellent location for such a purpose. The terrace has direct line of sight with several FM transmitters, Analog and DVB-T TV transmitters, GSM and UMTS base stations and several other stations (GPS location: latitude 44°26'01" N, longitude 26°03'27" E, MSL altitude 150m, relative altitude 30m). The headquarters of the governmental agency for special telecommunications is also located just a few hundreds of meters away from the measurement location. A bird's eye view of the surrounding area is presented in Figure 1.

Figure 1. Bird's eye view of the measurement location (Copyright (c) 2009 Microsoft Corporation and/or its suppliers, One Microsoft Way, Redmond, Washington 98052-6399 U.S.A.).

For the frequency bands below 1 GHz a wideband discone antenna (Sirio SD1300N, specified from 25 to 1300 MHz) was used, mounted on the building terrace. The antenna has an omnidirectional pattern in the horizontal plane and was connected using a low-loss RF cable to a high performance signal analyzer (Anritsu MS2690A - 50 Hz to 6 GHz, average noise level -155 dBm/Hz at 2 GHz), located in a laboratory on the last floor of the building. Although the length of the cable was approximately 20m, the cable attenuation was less than 5 dB. For the frequency bands above 1 GHz a directional antenna (Aaronia Hyperlog 4060, 400 MHz to 6 GHz) was used. In this case, a short cable of 1.5 m (SUCOFLEX 104PEA) was used and the insertion loss was lower than -1dB. During the measurements, the spectrum analyzer was configured as described in Table I.

TABLE I. SPECTRUM ANALYZER CONFIGURATION

Parameter	Value
Frequency sub-bands	**1.** 25-230 MHz **2.** 230-400 MHz **3.** 400-470 MHz **4.** 470-766 MHz **5.** 766-880 MHz **6.** 880-960 MHz **7.** 960-1525 MHz **8.** 1525-1710 MHz **9.** 1719-1880 MHz **10.** 1880-2200 MHz **11.** 2200-2400 MHz **12.** 2400-2500 MHz **13.** 2500-2690 MHz **14.** 2690-3400 MHz
Resolution/video bandwidth (RBW/VBW)	300 kHz / 300 kHz (sub-bands **2, 3, 5, 6, 8, 9, 11, 12, 13**) 1 MHz / 1MHz (sub-bands **1, 4, 7, 10, 14**)
Sweep time	5 ms
Reference level	0 dBm
Attenuation	10 dB
Detection type	Pos & Neg
Trace points	10001

The performed measurements covered the frequency range from 25 MHz to 3400 MHz, the whole band being further divided into 14 sub-bands according to the type of service and the bandwidth of the allocated signal.

The measurement equipment is shown in Figures 2 and 3.

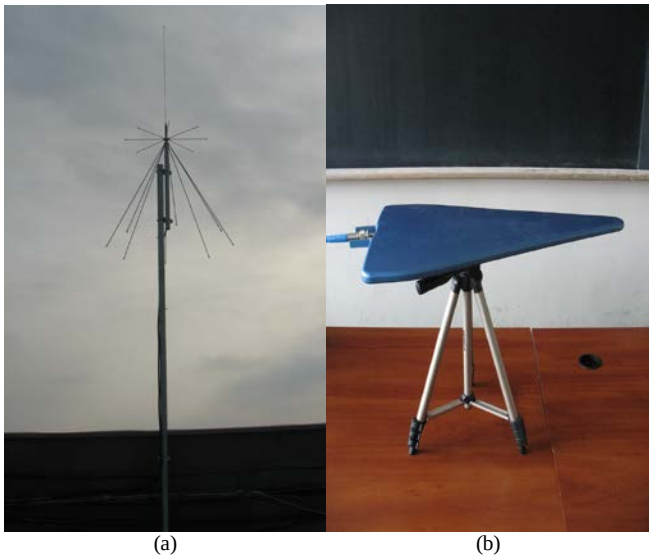

(a) (b)

Figure 2. Antennas used during the measurements: (a) Sirio SD1300N and (b) Aaronia Hyperlog 4060.

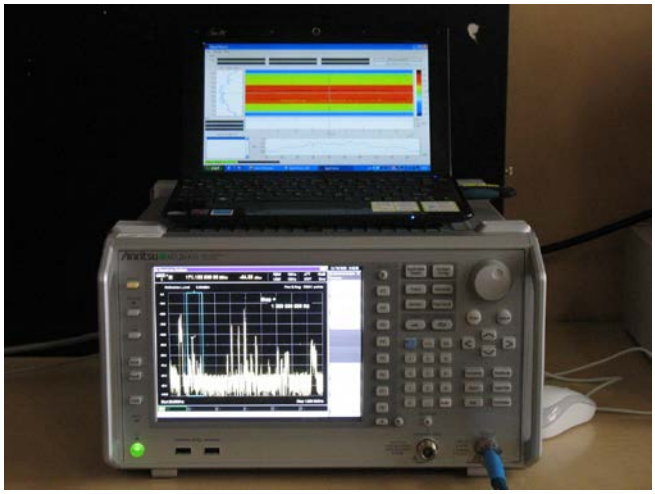

Figure 3. Signal analyzer as used during measurements.

The MathWorks MATLAB environment and the Anritsu Signal Viewer application were the software tools used for processing and analyzing the data obtained during the measurement campaign.

IV. MEASUREMENT RESULTS

As it was already described in Section II, the energy detection method is the only method that does not require any a priori knowledge about the evaluated signals, and this is the method that was used in order to evaluate the occupancy in the several frequency bands presented in Table I.

In order to estimate correctly the noise floor, a sliding window of 1000 samples was used for each of the frequency bands. A mean value of the samples contained in the sliding window was calculated and the lowest mean value, corresponding to an unoccupied frequency area, was chosen as the noise floor of the corresponding frequency band. To mitigate the effects of high-power noise samples in false activity detection, a second sliding window with a calculated width of 100 KHz was used in order to mean out such samples and to minimize the false alarm probability. To illustrate the effect of this second window, an example is presented in Figure 4 for the frequency band from 470 to 766 MHz.

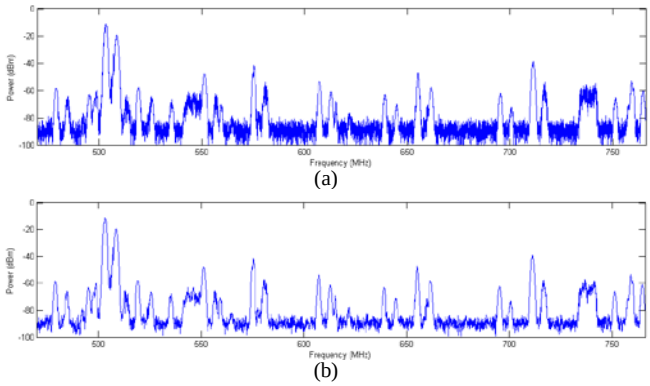

(a)

(b)

Figure 4. Spectral occupancy for the 470-766 MHz frequency band (a) before and (b) after applying the 100 kHz sliding window.

In Figure 4 (a) the original captured signal can be seen, and in Figure 4 (b) can be noticed the signal obtained after processing. In case of this frequency band, the width of 100 kHz chosen for the window results in a number 3 consecutive samples to be taken into account when processing the signal.

A parameter of great importance when using the energy detection method for taking decision about the availability of a certain frequency band is the value chosen for the energy threshold.

If the value used for the threshold is too high weak signals will be treated as noise and this would result in an underestimation of the actual occupancy. In Figure 5 (a), an example is presented for the frequency band from 470 to 766 MHz. The mean noise value is represented with the red line, and the value chosen for the threshold is represented with a green line. It can be noticed that when choosing a value of 11dB for the threshold, several low-power signals are below the threshold level.

On the other hand, choosing a too low value for the threshold will increase the false alarm probability caused by high-power noise samples and this would cause an overestimation of the actual occupancy. In Figure 5 (b), for the same frequency band a value of 3dB is chosen for the threshold, and several noise samples raise above the threshold level.

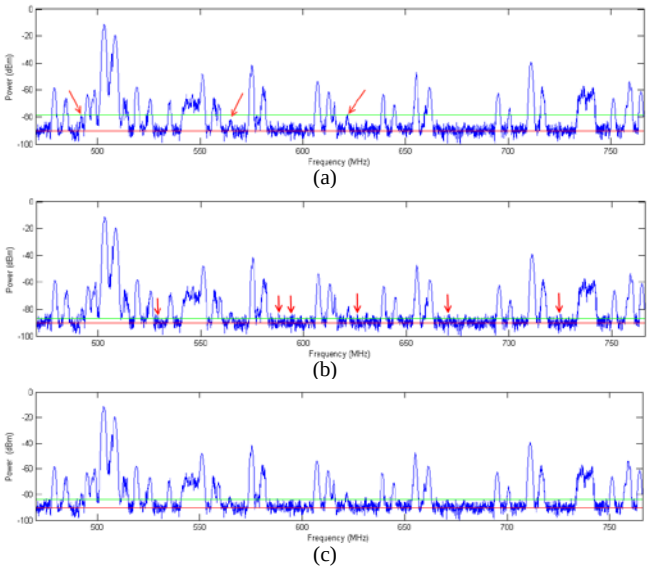

(a) (b) (c)

Figure 5. Spectral occupancy for the 470-766 MHz frequency band for 3 different values of the threshold: (a) 11dB (b) 3dB and (c) 5dB.

By analyzing the signals measured during the campaign, a value of 5 dB for the threshold was chosen, as it allows detection of the weakest measured signal and in the same time is high enough to avoid false detections. This situation is illustrated in Figure 5 (c).

The results listed in Table II were obtained by using this threshold value of 5dB for all the 14 different frequency sub-bands.

TABLE II. SPECTRUM OCCUPANCY IN THE 25-3400 MHZ FREQUENCY RANGE

Frequency range (MHz)	Possible applications according to TNABF [8]	Measured Occupancy (%)	Mean Occupancy (%)	
25 - 230	FM radio, Aero/Marine, Fixed/Mobile, Military, other	28.44	27.79	12.19
230 - 400	Military, Mobile	11.09		
400 - 470	Analogue/Digital Terrestrial Mobile, Meteorology, other	18.37		
470 - 766	Analogue TV, DVB-T	40.02		
766 - 880	Military, TV, DVB-T, Cordless, Military, other	12.30		
880 - 960	GSM, E-GSM, Military	46.80		
960 - 1525	Aero/Naval, Navigation, Radar, Military, Radio astronomy	2.36	8.56	
1525 - 1710	Satellite Mobile, Military, Meteorology	4.08		
1710 - 1880	GSM 1800, other	22.86		
1880 - 2200	UMTS/IMT 2000, DECT, other	14.50		
2200 - 2400	SAP/SAB, Military	2.89	3.80	
2400 - 2500	ISM, RFID, RLAN, other	9.42		
2500 - 2690	UMTS/IMT 2000, Military	2.21		
2690 - 3400	Military, Radar, Navigation, Meteorology, other	3.7		

Table II lists the effect of choosing different values for the threshold on the occupancy measured in the 25 to 230 MHz frequency band.

TABLE III. INFLUENCE OF THRESHOLD VALUE OVER MEASURED OCCUPANCY

Energy detection threshold (dB)	Measured occupancy (%)
3	41.53
5	28.44
7	22.32
9	19.60
11	18.18

As it can be noticed, the measured occupancy decreases when raising the value of the threshold, because the low-energy signals visible in Figure 4 are being ignored.

All the measurements have been carried out during daytime in weekdays, when higher values for spectral occupancy are expected, comparing to nighttime or weekends.

V. MEASUREMENT ANALYSIS

Although most of the frequency range between 25 MHz and 1GHz shows a relative high occupancy, there are bands with some potential for cognitive radio applications. The lowest occupancy percent was measured in the 230 to 400 MHz band (Figure 7), however most of this band is for the moment licensed for military applications.

The frequency band 470-766 MHz is currently used mostly for analog TV broadcasting. Several analog TV broadcasting stations can be noticed in Figure 9 (the level for the station located on 506 MHz is higher then average, as the broadcast antenna is located on the same building from where the measurements were performed). However, although for the moment the occupancy is quite high at 40.02%, this might change in the near future, with the introduction of DVB-T. Test broadcasting for DVB-T is already being performed in the Bucharest area, corresponding signals can be noticed in Figure 9 on 546 MHz (channel 30) and 738 MHz (channel 54). New measurements will have to be conducted in order to evaluate spectral occupancy in this frequency range, once the digital TV broadcasting technology will completely replace the analog one (analog TV broadcasting in Romania is only allowed until 1 January 2012, due to European regulations). Furthermore, the broadcast area for both DVB-T and analog TV stations is limited around big cities, which will result in a lower occupancy for this band in rural environment.

In the frequency band 766 to 880 MHz (Figure 10) only a test DVB-T broadcast station (778 MHz, channel 59) was detected during the measurements, although other possible applications are allowed conforming to the governmental agency responsible for frequency allocation in Romania [16].

The 880-960 MHz and 1710-1880 MHz (Figures 11 and 12) are licensed for the GSM 900 and 1800 systems. In the frequency bands corresponding to the downlink communication direction (925-960 MHz for GSM 900 and 1805-1880 MHz for GSM 1800) a high power level was

measured during the whole band, as the locations of base station antennas was close to the measurement location and the transmit power employed is considerably higher than the one used in case of mobile stations. Although in frequency bands corresponding to the uplink communication direction (880-915 MHz and 1710-1785 MHz) the measured occupancy was extremely low, it should be noted the measurement location and the low transmit power of mobile stations might cause an underestimation of the actual occupancy. CR equipment activating in these bands should have a detection mechanism capable of recognizing low-power signals with energy close to the noise floor, in order to avoid interference to primary users active in the area.

The overall spectrum occupancy measured in frequency bands located above 1 GHz was extremely low (mean occupancies of less than 10%), which make most of this frequency bands potential candidates for CR applications. Occupancies higher than 10% were obtained for sub-bands 9, where the GSM 1800 systems are licensed, and 10, licensed for UMTS/IMT 2000 systems. In both cases, it is again to be noticed that the measured occupancy is much higher for the downlink direction compared to the uplink direction, especially for the UMTS systems where spread spectrum signals are used.

The ISM band 2400 to 2500 MHz is a very good opportunity for testing CR prototype devices, as the measured occupancy is quite low (9.42%) and there are a multitude of commercially available hardware devices operating in this frequency range.

VI. Conclusion and Future Work

Results obtained during the measurement campaign conducted in an urban environment in Bucharest, Romania clearly indicate that there are several frequency bands that allow opportunistic access for future CR applications. The frequency range analyzed was 25 MHz to 3.4 GHz, and the mean occupancy ratio over the whole band was as low as 12.19%.

Although the values for spectrum occupancy were higher than the ones obtained for the frequency sub-bands above 1GHz, there were two sub-bands, 2 (230-400 MHz) and 5 (766-880 MHz), where the measured occupancy was lower, close to 10%.

In case of the frequency sub-bands above 1 GHz, there are several sub-bands where spectrum occupancy values lower than 5% were obtained (960 – 1525 MHz, 1525 – 1710 MHz, 2200 – 2400 MHz, 2500 – 2690 MHz, 2690 – 3400 MHz). All these bands offer good opportunities for testing of CR prototypes and development of CR networks.

In order to increase the relevance of the obtained data, measurements over longer periods of time and in wider frequency bands (up to 6 GHz) will be performed.

Related to the methodology used for choosing the threshold in case of the energy detection method, another fact that should be taken into account for future analysis is the mean sensitivity of the licensed user equipment that operates in the corresponding frequency band.

Although the results obtained up to now were collected exclusively in an urban environment, further measurement campaigns targeted at suburban and rural environments are intended, in order to obtain a complete picture of the perspectives for future CR applications.

Acknowledgment

This work was supported by the CNCSIS-UEFISCSU Romania under Grants PNII-RU-TE, no. 18/12.08.2010 and PN-II-"Idei" no. 116/01.10.2007.

References

[1] A. Marţian, I. Marcu, and I. Marghescu, "Spectrum Occupancy in an Urban Environment: A Cognitive Radio Approach, " in Proc. 6th Advanced International Conference on Telecommunications (AICT 2010), Barcelona, May 2010, pp 25-29.

[2] J. Mitola III, "Cognitive Radio for Flexible Mobile Multimedia Communications," in Proc. IEEE International Workshop on Mobile Multimedia Communications, pp. 3-10, 1999.

[3] A. Marţian, A. Achim, O. Fratu, I. Marghescu, "Analysis of Frequency Spectrum Usage from a Cognitive Radio Perspective, 3rd International Workshop on Cognitive Radio and Advanced Spectrum Management, " COGART 2010, November 08-10, 2010, Rome, Italy.

[4] M. A. McHenry, P. A. Tenhula, D. McCloskey, D. A. Roberson, and C. S. Hood, "Chicago spectrum occupancy measurements & analysis and a long-term studies proposal," in Proc. of Workshop on Technology and Policy for Accessing Spectrum (TAPAS), Boston, MA, USA, August 2006

[5] S. D. Jones, E. Jung, X. Liu, N. Merheb, and I.-J. Wang, "Characterization of spectrum activities in the U.S. public safety band for opportunistic spectrum access," in Proc. 2nd IEEE International Symposium on New Frontiers in Dynamic Spectrum Access Networks (DySPAN 2007), Apr 2007, pp. 137–146.

[6] M. H. Islam, C. L. Koh, S. W. Oh, X. Qing, Y. Y. Lai, C. Wang et al., "Spectrum Survey in Singapore: Occupancy Measurements and Analyses," in Proc. 3rd International Conference on Cognitive Radio Oriented Wireless Networks and Communications (CrownCom 2008), May 2008, pp. 1–7.

[7] M. Wellens, J. Wu, and P. Mähönen, "Evaluation of spectrum occupancy in indoor and outdoor scenario in the context of cognitive radio," in Proc. Second International Conference on Cognitive Radio Oriented Wireless Networks and Communications (CrowCom 2007), Aug 2007, p. 8.

[8] O. Holland, P. Cordier, M. Muck, L. Mazet, C. Klöck and T. Renk, "Spectrum Power Measurements in 2G and 3G Cellular Phone bands during the 2006 Football World Cup in Germany," IEEE Symposium on New Frontiers in Dynamic Spectrum Access Networks (DySPAN), April 2007, pp. 575 – 578.

[9] T. Renk, V. Blaschke, F. K. Jondral, "Time-dependent Statistical Analysis of Measurements for the Evaluation of Vacant Spectrum Bands," XXIX U.R.S.I. General Assembly, Chicago, Illinois, August 2008.

[10] R. I. C. Chiang, G. B. Rowe, and K. W. Sowerby, "A quantitative analysis of spectral occupancy measurements for cognitive radio," in Proc. IEEE 65th Vehicular Technology Conference (VTC 2007 Spring), Apr 2007, pp. 3016–3020.

[11] M. Lopez-Benitez, F. Casadevall, A. Umbert, J. Perez-Romero, R. Hachemani, J. Palicot and C. Moy, "Spectral Occupation Measurements and Blind Standard Recognition Sensor for Cognitive Radio Networks," Proc. 4th International Conference on Cognitive Radio Oriented Wireless Networks and Communications (Crowncom 2009), June 22-24, 2009, pp. 1-9.

[12] A. Ghasemi, E. S. Sousa, "Spectrum sensing in cognitive radio networks: the cooperation-processing tradeoff," in Wireless Communications and Mobile Computing, vol. 7, no. 9, Nov. 2007, pp. 1049-1060.

[13] C. Vlădeanu, A. Marţian, "Spectrum Sensing Algorithms used in Cognitive Radio Systems," in Cognitive Radio Technology and

Reconfigurable Communication Systems Workshop, 7th International Conference Communications 2008, Bucharest, June 2008, pp 21-26.

[14] B. Fette, Cognitive Radio Technology, 2nd Edition, Academic Press, 2009.

[15] K.-C. Chen, R. Prasad, Cognitive Radio Networks, John Wiley & Sons, 2009.

[16] Autoritatea Naţională pentru Administrare şi Reglementare în Comunicaţii, "Tabelul Naţional de Atribuire a Benzilor de Frecvenţă", available online at: http://www.igcti.ro/Portals/57ad7180-c5e7-49f5-b282-c6475cdb7ee7/TNABF%202009.pdf, January 2011.

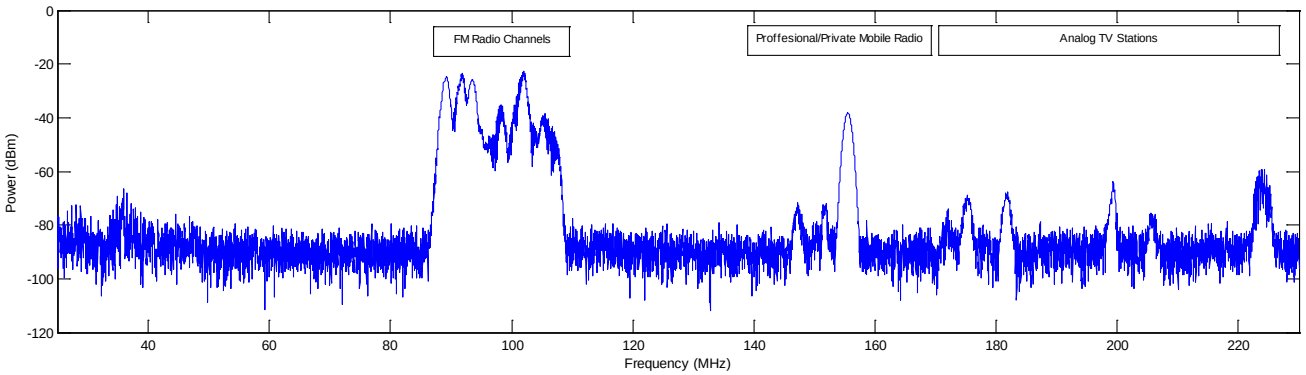

Figure 6. Instantaneous Spectrum Occupancy results: 25 to 230 MHz.

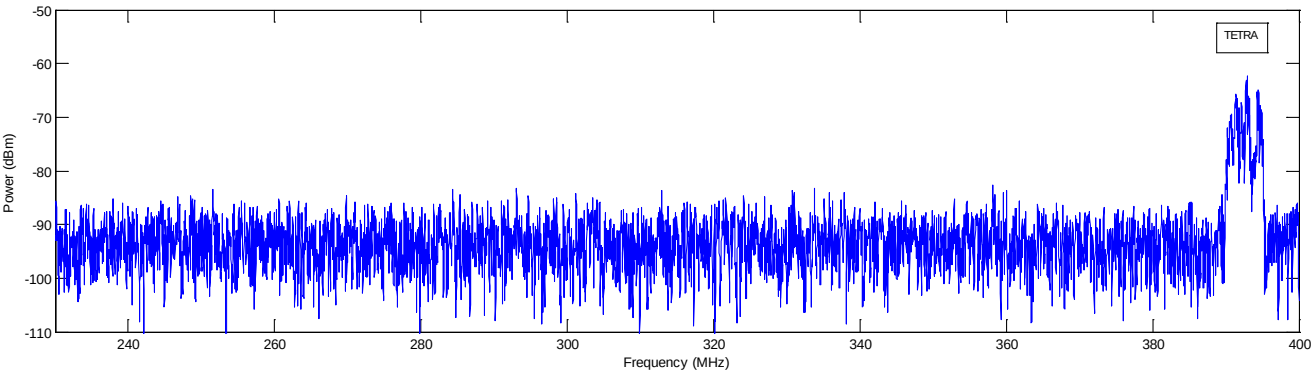

Figure 7. Instantaneous Spectrum Occupancy results: 230 to 400 MHz.

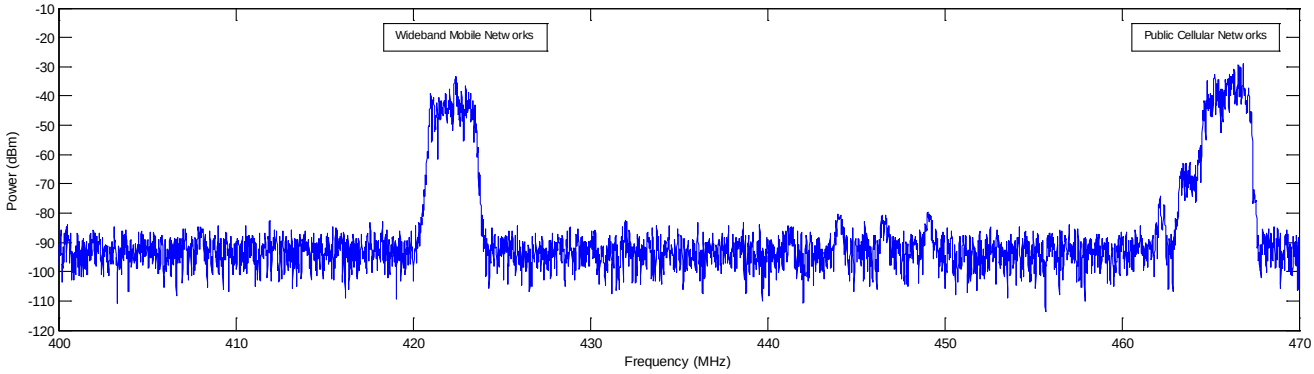

Figure 8. Instantaneous Spectrum Occupancy results: 400 to 470 MHz.

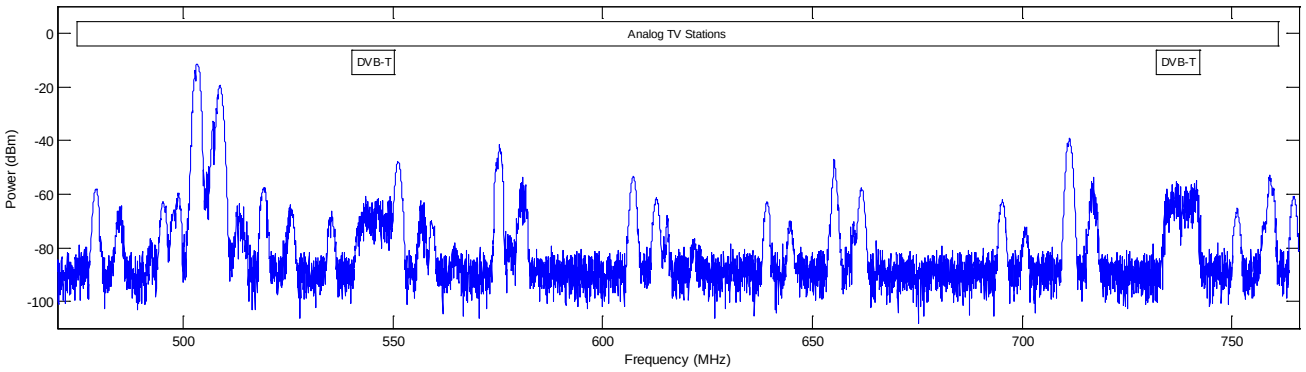

Figure 9. Instantaneous Spectrum Occupancy results: 470 to 766 MHz.

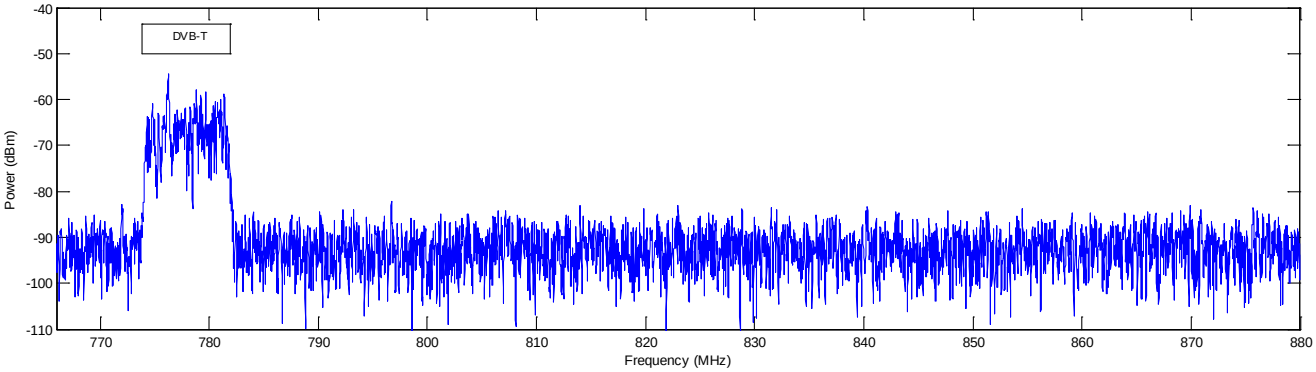

Figure 10. Instantaneous Spectrum Occupancy results: 766 to 880 MHz.

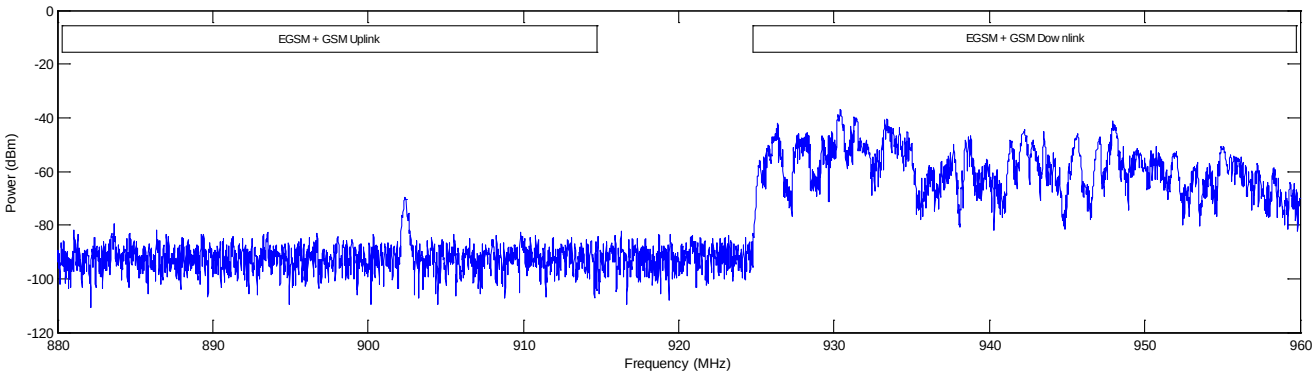

Figure 11. Instantaneous Spectrum Occupancy results: 880 to 960 MHz.

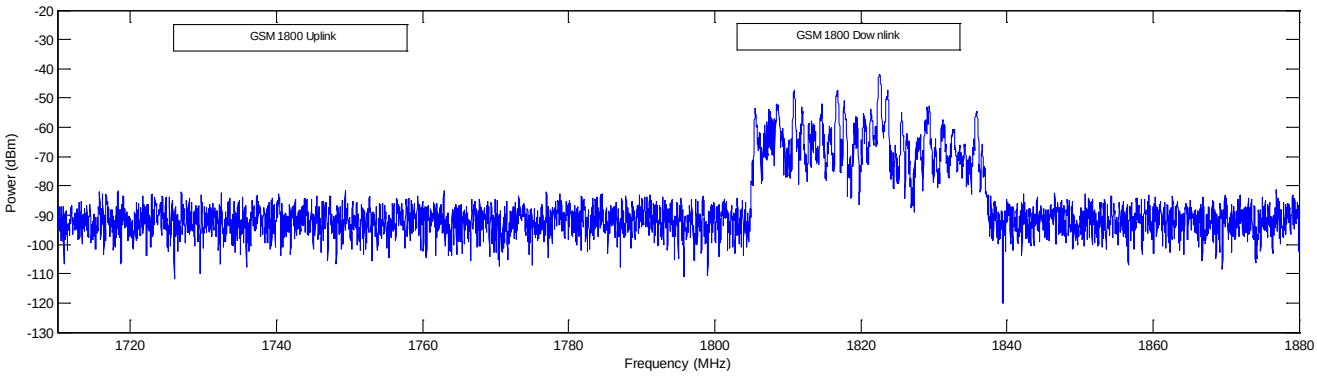

Figure 12. Instantaneous Spectrum Occupancy results: 1710 to 1880 MHz.

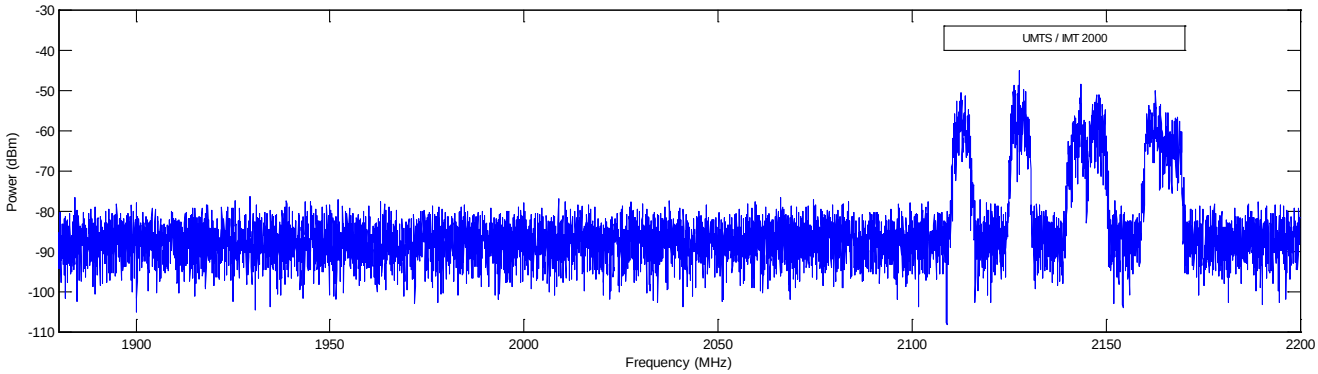

Figure 13. Instantaneous Spectrum Occupancy results: 1880 to 2200 MHz.

Decentralized Spectrum and Power assignment in OFDMA Femtocells: Exploiting Different Levels of Coordination

Francisco Bernardo*, Ramon Agustí†, Jorge Cordero*, Carlos Crespo*

*Signal Theory and Communications Department
Universidad de Sevilla
Seville, Spain
fbernardo@us.es; jcordero1@us.es; ccrespo@us.es

†Signal Theory and Communications Department
Universitat Politècnica de Catalunya
Barcelona, Spain
ramon@tsc.upc.edu

***Abstract*—This paper focuses on the task of spectrum assignment and the transmission power in the context of downlink OFDMA femtocell deployments. Concretely, the paper studies the impact of different levels of coordination between femtocells in a decentralized framework to perform spectrum and transmission power assignment. Two cooperative schemes are proposed, named non-communicative and communicative respectively. In the first case, each femtocell decide the spectrum and power assignment based on users' reported measurements, which are employed to sense intercell interference, including that from other femtocells or from macrocells in two-layer deployments. In the second case, femtocells are allowed to explicitly communicate other nearby femtocells the radio resource usage. Performance results have been obtained for a realistic indoor femtocell deployment with and without macrocell interference. The paper shows that both schemes based on self-organization can lead to sensible performance improvements over non-cooperative (selfish) schemes in terms of spectral efficiency and power consumption reductions. Finally, the dynamic response of the framework to changes in the network deployment has been analyzed.**

Keywords- femtocell; self-organization; OFDMA; coordination; performance tradeoff

I. INTRODUCTION

Self-organization is taking an important role in femtocell (FC) deployments [1][2]. Femtocells are small range and low cost user-deployed base stations introduced at a considerable amount of random locations such as users' homes and with end connectivity through a DSL (Digital Subscriber Line) backhaul. Differently from Wi-Fi access points, they are deployed in a network operator's frequency licensed band, allowing the extension of indoor coverage and thus increasing network capacity. However, FC deployments introduce several technical challenges that have to be overcome [3]. For instance, the assignment of frequency resources to FCs to mitigate intercell interference cannot be performed as in typical *macrocell* (MC) scenarios. In that case, the spectrum assignment task is carried out off-line during the network deployment phase, once the exact MCs' transmitter positions are known, usually requiring a lot of human supervision. On the other hand, the high number of FC transmitters and especially the random and distributed nature of the FC deployment would make unpractical the success of such manual configuration of the spectrum in use. Hence, it becomes necessary to include appropriate capabilities in each FC so that FCs can automatically reconfigure the spectrum assignment and minimize the human interaction. This is one of the main reasons to use self-organization to manage FC deployments.

Self-organization is the ability of a system composed of several entities to adopt a particular structure and perform certain functions to fulfill a global purpose without any external supervisor or central dedicated control entity [4]. In the field of mobile cellular networks, several tasks have been identified to adjust network parameters including *self-configuration* in pre-operational state, *self-optimization* in operational state, and *self-healing* in case of failure of a network element [5], bringing operational and capital expenditures reductions. Therefore, activities in several projects and standardization bodies are steered to study the automation of network procedures [6], [7].

The main characteristics of a self-organized system are its distributed nature and the localized interactivity between system elements. That is, each entity performs its operation based only on the information retrieved from other entities in its vicinity. Hence, self-organization clearly takes a relevant role in the context of FCs networks. For instance, [8] proposes a self-optimization scheme for frequency planning in the context of OFDMA (Orthogonal Frequency Division Multiple Access) FCs. It has been agreed that OFDMA radio access interfaces offer appealing properties such as robustness against multipath fading and high spectral flexibility. Then, as shown in [8], OFDMA FCs facilitate the development of such dynamic self-organization mechanisms, and proof of that is that they are being included in the latest specifications for LTE (Long-Term Evolution) system [9]. On the other hand, [10] presents a self-optimization scheme for the coverage (transmission power) in CDMA (Code Division Multiple Access) FCs in the presence of MC interference. However, it is expected that in OFDMA FCs, high transmission power reductions can be obtained. That is, the high spectral flexibility of OFDMA can allow finding spectrum assignments that enable a FC to operate in an 'interference free' state. Then, transmission power could be reduced from maximum power to a lower level for acceptable communications taking only into account thermal noise. Hence, energy saving is attained, being in line with recent trends within *green communications* [11] that pursue an efficient resource (energy) usage to reduce CO2 emissions.

More recently, other approaches to simultaneously optimize the spectrum assignment and transmission power in OFDMA FCs have been proposed [1][12]. However, the

impact of the different coordination methods between FCs in the decentralized resource assignment problem has not been addressed.

This paper proposes a decentralized framework to jointly self-optimize the spectrum assignment and the transmission power for the downlink of an OFDMA FC deployment within the coverage area of an OFDMA MC deployment, and analyzes the performance of several coordination levels between FCs. Concretely, two cooperative schemes where each FC takes into account the spectrum and power usage in nearby FCs are compared. The two strategies are named *communicative* and *non-communicative schemes* depending on whether an explicit exchange of information between FCs is allowed. We have tested the framework over a realistic indoor FC scenario with and without MC interference. Numerical results show that, compared with reference schemes, the self-optimization framework can improve overall spectral efficiency (in bits/s/Hz) while quality-of-service (QoS) of ongoing users' sessions is preserved. Moreover, the self-optimization of the transmission power allows to save energy and to reduce intercell interference. Also, an analysis of the dynamic response of the framework reveals that the communicative scheme can react better to changes in the FCs deployment than the non-communicative scheme. On the other hand, the communicative scheme requires from signaling between FCs to exchange the resource utilization messages.

In the following, Section II introduces the deployment scenarios in OFDMA FCs and the different levels of coordination. Next, Section III presents the self-organized framework whereas Section IV describes the self-optimization algorithms for spectrum assignment and transmission power. Then, the simulation model is presented in Section V, and obtained results are discussed in Section VI. Finally, Section VII states conclusions of this work.

II. OFDMA FEMTOCELL DEPLOYMENTS

In the following, the spectrum allocation and the different levels of coordination in OFDMA FCs are presented.

A. Spectrum Allocation

In general, OFDMA FCs will co-exist with large coverage operator-deployed OFDMA MCs, leading to a *two-layer deployment* (i.e., one layer for MCs and another for FCs). Since an OFDMA radio interface divides the available spectrum in several frequency subchannels, two or more cells using the same subchannel can interfere each other. This is particularly crucial in an OFDMA radio interface, because intercell interference dramatically reduces the data rate that users in a given cell can obtain. Therefore, intercell interference in the MC layer is mitigated through the use of Frequency Reuse Factors [13], where the available spectrum is distributed among MCs following a fixed regular pattern. Furthermore, interference between FCs in the FC layer cannot be in general neglected due to FCs' proximity, (e.g., in dense scenarios like buildings with at least one FC per home/office), and then appropriate interference avoidance methods are needed.

Nevertheless, one of the main challenges in the two-layer scenario is the management of the potential *cross-layer* intercell interference, due to the uncontrolled appearance of FCs from the network operator point of view. As depicted in Fig. 1, one of the simplest mechanisms to avoid the cross-layer interference is to employ an *orthogonal* spectrum deployment, where the macro- and femto- cell layers use different spectrum bands and spectrum management is independently performed for each layer. However, this deployment can reduce overall system capacity. On the contrary, *co-channel* spectrum assignment shares the available spectrum band between the MC and the FC layers, increasing the available capacity for each one but at the cost of complex management of the intercell interference. For instance, it has been determined that the MC coverage can decay dramatically around FCs due to the excessive interference leaked by FCs [14][15]. Moreover, it has been showed that [16] important capacity gains can be obtained in the MC layer by deriving indoor users to FC layer, where this gain depends on the MC transmit power configuration affecting the interference produced to the FC layer.

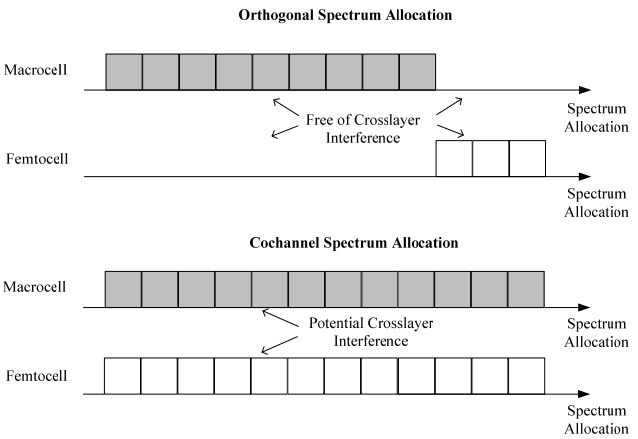

Figure 1. Possible spectrum allocations in OFDMA two-layer deployments

B. Levels of Coordination

For FC deployments, an operator-controlled spectrum assignment as in the MC case is unfeasible whereas decentralized approaches provide the necessary independency so that FCs can autonomously react to network changes. Nevertheless, some kind of coordination between FCs is needed to converge to appropriate solutions.

Different levels of coordination are possible depending on the information that a given FC handles to make its decision. This is sketched in Fig. 2 where three distinct coordination levels have been distinguished. First, resource assignment strategies can be classified between *non-cooperative* and *cooperative*. Non-cooperative strategies only take into account, for each FC, information from the own FC, without considering the actions taken by other cells in the surroundings. Then, they fall in a sort of selfish strategies and usually are used as reference approaches from comparison purposes. For instance, random schemes such as those used in [17][18] equally divide the available spectrum band into V portions,

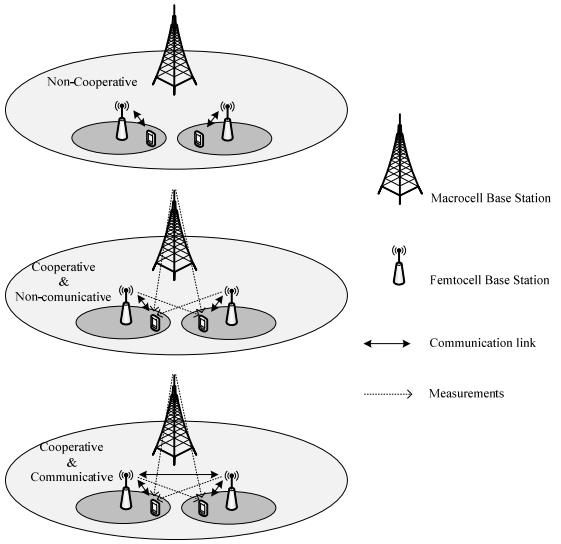

Figure 2. Levels of coordination between FCs.

and each FC randomly selects one of them. The greater V, the lower the probability that two adjacent FCs use the same portion, but also the lower the available capacity in each FC.

On the other hand, cooperative schemes do take into account information about resource assignment in other nearby cells in order to plan the spectrum assignment accordingly. Two subtypes can be distinguished named as *non-communicative* and *communicative*. The non-communicative scheme bases on the feedback of the users to analyze the spectrum and power usage in nearby cells including both other FCs and MCs. Hence it relies on users' *measurements reports* that are periodically sent to the FCs base station in uplink. On the other hand, the communicative scheme additionally allows that FCs can exchange explicit information regarding their spectrum and power usage. This can be done through the wireless interface or though the DSL backhaul. The main benefit of the communicative scheme is that a given FC manages the exact resource assignment decision taken by other cells in the surroundings, so that its decision could be more accurate and not only relies on users' measurements. In fact, we will see in the results section the impact of the measurements report period on the communicative and non-communicative strategies, showing that it could degrade the performance of the non-communicative schemes. However, communicative schemes suppose an additional signaling overhead for the wireless or DSL interface.

III. System Model and Functional Architecture

Fig. 3 depicts the system model and functional architecture for each OFDMA FC. Fig. 3(a) shows an *autonomous* FC surrounded by other cells (in general macro- and/or femto- cells). Each FC performs autonomous spectrum assignment and transmission power decisions with the objective of improving FC's spectral efficiency while guaranteeing FC users' QoS and optimizing power consumption.

An OFDMA radio interface is considered in downlink for users' data transmission, where a system bandwidth, W, is

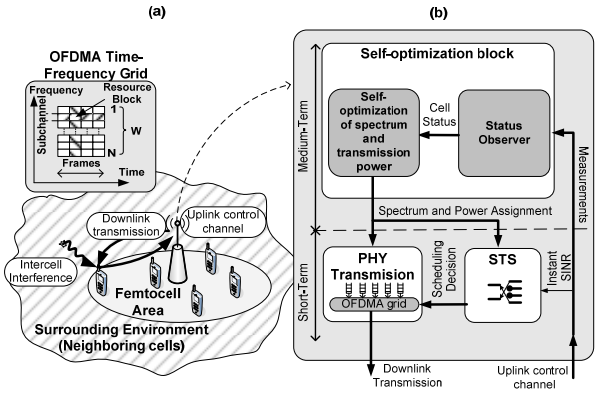

Figure 3. (a) Proposed system model and (b) functional architecture for a single FC with self-organization capabilities.

divided into N subchannels $\{1,\ldots,n,\ldots,N\}$. Hence the bandwidth of each subchannel is $B = W / N$ Hz. Moreover, time is divided into frames. The minimum radio resource block assignable to users is one subchannel per frame. On the other hand, there is an uplink control channel where users send instantaneous (frame-by-frame) measurements report messages. As it is explained in the following, these reports provide to the FC the means to approximate, *channel status* in the short-term to perform the link adaptation for each established downlink communication link, and *cell status* in the medium-term to perform reliable spectrum and power assignment.

The functional architecture is depicted in Fig. 3(b). It is a hierarchical architecture where the operation of the FC is divided into two timescales.

A. Short-term

In the short-term, the FC schedules users' transmissions into the OFDMA time-frequency grid following standard scheduling strategies, which are implemented in the Short-Term Scheduler (STS) functional block. Moreover, STS also performs link adaptation. That is, users' transmission bitrate is variable by means of Adaptive Modulation and Coding (AMC), where an appropriate modulation and coding scheme is associated to each instantaneous quality measurement of the channel (i.e., Signal to Interference plus Noise Ratio: SINR) [19]. The detailed SINR thresholds for each modulation and coding rate considered are given in Table I.

B. Medium-term

In the medium-term (seconds or tens of seconds), the FC changes (if needed) the usage of spectrum and transmission power. To this end, the *Self-optimization* functional block is introduced as depicted in Fig. 3(b).

The core of the self-optimization block is the *self-optimization algorithms* (explained in next section) that determine which subchannels the FC should use and the transmission power per subchannel. The FC executes these algorithms following a *self-optimization period* of L frames, so that each FC is periodically reacting to changes in its environment, that is, changes in the perceived interference affecting the performance of the FC.

TABLE I. ADAPTIVE MODULATION AND CODING TABLE

Modulation [bits/s/Hz]	Coding Rate	Achievable spectral efficiency [bits/s/Hz]	SINR threshold [dB]
-	-	0	< 0.9
2 (QPSK)	1/3	0.66	≥ 0.9
2 (QPSK)	1/2	1	≥ 2.1
2 (QPSK)	2/3	1.33	≥ 3.8
4 (16QAM)	1/2	2	≥ 7.7
4 (16QAM)	2/3	2.66	≥ 9.8
4 (16QAM)	5/6	3.33	≥ 12.6
6 (64QAM)	2/3	4	≥ 15.0
6 (64QAM)	5/6	5	≥ 18.2

The *Status Observer* module is in charge of building the *cell status* given as an input to the self-optimization algorithms. The cell status consists of (*i*) the average intercell interference plus thermal noise per subchannel $\overline{I}_n$, (*ii*) the average pathloss in downlink in the FC $\overline{PL}_{DL}$, and (*iii*) the average spectral efficiency $\overline{\eta}$ in bits/s/Hz. The average intercell interference per subchannel and downlink pathloss in the FC can be obtained from the measurement reports given by users. It is worth mentioning that these measurements are usual in mobile cellular systems to perform typical radio resource management procedures like, e.g., handovers [20]. Then users are periodically reporting these measurements averaged during a *measurements period* of l frames. In order to have the most up-to-date information, only the metrics obtained during last period prior the execution of the self-optimization algorithms are passed to them. Moreover, the average spectral efficiency can be estimated by the FC by averaging the quotient between the short-term FC throughput and the assigned bandwidth to the FCs during the last measurements period. Note that $\overline{I}_n$ can include both the MC and the other FC interference. Then, the proposed scheme will be able to adapt in a general co-channel MC and FC deployment.

Finally, notice that if two adjacent FCs execute simultaneously the self-optimization algorithms, then the stability of the framework would be compromised, since both FCs would try to change the spectrum and power assignment at the same time without knowing the final solution of the other FC respectively. Then, in order to minimize the probability that two FCs execute the self-optimization algorithms simultaneously, each FC randomly selects, from the next L frames after switch-on, the initial frame where the self-optimization period starts. Then, since large values of L are expected, then the probability that two adjacent FCs choose the same initial frame can be very low. Moreover, as it will be seen in the results section, it is desirable that $l \ll L$ so that the measurements taken during the last measurement period before the execution of the self-optimization algorithms reflect the latest stable up-to-date information. In other words, a short measurements period reduces the probability that neighboring FCs of a given FC change the spectrum and power assignment during the last measurement period, thus compromising the accuracy of the measurements.

IV. SELF-OPTIMIZATION ALGORITHMS

In the following, two strategies (non-communicative and communicative) to optimize the spectrum assignment and transmission power of a FC are presented.

A. Cooperative and non-communicative strategy

In the non-communicative strategy, only measurements reported by users to de FC base station are considered.

1) Spectrum assignment

Regarding the spectrum assignment, the strategy divides the decision into two stages. In the first one the algorithm decides the number of subchannels, C, that the FC needs in order to fulfill in average with users' throughput expectations. Assume that there are U users in the FC and that the u-th user is satisfied if the assigned throughput is above QoS target $th_{\text{target},u}$. Then, the number of subchannels is computed as:

$$C = \max\left\{\min\left\{\left\lceil \Delta \frac{\sum_{u=1}^{U} th_{\text{target},u}}{B\overline{\eta}} \right\rceil, N\right\}, 1\right\}, \quad (1)$$

where B is the subchannel bandwidth in Hz, and $\overline{\eta}$ is the average spectral efficiency (provided by Status Observer).

Basically, the expression in (1) computes C by dividing the total requested throughput in the FC between the estimated cell capacity for that FC. In addition, $\Delta > 1$ is a margin factor to allow the estimation of the number of subchannels to be conservative. That is, some extra subchannels could be needed to cope with instantaneous fluctuations of the wireless channel, affecting the spectral efficiency per subchannel, which could be punctually lower than $\overline{\eta}$. Finally, notice that C is bounded to a minimum of one subchannel and, to a maximum of N system available subchannels.

In the second stage, the spectrum assignment algorithm sorts the N available system subchannels in increasing order depending on the average intercell interference during the last period ($\overline{I}_n$). Then, the C first sorted subchannels are selected. Hence, the spectrum assignment algorithm in each FC tends to use the best subchannels according to the intercell interference perceived by its users. Finally, it is assumed that, after switch-on, a FC initially selects a random spectrum assignment.

2) Power assignment

Once the spectrum assignment is decided, the transmission power for each assigned subchannel, P_n, is adjusted as:

$$P_n(dBm) = \max\left\{\min\left\{\overline{I}_n + \overline{PL}_{DL} + \delta, P_{\max}\right\}, P_{\min}\right\}. \quad (2)$$

Based on the definitions given in the section before, the term $\overline{I}_n + \overline{PL}_{DL}$ stands for the transmission power needed in average to have an average SINR of 0 dB. Hence, the power

adjustment in (2) tends to set the transmission power so that an average SINR of δ dB is attained in the FC. Notice that P_n is maintained between the range $[P_{\min}, P_{\max}]$. $P_{\min}$ is a minimum power necessary to avoid excessive power reduction in the absence of intercell interference (a possible situation in an OFDMA interface depending on the subchannel assignment in the femtocell and other adjacent femtocells). On the other hand, $P_{\max}$ is the maximum power per subchannel in dBm due to maximum FC power limitation. Finally, it is considered that after switch-on a FC starts with $P_{\max}$ in all assigned subchannels.

B. Cooperative and communicative scheme

The communicative scheme takes into account explicit information exchanged between FCs. In this case, we assume that after the execution period of L frames each FC k informs the other FCs in the set of neighboring FCs, Ψ_k, about the set of subchannels, Φ_k, that the FC is planning to use. Each FC can build the set of neighboring FCs, Ψ_k, using the measurement information reported by its users. Also, in case that a MC layer is present (i.e., co-channel spectrum allocation), the FC will add to Ψ_k the strongest MC (attending to received channel power from MCs), m, and will compute Φ_m from measurements of the MC activity. Notice that, in this paper, direct communication of the FCs with the MC is not allowed. However, this communication could be exploited if, for instance, the operator broadcasts some information about the MC deployment to FCs through the DSL backhaul.

1) Spectrum assignment

As in the non-communicative strategy, the spectrum assignment algorithm is divided into two stages. In the first stage the number of subchannels needed C is computed following (1), which considered the requested throughput by users in the FC and the estimated capacity.

In the second stage, the spectrum assignment algorithm exploits the information collected from nearby FCs:

- First selects the subchannels that are not used by any FC in the set of neighboring FCs (i.e., all subchannels n that fulfill that $n \notin \Phi_j \ \ \forall j \in \Psi_k$).
- If the number of selected subchannels is still lower than C, then the FC selects from the remaining subchannels not selected in the previous step those with the lowest intercell interference $\overline{I}_n$.

Basically, the communicative algorithm pursues the same objective as the non-communicative one, since it tries, for a given FC, to minimize the interference received from other FCs (and strongest MC). What makes the difference is that the communicative algorithm uses the exact assignment in the set of neighboring FCs and this is key advantage regarding the adaptability of the algorithm as it will be seen in the results section.

2) Power assignment

As for the power assignment, it would be also possible for the FCs to exchange the transmission power per chunk and then it would be feasible to estimate the expected intercell interference received by users. However, this requires that users also report the estimated pathloss for all the cells in the set of neighboring FCs, thus increasing the signaling overhead. Then, we have opted for using the same procedure as for the non-communicative scheme where the intercell interference $\overline{I}_n$ per subchannel computed by Status Observer from measurements reports is used.

V. Simulation Model

We consider a downlink OFDMA-based scenario with a total of $N = 12$ subchannels of 375 kHz available in the system. The scenario is composed of 7 MCs and 12 FCs inside a building as depicted in Fig 4. MC radius is 500 m and the building is situated at approximately 200 m of the central MC. Each one of the offices has 20x20 m2, and the FC is located at the office's center. For indoor coverage, the COST 231 Multi-Wall Model (MWM) is used [21]. Height of the building's walls is 4 m. Inner walls are considered as 'narrow' walls (i.e., with small penetration losses), whereas external walls are considered as 'thick' walls. Penetration losses for doors and windows are also considered. Propagation model parameters and other default simulation values are presented in Table II.

On the other hand, indoor users in FCs are static and always have data ready to be sent (i.e., full-buffer traffic model), so that each user tries to obtain as much capacity as possible. However, a user is satisfied when a given throughput threshold $th_{\text{target},u}$ is reached. Finally, the well-known proportional fair scheduling [22] strategy is considered for resource assignment to users in the short-term according to functional architecture presented in Section III.

We will consider an orthogonal and co-channel spectrum allocation for the FC deployment. For the orthogonal spectrum allocation simply the MC layer is not considered, so that the N subchannels do not have MC interference. On the other hand, the co-channel allocation considers a MC deployment with a FRF3 spectrum assignment, i.e., the central MC uses one third of the spectrum and the rest of the MCs alternate one of the other 2 subbands.

Besides, we consider two distributions of the users in the FC scenario, named in the following as *homogeneous* and *heterogeneous* distributions. In the homogeneous distribution, 4 users are deployed in each office (i.e., FC) whereas in the heterogeneous distribution, half of the offices has 8 users and the rest 4 users.

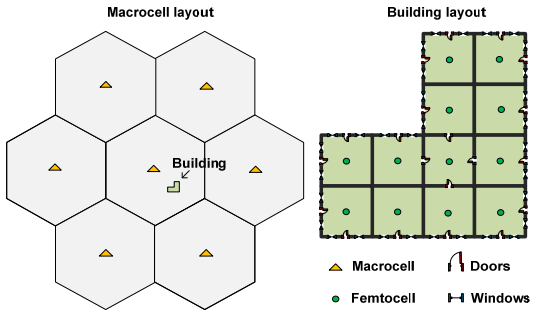

Figure 4. Scenario layout and building detail

TABLE II. SIMULATION PARAMETERS

Frame time T_f	2 ms
Subchannel bandwidth B	375 kHz
Carrier Frequency	2 GHz
Number of subchannels N	12 subchannels
UE thermal noise	-174 dBm/Hz
UE noise factor	9 dB
STS strategy	Proportional Fair
PF Averaging window	50 frames [22]
MC Radius	500 m
MC Antenna height	20 m
Power per subchannel (macro)	32.2 dBm
Minimum distance to FC	1 m
Antenna Patterns	Omnidirectional
Pmax	-0.7 dBm
Pmin	-7 dBm
Av. SINR target δ	16 dB
Margin factor Δ	1.3
Trigger period L	5000 frames
Measurements period l	500 frames
Path Loss model	Cost 231 multi-wall model
Penetration losses [external wall, inner wall, door, window]	[15,10,3,1] dB
Shadowing standard deviation	8 dB
Small Scale Fading Model	ITU Ped. A

VI. RESULTS

A. Tunig of the self-optimization algorithms

In this section we first assess the behavior of both the communicative and non-communicative schemes with regard to the value of the margin factor (Δ) and average target SINR (δ).

Fig. 5 and Fig. 6 show the evolution of the dissatisfaction probability (i.e., a QoS metric as the probability that the user's throughput is below the satisfaction throughput target), spectral efficiency, and transmission power consumption per subchannel for different values of Δ and δ respectively. These results are presented for the orthogonal and co-channel spectrum allocation and for 1024 and 2048 kbits/s (kbps) of requested throughput per user, with a homogeneous distribution

It can be seen in Figures that a better performance (i.e., lower dissatisfaction probability and transmission power and higher spectral efficiency) is achieved for an orthogonal spectrum allocation than for a co-channel allocation. This is because of the higher intercell interference that this latter allocation produces due to the presence of MCs.

More into details, it can be seen that increasing the margin factor Δ has a positive effect on dissatisfaction probability since this augments the number of estimated needed subchannels (see (1)). Hence more capacity is set per FC. However, this also increases the intercell interference between FCs (and also the MC) and thus the spectral efficiency is reduced. Also, the transmission power per subchannel is increased. Hence, there is a tradeoff on the selection of the margin factor. For instance a value around between 1.2 and 1.6 would be adequate for avoiding too high dissatisfaction probability and too low spectral efficiency. On the other hand, increasing the value of the target SINR δ in the power assignment algorithm (see (2)) has a logical positive impact on the dissatisfaction probability and spectral efficiency, since the power assignment tends to augment the average SINR in the FC. However, a too high target SINR does not translates into an improvement on dissatisfaction probability and spectral efficiency, and alternatively only produces an unnecessary increment of the transmitted power (and FC consumption). Thus, again, there is a tradeoff where in this case a value between 15 and 20 dB for the target SINR is adequate.

Nevertheless, the optimal values for Δ and δ can change depending on the scenario (e.g., the traffic load, the FCs deployment, etc.) and thus a static selection of these values can be inaccurate in some cases. Then self-tuning mechanisms for these parameters appear as a potential improvement that should be studied in future work.

B. Performance comparison

In the following, we compare the performance of the cooperative (communicative and non-communicative) schemes for spectrum and power assignment in FCs with a non-cooperative scheme. As stated previously in Section II.B, a random spectrum assignment with constant power is usually taken as a reference for a non-cooperative scheme in literature [17][18]. In this scheme, the spectrum is divided into V =3 equal portions and each FC randomly selects one of them to operate after switch-on.

Results are presented in terms of spectral efficiency, dissatisfaction probability, and transmission power consumption per subchannel. We have considered three different thresholds for the satisfaction throughput as 512, 1024, 2048 kbits/s, so that the behavior of the non-cooperative and cooperative strategies with different QoS requirements are assessed.

Fig. 7 and Fig. 8 show the performance comparison for the orthogonal and co-channel spectrum allocation respectively. Both Figures show the same qualitative performance, but, Fig. 8 attains lower spectral efficiency, slightly higher the dissatisfaction probability, and higher power consumption because of the presence of the MC layer, which increases the intercell interference. Fig. 7(a-c) and Fig. 8(a-c) show the performance comparison for the homogeneous distribution of the users in the building. Comparing the non-cooperative and the cooperative strategies, the cooperative schemes (communicative and non-communicative) demonstrates the best trade-off between QoS fulfillment and spectral efficiency. For instance, for 512 kbits/s satisfaction throughput, they obtain the best spectral efficiency with a reduced dissatisfaction probability. On the other hand, for 2048 kbits/s satisfaction throughput, each FC demands a higher number of subchannels to cope with the traffic demand, what translates into a higher intercell interference and hence into a reduction of the spectral efficiency. However, compared with the non-cooperative strategy, the cooperative schemes considerably reduce the dissatisfaction probability.

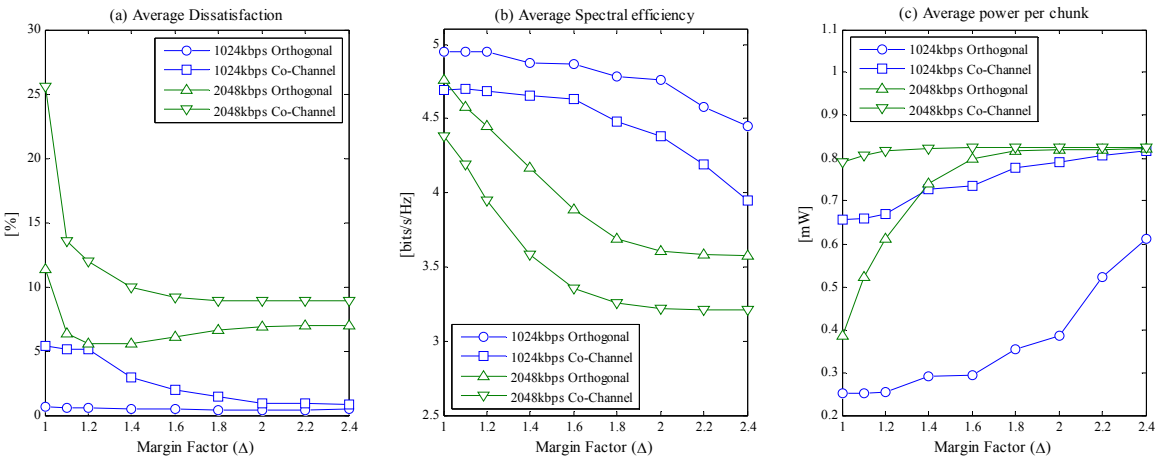

Figure 5. Impact of margin factor parameter on self-optimization algorithms performance

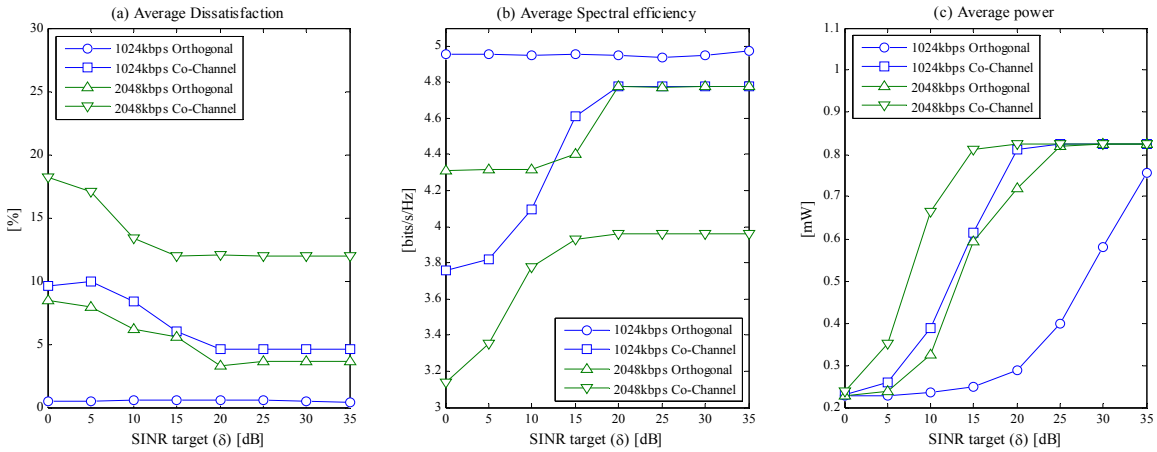

Figure 6. Impact of target SINR on self-optimization algorithms performance

Moreover, regarding the power consumption, the cooperative schemes can achieve important energy savings, especially in the orthogonal spectrum allocation and for low throughputs. In this case, due to low intercell interference, FCs can operate near the minimum power per subchannel with compromising neither the spectral efficiency nor the dissatisfaction probability. Notice that in the presence of MC interference (co-channel spectrum allocation) the FCs react by increasing the power per subchannel.

It is worth to remark the close performance that both the communicative and non-communicative schemes demonstrate, although a slightly better performance is attained by the communicative scheme. This reveals that both schemes are adequate for spectrum and power optimization in FCs attending to performance. However, results in next subsection reveal that other aspects should be taken into account such as the tradeoff between signaling overhead and dynamic response.

Moreover, it is important to highlight the effect of a heterogeneous spatial distribution of the traffic load as shown in Fig. 7(d-e) and Fig. 8(d-e). There, the benefits of the cooperative schemes are appreciable even with lower satisfaction throughputs than those achieved in the homogeneous case. Notice that, in general, a heterogeneous distribution of the load will be common in real scenarios. Thus, this calls for using adaptive approaches such as the proposed cooperative schemes.

Finally, as an example of the SINR improvements that self-organization could bring to FC deployments, Fig. 9 shows the SINR distribution in the proximities of the building for both the orthogonal and co-channel spectrum allocation. The spectrum and power assignments for the non-cooperative and the non-communicative schemes in the homogeneous distribution with 512 kbits/s are considered (analogous results have been found for the other tests and the communicative strategy). Points outside the building are taken as if they were connected to the central MC when applicable (co-channel). It can be seen that, the cooperative scheme considerably ameliorates overall FC's SINR with respect to the non-cooperative scheme. Concretely, in co-channel spectrum allocation the cooperative scheme does not create interference in the MC layer (brown color) whereas the non-cooperative scheme reduces in several dBs the SINR in the building's surroundings. It has been determined that in the former, FC layer self-organizes so that each FC uses different subchannels to those used by the central MC. However, it is appreciable a considerable reduction of the SINR in the FCs compared with the orthogonal spectrum allocation.

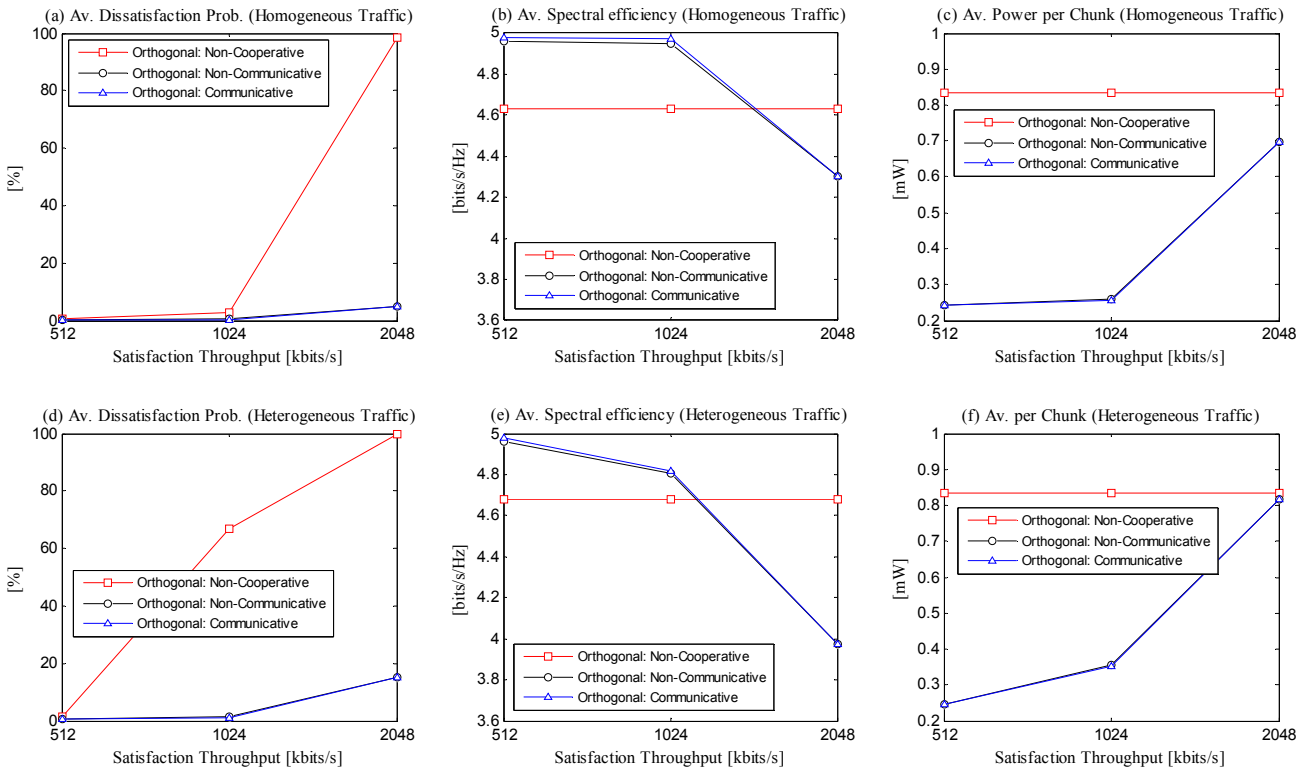

Figure 7. Performance comparision between random and self-organized schemes with orthogonal spectrum deployment.

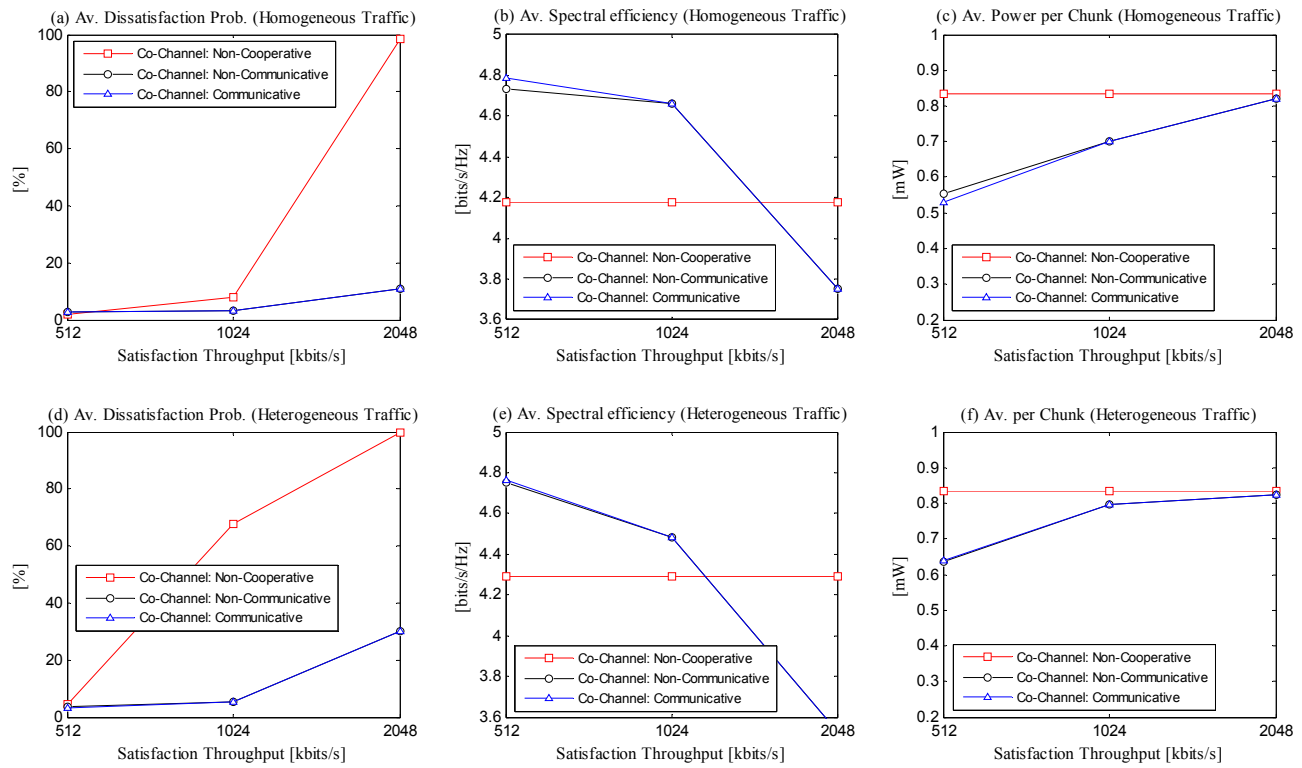

Figure 8. Performance comparision between random and self-organized schemes with orthogonal spectrum deployment.

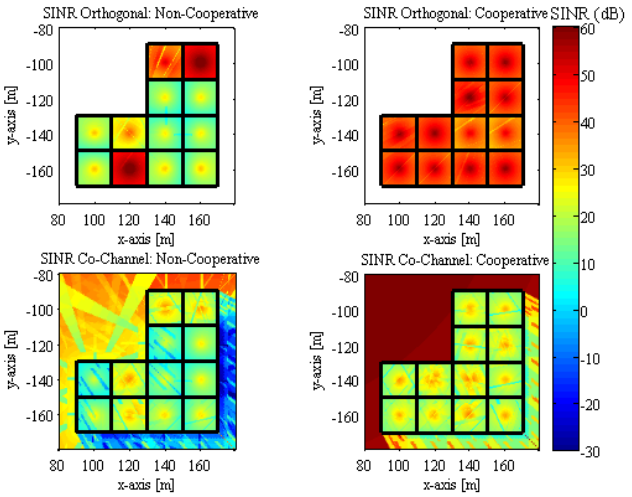

Figure 9. SINR comparision in the surroundings of the building.

It has been checked that, for each FC, this is mainly because of the interference produced by the other MCs, rather than by other FCs. Hence, in general, the interference from MCs distinct of the MC where FCs are deployed cannot be neglected.

C. *Dynamic response*

This section studies the dynamic response of the proposed framework, that is, the ability of the different FCs executing the self-optimization algorithms to adapt to changes in the network deployment. In the following, results are given for the orthogonal spectrum allocation with homogeneous traffic and a throughput target per user of 512 kbits/s.

Fig. 10 shows the adaptability (in terms of the time evolution of (a) dissatisfaction probability, (b) spectral efficiency and (c) transmission power per subchannel) of the non-cooperative, non-communicative and communicative schemes for the FC deployment. The figure shows a case where the central MC is activated at time instant 50 (time is normalized to the self-optimization period). Thus, at this moment, FCs in the building perceive an abrupt increment of the intercell interference in the subchannels used by the MC. Three different ratios of the measurements report period (l) to the self-optimization period (L) are evaluated. A high value (e.g., l/L =1) supposes that it is very probable that neighboring FCs of a given FC also change the spectrum and power assignment during the last measurement period. Hence, some averaged measurements during the last measurements period can be inaccurate.

It can be seen in all subplots of Fig. 10 that the response of the non-cooperative scheme does not depend on l/L, since the spectrum assignment is randomly selected without taking into account measurements. On the other hand, the non-communicative and communicative strategies show very different behaviors. For l/L =1, both algorithms demonstrate a very fast response to the increment on intercell interference. However, the non-communicative scheme reveals a poor performance since the measurements information that is taken is not up-to-date (i.e., neighbors of a FC were changing their resource assignment during the last measurements period). On the other hand, the communicative scheme achieves a good performance, since the spectrum assignment in a FC is based on the latest spectrum assignment sent by other FCs. Nevertheless, for l/L =0.1, both schemes show a very similar and good performance, although the response of the FC deployment to the activation of the central MC is slower. In this case, since $l \ll L$, it is less probable for a given FC that another neighbor FC changes the spectrum assignment during the last measurement period, thus supposing an improvement in performance of the non-communicative scheme.

Fig. 11 and Fig. 12 illustrate how the FCs in the building self-organize the spectrum and the power assignment after the activation of the central MC for l/L =1 and l/L =0.1 respectively. Figures show evolution of the average spectral efficiency for seven time instants around the activation of the central MC (time instant 50). Notice that, after MC activation, the spectral efficiency dramatically decays for all FC, but at time instant 70 (20 executions later), the spectral efficiency has increased for the communicative scheme. This is also the case for the non-communicative scheme in Fig. 12, although in Fig 11. the inaccuracy of the measurements avoids proper self-organization of the FC deployment.

Finally, it is important to remark that the success of the communicative scheme has an associated cost in terms of signaling overhead. Qualitatively, in order to communicate with adjacent FCs, each FC under the communicative scheme, has to transmit $\phi_k \cdot (Nb_s + b_{id}) \cdot (1/LT_f)$ bits/s. Here, ϕ_k is the number of neighboring FCs, b_s, is the number of bits needed to encode spectrum usage per subchannel, b_{id} is the number of bits devoted to code FC's identification, and T_f is the frame time and thus $(1/LT_f)$ is the update frequency that depends on the self-optimization period. On the other hand, the signaling needed for measurements in a given FC is $U \cdot (lNb_{\text{sinr}} + b_{In} + b_{PL}) \cdot (1/lT_f)$ bits/s, where U is the number of users in the FC, b_{sinr} are the bits needed to report instantaneous SINR per subchannel for frame-by-frame short-term scheduling, b_{In} and b_{PL} the bits needed to report intercell interference and pathloss respectively, and l the measurements period in frames.

Since the signaling for measurements is present in both the non-communicative and communicative schemes, and the signaling for communication of the FCs is exclusive of the communicative scheme, quotient between the signaling and for communication and the signaling needed for measurements can be used as a metric to analyze the signaling overhead of the communicative scheme. Fig. 13 shows this quotient for different values of ϕ_k, N and U, and with respect to the value of L. All magnitudes are encoded with 8 bits and $l = 500$ frames and T_f =2 ms. Certainly, the signaling overhead demonstrates an inverse relation with the self-optimization period L. Then low values of L can yield to a

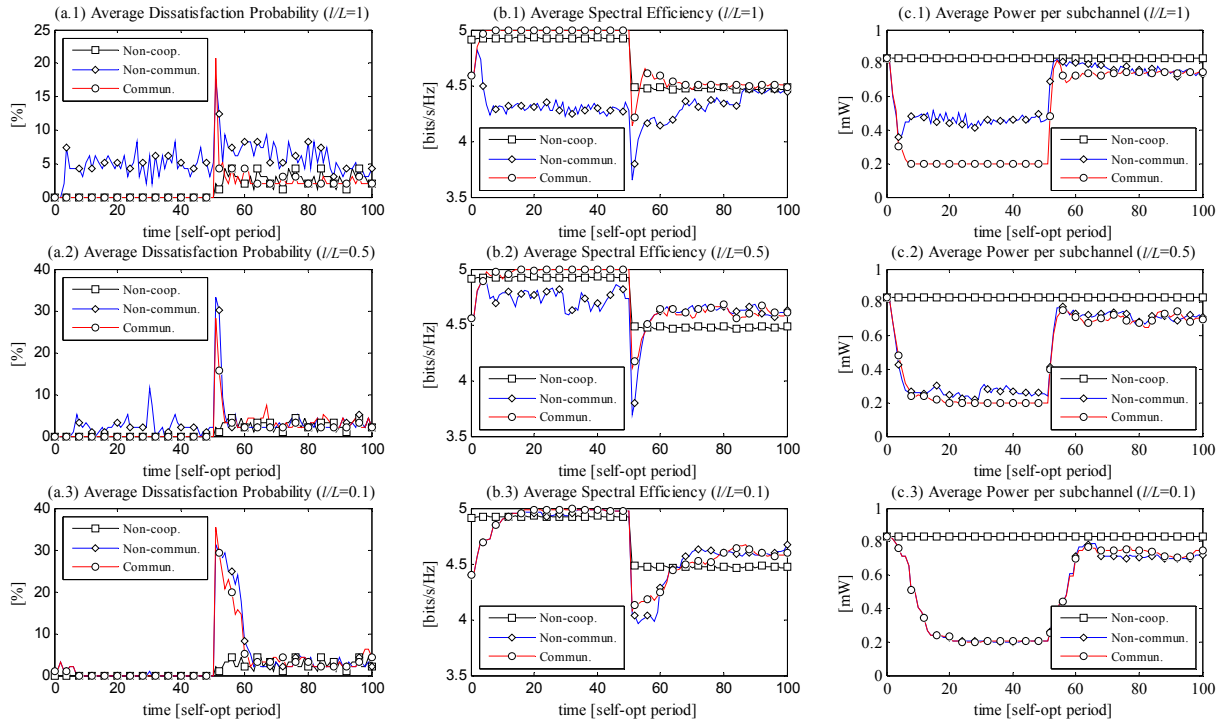

Figure 10. Dynamic response of the compared strategies under different ratios of the measurements and self-optimization periods

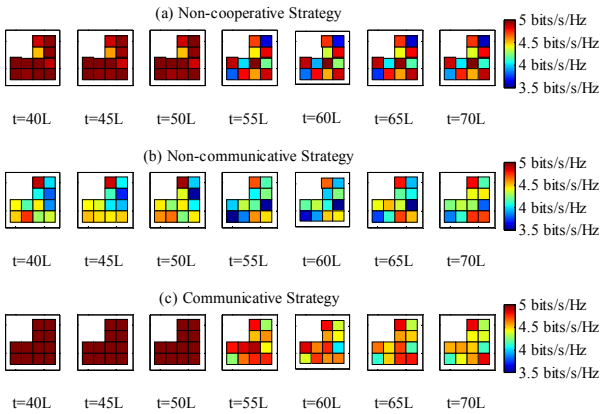

Figure 11. Average spectral efficiency per FC for compared schemes (*l*/*L*=1).

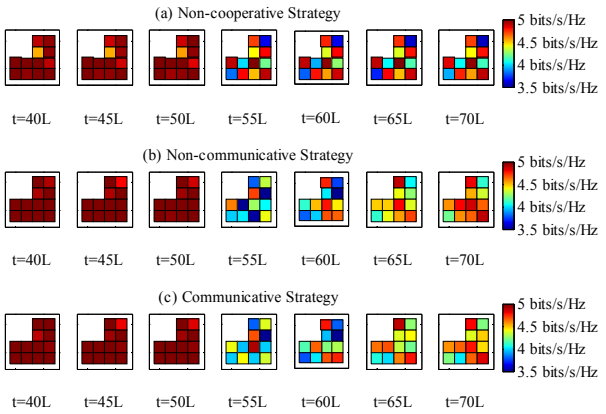

Figure 12. Average spectral efficiency per FC for compared schemes (*l*/*L*=0.1).

high signaling overhead of around 20%, especially for a low number of users and a high number of neighboring FCs as shown in Fig. 13. However, notice that for a high number of users in the FC, the signaling overhead tends to be negligible, since in this case the signaling for measurements is dominant.

VII. CONCLUSIONS

This paper has shown that self-organization is a suitable approach when facing resource management in OFDMA FC networks. Concretely, self-optimization algorithms for both spectrum and transmission power per OFDMA subchannel assignment have been proposed, showing that the inclusion of these algorithms can bring notable performance improvements, especially in two-layer deployments with MCs and heterogeneous spatial distribution of the traffic load.

Moreover, it has been determined that the effect of MCs distinct of the MC where FCs are deployed cannot be neglected. That is, those MCs could negatively interfere FCs producing a performance reduction. Hence, multicell MC deployments should be used in two-layer MC and FC per-

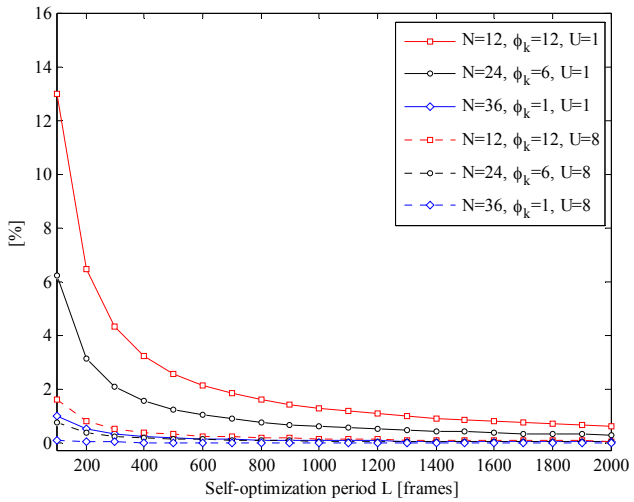

Figure 13. Signaling overhead of the communicative scheme over the non-communicative scheme

formance evaluations, rather than single-cell MC plus FCs, as usual in certain studies.

The paper has also studied the effectiveness of different levels of coordination between FCs. Communicative and non-communicative approaches have been compared, revealing that the performance of both schemes can be very close. However, when analyzing the dynamic response of the FC deployment under one scheme or the other, it has been observed that the relation between the measurements period and the self-optimization period can considerably degrade the performance of the non-communicative scheme. On the other hand, the communicative scheme demonstrates a robust behavior in this respect. The main drawback of the communicative scheme is the need of designing signaling interfaces between FCs, and the additional signaling that communication between FCs adds to the system. Finally, it is worth remarking the low complexity of the proposed self-optimization algorithms, showing that the simple inclusion of autonomous and adaptive mechanism could bring enormous performance benefits.

ACKNOWLEDGMENT

This work has been performed in the framework of the Spanish Research Council under COGNOS grant TEC2007-60985. Also, the European Regional Development Funds (FEDER) have supported this work.

REFERENCES

[1] F. Bernardo, R. Agustí, J. Cordero, and C. Crespo, "Self-optimization of Spectrum Assignment and Transmission Power in OFDMA Femtocells," Sixth Advanced International Conference on Telecommunications (AICT 2010), pp. 404-409, 2010

[2] J. Zhang and G. de la Roche, "Femtocells – Technologies and Deployment," Wiley, January 2010

[3] V. Chandrasekhar, J. Andrews, and A. Gatherer, "Femtocell networks: a survey," IEEE Commun. Mag., vol.46, no.9, pp.59-67, Sept. 2008

[4] C. Prehofer and C. Bettstetter, "Self-organization in communication networks: principles and design paradigms," IEEE Commun. Mag., vol.43, no.7, pp. 78-85, Jul. 2005

[5] E. Bogenfeld and I. Gaspard (editors) "Self-x in Radio Access Networks," Available at: https://www.ict-e3.eu/project/dissemination/whitepapers/whitepapers.html. Dec. 2008. [online][Last accessed 20/01/2011]

[6] INFSO-ICT-216284 Self-Optimisation and Self-Configuration in Wireless Networks (SOCRATES) Project, http://www.fp7-socrates.org/?q=node/1 [Last accessed 20/01/2011]

[7] D.N. Knisely, T. Yoshizawa, and F. Favichia, "Standardization of FCs in 3GPP," IEEE Commun. Mag., vol.47, no.9, pp.68-75, Sept. 2009.

[8] D. Lopez-Perez, A. Ladanyi, A. Juttner, and Jie Zhang, "OFDMA femtocells: A self-organizing approach for frequency assignment," IEEE 20th International Symposium on Personal, Indoor and Mobile Radio Communications, 2009, pp.2202-2207, 13-16 Sept. 2009.

[9] 3GPP TS36.300 v8.0.0 "Evolved Universal Terrestrial Radio Access (E-UTRA) and Evolved Universal Terrestrial Radio Access Network (E-UTRAN); Overall description; Stage 2", Mar. 2007

[10] H. Claussen, L. T. W. Ho, and L. G. Samuel, "Self-optimization of coverage for FC deployments," in Proc. Wireless Telecommunications Symposium (WTS), 2008.

[11] M. A. Marsan, L. Chiaraviglio, D. Ciullo, and M. Meo, "Optimal energy savings in cellular access networks," Proc. IEEE International Conference on Communications 2009 (ICC'09), GreenComm Workshop, Jun. 2009.

[12] Q, Su, et *al.*, "A distributed dynamic spectrum access and power allocation algorithm for Femtocell networks," International Conference on Wireless Communications & Signal Processing, 2009 (WCSP 2009), pp.1-5, 13-15 Nov. 2009

[13] Z. Wang and R.A Stirling-Gallacher, "Frequency reuse scheme for cellular OFDM systems," Electronics Letters, vol.38(8), pp.387-388, 2002

[14] J. Espino and J. Markendahl, "Analysis of Macro - Femtocell Interference and Implications for Spectrum Allocation," 20th Personal, Indoor and Mobile Radio Communications Symposium 2009 (PIMRC-09) Tokyo, Japan, 13-16 September, 2009

[15] J. Góra and T. E. Kolding, "Deployment Aspects of 3G Femtocells," 20th Personal, Indoor and Mobile Radio Communications Symposium 2009 (PIMRC-09) Tokyo, Japan, 13-16 September, 2009

[16] H. Claussen and D. Calin, "Macrocell Offloading Benefits in Joint Macro and Femtocell Deployments," 20th Personal, Indoor and Mobile Radio Communications Symposium 2009 (PIMRC-09) Tokyo, Japan, 13-16 September, 2009

[17] D. López-Perez, A. Valcarce, G. de la Roche, and J. Zhang, "OFDMA Femtocells: a roadmap on interference avoidance," IEEE Comm. Mag., vol.47, no.9, pp.41-48, Sept. 2009.

[18] V. Chandrasekhar and J.G. Andrews, "Spectrum allocation in tiered cellular networks," IEEE Trans. on Comm., vol. 57(10) pp. 3059 - 3068 Oct. 2009

[19] M.S. Al-Janabi, C.C. Tsimenidis, B.S. Sharif, and S.Y. Le Goff, "Adaptive MCS Selection with Dynamic and Fixed Subchannelling for Frequency-Coherent OFDM Channels," Int. Journal on Advances in Telecommnications, vol. 2(4), pp. 131-141, Mar. 2009

[20] E. Dahlman, S. Parkvall, J. Skold, and P. Beming, "3G Evolution,: HSPA and LTE for Mobile Broadband", Second Edition, Academic Press (Elsevier), 2008

[21] COST (European Co-operation in the Field of Scientific and Technical Research), COST 231 Book, Final Report. Chapter 4, Propagation Prediction Models.

[22] C. Wengerter, J. Ohlhorst, and A.G.E. von Elbwart, "Fairness and throughput analysis for generalized proportional fair frequency scheduling in OFDMA," IEEE 61st VTC 2005-Spring. Jun. 2005

Advanced Consideration of a Caller Pre-Validation Against Direct Spam Over Internet Telephony

Jürgen Müller and Michael Massoth
Department of Computer Science
Hochschule Darmstadt University of Applied Sciences
Darmstadt, Germany
e-mail: {juergen.mueller, michael.massoth}@h-da.de

***Abstract*—Spam over Internet Telephony as the distribution of unwanted voice messages over Voice over Internet Protocol networks is an upcoming threat. It is harder to prevent than e-mail spam since its content is not available before the victim is annoyed. This is even more difficult if the spam is sent directly to the victim's user equipment, bypassing the proxies of the service provider. Hence, this messages cannot be filtered, since the proxies are no longer participating in the transaction. This article presents a pre-validation mechanism, which ensures a minimum level of trust about the caller. It assumes that a legal registered user does not send any spam, since his service provider will penalize him if he does so. Therefore, the pre-validation mechanism sends some requests to the presence server of the provider and the user equipment of the caller to validate their existence. This enables the knowledge to allow a call attempt of an unknown user.**

***Index Terms*—Communication system security; Telephone equipment; Telephony; Spam**

I. Introduction

Spam over Internet Telephony (SPIT) is an upcoming problem in the internet and telecommunication society. This section gives a brief overview on SPIT. A lot of groups are affected. There are individuals and companies that use Voice over Internet Protocol (VoIP) because it is cheap. Additionally, there are spammers who want to send unsolicited calls.

Regarding a study of the German Federal Office for Information Security, about 98.5 % of e-mails received in Germany in 2008 were spam [2]. It would not be possible to use VoIP properly if this amount of spam would arrive in the VoIP networks. However, it is not described clearly if the whole 98.5 % are spam or unwanted e-mails in general.

The MessageLabs Intelligence Reports provides on a monthly basis the latest thread trend, including the spam propagation [3]. Therefore, the e-mail spam rate in the last 18 month was in an average on a level of about 90.5 %, as depicted in Figure 1.

In addition to annoyance, there is a big problem with cost caused by spam. According to a prediction of Ferris Research, the worldwide cost for spam grew up to $130 billion in 2009 [4].

A new kind of view on the spam phenomenon is given in a report by McAfee [5]. The authors describe herein that the whole amount of annual spam leads to a power consumption of 33 billion kilowatt-hours. That amount corresponds to the electricity used in 2.4 million homes in the United States of America.

VoIP has been designed to reduce telephony-related cost. First of all, providers want to save money, but this means a reduction of cost for spammers as well. Sending spam via internet telephony is much cheaper than sending it by a public switched telephone network.

Indeed, the distribution of e-mail spam is cheap as well. However, there is a major advantage of SPIT over e-mail spam: It is harder to detect. Therefore, more SPIT gets through to a callee than spam e-mails arrive in a mailbox.

The group of victims in addition grows. The number of residential, small- or home office VoIP subscribers grew 24 % in 2009 to 132 million worldwide [6]. 10.3 million of this VoIP users resides in Germany 2010 [7]. In the future, the total number of mobile VoIP users will reach 288 million by the end of 2013 [8].

This article is structured as follows: Section II introduces the process of SPIT and its two types. In Section III, all existing defense mechanisms that could be applicable against SPIT are introduced. The proposed caller pre-validation mechanism is introduced in Section IV. Section V describes how this mechanism could be attacked. Section VI contains a performance analysis of the proposed mechanism. A look forward and an introduction to future improvements are given in Section VII.

II. Background

It is important to know how SPIT works in order to understand it. As shown in Figure 2, there are three steps [9]. First of all, the spammer needs to collect addresses to send his messages to. The next step is the session establishment. The message itself is sent to the callee in the third step. The most relevant step is the address gathering, because this step enables the attack.

Fig. 2. The three steps of Spam over Internet Telephony [9].

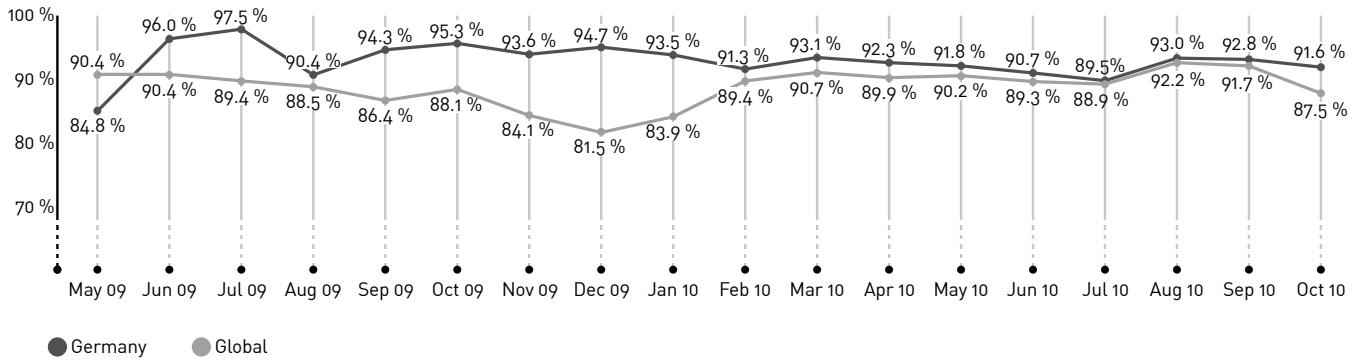

Fig. 1. E-mail spam rate between May 2009 and October 2010 [3].

A. Gathering Addresses

The question of interest is how spammers are able to acquire these addresses. Surveys show that there are at least five options to achieve this objective [9][10][11]:

- Trading: On the internet, there are several opportunities to buy whole lists of addresses. This is the easiest way to gather addresses.
- Harvesting: Spammers use so-called bots, which are automatically searching for addresses in the internet. This can be done by scanning page code for strings in special syntaxes. For example a SIP URI mainly consists of the sub strings "sip:" and the @-sign. Furthermore, spammers steadily get more addresses just by waiting.
- Active scanning (with permanent SIP URIs): The spammer needs a valid account in the network of the desired provider to launch this attack. However, he has to find out how addresses are put together among this provider. Next, the spammer starts an automated test call to each possible SIP URI. A successful call attempt identifies an assigned address.
- Active scanning (with temporary SIP URIs): This possibility is very similar to active scanning. The difference is that there is no message being sent via the infrastructure of the provider. Instead, they are sent directly to the callee's user equipment. Since spammers do not know the correct domain part of the temporary SIP URI, they have to figure out the range of IP addresses that are assigned by the corresponding provider. So, the spammer has to check each possible combination of user name and IP address.
- Passive scanning: An active scan implies the possibility of detection by a network administrator. Therefore, a spammer can host a web site or hotline and offer, for instance, a value-added service. Each user who wants to use that service has to register himself on the web site or to call a certain hotline. Every number who calls this hotline or is sent via the registration form can be stored for a SPIT attack.

The active scan attack is the most interesting source of addresses. A spammer could achieve three lists during his scan. The first one contains all addresses that are assigned and currently registered, i.e., the addresses that responded with a 200 OK response. A second list contains the addresses that are assigned but currently not registered, i.e., the addresses that responded with a 480 Temporarily Unavailable. The last list holds unassigned addresses that answered with a 404 Not Found response. The last one could be used for future scan attacks.

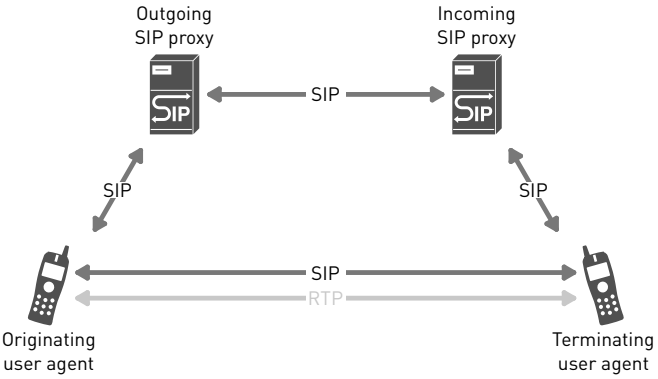

Fig. 3. The regular SIP trapezoid.

B. Session Establishment

The spammer could start to launch the spam attack itself, as soon as he collected enough addresses. Therefore, he has to establish a connection to each victim. He has two possibilities to establish these connections because he can gain two lists of assigned addresses (i.e., permanent and temporary SIP URI lists) [9]:

- SPIT via Proxy: The spammer uses the permanent SIP URI list to send his messages via the proxies of the provider.
  This so called SPIT via Proxy is the most usual form of SPIT. The messages sent by the spammer first arrive at proxies belonging to the provider, as shown in Figure 3. These proxies are able to take some actions against SPIT and redirect it to its destination.
  The provider is able to challenge the caller before he accepts his messages, too. So, only known and trusted users are able to participate in the system.
- Direct SPIT: A spammer usually does not want that

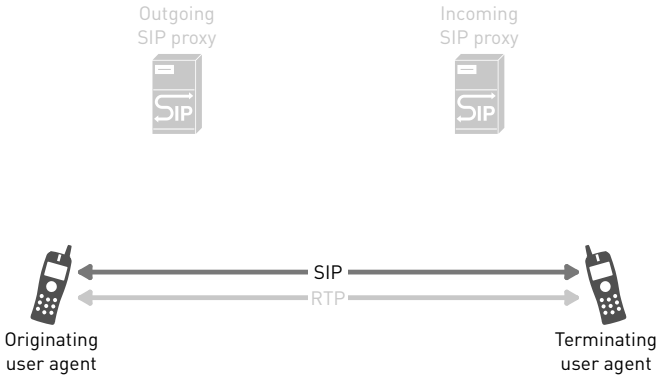

Fig. 4. SIP trapezoid within a direct connection.

his messages are rejected. Therefore, he can use the temporary SIP URI list.

Direct SPIT is a bit different from SPIT via Proxy, as shown in Figure 4. The message is sent directly to the callee's user equipment using the temporary SIP URI.

Where is the disadvantage for a detection system in this case? No proxy is involved in the message flow and no filtering can be applied to the message. Most user equipments are not designed to handle spam by themselves. It is very likely that spammers would use this form of SPIT because of these problems.

This is the reason why Direct SPIT is the most dangerous form of SPIT. A mechanism is needed that is able to analyze the message flow within the user equipment. However, there are only few processing resources in the user equipment for this kind of processing available.

The session establishment in the Direct SPIT scenario is much more dangerous, because no VoIP proxy is involved in this process. Indeed, temporary SIP URIs are only assigned for relatively short periods of time. Therefore, a spammer must possess a very up-to-date list of addresses to perform an attack this way. Nevertheless, a secure mechanism is required to prevent legitimate VoIP users from this attack due to the very high threat of it.

C. Sending Message

The transmission of the message itself can start after the connection is established. There are multiple possibilities for the sending process, related to the sort of message. They differ in terms of distribution or message type and can be described as follows:

- Call center: A call center consists of several people who talk to their customers personally. The assignment of a call center agent to a customer is usually performed by a computer system. Therefore, it can produce a lot of SPIT. However, such a call center requires a lot of money to operate, because of costs for employees, rooms, and equipment.
- Calling bot: A calling bot is a piece of software that establishes connections to the victims automatically. As soon as the session is built up, a prerecorded message is transmitted, then the session is terminated. It is inexpensive in comparison to a call center, because no staff or large rooms are required. Nevertheless, it is able to distribute a high amount of SPIT.
- Ringtone SPIT: Some user equipments are capable to understand the Alert-Info header field [12] of an INVITE request. It specifies an alternative ring tone to the user agent. The ring tone is referred to with a Uniform Resource Identifier (URI). This URI contains an audio advertisement as an alternative ring tone. Therefore, the callee does not have to accept the call to get the message. His own user equipment starts immediately to play this message to him.

The most problematic SPIT source is a call center, because legitimate call centers exist, too. This legitimate call centers traffic is hard to differentiate from those sent from illegal call centers.

Regardless of the SPIT source, additional purposes are possible. Most SPIT messages are sent with the intent to advertise a product or service. Unfortunately, there is the possibility of a SPIT message with the only aim to disturb the callee. Therefore, all kinds of annoying VoIP calls are considered as SPIT in the scope of this article.

D. Relevance of Spam over Internet Telephony

To determine the influence of SPIT on networks and society is difficult. Anyway, no empirical survey concerning SPIT exists so far.

One opportunity to find out its influence is to look at the impact of e-mail spam. Regarding to Jennings, costs caused by spam consists of three main components [4]. As depicted in Figure 5, the major component (85 %) is a loss of user productivity. This term refers to all costs, which are caused if an employee is not able to perform his work. An employee has to take a break from his work to check his e-mail account. He has to check each e-mail to be able to delete spam, to look for false positives, etc. Then he has to continue his original work after that, which needs some extra time.

It is highly probable that this will be a major factor regarding SPIT as well. It is even worse than that. An employee has to check his e-mails manually before he loses time of his original work. SPIT disturbs him for each incoming message, because his phone rings automatically.

Additionally, SPIT requires much more network resources than e-mail spam. This is because of the fact that VoIP consumes much more bandwidth than e-mails.

III. Related Work

There are a lot of techniques that could be applied against SPIT. However, only some of them are applicable to Direct SPIT. These techniques are introduced in this section.

A powerful technique against e-mail spam is content filtering. Unfortunately, this is not applicable against SPIT.

Content filters have a lot of time to check the mail before it is sent to the recipient. Unfortunately, the content of a call is not available in advance. However, SPIT has to be detected

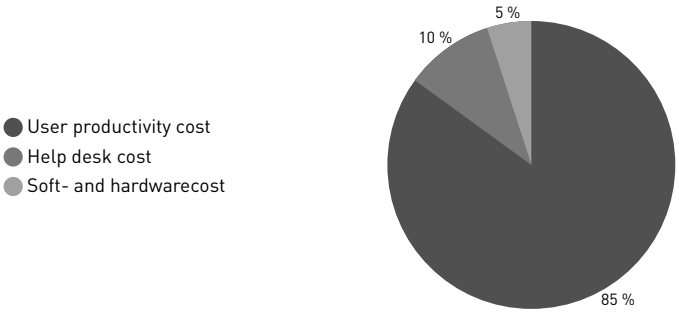

Fig. 5. Percentage of economic damage caused by e-mail spam [4].

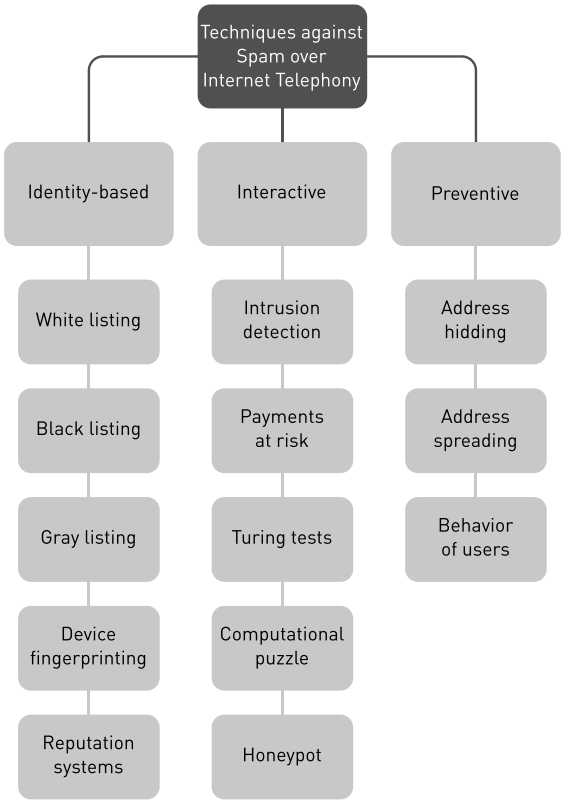

Fig. 6. Categories of techniques against SPIT.

before the phone is ringing, because the callee is actually annoyed when that happens.

So, it is important to look at the capabilities of the available user equipment. A usual phone is not able to process large amounts of data or to store much information. Some techniques against SPIT are depicted in Figure 6. These are discussed in more detail in the following.

A. Identity-based Techniques

Identity-based techniques attempt to avoid SPIT by the analysis of static information. They are able to fend spam utilizing only few resources in hardware and processing time. These techniques are the following:

- White listing: A white list is a list, which contains a collection of addresses of trusted users. Only calls from addresses that are present in this list are allowed to connect to the callee. The decision is made by comparing the address of the sender to the entries in this list.
  An attacker needs good knowledge about the social connections of his victim to bypass white listing. It is a very strong protection against unwanted communications, but on the opposite side is it too strong. All regular people cannot contact a protected user as long as they are not listed.
- Black listing: A black list is the technique opposite to white listing. All calls from addresses on the list are rejected.
  It is rather easy to bypass black listing. An attacker only has to change the source of his message, after he realizes that he is blocked. A service provider has to be very careful before he black lists a participant, because he must avoid listing a legitimate one.
- Gray listing [13]: The main disadvantage of black- and white listing is that the caller has to be known in advance. In this case, a gray list is applicable. Here, an initial call attempt is generally rejected. If the caller starts a second call attempt in a given time, his call gets connected to the callee.
  This technique is rather simple to bypass for an attacker by calling a second time if the first time misses. However, it is annoying for the caller to be rejected after an initial call attempt if he is not known in advance (e.g., a bank clerk).
- Device fingerprinting [14]: This technique analyzes the structure of the message or user equipment behavior to decide whether to accept the call attempt or not. Therefore, knowledge about behavior and message structure of well-known user equipment has to be available. The call attempt gets connected if its structure or the calling user equipment's behavior is successfully identified.
  This technique uses the assumption that spammers use their own self made soft phones, which are able to distribute more SPIT. An attacker who uses a common soft phone cannot be rejected by this technique. However, a spammer only has to imitate a known soft phone if he makes his own one.
- Reputation systems [15]: Each user gets an individual rating derived from user-based evaluations. Users with good ratings are allowed to call and users with bad ratings are blocked.
  This technique originates from e-commerce. Therefore, it suffers the same problems with reputation mafias. These try to increase (ballot stuffing) or decrease (bad mouthing) the reputation score [16]. This could be done by a botnet, for example.

The techniques belonging to this group are the easiest to implement in user equipment. Only device fingerprinting needs too much up-to-date information to work properly. So, it cannot be used to fend Direct SPIT directly.

TABLE I
CPT EXAMPLE FOR REQUEST INTENSITY [17].

	INVITE	REGISTER	ACK	CANCEL	BYE
Regular attack	30 %	10 %	30 %	10 %	10 %
Scan attack	40 %	5 %	40 %	10 %	5 %
SPIT	40 %	0 %	40 %	0 %	20 %
Denial of service	90 %	10 %	0 %	0 %	0 %
Password cracking	10 %	40 %	40 %	0 %	0 %
Firewall traversion	40 %	0 %	40 %	0 %	20 %

B. Interactive Techniques

Interactive techniques are designed to increase the cost for the distribution of SPIT. Their purpose is to raise that cost as much as possible to make SPIT too expensive for the sender. A description of these techniques follows:

- Intrusion detection [17]: This technique analyses the network traffic and compares it to usual traffic. It is designed for multiple network attack, but can also be used against SPIT. Intrusion detection cancels the call attempt if the traffic looks similar to an attack.
  The decision whether a flow is an attack or not is made with a conditional probability table (CPT). This CPT contains expected information about request intensity, error response intensity, number of destinations, etc. Many transmitted INVITE requests may be a probable indicator for SPIT, as depicted in Table I. Unfortunately, there is no knowledge about SPIT attacks and their behavior. Therefore, the CPT of the intrusion detection system can only be filled with information based on assumptions.
- Payments at risk [18]: The caller has to send a small amount of money to the callee. He gets his money back if the callee declares that the call was desirable. This technique leads to a direct increase of costs.
  Unfortunately, this technique generates a huge amount of financial transactions. Furthermore, it is problematic if the SPIT is initiated by a soft phone, which is remote-controlled by a bot.
- Turing tests [19]: A Turing test has the purpose to differentiate between human and machine. Therefore, a sound file is played to the caller. The sound file contains a short voice message, maybe in a dialect or containing background noise. Here, the sound file is relayed to a human, who solves it. The caller gets connected if he repeats this message correctly.
  This technique can be bypassed by a relay attack. Therefore, the sound file is relayed to a human, who solves it. This can be done by a call center, for example.
- Computational puzzle [15]: A computational puzzle is designed to increase the required hardware resources and calling time of the spammer. The calling user equipment has to calculate a task, which is very hard to solve. The caller gets connected after the correct result is transmitted.
  However, a computational puzzle is not able to prevent a victim from SPIT. The soft phone of a spammer is able to solve the task as well. Therefore, the result of a computational puzzle is only an increase of processing time at the caller.
- Honeypot [15]: Honeypots try to bind resources of spammers as long as possible. An incoming call is processed very slowly to bind the spammer's user equipment.
  A honeypot can be used as a SPIT monitoring system as well. It records all information about incoming SPIT and, therefore, allows an analysis of it.

Turing tests and computational puzzles are the weakest of these techniques. A spammer still gets connected even if a computational puzzle is in use. A Turing test does not represent a prevention for SPIT that is sent from a call centre. However, this group of techniques needs too many resources to run on user equipment and hence to be implemented within.

C. Preventive Techniques

Preventive techniques have the purpose to avoid SPIT before it occurs. The main goal is to keep spammers from gathering addresses.

Unfortunately, these techniques are not designed to work on user equipments. They concern the behavior of the user. This cannot be done by any equipment.

IV. CALLER PRE-VALIDATION MECHANISM

The callee's user equipment has to decide about the confidentiality of an incoming call. Therefore, a pre-validation mechanism is presented in this section.

A. Requirements

The pre-validation mechanism has to fulfill some requirements in order to be useful. Furthermore, it has to match some additional requirements, because it will be used in our research project Next Generation Telco Factory (NextFactor). They have the objective to enable a better integration as well as higher security. These requirements are the following:

- Standard compliant: The concept should work without any changes or preconditions to the equipment of the caller and service provider. A mechanism without this constraint would not work while the spammer uses a non-compliant soft phone or service provider. Furthermore, all requests should be used in their specified meaning.
- Open source software: The NextFactor research project uses open source software from its very beginning. This demands to use future open source components to fulfill the license requirements of the ones, currently in use. These yet used software is under the terms of the GNU General Public License version 2 (GPLv2) [20]. Therefore, the future software must also be compliant to this license.

These requirements should improve the quality of the resulting mechanism. The standard conformity is important, to ensure success.

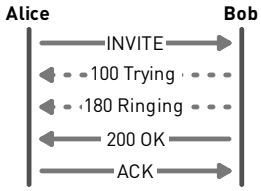

Fig. 7. Progression of a usual incoming call.

B. Analysis

Even with the lot of techniques presented in Section III, there is no feasible protection against Direct SPIT possible. The most techniques are designed to work in the proxies of the provider's network. Unfortunately, these proxies are bypassed by Direct SPIT. A technique is needed that is able to prevent Direct SPIT with the capabilities of usual user equipments.

Three problems could be identified:

- Lack of information in the user equipment: Most techniques require very up-to-date information to work properly. A listing technique cannot act against a spammer before the list does not know that he is a spammer. This information is much easier to distribute between proxies of the provider's network.
- Lack of processing power: For example, an intrusion detection mechanism requires too much processing power to run efficiently on a user equipment.
- Lack of time: The user equipment starts to ring immediately, after an initial INVITE request arrives, as shown in Figure 7. This is expressed with the optional 180 Ringing response sent back after the arriving INVITE request (and the also optional 100 Trying response). Therefore, there is no time left to do any validation. Nevertheless, it is still too late at the moment the phone starts ringing, because this disturbs the callee.

Let assume, that the callee's user equipment has enough time. It needs at least a little information about the caller, to verify his existence. There is only one INVITE request available at that time. Anyway, there is useful information about the caller in the SIP URI of the request (e.g., sip:alice@example.com):

- The user name (i.e., "alice").
- The name or IP address of the provider being used (i.e., "example.com").

It is important to keep the 180 Ringing response until validation succeeds. Therefore, the user equipment has time to validate the caller.

C. Concept

The user equipment has only a little information about the caller, as explained above. Now it has to validate its correctness. However, there is still no guarantee that SPIT will not occur. It can only be assured that the caller is registered. This is important, because it is very likely that spammers use Direct SPIT, since they do not want to use valid accounts. The named provider is able to admonish a user, after he sends SPIT if he is a registered user of the provider. There are two steps to perform after separating the 100 Trying and 180 Ringing response, as visible in Figure 8:

- Check the existence of the caller at the provider.
- Check the existence of the caller's user equipment.

The call attempt can be rejected if this information is not correct, because the caller is not trustable. The call establishment can proceed if the existence of the calling user is confirmed.

Therefore, a way to validate the existence of the user at the named provider is needed. The SIP Specific Event Notification [19] is helpful to do this. It provides several event packages for different scenarios. The following event package-based mechanism and event packages are applicable to the Direct SPIT:

- Presence event package [21]: This package allows getting information about the presence state of a user. A presence state is the willingness and ability of a user to communicate. It is widely common in instant messaging. The subscriber is notified if the requested user changes his presence state (e.g., from "present" to "away").
- INVITE-initiated dialog event package [22]: This package has the purpose to inform a subscriber if the requested user changes his dialog state. It is usable with all SIP messages that result in a dialog (e.g., INVITE, SUBSCRIBE). The requesting user gets a NOTIFIY request if such a dialog changes his state (e.g., "terminate").
- Dialog Event foR Identity VErification (DERIVE) [23]: This mechanism makes use of the INVITE-initiated dialog event package to verify that the current caller is in the correct state (i.e.,"Proceeding"). Besides, the state is verified that the caller is a known member of the alleged service provider. The outcome of the use of DERIVE can result in three cases.
  The call is verified if the SUBSRIBE request is answered with a 200 OK response. The correct state of the caller is confirmed in the following NOTIFY request.
  The call cannot be verified if the service provider of the caller does not support the Dialog Event Package. A 489 Bad Event response returns to show this. Nevertheless, the call attempt is accepted, because it is not mandatory to support this event package.
  The call attempt is suspicious if the answer indicates that

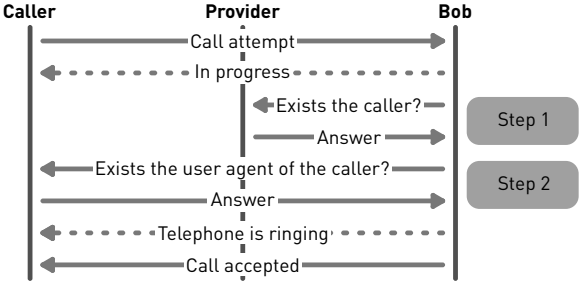

Fig. 8. Conceptual changes in a call attempt.

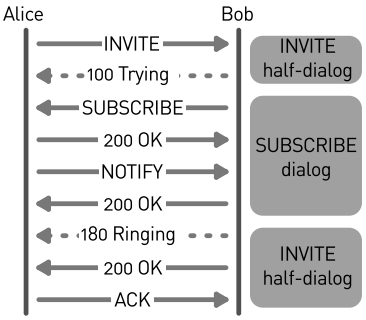

Fig. 9. Overview of DERIVE operation [23].

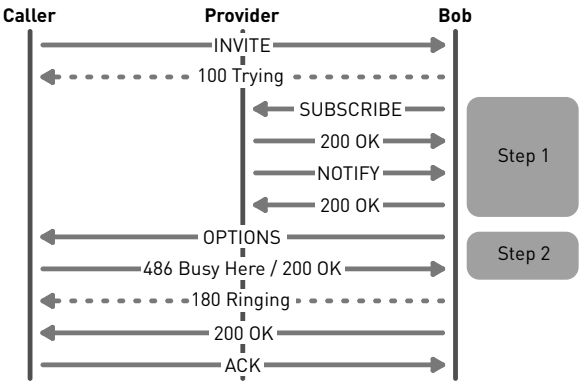

Fig. 10. Released changes in a call attempt.

the caller is not currently in the proceeding state. Therefore, the call attempt is rejected with a 434 Suspicious Call response.

The next validation step can be started if the user's existence at the provider has been validated. It is desired to validate the user equipment of the caller. This validation is important, because otherwise probable spammers are able to send messages with incorrect IP addresses.

Spammers are not able to start a bidirectional communication with an incorrect IP address, maybe it is only desired to disturb the callee. Therefore, spammers only have to send one INVITE request, because most user equipments starts to ring immediately.

A request can be sent to the calling equipment directly to validate the user equipment. The following three requests are the most suitable:

- MESSAGE: This request transmits a text message to its destination. The use of this request has some disadvantages. A second validation could be started if the recipient wants to validate the request as well. This leads to a loop if he uses the same validation. Additionally, it is possible to annoy a uninvolved third user if the caller sends an assigned IP address.
- INVITE: The purpose of the INVITE request is to establish a phone call. It has the same disadvantages as the MESSAGE request. Additionally, it is possible to connect the callee to a premium rate service with high rates, for example. However, the callee has to act by himself to become a victim of such an attack.
- OPTIONS: The OPTIONS request is normally used to determine the capabilities of user equipment. A communication is not established, so the disadvantages of the above requests do not apply here. The receiving user equipment does not act recognizably for its user and, therefore, does not annoy him.

D. Proof of Concept

The presented concept was implemented with Android 1.5 [24] and the VoIP client sipdroid 1.0.8 [25].

The Presence Event Package is used to validate the existence of the user at the provider, as depicted in Figure 10. This decision is made because the Dialog Event Package requests some information, which has nothing to do with the existence of the user. Using the presence state fits better to this task. It is a more expressive information about the "current" existence.

The validation of the user equipment is done by sending the OPTIONS request, because this is the only request without the disadvantage of possible annoyances. However, the contact header field of the NOTIFY request is validated before the OPTIONS request is sent. The OPTIONS request is not sent if it contains the temporary SIP URI of the caller. The existence of the user equipment is validated by comparing its address to the sender's address of the INVITE request, instead of sending the OPTIONS request. Therefore, the transmission time for this request is saved.

E. Restrictions

The presented mechanism is not able to work in every possible network configuration. Most of all, a presence server is required, which is not mandatory for a standard SIP configuration. However, future VoIP networks most likely include a presence server, as the IP Multimedia Subsystem (IMS) [26] concept becomes more popular. A 434 Suspicious Call response [23] could be sent out if the caller has no presence server available. Therefore, he gets adequate information why his call attempt is rejected.

Another scenario where no pre-validation is applicable is an anonymous caller. Anonymous calls are still known from public switched telephony. These calls are often mistrusted, because the callee expects that the caller has something to hide. In the sense of this behavior is it most fitting to sent a 433 Anonymity Disallowed response [27] to the caller. A caller who really wants to call the callee can see the reason of the rejection and call again without anonymity.

V. Attacking Scenario

The proposed caller validation has a main vulnerability. Let assume that the attacker has at least one valid account (i.e., sip:dummy@example.com) in the provider's network of the target, as depicted in Figure 11. The spammer calls Bob by his temporary SIP URI from a second unregistered account (i.e., sip:spammer@192.0.2.1). Then the INVITE request contains the information that it is allegedly sent from the registered

account. The provider confirms this request and sends a NOTIFY request, due to the fact that this account is registered.

This NOTIFY request must contain the header field "contact". It is not specified, which address has to be written in there. Hence, two possible scenarios can occur:

- The contact address in this message contains the temporary SIP URI of the registered account. Therefore, the user equipment rejects the call attempt, because it differs from the one in the INVITE request.
- The contact address does not contain the temporary SIP URI. Instead, there is maybe the address of the presence server. Now, the OPTIONS request is sent to the permanent SIP URI. However, this message is transmitted to the registered account of the spammer that really exists. So, the validation succeeds, too.

The proposed caller validation mechanism offers no protection in the second scenario. However, this attack works only if the presence server does not sent the temporary SIP URI of the spoofed account.

VI. Performance Analysis

It is obvious that the proposed mechanism requires more time to process than a normal call attempt. This section contains an analysis about this durational increase and its amount.

A. System Under Test

To determine the difference in processing time, a system with a 1.66 GHz dual core processor, 2 GB memory and a 6 Mbps internet connection was used. The SIP proxy of the provider was located in Denver (USA) Caller and callee were located in Darmstadt (Germany). The distance between Denver and Darmstadt is about 8,000 km, which results in 200 ms round-trip time with 17 hops. The caller pre-validation prototype was launched inside the Android Emulator.

B. Key Performance Indicator

One key performance indicator was defined to ensure stable and comparable measurement results. The start trigger of the time measurement is at the arrival of the INVITE request, as depicted in Figure 12. The stop trigger is at the sending of the 180 Ringing response.

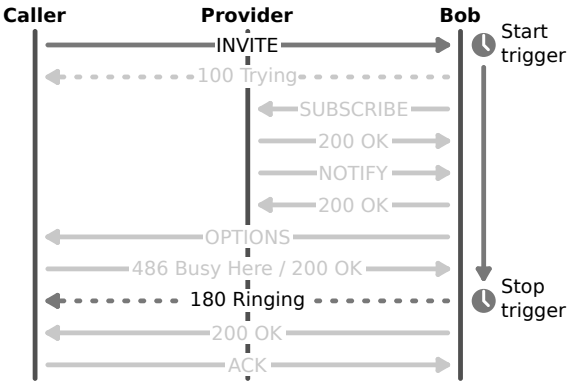

Fig. 12. Start and stop trigger of the service processing time.

The measurement takes place at the user equipment. This should reduce the distortion of the first and last message transmission to the caller, which does not depend on the pre-validation mechanism. The rest of the session establishing process was not measured, because it is the same as without caller pre-validation. The test sequence was repeated a hundred times.

C. Test Results

The regular sipdroid needs an average of 2.821 s to produce an answer, the prototype sends the answer after 5.240 s. A five-number summary of the results is listed in Table II and depicted in the box plot in Figure 13. It is obvious that the maximum results are outliers, because they are that much away from the box. Both clients show a similar behavior in processing and answering. This leads to the assumption that the mechanism has no negative influences on stability.

To confirm this assumption, the 95 % confidence interval was calculated. Itis shown in Table III and Figure 14. Both expected values are located within the same range. The main difference is that the caller pre-validation prototype requires about 2.5 s longer to process an answer. These 2.5 s contains a round-trip delay of 0.2 s per message to Denver and hence

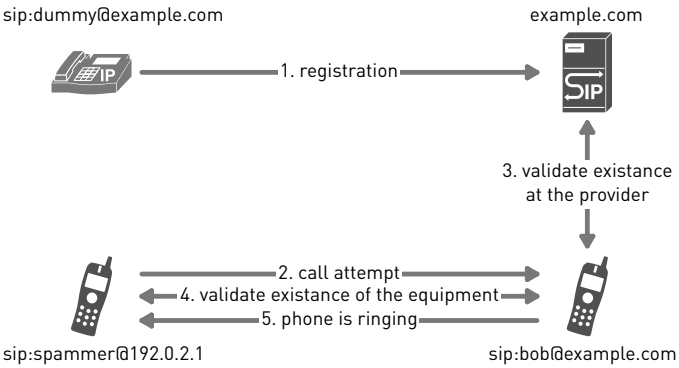

Fig. 11. Successful attacking scenario.

TABLE II
Five-number summary of the test results.

	Minimum	1. quartil	Median	3. quartil	Maximum
Sipdroid	2,405 s	2,531 s	2,837 s	3,000 s	3,538 s
Prototype	4,759 s	5,016 s	5,186 s	5,417 s	6,003 s

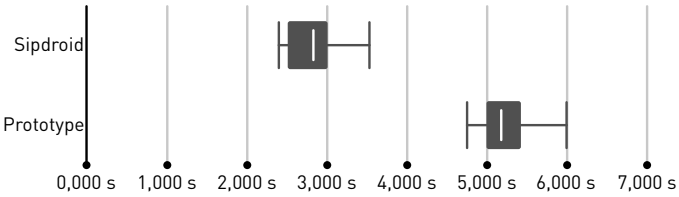

Fig. 13. Box plot.

TABLE III
VALUES OF THE 95 % CONFIDENCE INTERVAL.

	Lower	Average	Upper
Sipdroid	2,764 s	2,821 s	2,879 s
Prototype	5,181 s	5,240 s	5,298 s

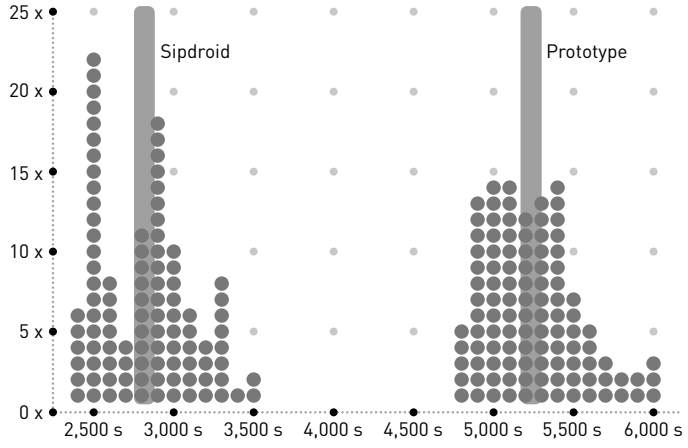

Fig. 14. 95 % confidence interval.

is smaller if a local provider is used.

These additional 2.5 s are only relevant to the caller. A callee never notices this time span, because his user equipment does not ring until it is done. Furthermore, this is an additional time needed for spammers. They can send less spam per hour if a huge number of their victims use this mechanism. So, this approach could be treated as an interactive technique to make spamming unprofitable.

It has to be mentioned that these results are based on a prototype that still needs some optimization. Its only purpose was to provide a proof of concept.

VII. Conclusion and Future Work

The defense against Direct SPIT is relevant for a large number of internet users who want to communicate over the internet via VoIP. The caller pre-validation mechanism introduced in this article is able to fend Direct SPIT sent from unregistered users. This is important because it is probable that spammers use Direct SPIT from unregistered accounts in order to be undetectable. However, the presented mechanism is only able to validate the correctness of the given user information. Furthermore, even a registered user is able to send SPIT. There is no guarantee that SPIT will not occur while using this mechanism. However, the caller's provider is capable to take measures against such users.

The prototype is currently in an alpha phase. It has to be implemented more efficiently, because a delay of 2.5 s is still a lot of time. This delay is indeed only observable for a caller – but this can be a legitimate caller, too. Therefore, the transmission of the SUBSRIBE and OPTIONS requests have to be made in parallel. The goal is to drop the delay to 50 % of the achieved value. The comparison of the temporary SIP URI in the NOTIFY and INVITE request can be performed after all responses have arrived.

Furthermore, an analysis has to be conducted regarding opportunities to fix the weakness in the attacking scenario described in Section V. If it is possible to fix the vulnerability, this would be included in the concept as well as in the prototype.

Additionally, the blocked callers could be added to a gray- or black list to save some time and processing power for an additional call attempt.

The prototype will be included into other VoIP clients as soon as it will be running robustly and more efficiently. Therefore, an implementation for a research project of the Department of Computer Science will be made.

VIII. Acknowledgements

We would like to thank Rachid El Khayari from the Fraunhofer Institute for Secure Information Technology for his wise support, which makes this work possible. We would also like to thank our valuable reviewers especially Torsten Wiens for his extensive and high quality comments.

References

[1] J. Müller and M. Massoth, "Defense against direct spam over internet telephony by caller pre-validation," in *Proceedings, The Sixth Advanced International Conference on Telecommunications (AICT 2010), 9-15 May 2010, Barcelona, Spain*, J. E. Guerrero, Ed. Los Alamitos, CA, USA: IEEE Computer Society, 2010, pp. 172–177.

[2] *The IT Security Situation in Germany in 2009*, Federal Office for Information Security, Bonn, Germany, Jan. 2009.

[3] *MessageLabs Intelligence August 2010*, MessageLabs, New York, NY, USA, Aug. 2010.

[4] R. Jennings, "Cost of spam is flattening," Ferris Research Blog, http://www.ferris.com/2009/01/28/cost-of-spam-is-flattening-our-2009-predictions/ 20.01.2011.

[5] *The Carbon Footprint of Email Spam Report*, McAfee, Santa Clara, CA, USA, 2009.

[6] M. Machowinski and D. Myers, "Trend toward hosted and business voip services seen across three new reports," Infonetics Research Press Release, Apr. 2010.

[7] Federal Association for Information Technology, Telecommunications and New Media, "Erstmals mehr als 10 millionen nutzer von internet-telefonie," Press statement, Apr. 2010.

[8] E. Potter, "Number of mobile voip users will approach 300 million by 2013," In-Stat Press Release, Mar. 2010.

[9] R. El Khayari, N. Kuntze, and A. U. Schmidt, "Spam over internet telephony and how to deal with it," in *Proceedings of the ISSA 2008 Innovative Minds Conference, 7 - 9 July 2008, School of Tourism & Hospitality*, H. S. Venter, M. M. Eloff, J. H. P. Eloff, and L. Labuschagne, Eds. Johannesburg, South Africa: University of Johannesburg, 2008.

[10] *Why Am I Getting All This Spam?*, Center for Democracy & Technology, Washington, DC, USA, Mar. 2003.

[11] T. Eggendorfer, *No Spam! Wie Spam gar nicht erst entsteht*, 1st ed. Frankfurt am Main, Germany: Software & Support, 2005.

[12] J. Rosenberg, H. Schulzrinne, G. Camarillo, A. Johnston, J. Peterson, R. Sparks, M. Handley, and E. Schooler, "Sip: Session initiation protocol," RFC 3261, IETF, Jun. 2002.

[13] E. Harris, "The next step in the spam control war: Greylisting," http://projects.puremagic.com/greylisting/whitepaper.html 20.01.2011.

[14] H. Yan, K. Sripanidkulchai, H. Zhang, Z.-Y. Shae, and D. Saha, "Incorporating active fingerprinting into spit prevention systems," in *3rd Annual VoIP Security Workshop, Berlin, Germany*. New York, NY, USA: ACM, 2006.

[15] J. Rosenberg and C. Jennings, "The session initiation protocol (sip) and spam," RFC 5039, IETF, Jan. 2008.

[16] C. Dellarocas, "Immunizing online reputation reporting systems against unfair ratings and discriminatory behavior," in *The 2nd ACM Conference on Electronic Commerce (EC 2000), Minneapolis, MN, USA – October 17 - 20, 2000*, A. Jhingran, J. K. MacKie-Mason, and D. Tygar, Eds. New York, NY, USA: ACM, 2000, pp. 150–157.

[17] M. El Baker Nassar, R. State, and O. Festor, "Intrusion detection mechanisms for voip applications," in *3rd Annual VoIP Security Workshop, Berlin, Germany*. New York, NY, USA: ACM, 2006.

[18] M. Abadi, A. Birrell, M. Burrows, F. Dabek, and T. Wobber, "Bankable postage for network services," in *Advances in Computing Science – ASIAN 2003: Progamming Languages and Distributed Computation, 8th Asian Computing Science Conference Mumbai, India, December 10-12, 2003, Proceedings*, ser. Lecture Notes in Computer Science, V. A. Saraswat, Ed., vol. 2896. Berlin / Heidelberg, Germany: Springer, 2003, pp. 72–90.

[19] H. Tschofenig, E. Leppanen, S. Niccolini, and M. Arumaithurai, "Completely automated public turing test to tell computers and humans apart (captcha) based robot challenges for sip," Internet-Draft, IETF, Feb. 2008, expired: 28.08.2008.

[20] *GNU General Public License Version 2*, Free Software Foundation, Boston, MA, USA, Jun. 1991.

[21] J. Rosenberg, "A presence event package for the session initiation protocol (sip)," RFC 3856, IETF, Aug. 2004.

[22] J. Rosenberg and H. Schulzrinne, "An invite-initiated dialog event package for the session initiation protocol (sip)," RFC 4235, IETF, Nov. 2005.

[23] J. Kuthan, D. Sisalem, R. Coeffic, and V. Pascual, "Dialog event for identity verification," Internet-Draft, IETF, Oct. 2008, expired: 28.04.2009.

[24] Open Handset Alliance, "Android.com," http://www.android.com/ 20.01.2011.

[25] P. Merle, "sipdroid - project hosting on sip/voip client for android," http://www.sipdroid.org/ 20.01.2011.

[26] Technical Specification Group Services and System Aspects, "Ip multimedia subsystem (ims); stage 2 (release 10)," 3rd Generation Partnership Project, Technical Specification TS 23.228 V10.3.1, Jan. 2011.

[27] J. Rosenberg, "Rejecting anonymous requests in the session initiation protocol (sip)," RFC 5079, IETF, Dec. 2007.

Dynamic Spectrum Sharing in Cognitive Radio Networks: a Solution based on Multiagent Systems

Usama Mir, Leila Merghem-Boulahia, Dominique Gaïti
ICD/ERA, UMR 6279,
Université de Technologie de Troyes,
12 rue Marie Curie, 10010 Troyes Cedex, France
{usama.mir, leila.merghem_boulahia, dominique.gaiti}@utt.fr

Abstract— **In modern day wireless networks, spectrum utilization and allocation are static. Generally, static spectrum allocation is not a feasible solution considering the distributed and dynamic nature of wireless devices, thus some alternatives must be ensured in order to allocate spectrum dynamically and to mitigate the current spectrum scarcity. An effective technology to ensure dynamic spectrum usage is cognitive radio, which seeks the unutilized spectrum holes opportunistically and shares them with the neighboring devices. Using cognitive radio capabilities, the nodes are not restrained to static spectrum utilization, rather they can choose it on demand. However, dynamic spectrum usage raises several challenges, which need to be addressed in detail. These challenges include efficient allocation of spectrum between licensed (or primary) and cognitive radio (or secondary) users in order to maximize spectrum utilization and to avoid device level interferences. To this extend, we develop a novel solution for spectrum allocation using multiagent system cooperation that enables secondary user devices to utilize the amount of available spectrum, dynamically and cooperatively. The key aspect of our design is the deployment of agents on each of the primary and secondary user devices that cooperate in order to have a better use of the spectrum. For cooperation, contract net protocol is used, allowing spectrum to be dynamically allocated by having a series of message exchanges amongst the devices. Simulation results show that our solution achieves up to 80% of the whole utility within the span of few messages, and provides an effective mechanism for dynamic spectrum allocation.**

Keywords- Multiagent Systems; Cognitive Radio; Dynamic Spectrum Sharing; Contract Net Protocol; Cooperation; Ad hoc Networks.

I. INTRODUCTION

In most of the modern day applications, radio spectrum allocation and sharing is a static function, in which the spectrum is assigned to a particular dominant primary (or licensed) user [3], for a long period of time in order to avoid interferences and collisions. Parallel to this, to deal with increasing user demands, dynamic spectrum allocation for new wireless networks is necessary. However, since existing wireless networks occupy extensive parts of the radio spectrum, there is no sufficient spectrum available to all the new unlicensed wireless networks [1] [25]. Thus, research has to be done to address this problem via dynamic sharing and assignment of spectrum. For example, in USA, Federal Communication Commission (FCC) considers to allow sharing of unused portions of TV bands to promote dynamic use of spectrum [2] [4].

One effective technology to alleviate the problem of static spectrum assignment and to maximize dynamic spectrum usage is cognitive radio (CR) [17], a radio in modern wireless systems, in which a CR (or a secondary user) node changes its parameters (transmission or reception) to share the spectrum dynamically and to avoid the interference with the other primary or secondary users. The parameter alteration is done by having some knowledge about the radio environment factors such as radio frequency (RF) signals, device level interferences, etc. To achieve efficient and dynamic allocation of spectrum between highly distributed CR devices, a balanced, simple and cooperative approach is necessary. Research is therefore in progress on exploring the cooperative spectrum sharing techniques in CR networks. Similar to CR network, a multiagent system (MAS) [21] [27] is a system composed of multiple autonomous agents, working individually or in groups (through interaction) to solve particular tasks. Like CR nodes, agents work dynamically to fulfill their user needs and no single agent has a global view of the network. Each agent maintains its local view and shares its knowledge (when needed) with other agents to solve the assigned tasks.

Recent advances in technology (especially in the domain of programmable integrated circuits and distributed artificial intelligence) have created an opportunity for us to develop a new class of intelligent, autonomous, and interactive CR devices [8]. These devices can then be used in a wide variety of network domains (WLAN [48], WRAN [49], MANETs [23]). In addition, an efficiently designed CR with a software agent deployed on it would be capable of interacting with neighboring radios to form a dynamic, loosely-coupled and infrastructure-less collaborative network. While CR physical architecture and its sensing capabilities have received considerable attention [5] [28], the question of how to share radio resources in cooperative scenarios is also an important research issue for current researchers [3] [8] [22].

Therefore, in this paper, a MAS based strategy is proposed for dynamic spectrum allocation. Specifically, we consider a

cooperative MAS [29] [36], in which the agents are deployed over primary and secondary[1] user devices. By cooperative MAS we mean that the primary user agents exchange a tuple of messages and help neighboring secondary user agents to improve their spectrum usage. Moreover, the cooperation mechanism we develop is similar to that of contract net protocol (CNP) [10] [30], in which the individual secondary user (SU) agent should send messages to the appropriate neighboring primary user (PU) agents whenever needed and, subsequently, the related PU agents should reply to these agents in order to make spectrum sharing agreements. We propose that the SU agents should take their decisions based on the amount of spectrum, time and price proposed by the PU agents and should start spectrum sharing whenever they find an appropriate offer (without waiting until the reception of all the neighboring PU agents' responses [14]). Then, after completely utilizing the desired spectrum, SU agents should pay the agreed price to the respected PU agents.

In fact, this work is divided into following four parts:

- First, we present a brief state of the art on various available approaches for spectrum sharing using multiagent systems, game-theoretical approaches and medium access control solutions.
- Second, we detail four different scenarios, in which spectrum sharing challenges need to be addressed in details. We also propose some initiative measures, which are necessary to be taken for efficient utilization of the available spectrum in the mentioned scenarios.
- Third, we present a cooperative framework with the related spectrum sharing algorithms. The proposed MAS is cooperative where PU agents exchange a series of messages to share their spectrum with the requesting SU agents. The more complex scenarios with agents' competitive behaviors will be examined as a part of our future study.
- Finally, we conduct extensive simulations to verify the working of the proposed cooperative algorithms for dynamic spectrum sharing in the context of cognitive radio networks.

The rest of the paper is organized as follows. The following section briefly presents related works. Section III presents four scenarios, in which dynamic spectrum sharing is a vital issue. In Section IV, we describe spectrum allocation problem with the help of an example. In Section V, we propose our model with the interlinked working of various modules and their related algorithms. The experimental setup, some results and discussions are given in Section VI. Section VII concludes our work with the future perspectives.

[1] The words cognitive, secondary and unlicensed user will be used interchangeably throughout the article.

II. PRIOR WORK

Research has been going around for several years in order to apply multiagent systems for decision making process and resource sharing. A rather new application of multiagent systems is for efficient allocation of spectral resources in CR networks. In TABLE I, we give the similarities between an agent and a CR. Basically, both of them are aware of their surrounding environments through interactions, sensing, monitoring and they have autonomy and control over their actions and states. They can solve the assigned tasks independently based on their individual capabilities or can work with their neighbors by having frequent information exchanges.

TABLE I. COMPARISON BETWEEN AN AGENT AND A CR

Agent	Cognitive radio
Environment awareness via past observations	Sensing empty spectrum portions and primary user signals
Acting through actuators	Deciding the bands/channels to be selected
Interaction via cooperation	Interaction via beaconing
Autonomy	Autonomy
Working together to achieve shared goals	Working together for efficient spectrum sharing
Contains a knowledge base with local and neighboring agents' information	Maintains certain models of neighboring primary users' spectrum usage

In literature, few strands of work have focused on spectrum sharing using MAS [13] [37]; but in these works, several limitations exist. For example, in [37], a MAS is used for information sharing and spectrum assignments. All the participating agents deployed over access points (APs), form an interacting MAS, which is responsible for managing radio resources across collocated WLANs. The authors have not provided any of the algorithms and results for their approach. The work in [13] considers a distributed and dynamic MAS based billing, pricing and resource allocation mechanism where the agents work as the auctioneers and the bidders to share the spectrum dynamically. The protocol used for radio resource allocation between the CR devices and operators is termed as *multi-unit sealed-bid auction*, which is based on the concept of bidding and assigning resources. The ultimate aim of using auctions is to provide an incentive to CR users to maximize their spectrum usage (and hence the utility), while allowing network to achieve Nash Equilibrium (a solution concept, where each user is assumed to know the equilibrium strategies of the other users, and no user has anything to gain by changing its own strategy). Auctions have traditional drawbacks of users' untruthful behaviors, which can cause serious drawbacks to the working of loyal users.

Game-theory has also been exploited for spectrum allocations in CR networks [6] [11] [18] [19] [39]. In game-theoretical approaches, each SU has one individual goal i.e., to maximize its spectrum usage and the Nash equilibrium is considered to be the

optimal solution for the whole network (or game). Furthermore, it incorporates two basic assumptions: first, the rationality assumption, that is, the participating primary and secondary users are rational so that they always choose strategies that maximize their individual gain. And, second, the users' common knowledge assumption, which includes the definitions of their preference relationship. These assumptions may behave well by allowing each user (or player) to rationally decide on its best action, although in most of the competitive games, sometimes users can provide false information in order to maximize their profits and thus can affect the whole network performance.

According to some current research works, spectrum sharing problems are similar to medium access control (MAC) issues [9] [32], where several users try to access the same channel and their access should be shared with the neighboring users to avoid the interferences. Generally, in MAC-based spectrum sharing solutions, when a CR user uses a channel, it sends a busy signal to the neighboring users through a control channel in order to avoid the interference. To estimate control signals, the authors of [20] suggest a fast fourrier transform-based radio design, which enables CR users to detect the carrier frequency of a control signal without causing any harmful collisions to the neighboring users. Others [23] suggest the use of a global plan to exchange the control information between CR devices. However, maintaining global plans needs a large amount of frequent information to be exchanged between CR users causing complex device level architectural overheads.

III. SPECTRUM SHARING SCENARIOS

Here, we provide some of the possible scenarios, which need the development of new solutions for dynamic spectrum sharing. These scenarios are addressed as a part of a Franco-German project TEROPP [46]. This project aims at developing various efficient spectrum management solutions. Up till now, our contribution to this project is the development of a cooperative approach for opportunistic spectrum allocation. In these scenarios, the current spectrum assignments are static and inter-device collision is a big issue. Therefore, efficient solutions are needed in order to enable dynamic spectrum usage and to avoid interferences. The scenarios are divided into four different domains as follows: (1) Spectrum sharing and interference avoidance in ISM bands, (2) Spectrum sharing in cellular networks, (3) Opportunistic spectrum utilization in TV bands, and (4) Spectrum allocation in ad hoc networks. After detailing and suggesting possible initiatives towards dynamic spectrum access, we will describe our cooperative framework as a solution to enable spectrum sharing under ad hoc network domain. Precisely, multi-hop architectures, topology changes and arrival and departure of nodes at any time are the reasons for developing a cooperative solution for dynamic spectrum sharing under ad hoc network setting.

A. Spectrum Sharing and Interference Avoidance in ISM Bands

Recently, WLAN [26] has been adopted as a common technology by internet home users and companies. Characterized by cheap devices and reasonable data-rates, WLANs can be deployed anywhere. Designed to operate over license-free ISM (Industrial, Scientific and Medical) bands, WLANs are restricted to employ only few orthogonal channels, which is more than enough to provide wireless access in a residential area. However, the huge increment in the number of WLANs operating in the same location introduced a new interference level that could be anarchic. This interference is considered to be the main limitation for WLANs performance and it introduces new challenges to all the neighboring technologies that operate in the ISM bands [26]. Similar problems may arise with the deployment of LTE femto-cells [40]. These small cells, located at a home or a building, can provide better coverage and higher capacity in indoor environments. However, they suffer from interference caused by the neighboring femto-cells. The common point of introducing these two cases is that the interference is most of the times unwanted and it needs to be avoided.

As an interference avoidance solution, we foresee a cooperative environment where the devices in a WLAN or LTE cell can have CR capabilities, which allow them to optimize frequency reuse. They can also select an alternative spectrum portion, in case of any interference. Then, they can send the newly searched spectrum portion information to the neighboring devices in order to avoid the possible collisions.

B. Spectrum Sharing in Cellular Networks

This scenario explains the spectrum sharing issues for cellular networks where the area is administrated by a central entity (such as a base station) and it is able to impose basic etiquettes to the users [7]. The mobile users (having CR capabilities), can perform signal measurements and can apply the etiquettes in order to contribute to an efficient use of the available spectrum. These etiquettes may be in the form of behavioral rules, such as, using correct MAC address, switching to a convenient base station and transmitting measurement reports. In such a context, distributed operational modes will be privileged and different overlay functions may be implemented such as rendezvous facilities [16], in order to optimize frequency reuse and to enable efficient usage of available bands.

A hospital can be considered as an application example of this scenario, where the number of users cannot be determined in a precise way. With the CR capability, a given terminal (a doctor's iPhone or a PDA) might be able to sense the best possible spectrum band. This band can then be shared and coordinated with the neighboring devices by having a series of interactions using multiagent systems and by taking into account the number of current users and their priorities. The shared band information can then be sent to the BS agent for the administrative purposes.

C. Opportunistic Spectrum Utilization in TV Bands

The European countries are working on improving their TV services by stopping the broadcast of PAL (phase alternative line) signals and using DVB-T (digital video broadcasting-transmitter) standards instead [41]. This process will create a sufficient amount of unused spectrum resources especially in the case of digital dividend [45]. Let us explain the exploitation of ultra high frequency (UHF) bands to understand the concept of numerical dividend. Generally, UHF bands are split in channels, where channels 21 to 69 were originally assigned to TV services. These channels are 8MHz in width, and the channel 21 corresponds to the bands 470-478 MHz. A DVB-T covers a city and its neighboring sectors, and uses 6 UHF channels to broadcast 36 TV programs. For example, in France, nearly 100 DVB-transmitters are used for broadcasting TV programs [42]. In a given place, we can expect that the TV services use only 6 among 49 UHF channels, leaving 43 channels as unutilized. These huge amounts of empty spectral resources justify the world interest for TV bands.

In a conference held under WRC'07 (World Radiocommunication Conference) [44], discussions about the utilization of the TV bands have already been started. The researchers have decided to assign the UHF channels 60 to 69 to IMT (International mobile telecommunication) services. Another initiative is taken by the European countries with the creation of the task group 4 (TG4) [43]. TG4 is responsible for measuring the performance of DVB-transmitters in order to utilize the unused TV bands opportunistically. These measurements will then be compared with the results obtained from mobile devices working in WiMAX.

To summarize, we provide here a few steps to be taken for the opportunistic utilization of spectral resources in digital dividend as following:

- At first, DVB-transmitters must have the capabilities of cognitive radios for sensing, characterizing and monitoring the unutilized TV bands. This is possible with the development of efficient signal processing techniques.
- Then, because DVB-transmitters normally share their spectral resources with the radio microphones, therefore more precise spectrum sharing techniques must be deployed.
- Finally, some techniques must be ensured in order to differentiate between a DVB-T and a microphone signal.

D. Spectrum Allocation in Ad hoc Networks

Here, we give an example of an SU equipped with CR capabilities and agent functionalities. The user is in a remote or an emergency situation, where it does not have direct access to radio resources and its access technology requires an energy that the user does not own. In this situation (as shown in Figure 1), SU senses the nearby signals of primary users PU1 and PU2 (step 1) and cooperates with the agents deployed on them (step 2). This cooperation process allows SU to act on primary users' responses by utilizing their available spectrum (step 3). Thus, the cognitive radio capability of an SU plays the role of interoperability, such that it can receive the information about neighboring users' spectrum bands and their access technology. Likewise, the role of the deployed agent is to cooperate and modify SU's software configuration by loading the necessary algorithms that fit the best to the current state (step 4).

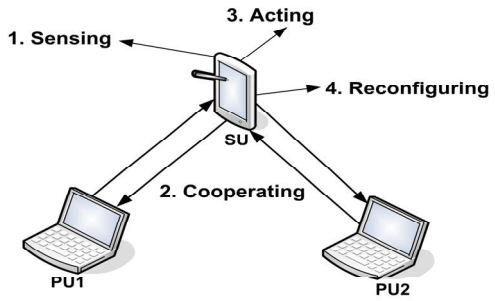

Figure 1. Description of an ad hoc scenario

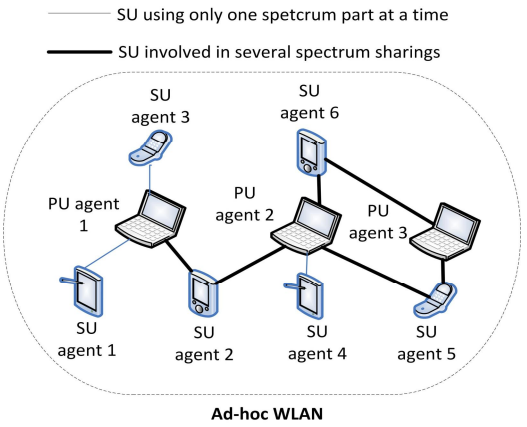

Figure 2. Ad hoc WLAN with three primary and six secondary users

IV. PROBLEM STATEMENT

In the above scenario, we have presented the role of an agent and a CR in an ad hoc emergency situation. However, considering a more general and practical perspective, we address the spectrum allocation challenges in a private ad hoc area or a well identified administrated perimeter such as a campus, a conference center or a hospital. Note that our proposed algorithms can also be easily applied for the emergency ad hoc network scenario.

. In our proposed scenario (Figure 2), there is an ad hoc WLAN [15], deployed in the area with sets of primary $PU = (PU_1, PU_2 \ldots PU_n)$ and secondary $SU = (SU_1, S_2 \ldots SU_m)$ users. To allow nodes to communicate, the agents are deployed

at each of them Whenever an SU device detects an empty portion of the spectrum as needed by its user, its agent starts communicating with the relative PU agent (having that empty spectrum part), until a spectrum sharing agreement is been made.

A. Formalization

Let $G = (N, A)$ be a directed network consisting of a set of mobile nodes N such that $(SU \cup PU) \in N$ and a set of directed arcs A. Each directed arc $(i, j) \in A$ connects a secondary user SU_i to a primary user PU_j. Similarly, we can denote the directed arc $(j, i) \in A$ to show the direction of connection from PU_j to SU_i. The secondary users are cooperating with the neighboring primary users to have a spectrum sharing deal. We assume that s_{ij} is the amount of spectrum a secondary user 'i' is desiring to get from a primary user 'j'. Similarly, t_{ij} is the amount of time, for which 'i' wants to utilize the spectrum and p_{ij} is the price it is willing to pay to 'j'. For the primary user 'j' on the other hand, s_{ji} is the amount of spectrum it is willing to share with 'i', t_{ji} is the respected time limit and p_{ji} is the price it is expecting to get after sharing its spectrum. We can formulate the above model for each secondary user 'i' as:

$$\text{Maximize} \sum_{(i,j)\in A} s_{ij} t_{ij} \qquad (1)$$

Subject to

$$\text{Minimize} \sum_{(i,j)\in A} p_{ij} \quad \forall\, SU \in N \qquad (2)$$

Similarly for primary users:

$$\text{Maximize} \sum_{(j,i)\in A} p_{ji} \qquad (3)$$

Subject to

$$\text{Minimize} \sum_{(j,i)\in A} s_{ji} t_{ji} \quad \forall\ PU \in N \qquad (4)$$

And

$$l_{ji} \le s_{ji} \le u_{ji}$$

where l_{ji} and u_{ji} are the lower and upper bounds of available spectrum of primary user 'j'. This means that the secondary user 'i' cannot ask for an amount of spectrum above this limit.

B. An Example

In static circumstances, the spectrum portions are assigned to primary users and in response the internet service providers get their spectrum price. As an example consider a primary user PU_j, who has bought a portion of a spectrum of the size of 8MB (Figure 3). During the peak office timings (t_0-t_1), the assigned portion may remain busy (or used) due to high user traffic such as for video conferencing and lecturing, but most of the other times (t_1-t_2 and t_3-t_n) the spectrum can remain unused. Obviously at free timings, PU_j can utilize its spectrum portion for other activities (e.g., watching video songs) but generally people prefer these kinds of activities to be performed on week-ends. With our proposed solution, a given secondary user SU_i will be able to choose the best spectrum band/channel dynamically. This choice is made in cooperation with the agent embarked on PU_j [35], by taking into account the amount of spectrum needed, the respected time limit and the related price.

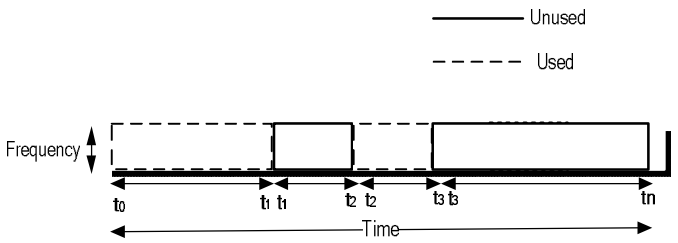

Figure 3. An example of a primary user's spectrum utilization during a day

V. COOPERATIVE SOLUTION FOR DYNAMIC SPECTRUM SHARING

In this section, we explain the proposed cooperative spectrum sharing scheme, with primary and secondary user's internal architectures and their algorithmic behaviors.

A. Agent

We start here by defining an agent as a dynamic and loosely coupled unit, having the capabilities of performing a task autonomously, based on the knowledge received from its environment and/or through other agents' interactions. These loosely-coupled units then work together to form a multi-agent system [21] [27]. Generally, an agent is appropriate and relevant for an SU node in a sense that it allows the introduction of various artificial intelligence (AI) techniques [12] to CR networks and helps an SU node to behave more efficiently by having frequent interactions with its neighboring devices. Once in place, cooperative multiagent systems have the potential of increasing the SU capabilities in a variety of ways. For example, a single SU agent is limited in its knowledge (and information) about spectrum access, but a bundle of SU agents can collectively identify spectrum holes and can communicate them to other nodes.

B. Contract Net Protocol

In multiagent literature, several approaches exist for cooperation [12]. Amongst these approaches, contract net protocol (CNP) [30] [34] is the most simple way for agents' cooperation and decision making. In CNP (Figure 4), the collection of agents is called *contract net* and several agents can form these nets in order to solve the assigned tasks. Each agent can either be a *manager* or a *contractor*. Basically, the *manager* agent initiates a task to the *contractor* agents by sending *Call for Proposals (CfPs)* messages. As a result, various eligible

contractors show their interest (in solving the task) by sending their *proposals*. The *manager* selects the best proposal (via *accept*) and the contract is then awarded to the selected contractor. The selected contractor solves the assigned task as agreed with the corresponding manager. Due to its simple and efficient nature, our proposed approach is based on bilateral message exchange and task allocation mechanisms of CNP.

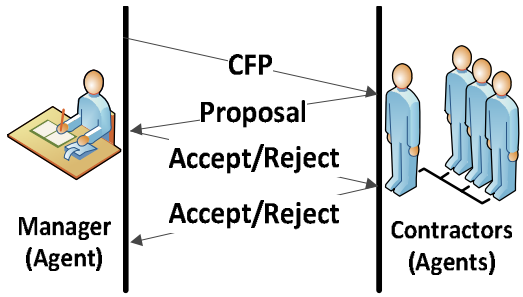

Figure 4. Message exchange in CNP

C. Working of the Proposed Solution

The SU based design (Figure 5 and algorithm. 1) consists of the following five different interlinked modules.

- First, the *dynamic spectrum sensor (DSS)* is used to sense the empty spectrum portions (or spectrum holes). Several techniques exist for spectrum sensing such as PU's weak signal and its energy detection [28], cooperative centralized detection [5], etc. For DSS, it is necessary that the sensing is performed by considering a real-time dynamic environment, because it is not obvious at what time a spectrum band is occupied or when it is free.

- The second module *spectrum characterizer (SC)* characterizes the spectrum holes based on the Shannon's theorem [33] to create a capacity based descending ordered list of all available PUs.

- *Secondary user interface (SUI)*, which is the third part sends a *request* message to the SU device agent, whenever a user wants to have a portion of spectrum (for internet surfing, watching high quality videos, etc).

- The fourth part, *agent's knowledge module (AKM)* gets PU characterization information from SC, which serves as a motivation for agents that subsets of PUs having vacant spectrum spaces are available. This list is not permanent rather it is updated and maintained on regular time intervals based on the information provided by SC module. Moreover, AKM creates a *CfP* message based on the inputs from *SUI* and *SC*:

CfP (SUID, s, t, d)

where *SUID* is the secondary user ID (or the secondary user's agent identification) and it is used to help PU to reply back to the corresponding SU, *s* is the amount of spectrum needed by the SU, *t* is the desired time limit (or holding time) for the spectrum utilization, and *d* is the deadline to receive the primary users' proposals.

- Finally, *agent coordination module (ACM)* geo-casts the *CfP* to the neighboring (and currently available) PU agents. By available PUs, we mean that the PU agents have not yet left the one-hop neighborhood and they have some unused spectrum to share. Moreover, *ACM* is also responsible for selecting the most suitable received *proposal*.

Having received the *CfPs*, the interested PU agents send their proposals to the corresponding SU agents. The proposal is in the following form:

Proposal (PUID, s, t, p)

where *PUID* is the primary user's agent identification, *s* is the amount of spectrum PU is willing to give to the respected SU, *t* is the proposed spectrum holding time, and *p* is the price PU is willing to receive. Note that the PU agent only contains *AKM* and *ACM* modules, where *AKM* manages the neighborhood information and *ACM* selects the most suitable *CfP* via cooperation.

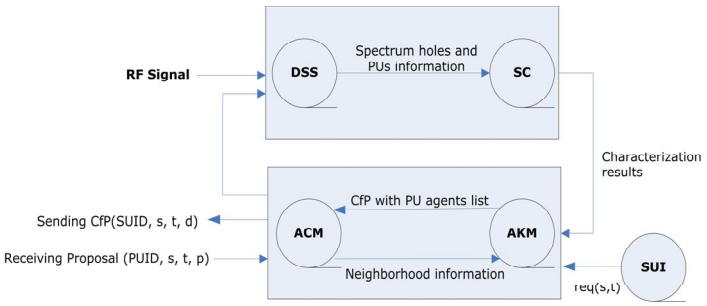

Figure 5. Working of CR and agent modules

Each PU maintains an ordered list of *CfPs* in its cache based on the values of *s* and *t* for the purposes of future cooperation (algorithm 2). At the same time, the receiving SU locally sorts fetched *proposals* and an *accept* message is sent to the most suitable proposal. The information of selected PU is also sent to *AKM* (of SU) for future interactions. In case of an *accept* message from the selected SU, the spectrum sharing is started based on agreed parameters from both the sides. PU can still respond to further *CfPs* if it wants its other unused spectrum portions to be shared. If the PU receives a *reject* message from SU, it continues sending proposals to further available *CfPs*, for which the deadline is not yet expired.

Algorithm 1: Behavioral Algorithm for an SU

```
Init – Let PU be the set of primary users in secondary user agent's
one-hop neighborhood and ℓ is the time interval based on the
information provided by the SC module in order to maintain capacity
based ordered list of primary users.
        /* SU characterizes each primary user on the basis of
        capacity*/
        For each i{ i∈ PU) } do
                Eval (SNR(i))
                /* SNR: is the primary user's signal to noise ratio
                obtained through DSS */
                Eval (B(i))
                /* B: bandwidth of PU given by DSS*/
                C(i)= B(i) log2 [1 + SNR(i)]
                /* c: capacity calculated using Shannon's
                theorem*/
        End For
        /*Sending of CfP message*/
        If PU != {}
                For each i ∈ PU
                        /*Geo-cast CfP*/
                        Send CfP (SUID, s, t, d) to PU(i)
                End for
        End If
        /*L is a list for saving received proposals*/
        For each received proposal 'm' do
                Characterize m using s(m)×t(m) / p(m) and add it in L
        End For
        If L={} and the deadline to receive proposals has expired
                Recreate CfP
        Else If L={i} where i is the only element in L and deadline
        for proposal reception has expired
                        Send an accept message to i
        Else
                        Send accept to primary user
                        corresponding to the best proposal
                        Send reject to all other primary users
        End If
```

Algorithm 2: Behavioral Algorithm for a PU

```
While busyflag = false do
        If received message = CfP
          /*K is a list for saving received CfPs*/
          For each received CfP 'n' do
                Characterize n using p(n) / (s(n)×t(n)) and add it in K,
                where p(n) is related price according to required
                spectrum
          End For
          For best CfP in K do
                Construct a proposal (PUID,s,t,p) and send it to
                corresponding secondary user
          End For
        End If
        If received message = accept
             Start spectrum sharing with selected secondary user
        End If
        If received message = reject OR some unused spectrum
        parts are still available
                Continue analyzing further CfPs for spectrum
                sharing
        Else
                Set busyflag = true
        End If
End While
```

Above we have presented a cooperative framework for spectrum allocation that can generate highly effective behavior in dynamic environments and achieve better utility of the participating agents. The proposed solution is based on multiagent system cooperation with the deployment of agents over primary and secondary users. The experimental evaluations presented in the following section will confirm the efficiency of our proposal for dynamic spectrum allocations.

VI. EXPERIMENTS AND RESULTS

In this section, we present some simulation results, conducted in order to validate the working and performance of the proposed spectrum allocation algorithms. We start by examining the achieved utility of both primary and secondary users and then compare the time values, for which the spectrum is being utilized. We also present the spectrum gain and loss with the amount of messages used for cooperation. The words (PU, PU agent, SU, SU agent respectively) are used interchangeably throughout the following section.

A. Simulation Setup

We perform our simulations under the assumption of a noiseless and mobile ad hoc network. By mobile ad hoc we mean that the nodes in the neighborhood of each of the SUs change. We randomly place a number of primary and secondary users in a specified area where each of the devices contains an agent deployed over it for cooperation purposes. For simplicity, two different fixed values of times (such as T1 and T2) are assumed, where "Time 1" (T1) represents the short-term case and "Time 2" (T2) is the longer period. When T1 is considered, the SU agents can ask for an amount of spectrum within one hour limit (i.e., $0 \leq T1 \leq 60$Minutes) and similarly this limit is within two hours, as in case of T2 (i.e., $0 \leq T2 \leq 120$Minutes). These two approximations capture the same amount of time values in real wireless environments without delving into complex situations. Our simulation starts with the total number of 6 SUs and 4 PUs, and for each next round there is an addition 10 agents (i.e., 6 SUs and 4 PUs). The simulation is conducted for 10 subsequent rounds, with a total of 20 hours per day, for both T1 and T2 respectively and the average values of parameters are taken to draw the graphs. The PU agent's utility is calculated as the price paid by SU agents for spectrum utilization divided by the amount of spectrum it has shared for the respected time period (holding time) as required by the SUs. The SU agent's utility is represented as its spectrum usage for the required time divided by the corresponding price paid to the PUs. Thus, by assigning weights or priorities to each of the mentioned parameters, the appropriate utility values for both the primary and secondary users are chosen.

We assume that each PU has random available spectrum portions and the neighborhood of SUs and PUs is randomly changing. Also, we follow the assumption that once agreed, PUs would not be able to withdraw their commitments and they

should share their spectrum with the corresponding SUs for the agreed time period. Further, the total number of cooperation messages (*CfP*, *proposal*, *accept* and *reject*) generated in the system, determine the cooperation cost. Thus, the cooperation strategy that is better (both between T1 and T2) in terms of less number of messages and, which gives good utility values is considered as the most cost efficient. The total number of resources successfully shared (over the number of resources required) presents the success rate, while the number of non-allocated spectrum portions (due to disagreements between primary and secondary user agents) measures the overall spectrum loss. All the experiments were realized using JADE [47] on a PC with 3GB memory and 2.4 GHZ dual processor.

B. Results

In Figure 6, we compare the average utility of each primary and secondary user at T1 with those at T2 for different numbers of users (10, 20, 30…). The figure depicts that when time limit is T2, the utilities are a bit less compared to the results obtained at T1. This is because the environment is mobile and some of the users are slightly hesitant to share their spectrum for longer periods. We observe that when there are 10 agents, the average utility values are almost identical for both T1 and T2, showing the optimal behavior. But in other cases, the average utility values are different, showing that the performance of agents in terms of their average utility values has decreased slightly with the increased number of agents.

Figure 7 illustrates the spectrum resource requirements and utilization over time periods T1 and T2. In the beginning (with 10 required resources), all of them are completely shared; whereas when the required spectrum resources arrives at the middle values (such as 30 to 40), approximately 90% of them are shared. This spectrum sharing trend continues following the same pattern reaching bigger values (such as 50 and 60), with achieved sum of resources comprised between 45 and 50. Thus, the performance degradation in terms of spectrum sharing is not high, even with large resource requirements.

Our approach is also relative to time, because in CR networks the spectrum holding time is one of the most important factors to be considered. Again, we run the simulation with several values of primary and secondary user agents. Figs. 8 and 9 plot the overall mean times (or holding time), for which the spectrum is required and utilized for a total of 10 to 120 agents. When time limit is T1, the results are almost fully satisfied, for 80 to 120 agents, while the time values are somewhat lesser at T2. Both the results are super linear and coherent with those of Figure 7, which displays that the spectrum sharing remains high even with the larger number of agents.

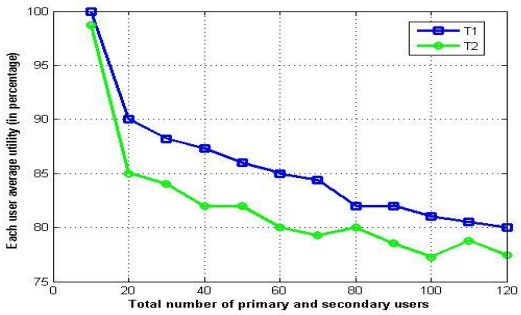

Figure 6. Agents' percentage utilities

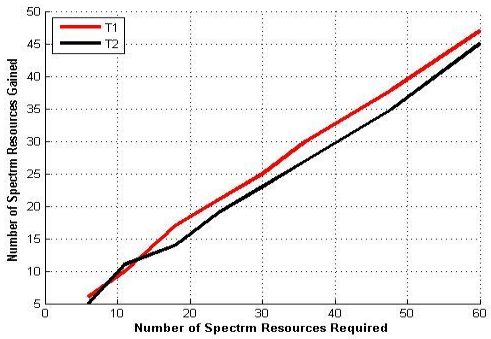

Figure 7. Spectrum resource requirement and utilization by SUs

Figure 10 depicts the maximum number of supported SUs by the neighboring PUs. Supported SUs are those, which have completely gained the required spectrum. We observe that when there are 10 to 15 PUs, the number of supported SUs is literally the same for both T1 and T2. This means, for limited number of agents even if the time values are high, the number of supported SUs is almost the same. However, with large number of agents (more than 50), the number of supported SUs at T2 are slimly lesser than T1. Therefore, in ad hoc situations, if we increase the time values along with an increment in number of agents, the results will be slightly less optimal.

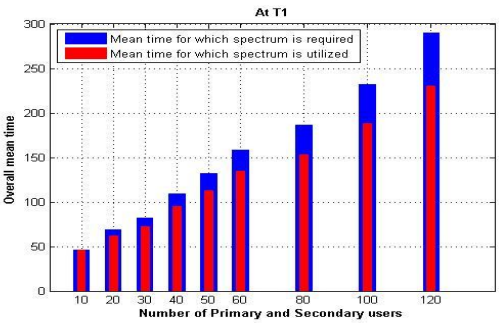

Figure 8. Spectrum holding time at T1

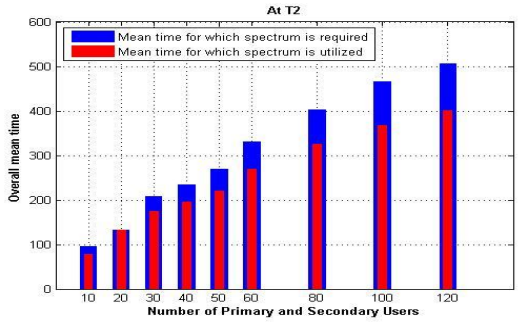

Figure 9. Spectrum holding time at T2

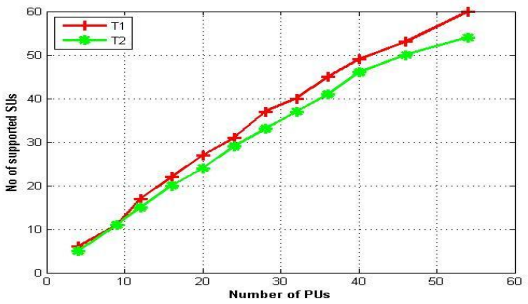

Figure 10. Supported SUs

The number of cooperation messages transmitted and received in the entire system with the success rate (in percentage) is shown in Figure 11 (and Table II). According to Figure 11, the values of exchanged messages are almost leveled off for the middle periods (from 30 to 70 agents). Further, Table II depicts that the average number of messages (per agent) remains between 4 to 5 even with the increased number of agents. We can also see that the approach is linear in terms of messages and success rate. Particularly when time limit is T2 (around 90 to 120 agents), the performance of the approach substantially degrades (reaching below 80%), but nevertheless it remains steady.

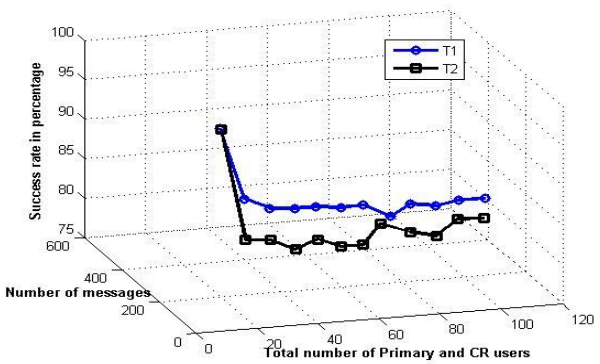

Figure 11. Number of messages with success rate

TABLE II. SUCCESS RATE AND NUMBER OF MESSAGES AT T1 AND T2

No of agents	Number of messages		Success rate (in %)	
	T1	*T2*	*T1*	*T2*
10	45	41	100	98.7
20	81	72	90	85
30	117	115	88.23	84
40	159	161	87.31	82
50	185	176	86	82
60	253	261	85	80
70	271	262	84.41	79.3
80	325	366	82	80
90	388	392	82	78.53
100	416	434	81	77.26
110	475	483	80.5	78.77
120	503	516	80	77.42

Another important aspect of our approach is the analysis of how the performance varies as the amount of participating agents increases. In this context, Figs. 12 and 13 show the overall spectrum loss, which is the loss caused by the unused spectrum, due to spectrum sharing disagreements. As the agents' demands augment, the percentage of spectrum loss grows on a steady pace. This is because some of the SUs are not able to find non-busy PUs or due to the relative change in their neighborhood. From the figures, it is also clear that the amount of overall spectrum loss (for both the time limits T1 and T2) is minimum (10 to 15%), when the number of users are at the middle stages (i.e., around 50). Spectrum loss then reaches bit higher values (16 to 22%), with increase number of agents, but still there is not a rapid degradation in the overall system performance. Note that the other factors such as collisions, device level interferences and delays are not considered here.

C. Discussion Related to Results

The above experiments and results prove that our solution is an effective one in order to provide dynamic spectrum sharing for CR networks and it can provide better utility of agents with the exchange of few cooperation messages. However, there are some important points related to our results, which need further discussion. First, we assume that the ad hoc environment is interference free; however, this assumption is not always true. In reality, the transmission power of most of the devices is so high that they can easily interrupt the working flow of neighboring devices, causing interferences. Thus, addressing spectrum sharing under interference enabled ad hoc networks is still an issue and several researchers are working on solving this issue to the modest details [31] [38].

Next issue is related to the limited number of agents we have used to perform our experiments. Since, JADE only allows a maximum of 100 to 120 agents on a single machine; therefore we have only shown the behavior of our approach with limited number of agents. In order to prove the consistent working of our model with large number of agents, we are working on

developing mathematical model based on Markov chain. This model will also help us to verify other parameters such as communication cost and agents' utility. Though, these mentioned issues need to be addressed in detail, still our model is flexible enough to replicate the real-world network settings where spectrum sharing can be performed in the similar cooperative way.

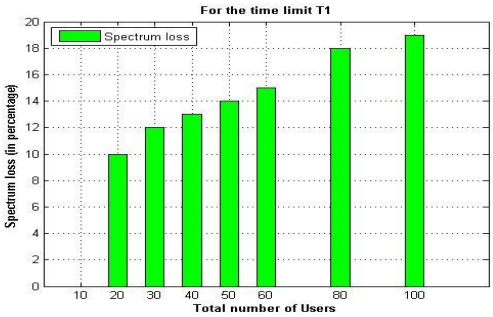

Figure 12. Spectrum loss at T1

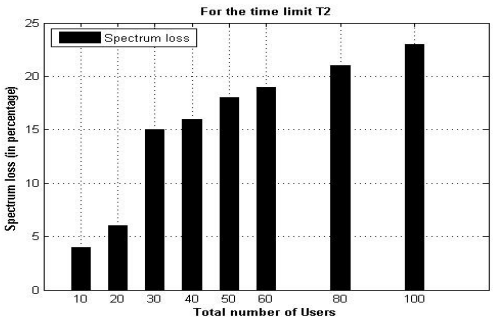

Figure 13. Spectrum loss at T2

VII. CONCLUSION AND FUTURE PERSPECTIVES

In this paper, we developed a cooperative framework for spectrum allocation that can generate highly effective behavior in dynamic environments and achieve better utility of the participating devices. The proposed approach is based on multiagent system cooperation and implemented by deploying agents on cognitive radio and primary user devices. Experimental evaluations confirm the efficiency of our algorithms for distributed and decentralized environments. The results show that the proposed approach can absorb the high spectrum sharing demands by introducing the cooperation between primary and secondary user devices. Furthermore, the proposed approach improves the overall utility and minimizes the spectrum loss with a minimum communication cost. The spectrum allocation success rate is almost 80% even with large number of agents. While we only proposed a specific cooperation strategy to maximize system utility, the proposed cooperation framework can be extended towards minimizing other key problems such as inter secondary user interferences and collisions. We intend to examine this problem as a part of our continuing work. We are currently working on a mathematical analysis of our approach using Markov chain. In addition, the proposed approach assumes that nodes are highly cooperative while in real systems, nodes can be selfish or competitive, so more precise work is needed to explore the competitive behaviors. We will also try to compare the results with game-theoretical approaches to have an even better validation of our work.

ACKNOWLEDGEMENT

This work was co-funded by ANR (French Research Agency) via grant ER502-505E ("Technologies for terminals in opportunistic radio applications") and by Higher Education Commission (HEC) Pakistan.

REFERENCES

[1] "Spectrum policy task force report," ET Docket No. 02–135, (November 2002).

[2] "Unlicensed Operation in the TV Broadcast Bands," Federal Communications Commission, First Report and Order and Further Notice of Proposed Rulemaking. 06-156, October 2006.

[3] B. Canberk, I.F. Akyildiz, and S. Oktug, "Primary user activity modelling using first-difference filter clustering and correlation in cognitive radio networks," Elsevier Science Journal on Ad hoc Networks, vol. 7, pp. 810-836, 2009.

[4] C. R. Stevenson, C. Cordeiro, E. Sofer, and G. Chouinard, "Functional requirements for the IEEE 802.22 WRAN standard," Technical Report, September 2005.

[5] D. Cabric, S.M. Mishra, and R.W. Brodersen, "Implementation issues in spectrum sensing for cognitive radios," Proc. Asilomar Conference on Signals, Systems and Computers, pp. 772–776, 2004.

[6] D. Niyato and E. Hossain, "Competitive pricing for spectrum sharing in cognitive radio networks: dynamic game, inefficiency of Nash equilibrium, and collusion," IEEE Journal on Selected Areas in Communications, vol. 308, pp. 192-202, 2008.

[7] D. Raychaudhuri and X. Jing, "A spectrum etiquette protocol for efficient coordination of radio devices in unlicensed bands," Proc. IEEE International Symposium on Personal Indoor (PIMRC 03), pp. 172–176, 2003.

[8] E. Jung and X. Liu, "Opportunistic spectrum access in heterogeneous user environments," Proc. IEEE New Frontiers in Dynamic Spectrum Access Networks (DySPAN 08), pp. 1-11, 2008.

[9] F. Akyildiz, W-Y. Lee, M. C. Vuran, and S. Mohanty, "NeXt generation/dynamic spectrum access/cognitive radio wireless networks: A survey," International Journal of Computer and Telecommunications Networking, vol. 50, pp. 2127-2159. 2006.

[10] F-S. Hsieh, "Developing cooperation mechanism for multi-agent systems with Petri nets," Engineering Applications of Artificial Intelligence Journal, vol. 22, pp. 616-627, 2009.

[11] G. Hosseinabadi, H. Manshaei, and J-P. Hubaux, "Spectrum sharing games of infrastructure-based cognitive radio networks," Technical report on LCA-REPORT-08-027, 2008.

[12] G. Weiss, "A modern approach to distributed artificial intelligence," MIT press, 2000, USA.

[13] H. J. Kloeck and F. Jondra, "Multi-agent radio resource allocation," ACM Mobile Networks and Applications, vol. 11, pp. 813-824, 2006.

[14] H. M. Kelash, H. M. Faheem, and M. Amoon, "A multiagent system for distributed systems management," Transactions on, Engineering, Computing and Technology, vol. 11, 2006.

[15] I. Doghri and H.K.-B. Ayed, "Towards fair P2P auctions over MANETs," Proc. International Conference on Computer and Information Technology, pp. 658-663, 2008.
[16] I. Romdhani, M. Kellil, H- Y. Lach, A. Bouabdallah, and H. Bettahar, "Mobility-aware rendezvous point for mobile multicast sources," Proc. International Wired/Wireless Internet Communications conference (WWIC 04), pp. 62-73, 2004.
[17] J. Mitola, "Cognitive radio: an integrated agent architecture for software defined radio," PhD Thesis, KTH Royal Institute of Technology, Sweden, 2000.
[18] J. O'Neel, "Analysis and design of cognitive radio networks and distributed radio resource management algorithms." PhD Thesis, Virginia Tech, USA, 2006.
[19] J. Zhang and Q. Zhang, "Stackelberg game for utility-based cooperative cognitive radio networks," Proc. ACM International Symposium on Mobile Ad hoc Networking and Computing (MOBIHOC 09), pp. 23-32, 2009.
[20] K- C. Huang, X. Jing, and D. Raychaudhuri, "MAC protocol adaptation in cognitive radio networks: an experimental study." Proc. International Conference on Computer Communications and Networks (ICCCN 09), pp.1-6, 2009.
[21] K. P. Sycara, "Multiagent systems," Artificial Intelligence Magazine, vol. 19, pp. 79-92, 1998.
[22] K.R. Chowdhury, M.D. Felice, and I.F. Akyildiz, "TP-CRAHN: A transport protocol for cognitive radio ad hoc networks," Proc. IEEE Conference on Computer Communications (INFOCOM' 09), pp. 2482-2490, 2009.
[23] L. Ma, X. Han, and C-C. Shen, "Dynamic open spectrum sharing MAC protocol for wireless ad hoc networks," Proc. IEEE New frontiers Dynamic Spectrum Access Networks (DySPAN'05), pp. 203-213, 2005.
[24] L. Panait, and S. LukeOn, "Cooperative multi-agent systems learning: state of the art," Proc. Autonomous Agents and Multi-Agent Systems (AAMAS'05), pp. 387–434, 2005.
[25] M. Mchenry, "Spectrum white space measurements," New America Foundation Broadband Forum, June 2003.
[26] M. Sawan, H. Yamu, and J. Coulombe, "Wireless smart implants dedicated to multichannel monitoring and microstimulation," IEEE Circuits and Systems Magazine, vol. 5, pp. 21-39, 2005.
[27] M. Wooldridge, "An Introduction to Multiagent Systems," John Wiley & Sons Press, 2002, England.
[28] N. Sahai, Hoven, and R. Tandra, "Some fundamental limits in cognitive radio," Proc. Allerton Conference on Commonunication, Control and Computing, 2004.
[29] P.J. Denning and C. Martell, "Coordination," Springer Verlag, 1998, USA.
[30] R. G. Smith, "The contract net protocol: High-level communication and control in a distributed problem solver," IEEE Transactions on Computation, vol. 29, pp. 1104–1113, 1980.
[31] S. J. Kim and G. B. Giannakis, "Optimal resource allocation for MIMO ad hoc cognitive radio networks," Proc. International Conference on Communication, Control and Computation, pp. 39-45, 2008.
[32] S. Kumar, V. S. Raghavan, and J. Deng, "Medium access control protocols for ad hoc wireless networks: a survey," International Journal of Ad hoc Networks, vol. 4, pp. 326-358, 2006.
[33] T. C. Clancy, "Dynamic Spectrum Access in Cognitive Radio Networks," PhD Thesis, University of Maryland, USA, 2006.
[34] T. Sugawara, T. Hirotsu, S. Kurihara, and K. Fukuda, "Effects of fluctuation in manager-side controls on contract net protocol in massively multi-agent systems," Proc. IEEE International Conference on Distributed Human-Machine Systems (DHMS'08), 2008.
[35] U. Mir, L. Merghem-Boulahia, and D. Gaïti, "Utilization of a cooperative multiagent system in the context of cognitive radio networks," Proc. IEEE International Workshop on Modelling Autonomic Communications Environments (MACE'09), pp. 100-104, 2009.
[36] U. Mir, L. Merghem-Boulahia, and D. Gaïti, "A cooperative multiagent based spectrum sharing". in Proc. Advanced International Conference on Telecommunications (AICT'10), pp. 124-130, Barcelona, 2010.
[37] X. Jiang, H. Ivan, and R. Anita, "Cognitive radio resource management using multi-agent systems," Proc. Conference on Consumer Communications and Networking, (CCNC'07), pp. 1123-1127, 2007.
[38] Y. Su and M. Schaar, M, "A new perspective on multi-user power control games in interference channels," IEEE Transactions on Wireless Communications, vol. 8, pp. 2910–2919, 2009.
[39] Z. Ji and K. Liu, "Dynamic spectrum sharing: A game theoretical overview," IEEE Communications Magazine, vol. 45, pp. 88-94, 2007.
[40] http://mobiledevdesign.com/tutorials/lte-femtocells-0603/, Feb. 03, 2011
[41] http://www.dvb.org/ , Jan. 12, 2011
[42] http://www.dvb.org/about_dvb/dvb_worldwide/france/, Jan. 31, 2011
[43] http://www.ero.dk/TG4, June. 06, 2010
[44] http://www.itu.int/ITU-R/index.asp?category=conferences&rlink=wrc-07&lang=en, Sept. 02, 2007
[45] http://ec.europa.eu/information_society/policy/ecomm/radio_spectrum/topics/reorg/pubcons_digdiv_200907/index_en.htm, Sept. 04, 2009
[46] TEROPP,http://era.utt.fr/fr/projets_de_recherche/carnot_teropp.html, Jan. 11, 2011
[47] http://jade.tilab.com/, July. 07, 2010
[48] http://ayman.elsayed.free.fr/msc_student/wlan-tutorial.pdf, June 2002
[49] http://ieeexplore.ieee.org/stamp/stamp.jsp?tp=&arnumber=4085653, Feb. 08, 2007

APPENDIX

Abbreviations

ACM agent coordination module, 6
AI artificial intelligence, 5
AKM agent's knowledge module, 6
APs access points, 2
CfP call for proposal, 6
CNP contract net protocol, 2
CR cognitive radio, 1
DSS dynamic spectrum sensor, 6
DVB-T digital video broadcasting- transmitter, 4
FCC federal communication commission, 1
ISM industrial, scientific and medical, 3
JADE java application development framework, 8
LTE long term evolution, 3
MAC medium access control, 3
MANETs mobile ad hoc networks, 1
MAS multiagent system, 1
PAL phase alternative line, 4
PDA personal digital assistant, 3
PU primary user, 2
PUID primary user's agent identification, 6
RF radio frequency, 1
SC spectrum characterizer, 6
SU secondary user, 2
SUI secondary user interface, 6
SUID secondary user's agent identification, 6
TG4 task group 4, 4
UHF ultra high frequency, 4
WRAN wireless regional area network, 1
WLAN wireless local area network, 1
WRC world radiocommunication conference, 4

Low Complexity Enhanced Hybrid Spectrum Sensing Architectures for Cognitive Radio Equipment

Ziad Khalaf, Amor Nafkha, and Jacques Palicot
SUPELEC/IETR
SUPELEC,Avenue de la Boulaie,CS 47601
35576 Cesson Sévigné Cedex, France
Email: {ziad.khalaf,amor.nafkha,jacques.palicot}@supelec.fr

Mohamed Ghozzi
R-Interface, Ercom Group
9 Grand'Rue 13002 Marseille, France
Email: mohamed.ghozzi@ercom.fr

***Abstract*—Spectrum sensing enables detecting opportunities in licensed bands in order to access unused portions of the licensed spectrum. In this paper we propose two low complexity detectors based on a combination of two well-known and complementary signal detection mechanisms: energy detection and mono-cycle detection, which exploits cyclostationarity property of the signals. In the first algorithm the mono-cycle detector iteratively corrects the thresholds of a double threshold energy detector, that will finally converge to the performance of the mono-cycle detector. The second algorithm uses the mono-cycle detector to directly estimate the noise level N_0, which is used to fix the threshold of the radiometer. Simulation results conducted on different environments show promising performances of the proposed detectors especially in low SNR.**

***Index Terms*—Cognitive Radio, Spectrum sensing, Energy detector, Detection features.**

I. Introduction

The term "Cognitive Radio", defined by J.Mitola [2] was reused by the FCC [3] to define a class of radio systems that continuously perform spectrum sensing, dynamically identify vacant (unused) spectrum and then operate in this spectrum at a time when it is not used by incumbent radio systems.

The increasing in telecommunication services number and rates has led to a growing demand of spectrum resources. The objective of cognitive terminals is to obtain independently and dynamically radio frequencies to access the network. Large parts of the spectrum allocated to licensed radio services (referred to as primary users, PUs) have exclusive access rights. However, secondary users (SUs) can still access opportunistically to the spectrum held by the PUs when they are not using it.

As they do not have full access rights, SUs must guarantee to not cause harmful interference to PUs. Hence they need to monitor the spectrum continuously to detect if PUs resumed their communications. For that purpose, it has been suggested by the FCC to use Cognitive Radio based technology to help SUs filling these requirements. In that case Cognitive Radios (CRs) must stop and transfer their activities to another vacant band. CRs need to be more sensitive than PUs and efficient at lower SNR to detect PUs signals.

Various spectrum sensing techniques have been presented as noticed in [4] including *the classical likelihood ratio test (LRT) [5], energy detection (ED) [5]–[7], matched filtering (MF) detection [5], [8], cyclostationary detection (CSD) [9]–[13],* and some newly emerging methods such as *eigenvalue-based sensing [14]–[16], wavelet-based sensing [17], covariance-based sensing [18], and blindly combined energy detection [19]*. In this paper, our focus is on energy and cyclostationary detection. However, for other different methods of spectrum sensing in cognitive radio, we advise the readers to refer to [4], [20]. Energy detection is the simplest detection method but needs the exact knowledge of the noise level N_0; furthermore, a wrong estimation is known to seriously impact the detection performance [6]. Cyclostationary detection was proposed as an alternative since noise is stationary whilst telecommunication signals are rather cyclostationary. The advantage of cyclostationary methods is that it does not need any knowledge about the noise level N_0 and allows the detection at low SNR. However, one major drawback of cyclostationary detection is that it requires high computation time and needs a high sampling rate. In this paper, we propose a modified version (M-HSD) of the HSD proposed in [1], and an Enhanced HSD (EHSD) algorithms that combine cyclostationary and energy detection, to detect the free spectrum. Taking into consideration the limitations of the energy detector performance due to presence of noise uncertainty and background interference, the idea of this paper is to reduce the uncertainty over the noise level N_0 using the help of cyclostationary detection. Two kind of strategies can be applied, the first one (M-HSD) uses an iterative approach: at the beginning of the sensing, we can usually fix two thresholds ξ_1 and ξ_2 for the energy detector. Then, the detection is given by the following process: if the energy detector criteria is greater (*resp.* smaller) than ξ_2 (*resp.* ξ_1) then this indicates the presence (*resp.* absence) of the primary user signal. Else if the energy detector criteria is inside the interval $[\xi_1, \xi_2]$, then cyclostationary detection can be applied and based on its decision, the hybrid architecture can iteratively adjust the thresholds of the energy detector, to finally converge to the performance of the cyclostationary

detector. The second approach (EHSD) consists in directly estimating the noise level N_0 using the cyclostationary detector and uses this estimation to obtain the appropriate threshold of the radiometer.

The remaining part of the paper is organized as follows. In Section II, we present the system model adopted throughout this work. We briefly describe energy and cyclostationary detectors in Section III. The proposed HSD architecture will be recalled in Section IV. The M-HSD architecture will be presented in Section V. In section VI, EHSD algorithm is proposed. Section VII presents simulation results and discussions. Finally, Section VIII presents the conclusions of this study and makes some suggestions for future work.

II. System model

The spectrum sensing detection problem consists of collecting a set of N samples $y_1, y_2, ..., y_N$ from a given frequency band B, processing the data by a Neyman-Pearson receiver, which takes the form of a Likelihood Ratio Test (LRT) and deciding for that frequency band whether or not a primary user is present. Let $\mathbf{y}$ denotes the vector formed by N samples, $\mathbf{y} = [y(1), .., y(N)]^t$, where the samples are realizations of the random variables $Y_1, Y_2, ..., Y_N$, respectively. The LRT compares a statistic λ to a fixed threshold ν. The statistic λ is the ratio between the joint Probability Density Function (PDF), $p_Y(\mathbf{y}|H_1)$, of the N samples given that a primary user is present and the joint PDF, $p_Y(\mathbf{y}|H_0)$, of N samples given that no primary user is present. H_1 and H_0 denote the binary hypotheses that a primary user is present and absent, respectively. This ratio is called Likelihood Ratio (LR). The threshold ν is determinated by constraining the probability of false alarm to a specified value.

The binary hypotheses (H_0, H_1) are defined in a way such that, under hypothesis H_1 and $k \in [1, .., N]$, the k^{th} collected sample, $y(k)$, is composed of a primary user signal sample, $x(k) \sim \mathcal{N}(0, \sigma_x^2)$, affected in different ways by the channel, $h(k) \sim \mathcal{N}(0, 1)$, plus an additive Gaussian noise sample, $n(k) \sim \mathcal{N}(0, \sigma_n^2)$, where $\mathcal{N}(m, \sigma^2)$ denotes the normal distribution with mean m and variance σ^2. Under hypothesis H_0, the k^{th} sample, $y(k)$, consists of the additive Gaussian noise sample $n(k)$. Hence,

$$\begin{cases} H_0 : y(k) = n(k) \\ H_1 : y(k) = h(k)x(k) + n(k) \end{cases}$$

The LRT then takes the form

$$\lambda = \frac{p_Y(\mathbf{y}|H_1)}{p_Y(\mathbf{y}|H_1)} \lessgtr_{H_1}^{H_0} \nu$$

For $\lambda > \nu$, H_1 is decided, otherwise H_0 is decided. Assuming that the samples are statistically independent, the joint PDF $p_Y(\mathbf{y}|H_i)$; $i \in \{0, 1\}$, is nothing but the product of the N marginal PDFs of the samples. Specifically,

$$p_Y(\mathbf{y}|H_i) = \prod_{k=1}^{N} p_{Y_k}(y_k|H_i);\ i \in \{0, 1\}$$

The performance of any spectrum sensing methods is indicated by two probabilities: the detection probability, P_d, which defines the probability of the sensing algorithm having detected the presence of the primary signal under the hypothesis H_1; probability of false alarm, P_{fa}, which defines the probability of the sensing algorithm claiming the presence of the primary signal under the hypothesis H_0. In the hypothesis testing problem, where we have to decide whether the primary signal is present or absent, two kinds of errors can occur:

- A false alarm occurs when it is decided that the primary signal is present even though it is not.
- A miss detection occurs when it is decided that the primary signal is not present even though it is.

The performance, of sensing algorithm, is usually presented using a family of curves showing the detection probability P_d as function of the false alarm probability P_{fa} (*Cf.* Figure 1). The test is good when these curves are located above the chance line that characterizes pure hazard. In literature, this representation is called ROC curve (*R*eceiver Operational Characteristic) [21].

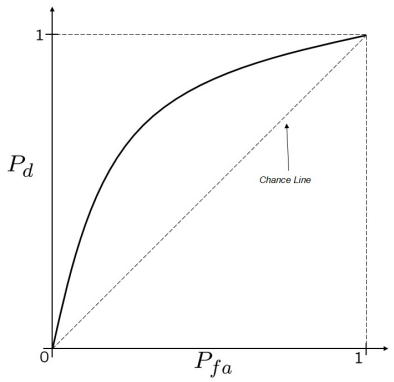

Fig. 1. Example of ROC curve showing the probability of detection P_d according to the probability of false alarm P_{fa}

III. Sensing Methods

A. Generalities

The optimal sensing detector needs to know the values of channels gain, noise and primary user's variance. In practice, we may have no knowledge about the values of some or all of these parameters. In these cases, an approximation of the optimal test is done in the case of Gaussian signals with low level compared to noise (assumed white and Gaussian). It is given by the locally optimal test [21], which uses only second order statistics of the signal. Application of Taylor's theorem yields the following statistical test:

$$Z = \frac{1}{N_0^2 T} \int_{-T/2}^{T/2} \int_{-T/2}^{T/2} R_{xx}(u, v) y(u) y(v) du dv \lessgtr_{H_1}^{H_0} \xi \quad (1)$$

With $R_{xx}(u, v)$ is the autocorrelation function and T is the listening duration before the detector takes any decision. Thus, the new detector calculates a quadratic transformation of

the received signal and compares the result to a detection threshold. However, in the case of low SNR, it is shown in [22] that this locally optimal detector remains valid even in the case where the signals of interest are not Gaussian. Depending on the chosen statistical model of the observation $x(t)$, two types of detectors can be derived. For a stationary model, the detector is the energy detector or radiometer. It is a simple detector with low complexity and reduced time of computation, but has the disadvantage of being sensitive to a bad estimate of the noise level N_0. For a cyclostationary model of $x(t)$, the detector is the mono or multi-cycles detector. This detector is able to detect in low SNR, and is insensitive to the poor estimate of noise level, but has the disadvantage of an important computing time.

B. Energy Detection

When the statistical model of the signal of interest $x(t)$ is chosen to be stationary, the autocorrelation function $R_{xx}(u,v)$ becomes dependent only of the difference $u-v$ and it can be written under this form: $R_{xx}(u,v) = R_{xx}(u-v)$.

By performing variable changes according to:

$$u = t + \frac{\tau}{2}$$
$$v = t - \frac{\tau}{2} \tag{2}$$

we obtain the following local optimal detector form [23]:

$$Z_{ro} = \frac{1}{N_0^2} \int_{-\infty}^{\infty} R_{xx}(\tau) R_{yy}(\tau)_T d\tau \tag{3}$$

where $R_{yy}(\tau)_T$ is the correlogram of $y(t)$ defined by :

$$R_{yy}(\tau)_T \triangleq \begin{cases} \frac{1}{T} \int_{-(T-|\tau|)/2}^{(T-|\tau|)/2} y(t-\frac{\tau}{2}) y(t+\frac{\tau}{2}) dt, & |\tau| \leq T \\ 0 \text{ elsewhere} \end{cases}$$

Using the Parseval theorem [5] applied to (3), the statistical test becomes:

$$Z = \frac{1}{N_0^2} \int_{-\infty}^{\infty} S_{xx}(f) P_T(f) df \tag{4}$$

With $P_T(f)$ the peridogram of $y(t)$ given by:

$$P_T(f) = \frac{1}{T} \mid Y_T(f) \mid^2$$

and

$$Y_T(f) = \int_{-T/2}^{T/2} y(t) \exp^{-i2\pi ft} dt$$

Hence the local optimal detector computes the periodogram of the observed signal $y(t)$. The obtained result is then correlated with the ideal. Since the power spectral density $S_{xx}(f)$ cannot be known *a priori*, we replace it in (4) by a non zero constant S_0 over all the band $[-B/2, B/2]$ of the received signal to obtain the new statistical test:

$$Z_r = \frac{S_0}{N_0^2} \int_{-B/2}^{B/2} P_T(f) df \tag{5}$$

The obtained detector is called radiometer or energy detector whose statistical test is proportional to the energy of the received signal. The application of the Parseval theorem to (5) results in the following statistical test in the time domain:

$$Z_r \propto \frac{1}{T} \int_0^T y(t)^2 dt \tag{6}$$

Where the symbol $\propto$ indicates proportionality. Urkowitz [7] studied the energy detector with the statistic test X, which is equal to second term of equation (6). The block diagram of a radiometer is given in Figure 2. Urkowitz studied also the expression of the probability density function of the statistic X and showed that for a large time-bandwidth product ($BT > 250$) the statistic X follows a Gaussian law under both conditions: noise alone, or signal plus noise, with mean μ_{j+1} and variance σ^2_{j+1} ($j \in \{0,1\}$) given by:

$$\begin{array}{lll} H_0 & \mu_1 = N_0 BT, & \sigma_1^2 = N_0^2 BT \\ H_1 & \mu_2 = N_0 BT(SNR+1), & \sigma_2^2 = N_0^2 BT(2SNR+1) \end{array} \tag{7}$$

where SNR refers to the *signal to noise ratio* defined as:

$$SNR = \frac{E_x}{N_0 B}$$

with E_x the power of the signal $x(t)$ over the duration T. The probability of detection P_d and of false alarm P_{fa} becomes:

$$P_{fa} = Q\left\{\frac{\xi - \mu_1}{\sigma_1}\right\}$$

and

$$P_d = Q\left\{\frac{\xi - \mu_2}{\sigma_2}\right\}$$

with

$$Q(u) = \frac{1}{\sqrt{2\pi}} \int_u^{\infty} \exp^{-v^2/2} dv$$

Then, for a desired false alarm probability $P_{fa,des}$, we can compute the adequate detection threshold ξ_0 using the following equation:

$$\xi_0 = \mu_1 + \sigma_1 Q^{-1}(P_{fa,des}) = G(P_{fa,des}) N_0 \tag{8}$$

with:

$$G(P_{fa,des}) = BT + \sqrt{BT} Q^{-1}(P_{fa,des})$$

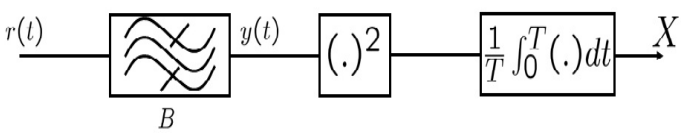

Fig. 2. Block scheme of the energy detector.

1) Energy detection limits: The good performance of the radiometer is accurate if the noise spectral density N_0 is perfectly known at the receiver. In a classical communication between transmitter and receiver, there is a preliminary exchange of data, which are known by the receiver, who is able to determine a good estimation of the noise level N_0. This cooperative aspect between transmitter and receiver is unfortunately absent in the case of detection of free bands because no data exchange is driven between terminals in opportunistic radio access. Subsequently, the estimated noise level $\hat{N}_0$ is not exempt from error especially when the tested band is occupied. As the detection threshold is proportional to N_0 (*Cf.* (8)), it can not be determined with accuracy, leading to more degradation of the radiometer performance.

2) Ideal Radiometer Performance: Let $P_{d,des}$ designate, the desired detection probability, $u' = Q^{-1}(P_{d,des})$ and $v' = Q^{-1}(P_{fa,des})$. It is shown in [6] that for large time-bandwidth product BT, the minimum signal to noise ratio snr_m that guarantees a desired probability of false alarm $P_{fa,des}$ and a desired probability of detection $P_{d,des}$ is given by:

$$snr_m = \frac{v'}{\sqrt{BT}} + \frac{u'}{BT}\left[u' - \sqrt{u'^2 + BT + 2v'\sqrt{BT}}\right]$$

The variation of this ratio depends on the time-bandwidth product BT as shown in Figure 3.

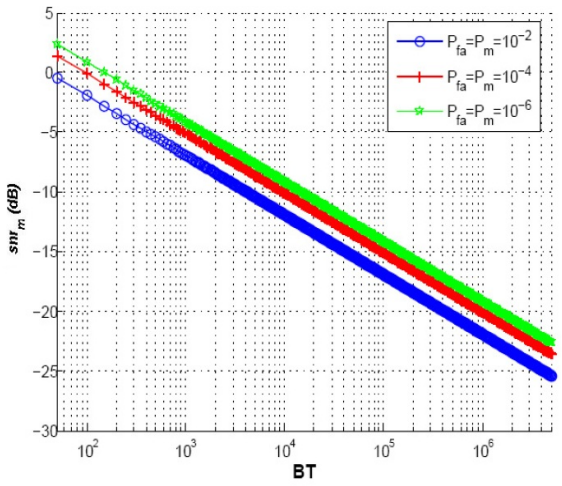

Fig. 3. the variation of the minimum signal to noise ratio snr_m that guarantees the desired probability of false alarm P_{fa} and a desired probability of miss detection P_m, versus the time-bandwidth product BT. When the noise level N_0 is perfectly known, snr_m decreases as the product BT increases.

For different values of probability $P_{fa,des}$ and probability of detection $P_{d,des}$, the required snr_m for detection decreases as the time-bandwidth product BT increases. It should be noted that BT is proportional to the number of observations available when the received signal is sampled.

3) Non Ideal Radiometer: Let $\hat{N}_0$ be an estimated value of the noise level N_0 and $\hat{\xi}_0$ the corresponding threshold of detection. In the case of an under-estimation of N_0 *i.e.*, $\hat{N}_0 < N_0$, Figure 4 shows that a bad decision is performed when the energy X of the signal is located in the interval $[\hat{\xi}_0, \xi_0]$. In the case of free bands detection, this bad decision results in the declaration of an occupied strip while it is free, causing an increase of the probability of false alarm.

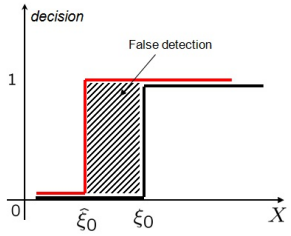

Fig. 4. Decision error in the case of an under-estimation of noise level N_0. This bad decision results in the declaration of an occupied strip while it is free, causing an increase of the probability of false alarm.

However, in the case of an over-estimation of noise level N_0 *i.e.*, $\hat{N}_0 > N_0$, Figure 5 shows that a wrong decision is made when the energy of the received signal X is located in the interval$[\xi_0, \hat{\xi}_0]$. In terms of free bands detection, this error results in declaring that the tested band is free, while it is occupied, which provides a more important missing probability. Consequently, the uncertainty on the noise level

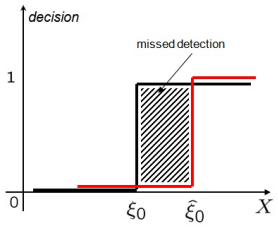

Fig. 5. Decision error in the case of an over-estimation of noise level N_0. This error results in declaring that the tested band is free, while it is occupied, which provides a more important missing probability, and causes interference to the PU.

leads in one case to an under-exploitation of free bands by secondary users and in another case to more interferences generated to the primary users. To overcome undesirable effects of uncertainty on the value of N_0, it has been proposed in [6] to use a different detection threshold given by:

$$\hat{\xi}_0 = U\xi_0$$

Where U is the peak-to-peak uncertainty on the estimation of noise level N_0 given by:

$$U = \frac{1+\epsilon_2}{1-\epsilon_1} \geq 1$$

Here, ϵ_1 and ϵ_2 give the range of uncertainty on the estimation of N_0:

$$(1-\epsilon_1)N_0 \leq \hat{N}_0 \leq (1+\epsilon_2)N_0$$

Thus, the expression of snr_m [6] becomes:

$$snr_m \approx (U-1) + O\left(\frac{1}{\sqrt{BT}}\right)$$

The term $(U-1)$ determinates the minimum SNR under, which detection is more regardless of possible parameters $P_{fa,des}$, $P_{d,des}$ and the observation time T of the detector. In the particular case where $P_{fa,des} = 1 - P_{d,des} = 0.01$, Figure 6 shows the evolution of the snr_m as a function of BT for different values of U. Whatever U nil or not, the value of snr_m decreases as the BT product increases. In contrast, if $U \neq 0$ (presence of uncertainty), the decay tends asymptotically to its limit $U-1$. For example, for $U = 3$ dB, the value of snr_m limit is 2 dB. Despite its low complexity and ease of implementation, the radiometer does not perform a reliable detection of free bands especially if the uncertainty regarding the noise level is important or the SNR is low.

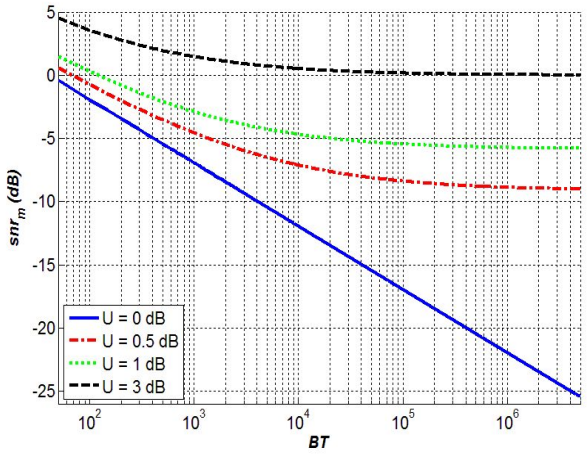

Fig. 6. When the value of U is different from zero (presence of uncertainty), the value of snr_m decreases as the BT product increases, and tends asymptotically to its limit $U-1$.

C. Cyclostationary Detection

When the cyclostationary model is adopted for the signal of interest $x(t)$, the autocorrelation function $R_{xx}(u,v)$ is expressed as a function of the cyclic autocorrelation

$$R_{xx} = \sum_{\alpha} R_{xx}(\alpha, u-v) \exp^{i\pi\alpha(u+v)} \qquad (9)$$

By replacing $R_{xx}(u,v)$ in (1) by its expression in (9), and by performing variables changes according to (2), we obtain the statistical test of the multi-cycle's coherent detector:

$$Z_{mc} = \sum_{\alpha} \frac{1}{N_0^2} \int_{-B}^{B} R_{xx}(\alpha,\tau)^* R_{yy}(\alpha,\tau)_B d\tau$$

With $R_{yy}(\alpha,\tau)_B$ is the cyclic periodogram of the observation $y(t)$ whose expression is presented in [24]. The local optimal detector computes the correlogram of the observation over all cyclic frequencies contained in the detected signal and the obtained result is then correlated with the ideal cyclic autocorrelation of the expected signal.

In the frequency domain after applying Parseval's theorem, this statistic test is written as follows:

$$Z_{mc} = \sum_{\alpha} \frac{1}{N_0^2} \int_{-\infty}^{\infty} S_{xx}(\alpha,f)^* S_{yy}(\alpha,f)_B df$$

With $S_{yy}(\alpha,f)_B$ is the cyclic periodogram of the observation $y(t)$. In practice, the implementation of the multi-cycles detector is impossible due to the non-knowledge of the ideal functions $R_{xx}(\alpha,\tau)$ or $S_{xx}(\alpha,\tau)$ of the signals to detect. In fact, their phases can not be known in advance because the expected signals are random. To overcome this indeterminacy on the phase, two alternatives are possible [24]. In the first alternative, the implementation of the statistic Z_{mc} occurs in an adaptive manner. This means that for each calculation of Z_{mc}, a phase search is made according to the maximization of the statistic Z_{mc}. If this is not enough, a second alternative is to detect a single frequency at a time:

$$Z_{\alpha} = \Big| \int_{-\infty}^{\infty} S_{xx}(\alpha,f)^* S_{yy}(\alpha,f)_B df \Big| \underset{H_1}{\overset{H_0}{\lessgtr}} \xi$$

For $\alpha = 0$, the obtained detector is the optimal radiometer. For $\alpha \neq 0$, the detector is called coherent mono-cycle detector. In a noisy environment of a known spectral density N_0, Gardner [10] and Izzo [25] show that, the optimal radiometer detector (with perfect knowledge of N_0) is better than the coherent mono-cycle detector. In [26], different noise models was considered: Gaussian, non-Gaussian, white and non-white. The author concluded that in a realistic situation characterized by a variable noise level, the optimal performance of the radiometer is becoming significantly degraded and significantly lower than those of mono-cycle detector. Furthermore, the author shows the superiority of mono-cycle detector in a noisy environment characterized by additive interference. In literature, many other cyclic methods of detection / estimation exist. For example, Zivanovic and Gardner [11] define the degree of cyclostationarity of a random process by:

$$DCS = \frac{\sum_{\alpha \neq 0} \int_{-\infty}^{\infty} |R_{xx}(\alpha,\tau)|^2 d\tau}{\int_{-\infty}^{\infty} |R_{xx}(0,\tau)|^2 d\tau}$$

It involves measuring the distance between the correlation of the process of interest and the correlation of the most close stationary process. We can also define the degree of cyclostationarity to a process on a specific frequency α by:

$$DCS^{\alpha} = \frac{\int_{-\infty}^{\infty} |R_{xx}(\alpha,\tau)|^2 d\tau}{\int_{-\infty}^{\infty} |R_{xx}(0,\tau)|^2 d\tau}$$

Although the authors of [11] did not mention the problem of detection, this notion of degree of cyclostationarity can be useful for detection by comparing DCS (or DCS^{α}) to a threshold value given by a criterion such as P_{fa} is constant. Hurd and Gerr [27] proposed a test for the presence of cyclostationarity based on the calculation of the normalized spectral correlation:

$$\gamma(\alpha_p, \alpha_q, M) = \frac{|\sum_{m=0}^{M-1} I_N(\alpha_{p+m}) I_N^*(\alpha_{q+m})|^2}{\sum_{m=0}^{M-1} |I_N(\alpha_{p+m})|^2 \sum_{m=0}^{M-1} |I_N(\alpha_{q+m})|^2}$$

with $I_N(\alpha) = \sum_{n=0}^{N-1} x(n) exp^{(-i\pi\alpha)}$, $\alpha_k = 2\pi k/N$ and M a smoothing parameter. The presence on the plot of $\gamma(\alpha_p, \alpha_q, M)$ varying with α_p of dark lines parallel to the diagonal indicate the cyclostationarity of the signal $x(t)$. Hence the detection is performed in a visual manner.
Dandawate and Giannakis [13] proposed tests for the presence of cyclostationarity at a given frenquency based on the following decision rule:

$$Z \propto \hat{\boldsymbol{C}}_{kx}^{(T)} \boldsymbol{\Sigma}_{kx}^{-1} \hat{\boldsymbol{C}}_{kx}^{(T)\prime} \underset{H_1}{\overset{H_0}{\lessgtr}} \xi_G$$

where $\hat{\boldsymbol{C}}_{kx}^{(T)}$ is an estimation vector of the k^{th} order cumulants of the process $x(t)$, $\hat{\boldsymbol{C}}_{kx}^{(T)\prime}$ the transpose of the vector $\hat{\boldsymbol{C}}_{kx}^{(T)}$, $\boldsymbol{\Sigma}_{kx}$ the covariance matrix of $\hat{\boldsymbol{C}}_{kx}^{(T)}$ and ξ_G the detection threshold. Unlike the two previous methods, the authors find the distribution of the statistic Z under the two hypotheses H_0 and H_1. This allows, thereafter, to calculate for a given probability of false alarm the appropriate threshold ξ_G. Very present in the literature, this test is used in the recognition of standards accessible to software radio terminals [28] or in the detection of free channels on the GSM frequency band [29]. In these examples, systems to be detected are *a priori* known permitting a cyclostationarity test over a reduced number of frequencies. In this paper, we choose to retain this test of cyclostationarity to be the cyclic detector used in our different proposed solutions, which will be discussed in the next sections.

D. Limits of the sensing methods

The last two methods (Energy and cyclostationary detection) present many advantages but have some limits; in fact when a band is tested, the detection system delivers a decision such as free or occupied band, without giving more details on the contents of this band in particular in the case of occupation of this band. However, a band may not be completely occupied *i.e.*, sub-intervals of this band are free as we can see from the example of Figure 7. Subsequently, a limitation of this solution is that existing communication opportunities may be missed when the tested bandwidth is much larger than the size of these opportunities.

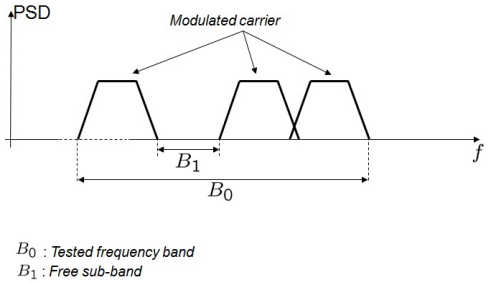

Fig. 7. Example of missed opportunity for communication in the case of a large tested range of frequencies

IV. Hybrid Detector

A. Generalities

As we have seen in Section I, the secondary user undertakes to not create interference to primary users by unwanted access to their frequency bands. For that purpose, secondary users have to perform periodic verifications of these bands. The more often these verifications are done, the lower becomes the risk of interference. Subsequently, periodic scanning of the spectrum is subjected to time constraint especially that the number of bands shared with the primary user can be important.

	Computational complexity	insensitivity of noise	*a priori* knowledge	Detection in low SNR
radiometer	+	-	noise level N_0	-
cyclostationary Detector.	-	+	cyclic frequencies	+

TABLE I
Comparison of properties of energy (Radiometer) and cyclostationary detector. The (+) indicates a advantage and (-) indicates an inconvenient

B. detector architecture

Table I gives features comparison between energy and cyclostationnarity detectors. Except its noise sensitivity, which degrades its detection in low SNR, energy detector is the best solution to detect free bands because no *a priori* information is needed. Furthermore, it is a very simple method to implement. On the contrary, cyclostationnarity detection is very robust but computationnaly extensive and needs the prior knowledge of cyclic frequencies in order to take a quick decision. If this information is unknown, the process becomes too much complicated and it will not be possible to implement it (today) in a real time manner. However, reading carefully table I, it appears that these two methods are complementary. Therefore it is the reason why we propose our hybrid architecture in [1], which permits to detect quickly with minimum *a priori* information free bands, by taking advantage of both methods. This hybrid architecture, which is presented in Figure 8 is an iteratively adaptative architecture as it is explained in [1]. In the next section we introduce the M-HSD algorithm, which is the same as the HSD proposed in [1] but this time we added $buffer_1$ and $buffer_2$ in order to take soft decisions over the modifications of the thresholds ξ_1 and ξ_2. The benefit of using buffers gives stability for operating at low $SNRs$ as it is explained in the next section.

V. Decision rule of the M-HSD algorithm

We first assume that N_0 is constant with respect to time. Let X_i be the energy of the received signal $x(t)$ during an observation time T after the iteration i, B the bandwidth of the tested band, ξ_1 and ξ_2 two thresholds that are first initialized at 0 and $+\infty$ respectively. ξ_G, which is the threshold of the

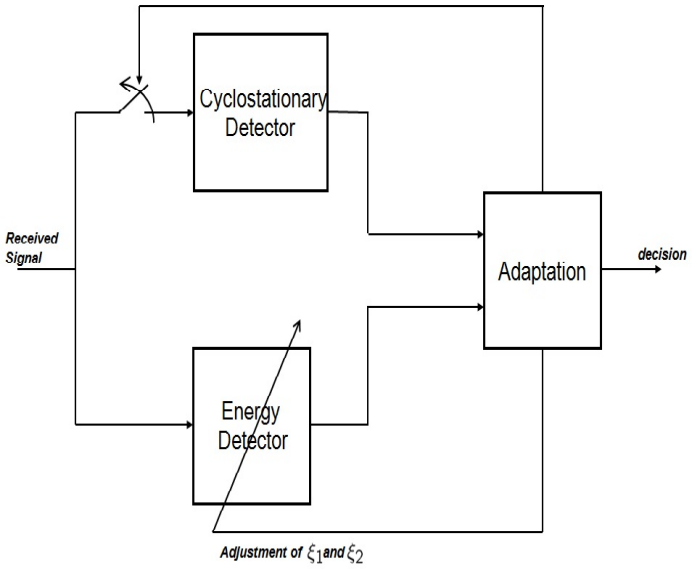

Fig. 8. Hybrid Spectrum sensing Detector (HSD) architecture as it was proposed in [1].

cyclostationary block that is defined in order to respect the desired $P_{fa,des}$, is fixed using the central χ^2 table as described in [13].

At the beginning of the sensing, the energy detector calculates the energy X of the received signal after an observation time T. Then if X falls inside the interval $[\xi_1, \xi_2]$, the energy detector can not make a direct decision of type *signal present* or *signal absent*. In that case, the adaptation stage presented in Figure 8 will call the cyclostationary block (which *a priori* knows the cyclic frequency α of the signal of interest) to make the decision. After the decision of the cyclic test is taken, if it is of the type *signal present* (*resp. signal absent*), the calculated value X is then saved in a buffer called $buffer_2$ of size N_2, (*resp.* $buffer_1$ of size N_1).

The algorithm continues in the same way except when $buffer_2$ (*resp.* $buffer_1$) is full. In this case, the adaptation stage starts to modify the value of the threshold ξ_2 (*resp.* ξ_1) according to the average of $buffer_2$, (*resp.* $buffer_1$) and then the oldest value in the buffer will be replaced by the new calculated one (X_i after the iteration i).

At any time, if the calculated value X is outside the interval $[\xi_1, \xi_2]$, the adaptation stage will take automatic decision of type *signal absent* (resp. *signal present*) depending on whether X is less than ξ_1 (resp. greater than ξ_2) avoiding the use of the cyclic test.

The process is repeated making the interval $[\xi_1, \xi_2]$ smaller and smaller. Two cases, high and low SNR, need to be studied in order to analyze the M-HSD architecture limits, which will be explained in the next paragraph. Figure 9 shows the algorithm of the M-HSD method.

It should be noted that at low SNR, the test of "Dandawate and Giannakis" can easily make errors (the two types of errors described in part II), so the values that should be saved in $buffer_1$ might be saved in $buffer_2$ and inversely. But the use of buffers can make a "dilution" of these errors over the values of ξ_1 and ξ_2.

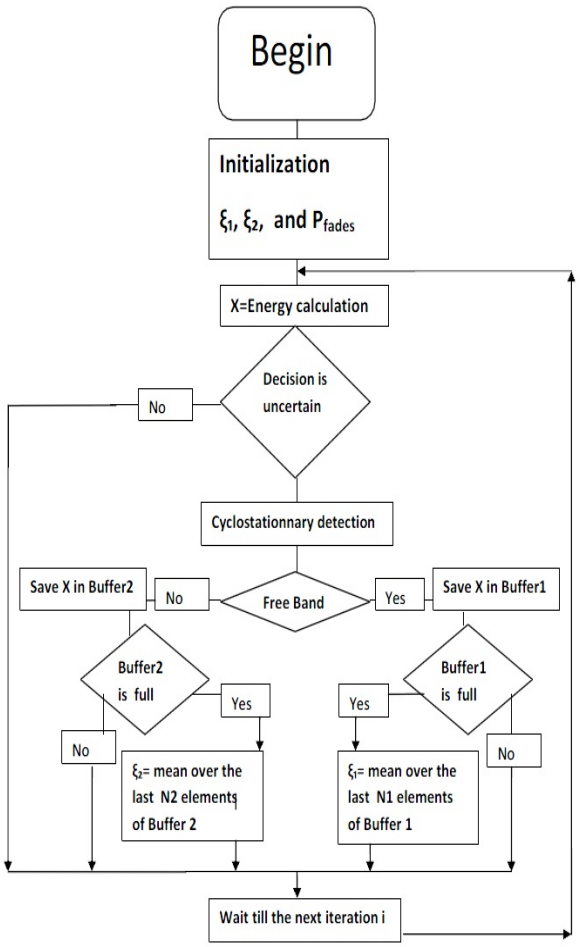

Fig. 9. The M-HSD algorithm (a Modified version of the HSD algorithm [1]). The major modification is the addition of $buffer_1$ and $buffer_2$ in order to make soft modifications over ξ_1 and ξ_2.

Using the M-HSD algorithm, will practically reduce the complexity from that of a cyclostationary detector: $O(N^2 + 0,5Nlog_2N)$, before the buffers are full, to the one of a radiometer: $O(Nlog_2N)$ at the convergence phase. At this point, the M-HSD detector will present a detection performance close to that of the cyclostationary detector.

A. Analytical Study of the M-HSD algorithm Using Order Statistics

In this section, for simplicity reasons, we assume that the buffers' size is one. In order to study the M-HSD architecture in a statistical point of view, we will use the order statistics tool. The K^{th} order statistic of a statistical sample denoted $X_{(k)}$ is equal to its K^{th} smallest value. The first order statistic (or smallest order statistic) is always the minimum of the

sample, that is:

$$X_{(1)} = min\{X_1, ..., X_n\}$$

Similarly, for a sample of size n, the n^{th} order statistic (or largest order statistic) is the maximum, that is:

$$X_{(n)} = max\{X_1, ..., X_n\}$$

if $f(x)$ is the probability density function of the random variable X and $F(x)$ its cumulative distribution function, then it is shown in [30] that the density probability of the k^{th} order statistic is given by:

$$f_{X_{(k)}}(x) = \frac{n!}{(k-1)!(n-k)!} F(x)^{k-1} (1 - F(x))^{n-k} f(x) \quad (10)$$

for the special case $k = 1$, (10) becomes:

$$f_{X_{(1)}}(x) = n[1 - F(x)]^{n-1} f(x) \quad (11)$$

and for $k = n$, (10) becomes:

$$f_{X_{(n)}}(x) = nF(x)^{n-1} f(x) \quad (12)$$

Now, using the distributions of X under H_0 (resp. X under H_1) from (7) in (11) (resp. (12)), we can obtain the distributions of ξ_1 and ξ_2 (in (13) and (14) respectively) after n iterations of the algorithm M-HSD under the hypotheses H_0 and H_1 respectively:

$$f_{\xi_1(k=1)}(x) = \frac{n}{2\sigma_1\sqrt{2\pi}} \left[1 + erf\left(\frac{x-\mu_1}{\sigma_1\sqrt{2}}\right)\right]^{n-1} e^{-\frac{1}{2}\left(\frac{x-\mu_1}{\sigma_1}\right)^2} \quad (13)$$

and :

$$f_{\xi_2(k=n)}(x) = \frac{n}{2\sigma_2\sqrt{2\pi}} \left[1 - erf\left(\frac{x-\mu_2}{\sigma_2\sqrt{2}}\right)\right]^{n-1} e^{-\frac{1}{2}\left(\frac{x-\mu_2}{\sigma_2}\right)^2} \quad (14)$$

B. M-HSD algorithm limits

- *High SNR case:* if the signal is received at a good SNR, the performance of the cyclic test will be ideal (P_{fag} close to zero and P_{dg} close to one where P_{fag} and P_{dg} are respectively the observed false alarm and detection probability of the cyclostationary block). So the saved values in each buffer will be from the same population (signal in $buffer_2$ and noise in $buffer_1$). The variables ξ_1 and ξ_2 will never meet and ξ_1 will always be smaller than ξ_2. This is due to the fact that the signal is well separated from the noise as shown in Figure 10, which represents the variation of the probability density function of ξ_1 and ξ_2 for different number of iterations at 0 dB. Figure 11 represents the expected values of the distribution of ξ_1 under H_0 and ξ_2 under H_1 over the number of iterations (obtained using (14) and (13)). It is clear that ξ_1 and ξ_2 are not going to meet even after a huge number of iterations (10^9 iterations, *Cf.* Figure 10). Then after the convergence of the M-HSD algorithm, the cyclic block will be very rarely used because it is very rare that the statistic X_i falls between ξ_1 and ξ_2 leading to a radiometer complexity and to perfect decisions.

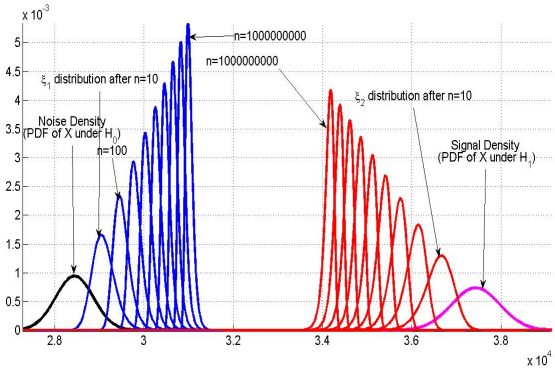

Fig. 10. The variation of the probability density function of ξ_1 (resp. ξ_2) under H_0 (resp. H_1) for different number of iterations at 0 dB, plotted using (13) (resp. (14)).

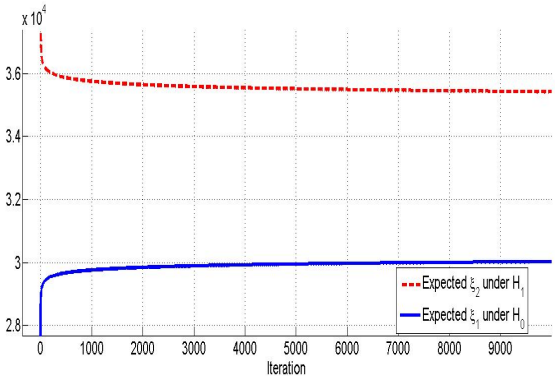

Fig. 11. The expected values of ξ_1 (resp. ξ_2) under H_0 (resp. H_1) as function of the iterations number n at 0 dB, plotted using a numerical calculus using (13) (resp. (14)) and the Matlab tool.

- *Low SNR case:* If the signal is received at a low SNR, the received signal will be very close to the noise level, then ξ_2 will soon be less than ξ_1 after a small number of iterations as we can see in Figure 12. Moreover, with low SNR, the cyclic test can easily misdetect in it decisions (for example the values saved in the buffers may not be from the same population). In this case, it would be better to change ξ_2 instead of changing ξ_1. This fact induces a strong degradation of the detection performance. Once ξ_1 becomes greater than ξ_2, the M-HSD algorithm will fix $\xi_1 = \xi_2$ and will stop its evolution. In this case the M-HSD algorithm has reached its detection limit.

VI. The Enhanced HSD algorithm (EHSD)

An Enhanced architecture of this last one can be studied as well to improve the detection at lower SNR. It consists in directly estimating the noise level $\hat{N}_0$. We will keep the same algorithm of the M-HSD architecture but with just making few modifications: N_1 will be chosen to be big enough to make a good estimation of the noise level N_0. Moreover, we will keep ξ_2 in the architecture to reduce the detection complexity as much as possible. Directly when $buffer_1$ is full, we will calculate its mean $\hat{\mu}_1$. Then, the EHSD algorithm will use the

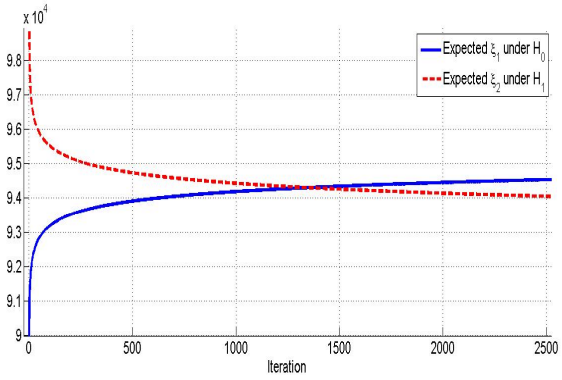

Fig. 12. The expected values of ξ_1 (resp.ξ_2) under H_0 (resp. H_1) as function of the iterations number n at -10 dB, plotted using a numerical calculus using (39) (resp. (40)) and the Matlab tool. We can observe that ξ_2 will soon be less than ξ_1 after a small number of iterations at low SNR.

following equation to estimate N_0:

$$\hat{N}_0 = \frac{\hat{\mu}_1}{BT}$$

Using this estimation of $\hat{N}_0$, we can estimate $\hat{\xi}_0$ that guarantees the $P_{fa,des}$ from the equation bellow:

$$\hat{\xi}_0 = G(P_{fa,des})\hat{N}_0$$

EHSD is a little more complex than M-HSD, because we will need to repeat the cyclostationary test at least N_1 times to be able to estimate $\hat{\xi}_0$, (the size of $buffer_1$ in the EHSD algorithm is usually bigger than the size of $buffer_1$ in the M-HSD algorithm). Figure 13 shows the algorithm of the EHSD method.

A. EHSD Performance

Let D_0 (resp. D_1) designate the event that the cyclic detector has chosen H_0 (resp. H_1). If we assume that for a given SNR the cyclic detector can make false alarms under H_0 and good detections under H_1 independently of the value of the calculated variable X, then we can write:

$$E(X|H_1, D_0) = \mu_2 \tag{15}$$

and

$$E(X|H_0, D_0) = \mu_1 \tag{16}$$

where E(.) denotes the expectation operator.
Recall the partition probability theorem stated below:

$$\begin{aligned} E(X|D_0) =& P(H_1|D_0)E(X|H_1, D_0) \\ &+ P(H_0|D_0)E(X|H_0, D_0) \end{aligned}$$

Using the assumptions of (15) and (16), we can write:

$$E(X|D_0) = P(H_1|D_0)\mu_2 + P(H_0|D_0)\mu_1 \tag{17}$$

by applying Bayes equality we can write:

$$P(H_1|D_0) = \frac{P(D_0|H_1)P(H_1)}{P(D_0)} \tag{18}$$

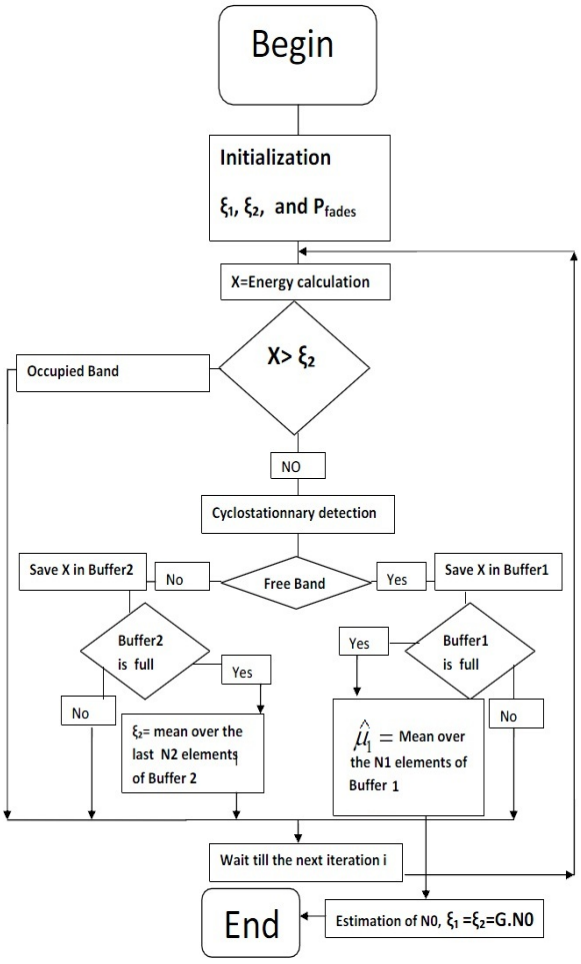

Fig. 13. Algorithm of the EHSD architecture. Only few modifications over the M-HSD algorithm are done.

$$P(H_0|D_0) = \frac{P(D_0|H_0)P(H_0)}{P(D_0)} \tag{19}$$

We can express the probability that the cyclic detector chooses H_0 in terms of $P(H_1)$, $P(H_0)$, P_{fag}, and P_{dg}:

$$P(D_0) = (1 - P_{fag})P(H_0) + (1 - P_{dg})P(H_1) \tag{20}$$

now considering the following definition:

$$\gamma = \frac{P(H_0)}{P(H_1)}$$

where γ represents the characteristic of the environment (free or occupied). Using (18), (19) and (20), equation (17) becomes:

$$E(X|D_0) = (1 - \delta)\mu_2 + \delta\mu_1 \tag{21}$$

where

$$\delta = \frac{1 - P_{fag}}{1 - P_{fag} + \frac{1-P_{dg}}{\gamma}}$$

Or for all δ we have:

$$(1-\delta)\mu_2 + \delta\mu_1 \geq \mu_1$$

Therefore we conclude that:

$$E(X|D_0) \geq \mu_1$$

This means that we always have an over estimation of the noise level N_0 ($\hat{\xi_0} \geq \xi_0$), wish implies that the false alarm constraint will always be respected in the EHSD method (the observed false alarm is then less or equal to the desired false alarm). Using (21) we can find a theoretical approximation for the expression of the relative error over the estimated threshold $\hat{\xi_0}$ defined by $Error_{rel} = \frac{\hat{\xi_0}-\xi_0}{\xi_0}$, as function of the SNR.

For large N_1, we can write:

$$\hat{\mu_1} \approx E(X|D_0)$$

then:

$$\hat{N_0} \approx \frac{E(X|D_0)}{TW}$$

Using the result given by (21) we can write:

$$\hat{N_0} \approx \frac{(1-\delta)\mu_2 + \delta\mu_1}{TW}$$

so $Error_{rel}$ can be approximated by:

$$Error_{rel} \approx \frac{\frac{G}{TW}((1-\delta)\mu_2 + \delta\mu_1) - \frac{G}{TW}\mu_1}{\frac{G}{TW}\mu_1}$$

after simplifying it, we will obtain:

$$Error_{rel} \approx \frac{SNR}{\gamma\frac{1-P_{fag}}{1-P_{dg}} + 1} \quad (22)$$

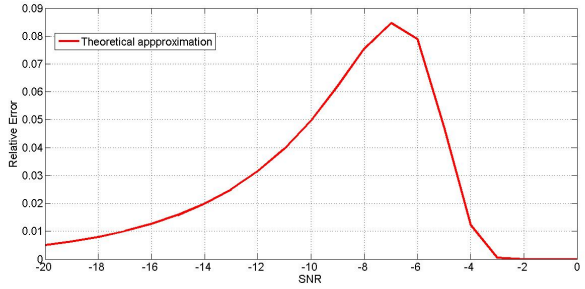

Fig. 14. The theoretical approximation of the relative error over the threshold ξ_0, simulated using the approximation (22).

Observing the curve in Figure 14, we can check that for high $SNRs$ (when the cyclic test is perfect), the term $1 - P_{dg}$ goes to zero as well as global expression of $Error_{rel}$. In that case, an excellent estimation of ξ_0 can be done. For lower SRN, the term $1 - P_{dg}$ is not zero anymore because the cyclostationary test is no more an ideal test inducing an error over the estimation of ξ_0. This error reaches its maximum before it starts to decrease because the SNR term becomes very small. Physically this error reduction is due to the fact that the signal is too weak and thus close to the noise level.

VII. Simulation Results and Discussion

In the simulations, we used a 4-PSK modulation at 20 Khz where $\alpha = \frac{1}{T_s}$ is the cyclic frequency used in the cyclostationary detector *a priori* known, and T_s refers to the symbol period of the 4-PSK. We set N_1 and N_2 equal to 30 in the simulation of the M-HSD algorithm, while for the EHSD algorithm, we used $N_1 = 100$ and $N_2 = 30$. The time-bandwidth product BT is equal to 4500 and an equiprobabilist environment ($\gamma = 1$) was used, unless otherwise stated while simulating the different architectures.

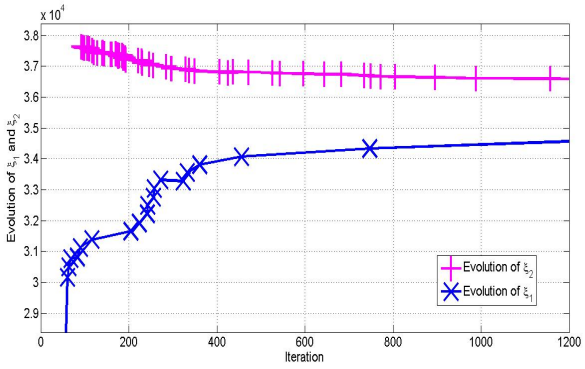

Fig. 15. The variation of ξ_1 and ξ_2 at -5 dB using M-HSD algorithm, with $\gamma = 1$, $N_1 = 30$, and $N_2 = 30$. Each mark on the curves indicates a modification of ξ_1 and ξ_2. One can notice that the cyclostationary test is less and less used, as the number of iterations increases, inducing a lower complexity.

Figure 15 presents the evolution of ξ_1 and ξ_2 over the iterations of the M-HSD algorithm at -5 dB. We have fixed ξ_G to guarantee a P_{fa} less than 1%. Each mark on the curves in Figure 15 indicates a modification of ξ_1 or ξ_2. We can observe that there are lots of marks at the beginning, which means that the cyclostationary test is frequently used at this stage, but after a while, the cyclostationary test is much less utilised inducing a lower complexity.

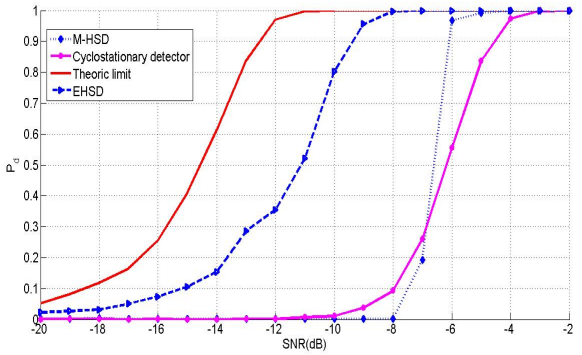

Fig. 16. Simulated detection probability as function of SNR of the M-HSD (using N_1=N_2=30), and EHSD (using N_1=100, and N_2=30) architectures with a $P_{fa,des}$ fixed at 1%, also compared to the cyclic test and to the ideal radiometer under the same conditions.

In order to compare detection performances of the different above mentioned techniques, we simulate the variation of the

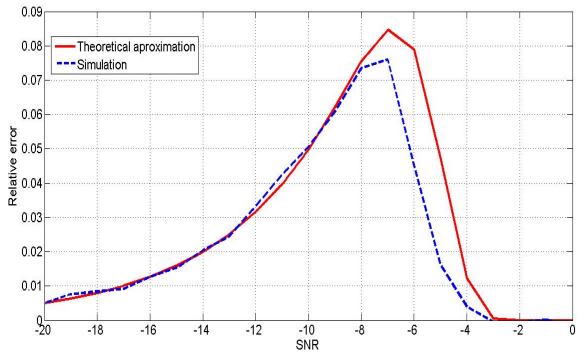

Fig. 17. Simulation result of the relative error of the estimated threshold $\hat{\xi}_0$ as function of the SNR using the EHSD algorithm, compared to the theoretical approximation given in (22).

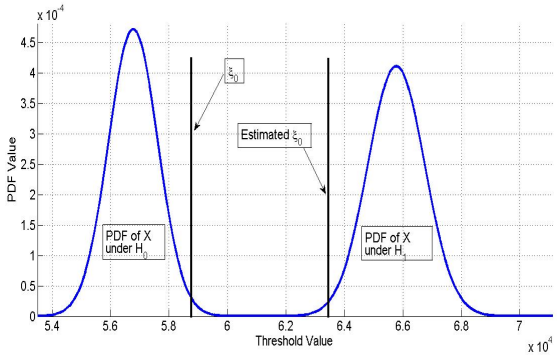

Fig. 18. The distribution of the statistic X under the two hypothesis H_0 and H_1 obtained using (7) of Urkowitz at -8 dB. We have found that in this situation $\hat{\xi}_0$ is located on the tail of the PDF of X under H_1, that is why we can still obtain good detection performance although the estimation error over ξ_0 is maximal.

probability of detection as function of SNR, for the M-HSD and EHSD, using the same $P_{fa,des} = 1\%$. We also compare the obtained results with the curves representing the performance of the cyclic test and the ideal radiometer. The simulated results are shown in Figure 16, where we can observe that the performance of the M-HSD algorithm are near the cyclostationary detector, which means that M-HSD has reached the performance of the cyclic test with a radiometer complexity. Now if we take a look at the EHSD algorithm performance, which also has a radiometer complexity at steady state, we can see that it is able to detect at 100%, with an observed P_{fa} smaller 1% starting at -8 dB, versus -3 dB for the cyclic test, and so achieving a gain of 5 dB in terms of SNR. It should be noted that the EHSD algorithm is a little more complex than M-HSD algorithm at the beginning of the sensing process since it needs a larger $buffer_1$ to achieve a good estimation of N_0.

Figure 17 validates the approximation given in (22) of the relative error of the threshold $\hat{\xi}_0$ as function of the SNR. This approximation is very close to the simulation results especially at low and high SNR. It can be concluded that when the cyclostationary test starts detecting at 100% (at -3 dB), we can have then a perfect estimation of ξ_0. An important remark is that for example, at -8 dB, we have a maximum error over the threshold estimation and we can still detect at 99% (*Cf.* Figure 16). This fact is explained by Figure 18, that shows the PDF of X under both, H_0 and H_1 at -8 dB using (7). We can observe that these densities are still well separated at -8 dB. In consequence this error of estimation does not have a significant impact over the detection performances. At the matter of fact we can observe that $\hat{\xi}_0$ is located on the tail of the PDF of X under H_1.

A. The Influence of the Environment γ over the Performance of the M-HSD and EHSD Algorithms

As we have already seen, the state of the channel (free or occupied) can be characterized by the variable γ as the ratio between $P(H_0)$ and $P(H_1)$. If we look closely at Figure 12, we note that the point of intersection of the two curves that presents the expectation of ξ_1 and ξ_2, under respectively H_0 and H_1, does not depend solely on the SNR of the received signal but also on how the sequence of the events *free channel* or *occupied channel* is occurring while using the M-HSD algorithm. Also if we look at (22), which gives the relative error in estimating the optimal threshold when using the EHSD algorithm, we can check that it depends also on the environment characteristic γ. This is the reason why it is interesting to observe the influence of the environment over the performance of our different proposed architectures.

We have used two extreme simulation environments to observe the variation of the performance of the M-HSD detector. The first is $\gamma = 99$ $(P(H_0) = 99\%)$ and the second is $\gamma = 0.01$. We observe in Figure 19 that the performance effectively varies depending on the environment γ. For $\gamma = 99$, which signifies that 99% of the time the band is free, ξ_1 keeps increasing, causing a reduction of the detection performance. This environment $(\gamma >> 1)$ is not that one favorable for the M-HSD algorithm because it will have its detection performance close to the cyclostationary detector (at-4 dB M-HSD detects up to 100% versus -3 dB for the cyclic detector), so the major advantage in this case is the lower complexity of the M-HSD algorithm.

However, when $\gamma = 0.01$ $(P(H_1) = 99\%)$ ξ_2 keeps decreasing, which allows better detection results. In this case a gain of 2 dB is observed compared to the cyclic detector. Moreover M-HSD is still less complex, and detects significantly better than the cyclostationary detector. Then, we conclude that the M-HSD algorithm ensures a gain between one and two dB over the detection performance of the cyclic detector with a decreasing complexity.

Now we simulate the EHSD architecture in both environments, $\gamma = 99$ and $\gamma = 0.01$. For $\gamma = 99$, the observed performance in Figure 20 is close to the ideal radiometer performance. This result is explained in (22), which shows that the relative error is inversely proportional to γ. So for $\gamma = 99$ this error is almost zero for all the SNR. Therefore the

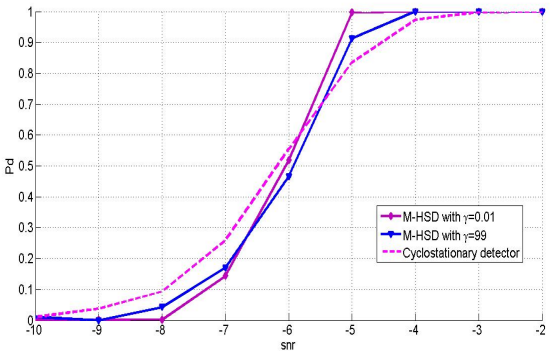

Fig. 19. Simulated detection probability under different SNRs, of the M-HSD (using N_1=N_2=30), with $P_{fa,des}$ fixed at 1% using $\gamma = 99$ and $\gamma = 0.01$, also compared to Giannakis test under the same conditions.

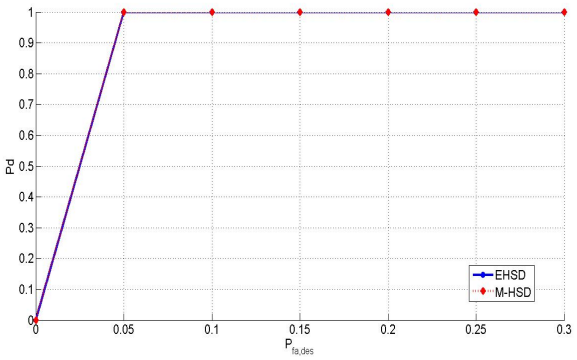

Fig. 21. ROC curves of the M-HSD and the EHSD at -5 dB, for $\gamma = 1$. We observe that in these conditions M-HSD and EHSD present the same performance.

estimated threshold $\hat{\xi}_0$ is very close to the optimal threshold ξ_0, which explains the obtained result. As for $\gamma = 0.01$, the same formula (22) shows that for low SNR the relative error over the estimation of the optimal threshold is high because γ is less than 1. But for high SNR, we have P_{dg} close to one, which makes the relative error decreases to zero. Then we can observe that the performance of the EHSD is always better than that of the M-HSD algorithm. In fact there is always a minimum gain of 2 dB over the cyclic detector, and if the environment is favorable ($\gamma >> 1$) to the EHSD algorithm, we may even reach the performance of the ideal radiometer.

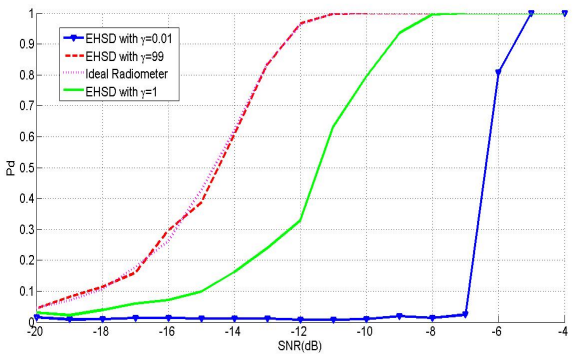

Fig. 20. Simulated detection probability under different SNRs, of the EHSD (using N_1=100, and N_2=30), with $P_{fa,des}$ fixed at 1% using $\gamma = 99$, $\gamma = 1$ and $\gamma = 0.01$, also compared to the ideal radiometer under the same conditions.

Another way of comparing performance is to plot the ROC curves already defined in part II. For $\gamma = 1$, we simulate for different $SNRs$ the ROC curve of both M-HSD and EHSD. For a relatively good SNR (-5 dB), we can check in Figure 21 that both architectures present the same performance. But for lower SNR (-10 dB), we can observe in Figure 22 the superiority of the EHSD over the M-HSD algorithm in terms of detection. Although both EHSD and M-HSD converge to a radiometer complexity at steady state, EHSD has always better performance than M-HSD. Therefore it is better to use EHSD instead of M-HSD.

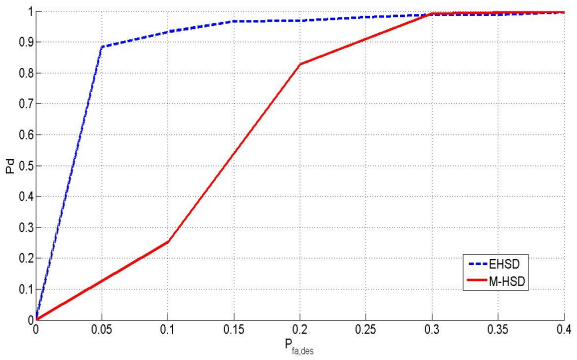

Fig. 22. ROC curves of the M-HSD and the EHSD at -10 dB, for $\gamma = 1$. We observe that in these conditions EHSD presents better detection performance compared to M-HSD.

VIII. Conclusion

Spectrum sensing is subject to time constraints. For this reason, we have proposed adaptive architectures, which combine two systems. The first system is a low complexity detector, but it is very sensitive to a bad estimation of the noise level N_0. As for the second, it is a more complex system based on cyclostationary detection, but it is insensitive to a poor estimation of N_0. These new adaptive architectures allow the sensing at lower SNR and with a decreasing algorithmic complexity. In a Gaussian noise environment the obtained results are promising as it was shown by the performed simulations. Future work will include the study of different channel types with a variable N_0. A study of the convergence time and power consumption of the proposed architectures are under investigation.

Acknowledgment

The authors would like to thank Wassim Jouini for his comments and insightful discussions regarding this work.

References

[1] Z. Khalaf, A. Nafkha, J. Palicot, and M. Ghozzi, *Hybrid Spectrum Sensing Architecture for Cognitive Radio Equipment*, AICT'10, May 2010, Barcelona, Spain.

[2] J. Mitola, *Cognitive Radio An Integrated Agent Architecture for Software Defined Radio*, PhD thesis, Royal Institute of Technology (KTH), May 2000.

[3] Spectrum Efficiency Working Group. Report of the Spectrum Efficiency Working Group. Technical report, FCC, November 2002.

[4] Y. Zeng, Y. Liang, A. T. Hoang, and R. Zhang, *A Review on SpectrumSensing for Cognitive Radio: Challenges and Solutions*, EURASIP Journal on Advances in Signal Processing Volume 2010, Article ID 381465, October 2009.

[5] S. M. Kay, *Fundamentals of Statistical Signal Processing: Detection Theory*, vol. 2, Prentice Hall, Upper Saddle River, NJ, USA, 1998.

[6] P.M. Fishman, *Radiometric detection of spread-spectrum signals in noise of uncertain power, IEEE Transactions on Aerospace and Electronic Systems*, vol. 28, pp. 654-660, July 1992.

[7] H. Urkowitz, *Energy detection of unknown deterministic signals*, Proceedings of the IEEE, vol. 55, no. 4, pp. 523-531, 1967.

[8] H. S. Chen, W. Gao, and D. G. Daut, *Signature based spectrum sensing algorithms for IEEE 802.22 WRAN*, in Proceedings of the IEEE International Conference on Communications (ICC 07), pp. 6487-6492, Glasgow, Scotland, June 2007.

[9] M. Ghozzi, *Détection cyclostationnaire des bandes de fréquences libres.* PhD thesis, 2008.

[10] W.A. Gardner and C.M. Spooner, *Signal interception: Performance advantages of cyclic feature detectors*, *IEEE Transaction on Communications,* vol. 40, January 1992.

[11] W.A. Gardner and G. Zivanovic, *Degrees of cyclostationary and their application to signal detection and estimation*, Signal processing, vol. 22, March 1991.

[12] W. A. Gardner, *Exploitation of spectral redundancy in cyclostationary signals*, IEEE Signal Processing Magazine, vol. 8, no. 2, pp. 14-36, 1991.

[13] A.V. Dandawate and G.B. Giannakis, *Statistical tests for presence of cyslostationarity*, IEEE Transactions on Information Theory, vol. 42, pp. 2355-2369, September 1994.

[14] Y. H. Zeng and Y.-C. Liang, *Eigenvalue-based spectrum sensing algorithms for cognitive radio*, IEEE Transactions on Communications, vol. 57, no. 6, pp. 1784-1793, 2009.

[15] F. Penna, R. Garello, and M. A. Spirito, *Cooperative spectrum sensing based on the limiting eigenvalue ratio distribution in wishartmatrices*, IEEE Communications Letters, vol. 13, no. 7, pp. 507-509, 2009.

[16] L. S. Cardoso, M. Debbah, P. Bianchi, J. Najim, *Cooperative Spectrum Sensing Using Random Matrix Theory*, invited paper, Proc. ISPWC 2008, May 2008, Santorini, Greece.

[17] Z. Tian and G. B. Giannakis, *A wavelet approach to wideband spectrum sensing for cognitive radios*, in Proceedings of the 1st International Conference on Cognitive Radio Oriented Wireless Networks and Communications (CROWNCOM 07), Mykonos, Greece, June 2007.

[18] Y. H. Zeng and Y.-C. Liang, *Spectrum-sensing algorithms for cognitive radio based on statistical covariances* IEEE Transactions on Vehicular Technology, vol. 58, no. 4, pp. 1804-1815, 2009.

[19] Y. H. Zeng, Y.-C. Liang, and R. Zhang, *Blindly combined energy detection for spectrum sensing in cognitive radio*, IEEE Signal Processing Letters, vol. 15, pp. 649-652, 2008.

[20] A. Sahai, S. M. Mishra, R. Tandra, and K. A. Woyach, *Cognitive radios for spectrum sharing*, IEEE Signal Processing Magazine, vol. 26, no. 1, pp. 140-145, 2009.

[21] H.L. Van Trees, *Detection, estimation, and modulation theory, Part III.* Wiley, 1971.

[22] D. Middleton, *Canonically optimum threshold detection*, IEEE Transactions on information Theory, vol. 12, pp. 230-243, April 1966.

[23] B. Zayen, A. Hayar, K. Kansanen, *Blind Spectrum Sensing for Cognitive Radio Based on Signal Space Dimension Estimation*, ICC'09, IEEE International Conference on Communications, June 14-18, 2009, Dresden, Germany.

[24] W.A. Gardner, *Introduction to random processes with applications to signals and systems.* New York : McGraw-Hill, 1989.

[25] L. Izzo, L. Paura and M. Tanda, *Signal interception in non-gaussien noise*, IEEE Transaction on Communications, vol. 40, pp. 1030-1037, June 1992.

[26] P. Rostaing, *Détection de signaux modulés en exploitant leurs propriétés cyclostationnaires : Application aux signaux sonar.* PhD thesis, Université de Nice - Sophia Antipolis, 1997.

[27] H.L. Hurd and N.L. Gerr, *Graphical methods for determining the presence of periodic correlation* Journal of Time Series Analysis, vol. 12, no. 4, pp. 337-350, 1991.

[28] M. Öner and F. Jondral, *Air interface recognition for a software radio system exploiting cyclostationarity*,in Proc. IEEE PIMRC'04, Barcelona, Spain, vol. 3, pp. 1947-1951, September 2004.

[29] M. Öner and F. Jondral, *Extracting the channel allocation information in a spectrum pooling system exploiting cyclostationarity*, in Proc. IEEE PIMRC'04, vol. 1, pp. 551-555, September 2004.

[30] A. Papoulis and S.U.Pillai, *Probability, Random Variables and Stochastic Processes*, Mc Graw Hill, 2002.

Software Defined Radio Certification in Europe: Challenges and Processes

Gianmarco Baldini
Security Technology Assessment Unit
Joint Research Centre, European Commission
Ispra, Italy
email: gianmarco.baldini@jrc.ec.europa.eu

Dimitrios Symeonidis
Security Technology Assessment Unit
Joint Research Centre, European Commission
Ispra, Italy
email: dimitrios.symeonidis@jrc.ec.europa.eu

***Abstract*— Standardization and certification of Software Defined Radio technologies are closely related. This paper describes the current standardization efforts for Software Defined Radio technologies in Europe and the related certification processes with a specific focus to the public safety and military domain. This paper describes the regulatory and technical requirements for the certification of Software Defined Radio in the European context, which is characterized by various political entities and governmental institutions. We describe the development of an European Software Defined Radio certification process through a networked approach and we identify the main components including the Development and Testing tools, References Implementation, the Waveform Repository and the Issue Tracking system. The main stakeholders in the certification processes are identified and their roles are described. This paper describes also two specific certification processes, which are particularly important for Software Defined Radio technology: performance benchmark certification and security certification. Performance benchmark certification is used to evaluate the performance of Software Defined Radio against specific technical requirements. Security certification is needed to ensure that the Software Defined Radio platform and the waveforms validate security requirements. The conclusion is that Software Defined Radio certification at European level requires a comprehensive framework, which includes organizational, procedural and technical elements[1].**

Keywords - Software Defined Radio, Certification, Performance Benchmarking

I. INTRODUCTION

The concept of Software Defined Radio dates back to the 1992 when Joseph Mitola described it in [2].

For a number of years the focus of software defined radio (SDR) research was on military applications. The JTRS (Joint Tactical Radio Systems) program [3] and [4] is intended to permit the Military Services to operate together in a "seamless" manner via wireless voice, video, and data communications through all levels of command, including direct access to near real-time information from airborne and battlefield sensors.

JTRS is envisioned to function more like a computer than a conventional radio and is to be upgraded and modified to operate with other communications systems by the addition of software as opposed to redesigning hardware - a more costly and time-consuming process. A single JTRS radio with multiple waveforms can replace many separate radios, simplifying maintenance. The additional advantage is that because JTRS is "software programmable", they will also provide a longer functional life. Both features can offer potential long-term cost savings to the military organizations.

For the public safety community, SDR developments were primarily part of the internal research and development activities of land mobile radio vendors. The Public Safety domain was not the primary focus of SDR industrial vendors. However, several incidents over the past several years have suggested that public safety community may use evolving SDR and cognitive radio technology to address critical public safety communications challenges.

Interoperability has been a long-standing challenge in public safety communications. We have numerous examples in which responders with incompatible radios have been unable to communicate during a natural disaster or an emergency/crisis situation. The challenges of interoperability in public safety communication have been described by a number of sources including [5] and [6].

The application of SDR to mitigate or resolve interoperability barriers in the Public Safety domain has been the focus of the FP7 PASR WINTSEC project [7].

The WINTSEC (Wireless INTeroperability for SECurity) project aims to explore a mix of complementary solutions to overcome the barriers for wireless interoperability across different security agencies, taking into account the constraints of the security services and legacy systems and equipment. WINTSEC studies the deployment of standardized Internetworking layer at Core Network level and Software Defined Radio (SDR) added value for Base Station and Terminal. WINTSEC addresses information assurance, elaborates the European "SDR Architectural Framework" and the concepts for the "SDR Certification Environment".

[1] the views expressed are those of the authors and cannot be regarded as stating an official position of the European Commission.

Certification of the equipment and software is an essential process in the Public safety or Defence domains. This is particularly important for the introduction of new technologies like SDR, which must be validated against specific operational and technical requirements.

Because of its high degree of reconfigurability and ease of programming, SDR is a technology enabler for cognitive radio (CR). Cognitive radio is a radio or wireless communication device that is able to change dynamically its transmission or reception parameters by using the information collected or sensed on the external environment. Cognitive radios can also potentially enable Dynamic Spectrum Allocation (DSA), where the allocation of spectrum bands to communication services can change depending on time and context (see [8] and [10]). The use of SDR as an enabler of CR makes the certification activity even more important, because a badly configured or faulty SDR can negatively affect other wireless communication services in the same coverage area through harmful wireless interference. The need for a certification process for SDR as a CR and DSA enabler, are described in [9] as part of the standardization work of IEEE P1900.3.

Reference [9], identifies four testing areas for certification:

- Over the Air. A Provisioning Testing, which verifies the ability of a device to correctly obtain & install applications over the air.
- Security Testing to ensure that security requirements are validated.
- Performance Testing to validate the time constraints and
- Stress testing to verify the robustness of the implementation when stretched to the limits of system resources.

The paper acknowledges that SDR certification is a difficult task because SDR is a complex system with a large potential state space. The validation and certification of non-functional attributes (e.g., security) is particularly challenging for SDR products.

The complexity of SDR certification is also discussed in [11], where the vast amount of SW and HW combinations is identified as one of the biggest challenge in the certification process.

A preliminary study on SDR standardization and certification is provided by the same authors in [1], but the paper does not address performance benchmarking and security certification, which is investigated in this paper.

This paper will provide a survey of the SDR standardization and certification status in Europe and a proposal for a SDR certification framework and related tools.

The paper is structured in the following sections: section II describes the status of SDR standardization and certification in USA and Europe with the identification of the main challenges. The certification framework is proposed in section III, which describes the main elements of the SDR certification process including the reference implementations, the certification of API compliance, certification tools, the structure of the certification network, the waveform libraries and the issue tracking workflow. Two specific certification processes are then presented in the following sections. Benchmark certification is described in section IV, while security certification is described in section V. Finally section VI concludes the paper.

II. SDR STANDARDIZATION AND CERTIFICATION

The initial drive for standardization has been the JTRS program, which proposed the Software Communications Architecture (SCA) as a framework to integrate the hardware and software components.

SCA is a framework for developing SDR systems and we can define a framework as a set of cooperating classes that make up a reusable design for a specific class of software.

The interfaces among the classes and the other elements of the framework must be clearly defined to facilitate the activity of development, integration and validation.

The goals of the SCA are to:

a) provide portability of applications between different SCA implementations,
b) Reduce development time of new waveforms through the ability to reuse design modules;
c) Build on evolving commercial frameworks and architectures.

SCA is based on CORBA as a middleware to provide the communications among the main components and functions of the framework, which are:

- Radio management functions,
- Domain Manager,
- Application Factories,
- Applications,
- Device Managers and
- Devices

The portability concept is quite important for SCA and it is a basis for the certification process. SCA and SDR are mostly investigated in the Wireless Innovation Forum, which is (from reference [12]):

"Established in 1996, the Wireless Innovation Forum™ is a non-profit international industry association dedicated to promoting the success of next generation radio technologies. The Forum's 100-strong membership comprises world class technical, business and government leaders from EMEA, Asia and the Americas who are passionate about creating a revolution in wireless communications based on reconfigurable radio. Forum members span commercial, defense and civil government organizations at all levels of the wireless value chain and include service providers, operators, manufacturers, developers, regulatory agencies, and academia." The Wireless Innovation forum is very active in the Defence domain even if a number of deliverables have been created for the Public Safety and Commercial domain as well.

In USA, the Federal Communication Commission (FCC) has adopted rule changes to address the certification of SDR

equipment in [13], where SDR is considered a new class of equipment with streamlined equipment authorization. The purpose of the action is to modify certification rules to accommodate the flexibility offered by SDR. Specifically, FCC amended the equipment authorization rules to permit equipment manufacturers to make changes in the frequency, power and modulation parameters without the need to file a new equipment authorization application with the Commission. The action also permitted electronic labeling so that a third party may modify a radio's technical parameters without having to return it to the manufacturer for re-labeling. The certification rules were updated in [14] to further facilitate the development and deployment of SDR and CR. Specifically, the action eliminated the rule for a manufacturer to supply radio software to the Commission upon request because this may become an unnecessary barrier to entry.

The action also required the manufacturer to supply a high level operational description of the radio software that controls its RF characteristics for SDR certification. Security aspects were also addressed by requesting software controls to limit operation to authorized frequency bands.

In [14], FCC does not allow the Telecommunications Certification Bodies (TCBs) to certify SDR equipment. SDR certification is required to be carried out at FCC labs. The reason is because software defined radio is a new technology; TCBs will not be permitted to certify software defined radios until the Commission has more experience with them and can properly advise TCBs on how to apply the applicable rules.

The European context is more complex because of the geopolitical diversity and the presence of national certification centers and processes.

The European Software Radio Architecture (ESRA) is an on going standardization activity at European level. The goals are to ensure waveform portability and SDR reconfigurability. The ESRA standardization activity will be implemented through existing projects at European level like ESSOR [15], WINTSEC and its follow-up EULER, which is focused on the application of SDR for improved joint interoperability in Public Safety and defense.

Many organizations and industries in Europe are involved in this process. The (EDA) European Defence Agency is a main player in this process.

At the same time, ETSI (European Telecommunications Standards Institute) started a similar initiative to conduct feasibility studies for the standardization of a wider concept of SDR technology called RRS (Reconfigurable Radio Systems), which are defined as follows (from [16]):

"The group of technologies for Cognitive Radio and for Software Defined Radio are all technologies for Reconfigurable Radio Systems (RRS). Such systems exploit the capabilities of reconfigurable radio and networks and self-adaptation to a dynamically changing environment, with the aim to ensure end-to-end connectivity."

In comparison to EDA, which is focused on the military and public safety domain, the main target domains of ETSI RRS are the commercial domain and the public safety domain. ETSI RRS is composed by four working groups: WG1 for system design, WG2 for handset architecture, WG3 for functional architecture and WG4 for Public Safety domain.

From a standardization point of view, the ETSI RRS is performing work that is complementary to the IEEE SCC41 and IEEE 802 activities, with a focus on SDR standards beyond the IEEE scope, CR/SDR standards addressing the specific needs of the European Regulatory Framework and

CR/SDR TV White Space standards adapted to the digital TV signal characteristics in Europe.

Currently, there are no specific working items on the certification of SDR/CR equipment, but the TC maintains a close link with other ETSI TCs and organizations to ensure conformance of SDR/CR to the European regulatory framework. Technical standards on the SDR architecture are currently under definition.

The main challenge of SDR certification in Europe is currently the lack of technical standards for SDR/CR technology against which certification should be executed.

The WINTSEC project has laid the foundations of ESRA, which however has not yet reached the level of a standard but rather an architectural framework; the items defined in the ESRA document are not actual requirements but mere recommendations. The ongoing EULER project [17], which is expected to provide further ESRA recommendations extensions, will not also propose a standard.

However, certification is valid against a published standard; no certification can exist against an architectural framework. The consequence is that any certification guidelines described in the deliverables of the WINTSEC project are designed against a future, ESRA-derived standard, and that they are described as "compliance evaluation procedures" rather than "certification procedures".

The concept of compliance evaluation is significantly less rigid than the concept of certification for a number of reasons: a) evaluation is a much more informal, less authoritative procedure where the steps and requirements can be adapted to each specific test case; b) compliance evaluation can be performed on any relatively mature version of the product under test as it deals mostly with general properties of it, rather than specific details; c) the result of evaluation is a report elaborating on the estimate of each property's compliance to the guidelines; d) evaluation procedures are often related to new, rapidly evolving technological domains, where a standard and certification procedure would quickly become outdated or hinder development.

It is advisable that a set of guidelines/directives accompanied by compliance evaluation procedures evolves into a standard and certification procedure as the technological domain involved matures.

In Europe, certification of wireless equipment is driven by the Radio and Telecommunications Terminal Equipment Directive (R&TTE) that came into force in April 2000 in Europe. With the exception of a few categories of equipment, the Directive covers all equipment, which uses the radio frequency spectrum. A basic requirement is that radio equipment shall be so constructed to effectively use the spectrum allocated to terrestrial/space radio communication and orbital resources so as to avoid harmful interference. The adaptation of the R&TTE directive for SDR technology has been investigated by the Telecommunications Conformity Assessment and Market Surveillance Committee (TCAM), which is the standing Committee assisting the European Commission in the management of the R&TTE Directive 99/5/EC. In TCAM, the specific sub-group TGS (TCAM Group on SDR) was created to investigate SDR regulation with respect to the R&TTE Directive. Based on a TGS report provided to TCAM in 2006 ("Conclusions concerning the regulatory aspects of SDR with respect to the R&TTE Directive"), and on discussions in TCAM, the European Commission draw some conclusions to particular discussion points, but the discussion was not finalized.

Two deployment models for SDR technology are considered:

- Vertical mode, where the terminal reconfiguration can only be done (and authorized) through the equipment manufacturer (who also takes the responsibility).
- Horizontal model, where the reconfigurations can be authorized by different actors. The software only needs a declaration of standard compliance. This responsibility can be taken by different actors.

The following conclusions were presented:

- For downloaded SW, a digital marking (e.g., CE marking) is recommended.
- It is recommended to maintain, in the SDR devices, a history of software changes.
- SDR equipment would be considered as a "relevant component", in the meaning of Article 2 of the R&TTE Directive.
- Harmonized standards covering SDR devices should contain countermeasures against illegal programming and hacks for equipment, which are at risk.

Future versions of the R&TTE Directive may incorporate additional elements for SDR certification.

In summary, we can identify the following challenges for SDR certification in Europe:

- SDR technical standards should be defined for all the relevant domains: military/public safety and commercial.
- Identify who should have the responsibility of the final product or its components including software waveforms, SDR HW platform and software framework (e.g., SCA). This is especially important for a horizontal market.
- The European SDR certification process should address the geopolitical diversity of Europe and the existing national organizations and certification centers.
- Ensure that SDR technology validates harmonized radio-spectrum regulations at European level and non-harmonized regulations at national level.
- Ensure that all the certified waveforms and SDR platforms are managed in a controlled environment and accessible to end-users across Europe.

III. PROPOSAL OF A SDR CERTIFICATION FRAMEWORK

The purpose of this section is to describe a SDR certification framework, which is able to address the challenges, describes in the previous section.

The certification framework is based on the following elements:

- Reference implementation, which complements existing or future standards on SDR. Reference implementations are useful to resolve ambiguities in the standards definition.
- Procedures and tools to certify API compliance
- Use of Reference platforms against which waveforms should be certified.
- A European certification network to address the geopolitical diversity of Europe.
- A repository of waveform libraries, which can be accessed by end-users across Europe.
- A waveform usage and issue tracking to manage issues and changes in the versions of the waveforms.

The SDR certification framework addresses the horizontal model, which is the most complex of the SDR certification and deployment models.

The following stakeholders are identified:

- SDR HW platform manufacturers, which are responsible for designing and deploy the SDR HW platforms
- The SW waveforms designers, which are responsible for the creation of SW waveforms in accord to specific standards and specifications.
- The telecom provider, which provides the network deploying SDR technology.
- The user/subscriber of the SDR platform and the network.

- The administrative organizations, which include the European and national spectrum regulators and the authorities, which manage the use (and certification) of SDR technology in the market.
- The certification authorities, which may be industry or government representatives.

A. Reference Implementation

Naturally, a large effort is made during the design of a standard to be as concise, consistent and complete as possible. However, it is realistically *inevitable* that any standard contains ambiguities, gaps or sometimes even contradictions in its definition. This runs contrary to the goal of standard compliance, which is seamless interoperability between components or systems.

A trend that is becoming more and more prevalent is for any standard to be complemented by a reference implementation. This is an open, free and complete software implementation of the standard, usually defined by a neutral, impartial, independent and trusted entity. The goal of such an activity is to clarify the standard, while at the same time encouraging wide adoption.

Any ambiguities in the wording of the standard should be easily resolvable by consulting the source code of the reference implementation. Furthermore, any contradictions inside the standard definition should be discovered during the development of the reference implementation, and the standard drafting body (or consortium) should be notified, in order to rectify them. It is therefore evident that two-way flow of information between the standard drafting body and the developers of the reference implementation is necessary to improve the quality of the standard.

The reference implementation should be thoroughly documented, as the goal is clarity. A high-level language should be preferred, since code readability should be preferred over efficiency in a reference implementation. Finally, the code should be extensively cross-referenced to the articles and clauses of the related standard, in order to improve the tracking of the design choices in the reference implementation.

B. Certifying API Compliance

The outcome of a software standard is often a set of Application Programming Interfaces (APIs), which allow other programs or modules to interface with and exploit the capabilities of software components. Therefore, an important activity of the certification process for standard compliance is to check compliance to the resulting API.

Certification of a component's compliance to a given API is usually done by executing a software test tool (or set of tools) that thoroughly checks the existence of all the functions and data structures defined in the API in the component under test and their robustness (stress testing). For example a method might be called with a predefined set of arguments, and the result would be compared to the expected result. This is commonly called Unit Testing. Part of the stress testing process might be calling methods with erroneous/invalid input parameters; in this case, an error should be returned by method and the software executable under test should not enter in an undefined state. For example, the software executable should not crash or hang.

Unit testing has a set of limitations: it can only follow a limited number of execution paths, and therefore it can only test for the existence of a limited number of errors. In other words, unit testing cannot guarantee the absence of errors.

Finally, while unit testing can confirm the existence and correct operation (under normal conditions and under stress) of all the methods and objects in an API, it cannot test for the existence of additional methods and/or objects (extensibility).

Development tools could also be used for testing and validation of the waveform and SDR framework (e.g., SCA) code. In the early days of computer programming, source code was written in a single long file using a plain text editor. The target had single processor architecture. Today, especially in the SDR context, the common practice is to create first a platform-independent model of a component, then a platform-specific model, and then generate code for multiple architectures (e.g., GPP, DSP and FPGA).

Therefore, complex and powerful Integrated Development Environments (IDEs) are used throughout the industry. These IDEs provide a long series of additional features to the developer, such as syntax highlighting, auto completion, build automation, debugging, version control, built-in documentation, configuration management and others.

Often these tools include (either built-in, or in the form of plug-ins) compliance testing functionalities for a specific standard. This is highly beneficial for the process of pre-certification, as it allows developers to test their code for standard compliance parallel to their coding efforts (two of the four basic Extreme Programming activities), rather than test for compliance towards the end of the development process, when it actually might be too late. The reference implementation might be instrumental in this compliance testing process.

Example of Development and Testing Tools are the CRC's SCA Architect and Prismtech's Spectra CX, which are both based on the Eclipse IDE.

C. Reference Platforms

While part of the certification testing of a waveform's components might occur on the source code or the configuration/interface files, some of the tests will inevitably need to be run on the full, ported waveform, which is downloaded and activated on the SDR platform.

While it would be possible to select a high-quality SDR platform (i.e., the reference platform), against which all waveforms should be run for certification testing, several problems arise from this approach:

1. Such a choice would give the manufacturer of the SDR platform an undeniable and unfair advantage over their competitors, as they would be able to claim to be the “preferred platform provider”. Furthermore, such a choice would tie the European

SDR Certification community to a single vendor, denying all the benefits of market competition like costs reduction, supply chain diversification, etc).

2. The standard must be meticulously implemented in the waveform and reference platform. Otherwise, a single reference platform would create a de facto standard, which might slightly differ from the paper standard; waveform developers would be forced to comply with this de facto standard to pass certification.

As a solution to these problems, it is suggested to adopt multiple reference platforms for certification testing. A waveform under test would be ported, loaded and run on multiple platforms. A certification failure on a single platform would require further examination, but might hint to an incompatibility of the underlying platform. Instead, certification failure on two or more platforms would still require further examination, but it would indicate that most probably the error lies in the waveform under test.

The relationship among the various certification activities is described in Figure 1.

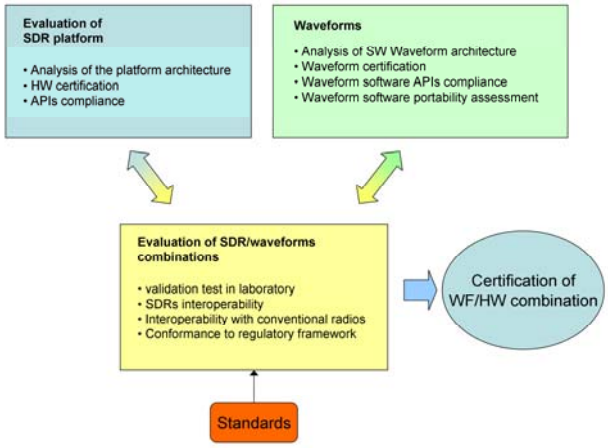

Figure 1 The relationships among different certification areas.

In the first phase, the SDR platforms and the waveforms are separately tested and certified for compliance to the standards. If these steps are successful, the next phase is the certification of the combinations of SDR platforms (i.e., HW) and Waveforms (i.e., SW).

An important certification activity is the conformance to the regulatory framework (e.g., the spectrum regulations) for the areas where the SDR Platforms and Waveforms are supposed to operate. For example, the SDR should not generate harmful interference to licensed users.

The validation activity should also include the case of roaming where a SDR device is used in different contexts with different national spectrum regulations.

At the end of the certification process, the certification body should release a compliance certificate, which includes the spectrum regulations considered in the testing activity.

D. SDR Certification Network

The technical requirements for the certification of SDR and its components must be mapped to a certification procedure. SDR certification tools need to be developed, either from scratch, or (more likely) building upon existing certification tools (e.g., the xUnit test framework). Then these procedures can be executed (using test tools) on a network of certification centers throughout Europe.

Some characteristics of this network:

- A centralized certification authority would not execute actual certification of products; instead it would prepare, monitor and accredit the certification centers, making sure that they are compliant to the shared certification procedures and tools.
- Location transparency of the certification process is a necessary requirement. It means that it shouldn't be easier to pass certification at one centre rather than another.
- Certification laboratories might be included in the process; these would be industrial champions or centres of excellence in a specific technological area (e.g., FPGAs), and would perform partial certification in that area for components developed by themselves or others. This is an extension of the concept of self certification.
- Redundancy should be considered to address occasionally increasing certification workload, or problems in the certification process.

A description of the structure of the European SDR certification network is provided in Figure 2, where Waveform and SDR platform certification centers are dependent on the national certification centre, which are connected to the centralized certification and accreditation authority. Note that centre for the validation against spectrum regulations can be affiliated both to a national centre and the centralized centre to include testing of roaming functionality among different nations.

The optimum number of certification centers is difficult to decide: some European larger countries might choose to create more than one certification centre, while smaller countries may decide to share the cost with other countries, or depend on larger countries for their certification needs.

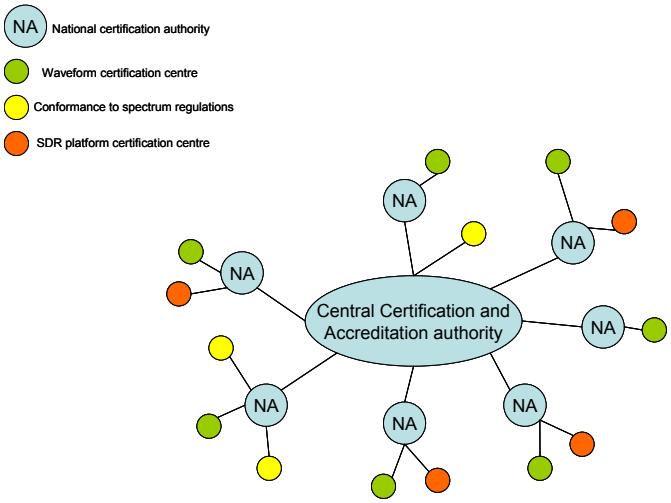

Figure 2 The structure of a potential European SDR certification network

In addition to the benefits of redundancy and national independence achieved by having a network of certification centers instead of a single one, the network would mitigate the risk of a slightly different, de facto standard created by a single certification centre as in the case of multiple reference platforms.

Finally, it would be mutually beneficial to maintain a close relationship with the US SDR certification centers (e.g., JTeL), to exchange know-how and possibly share procedures and tools.

E. Waveform Libraries

The creation of a central repository to maintain and distribute software modules is a common practice today. This approach provides the following advantages:

- A central repository provides more control for the storage and maintenance of certified software modules.
- The customers have easier access to a central repository.
- It is easier to implement automatic download and updates for new versions/features.
- It is easier to apply specific signatures on the certified software modules.

A similar approach is proposed to store the certified SDR Waveforms: a common, centralized repository (called "Waveform Libraries") of all the waveforms that have passed certification against the standards. This would facilitate over-the-air (OTA) downloads of complete waveforms as well as upgrades of waveforms and components. At the same time this repository would be a valuable tool during the certification process, by storing the results of the tests and keeping a history of past certifications.

Because of the presence of various administration authorities in Europe, it is suggested to have a distributed, redundant architecture for this repository, possibly with one instance per certification centre and one per national authority; limited, stripped-down versions of the repository might even be included in the local, encrypted storage of the SDR base stations and terminals in the field.

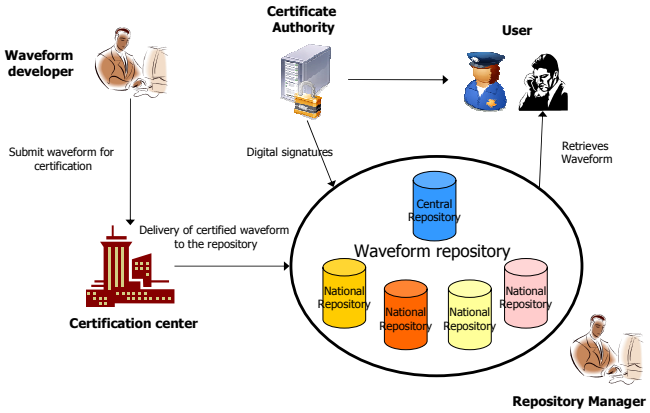

Figure 3 Waveform Repositories

Such a repository could include source code, binary files of the waveforms, or both. Additionally, it would certainly include configuration files, model/interface files (UML, IDL, etc), other meta-data related to deployment and use (such as performance requirements), and documentation files both for the porting/certification process and for the deployment/usage.

Some additional tags should accompany each waveform in the repository: information about certification status, the version of the standard with which the waveform complies, the communications protocol implemented, the license scheme, the owner of the waveform, etc. It will also include the information on the SDR platforms against which the waveform has been certified.

The structure of the waveform libraries is described in Figure 3, where the main stakeholders are present. The waveform developer submits the waveform for certification to the certification centre. After the certification, the waveform is stored in the national and centralized repository together with the information described above. The certificate authority can add digital signatures to the waveform to guarantee the security for the software download. Finally, the customer can collect or download the waveforms.

F. Waveform Usage & Issue Tracking

Alongside the waveform libraries discussed above, two additional tools are needed in the European SDR ecosystem to keep track of waveform usage and reported issues.

One tool is used to track waveform usage in customers. Tracking waveform usage would be useful to understand the needs of the end-users/customers, to introduce upgrades (using a push-mode, rather than a pull-mode in order to deploy upgrades to all the users of a specific waveform or component), and possibly also for licensing and fees collection. A waveform usage directory (WUD) could be

used to identify gaps in the SDR ecosystem and it would allow the central authorities to know which customers are using the waveforms. This tool can also be used to improve the efficiency of technical support and customization, but identifying which categories of customers are using specific waveforms.

The other tool is a centralized issue tracking system (ITS) that is integrated with the Waveform Libraries and the WUD. Its objective is to report and track any issue related to the malfunction of certified SDR platforms and waveforms or a request for an enhancement. The centralized ITS will store the list of all the available waveforms and it will allow customers to report issues.

The ITS will be based on a classical issues tracking flow. Once a new issue is reported by a customer, the issue tracking process will verify whether the issue reported is a known issue (i.e., a duplicate of another issue already registered in the ITS), if it is an enhancement request, if it is not really a waveform issue, but a deployment/configuration issue on the side of the end-user, or if it actually is a new issue that needs to have the developer's attention. When an issue is resolved by the developer, the ITS combined with the WUD would allow for efficient distribution of the update to all the users of the affected waveform or component.

Finally, the centralized Issue Tracking System would allow the involved partners and supervising authorities to collect statistics about the quality of the waveforms and waveform components (thus measuring the performance of waveform developers), as well as the performance of the support organizations.

IV. PERFORMANCE BENCHMARKING CERTIFICATION

SDRs are generally considered soft real-time systems, in the sense that signal processing has to keep up with the data rate of the communications system. In other words, the result of a calculation must not only be accurate, but it must also be completed by a certain deadline, otherwise it will not validate the operational requirements.

Each SDR waveform has specific performance requirements that need to be fulfilled, in order for it to run in real-time. These requirements might include definite processing speed from a processing core, a certain bandwidth or latency between processing cores, or the availability of certain components (e.g., an OCXO, or an RF front-end with a certain frequency range).

A. Performance Metrics

In order to compare the performance available on the platform with the performance required by the waveform, it is necessary to have a common way of describing and measuring these performance requirements and capabilities.

This task is more or less complex if an SDR Set operates in single-mode than when it operates in multi-mode. With single-mode we mean that a single waveform will execute on the platform at any single moment, while with multi-mode we mean that multiple waveforms will execute on the platform at any single moment, with voice, video and data bridges between them. A terminal will probably operate in single mode most of the time, while a base-station is most likely to operate in multi-mode.

In multi-mode, we should differentiate between the nominal (zero-load) performance that the platform can provide, and the actually available performance when one or more waveforms are already running on the platform.

B. Performance Benchmarking

Measuring the performance capacities of an SDR platform and the performance requirements of a SDR waveform is a valuable activity both during design phase and deployment phase.

Specifically, performance benchmarking during the design phase of a platform or of a waveform can allow developers to identify components that are performance hogs and focus their optimization efforts on these bottlenecks. On the other hand, performance benchmarking is essential when making purchasing or waveform porting decisions: it enables authorities to determine the feasibility of a waveform porting onto a platform by providing assurance that the waveform performance requirements will be satisfied by the platform hardware and software resources. Furthermore, once porting feasibility has been guaranteed, benchmarking can drive the adaptation effort of the porting.

Therefore the benchmarking has to start early in the design or porting process in order to limit the cost and time of the porting effort.

C. Processing Cores Benchmarking

CPU benchmarking might be the most widely studied and applied type of benchmarking in the computer industry. A wide selection of both open-source and proprietary solutions are available for CPU benchmarking; some of these tools are based on integer or floating point arithmetic, others on linear algebra operations, and others still on compression or audio/video encoding algorithms.

Here we mention only three of the most widely accepted CPU benchmarks: EEMBC's Coremark, HPL (High Performance Linpack) and Livermore loops. With minor modifications these tools could be ported to the SDR domain and be used in benchmarking GPPs/FPGAs and DSPs in SDR platforms.

Each SDR HW component may be used for specific tasks. For example, DSPs concentrate mainly on FIR/IIR filters, FFT calculations and codec implementations, so naturally these are the kinds of operations benchmarked. An example of DSP benchmarking is BDTi's DSP Kernel Benchmarks: a proprietary solution that executes 12 different types of benchmarks on each processor.

However, many of the graphics cards used for gaming PCs can be considered DSPs. In fact, several efforts are currently under way to exploit the DSP potential of commercial graphics processing units (GPUs) using either

nVidia's CUDA or Apple's OpenCL for signal processing. Furthermore, General Purpose Graphics Processing Unit (GPGPUs) such as the Cell processor (found in Sony's Playstation 3) or Intel's Larrabee show promising potential for mixed generic and signal processing applications, which makes them a good fit for SDR applications. See [18] for a description of the use of GPGPU to realize SDRs on desktop computers with distributed resources. In both the above cases, a multitude of benchmarking tools already exists.

D. *Benchmarking the entire SDR platform*

In addition to the procedures discussed above, which target specific components of an SDR platform, it is important to complement them with benchmarks that test the SDR platform as a whole; these types of tests often reveal bottlenecks that might go undetected by examining individual components separately.

The MPrime application is one such test. MPrime was originally developed to search for prime Mersenne numbers; however, due to the very intense performance requirements it imposes on the underlying platform, it is often used to stress-test computing systems for stability. Other such stress-testing tools are the FurMark (a closed-source, Windows-only fur-rendering performance and stability test for the GPU), or distributed computing clients such as the University of Berkeley's BOINC.

Another tool that could be used for benchmarking the SDR platform as a whole is the Phoronix suite (see Figure 4), probably the most widely used open-source test suite for Linux operating systems. It includes tests for the processor, memory, disk, and graphics and also for the system as a whole.

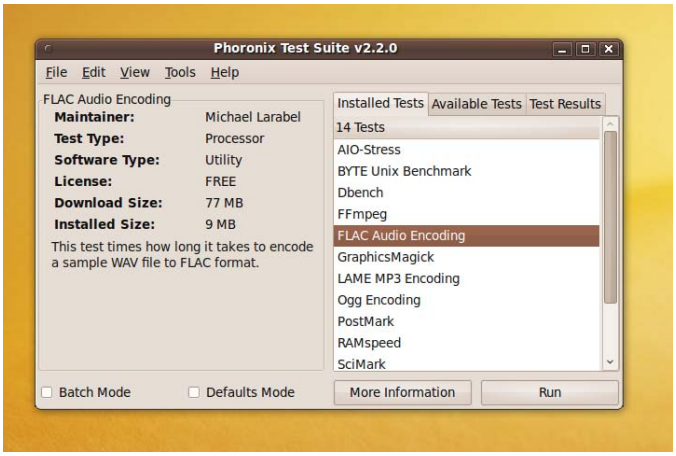

Figure 4 Phoronix Test Suite v2.2.0.

E. *Power consumption benchmarking*

Another architectural area, which requires performance benchmarking, is power consumption/power efficiency. This is an issue that is increasingly seeing the attention of both industry and academia, and a rather problematic area for the SDR domain (especially for handheld/portable radios) due to lower power efficiency of the more generic hardware (both processing and RF) used in SDR compared to the specialized hardware used in traditional legacy communications systems.

An example of benchmark tool for power consumption is PowerTop, an open-source tool released by Intel in 2007 as part of the LessWatts effort. PowerTop measures and tries to estimate the power consumption of software processes and device drivers, thereby identifying the culprits and guiding the effort of developers to minimize power consumption. This tool was successfully used in improving the power consumption of the Firefox browser and of several device drivers and kernel subsystems.

F. *Benchmarking of SDR waveforms*

While measuring the performance of a SDR platform is useful in the design, purchasing and waveform porting phases; it is instrumental to measure also the performance of an SDR waveform before porting or deployment.

OProfile is a system-wide profiler for Linux systems, which allows developers to receive real-time statistics about the resource usage of all a waveform's components with low overhead (usually less than 1%), in addition to several post-processing tools for analyzing these statistics. OProfile uses hooks in the Linux kernel to raise interrupts, and can be used both on x86 and on ARM processors.

OProfile is sponsored by some major companies such as IBM and RedHat. An OProfile plug-in exists for the Eclipse development framework, on which both Prismtech's and Zeligsoft's SDR development environments are based.

G. *Benchmark cheating*

Several incidents have been reported in recent years of cheating in CPU benchmarks, 3D accelerator benchmarks, Java VM benchmarks and others. This is commonly called as "benchmark cheating". It is therefore important that statistically rigorous techniques are used when evaluating the performance of SDR components and systems in order to avoid deceptive advertising and other irregularities:

- Run not one, but multiple different benchmark tools on the target in order to avoid "on-demand" benchmarks, i.e., benchmarks that favor one system vendor over the others.

- Run each of the benchmark tools on the device-under-test (DUT) a sufficiently large number of times, and clearly describe the statistical analysis on the vector of the results that led to the final benchmark output, so as to avoid e.g., reporting of only the best result obtained or arbitrarily discarding unfavorable results.

Finally, [19] describe tools from theoretical computer science including randomization, one-way functions, and trapdoor functions, which are used to improve the robustness of benchmarks against cheating.

V. SECURITY CERTIFICATION

As described in the previous sections, software portability should include security mechanisms, which guarantees the authenticity of the waveform and the trust of the SDR platform and waveforms.

The certification process is based on certification criteria, which are defined on the basis of regulations, standards and industry specifications. There are usually two certification processes: one process to certify the SDR platform, which includes the HW platform, RTOS and software framework and the second process for the waveform certification. Additionally, a certification process should be established for the security requirements. Security certification is an essential protection against security threats like download of malicious software, masquerading of a SDR node and denial of service (DoS). The security certification process for SDR can be based on similar processes already defined in the computing domain like the Common Criteria [20]. Among other things, Common Criteria are used to develop Protection Profiles, which identify the security requirements, and Assurance Levels, which describe the rigor of testing and evaluation. The combination of Protection Profiles and Assurance Levels results in a Security Target against which the certification process can evaluate a product. This model is appropriate for the future use of SDR in different markets: military, public safety and commercial with different security requirements and equipment costs. For each domain, we can define different types of protection profiles and security targets.

In comparison to conventional wireless equipment, the security certification process is particularly complex for SDR equipment because of the complexity of the technology and because various stakeholders could be involved in the certification process. A description of the challenges in the certification of non-functional requirements like security is provided in [9], which notes that certifications for security requirements are intrinsically different and more complex from those covering functional or process requirements, as they need to model the user as malicious for all the potential security threats and this increases the number of test cases.

An additional level of complexity is the presence of supplementary stakeholders like the certificate authority, which should be part of the certification process. The number and the role of the stakeholders depend on the related domain: military, public safety and commercial domain. In the military and public safety domains there are usually well defined security certification processes for conventional equipment, which can be adapted to SDR technology.

VI. CONCLUSIONS AND FUTURE WORK

Standardization is still an ongoing process, with multiple stakeholders involved. The goal of a European SDR standard is to facilitate waveform portability and system interoperability. To ensure these benefits, a network of certification centres accompanied by the relevant certification procedures and tools needs to be developed. These concepts were studied in the context of a European SDR Architectural Framework inside the WINTSEC project. The importance of performance metrics was described, as they're particularly important in order to validate the operational requirements in the public safety domain. Possible pitfalls were identified, including sensitive issues, either political or commercial. The need for Waveform Libraries, as well as a Waveform Usage & Issue Tracking directory were explained. Performance and Security aspects are particularly important in SDR technologies This paper described metrics, processes and tools for Performance benchmarking with special focus on mitigating the risk of performance cheating. This paper also described SDR security certification and the relationship to Common Criteria.

Future work will focus on the definition of a comprehensive framework for security certification of SDR equipment. The framework will include identification of the main stakeholders and related roles, certification processes and the link to the standardization activity.

ACKNOWLEDGMENT

Part of this work was performed in the project WINTSEC which has received research funding from the European Community's Seventh Framework program. This paper reflects only the authors' views and the European Community is not liable for any use that may be made of the information contained therein.

REFERENCES

[1] D. Symeonidis and G. Baldini, "European Standardization and SDR Certification," (AICT 2010), The Sixth Advanced International Conference on Telecommunications, pp. 136-141, May 9-15, 2010, Barcelona, Spain.

[2] J. Mitola III, "Software radios-survey, critical evaluation and future directions ," Telesystems Conference, 1992. NTC-92., National , vol., no., pp.13/15-13/23, 19-20 May 1992.

[3] D. R. Stephens, B. Salisbury and K. Richardson, “JTRS infrastructure architecture and standards,” in Military Commun. Conf., 2006.MILCOM 2006, Oct. 2006, pp. 1–5.

[4] “The Joint Tactical Radio System (JTRS) and the Army’s Future Combat System (FCS): Issues for Congress” by Andrew Feickert. CRS Report for Congress. Order Code RL33161. November 17, 2005.

[5] “Why Can’t We Talk? Working Together To Bridge the Communications Gap To Save Lives”. A Guide for Public Officials by US National Task Force on Interoperability. February 2003.

[6] US SAFECOM program. Web site http://www.safecomprogram.gov. Last accessed 03/01/2011.

[7] V Blaschke, F. K. Jondral and S. Nagel, "Wireless Interoperability for Security - WINTSEC," Nov. 2007, Software Defined Radio Technical Conf. Product Exposition November 2007.

[8] J.M. Chapin, and W.H. Lehr, "Cognitive Radios For Dynamic Spectrum Access - The Path to Market Success for Dynamic Spectrum Access Technology," Communications Magazine, IEEE, vol.45, no.5, pp.96-103, May 2007.

[9] J. Giacomoni and D.C. Sicker, "Difficulties in providing certification and assurance for software defined radios," New Frontiers in Dynamic Spectrum Access Networks, 2005. DySPAN 2005. 2005 First IEEE International Symposium on, vol., no., pp.526-538, 8-11 Nov. 2005.

[10] I. F. Akyildiz, W. Lee, M. C. Vuran and S. Mohanty, "NeXt generation/dynamic spectrum access/cognitive radio wireless networks: a survey". *Computer Networks* 50, 13 (Sep. 2006), 2127-2159.

[11] T. Ulversoy, "Software Defined Radio: Challenges and Opportunities," Communications Surveys & Tutorials, IEEE , vol.12, no.4, pp.531-550, Fourth Quarter 2010.

[12] Wireless Innovation Forum (ex Software Defined Radio Forum). http://www.wirelessinnovation.org. Last accessed 03/01/2011.

[13] Federal Communication. Commission, "In the matter of Authorization and Use of Software Defined Radios, First Report and Order," Sept. 2001, FCC 01-264, ET Docket No. 00-47.

[14] Federal Communications Commission, "In the matter of facilitating opportunities for flexible, efficient, and reliable spectrum use employing cognitive radio technologies, report and order," Mar. 2005, FCC 05-57, ET Docket No. 03-108.

[15] ESSOR project announcement on European Defence Agency website, http://www.eda.europa.eu/genericitem.aspx?area=News&id=54. Last accessed 03/01/2011.

[16] ETSI Reconfigurable Radio System Technical Committee. www.etsi.org.. Last accessed 03/01/2011.

[17] EULER project website, http://www.euler-project.eu/. Last accessed 03/01/2011.

[18] P. Szegvari and C. Hentschel, "An Universal Framework for Scalable Software Defined or Cognitive Radios Running on Desktop Computers" December. 2009, SDR'09 Technical Conference & Product Exposition.

[19] J. Cai, A. Nerurkar and Min-You Wu, "Making benchmarks uncheatable," Computer Performance and Dependability Symposium, 1998. IPDS '98. Proceedings. IEEE International , vol., no., pp.216-226, 7-9 Sep 1998.

[20] NIAP Common Criteria Evaluation and Validation Scheme. Available: http://www.niap-ccevs.org/cc-scheme/. Last accessed 18/01/2011.

A Mathematical Framework for the Performance Evaluation of an All-Optical Packet Switch with QoS Differentiation

John S. Vardakas*,Ioannis D. Moscholios†, Michael D. Logothetis*, and Vassilios G. Stylianakis*
*WCL, Dept. of Electrical and Computer Engineering
University of Patras, Patras, 265 04, Greece,
Emails: {jvardakas,m-logo,stylian}@wcl.ee.upatras.gr
†Dept. of Telecommunications Science and Technology
University of Peloponnese, 221 00, Tripolis, Greece,
Email: idm@uop.gr

***Abstract*—In this paper we propose a mathematical framework for the performance evaluation of an all-optical packet switch, in terms of packet blocking probability. We provide the analytical models for several QoS differentiation schemes, including wavelength conversion, packet dropping, pre-emptive dropping, fiber delay lines, and wavelength reservation. We demonstrate the accuracy of the proposed models by comparing the analytical results with that of simulation; the results are found to be quite satisfactory.**

***Keywords*-optical packet switching; wavelength division multiplexing; packet blocking probability; markov chains; quality of service.**

I. Introduction

Wavelength Division Multiplexing (WDM) is the most promising solution for the efficient utilization of the enormous bandwidth of an optical fiber [2]. In WDM optical networks, the bandwidth of an optical fiber is partitioned into multiple data channels, in which different messages can be transmitted simultaneously. Nowadays, the WDM technology is deployed in point-to-point architectures, where electronic devices are used to switch optical signals. However, traditional electronic packet switches are not suitable for handling such high bandwidth due to limitations of electronic processing speeds and due to the significant cost of high speed Optical-Electronic-Optical (O-E-O) converters [3]. Optical Packet Switching (OPS) is a promising sub-wavelength switching approach, since it is capable of dynamically allocating network resources with fine granularity and excellent scalability. In OPS networks the packet payload remains in the optical domain during the entire packet transmission from the origin to the destination node [4]. Even though the packet payload is switched transparently without O-E-O conversion, the packet header requires electronic processing. A long term approach of the OPS is to process, buffer and forward the entire packet (both header and payload) in the optical domain.

A vital problem in OPS networks is the resolution of packet contention which occurs at a switching node whenever two or more packets are switched on the same output wavelength, at the same time. In electrical packet-switched networks, contention is resolved with the store-and-forward technique, where packets that lost the contention are stored in a memory module, in order to be sent out at a later time to an available output port. This is possible because of the availability of electronic Random-Access Memory (RAM). Since there is no equivalent all-optical RAM technology, optical packet switches need to implement different approaches for contention resolution.

In OPS networks, popular contention resolution schemes include the use of Fiber Delay Lines (FDLs) [5], [6], wavelength conversion [7], [8] and deflection routing [9]. FDLs provide constant delay to optical packets, to avoid packet blocking and loss, when all output ports are busy upon packet arrival. Even though employing FDLs makes the switch bulky and expensive, especially in cases where large amount of data needs to be buffered [10], packet contention finds a straightforward solution by incorporating FDLs readily. Wavelength converters are used in an OPS switch to resolve optical packet blocking by transmitting a contending optical packet on another wavelength of the same fiber. Deflection routing is another way to minimize packet losses by routing packets, which lose the contention, to nodes different than their preferred next hop nodes, with the prospect that they will eventually reach their destinations [11]. The latter solution is not preferred in delay-sensitive services, such as real-time or interactive applications, because it may cause packet misordering upon arrival at the destination node.

Apart from wavelength conversion which is the most promising solution for optical packet blocking, other resolution schemes such as wavelength reservation, packet dropping and pre-emptive drop policy, must be employed, in order to provide Quality of Service (QoS) differentiation. Wavelength reservation is an access restricted scheme, where a number of wavelengths are reserved to benefit high priority service-classes [12]. In packet dropping, packets belonging to low priority service-classes are dropped with a certain probability, before destined to an output port [13]. In the

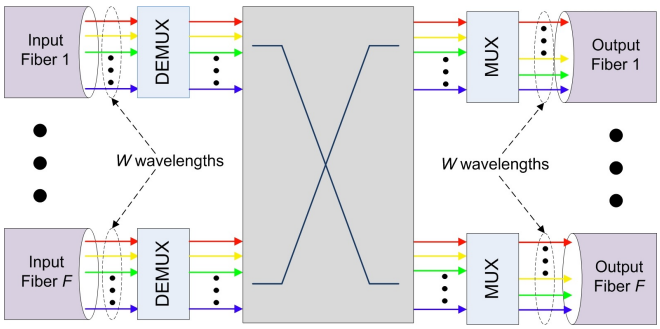

Figure 1. Generic configuration of an all-optical packet switch with F input/output fibers and W wavelengths per fiber.

pre-emptive drop policy, high priority packets pre-empt low priority packets (currently in transmission) in the case of contention.

The performance evaluation of an OPS switch, in terms of Packet Blocking (Loss) Probability (PBP), attracts notable research efforts [12]-[17]. We concentrate on Øverby's works [12]-[15], where analytical models for the PBP calculation in an all-optical packet switch, under the aforementioned QoS differentiation schemes, are presented. In [14], Øverby studied QoS differentiation schemes with wavelength converters for an asynchronous bufferless OPS switch, while the absence of wavelength converters was investigated in [15]. In all cases only two service-classes were considered (low and high priority) with infinite number of traffic sources. The utilization of FDLs in a slotted optical shared-buffer cross-connect is studied in [16], where a single service-class is considered. In [17] the authors present an analytical model for the calculation of the PBP in an all-optical packet switch equipped with tunable optical wavelength converters shared per output fiber that supports service-classes with different priorities.

In this paper, we extend our work presented in [1] and we propose analytical loss models for the PBP calculation in an all-optical packet switch that accommodates multiple service-classes of finite population, and supports QoS differentiation among them. The finite population assumption is essential, because the number of input ports in an all-optical packet switch is limited. Our study begins with the PBP determination in an all-optical packet switch with full wavelength conversion capability. The switch may operate without any QoS differentiation scheme, or adopt the intentional packet dropping policy, or the wavelength reservation policy (a number of wavelengths are reserved for each service-class). In addition, we study the all-optical packet switch which utilizes a number of FDLs in each output wavelength, by considering two cases: i) Packets belonging to a low priority service-class are intentionally forwarded to an FDL, before attempting to reach an output wavelength. In this way their arrival rate is reduced and therefore the probability that high-priority packets will occupy an output wavelength is increased. ii) Packets of a low priority service-class are not allowed to access the output wavelengths, when the number of occupied output wavelengths exceeds a predefined threshold. In that case, packets of the high-priority service-class are forwarded to an FDL.

Furthermore, we study the case of the absence of wavelength converters in the switch, where the QoS differentiation is employed either with the intentional packet dropping policy, or the pre-emptive drop policy. All the proposed models are computationally efficient since they are based on simple recurrent formulas. Our analysis is validated through simulation; the accuracy of the proposed models is found to be quite satisfactory.

The rest of the paper is organized as follows. In Section II, we present the analytical model for the PBP calculation in with full wavelength conversion capability in the case where i) no QoS differentiation scheme is applied (subsection II.A), ii) the intentional packet dropping policy is applied (subsection II.B), iii) the wavelength reservation policy is applied (subsection II.C), iv) the combination of the wavelength reservation policy and the intentional packet dropping policy is applied (sub-section II.D), and v) a number of FDLs is equipped in the switch (sub-section II.E). In Section III we present the analytical model for the PBP calculation in an all-optical switch without wavelength conversion capability i) under the intentional packet dropping policy (subsection III.A), and ii) under the pre-emptive drop policy (subsection III.B). Section IV is the evaluation section. Finally, we conclude is Section V.

II. All-Optical Packet Switch With Wavelegnth Conversion Capability

Fig. 1 shows the considered architecture of an all-optical packet switch with full wavelength conversion capability. The switch has F input and output fibers, while each input/output fiber supports W wavelengths. The bandwidth capacity of each wavelength is C bits/sec. Each one of the output fibers corresponds to a specific destination node. The OPS network accommodates K service-classes with different QoS priorities; service-class 1 has the lowest priority, while service-class K has the highest priority. Arriving packets at the switch are switched to the appropriate output fiber according to the packet header which is processed electronically. Since wavelength conversion is supported by the switch, a packet can be switched to any wavelength of the destination fiber, as long as at least one wavelength is available at the time instant the packet arrives at the switch. The arrival rate of service-class k packets ($k \in [1, K]$) is denoted as λ_k. We assume that the length of the packets is exponentially distributed with mean l_p, which is the same for all service-classes. The latter assumption is adopted in order to define the same service-time for each service-class; therefore, if a packet is accepted for service through an available wavelength, the time that this wavelength is

occupied is $\mu^{-1} = l_p/C$, where μ is the service rate of the wavelength, (exponentially distributed). In the following subsections we present the analytical models for the PBP calculation both without any QoS differentiation scheme, and with QoS differentiation schemes: the intentional packet dropping policy, the wavelength reservation policy, and the utilization of FDLs. Although our analysis targets at the PBP calculation in one destination fiber, it can be applied to any output fiber of the all-optical packet switch.

A. Absence of QoS differentiation scheme

The absence of a QoS differentiation scheme means that all service-classes have the same priority; therefore, the PBP is the same for all service-classes. The calculation of the PBP is based on the knowledge of the occupancy distribution of the wavelengths in the fiber. To this end, we formulate a Markov chain with the state transition diagram of Fig. 2, where state *i*represents the number of occupied wavelengths in the fiber. We denote the total packet arrival rate from an input wavelength by$\lambda = \sum_{k=1}^{K} \lambda_k$.We also indicate the number of input wavelengths that offer traffic to the fiber under study, as $R_f, f \in [1, F]$, where $R_f = F \cdot W$, if we assume that all output fibers have the same traffic load. The transition from state [*i*-1] to state [*i*] of the Markov chain occurs [*Rf*-(*i*-1)]·λ times per unit time. This is because in state [*i*-1] the number of input wavelengths which have not been used for a connection establishment with an output port is $R_f - (i-1)$, while the call arrival rate is aggregated to λ, since a packet from any service-class is required for the occupation of the wavelength. The reverse transition, from state [*i*] to state [*i*-1] is realized *i* times per unit time, where μ is the service rate of a wavelength. The probability *P*(*i*) that *i* wavelengths are occupied in the fiber can be derived from the rate balance equations of the state transition diagram of Fig. 2. We use the classical method for deriving the distribution *P*(*i*) which is described in [18]. More specifically, from the global balance equations (rate-out = rate-in), we obtain the following steady-state equation:

$$P(i-1)[(R_f-(i-1))\lambda] + P(i+1)[(i+1)\mu] = \\ = P(i)[(R_f-i)\lambda + i\mu] \quad (1)$$

where $P(i) = 0$ for $i < 0$ and $i > W$. By writing (1) for $i = 0$ to $i-1$, and summing up side by side, we get the following recurrent formula:

$$P(i) = \frac{\lambda}{\mu}\frac{R_f-(i-1)}{i}P(i-1) \quad (2)$$

Consecutive applications of (2) yields the equation that gives the probability *P*(*i*) that *i* wavelengths (*i*=0,1,…,*W*) are occupied in the output fiber:

$$P(i) = \left(\frac{\lambda}{\mu}\right)^i \cdot \frac{\prod_{j=1}^{i}[R_f-(j-1)]}{i!} \cdot P(0) \quad (3)$$

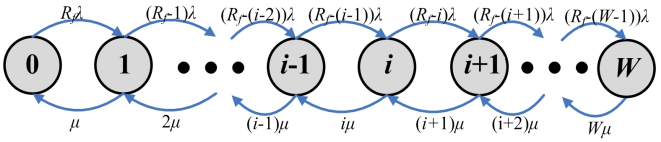

Figure 2. State transition diagram of the number of occupied wavelenths in the output fiber f, for the case of no QoS differentiation scheme.

The probability *P*(0) that the fiber is empty can be derived using the normalization condition,

$$\sum_{i=0}^{W} P(i) = 1 \quad (4)$$

Therefore, the probability *P*(0) is given by the following formula:

$$P(0) = \left[\sum_{n=0}^{W}\left(\frac{\lambda}{\mu}\right)^n \frac{\prod_{j=1}^{n}[R_f-(j-1)]}{n!}\right]^{-1} \quad (5)$$

It should be noted that the distribution of (3) is the well-known Engset distribution. The PBP is determined by (3) when *i*=*W*, i.e. *P*(*W*), since an input packet cannot be serviced when all the wavelengths are occupied. As a result, in the absence of any QoS differentiation scheme, the PBP is the same for all service-classes.

B. The intentional packet dropping policy

In the intentional packet dropping policy, a service-class k packet is dropped with a constant probability p_k, before reaching the output fiber. Since the first service-class has the lowest priority and the *K*-th service-class has the highest priority, $p_1 > p_2 > ... > p_K = 0$ i.e. a *K*-th service-class packet cannot be dropped. In order to favor specific service-classes, the values of the dropping probabilities p_k should be selected appropriately. In this case, the occupancy distribution of the wavelengths in the fiber could be derived from the state transition diagram of Fig. 2, with the substitution:

$$\lambda = \sum_{k=1}^{K} \lambda_k(1-p_k) \quad (6)$$

Following the same concept as in the case of no QoS differentiation scheme, the distribution of the occupied wavelengths in the output fiber is given by (3) and (5), where λ is given by (6). The PBP of a service-class k packet is given by:

$$B_k = p_k + (1-p_k)P(W) \quad (7)$$

since a service-class k packet can be blocked when the system is at any state with probability p_k, or at the last state (when all wavelengths are occupied) with probability $(1-p_k)P(W)$. Especially for the *K*-th service-class, the PBP

is determined by $P(W)$, given that the K-th service-class has the highest priority and $p_k = 0$.

C. The Wavelength Reservation Policy

In the wavelength reservation policy a number of wavelengths in the output fiber is reserved exclusively for each service-class. More precisely, a service-class k packet is accepted for service, when more than tk wavelengths are available in the fiber. In order to reduce the PBP of the high priority service-classes, we assume that $t_1 > t_2 > ... > t_K$.The occupancy distribution of the fiber is described by the Markov chain of Fig. 3, where the arrival rate $\lambda(i)$ is given by:

$$\lambda(i) = \sum_{k=1}^{K} \lambda_k D_k(i) \tag{8}$$

where $D_k(i)$ is a parameter that equals to 1, if the number of the free wavelengths is less than or equal to t_k, or equals to 0, if the number of the free wavelengths is more than t_k; therefore, from the state transition diagram of Fig. 3 we derive the recursive formula:

$$P(i) = \frac{(R_f - (i-1))}{\mu \cdot i} \sum_{k=1}^{K} \lambda_k D_k(i-1) \cdot P(i-1) \tag{9}$$

where:

$$D_k(i-1) = \begin{cases} 1, & \text{for } i \leq W - t_k \\ 0, & \text{for } i > W - t_k \end{cases} \tag{10}$$

Eq. (9) can be solved by setting $P(0)$=1, ($P(i)$=0, i<0), and normalizing each value over the summation $\sum_{i=0}^{W} P(i)$. The PBP calculation of service-class k is based on the summation of the probabilities of the blocking states [W-t_k] to [W], and is given by the formula:

$$B_k = \sum_{j=W-t_k}^{W} P(j) \tag{11}$$

D. A combination of the intentional packet dropping and the wavelength reservation policies

Under the intentional packet dropping policy, a low priority packet is dropped with a constant probability, even when the number of the occupied wavelengths is low (at the time instant of the dropping). An alternative solution could be the activation of the intentional packet dropping policy, only when the number of occupied wavelengths in the fiber exceeds a pre-defined threshold. In this way we favor the high priority service-classes only when the number of the available output wavelengths is low. Since the first service-class has the lowest priority and the K-th service-class has the highest priority, the dropping probabilities for the K service-classes are defined as $p_1 > p_2 > ... > p_K = 0$, while the thresholds for the activation of the dropping policy are defined as $t_1 > t_2 > ... > t_K = 0$; therefore packets of the highest priority cannot be dropped. In this case, the occupancy distribution of the fiber is described by the Markov chain of Fig. 3, where the arrival rate of packets is given by (6) only when the number of the occupied wavelengths exceeds the threshold W-t_k for the specific service-class, while, the arrival rate of service-class k packets equals to λ_k, only when the number of the occupied wavelengths in the fiber is less than W-t_k, therefore:

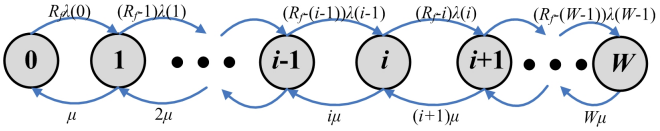

Figure 3. State transition diagram of the number of occupied wavelenths in the output fiber f, for the case of QoS differentiation scheme.

$$\lambda(i) = \begin{cases} \sum_{k=1}^{K} \lambda_k (1 - p_k), & \text{if } i \geq W - t_k \\ \sum_{k=1}^{K} \lambda_k, & \text{if } i < W - t_k \end{cases} \tag{12}$$

Following the same concept as in the case of no QoS differentiation scheme and based on the state transition diagram of Fig. 3 we derive the recursive formula:

$$P(i) = \frac{(R_f - (i-1))}{\mu \cdot i} \lambda(i-1) \cdot P(i-1) \tag{13}$$

Eq. (13) can be solved by setting $P(0)$=1, ($P(i)$=0, i<0), and normalizing each value over the summation $\sum_{i=0}^{W} P(i)$. The PBP calculation is based on the fact that a service-class k packet can be blocked at any one of the states from [W-t_k] to [W] with probability p_k, or at the last state (when all wavelengths are occupied) with probability (1-p_k)$P(W)$:

$$B_k = \sum_{j=W-t_k}^{W} p_k P(j) + (1 - p_k) P(W) \tag{14}$$

It should be noted that if t_2=W, then the set of equations (12)-(14) calculates the PBP in an all-optical switch, which supports 2 service-classes, under the intentional packet dropping policy (sub-section II-B), using the same values for the dropping probabilities p_k. Furthermore, if $p_2 = 1$, the same set of equations calculates the PBP in an all-optical switch, which supports 2 service-classes, under the wavelength reservation policy (sub-section II-C), using the same values for the parameters t_k.

E. Utilization of FDLs

Optical buffering using FDLs could be used in several ways in order to provide QoS differentiation. We consider two cases in which the OPS network supports 2 service-classes with different priorities. In the first case, only low priority packets are forwarded to FDLs before attempting to reach an output wavelength. In the second case, when the number of occupied wavelengths exceeds a pre-defined

threshold, packets that belong to the high priority service-class are forwarded to an FDL module before attempting to reach an output wavelength. In the following sub-sections we provide the analysis for the PBP calculation in both cases.

1) Delaying low priority packets through FDLs: We consider the case where low priority packets are forwarded to FDLs before attempting to reach an output wavelength. In this way the arrival rate λ_1 of the low priority packets is reduced and the high priority packets have increased probability to reserve an output wavelength. We assume that each wavelength is equipped with a module that contains an equal number of *L* FDLs. The length of each FDL is denoted by l_{FDL}; thus, the delay that a packet suffers during its transmission through an FDL is equal to the transmission delay plus the propagation delay of a packet:

$$h = \frac{l_p}{C} + \frac{l_{FDL}}{\tilde{c}} = \frac{l_p}{C} + \frac{l_{FDL} \cdot \tilde{n}}{c_o} \tag{15}$$

where $\tilde{c} = c_o/\tilde{n}$ is the speed of light in the optical fiber, *co* is the speed of light in the vacuum ($3 \cdot 10^8$m/sec) and $\tilde{n}$ is the refractive index of the optical fiber. Since the mean length packet l_p is exponentially distributed and $l_{FDL} \cdot \tilde{n}/_{c_o}$ is constant, *h* is also exponentially distributed.

The procedure of the postponement of the low priority packets through an FDL can be modeled as a loss system with a finite number of input traffic sources and *L* FDLs as the number of servers, as shown in Fig. 4. The number of the input traffic sources for each set of FDLs is not constant; it is a function of the number *i* of occupied wavelengths and consequently, the number of the input traffic sources to the FDL module of a wavelength is (R_f -*i*). Moreover, the arrival rate of each input traffic source is λ_1, since, only packets from the first service-class enter FDLs and the service time of FDLs is equal to *h*. This system can be described analytically by the Engset distribution:

$$q_i(j) = (\lambda_1 \cdot h)^j \cdot \frac{\prod_{m=1}^{j} [(R_f - i) - (m-1)]}{j!} \cdot q_i(0) \tag{16}$$

The probability $q_i(0)$ that FDLs are empty, when *i* wavelengths are occupied in the output fiber, can be derived using the normalization condition, $\sum_{m=0}^{L} q_i(m) = 1$. The probability that a low priority packet will find all *L* FDLs occupied is given by $q_i(L)$; in this case the low priority packet is blocked and lost.

Since the number of the input ports to an FDL module is a function of the occupied wavelengths, it is possible that in case of high wavelength occupancy, the low priority packets can not be blocked because of the unavailability of an FDL; they are only delayed by their transmission through an FDL. This situation occurs when the number of the input traffic sources is less than the numbers of FDLs in the FDL module. Therefore, the rate by which the packets egress the FDLs and request access to the wavelength is $L \cdot 1/h$, when the number of input ports is larger than *L*; if this number is less than *L*, no packets are blocked in the FDLs and the egress rate of the packets is $(R_f - i) \cdot 1/h$. This rate is added to the rate of the high priority packets, which is $(R_f - i) \cdot \lambda_2$. In the case of $(R_f - i) < L$, in order to achieve the reduction of the arrival rate of the low priority packets, this delay has to be larger than the inter-arrival time of the packets. The total arrival rate of packets, when *i* output wavelengths are occupied in the output fiber, is given by:

$$\lambda(i) = \begin{cases} (R_f - i) \cdot \lambda_2 + L \cdot \frac{1}{h} & \text{if } L < (R_f - i) \\ (R_f - i) \cdot \left(\lambda_2 + \frac{1}{h}\right) & \text{if } L \geq (R_f - i) \end{cases} \tag{17}$$

In order to calculate the distribution of the occupied wavelengths in the output fiber we construct the Markov chain of Fig. 5. By following the same procedure as in the case of no QoS differentiation scheme and based on the state transition diagram of Fig. 5, we derive the recursive formula:

$$P(i) = \frac{\lambda(i-1)}{i \cdot \mu} \cdot P(i-1) \tag{18}$$

Eq. (18) can be solved by setting *P*(0)=1, (*P*(*i*)=0, *i*<0), and normalizing each value over the summation $\sum_{i=0}^{W} P(i)$. The PBP of low and high priority service-classes are respectively given by:

$$\begin{array}{l} B_1 = \sum_{i=0}^{W-1} P(i) \cdot q_i(L) + P(W) \\ B_2 = P(W) \end{array} \tag{19}$$

since a low priority packet can be blocked when the system is at any state with probability $q_i(L)$ (blocked in the FDL module), or at the last state (when all wavelengths are occupied) with probability *P*(*W*).

2) Combining the wavelength reservation policy with the utilization of FDLs: We consider the case where the number of wavelengths is divided into two groups. The first group consists of $W - W_T$ wavelengths which are available for servicing packets of both service-classes. If the number of the occupied wavelengths in the output fiber exceeds the threshold $W - W_T$, then only packets of the high priority service-class are forward to an FDL module. Each one of the remaining W_T wavelengths (of the second group of wavelengths) is equipped with *L* FDLs. Packets that egresses the FDLs are able to attempt reaching one of the W_T wavelengths. Following the assumptions for the FDLs, presented in the previous sub-section, we define the arrival rate of the packets, when *i* output wavelengths are occupied as:

$$\lambda(i) = \begin{cases} (R_f - i) \cdot (\lambda_1 + \lambda_2) & \text{if } i \leq W - W_T \\ L \cdot \frac{1}{h} \text{ if } i > W - W_T \text{ and } L < (R_f - i) \\ (R_f - i) \cdot \frac{1}{h} \text{ if } i > W - W_T \text{and} L \geq (R_f - i) \end{cases} \tag{20}$$

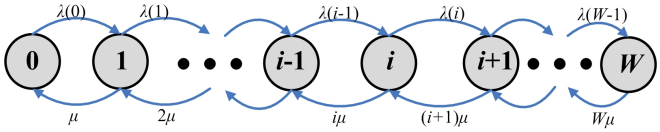

Figure 4. State transition diagram of the number of occupied wavelenths in the output fiber f, for the case where the all-optical switch utilizes an FDL module.

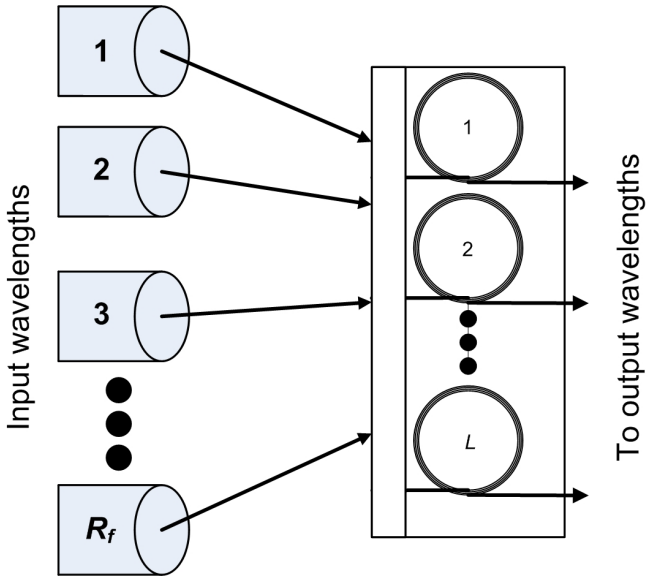

Figure 5. Schematic diagram of the module of L FDLs and R_f input wavelengths.

The distribution of the occupied wavelengths in the output fiber is given by (18) where the arrival rate $\lambda(i)$ is given by (20). The PBP of the low priority service-class is given by the summation of the probabilities of the blocking states $[W - W_T + 1]$ to $[W]$:

$$B_1 = \sum_{i=W-W_T+1}^{W} P(i) \tag{21}$$

The PBP calculation of the high priority service-class is based on the fact that a packet can be blocked in the FDL module at any one of the states from [W-t_k+1] to [W-1] with probability $q_i(L)$ (given by (16)) or at the last state (when all wavelengths are occupied) with probability $P(W)$:

$$B_2 = \sum_{i=W-W_T+1}^{W-1} q_i(L) \cdot P(i) + P(W) \tag{22}$$

III. All-Optical Packet Switch Without Wavelength Conversion Capability

The analysis of an all-optical switch without wavelength conversion capability could be considered as a special case of the analysis of an all-optical switch with wavelength conversion capability, presented in Section II. More precisely, we focus on the determination of the occupancy distribution of one output wavelength; therefore this analysis could be used to any output wavelength of any output fiber. In the following subsections we present the analytical models for the PBP calculation in an all-optical packet switch that operates under the intentional packet dropping policy, or the pre-emptive drop policy.

A. The Intentional Packet Dropping Policy

We assume that the switch operates under the intentional packet dropping policy; therefore a service-class k packet is dropped with a constant probability p_k, before reaching the output fiber. Since an output wavelength can be idle (state 0) or busy (state 1), we formulate a Markov chain with the state transition diagram of Fig. 6, where the total arrival rate is given by (6) and $R_{f,w}$ denotes the number of input wavelengths that offer traffic to the wavelength under study. By solving the Markov chain of Fig. 6, we derive the steady-state probabilities:

$$\begin{aligned} P(0) &= \frac{\mu}{R_{f,w}\lambda+\mu} \\ P(1) &= \frac{R_{f,w}\lambda}{R_{f,w}\lambda+\mu} \end{aligned} \tag{23}$$

Following the same analysis as in the full wavelength conversion case, the PBP of service-class k packets is given by:

$$B_k = p_k + (1 - p_k) \cdot P(1) \tag{24}$$

B. The Pre-Emptive Drop Policy

In the pre-emptive drop policy, high priority packets pre-empt low priority packets currently in transmission in the case of contention. In our study, we assume that the all-optical network supports 3 service-classes. When the wavelength under study is occupied, packets that belong to service-class 1 will be blocked, while packets that belong to the other two service-classes are permitted to interrupt the transmission of a service-class 1 packet, and pre-empt the wavelength. We assume that the successful pre-emption of a service-class 1 packet by a packet that belongs to service-class 2 and 3 is realized with probability p_2 and p_3, respectively. We define that service-class 3 packets have higher priority than service-class 2 packets, therefore $p_2 < p_3$. By fine-tuning the values of p_2 and p_3 we can adjust the PBP of service-class 2 and 3, respectively, to any desired level.

In order to model the all-optical switch without wavelength conversion capability, under the pre-emptive drop policy, we construct the Markov chain of Fig. 7. State [0, 0] is the idle state, while states [1, 1], [1, 2] and [1, 3] indicate the states where the wavelength is occupied by a service-class 1, 2 or 3 packet, respectively. When the system is idle, it is transferred to state [1, m], m=1, 2, 3, $R_{f,w} \cdot \lambda_m$ times per

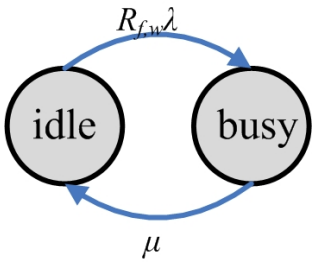

Figure 6. State transition diagram of the number of occupied wavelenths in the output fiber of the switch without wavelength conversion, under the intentional packet dropping policy.

unit time, where $R_{f,w}$ is the number of input wavelengths that offer traffic to the wavelength under study. When the system is at state [1, 1], it can be transferred to state [1, 2] $R_{f,w} \cdot \lambda_2 \cdot p_2$ times per unit time. This transition refers to the case where a service-class 1 packet is pre-empted by a service-class 2 packet. Similarly, when the system is at state [1, 1], it can be transferred to state [1, 3] $R_{f,w} \cdot \lambda_3 \cdot p_3$ times per unit time, when a service-class 3 packet pre-empts a service-class 1 packet. Solving the Markov chain of Fig. 7, we obtain the following state probabilities:

$$
\begin{aligned}
P(0,0) &= \frac{\mu}{R_{f,w}(\lambda_1+\lambda_2+\lambda_3)+\mu} \\
P(1,1) &= \frac{\lambda_3 R_{f,w}\mu}{(R_{f,w}(\lambda_1+\lambda_2+\lambda_3)+\mu)(\lambda_3 R_{f,w}p_3+\lambda_2 R_{f,w}p_2+\mu)} \\
P(1,2) &= \frac{\lambda_2 R_{f,w}(\lambda_3 R_{f,w}p_3+p_2 R_{f,w}(\lambda_3+\lambda_2)+\mu)}{(R_{f,w}(\lambda_1+\lambda_2+\lambda_3)+\mu)(\lambda_3 R_{f,w}p_3+\lambda_2 R_{f,w}p_2+\mu)} \\
P(1,3) &= \frac{\lambda_3 R_{f,w}((\lambda_3+\lambda_1)R_{f,w}p_3+\lambda_2 R_{f,w}p_2+\mu)}{(R_{f,w}(\lambda_1+\lambda_2+\lambda_3)+\mu)(\lambda_3 R_{f,w}p_3+\lambda_2 R_{f,w}p_2+\mu)}
\end{aligned}
\tag{25}
$$

A service-class 3 packet is blocked when the system is at state [1, 3] or either at state [1, 2], or at state [1, 1] and pre-emption fails. Similarly, a service-class 2 packet is blocked when the system is at state [1, 2] or either at state [1, 3], or state [1, 1] and pre-emption fails. A service-class 1 packet is blocked when the system is at states [1, 2] or [1, 3] or [1, 1] and pre-emption by a service-class 2 or 3 packet successfully occurs. Therefore the PBP of the three service-classes (B_1, B_2 and B_3, respectively) can be calculated using the formulas:

$$
\begin{aligned}
B_1 &= P(1,3) + P(1,2) + P(1,1)(1 + \tfrac{p_3\lambda_3}{\lambda_1} + \tfrac{p_2\lambda_2}{\lambda_1}) \\
B_2 &= P(1,3) + P(1,2) + (1-p_2)P(1,1) \\
B_3 &= P(1,3) + P(1,2) + (1-p_3)P(1,1)
\end{aligned}
\tag{26}
$$

IV. Evaluation

In this section, we evaluate the proposed analytical models through simulation. To this end, we simulate the different functions of the all- presented in section II and III, by using the Simscript II.5 simulation tool [19]. We examine the blocking performance of the all-optical packet switch, with or without wavelength conversion, by providing two application examples.

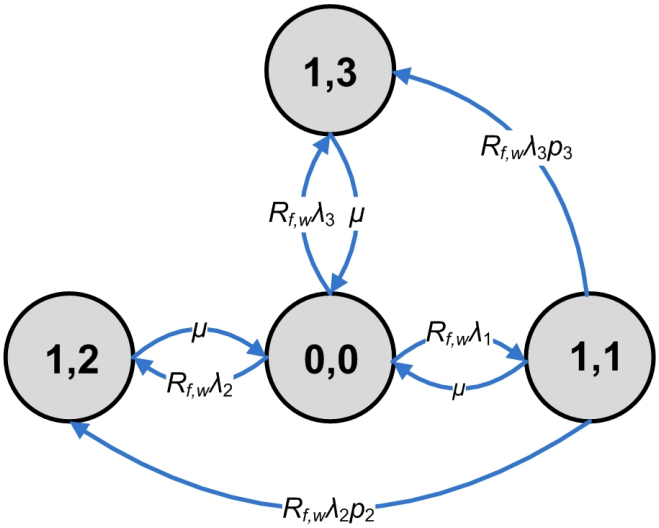

Figure 7. State transition diagram of the number of occupied wavelenths in the output fiber of the switch without wavelength conversion, under the pre-emptive drop policy.

In the first example we consider an all-optical packet switch with wavelength conversion capability. The number of the input/output fibers are *F*=10, while each fiber supports *W*=8 wavelengths. The capacity of each wavelength is *C*= 10 Gbit/sec. Packets that belong to *K*=2 service-classes arrive at the switch and they are switched to the appropriate output fiber. We calculate the PBP in one output fiber, while considering that an equal traffic load is offered to every output fiber, i.e. $R_f = F \cdot W$. The length of the packets that belong to all service-classes is exponentially distributed with mean value of 15 Kbytes. In Table I we present analytical and simulation PBP results for the case of no QoS differentiation policy versus the arrival rate per idle input wavelength. Since no QoS differentiation scheme is considered, the PBP is the same for the two service-classes. The comparison between analytical and simulation results reveals that the accuracy of the proposed analytical model is completely satisfactory.

The effect of the application of the intentional packet

Table I
Analysis Versus Simulation For The PBP In The Case Of No QoS Differentiation Scheme

Arrival rate (packets/sec)		Packet Blocking Probability (PBP)		
1^{st} serv.	2^{nd} serv.	Analysis(%)	Simulation	
			Mean (%)	95% Conf. Interval
500	1000	0.00766	0.00756	6.2×10^{-5}
750	1250	0.04858	0.04820	7.5×10^{-4}
1000	1500	0.17883	0.17742	2.6×10^{-3}
1250	1750	0.48379	0.47999	5.6×10^{-3}
1500	2000	1.04937	1.04114	9.1×10^{-3}
1750	2250	1.94094	1.92571	2.8×10^{-2}
2000	2500	3.18720	3.16220	4.3×10^{-2}

dropping policy to the PBP is shown in Table II. A packet that belongs to the first service-class is dropped with a constant probability p_1=0.05, while packets that belong to the second service-class cannot be dropped. As Table II shows, the model's accuracy is satisfactory. We notice that the PBP of the second service-class is reduced, compared to the corresponding results of Table I, while the PBP of the first service-class is increased. This is due to the fact that 5% of the first service-class packets are dropped, before reaching an output wavelength; therefore packets that belong to the second service-class have privileged access to the output wavelengths. Moreover, in Figs. 8 and 9 we present analytical PBP results for both service-classes, respectively, versus the packet arrival rate, for various values of the dropping probability p_1. We consider 7 arrival-rate points (1, 2, ..., 7) in the x-axis of Figs. 8 and 9. Point 1 corresponds to$\lambda = (500,\ 1000)$packets/sec, and in the successive points the values of λ_1, λ_2 are equally increased by 250 packets/sec. The last Point 7 corresponds to (2000, 2500). Comparison of the results of Figs. 8 and 9 clearly reveals that the PBP of the first service-class strongly increases with the increase of the dropping probability p_1, while the PBP of the second service-class is softly affected by this increase.

The effect of the wavelength reservation policy on the PBP is presented in Table III. We assume the same scenario for the all-optical switch as in the two previous cases, while t_1=1 out of W=8 wavelengths are reserved for the packets of the second service-class (note that t_2=0). As the results reveal, the accuracy of the presented analytical model is quite satisfactory.

The impact of the increase of the wavelength threshold t_1 to the PBP of both service-classes can be monitored in Figs. 10 and 11. In particular, Figs. 10 and 11 illustrate the PBP of both service-classes against the arrival rate, for different values of the threshold t_1. We employ the same arrival-rate points, as the ones used in Figs. 8 and 9. The study of these figures reveals that the increase of t_1 results to the PBP decrease of the second service-class; the reverse performance is observed for the PBP of the first service-class. The explanation for this behavior is as follows: for high values of t_1 more wavelengths are reserved for the second service-class, thus packets that belong to this service-class have increased probability to access the output wavelengths of the output fiber, compared to packets that belong to the first service-class.

Table II
ANALYSIS VERSUS SIMULATION FOR THE PBP IN THE CASE OF THE INTENTIONAL PACKET DROPPING POLICY

Arrival rate		PBP 1^{st} service-class		PBP 2^{nd} service-class	
1^{st}	2^{nd}	Analysis(%)	Simulation	Analysis(%)	Simulation
500	1000	5.0058	$4.964\pm6.9\times10^{-2}$	0.006	$0.006\pm3.4\times10^{-5}$
750	1250	5.0374	$4.995\pm6.6\times10^{-2}$	0.039	$0.039\pm1.7\times10^{-4}$
1000	1500	5.1428	$5.099\pm7.1\times10^{-2}$	0.151	$0.149\pm2.3\times10^{-3}$
1250	1750	5.3932	$5.348\pm4.2\times10^{-2}$	0.414	$0.411\pm6.2\times10^{-3}$
1500	2000	5.8662	$5.817\pm1.5\times10^{-2}$	0.912	$0.904\pm2.1\times10^{-2}$
1750	2250	6.6243	$6.569\pm4.5\times10^{-2}$	1.709	$1.696\pm2.9\times10^{-2}$
2000	2500	7.7002	$7.636\pm6.0\times10^{-2}$	2.842	$2.819\pm6.0\times10^{-2}$

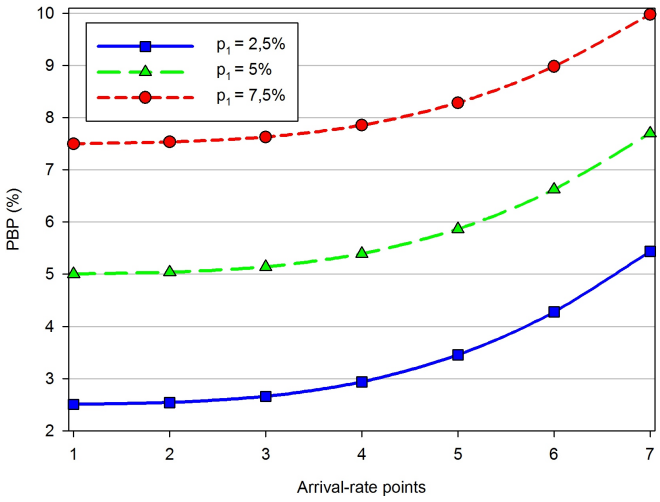

Figure 8. Analytical PBP results versus the arrival rate for different values of the dropping probability p1, for the first service-class of the first example, under the intentional dropping policy.

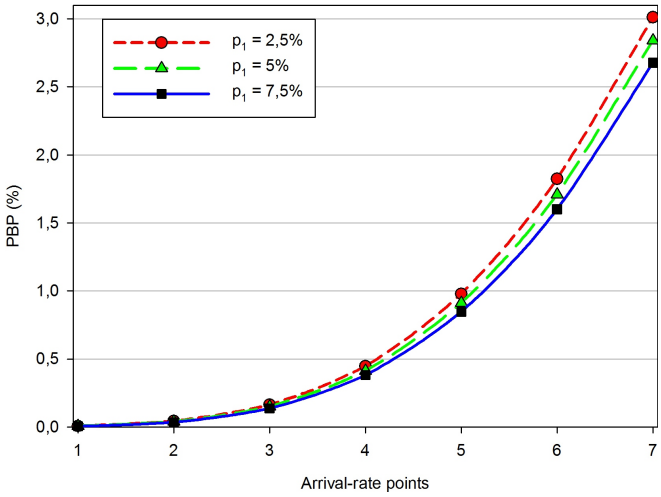

Figure 9. Analytical PBP results versus the arrival rate for different values of the dropping probability p_1, for the second service-class of the first example, under the intentional dropping policy.

The evaluation of the combination of the intentional packet dropping policy and the wavelength reservation policy is realized through the comparison of analytical and simulation PBP results versus the packet arrival rate, as presented in Table IV. The results were obtained under the first application example, while the dropping probability of the first service-class is p_1= 0.05 and t_1 = 1 out of 8 wavelengths are reserved for the second service-class. As the results of the Table IV reveal, the accuracy of the proposed analytical model is quite satisfactory. Since the results of

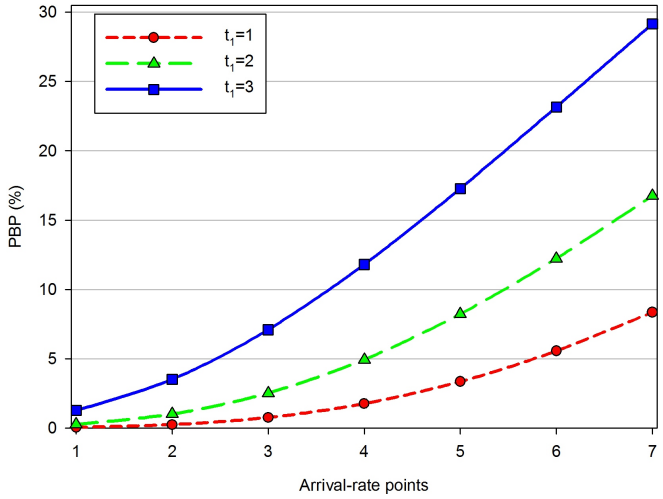

Figure 10. Analytical PBP results versus the arrival rate for different values of the threshold t_1, for the first service-class of the first example, under the intentional packet dropping policy.

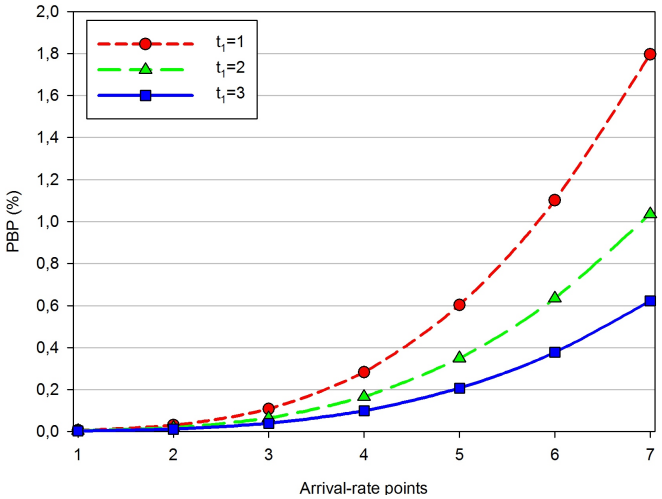

Figure 11. Analytical PBP results versus the arrival rate for different values of the threshold t_1, for the second service-class of the first example, under the intentional packet dropping policy.

Table IV were obtained by considering that only t_1=1 out of 8 wavelengths are reserved for the second service-class, there is a small benefit for packets of this service-class, over packets of the first service-class. The effect of the number of wavelengths that are reserved for the high priority service-class is depicted in Figs. 12 and 13. More precisely, Figs. 12 and 13 show the PBP of the two service-classes, respectively, versus the arrival rate, for different values of the threshold t_1, while the dropping probability p_1 is kept constant and equal to 0.05. As the results of Figs. 12 and 13 reveal, the increase of the value of t_1 has a small influence on the PBP performance of the high priority second service-class. On the other hand, increasing t_1 results in higher PBP values for the low priority service-class. Therefore, in order to benefit the high priority service-class, both the dropping probabilities p_k and the thresholds t_k should be carefully adjusted.

The first application example is also employed in order to evaluate the analytical models for the PBP calculation in an all-optical switch that utilizes FDLs. In the case where low priority packets are delayed by their transmission through a number of FDLs, we consider that each wavelength in the output fiber is equipped with a module that contains an equal number of $L = 4$ FDLs. The length of each FDL is denoted by $l_{FDL} = 5$ km, while the refractive index of the fiber that is used for the construction of the FDLs is *n*=1.55. In Table V we present analytical and simulation PBP results for the two service-classes against the arrival rate. The comparison of analytical and simulation results reveals that the accuracy of the proposed analytical model is satisfactory.

We also study the effect of the number of the FDLs in each FDL module, to the PBP of both service-classes. Fig. 14 presents analytical PBP results of both service-classes, versus the number of FDLs. We assume that the length of each FDL is $l_{FDL} = 5$ km, while the packet arrival rate of both service-classes is (λ_1, λ_2)=(300,500) packets/sec. Fig. 14 shows that when more FDLs are used in the FDL module, the PBP of the low priority service-class decreases; the reverse behavior is observed for the high priority service-class. For higher number of FDLs the PBP of both service-classes becomes the same and increases with further increase of the number of FDLs. This is due to the fact that when

Table III
ANALYSIS VERSUS SIMULATION FOR THE PBP IN THE CASE OF THE WAVELENGTH RESERVATION POLICY

Arrival rate		PBP 1^{st} service-class		PBP 2^{nd} service-class	
1^{st}	2^{nd}	Analysis(%)	Simulation	Analysis(%)	Simulation
500	1000	0.0518	$0.0512 \pm 5.5 \times 10^{-4}$	0.0051	$0.0050 \pm 8.9 \times 10^{-5}$
750	1250	0.2485	$0.2459 \pm 2.1 \times 10^{-3}$	0.0299	$0.0295 \pm 1.1 \times 10^{-4}$
1000	1500	0.7611	$0.7534 \pm 5.4 \times 10^{-3}$	0.1074	$0.1058 \pm 4.4 \times 10^{-3}$
1250	1750	1.7585	$1.7407 \pm 2.1 \times 10^{-2}$	0.2828	$0.2787 \pm 8.2 \times 10^{-3}$
1500	2000	3.3528	$3.3189 \pm 3.5 \times 10^{-2}$	0.6023	$0.5937 \pm 1.9 \times 10^{-2}$
1750	2250	5.5705	$5.5142 \pm 5.9 \times 10^{-2}$	1.1011	$1.0854 \pm 6.7 \times 10^{-2}$
2000	2500	8.3572	$8.2728 \pm 9.0 \times 10^{-2}$	1.7961	$1.7704 \pm 8.4 \times 10^{-2}$

Table IV
ANALYSIS VERSUS SIMULATION FOR THE PBP IN THE CASE OF THE COMBINATION OF THE WAVELENGTH RESERVATION AND THE INTENTIONAL PACKET DROPPING POLICY

Arrival rate		PBP 1^{st} service-class		PBP 2^{nd} service-class	
1^{st}	2^{nd}	Analysis(%)	Simulation	Analysis(%)	Simulation
500	1000	0.0097	$0.0096 \pm 2.2 \times 10^{-4}$	0.0074	$0.0073 \pm 5.4 \times 10^{-3}$
750	1250	0.0573	$0.0565 \pm 5.8 \times 10^{-3}$	0.0464	$0.0459 \pm 3.5 \times 10^{-3}$
1000	1500	0.2061	$0.2032 \pm 8.9 \times 10^{-3}$	0.1735	$0.1717 \pm 6.8 \times 10^{-3}$
1250	1750	0.5434	$0.5356 \pm 1.8 \times 10^{-2}$	0.4697	$0.4650 \pm 2.5 \times 10^{-2}$
1500	2000	1.1566	$1.1401 \pm 3.0 \times 10^{-2}$	1.0197	$1.0094 \pm 4.0 \times 10^{-2}$
1750	2250	2.1091	$2.0789 \pm 4.1 \times 10^{-2}$	1.8874	$1.8683 \pm 5.8 \times 10^{-2}$
2000	2500	3.4251	$3.3761 \pm 8.0 \times 10^{-2}$	3.1014	$3.0701 \pm 6.8 \times 10^{-2}$

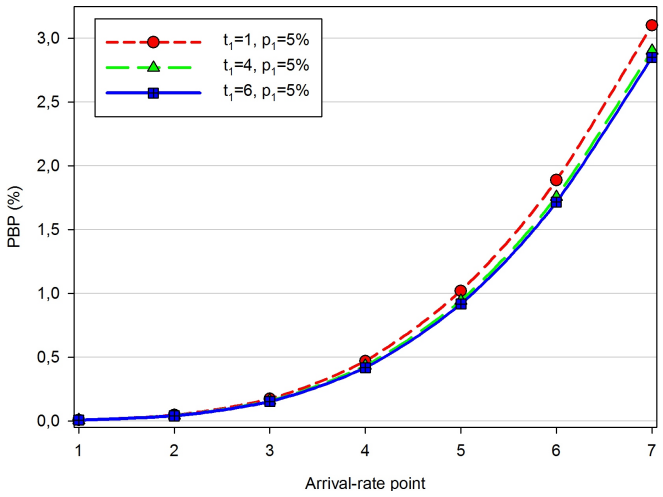

Figure 12. Analytical PBP results versus the arrival rate for different values of the threshold t_1, for the first service-class of the first example, under the wavelength reservation with intentional packet dropping policy.

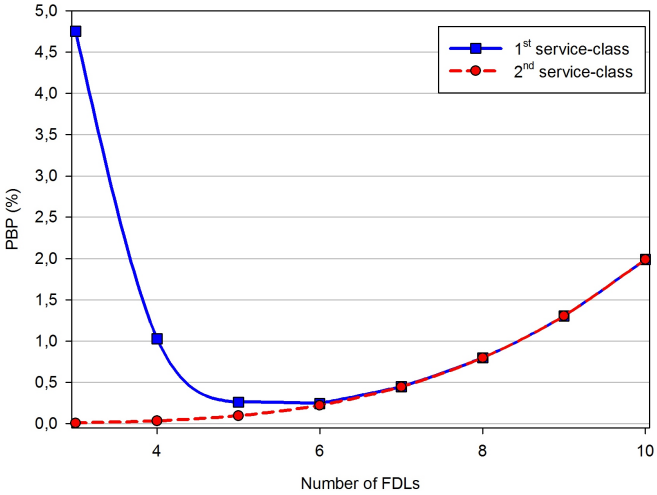

Figure 14. Analytical PBP results versus the number of FDLs for the two service-classes of the first example, for the case of delaying low priority packets through FDLs.

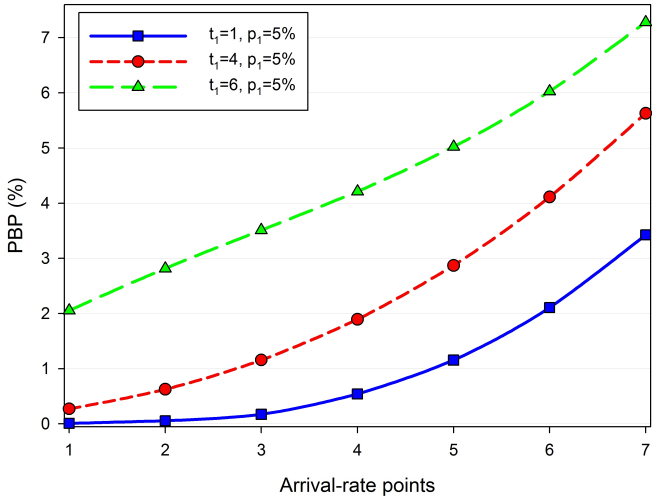

Figure 13. Analytical PBP results versus the arrival rate for different values of the threshold t_1, for the second service-class of the first example, under the wavelength reservation with intentional packet dropping policy.

few FDLs are employed, most of the low priority packets are blocked in the FDL module and high priority packets have increased probability to find an available output wavelength. By installing more FDLs in the FDL module, the difference between the PBP of both service-classes is reduced, while higher number of FDLs corresponds to higher input packet sources to the switch, which results in higher PBP for both service-classes.

Apart from the number of FDLs installed in each FDL module, another parameter that affects PBP is the length of each FDL. In Fig.15 we present analytical PBP results of both service-classes versus the length of an FDL. We assume that each FDL module consists of $L = 4$ FDLs, while the packet arrival rate of both service-classes is (λ_1, λ_2)=(300,500) packets/sec. Fig. 15 shows that the increase of the FDL length results in a PBP decrease of the high priority service-class, while the PBP of the low priority service-class has a decrease up to a certain value of the FDL length; after this point the PBP increases. The explanation for this behavior is as follows. When the FDL length is small, the delay that low priority packets experience is low and therefore the rate by which packets egress the FDL is high, compared to the rate when the FDL length is large. In the latter case, fewer low priority packets request service through an output wavelength; therefore high priority packets have privileged access to the output wavelengths.

The analytical model for the combination of the wavelength reservation policy with the utilization of FDLs is evaluated by comparing analytical and simulation results, as they are presented in Table VI. In particular, in Table VI we present analytical and simulation PBP results, for different values of packet arrival rate, for both service-classes. We consider the first application example, while each wavelength in the output fiber is equipped with a module that contains an equal number of $L = 4$ FDLs. Also, the length of each FDL is denoted by $l_{FDL} = 5$

Table V
ANALYSIS VERSUS SIMULATION FOR THE PBP IN THE CASE OF DELAYING LOW PRIORITY PACKETS THROUGH FDLS

Arrival rate		PBP 1^{st} service-class		PBP 2^{nd} service-class	
1^{st}	2^{nd}	Analysis(%)	Simulation	Analysis(%)	Simulation
200	400	0.2887	$0.2845 \pm 3.2 \times 10^{-4}$	0.0245	$0.0241 \pm 2.4 \times 10^{-4}$
300	500	1.0291	$1.0144 \pm 2.1 \times 10^{-3}$	0.0344	$0.0339 \pm 2.5 \times 10^{-4}$
400	600	2.3961	$2.3619 \pm 3.3 \times 10^{-3}$	0.0474	$0.0467 \pm 3.2 \times 10^{-4}$
500	700	4.3752	$4.3127 \pm 5.8 \times 10^{-3}$	0.0639	$0.0630 \pm 5.5 \times 10^{-4}$
600	800	6.8585	$6.7605 \pm 9.1 \times 10^{-3}$	0.0847	$0.0835 \pm 7.6 \times 10^{-4}$
700	900	9.7035	$9.5648 \pm 4.2 \times 10^{-3}$	0.1103	$0.1087 \pm 1.3 \times 10^{-3}$
800	1000	12.771	$12.589 \pm 6.6 \times 10^{-2}$	0.1414	$0.1394 \pm 2.1 \times 10^{-3}$

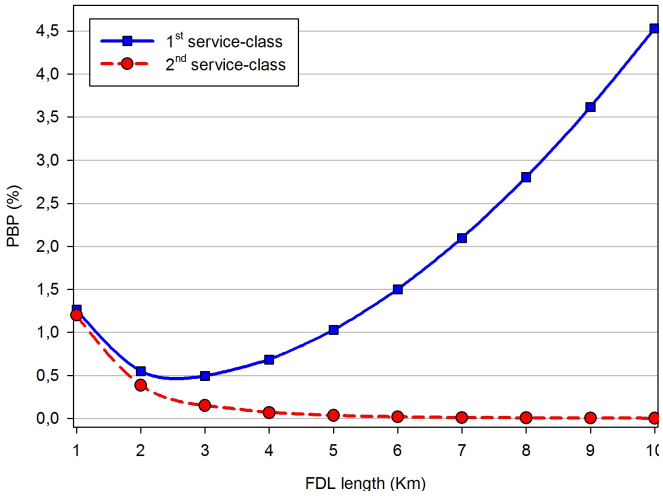

Figure 15. Analytical PBP results versus the length of each FDL for the two service-classes of the first example, for the case of delaying low priority packets through FDLs.

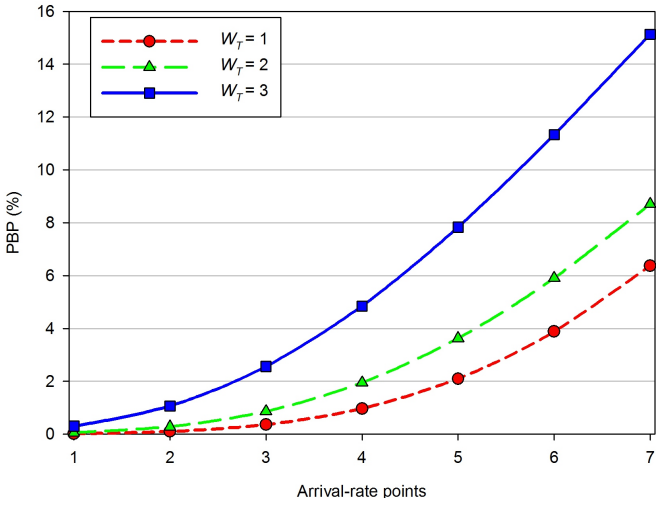

Figure 16. Analytical PBP results for the first service-class of the first example, under the combination of the wavelength reservation policy and the utilization of FDLs.

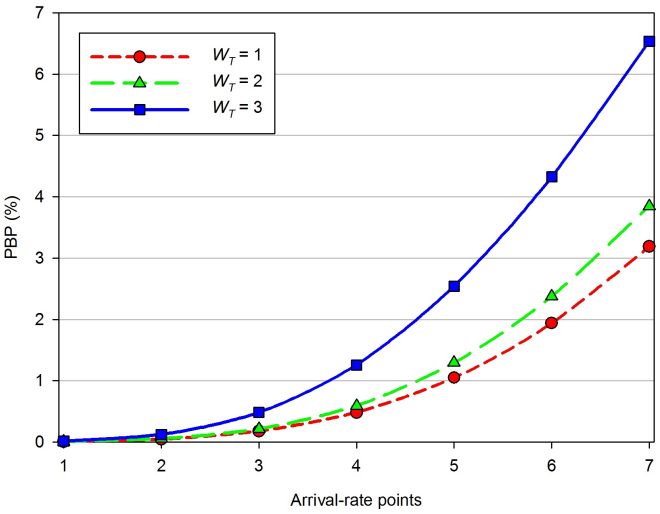

Figure 17. Analytical PBP results for the second service-class of the first example, under the combination of the wavelength reservation policy and the utilization of FDLs.

km and 2 out of 8 wavelengths are reserved for the high priority service-class. As the results reveal, the accuracy of the proposed analytical model is satisfactory. We also study the impact of the wavelength threshold W_T to the PBP. To this end, Fig. 16 and 17 presents analytical PBP results of both service-classes, respectively, versus the arrival rate, for different values of the parameter W_T. We consider 7 arrival-rate points (1, 2, ..., 7) in the x-axis of Figs. 16 and 17. Point 1 corresponds to $(\lambda_1, \lambda_2) = (500, 1000)$ packets/sec, and in the successive points the values of λ_1, λ_2 are equally increased by 250 packets/sec. Thus, Point 7 corresponds to (2000, 2500). As it was anticipated, the increase of W_T results in the increase of the difference of PBP of the two service-classes, since more wavelengths are dedicated to exclusively service high priority packets.

In the second application example, we consider an all-optical switch without wavelength conversion capability. The number of the input fibers are again F=10, while each fiber supports W=8 wavelengths. The capacity of each wavelength is C= 10 Gbit/sec. Packets that belong to K=3 service-classes arrive at the switch and they are switched to the same output wavelength. We study the blocking performance of a single wavelength, considering that an equal traffic load is offered to every output fiber, i.e. $R_{f,w} = F \cdot W$. The dropping probability of the second and third service-classes is $p_2 = 0.01$ and $p_3 = 0.02$, respectively, while packets from the first service-class are not dropped. In Fig. 18 we present analytical PBP results of the three service-classes, where the arrival rate is the same for all service-classes. As the results reveal, packets of the second and third service-classes suffer higher blockings, compared to packets of the first service-class. The same scenario is used to study the pre-emption drop policy. The successful pre-emption of a service-class

Table VI
ANALYSIS VERSUS SIMULATION FOR THE PBP IN THE CASE OF THE COMBINATION OF THE WAVELENGTH RESERVATION AND THE UTIZATION OF FDLS

Arrival rate		PBP 1^{st} service-class		PBP 2^{nd} service-class	
1^{st}	2^{nd}	Analysis(%)	Simulation	Analysis(%)	Simulation
500	1000	0.0615	$0.0606 \pm 1.4 \times 10^{-4}$	0.0091	$0.0090 \pm 2.2 \times 10^{-4}$
750	1250	0.2879	$0.2838 \pm 5.5 \times 10^{-4}$	0.0557	$0.0552 \pm 7.7 \times 10^{-4}$
1000	1500	0.8611	$0.8488 \pm 4.9 \times 10^{-3}$	0.2148	$0.2126 \pm 1.3 \times 10^{-3}$
1250	1750	1.9447	$1.9169 \pm 7.3 \times 10^{-3}$	0.5937	$0.5877 \pm 2.8 \times 10^{-3}$
1500	2000	3.6289	$3.5770 \pm 3.1 \times 10^{-2}$	1.2946	$1.2815 \pm 6.9 \times 10^{-3}$
1750	2250	5.9101	$5.8256 \pm 4.5 \times 10^{-2}$	2.3779	$2.3538 \pm 2.8 \times 10^{-2}$
2000	2500	8.7080	$8.5835 \pm 6.6 \times 10^{-2}$	3.8501	$3.8112 \pm 8.2 \times 10^{-2}$

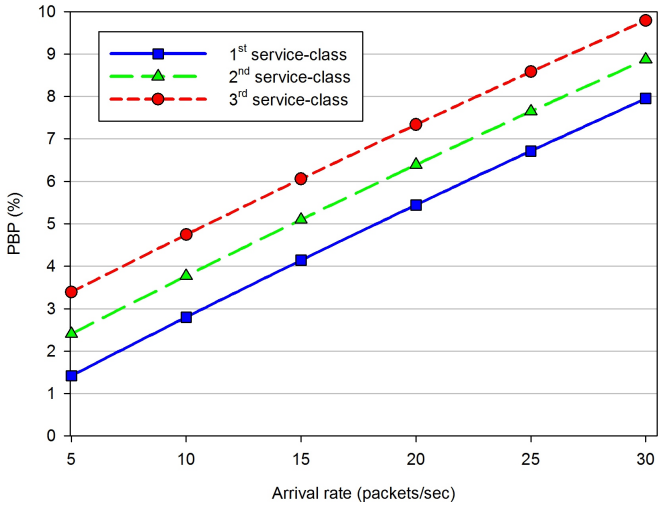

Figure 18. Analytical PBP results for the three service-classes of the second example, under the intentional packet dropping policy.

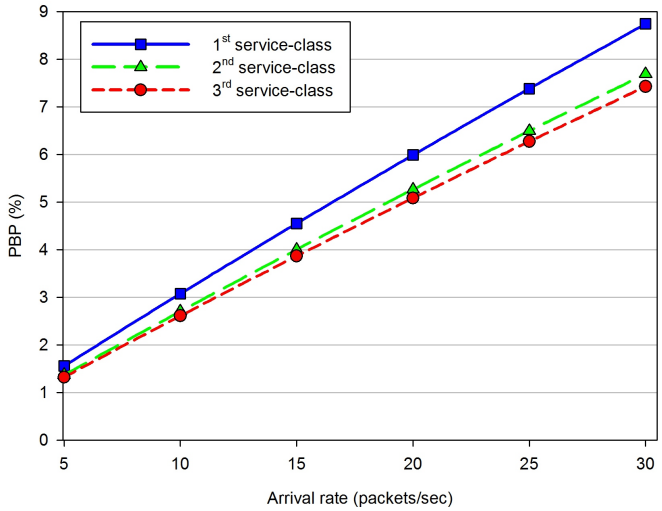

Figure 19. Analytical results PBP for the three service-classes of the second example, under the pre-emption drop policy.

3 packet by a packet that belongs to service-class 2 and 1 is realized with a probability $p_2 = 0.1$ and $p_1 = 0.2$, respectively. In Fig. 19 we present analytical PBP results of the three service-classes. As the results reveal, the PBP of the 3rd service-class is higher, compared to the PBP of the 1st and 2nd service-classes.

V. Conclusion

In conclusion, we propose analytical models for the calculations of PBP in an all-optical packet switch, under several QoS differentiation schemes. Packets that belong to multiple service-classes arrive from a finite number of input ports and attempt to gain access to an output wavelength. PBP is derived by the steady-state equation of one-dimensional Markov chains. The accuracy of the proposed calculations is quite satisfactory as was verified by simulations. In our future work we shall extend this analysis, in order to further study the effect of the implementation of FDLs and examine the deflection routing to the blocking performance of the all-optical switch.

Acknowledgment

This work was supported by the research program Caratheodory, of the Research Committee of the University of Patras, Greece.

References

[1] J. S. Vardakas, I. D. Moscholios, and M. D. Logothetis, "An analytical Study of an All-Optical Packet Switch with QoS Support", in Proc. of the 6^{th} IARIA Advanced International Conference on Telecommunications - AICT 2010 , Barcelona, Spain, May 9-14, 2010.

[2] B. Mukherjee, "Optical WDM networks", Springer, 2006.

[3] N. Bouabdallah, "Sub-wavelength solutions for next generation optical networks", IEEE Communications Magazine, August 2007, pp. 36-43.

[4] R. V. Caenegem, D. Colle, M. Pickavet, P. Demeester, K. Christodoulopoulos, K. Vlachos, E. Varvarigos, L. Stampoulidis, D. Roccato, and R. Vilar, "The design of an all-optical packet switching network", IEEE Communications Magazine, November 2007, pp. 52-61.

[5] N. H. Harai, N. Wada, F. Kubota, and Y. Shinoda, "Multistage fiber delay line buffer photonic packet switch for asynchronously variable-length packets", IEICE Transactions on Communications, vol. E88-B, no. 1, January 2005, pp. 258-265.

[6] D. Hwrter, M. C. Chia, and Andonovic, "Buffering optical packet switches", IEEE/OSA Journal of Lightwave Technology., vol. 16, no. 12, December 1998, pp.2081-2094.

[7] S. L. Danielsen, P. B. Hansen, and K. E. Stubkjear, "Wavelength conversion in optical packet switching", IEEE/OSA Journal of Lightwave Technology, vol. 16, December 1998, pp. 20952108.

[8] V. Eramo and M. Listanti, "Packet loss in a bufferless optical WDM switch employing shared tunable wavelength converters", IEEE/OSA Journal of Lightwave Technology, vol. 18, December 2000, pp. 18181833.

[9] S. Yao, B. Mukherjee, S.J.B. Yoo, and S. Dixit, "A unified study of contention-resolution techniques in optical packet-switched networks", IEEE/OSA Journal of Lightwave Technology, vol. 21, no. 3, March 2003, pp. 672683.

[10] Z. Zhang and Y. Yang, "Performance modeling of bufferless WDM packet switching networks with limited-range wavelength conversion", IEEE Transactions on Communications, vol. 54. no. 8, August 2006, pp. 1473-1480.

[11] J. P. Jue, "An algorithm for loopless deflection in photonic packetswitched networks", in Proc. of IEEE International Conference on Communications, ICC 2002, vol. 5, New York, USA, 28 April - 2 May 2002.

[12] H. Øverby and N. Stol, "A teletraffic model for service differentiation in OPS networks", in proc. of the 8th Optoelectronic and Communications Conference, Shanghai, China, 13-16 October 2003, pp. 677678.

[13] H. Øverby, N. Stol and M. Nord, "Evaluation of QoS differentiation mechanism in asynchronous bufferless optical packet-switched networks", IEEE Communications Magazine, vol. 44, no. 8, August 2006, pp. 52-57.

[14] H. Øverby, and N. Stol, "QoS differentiation in asynchronous bufferless optical packet switched networks", Wireless Networks, vol. 12 no. 3, 2006, pp. 383-394.

[15] H. Øverby and N. Stol. "Quality of service in asynchronous bufferless optical packet switched networks", Telecommunication Systems, 27(24), 2004, pp. 151179.

[16] A. G. Fayoumi and A. P. Jayasumana, "A surjective-mapping based model for optical shared-buffer cross-connect", IEEE/ACM Transactions on Networking, vol. 15, no. 1, February 2007, pp. 226-233.

[17] V. Eramo, M. Listanti and R. Tiberio, "Performance evaluation of QoS-aware optical packet switches", in Proc. of IEEE International Conference on Communications (ICC 2008) , Beijing, China, 19-23 May 2008.

[18] H. Akimaru, K. Kawashima, "Teletraffic theory and applications", Springer-Verlag, 1993.

[19] Simscript II.5, http://www.simscript.com/

A Media Delivery Framework for On Demand Learning in Manufacturing Processes

Martin Zimmermann
Production Systems Engineering
University of Applied Sciences Offenburg
77654 Offenburg, Germany
m.zimmermann@fh-offenburg.de

Abstract — **This paper presents a streaming-based E-Learning environment where closer integration between learning and work is achieved by integrating multimedia services into manufacturing processes. It contains a comprehensive and detailed explanation of the proposed E-Learning streaming framework, especially the adaption of streaming services to mobile environments. We first analyze several scenarios where E-Learning streaming services can be integrated into manufacturing processes. To allow systematic and tailor-made integration, we develop a model and a specification language for E-Learning streaming services and apply the model using practical scenarios from real manufacturing processes. Adaption of multimedia streaming services to mobile devices is discussed based on Synchronized Multimedia Integration Language (SMIL). Last, we comment on the benefits of using E-Learning streaming services as part of manufacturing processes and analyze the acceptance of the developed system. The key components of our E-Learning environment are 1) an xml based streaming service specification language, 2) adaption of multimedia E-Learning services to mobile environments, and 3) Web Services for searching, registration, and creation of E-Learning streaming services.**

Keywords - Just-in-time Learning, Media Streaming Services, Manufacturing Processes, Mobile Devices, Push Service, Pull Service, SMIL, Web Services.

I. INTRODUCTION

This article is an extended and revised version of the conference paper entitled "On Demand Learning in Manufacturing Processes" [1]. It contains a more comprehensive and detailed explanation of the proposed E-Learning framework, especially the adaption of multimedia streaming services to mobile environments.

Most E-Learning projects tend to separate learning activities from everyday work. This paper presents an approach where closer integration between learning and work is achieved by integrating multimedia services into manufacturing processes. A major challenge to which companies must respond is the integration of advanced E-Learning technologies. What is actually needed is a learning "on demand", embedded into work processes, responding to both requirements from the work situation and from employee interests, a form of learning crossing boundaries of e-learning and performance support.

The goal of E-Learning services integration in manufacturing processes is, through the development of new IT solutions, to accelerate and enhance the ability of manufacturing industry to capitalize on the emergence of a powerful global information infrastructure.

Manufacturing processes involve the control and management of manufacturing systems ranging from basic assembly processes to the high-tech manufacture of pharmaceutical, telecommunications and electronic equipment. Categories for such manufacturing processes are assembly line / flow shop, and cellular manufacturing / group technology. As an example, in case of assembly line based processes a line of dissimilar machines are grouped in the line (sometimes more than one to balance flow). Innovation, productivity, flexibility, and continuous improvement are key ingredients to success in the constantly evolving world of manufacturing.

Multimedia networking services support monitoring, controlling and supervising production processes in order to achieve high levels of efficiency and environmentally friendly production. The new flexibility of workers and work environments makes traditional conceptions of training in advance, in rather large units and separate from work activities, more and more obsolete. Manufacturing scenarios where E-Learning services can be integrated are shown in Fig. 1.

Computer networks provide a rich environment for constructing such interactive, intelligent, active, and collaborative learning environments. They offer certain distinguished advantages over traditional learning environments. In a traditional learning environment, employees are required to gather at a certain time and place to attend a lesson. In contrast, on demand-based learning allows employees from geographically separated locations to join lessons.

The proposed method adopts the client-server architecture to support multimedia content transmission. A media server may be a single machine or a group of machines to manage contents of the Internet-based learning system. It handles requests from users for push and pull services. In particular, it determines and schedules the required e-learning contents with optimal details to transmit to the users.

The following E-Learning streaming services can be identified:

- Pull (on demand) service: Allows on demand access to remote E-Learning content, e.g., video content illustrating configuration of a Computerized Numerical Control (CNC) machine.
- Push service: As an example, a push channel from a remote expert to the manufacturing personal ("how to configure / operate a machine"). Live audio and video (expert) as well as media files can be delivered (see Fig. 1).
- Push service: For recording a failure scenario during a manufacturing process (by recording the voice comments of a worker and by recording the machine status by video). This multimedia documentation can be used later to analyse details.

A further service type are peer to peer and multiparty conferences, e.g., for maintenance and remote diagnosis: teleoperation and remote diagnosis and maintenance of distant plant and production equipment can be achieved by using peer to peer E-Learning streaming services.

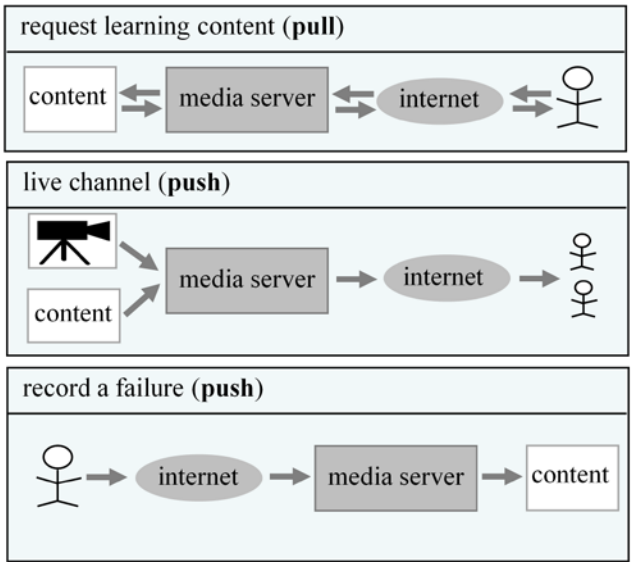

Figure 1. E-Learning services in manufacturing processes

The remainder of this document is as follows. Section II makes a comparative digest into related work in this field of interest. In Section III, we discuss a XML-based language, which allows specification of E-Learning streaming services while Section IV presents a generic SMIL-based adaptation methodology suitable to adapt E-Learning services to different access mechanisms, device capabilities and user preferences. Section V outlines the architecture and describes the major components and technologies to solve the problems stated in Section I. Finally, Section VI gives a brief summary and concludes with a note on future work.

II. RELATED WORK

Khasawneh et al. present a framework for an on-demand E-learning management system that make use of broadband network for the delivery of distributed "educational activities" such as distributed courses, tutoring sessions, lectures, workshops, etc. [2]. The developed scheme is tailored towards personalized learning using distributed information in a dynamic and heterogeneous learning setting, i.e., a connected network of learning management entities and educational systems where learners are individually supported in accessing distributed resources. However it is restricted to on demand scenarios and multimedia files.

Borissova et al. introduce a framework for design and development of an interactive multimedia E-learning system for engineering training [3]. The main goal of the project is to encourage low cost developing of effective and customized e-learning systems for engineering training by using popular and inexpensive software tools especially for virtual simulation of engineering system operations.

The Venice [4] project proposes a Web Services-based framework for VoIP applications. By using a service oriented architecture, the authors aim at easing the integration of supplementary services, the compatibility between different signaling layer protocols for call control and the installation of software updates on client devices. However, the Venice project is specifically tailored to VoIP scenarios, i.e., the authors do not address reusability between different multimedia applications nor provide a generic platform for the development of these.

Based on a distributed messaging middleware, the Global Multimedia Collaboration System (Global MMCS) [5][6] provides a framework for an audio/video collaboration system, which bridges the gaps between nowadays multimedia applications by providing a common signaling protocol with gateways to existing protocols like SIP or H.323 [10]. However, the authors do not address other multimedia applications and the reuse of components between these.

In [7], an approach is suggested to combine the areas of e-learning and Web Services, by providing electronic learning offerings as (individual or collections of) Web Services as well. It elaborates on this by showing how content providers and content consumers (i.e., learners) can communicate appropriately through a Web Service platform with its common description, publication, and retrieval functionalities. However, it does not support live channels.

The JSR 309 [16] is designed to provide server-based Java applications with multimedia capabilities. It targets a large range of applications from simple ring-back tone applications to complex conferencing applications, by providing: media network connectivity to establish media streams, IVR functions to play/record/control multimedia contents from file or streaming server, ways to join/mix IVR function to network connection to create conferences and call bridges. However the proposed API approach is restricted to Java based applications and it does not support enhanced VoIP functions, e.g., ring groups or call queues. It mainly provides low level objects like players, recorders, mixers and connections that developers can manipulate or combine together to obtain all the multimedia capabilities.

Scholz et al. present a generic framework for multimedia applications consisting of a set of reusable Web Service components, a modeling language based on finite state

automata and a compiler [17]. The authors concentrate on the signaling plane protocols, especially their similar structure and purpose, i.e., the definition of possible states for both, client and server, and the transitions between these states via the exchange of messages.

Chou et al. describe a service-oriented communication (SOC) paradigm based on Web Services for real-time communication and converged communication services over IP [11]. This approach extends Web Services from a methodology for service integration to a framework for SOC. In particular, it introduces the generic Web Services-based application session management (WS-session), the two-way full duplex Web Services interaction for communication, and the development of Web Services Initiation Protocol.

In [12], a mobile streaming media CDN (Content Delivery Network) architecture is presented in which content segmentation, request routing, prefetch scheduling, and session handoff are controlled by SMIL [13] (Synchronized Multimedia Integrated Language) modification. The approach concentrates on the segmentation aspect, which is important for mobile users.

Oliveira et al. present a proposal to solve the problem of the adaptation of multimedia services in mobile contexts [19]. The approach combines context-awareness techniques with user interface modeling and description to dynamically adapt telecommunications services to user resources, in terms of terminal and network conditions. The solution is mainly characterized by the approach used for resolving the existing dependencies among user interface variables, which is based on the constraints theory, and by the mechanism for acquiring the user context information, which uses the Parlay/OSA interfaces.

III. SPECIFICATION OF E-LEARNING SERVICES

To overcome the restrictions of traditional learning environments discussed in Section I, we present a novel concept for a model-driven development and deployment of E-Learning streaming services. Its central idea is the specification of E-Learning services in terms of manufacturing resources, media objects, and delivery policies. By using Web Services for composition of E-Learning streaming services, we facilitate reuse, customizability and technology-independence.

A. Media Streaming Model

The information model in Fig. 2 represents a model of our E-Learning streaming services (UML class diagram). Different fundamental components (represented by rectangles) of the system are shown in the form of classes and relationships.

Manufacturing processes are composed of manufacturing resources, e.g., manufacturing automation devices, equipment & machinery, material & manufactured parts, and manufacturing personnel. E-Learning streaming services are related to such manufacturing processes and / or single manufacturing resources. As an example, for a single machine a video on demand can be requested by the manufacturing personal to study the detailed configuration steps for such a machine.

According to the model in Fig. 2 an E-Learning service can be described by its media objects (e.g., audio and / or video objects), related manufacturing resource, distribution and replication policy, and the quality of service used for content delivery. Media streams can also be categorized according to how the media objects are delivered.

Fig. 2 shows how pull services, push services and conference services inherit from the E-Learning base class. This generalization relationship indicates that these sub classes are considered to be a specialized form of the super class (E-learning). In pull services data delivery is initiated and controlled from a client whereas in push services a server initiates data transfer and controls the flow. Content Caching means to replicate media objects across different E-Learning servers. Such content caches improve application performance by storing frequently requested content closer to end users of the content and by offloading servers from repetitive requests.

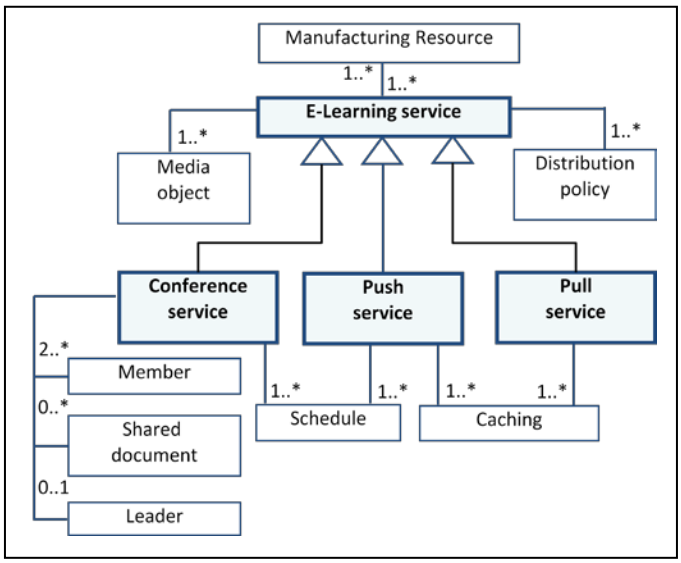

Figure 2. E-Learning service model

Conference services support scheduled and ad-hoc conferences. Such conferences contain the following attributes: date and time when the conference will take place, the invited participants and as an optional part the leader, the agenda as well as conference documents.

B. Use Case: Live training

The following scenario (Fig. 3) illustrates one of our implemented key use cases, a technical training (how to configure and operate a machine) for a computerized numerical control machine (CNC) as the related manufacturing resource.

The operator shows the handling of a machine to the distributed audience (video). A background speaker (at a separate location, e.g., office) explains the configuration steps (video / audio). To enable the interaction between the speaker and the learning community, each participant is offered an audio back channel. In the scenario there are different QoS requirements, e.g., for the video transmission showing the manufacturing machine a high resolution and frame rate is required.

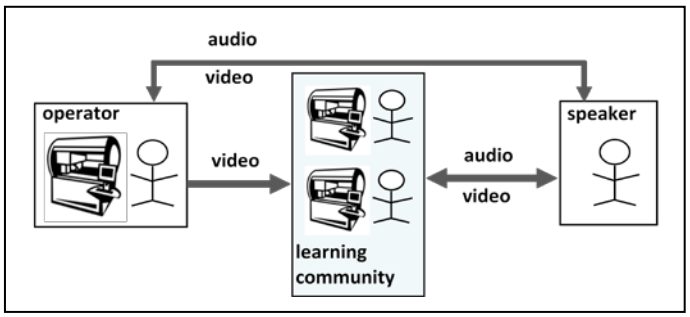

Figure 3. Example E-Learning scenario

C. XML Specification

For the specification of the properties of an E-Learning service we use XML. A specification of an E-Learning service is a structured composition of autonomous objects (see Fig. 4):

- Resources or manufacturing processes (category, type, keywords).
- A collection of media objects, e.g., audio and video objects (live or files) together with temporal relationships.
- Distribution policy, e.g., push or pull
- Roles and related media objects, e.g., speaker role.

This information can be used later, e.g., by the manufacturing personal, for searching and accessing E-Learning services.

Fig. 4 illustrates the specification of the live training scenario introduced in subsection A. The first part contains the description of manufacturing resources related to the E-Learning service. The list of media objects, which are used in the service is part of the section `<MediaObjects>` together with the type, bitrates and source.

For specification of temporal relationships we introduce two timing elements: `<seq>` and `<par>` similar to SMIL [13]. Both elements represent timing containers: they influence how the timing of their children is defined. A `<seq>` (sequential) container specifies that its children get processed sequentially: each child, whether it contains media objects or hierarchical structure, is processed when its predecessor ends. Fig. 4 shows the top-level sequential behavior in our E-Learning service: A `<par>` element specifies that its children play in parallel. Two videos and one audio fragment are rendered starting at the default time of the beginning of the `<par>` container.

The section `<DistributionPolicy>` defines the details of media delivery policy. The media streams in Fig. 4 are delivered based on a push policy. This includes also the definition when the media objects must be delivered (date and time), together with the available bit rates. There is also a recording option that allows creation of an archive recording while the live stream is going on.

Finally the roles, e.g., the speaker role are introduced together with a list of media streams, which are consumed and supplied by each role. As an example, the speaker role is a consumer of a video and an audio stream delivered by the role operator.

```
<StreamingService>

<ManufacturingResources>
   <resource  category = ″num control machine″ />
   <keywords>live training </keywords>
</ManufacturingResources>

<MediaObjects>
<par>
  <video id = ″videoSpeaker″ type = ″live″
                bitrate= … src =  … />
  <audio id = ″audioSpeaker″ type = live″
                bitrate= … src = …/>
  <video id = ″videoOperator″ type = ″live″
                bitrate= … src =  … />
   . . .
<par>
</MediaObjects>

<DistributionPolicy>
  <push codec=″MPEG4″ date= …  time=…
        recording=″yes″  file = …
  </push>
</DistributionPolicy>

<Roles>
   <role name=″Speaker″/>
     <consumerOf>
        <video id=″videoOperator″ />
        <audio id = ″audioLearningCommunity″… />
     </consumerOf>
     <supplierOf>
        . . .
     </supplierOf>
   </role>
   . . .
</Roles>
. . .
</StreamingService>
```

Figure 4. E-Learning service specification

IV. SMIL-BASED MULTIMEDIA INTERFACES

While the modeling and specification approach presented in the previous section specifically focuses on design time of E-Learning streaming services, this section presents a SMIL-based approach for adaption of multimedia streaming services to mobile devices. After a brief discussion of key differences between traditional devices and mobile devices, we present our concept in detail.

A. Multimedia Devices

The acceptance of new E-Learning services will only be effective if the users have the possibility to access them anywhere, and in any technological circumstances. Ubiquitous access to E-Learning services is becoming increasingly important with the proliferation of wireless devices and technologies. This requirement means that there is a significant challenge of being able to transform E-Learning services in

order to adapt them to a great variety of delivery contexts, i.e., various devices.

Examples in our manufacturing scenarios include:

- Mobile devices that are used by a problem solution team to display just in time information that is relevant to manufacturing problem, e.g., a previously recorded video showing a failure scenario.
- Ubiquitous collaborative learning via cell phones or PC tablets that allow the learner to play an active role in both the knowledge building process and decision making anywhere, anytime.
- Mobile technologies can provide situated learning by extending the learning/training environment beyond the production areas into authentic and appropriate contexts of use.

However, there are a number of key differences between a traditional device such as a PC and a mobile device, such as a PDA. These include especially screen size and resolution, data input capabilities, as well as browser features.

The screen size and resolution capabilities of a traditional PC are quite different from that on a mobile device. PCs have large screens of 15 inches or more with typical display resolutions of 1280 x 1024 or higher. Mobile display resolutions start at around 128 x 128, barely 1/100th of the available resolution on a PC. Although mobile device display resolutions on smart-phones are typically 240 x 320 and can reach 640 x 480 or greater, the physical size of the display is limited by the requirement to have a small pocket-sized device. Increasing the resolution provides more dots-per-inch, but delivers limited benefit on such a small screen. The available screen estate is important when designing E-Learning services for mobile devices, and simply reformatting existing content is not appropriate.

The data input capabilities on mobile devices are restricted compared to PCs. Most mobile devices have only a numeric keyboard and entering text requires multi-tap key entry. The data input constraints should be considered when designing the mobile application, and data entry should be as limited as possible.

B. Adaption of Multimedia Streaming Services

Among the alternatives that may be considered as standardized multimedia formats, i.e., HTML5, MHEG, MPEG-4 and SMIL, we decided to choose SMIL. The main reason behind this choice is the SMIL-based E-Learning streaming specification language (Section III), which is also based on SMIL. The well-designed and extensive SMIL language elements for adaption of multimedia streaming services to mobile devices is another reason.

SMIL (Synchronized Multimedia Integration Language) is a W3C recommended XML-based markup language, which facilitates the construction of accessible multimedia applications for the internet and mobile devices. Collections of XML elements and attributes can be used to describe the temporal and spatial coordination of one or more media objects. SMIL defines markup for timing, layout, animations, visual transitions, and media embedding, among other things. SMIL allows the presentation of media items such as text, images, video, and audio, as well as links to other SMIL presentations, and files from multiple web servers.

A SMIL application references to media objects, not the media data itself, and instructions on how those media objects should be combined spatially and temporally. Relations between media objects (and substructures) are described, and the computation of the timeline follows from this. The main temporal composition operators available are parallel composition, sequential composition and selection of optional content. Composition is hierarchical: nodes cannot become active unless all of their ancestors are active. The declarative containment model has one large advantage: SMIL presentations can adapt automatically to varying bandwidth conditions and alternate content with different durations. The hierarchical temporal composition model represents also a container for timed metadata, and allows structure-based deep linking into the content.

There are several alternatives available for making an E-Learning service compatible with different (mobile) devices:

- Resize the base layout: requires analyzing the used mobile devices and creating a layout that is not bigger than the most restrictive presentation environment. This is very safe strategy, but it can lead to frustration among E-Learning participants who have more sophisticated devices.
- Use device default layout: if no layout section is defined in a presentation, the SMIL player can place objects where it thinks they fit best. While this sounds attractive, it usually results in all content being stacked on top of all other content. The result is rarely pleasing or useful.
- Explicitly allow media objects to be scaled: SMIL provides values for media object placement that allow media objects to be scaled. While this is potentially useful, small devices will often have trouble when scaling media objects and especially video.
- Define multiple layouts using SMIL content control: this is the most useful way of handling multiple devices. SMIL provides a wealth of facilities for providing alternative layouts within one application.

In the following, we illustrate how to apply multiple layouts based on SMIL. One valuable SMIL feature in this context, especially for mobile devices, is the content control. It can be used to select over a number of layouts or media objects based on system properties. It is based on the switch element, which allows only one of its child elements to be chosen, the first one which is acceptable. It can be used anywhere in a SMIL document.

The general layout and some positioning models used in our E-Learning example are shown in Fig. 5. SMIL supports the notion of a top-level container window (called either the root-layout or top-Layout, which contains one or more regions. Each region defines a rectangular collection of pixels and a region stacking order (called the z-index).

The layout contains the root-layout container window (not shown) and several media rendering regions. Some of the regions are assigned an explicit stacking order, others take the default of their parent (in this case, the default for the root is '0'). Each region contains positioning information when screen space is used.

Fig. 5 illustrates three layout strategies for different devices. Depending on the available display area, the video objects part of the E-Learning service are handled in a different way. A standard layout containing three regions (Fig. 5 a): Two video regions, one for the speaker and one for the operator; an additional region for a text object, illustrating additional information, e.g., specification of configuration steps in a manufacturing scenario.

Fig. 5 illustrates also two different layout strategies for mobile devices:

- Fig. 5 c shows a simple positioning model on a small device where only the video of the operator is visible (accompanied by the speaker audio);
- The layout in Fig 5 b shows an overlapping layout, i.e., the small video (speaker) is part of the main video region. SMIL handles such overlaps by giving all regions z-index stacking levels. When two regions overlap, the region with the higher z-index "covers" the other with its overlap. In environments where bandwidth is restricted a image of the speaker could be played instead of the speaker's video.

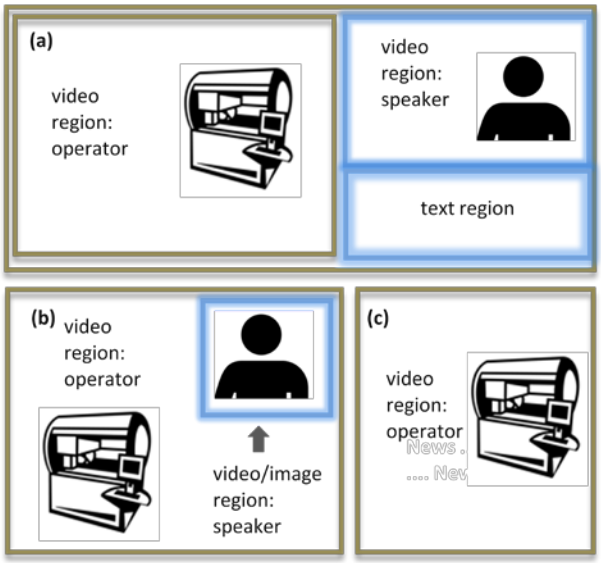

Figure 5. Layout strategies for different devices

The code fragment in Fig. 6 provides an overview of how SMIL handles layout such diversity of devices. One consideration for mobile devices is to add additional content control to address the needs of small devices.

Fig. 6 shows several layout sections within a common switch statement. Every visual media object must be assigned to a region, which is a rectangular area that is places within the root-layout area. The first section contains the standard layout, which has been designed for a display area of 1024 pixels high and 1280 pixels wide (or greater). If this room is available, then the base layout will always be used, i.e., two video regions and an additional text region (not shown in Fig. 6). If a smaller display is available, a second layout is used. This layout could use relative values instead of absolute positioning. It also could allow certain media to be scaled. Rather than using the id attribute of the region element to define region names, the `regionName` attribute is used. This allows multiple layouts to be defined that create regions with the same name. In the body section, a reference to a region is made. The player will select the appropriate layout for the device used during playback.

```
<switch>
<layout systemScreenSize="1024X1280">
... define a standard layout ...
... 3 regions: 2 video regions and   ...
... 1 text region  ...
  <region regionName="videoOperator"
       left="0" width="784 . . . />
  <region regionName="videoSpeaker" . . .
       left="784" . . ./>
</layout>

<layout systemScreenSize="480X640">
... define a smaller layout ...
... 2 overlapping video regions ...
    <region regionName="videoOperator"
       left="0" . . . z-index="1" />
    <region regionName="videoSpeaker" . . .
       left="0" z-index="2"/>
</layout>

<layout>
... define a small and simple layout ...
... 1 video region ...

</layout>
<switch>
```

Figure 6. Layout strategies in SMIL

There are several SMIL profiles developed for use on mobile telephones. While these provide general guidance to manufacturer and industry standardization groups, most handset vendors do not directly implement SMIL. Instead, the embed SMIL functionality in layered standards that include signally, packaging and transport protocols that are optimized for mobile handsets. One such layer set of protocols is developed by 3GPP: the third-generation partnership platform. One common packaging of SMIL in this environment is via MMS, the multimedia messaging system.

SMIL 3.0 contains elements and attributes which provide for runtime content choices and optimized content delivery:

- `BasicContentControl`: contains content selection elements and predefined system test attributes.
- `CustomTestAttributes`: contains author-defined custom test elements and attributes.
- `PrefetchControl`: containing presentation optimization elements and attributes.

- `SkipContentControl`: specifies attributes that support selective attribute evaluation.
- `RequiredContentControl`: defines the `systemRequired` attribute to specify the namespace prefixes of modules required to process a particular SMIL file.

For example, the `BasicContentControl` attributes define a list of test attributes that can be added to language elements, as allowed by the language designer. Conceptually, these attributes represent Boolean tests. When any of the test attributes specified for an element evaluates to false, the element carrying this attribute is ignored.

The example in Fig. 7 is based on test attributes part of `BasicContentControl`. It uses the bandwidth related `<switch>` statement with one that considers display size as well. The second video (speaker video) in Fig. 7 will only be activated if the bitrate is 34400 (or greater) and the screen size is at least 480x640.

```
...
<par>
   <video src="videoOperator.mpg" ... />
   <switch>
      <video region="videoSpeaker"
             src="videoSpeaker.mpg"
             systemBitrate="34400"
             systemScreenSize="480X640"/>
    </switch>
</par>
...
```

Figure 7. Bandwidth related switch statement

We tested the E-Learning scenarios in two devices, a PDA and a laptop, both with the Microsoft Internet Explorer browser as the SMIL player. Microsoft Internet Explorer implements the SMIL profile designated by XHTML+SMIL. This choice had the advantages of being supported by a disseminated browser (even in PDAs and other mobile devices) and of supporting the Web forms mechanism, which was an essential condition for implementing user input capabilities. The main disadvantage was related with the different approach taken by the XHTML+SMIL profile for managing the presentation spatial layout. This profile bases its layout functionality on the XHTML and Cascading Style Sheets layout model and does not use the construction defined by the layout language elements of the SMIL szandard. However, the presentations generated by both approaches are equivalent, in what concerns spatial layout.

V. SERVICE ORIENTED ARCHITECTURE

This section presents an open and flexible service-oriented architecture for the dynamic composition and execution of E-Learning streaming services. First, we introduce a set of Web Services and explain how a streaming service is initialized including the dynamic creation and composition of remote streaming components. Then, media streaming to Apple iPhone is illustrated as an example. Finally, we highlight details on the experiences from the E-learning designer's point of view as well as from the end user perspective.

A service-oriented architecture (SOA) is basically a set of services interacting with each other and coordinating some activity. Service providers and service consumers are the two main entities acting on behalf of a user. The Web Service technology additionally addresses a standardized description of a service's functionality using an XML dialect [14]. Using the Web Service Description Language (WSDL) [8], a service provider describes the functionality (interface) of a service in a platform, language, and operation system neutral way while a service requestor talks to these services using SOAP over HTTP (or other transport protocols).

A. E-Learning Streaming Services

Streaming services are managed by a set of Web Services (see Fig. 8). Such a Web Service is a URL-addressable software resource that performs operations and provides answers. In our case, the operations offered by the service interface are (see Fig. 8):

- `searchStreamingService`: allows searching a streaming service (based on the elements and attributes which form the xml service specification (e.g., category of a manufacturing resource, type of media object, distribution policy, etc.).
- `registerStreamingService`: enables validation and registration of new streaming services
- `createStreamingService`: instantiates streaming software components and establishes interconnections between components.
- `startStreamingService`: the operation is typically invoked by a scheduler (in case of push based services, driven by date and time values).
- `subscribeToStreamingService`: allows users to subscribe to (future) streaming services (e.g., a remote video based training related to a certain CNC machine). When a new media streaming service is registered or started, a user will be notified automatically by the service manager (as soon as such a service has been registered to the xml database).

OPERATION	PARAMETERS	RESULT
registerStreamingService	service specification (xml)	result code
createStreamingService	service id	result code
searchStreamingService	keywords, category time, date delivery policy (e.g. pull)	list of services
requestStreamingService	service id	result code [rtsp channel]
subscribeToStreamingService	keywords. category time, date delivery policy (e.g pull)	result code [future notifications]
startStreamingService	service id	result code

Figure 8. Operations part of the Web Service

After searching a streaming service, the client (e.g., RTSP media player) requests depending on its role the related SMIL specification which defines the layout and temporal relationships between media objects. In the next step (step 7 in

Fig. 9) it will set up three network channels with all involved RTSP servers. Media data is delivered using the RTP over UDP, as shown in Fig. 9, step 8.

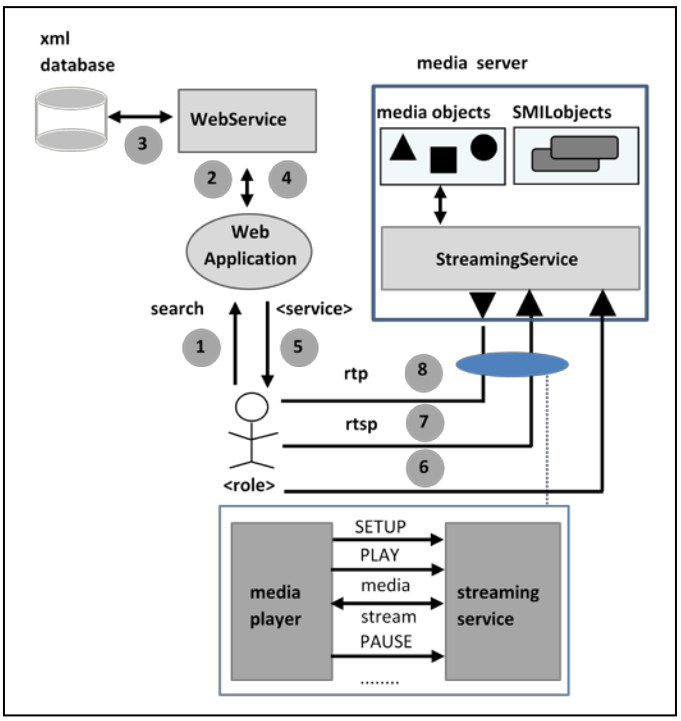

Figure 9. E-Learning Web Services

A full-duplex TCP connection is used for control and negotiation. A simplex UDP channel is used for media data delivery using the RTP packet format. A full-duplex UDP channel called RTCP is used to provide synchronization information to the client and packet loss information to the server. RTSP initiates and controls delivery. The XML service description includes references to media streams, using the URL method rtsp.

According to our service specification language, the following properties of E-Learning services can be used as part of a query:

- Manufacturing resources, e.g., category or keywords
- Media objects properties, e.g., recorded live training
- Distribution policy, e.g., on demand service
- QoS properties, e.g., bitrate, or used codec
- Date / time duration attributes

B. *Software Components*

Our approach is based on a clear separation of a streaming service specification and its implementation by a distributed application and can be used for different streaming paradigms, e.g., push and pull services.

The following figure (Fig. 10) illustrates the user interface and the management interface. The services are managed by a service manager, which provides in the current implementation a simple interface to search, and start (request) services. Moreover, a management interface enables creation of new services, and deletion of existing services. Service specifications are stored as XML documents in a XML database.

A new e-Learning streaming service specification is first analyzed by a Web Service (operation create). Driven by a component library, which contains existing streaming components, such as encoders, media servers, etc., and a set of configuration rules, a Web Service creates a distributed streaming application configuration. Based on such a service specification, the service manager also supports retrieval of existing services.

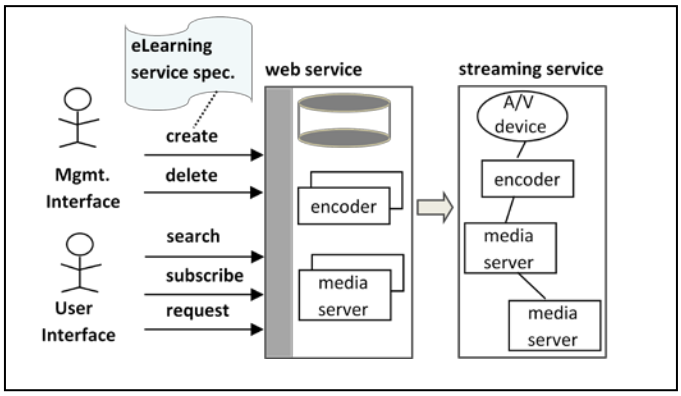

Figure 10. User interface and management interface

Push services are started automatically according to the specified date and time values. Starting a service means to create the required streaming components, e.g., an encoder and a media server component as well as to establish the communication relationships. Before a new service is created, a consistency checker is responsible to test the availability of nodes, and media objects according to the definition as part of a service specification. A service specification is then analyzed by a Web Service, which will select appropriate streaming software components.

Multimedia services are stored as XML documents in a XML database. We use Apache's Xindice, which is a database designed from the ground up to store XML data or what is more commonly referred to as a native XML database. Advantages are: faster for XML than other databases, no mapping to relational required, quick fragment retrieval provided, and optimized XML querying supported.

The prototype has been implemented using the PHP programming language and the PHP Web Services Development Pack nusoap [9] for the creation of and access to Web Services. We use the existing media server components from RealNetworks, and the OSS software Asterisk [15] as a VoIP server. The first (subjective) test results based on implementation of push and pull services as well as conference management are very promising. However, the used OSS VoIP system Asterisk does not offer scheduled conferences, i.e., a direct mapping to the Asterisk conference management functions is not possible. Information related to scheduled

conferences is stored in a xml database. As the prototype is still under development, an objective measurement of processing time and delay has not yet been made.

C. Streaming to Mobile Devices

We use a commercial media delivery platform from RealNetworks (Helix Mobile Server) [20] which supports live and on-demand streaming of 3GPP content to any standards-compliant media player. The server supports 3GPP Release 4 Specifications including the .3gp file format and the payload formats associated with MPEG-4, AMR, AAC and H.263. It also implements 3GPP Release 5 Specifications including AMRwideband and enhancements for RTP and RTSP. The Helix Media Delivery Platform supports the various methods used by the Apple devices to access media complete with support for Android, Symbian and Windows 7 Mobile OS clients.

Another reason why we decided to use Helix Mobile Server is the Custom Statistics Reporting facility. When deploying media streaming services to mobile devices, it is important to have accurate statistical information on client usage. The Helix Media Delivery platform, i.e., the Helix Mobile Servers as well as Helix Clients have a statistics-reporting mechanism through which media players can relay back playback statistics to the media server, either at end of a session or on an interval basis. This feature is used to gather statistics about usage of E-Learning streaming services.

We do not use Java Media Framework, because it is not stable enough, especially for long running streaming applications.

In the following, media streaming to Apple iPhone is illustrated as an example. From the user's point of view, the starting point of such a scenario for mobile environments is the request of a SMIL file, which contains the layout specification and the required audio and video files. In the case of Apple mobile devices, the methods used for accessing media objects is very different than delivering content through RTSP (as other mobile clients use) or RTMP (as Adobe flash media players use). Apple has implemented a client-driven system for downloading full or segmented audio and video files through the HTTP or HTTPS protocol. With on-demand media files, these are delivered to the Apple device by converting the original source media file into a series of 10 second segmented media files encapsulated in a MPEG-2 media stream (.ts container) and making them available to be delivered to the client through http or https.

After creating the MPEG-2 TS segments, an index file (.m3u8) is created (or updated if the content is live) that lists the order of and URLs to each segmented media file (Fig. 11). This index file is also known as a playlist and will also include some additional information about the content itself (segment length, if content is encrypted where the decryption key can be found, multirate bandwidth information etc). After receiving the index file, the iPhone OS media client downloads each segment files listed in the playlist using HTTP(S) and plays back the media in order listed. Once the device reads the playlist and works out the bandwidth available (if required for a multi-rate clip) the client then requests the relevant .TS media segment for playback to start (step 5 in Fig. 11 below).

Helix Media Server has the ability to on-the-fly segment (and optionally encrypt) a correctly formatted on-demand media file into the structure required by the Apple device (.ts media segments and m3u8 playlist as seen in step 4 in Fig. 11 above). This process happens instantaneously on the first request by an Apple device (step 3 in Fig. 11) and the playlist is then sent back to the device (step 5 in Fig. 11).

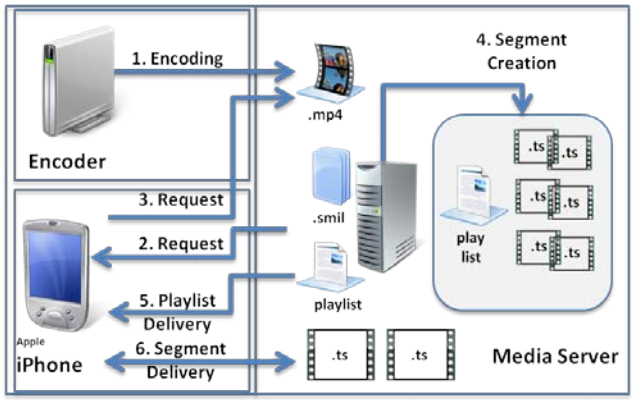

Figure 11. Streaming to Apple mobile devices

Once the device received the playlist and calculated the available bandwidth (if required for a multi-rate E-Learning service) the client then requests the relevant .ts media segment for playback to start (step 6 in Fig. 11).

D. User Experience

The goal of the project was also to evaluate the user interfaces and the usage of the E-Learning streaming services. Two actors have to be regarded to analyze the acceptance of the system: the designer of an E-Learning streaming service (i.e., person responsible for specification of E-Learning streaming services in terms of manufacturing resources, media objects, delivery options, and device adaption policies) as well as the end user accessing on-demand or push streaming services. As in any E-Learning environment streaming services also need to be user centered taking into account the user's characteristics and abilities interacting with the environment and learning materials, and comply with usability.

Designers of E-Learning streaming services have a strong tendency towards reusing designs that worked well for them in the past. However, currently our system does not provide templates for typical E-Learning scenarios. Additionally, the E-Learning specification based on XML files, especially the adaption part which deals with mobile devices was not well accepted. Based on the XML schema for the specification language a graphical user interface will be implemented better suited and more accepted by developers of streaming services.

In a production environment robust and easy to use search functions are one of the key requirements. Our original search functions had to be improved. Context-driven search results, driven by the concrete manufacturing resources, which are part

of a single work place are regarded to be important for the machine operators. As an example, depending on the available machine(s), which are part of a single work place, the search functions have to offer the "right" E-Learning services related to the given local manufacturing resources.

The most accepted E-Learning streaming services are on demand video services. From the production management point of view, push services are essential for quality improvements. Such services allow a "just in time" documentation of occurred failures, during runtime of a machine by ad hoc video and audio recordings. These recordings can be analyzed later and appropriate solutions can be developed to improve manufacturing processes.

The challenge of mobile devices is to understand and explore how best they can be used to support learning, training, and performance support. The use of mobile technologies should not be viewed as isolated activities; instead, they should be viewed as richly ubiquitous, and effective collaborative devices having during maintenance, or helping to diagnose during a manufacturing process problem solving effort.

As well as the limited screen size and data input capabilities, the use cases for mobile devices should also be considered when designing E-Learning services and content for mobile devices. Services which are used on-the-go should be made available on the mobile. Just taking an existing PC-based E-Learning service and reformatting it for the mobile phone is rarely the right solution.

Due to the variation in screen resolution and browser markup support, it is necessary to optimize E-Learning content for the specific type of mobile device. This involves designing an appropriate layout for mobile devices, i.e., applying the appropriate mobile page flow, etc. It is also necessary to resize videos and images based on the device resolution.

In order to optimize the content based on the mobile device type, it is necessary to identify the type of device or browser. This can be done automatically using the SMIL attributes for content control. When the device is identified, the characteristics of that device required for content optimization can be retrieved from the SMIL application. The necessary information includes screen resolution, the number and size of regions, etc.

The following research questions are essential for user acceptance of mobile devices:

- What types of training and / or performance support can be effectively delivered via mobile devices that are consistent with the E-Learning environment for manufacturing processes?
- How is the mobile technology training/performance support integrated within the identified E-Learning environment, taking into consideration the identified E-Learning environment's system architecture?
- What are the existing mobile technologies "best practices" that can be applied to the identified E-Learning environment?

The most interesting metric for the media server performance is the number of concurrent users the server can support. In [22], several streaming use cases are described and tested to report the number of successful streams as well as streams that failed to complete correctly. Streams that died or could not even start were reported as errors. Performance results indicate that the network connection is the bottleneck for HTTP streaming while the CPU is the bottleneck for RTSP based streaming. However, in our case we have a maximum number of 10 parallel streams, i.e., we could not observe any server bottlenecks.

VI. CONCLUSION AND FUTURE WORK

In this paper, we have presented a service-oriented architecture for E-Learning streaming services – realized using Web Services technology. The major contributions and extensions of our approach aim to provide a high level specification of E-Learning services in terms of user roles, media objects, distribution policies, etc. The introduced Web Service supports creation of tailor-made media streaming applications, using existing software components, e.g., media server or VoIP software components.

The work presented in this paper is also proposal to solve the problem of the dynamic adaptation of multimedia services in heterogeneous device contexts, especially in case of mobile devices. We presented a generic SMIL-based adaptation methodology suitable for the adaptation of multimedia services according to different conditions of access devices and networks.

We report the current status of our prototype. The prototype has shown that our XML based language is well suited for automatic generation of implementations. At implementation level, the different aspects are integrated in a general object-oriented architecture supporting modularity and reuse of software. The deployment of new service operations is very easy to accomplish due to the modular structure of the service oriented architecture and the well designed and easy to use PHP development pack nusoap.

Currently, the evolution of E-Learning is mainly driven by then convergence of two traditionally separate worlds: just in time learning and Web 2.0 tools, such as social networks. Learning takes place through conversations about content and grounded interaction about problems and actions, i.e., employees learn from each other through communities of practice, blogs, wikis, and other forms of self-published content. Another trend that has emerged in E-learning over the past years is that there has been a steady shift away from traditional PCs to mobile devices. The type of mobile learning we expect in the future will be much more akin to performance support - checklists, quick guides and short 'how to' videos, e.g., a video illustrating configuration or handling of a complex machine.

Future work will concentrate on the extension of the service model to support additional functionality, e.g., application sharing as well as the integration of authentication services (authentication of users). Another objective is to improve the search functions by a recommendation system to identify interesting E-Learning material based on the current context

(e.g., location) and the user's personal ontology, similar to the approach introduced by Woerndl et al. [21].

ACKNOWLEDGEMENTS

The proposed framework is part of a multimedia project, financed by the state government of Baden-Württemberg in Germany.

REFERENCES

[1] M. Zimmermann, "On Demand Learning in Manufacturing Processes - Implementation by Integrated Multimedia Streaming Services", AICT 2010, pp. 106-111, 2010 Sixth Advanced International Conference on Telecommunications, 2010.

[2] B. Khasawneh and S, A. El-Seoud, "Framework for on-demand e-learning resources allocation and distribution", OERAD International Journal of Computing & Information Sciences, Vol. 4, No. 2, 2006.

[3] D. Borissova and I. Mustakerov, "A Framework of Multimedia E-Learning Design for Engineering Training", ICWL 2009, in LNCS 5686, pp. 88–97, 2009, Springer, Berlin Heidelberg, 2009.

[4] M. Hillenbrand, J. Götze, and P. Müller, Voice over IP - Considerations for a Next Generation Architecture. In EUROMICRO-SEAA, pp. 386–395, IEEE Computer Society, 2005.

[5] A. Uyar, W. Wu, H. Bulut, and G. Fox, "Service-Oriented Architecture for a Scalable Videoconferencing System", In Proc. of IEEE Int. Conf. on Pervasive Services 2005, pp. 445–448, IEEE Computer Society, 2005.

[6] W. Wu, G. Fox, H. Bulut, A. Uyar, and T. Huang, "Service Oriented Architecture for VoIP conferencing", In Int. Journal of Communication Systems, Special Issue on Voice over IP - Theory and Practice, volume 19, pp. 445–462, John Wiley & Sons, 2006.

[7] G. Vossen, P. Westerkamp, "E-Learning as a Web Service," ideas, Seventh International Database Engineering and Applications Symposium (IDEAS'03), 2003.

[8] E. Christensen, F. Curbera, G. Meredith, and S. Weerawarana, "Web Services Description Language (WSDL) 1.1", http://www.w3.org/TR/wsdl, 2001

[9] http://sourceforge.net/projects/nusoap/, Retrieved December 29, 2010, from http://sourceforge.net/projects/nusoap

[10] ITU. Recomm. H.323 (1999), "Packet-based multimedia communications systems".

[11] L-L. Wu Chou and L. Feng, "Web Services for communication over IP", In: Communications Magazine, IEEE, Volume: 46, Issue: 3, 136-143, 2008.

[12] T. Yoshimura, "Mobile Streaming Media CDN Enabled by Dynamic SMIL", WWW2002, May 7-11, 2002, Honolulu, Hawaii, USA, ACM 1-58113-449-5/02/0005, 2002.

[13] SMIL: http://www.w3.org/TR/smil20, Retrieved December 29, 2010, from http://www.w3.org/TR/smil20.

[14] D. Fallside, "XML Schema Part 0: Primer", http://www.w3c.org/TR/xmlschema-0, 2001.

[15] Asterisk: The Open Source Telephony Project, http://www.asterik.org

[16] T. Ericson and M. Brandt, "JSR 309 - Overview of Media Server Control API", Public Final Draft, Media Server Control API v1.0, 2009.

[17] A. Scholz, "WS-AMUSE - Web Service architecture for multimedia services", International Conference on Software Engineering, In Proceedings of the 30th international conference on Software engineering, Leipzig, Germany, 2008.

[18] http://java.sun.com/javase/technologies/desktop/media/jmf/index.jsp, Retrieved December 29, 2010, http://java.sun.com

[19] J. M. Oliveira and E. Carrapatoso, "Dynamic Generation of SMIL-Based Multimedia Interfaces", JOURNAL OF MULTIMEDIA, Vol. 3, No. 4, 2008.

[20] RealNetworks, Inc., "Helix Media Delivery Platform for Mobile Networks", RealNetworks White Paper, Series Version 2.1, 2010.

[21] W. Woerndl, G. Groh, and A. Hristov, "Individual and Social Recommendations for Mobile Semantic Personal Information Management", International Journal on Advances in Internet Technology, vol 2 no 2&3, ISSN: 1942-2652, 2009.

[22] Y.-J. Lee., O.-G. Min, and H.-Y Kim, "Performance evaluation technique of the RTSP based streaming server", Proceedings of the Fourth Annual ACIS International Conference on Computer and Information Science (ICIS), 2005.

Distributed Control and Signaling using Cognitive Pilot Channels in a Centralized Cognitive Radio Network

Nicolás Bolívar and José L. Marzo
Broadband Communications and Distributed Systems Group (BCDS)
Universitat de Girona
Girona, Spain
E-mail: nbolivar@eia.udg.edu, joseluis.marzo@udg.edu

***Abstract*—In this paper, a cognitive radio network (CRN) model is presented. In this model, the control of the CRN is distributed among the frequency spectrum considered for transmission using cognitive pilot channels (CPCs). This control is performed by using frequency-division and time-division multiplexing techniques. Frequency-division is used to divide the spectrum into predetermined frequency slots in which cognitive radio users (CRUs) communicate. Then, the frequency slots are divided into sub-frequency slots, some of which are defined as CPC and used by the CRUs to communicate with a central cognitive base station (CCBS) and to determine availability in a frequency slot. Time-division is used to determine if a primary user (PU) has accessed the channel used by CRUs. Using this time-division approach, presence of PUs is detected. We have designed a CRN able to work with today's available technologies and CRU devices that use different frequency bands of operation. Since in terms of energy, this control can be very inefficient because at specific periods of time the network might be completely used, a method for energy reduction in a centralized cognitive radio network (CRN) is presented. Results of the performance of the network will be presented in terms of the number of CRU and the time these CRUs use the CPCs for control.**

Index Terms*— *Cognitive Pilot Channel; Cognitive Radio Networks; Dynamic Spectrum Access; Medium Access Control

I. INTRODUCTION

A basic model for controlling and signaling a Cognitive Radio Network (CRN) was presented in [1]. Considering that fixed spectrum licensing has produced apparent scarcity in the wireless frequency spectrum [2-3], strategies such as Cognitive Radio (CR) have been suggested for efficient spectrum occupation. The CR systems have the ability to detect free frequency slots in the spectrum, i.e. "white spaces", and to allocate the CR communications in these white spaces by using dynamic spectrum access (DSA) mechanisms [4-6]. CR has already been considered as the main technology for IEEE standards, such as IEEE 802.22, which is the standard for Wireless Regional Area Network (WRAN) using white spaces in the TV frequency spectrum and for standards related to DSA networks that are comprised in the IEEE SCC41 [2-3, 6].

In general, a CRN should be able to perform 4 tasks efficiently, spectrum sensing, spectrum decision, spectrum sharing, and spectrum mobility [5]. Spectrum sensing refers to the identification of the most likely white spaces in a specific time. Spectrum decision refers to the process of deciding in which white spaces to allocate communications [5]. The spectrum sharing function consists on maximizing the cognitive radio users (CRUs) performance without disturbing Primary Users (PUs) and other CRUs; this is one of the main challenges for opportunistic spectrum access (OSA) in CRN [5, 7]. Spectrum mobility is the CRU ability to leave the frequency portion of the spectrum occupied when a PU starts using the same frequency portion and then, to find another suitable frequency slot for communication [5]. Spectrum sensing and spectrum mobility must be guaranteed in order to implement an efficient CR Medium Access Control (MAC).

Several CR MAC protocols have been developed over the premise of the presence of a dedicated common control channel [8, 9]. In this CR MAC approach, all CRU must be able to communicate in this common control channel. Thus, the CR capacity is under-utilized, since data communications cannot be sent or received on the common control channel. The CR MAC protocols that improve this performance are based on multi-channel MAC protocols. This approach can be considered for efficient spectrum utilization because the CRN must operate in different frequency bands. The main difference between multi-channel and CR MAC protocols is that in the CR MAC protocols, the presence of PUs is considered. Multi-channel MAC protocols can be categorized in dedicated control channel, split phase, common hopping, and default hopping [10]. Other than the aforementioned dedicated control channel approach, these multi-channel MAC protocols need some kind of user synchronization to determine the control channel beforehand. Furthermore, in multi-channel MAC protocols, all CRU must be able to use the same frequency channels, which is not always the case in heterogeneous systems. A comparison among our proposal, CPCDF-MAC, multi-channel MAC protocols from [10] and existing CR MAC protocols from [8] is shown in Table I.

TABLE I. COMPARISON AMONG CR MAC PROTOCOLS

Protocol	Specific Control Channel	Time Synchronization Needed	Multiple Transceivers	Support for Heterogeneous Frequency Devices
Common Control Channel	Yes	No	No	No
Common Hoping/ Default Hoping Sequence	No	Yes	No	Partial
OSA-MAC	Yes	Yes	No	No
HC-MAC/ OS-MAC	Yes	No	No	No
CPCDF-MAC (Proposal)	No	Yes	Yes	Yes

The utilization of beacons was suggested as a solution for spectrum sharing in [11], using these beacons to control the devices medium access into the frequency bands. Architectures with more than one beacon have been proposed to improve performance [12]. Decisions based on channel occupancy are performed by combining the information obtained in these beacons using data fusion techniques. The most common data fusion techniques to decide whether a particular frequency band is occupied are voting rules and logical operations [13]. In these proposals, the beacons are sent by the PU through a cooperative control channel or a beacon channel, with the latter being considered a better option in [14]. This approach has two main disadvantages for implementation in a CRN with today's available technologies; the first is that a new set of primary users must exist or new hardware must be developed since the PUs should inform the nearby CRU about their presence, and the second disadvantage is that a new channel must be reserved for the beacon signals.

A cognitive pilot channel (CPC) is a solution proposed in the E2R project for enabling communication among heterogeneous wireless networks. The CPC consists on controlling frequency bands in a single or various "pilot" channels, which is analogue to the beacon proposal. In both CPC and beacons proposal, there are "in-band" transmission, i.e. information transmitted in the same logical channels of the data transmission, and "out-band" transmission, i.e. information transmitted in different channels of the data transmission. Studies have been conducted in [15-18] to define the quantity of information that should be transmitted in the CPC, the bandwidth for each CPC, and the "out-band" and the "in-band" transmission or other solutions with a combination of both. The IEEE P1900.4 group, part of the IEEE SCC41, has accepted CPC as part of the architecture for the CR Access [16].

In the E2R project, for achieving communication between heterogeneous nodes and networks, and also scalability, a large band is divided into several sub-bands with one local CPC (LCPC). This LCPC is used for accessing a network, and informing the devices about the operator, frequencies and radio access technologies in this network [15-16]. In [17], CPC is considered for radio environment discovery, reconfiguration support and terminal radio environment information and context awareness. We expand the use of CPC in order to control the CRN. The objective is to build a CRN using today's available technologies that are able to support heterogeneous frequency CRU devices, i.e. CRU that use different operation frequencies, while using the spectrum as effectively as possible.

To control the CRN, joint time and frequency control for assuring effective spectrum sharing are used. For transmitting channel availabilities, network discovery and channel petitions, a frequency-based approach using beacons in a CPC is proposed. The utilization of the CPCs instead of a dedicated control channel allows heterogeneous systems to communicate in our CRN. In a first approach, a central cognitive base station (CCBS) sends beacons via parallel communication in sub-channels of all available frequency slots. With this approach, the use of all available frequency bands for communications was guaranteed. When a CRU requested access in the CRN, the CRU already knew which channels were available because of these beacons. However, in terms of energy, transmitting through every available channel would be inefficient. This is because the entire wireless spectrum channels would be occupied in a specific moment. Considering this problem, new alternatives are explored to reduce the energy used for signaling cognitive radio users (CRU) channel availability.

Among the strategies that might be applied to decrease this amount of energy are: reducing the number of channels and/or amount of time/symbols used for signalization, and recognizing patterns of transmission. Since the network is centralized, collisions on entrance of CRUs are reduced. Considering that CRUs might also be capable of recognizing patterns of occupancy, to reduce the energy used for sensing, signaling and transmission. For this reason, Cognitive Radio technology has also been considered as an alternative to reduce energy consumption for wireless communications [19]. In [20], we explained the use of a distributed control and a centralized database for reducing the amount of energy used to signal this availability in the CRN. A complementary control based on a time-division approach, in which the PU entrances are detected via time slots, is also used. Finally, in this paper we present the performance of the network using this energy reduction method in our CRN with distributed control.

The remainder of this paper is organized as follows: Section II introduces the model of the network. Section III presents the expected results of our proposal and Section IV provides a discussion of our work.

II. PROPOSED MODEL

A. CCBS Control Architecture

The proposed model of the CRN is an infrastructure-based architecture for effective spectrum access, sharing and management. The main reason for using a centralized model is to concentrate wideband spectrum sensing and spectrum decision in the central station and, as a consequence, to

reduce operations and the hardware required in the CRU devices. A basic representation of the centralized CRN model can be seen in Fig. 1. The elements of our CRN are the CCBS and the CRUs, which operate and coexist with the PUs.

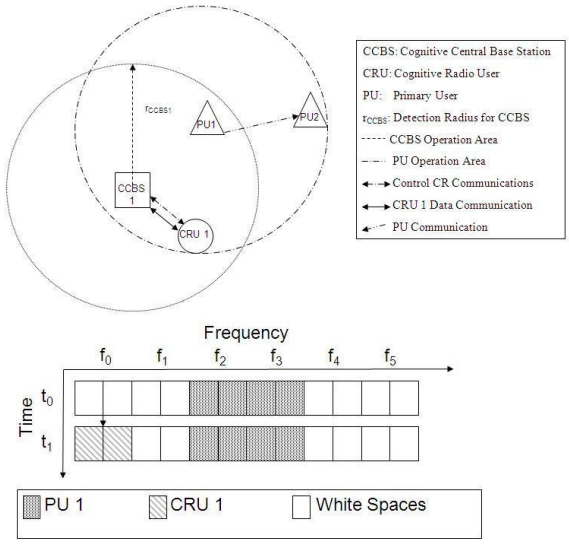

Fig. 1. CRN Model

In Fig. 1, CRU1 is communicating with the CCBS (CCBS1), while PU1 is communicating with PU2. PU1 transmission is within the range of the CCBS1 and CRU1. This means that the communication between CRU1 and CCBS1 must be performed in a different frequency slot than the one that the PUs is using. Hence, in order to ease CR operation, a CR radio spectrum model that uses fixed frequency slots for both CR frequency sensing and CR medium access is proposed. A frequency/time representation of the corresponding scenario is also shown in Fig. 1.

In the proposed architecture, we assume that the management of the network is performed in the CCBS, which permits to reduce the amount of processes from the CR users (CRU)' terminals and therefore, keeping those terminals simple while using today's available technologies. We address the spectrum sharing problem, since we assume that the CCBS decides which channel to assign for each CRU, according to the available channels and the characteristics of the CRU. The architecture of a CCBS is shown in Fig. 2.

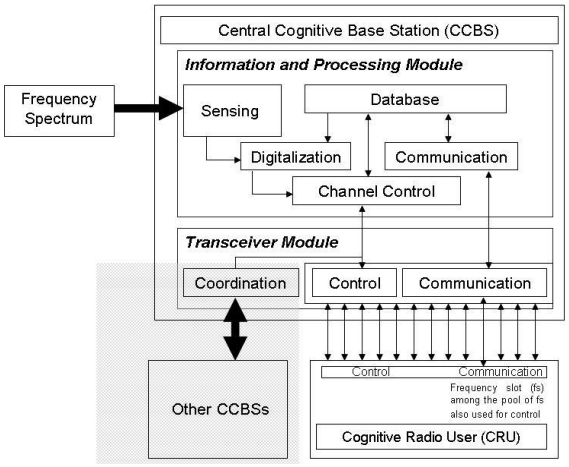

Fig. 2. CCBS Control Architecture

The CCBS is composed of two major modules, information and processing module and transceiver module is proposed. The information and processing module is divided in five sub-modules: sensing, database, digitalization, channel control and communications. In the sensing sub-module, the CCBS scans the analog radio frequency spectrum, which is assumed to be perfectly and continuously sensed. In the digitalization sub-module, the analog sensed signal is digitalized within predefined frequency slots. An Analog/Digital (A/D) converter is used considering the thresholds determined for each channel according to the location. A logical "1" is then assigned if a communication exists in a frequency slot; otherwise a logical "0" is assigned. This information is stored as a vector in the database sub-module, which also provides the specifications of the location that are loaded into the digitalization sub-module. In addition, the database sub-module stores information related to the CRU frequency assignments from the channel control and the communication sub-modules. The channel control sub-module uses a frequency subdivision of the frequency slots (sub-frequency slots). In those sub-frequency slots, CCBSs and CRUs exchange both control and data information. The channel control sub-module is responsible for controlling which CRUs are communicating and the frequency slots used. In this sub-module, CRUs are assigned free frequency slots to communicate. This information is sent in a vector to the control of the transceiver module, while it is also kept in the database. Fig. 3 shows the division in frequency and sub-frequency slots. Finally, the communications sub-module is responsible of data communication, which uses the frequency slot that has been defined in the previous sub-module.

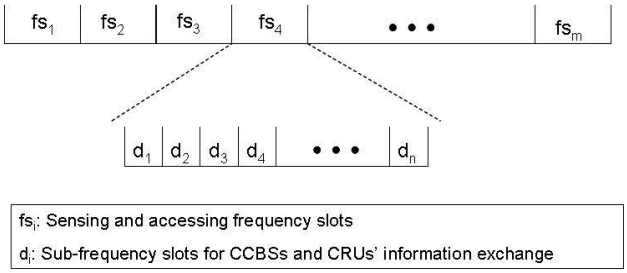

Fig. 3. Frequency slot and sub-frequency slot division of the spectrum

The Transceiver Module is divided into 3 sub-modules, control, communication and coordination. These sub-modules are responsible for communicating the information coming from the information and processing module with the control module of the CRUs, the communication module of the CRUs, and with other CCBSs for cooperation, respectively. This architecture allows cooperation among the base stations of adjacent CRNs by using in each sub-channel a logical OR with the data from other CCBS. However, in this paper we are not considering the possible coordination among CRN.

In this paper, only the CRN control is studied; the control algorithm for the CCBS is represented in Fig. 4. In this figure, the frequency spectrum sensing and A/D conversion block represent the equivalent processes that are shown in the CCBS Algorithm. On the other hand, the channel control block from Fig. 2 is divided into CCBS Control Broadcast Transmission, CCBS-CRU Control Communication and the time synchronization needed. It is worth to mention that both database storage and information and control transmission/reception are considered for the algorithm as part of the CCBS Control Broadcast Transmission and CCBS-CRU Control Communication processes.

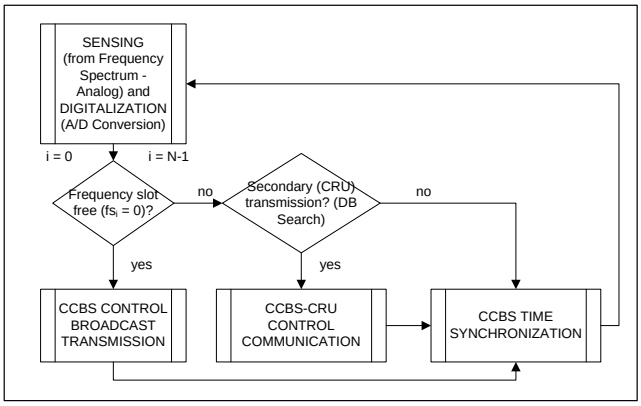

Fig. 4. CCBS Algorithm per each frequency slot i (fs_i)

In the following section, the control of the system is explained, considering the control processes of the CCBS Algorithm. The algorithm is also related to each of the required dynamic functionalities for CRN, Dynamic Spectrum Access (DSA), Dynamic Spectrum Sharing (DSS) and Dynamic Spectrum Management (DSM) [7].

B. CCBS – CRU Control

The CCBS-CRU Control Communication is performed under three different scenarios, CRU network discovery, CRU medium access and while CRU data communication is being transmitted. DSA is present for the first two scenarios, DSS for the last two, while DSM only occurs for the last one. For the CR network discovery and from the CRU perspective, the process is as follows. When a new CRU enters into a CCBS range, this CRU scans in its possible transmission channels, and sends in an available channel an identification frame that consists on: petition to enter, ID of the device, and type of device. This frame is sent in a frequency-based approach, since a CRU can enter for the first time to the network at any moment. When the CCBS receives this request, acknowledges the CRU type of device, keeps this information into memory, and sends a confirmation message. The CRU then waits for confirmation of the corresponding CCBS, and synchronizes itself with the CCBS.

From the CCBS perspective, a broadcast signal is first sent in one or more of all the available frequency slots in which CRUs are able to communicate. This is the CCBS Control Broadcast Transmission process in Fig. 4. Since a CRU can enter to the CRN at any moment, time synchronization does not exist yet, and a frequency beacon mechanism is proposed. This consists in a two bit signal sent in the first two sub-frequency slots shown in Fig. 3 of all the available channels. The set of values corresponding to control are detailed in Table II.

TABLE II. DISTRIBUTION OF CONTROL BITS FOR THE PROPOSED ARCHITECTURE

Bit 1/Bit 2	Process
00	CCBS and CRU coordination for using a channel
01	CRU request to use a channel
10	CCBS announcing availability
11	Frequency Slot occupied, CRU must leave immediately

When a CRU is trying to use the CRN, a message containing the identification frame is received from the CRU, and the process in the CCBS consists on determining if the information received is valid, i.e. no errors in the reception, if the CRU can access the CRN, and if both conditions are fulfilled, the CRU is accepted and its presence in the network is stored in the database.

According to the channel and device characteristics, the CRU medium access might be performed in a time-based approach or a frequency-based approach. Since the analysis for the 2 bit message is the same for both frequency division and time division based approaches, the case for the frequency-based approach is explained, without losing generality. The process for the CRU Medium Access to the network is then similar to the previously shown process for

network admission. The differences are that the CRU is already present in the network, so there is no need to communicate the identification frame again and that after being admitted in a channel, data communication is the process that continues in the next time slot. The CCBS-CRU Control Communication process can be described then as in Fig. 5. When the CCBS receives information from a CRU in a communication channel, the CCBS compares this information with its database. If the CCBS does not identify this information as coming from a known CRU, the CRU admission process is started. If the CRU is already registered in the CRN, but this CRU is not communicating, the CRU confirmation process is activated. In the case this CRU has been already assigned a frequency slot, the data communication process is performed.

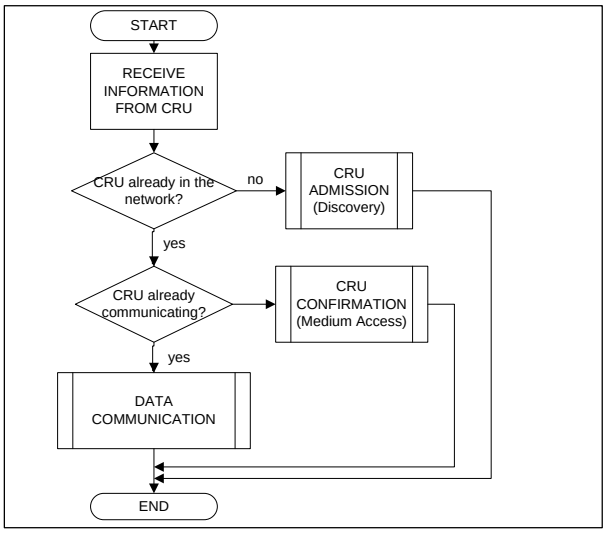

Fig. 5. CRU Admission in the CRN from the CCBS perspective

When a CRU data communication is already established, and since PU communication can enter at any moment, a time-based approach is implemented in order to discover PU presence. This frequency and time system allows the elimination of a dedicated control channel for spectrum sharing. Using the slotted predefinition, if a transmission is received in a moment no transmission should be performed, we assume that a PU is communicating and, then, the channel is evacuated and the process of assigning a channel restarts, keeping into memory the last information that was going to be transmitted. For effective use of the wideband spectrum, we also propose a multi-channel approach, since several cognitive users might communicate in different channels. For the analysis of the system, we consider each communication channel separately, since it is transparent for the CRU in which channel is transmitting. An example of the time-based approach for determining PU entrance in the operation range of a CRN is depicted in Fig. 6, which shows the utilization in time of a frequency slot by both PU and CRUs.

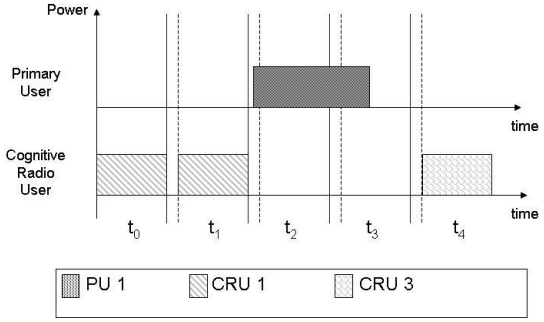

Fig. 6. Frequency slot utilization by both PU and CRUs (in time)

In [20], two additional characteristics are added to the CRN model of [1] to reduce broadcast transmissions. The first one is that CRU synchronization will be performed as follows: Since CRUs know the duration of the time slot, the CRU will search during a time slot in its channels for continuous transmission. If a CRU finds a PU-free channel, the device will send a signal for announcing that this CRU wants to access the network. A channel occupied by a CRU will be identified because of the time slots used for control, so this scheme will not introduce collisions among CRUs.

The second reduction consists on using the ability the CCBS has to identify the channels every CRU in the network is able to use. In this manner, the CCBS will only send a new broadcast transmission for each channel petition. This means that now, the entire wireless frequency spectrum considered for the CRN domain will not be used at several moments.

Using these alternatives, the flux diagram from Fig. 5 presents two cases: a CRU wants to access the CRN, and another CRU exists in one of the CRU devices' available channels. In this case, the new CRU senses the occupation, and when the device senses no transmission, it synchronizes with the CRN and could send its network admission petition or use a free channel to transmit, since the CRU device is already synchronized in time with the CRN.

The other case is that no CRU is communicating in the network within the available channels for the new CRU device. In this situation, only PUs could be using the channels; this means that the CRU is not able to recognize the time slot that must be used for synchronization. The CRU then uses its time sensing capability to detect that a channel is being occupied for more time that the time-slot duration, so the CRU does not transmit through that channel. Next, the CRU device must find another channel to synchronize. If there is no available channel for this CRU, this device cannot access the CRN. When an available channel is found, the CRU then simply sends a petition to use the channel that the CCBS responds in the corresponding time slot, so the new CRU can be now synchronized to the network.

In Fig, 7, an example of the CRU admission in the CRN is shown by using the same example as in Fig. 5. CRU 3, which has three channels for communications, "senses" its environment. Channel 1 is being used by a PU, so this

channel is unavailable to CRU transmission. Channel 2 is occupied by CRU1. This makes the channel unavailable for CRU 3 use, but CRU 3 can detect the time slot position using CRU 1 transmission. Using that information, CRU 3 can access Channel 3 in time t2.

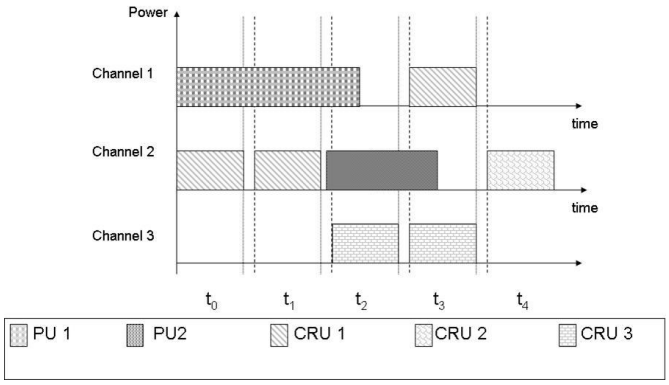

Fig. 7. Frequency slot utilization by both PU and CRUs (in time)

III. RESULTS

In this section, the difference in expected transmission generated by both CRU interference to PU, and CRUs not having a frequency slot (channel) to transmit, which will be called transmission errors, will be analyzed. Due to the fact that none of the CR-MAC protocols shown in Table I present support for heterogeneous devices, no comparison is performed in this section. Results will be presented in terms of the number of CRU users and the relation of time dedicated for the Cognitive Control Algorithm.

In [20], a simulation is then performed in MATLAB to show the obtained results. The values used are the following: number of channels (n) = 128, number of sub-channels (m) = 256, control time/ (control + data) time = 1/10, and time duration (td) = 500 units of time. In Fig. 8, channel occupancy and power used when the CCBS sends broadcast signaling to announce availability is shown.

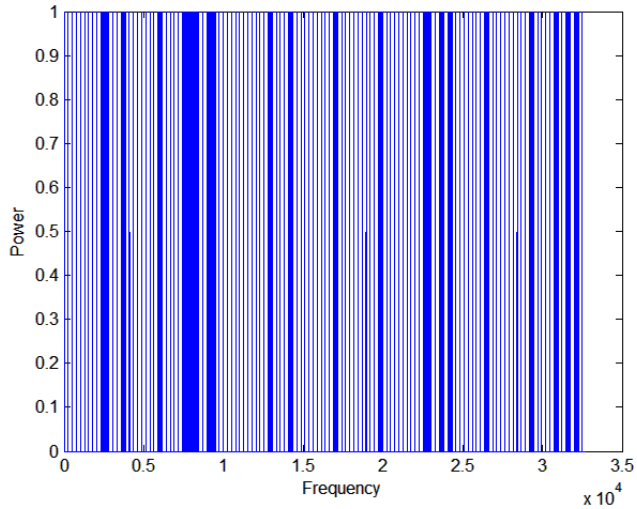

Fig. 8. Power used in the model presented in [3] in t = 481, when CCBS sends broadcast transmission.

As expected, when CCBS sends broadcast transmission, every channel is occupied either by PUs (thick blue lines) or the CCBS broadcast transmission (thin lines). In Fig. 9, the power used and channel occupancy in the proposal is shown.

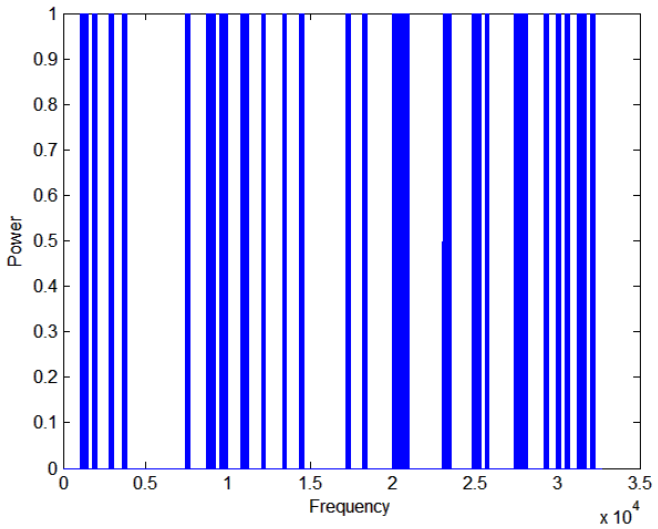

Fig. 9. Power used in the new model in t = 481, when CCBS in [3] would send broadcast transmission.

In Fig. 9, power used with the new model when CCBS in [1] would be sending broadcast transmission is shown. In this case, thick lines represent PU transmission, while thin lines represent CRU sending information to the CCBS. CRU lines in this case are thicker than in the previous model, since more information is sent in the first communication. This data is not sent later, as in [1], unless the information is asked to be submitted again by the CCBS

The results show that in [20], in terms of energy reduction, the modifications provide the advantage of eliminating CCBS broadcasting transmission in all available channels, as explained in the previous section. This means a reduction per unit of time of (number of available channels) x (broadcasting transmission time) x (power used for beacon transmission).

The reduction might be also seen when CRUs are communicating or requesting communications. As some CRUs might be using or requesting channels, the energy decrease is not as straightforward as in the admission process. This reduction depends not only on the usage of the network, but on the numbers of requests at a specific moment.

An important measure for a CRN is how much information in terms of bits is lost due to interference to PU and how much CRUs interferes PUs. Using the same parameters, n = 128, m = 256, td = 500, a simulation is performed. In Fig. 10, the information lost for the new model due to PU and CRU interference is shown.

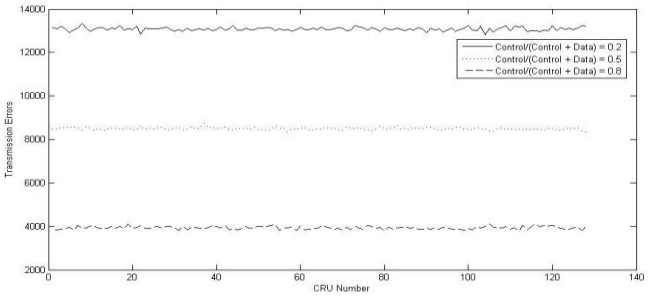

Fig. 10. Transmission Errors

The results show that transmission errors decrease when the portion of the time that is used for control increases; however, the data that could be transmitted in the same amount of time also decreases. Effective transmission errors, which we define as Eff. Trans. Errors = Transmission Errors/Data Transmitted, might provide then a better guidance for choosing a Control/(Control+Data) rate for the CRN. Fig. 11 shows the effective transmission errors per CRU number.

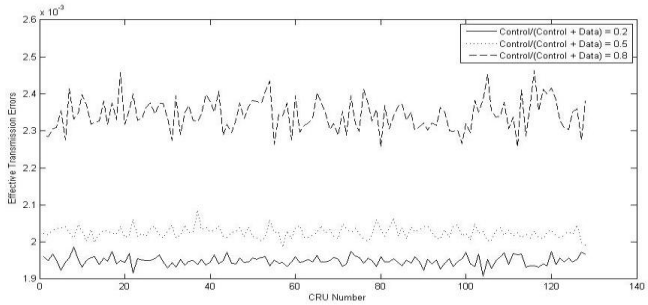

Fig. 11. Effective Transmission Errors

Results are very similar for different control time / control plus data time ratios. This is expected from the construction of the algorithm. Errors due to channel unavailability, defined as availability errors, in average, are shown in Fig. 12.

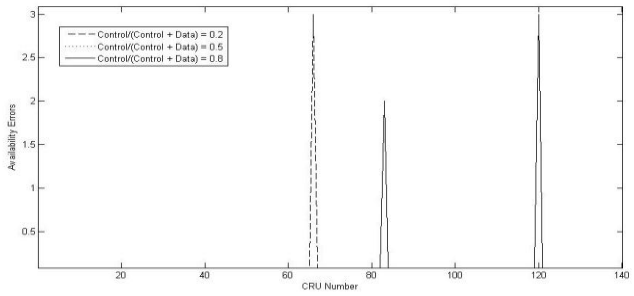

Fig. 12. Availability Errors

Results from Fig. 12 show that the availability errors are quite random; however, when the number of repetitions increases, we might conclude these errors are dependent on the CRU Number since more users might be trying to use the same number of channels. Combining these results with the ones from Fig. 11, and since the idea is to transmit as much data and less control information as possible, we conclude that it is possible to construct a CRN using a CPC with a low Control/(Control+Data) ratio.

IV. DISCUSSION

The results indicate that a basic CR-MAC protocol can be implemented through CPC channels. Using this premise, a CRN composed by total heterogeneous wireless frequency devices could be developed. A comparison with a common control channel based CR-MAC, for future work, will permit to infer if better results could be obtained combining a common control channel approach with the CPC approach.

The expected results are that controlling a CRN using a CPC, while not significant, still affect the performance of the PU compared to a CRN controlled by a common control channel, while allowing the presence of heterogeneous frequency CRU. Lowering the transmission and availability errors is also a must in future proposals. The results will be compared with the obtained in other CPC proposals such as in [16] and [18].

The results also indicate that a reduction in energy transmission due to signalization can be achieved by using the basic CRU sensing properties. Since the CRU can only detect values above a specific threshold for a determined period of time, the CRU might detect PU transmission due to its continuity, and CRU transmission due to its periodicity. Using that property, broadcasting transmissions, which are the ones that contribute to energy waste are reduced. Another advantage of using this property is that the CCBS is already aware of the available channels of each CRU. This is because in the admission process, each CRU has already indicated its characteristics. Considering that the CCBS has this knowledge, direct channel assignation can be performed, so broadcast transmission is also reduced.

On the other hand, broadcasting signaling would still be needed in some cases. The minimum number of channels to communicate with all CRUs in the CRN can be found according to the characteristics of the CRU, and the access control would be performed through those channels. Further works will be developed in this area to find the trade-offs for applying this combined approach while still guaranteeing effective heterogeneous communication.

ACKNOWLEDGMENT

The authors would like to thank Enrique Rodríguez-Colina for all his collaboration in the description of the model used in this paper. Part of this work was supported by the Department of Universities, Research and Information Society (DURSI) of the Government of Catalonia, European Social Funds (SGR-1202); by a FI Grant from the Government of Catalonia, in accordance with the Resolution IUE/2681/2008, and also by the Spanish Government (TRION MICINN TEC2009 - 10724)

REFERENCES

[1] N. Bolívar, J. L. Marzo and E. Rodríguez-Colina, "Distributed Control using Cognitive Pilot Channels in a Centralized Cognitive Radio Network," in the Sixth Advanced International Conference in Telecommunications, pp. 30-34, May 2010, ISBN: 978-0-7695-4021-4.

[2] Overview of SCC41 and the 1900.x Working Groups. IEEE. http://grouper.ieee.org/groups/scc41/. Retrieved 2011-01-18.

[3] M. Muck, S. Buljpre, P. Martigne, A. Kousaridas, E. Patouni, M. Stamatelatos, K. Tsagkaris. J.Yang, O. Holland, "IEEE P1900.B: Coexistence Support for Reconfigurable, Heterogeneous Air Interfaces," in IEEE Dyspan 2007, pp. 381-389, April 2007.

[4] J. Mitola III and G. Q Maguire, Jr., "Cognitive Radio: Making Software Radios More Personal," IEEE Personal Communications (Wireless Communications), vol.6, no. 4, pp. 13-18, August 1999.

[5] I. F. Akyildiz, W. Y. Lee, M. C. Buran, and S. Mohanty, "A survey on spectrum management in cognitive radio networks," IEEE Communications Magazine, vol. 46, no. 4, pp. 40-48, April 2008.

[6] IEEE 802 LAN/MAN Standards Committee 802.22 WG on WRANs (Wireless Regional Area Networks). IEEE. http://www.ieee802.org/22/. Retrieved 2011-01-18.

[7] F. Wang, M. Krunz, and S. Cui, "Spectrum Sharing in Cognitive Radio Networks," in IEEE 27th Conference on Computer Communications, INFOCOM 2008, pp. 36-40, April 2008.

[8] H. Wang, H. Qin, and L. Zhu, "A Survey on MAC Protocols for Opportunistic Spectrum Access in Cognitive Radio Networks," in IEEE International Conference on Computer Science and Software Engeneering 2008, pp. 214-218, December 2008.

[9] S. - Y. Lien, C. - C. Tseng, and K. - C. Chen, "Carrier Sensing based Multiple Access Protocols for Cognitive Radio Networks," in IEEE Conference on Communications 2008, ICC 2008, pp. 3208-3214, May 2008.

[10] A. Yau, P. Komisarczuk, and P. D. Teal, "On Multi-Channel MAC Protocols in Cognitive Radio Networks," in Australasian Telecommunication Networks and Applications Conference 2008, ATNAC 2008, pp. 300-305, December 2008.

[11] A. P. Hulbert, "Spectrum Sharing Through Beacons," in IEEE 16th International Symposium on Personal, Indoor and Mobile Radio Communications, pp. 989-993, September 2005.

[12] S. Mangold, A. Jarosch, and C. Monney, "Operator Assisted Cognitive Radio and Dynamic Spectrum Assignment with Dual Beacons – Detailed Evaluation," in First International Conference on Communication System Software and Middleware 2006, pp. 1-6, August 2006.

[13] Z. Quan, S. Cui, H. V. Poor, and A. H. Sayed, "Collaborative Wideband Sensing for Cognitive Radios," IEEE Signal Processing Magazine, vol. 25, no. 6, pp. 60-73, November 2008.

[14] A. Ghasemi, and E. S. Sousa, "Interference Aggregation in Spectrum-Sensing Cognitive Wireless Networks," IEEE Journal of Selected Topics in Signal Processing, vol 2, no. 1, pp. 41-56, February 2008.

[15] End to end efficiency. E3. https://ict-e3.eu/project/technical_highlights/5_enablers/enablers_2009_10.html. Retrieved 2011-01-18.

[16] M. Filo, A. Hossain, A. R. Biswas, R. Piesiewicz, "Cognitive Pilot Channel: Enabler for Radio Systems Coexistence," Second International Workshop on Cognitive Radio and Advanced Spectrum Management 2009, CogART 2009, pp. 17-23, May 2009.

[17] End to End Reconfigurability II (E^2R II) White Paper, "The E^2R II Flexible Spectrum Management (FSM) Framework and Cognitive Pilot Channel (CPC) Concept – Technical and Business Analysis and Recommendations," pp. 1-52, November 2007.

[18] O. Sallent, J. Pérez-Romero, R. Agustí, P. Cordier, "Cognitive Pilot Channel Enabling Spectrum Awareness," IEEE Conference on Communications Workshops 2009, ICC Workshops 2009, pp. 1-6, June 2009.

[19] J. Palicot, M. Katayama, A. Nafkna, G.Ravera, M.Massoth, J. Perez-Romero, "Challenges in Advanced Communications and Services," Panel AICT 2010, IARIA Panels, May 2010.

[20] N. Bolívar and J. L. Marzo, "Energy Reduction for Centralized Cognitive Radio Networks with Distributed Cognitive Pilot Channels," Accepted at 2010 Latincom, September 2010.

An Improved Multi-band Speech Enhancement Method for Colored Noise Estimation and Reduction

Radu Mihnea Udrea, Dragos Nicolae Vizireanu, Claudia Cristina Oprea, Ionut Pirnog
Telecommunications Department
"Politehnica" University of Bucharest
313, Splaiul Independentei, Sector 6, 060042
Bucharest, Romania
mihnea@comm.pub.ro, nae@comm.pub.ro, cristina@comm.pub.ro, ionut@comm.pub.ro

***Abstract*—There are many situations where speech is affected by different kind of acoustic noise. We propose an improved spectral subtraction method for the reduction of colored acoustic noise added to the speech. Our implementation uses a multi-band spectral over subtraction method to reduce the colored noise. We use a non-linear Bark scale distribution to estimate the over-subtraction factor. The noise power spectral density is estimated, using a time-recursive algorithm, by tracking the minimum of the noisy speech spectrum in each frequency band. Simulations show a better quality in terms of Itakura Saito distance and perceptual evaluation of quality for the enhanced speech. Using the proposed speech enhancement method, a very good speech quality with less musical noise and with minimal speech distortion is obtained.**

Keywords-speech enhancement; spectral subtraction; noise estimation; critical band.

I. INTRODUCTION

The speech signal is often accompanied by the background noise of the environment. There are many negative effects when processing the degraded speech for some applications like: voice command systems, voice recognition, speaker authentication, hands-free systems.

The main objective of speech enhancement is to improve the perceptual aspects of speech such as overall quality or intelligibility. Enhancement techniques can be classified as single channel and dual channel or multi channel enhancement techniques. Single channel enhancement techniques apply to situations in which only one acquisition channel is available. In multi channel enhancement techniques, a reference signal for the noise is available and hence adaptive noise cancellation technique can be applied.

The spectral subtraction method is a well-known single channel noise reduction technique. The basic spectral subtraction technique proposed by Boll [2] apply subtraction of the noise spectrum estimate over the speech spectrum. The conventional power spectral subtraction method substantially reduces the noise levels in the noisy speech. However, it also introduces an annoying distortion in the speech signal called musical noise. Due to the inaccuracies in the short-time noise spectrum estimate, large spectral variations exist in the enhanced spectrum causing these distortions.

Berouti [3] proposed an important variation of spectral subtraction for reduction of residual musical noise. The proposed method subtracts an overestimate of the noise power spectrum from the speech power spectrum. This operation minimizes the presence of residual noise by decreasing the spectral excursions in the enhanced spectrum. The over-subtraction factor provides a degree of control over the noise removal process between periods of noise update.

A nonlinear approach to the subtraction procedure was proposed in recent studies [4], [5], [6], [7], which takes into account the variation of the signal-to-noise ratio across the entire speech spectrum. The real-world noise spectrum is not flat, therefore the noise signal does not affect the speech signal uniformly over the whole spectrum. Hence, it becomes imperative to estimate a suitable factor that will subtract just the necessary amount of the noise spectrum from each frequency sub-band, to prevent destructive subtraction of the speech while removing most of the residual noise.

Noise spectrum estimation is also a challenging situation. Several noise-estimation algorithms have been proposed for speech enhancement applications. For rather stationary noise sources, the noise power spectral density (PSD) can be estimated by tracking the minimum of the noisy speech spectrum in each frequency band [8], [9]. However, in case of non-stationary noise sources, more advanced methods can be used [10].

In this paper we used a modified spectral over-subtraction approach that allows better and more suppression of the noise. We propose to use the noise PSD estimation to compute the *a posteriori* SNR in each frequency subband. Then we calculate the corresponding over-subtraction factor and we apply the nonlinear multi-band spectral subtraction that reduces colored noise, using a different over-subtraction factor in each frequency band.

This paper is organized as follows: a overview of the spectral subtraction methods is presented in Section II. Section III presents the human auditory system and the critical band and Bark scale model of speech analysis. Section IV describes the time-recursive averaging type of algorithms in which the noise spectrum is estimated in order to be used by the spectral subtraction method. Section V presents the improved multi-band spectral over-subtraction

method proposed to reduce the colored noise. Section VI shows implementation details and experimental results.

II. SPECTRAL SUBTRACTION METHODS

A. Basic Spectral Subtraction Method

The spectral subtraction method proposed by Boll [2] consists in obtaining an estimate of the noise-free signal spectrum by subtracting an estimate of the noise spectrum from the input noisy signal spectrum. The background noise is considered acoustically added to the speech. It is assumed that the background noise remains locally stationary to the degree that its spectral magnitude expected value prior to speech activity equals its expected value during speech activity.

The noise is assumed to be uncorrelated and additive to the speech signal. An estimate of the noise signal is measured during silence or non-speech activity in the signal. We assume that the speech signal $s(n)$ has been degraded by the additive noise signal $d(n)$,

$$y(n) = s(n) + d(n). \tag{1}$$

Taking the Discrete Fourier Transform (DFT) of $x(n)$ gives

$$Y(k) = S(k) + D(k). \tag{2}$$

The estimate of the noise spectrum is obtained during speech pauses (SP) when

$$y_{SP}(n) = d(n). \tag{3}$$

Noise spectrum can be estimated as the average value of $|Y_{SP}(k)|$ over the speech pauses frames

$$\left|\hat{D}(k)\right| = \frac{1}{M}\sum_{i=0}^{M-1}\left|Y_{SP_i}(k)\right|, \tag{4}$$

where M is the number of consecutive frames of SP.

The estimate of the clear speech spectrum magnitude can be obtained as

$$\left|\hat{S}(k)\right| = \left|Y(k)\right| - \left|\hat{D}(k)\right|. \tag{5}$$

The phase $\theta_Y(k)$ of the input signal is used for reconstruction of the estimated signal spectrum based on the fact that for human perception the short time spectral magnitude is more important than the phase for intelligibility and quality. This conclusion was made by Lim and Wang in their work [11], when using the actual phase rather than the degraded speech phase does not improve the quality of the enhanced speech.

Therefore,

$$\hat{S}(k) = \left|\hat{S}(k)\right| e^{j\theta_Y(k)}. \tag{6}$$

The time reconstructed speech signal is obtained taken the Inverse Discrete Fourier Transform of $\hat{S}(k)$.

Since the noise spectrum cannot be directly obtained, there are some significant variations between the estimated noise spectrum and the actual noise content present in the instantaneous speech spectrum. This residual spectral content manifest themselves in the reconstructed time signal as varying tonal sounds resulting in a musical disturbance of an unnatural quality. This sounds like a musical noise and is the main drawback of the spectral subtraction method.

B. Generalized Spectral Subtraction

A generalized form of the basic spectral subtraction was proposed by Berouti [3]. The estimate of the enhanced speech is given by

$$\left|\hat{S}(k)\right| = \left(\left|Y(k)\right|^p - \alpha\left|\hat{D}(k)\right|^p\right)^{1/p}, \tag{7}$$

where p is the exponent of the spectrum and α is a multiplication factor used for over-subtraction of noise spectrum estimate. For $\alpha = 1$ and $p = 2$ we have the *Power Spectral Subtraction* method.

Power spectral relation after taking DFT from (1) gives

$$\begin{aligned} |Y(k)|^2 = &|S(k)|^2 + |D(k)|^2 + \\ &+ S(k)D^*(k) + S^*(k)D(k) \end{aligned} \tag{8}$$

where $S^*(k)$ and $D^*(k)$ are complex conjugates of $S(k)$ and $D(k)$ respectively.

Because in our system only the power of the input noisy signal $|Y(k)|^2$ can be evaluated, the rest of terms are approximated by their average during non-speech activity period.

If $d(n)$ is uncorrelated with $s(n)$, then

$$E\{S(k)D^*(k)\} = 0 \text{ and } E\{S^*(k)D(k)\} = 0. \tag{9}$$

The short time power spectrum of the noisy speech can be approximated by

$$\left|Y(k)\right|^2 \approx \left|S(k)\right|^2 + \left|D(k)\right|^2. \tag{10}$$

The noise PSD $\hat{\sigma}_d^2(k)$ is estimated as the average value of the noise power spectrum taken during non-speech activity periods.

$$\hat{\sigma}_d^2(k) \simeq E\left\{\left|D(k)\right|^2\right\}. \quad (11)$$

A significant improvement to minimize the presence of residual noise and musical noise in the processed speech was proposed by Berouti et al. [3]. The average noise power spectrum is multiplied by the over-subtraction factor α and subtracted from the noisy speech spectrum in order to minimize the residual and musical noise:

$$\left|\hat{S}(k)\right|^2 = \left|Y(k)\right|^2 - \alpha \cdot \hat{\sigma}_d^2(k), \quad \alpha \geq 1. \quad (12)$$

This method improves the noise suppression better than basic spectral subtraction technique and also eliminates the musical noise. Besides it adapts to wide range of signal to noise ratios.

After subtracting an overestimate of the noise power spectrum the resulting estimated speech spectrum is down-limited at a minimum β level (spectral floor):

$$\left|\hat{S}(k)\right|^2 = \begin{cases} \left|\hat{S}(k)\right|^2, \text{ if } \left|\hat{S}(k)\right|^2 > \beta \cdot \hat{\sigma}_d^2(k) \\ \beta \cdot \hat{\sigma}_d^2(k), \text{ otherwise} \end{cases}, \quad (13)$$

where the spectral floor parameter was set to $\beta = 0.001$.

These modifications lead to minimizing the perception of the narrow spectral peaks by decreasing the spectral excursions and thus lower the musical noise perception.

To reduce the speech distortion caused by large values of α, its value is adapted from frame to frame. The basic idea is to take into account that the subtraction process must depend on the *a posteriori* SNR of the frame, in order to apply less subtraction with high *a posteriori* SNR and vice versa.

The *a posteriori* SNR is calculated for every frame with:

$$\gamma = 10\log_{10}\frac{\sum_{k=0}^{N-1}\left|Y(k)\right|^2}{\sum_{k=0}^{N-1}\hat{\sigma}_d^2(k)}, \quad (14)$$

where N is the number of frequency bins of DFT.

The over-subtraction factor α can be calculated [8] as:

$$\alpha = \begin{cases} 1 & \gamma \geq 20\text{dB} \\ \alpha_0 - \frac{3}{20}\gamma & -6\text{dB} \leq \gamma < 20\text{dB} \\ 4.9 & \gamma < -6\text{dB} \end{cases}, \quad (15)$$

where $\alpha_0 = 4$ is the desired value of α at $\gamma = 0\text{dB}$.

The over-subtraction factor gives a degree of adaptation from frame to frame, but it may reduce speech spectral information in the same frame for frequency domains where noise PSD is lower, if noise spectrum is not flat.

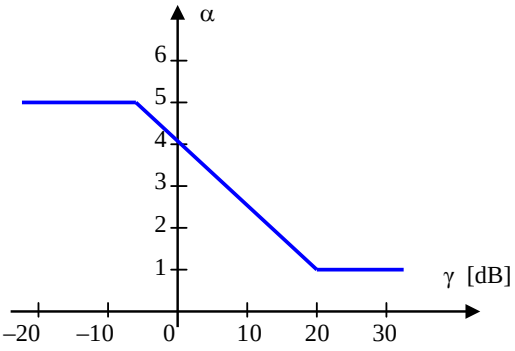

Figure 1. The over-subtraction factor α dependence over the a posteriori SNR γ.

C. Multi-Band Spectral Subtraction

In real environments, the noise spectrum is not uniform for all frequencies. For example, in the case of engine noise, most of the noise energy is concentrated in the low-frequency area. To take into account the fact that colored noise affects the speech spectrum differently at different frequencies, a multi-band linear frequency spacing approach to spectral over-subtraction was proposed in [5].

The speech spectrum is divided into a number of non-overlapping bands, and spectral subtraction is performed independently in each band. The estimate of the clean speech spectrum in the i-th band is obtained by:

$$\left|\hat{S}_i(k)\right|^2 = \left|Y_i(k)\right|^2 - \alpha_i \cdot \hat{\sigma}_d^2(k), \; \nu_i < k < \nu_{i+1}, \quad (16)$$

where k is the frequency bin, ν_i and ν_{i+1} are the beginning and ending frequency bins of the i-th frequency band and α_i is the over-subtraction factor of the i-th band. The over-subtraction factor α_i is a function of the *a posteriori* SNR γ_i of the i-th frequency band.

$$\gamma_i = 10\log_{10}\frac{\sum_{k=\nu_i}^{\nu_{i+1}}\left|Y_i(k)\right|^2}{\sum_{k=\nu_i}^{\nu_{i+1}}\hat{\sigma}_d^2(k)}. \quad (17)$$

The over-subtraction factor α_i may be calculated for each frequency band as:

$$\alpha_i = \begin{cases} 1 & \gamma_i \geq 20\text{dB} \\ 4 - \frac{3}{20}\gamma_i & -6\text{dB} \leq \gamma_i < 20\text{dB} \\ 4.9 & \gamma_i < -6\text{dB} \end{cases}, \quad (18)$$

The negative values of the estimated spectrum were floored using (13).

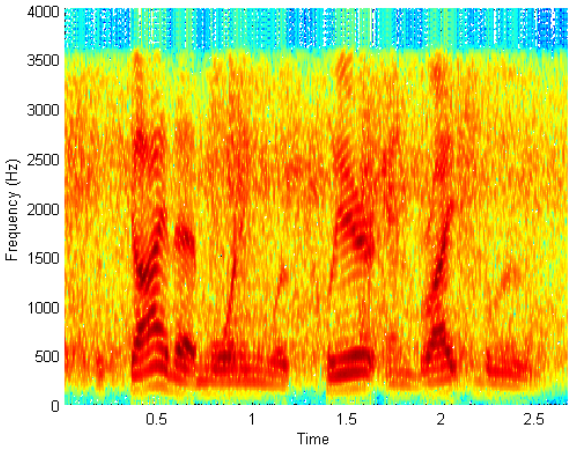

Figure 2. Spectrogram of speech affected by colored noise.

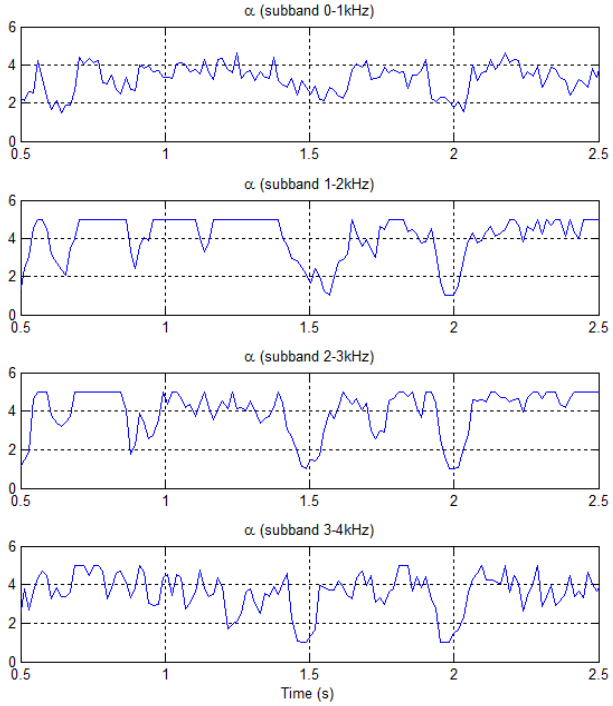

Figure 3. Over-subtraction factor α computed for four linearly-spaced frequency subbands.

In Fig. 2 it is plotted the spectrogram of speech sentence "The sky this morning was clear and light blue" affected by colored noise. Fig. 3 shows the over-subtraction factor computed after dividing the frequency domain into four linearly-spaced frequency subbands. It can be seen that the over-subtraction factor takes different values depending on the SNR in each frequency subband, allowing a better distribution of noise reduction over the entire frequency domain.

Because the human ear sensibility depends nonlinearly on the frequency, a nonlinear frequency spacing approach for multi-band over-subtraction factor estimation is proposed in this paper. The method is presented in Section V.

III. CRITICAL BANDS AND BARK SCALE

The human auditory system is a highly complicated mechanism. During the last decades, a considerable progress has been made within the research of the human hearing. The field of psychoacoustics examines directly the relationships between acoustic stimuli and the associated sensations. The concept of hearing area refers to the ranges of frequency and sound pressure values within which the human ear generally perceives sound.

The absolute threshold of hearing, also known as the threshold in quiet, signifies the minimum sound pressure level of a pure tone that is enough for the tone to be audible in the absence of any interfering voices, i.e., in quiet.

A prominent contributor to the idea of auditory filters was Fletcher who measured the detection threshold of a sinusoidal signal in the presence of a bandpass noise masker. In his experiment, the noise power density was held constant and its centre frequency was always the same as the signal frequency. As the noise bandwidth was increased, the threshold of the signal also increased at first, but after a certain noise bandwidth had been achieved, the signal threshold levelled off.

Basically, the power spectrum model suggests that the peripheral auditory system contains a bank of linear overlapping bandpass filters called auditory filters. It is assumed that when trying to detect a signal in a noisy environment, only one filter whose centre frequency is close to the frequency of the signal is being used. According to the model, this auditory filter blocks out most of the noise and only the part passing through the filter affects the masking of the signal. In reality, the perception of complex signals, e.g. speech, depends on the outputs of several auditory filters and not just one.

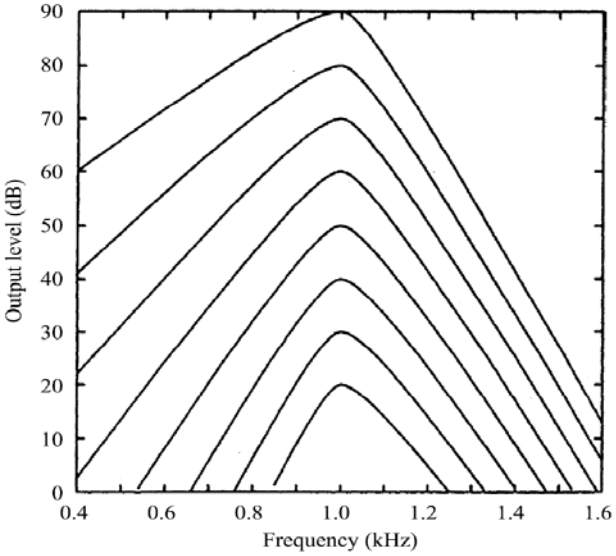

Figure 4. Shape of the auditory filter [12].

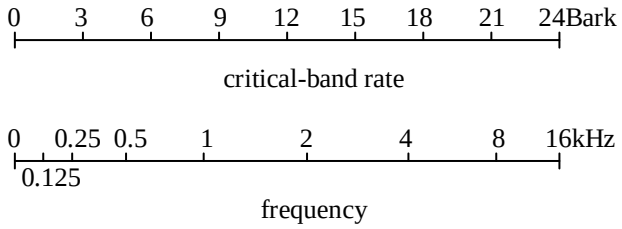

Figure 5. Frequency in Hertz and the critical-band rate scale in Bark [13].

The assumption of linear auditory filters is also incorrect since, strictly speaking, the shape of the filter changes slightly with the input level. As the level of the stimulus is increased, the slope on the low-frequency side of the auditory filter becomes less sharp while the high-frequency skirt becomes steeper. This is illustrated in Fig.4.

In his band-widening experiment, Fletcher introduced the concept of critical bandwidth (CB), denoting the noise bandwidth limit at which the detection threshold of the signal (tone) ceased to increase. For simplicity, he thought that the auditory filter could be approximated as having a rectangular shape and a passband width equal to CB. Fletcher suggested that, with this rectangular model, CB could be evaluated by measuring the threshold of a sinusoidal signal in broadband white noise [12]. In this method, the power of the tone and the power spectral density of the noise masker are first measured. The noise power within the same critical band with the signal is then equal to the product of the measured power spectral density and the CB of the band in question.

The critical bandwidth can also be explained based on the physical structure of the inner ear. Each point on the basilar membrane (BM) responds only to a certain range of frequencies, which leads to the idea that these different points correspond to auditory filters with different centre frequencies [12].

A commonly used scale for specifying the critical bands is the Bark scale which divides the audible frequency range of 16 kHz into 24 bands. Fig. 5 illustrates the relationship between the frequency in Hertz and the critical-band rate in Bark [13].

An approximate analytical expression to describe the conversion from linear frequency, *f*, into the critical band number *z* (in Bark) is [13]:

$$z(f) = 13\arctan\left(0.76 f\right) + 3.5\arctan\left(f / 7.5\right)^2, \quad (19)$$

and the critical bandwidth (in Hz) for a given centre frequency can be evaluated by

$$BW\left(f\right) = 25 + 75\left(1 + 1.4 f^2\right)^{0.69}. \quad (20)$$

In the above equation *f* is given in kHz. By the definition of the Bark scale, each critical band has a width of one Bark.

Table 1 shows the correspondence between Bark scale and the frequency limits for the corresponding CB [13].

Table 1. CRITICAL BANDWIDTH AS A FUNCTION OF CENTER FREQUENCY AND CRITICAL BAND [13].

CB rate	Center frequency	Frequency	CB bandwidth
Bark	***Hz***	***Hz***	***Hz***
0	50	20	80
1	150	100	100
2	250	200	100
3	350	300	100
4	450	400	110
5	570	510	120
6	700	630	140
7	840	770	150
8	1000	920	160
9	1170	1080	190
10	1370	1270	210
11	1600	1480	240
12	1850	1720	280
13	2150	2000	320
14	2500	2320	380
15	2900	2700	450
16	3400	3150	550
17	4000	3700	700
18	4800	4400	900
19	5800	5300	1100
20	7000	6400	1300
21	8500	7700	1800
22	10500	9500	2500
23	13500	12000	3500
24		15500	

IV. NOISE ESTIMATION

The noise signal typically has a nonuniform effect on the spectrum of the speech. Each spectral component will typically have a different effective SNR. Consequently, we can estimate and update individual frequency bands of the noise spectrum whenever the effective SNR at a particular frequency band is extremely low. This observation led to the recursive-averaging type of algorithms [8],[9] in which the noise spectrum is estimated as a weighted average of past noise estimates and the present noisy speech spectrum.

The time-recursive algorithms have the following form:

$$\hat{\sigma}_d^2\left(\lambda,k\right) = \delta\left(\lambda,k\right)\hat{\sigma}_d^2\left(\lambda-1,k\right) + \left(1-\delta\left(\lambda,k\right)\right)\left|Y\left(\lambda,k\right)\right|^2, \quad (21)$$

where $\left|Y\left(\lambda,k\right)\right|^2$ is the speech magnitude spectrum squared (periodogram), $\hat{\sigma}_d^2\left(\lambda,k\right)$ denotes the estimate of the noise power spectral density (PSD) at frame λ and frequency k

and $\delta(\lambda,k)$ is the smoothing factor, which is time and frequency dependent.

In [9], the smoothing factor $\delta(\lambda,k)$ is chosen to be a sigmoid function of the *a posteriori* SNR $\gamma_k(\lambda)$:

$$\delta(\lambda,k)=\frac{1}{1+e^{-\tau(\gamma_k(\lambda)-1.5)}}, \quad (22)$$

where the τ is a parameter with values in the range $15\le\tau\le30$, and $\gamma_k(\lambda)$ is an approximation of the *a posteriori* SNR given by:

$$\gamma_k(\lambda)=\frac{|Y(\lambda,k)|^2}{\frac{1}{10}\sum_{m=1}^{10}\hat{\sigma}_d^2(\lambda-m,k)}. \quad (23)$$

Also, a different function was proposed for computing $\delta(\lambda,k)$:

$$\delta(\lambda,k)=1-\min\left[1,\frac{1}{\gamma_k(\lambda)}\right], \quad (24)$$

used to ensure that $\delta(\lambda,k)$ is in the range of $[0,1]$.

The recursive algorithm given in (21) and (24) can be explained as follows:

- If speech is present, the *a posteriori* estimate $\gamma_k(\lambda)$ will be large and therefore $\delta(\lambda,k)\approx1$. Consequently, we will have $\hat{\sigma}_d^2(\lambda,k)\equiv\hat{\sigma}_d^2(\lambda-1,k)$ according to (21). The noise update will cease and the noise estimate will remain the same as the previous frame's estimate.
- If speech is absent, the *a posteriori* estimate $\gamma_k(\lambda)$ will be small and therefore $\delta(\lambda,k)\approx0$. As a result, $\hat{\sigma}_d^2(\lambda,k)\equiv|Y(\lambda,k)|^2$ and the noise estimate will follow the PSD of the noisy spectrum in the absence of speech.

The main advantage of using the time smoothing factor $\delta(\lambda,k)$ given by (22) or (24), as opposed to using a fixed value for $\delta(\lambda,k)$, is that these factors are time and frequency dependent. This means that the noise PSD will be adapted differently and at different rates in the various frequency bins, depending on the estimate of the *a posteriori* SNR $\gamma_k(\lambda)$ in that bin. This is particularly suited in situations in which the additive noise is colored.

A different and simpler approach [14] to recursive averaging noise estimation is to choose a fixed smoothing factor and to control the update of the noise PSD based on the comparison of the estimated a posteriori SNR to a threshold.

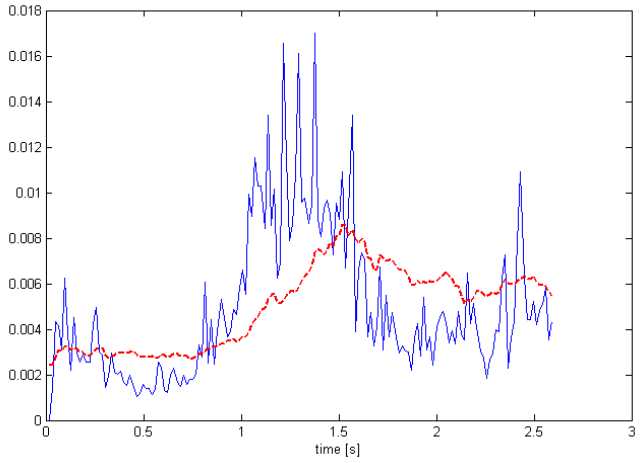

Figure 6. Estimated noise PSD (dashed line) for a frequency bin $k=30$ compared with real noise spectral distribution (continuous line).

$$\hat{\sigma}_v^2(\lambda,k)=\begin{cases}\delta\cdot\hat{\sigma}_v^2(\lambda-1,k)+(1-\delta)|Y(\lambda,k)|^2, & \text{if } \gamma_k(\lambda)<\varepsilon\\ \hat{\sigma}_v^2(\lambda-1,k), & \text{otherwise}\end{cases} \quad (25)$$

If the a posteriori SNR $\gamma_k(\lambda)$ is found to be smaller than a specified threshold ε, suggesting speech absence, then the noise spectrum is updated, else, if the a posteriori SNR is found to be larger than a specified threshold, suggesting speech presence, then the noise spectrum update is stopped.

The threshold ε can have significant effect on the noise spectrum estimation. If ε is chosen too small, then the noise spectrum is not updated often enough and is underestimated. Else, if ε is chosen too large, then the noise spectrum is overestimated. Simulations in [14] showed that choosing $\varepsilon=2.5$ gave a good compromise.

The estimated power of the noise is computed from the noise PSD of each frame:

$$\hat{\sigma}_v^2(\lambda)=\frac{1}{N}\sum_{k=0}^{N-1}\hat{\sigma}_v^2(\lambda,k), \quad (26)$$

where *N* is the number of frequency bins.

In Fig. 6 there are represented the estimated noise PSD (with red-dashed line) for a frequency bin $k=30$ compared with real noise spectral distribution (represented with continuous line) at the same frequency bin.

V. The Proposed Over-subtraction Method

The main drawback of the spectral subtraction method is the residual noise resulted as the difference between the estimated noise spectrum and the actual noise content present in the instantaneous speech spectrum. This residual spectral content manifest themselves in the reconstructed time signal as varying tonal sounds resulting in a musical like noise.

This residual noise can be reduced by a good estimation of the noise PSD and by using the multi-band spectral over-subtraction. Because the human ear sensibility depends nonlinearly on the frequency, a nonlinear frequency spacing approach for multi-band over-subtraction factor estimation is proposed in this paper.

The speech spectrum is divided into *N* non-overlapping bands over the Bark scale of frequency distribution, and spectral subtraction is performed independently in each band. Also, for the noise spectrum estimate, we used the noise PSD estimated $\hat{\sigma}_d^2(\lambda,k)$ at frame λ and frequency k using (21) or (25).

The estimate of the clean speech spectrum in the *i*-th band is obtained by:

$$\left|\hat{S}_i(k)\right|^2 = \left|Y_i(k)\right|^2 - \alpha_i \cdot \hat{\sigma}_d^2(\lambda,k)\,,\ \nu_i < k < \nu_{i+1}\,, \qquad (27)$$

where ν_i and ν_{i+1} are the beginning and ending frequency bins of the *i*-th frequency critical band according to Table 1, and α_i is the over-subtraction factor of the *i*-th critical band.

The over-subtraction factor α_i is a function of the *a posteriori* SNR γ_i of the *i*-th frequency band.

In this paper we propose to use the time-recursive estimation of the *a posteriori* SNR $\gamma_i(\lambda)$ at frame λ for the *i*-th frequency band:

$$\gamma_i(\lambda) = 10\log_{10}\frac{\sum_{k=w_i}^{w_{i+1}}\left|Y(\lambda,k)\right|^2}{\sum_{k=w_i}^{w_{i+1}}\hat{\sigma}_d^2(\lambda,k)}\,. \qquad (28)$$

The over-subtraction factor α_i is calculated for each frequency band as

$$\alpha_i = \begin{cases} 1 & \gamma_i(\lambda) \geq 20\text{dB} \\ 4 - \frac{3}{20}\gamma_i(\lambda) & -6\text{dB} \leq \gamma_i(\lambda) < 20\text{dB}\,. \\ 4.9 & \gamma_i(\lambda) < -6\text{dB} \end{cases} \qquad (29)$$

In the frequency domain of 0-4 kHz, specific for the speech signal, there are 16 critical bands. Experiments showed that there is computational inefficient to separate the spectrum into such a large number of intervals. An equivalent performance is obtained if there are grouped together 3 or 4 critical bands, therefore the spectrum analysis to be performed in a total number of 4 or 5 frequency domains, keeping the nonlinearity frequency spacing given by the human auditory system.

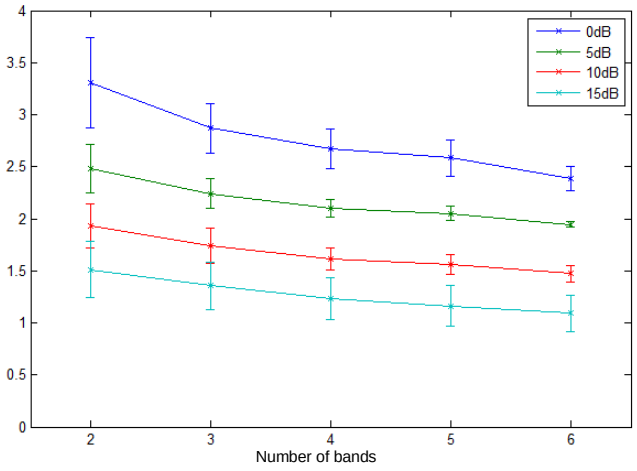

Figure 7. The Itakura-Saito (IS) distance for a variable number of frequency band analysis

VI. Implementation and Experimental Results

The speech signals, sampled at a frequency of 8 kHz, are degraded by the various noise types with segmental SNR's of -5 and 0 dB. Different types of noise taken from the Noisex92 database [15] are added to the speech signal. The noise is chosen with varying spectral distribution simulating colored noise (car engine, factory noise, babble noise).

We used both linear and nonlinear frequency spacing for multi-band spectral over-subtraction, in which the over-subtraction factor α_i is computed as in equation (29) for each frequency band. To determine the number of bands that gives an optimal speech quality, we varied the number of bands from 1 to 8 and examined speech enhancement using both types of frequency spacing.

Objective and subjective quality evaluation methods were applied to establish the performance of the algorithms presented in this study.

The Itakura-Saito (IS) distance method is used as an objective measure to evaluate the performance of the algorithm. The IS measure is based on the similarity or difference between the all-pole model of the clean signal and the corrupted or processed speech signal.

In Fig. 7, the mean IS values are plotted as a function of the number of bands. These values are obtained using the proposed time-recursive estimation for the *a posteriori* SNR used in the over-subtraction factor and a multi-band linear scaled frequency at 0, 5, 10 and 15 dB SNR An improvement in terms of the IS distance can be seen when the number of bands increases from one to six; afterwards, the improvement in quality is no longer perceivable.

Also, we used the ITU-T Recommendation P.862 (PESQ) [16] to obtain a perceptual evaluation of the enhanced speech quality. The Mean Opinion Score (MOS) obtained in the evaluation process is between 0 and 5 where 0 represents a very annoying distortion of the perceived signal and 5 represents imperceptible quality degradation.

Table 2. PESQ MOS EVALUATION FOR THE ENHANCED SPEECH QUALITY

Input SNR	Spectral Subtraction	Standard multi-band spectral subtraction					Time recursive estimation for multi-band spectral subtraction				
No. of bands		*2*	*3*	*4*	*5*	*6*	*2*	*3*	*4*	*5*	*6*
0dB	1.75	1.79	1.82	1.85	1.84	1.84	1.88	1.87	2.00	2.03	2.01
5dB	1.85	1.90	1.99	1.97	1.98	1.97	1.99	2.00	2.07	2.05	2.03
10dB	2.26	2.41	2.44	2.46	2.45	2.40	2.49	2.49	2.55	2.52	2.50
15dB	2.82	2.86	2.88	2.90	2.89	2.84	2.92	2.93	2.95	2.93	2.92

In Table 2 the simulations show that for a single band analysis the results are similar with the standard spectral over-subtraction method. The MOS is increasing when using more than one band, having a maximum when there are four bands, for both methods. Increasing the number of bands more than four bands does not give an increasing of quality since the resolution in frequency analysis is getting worse. A better quality can be noticed for the time recursive estimation of the noise PSD.

Subjective listening tests indicate that, using the multi-band approach and the time-recursive estimation, a very good speech quality with less musical noise and with minimal speech distortion is obtained.

Fig. 8 and Fig. 9 show the spectrograms for speech of speech sentence "The sky this morning was clear and light blue" affected by train noise and car engine noise, at a SNR of 10dB, and the spectrograms of the enhanced speech obtained with standard spectral subtraction, spectral over-subtraction using single-band subtraction factor, multi-band spectral over-subtraction using four linearly-spaced frequency bands, multi-band spectral over-subtraction using four non-linear Bark spaced bands and multi-band spectral subtraction using the time-recursive estimation of the noise PSD.

CONCLUSIONS

This paper presents an improved spectral subtraction method that takes into account the non-uniform effect of colored noise on the speech spectrum. A nonlinear frequency spacing approach for multi-band over-subtraction factor estimation is based on the fact that human ear sensibility varies nonlinear in frequency spectrum. This gives a better perceived quality to the enhanced speech.

Also, time-recursive estimation of the noise PSD is used to compute the multi-band over-subtraction factor in the nonlinear frequency spacing approach. The proposed method reduces the residual musical tones that appear in the case of conventional power spectral subtraction. Simulations with different types of noise show a better quality for the enhanced speech when using time recursive multi-band spectral subtraction.

ACKNOWLEDGMENT

The work has been funded by the Sectoral Operational Programme Human Resources Development 2007-2013 of the Romanian Ministry of Labour, Family and Social Protection through the Financial Agreement POSDRU/89/1.5/S/62557.

REFERENCES

[1] R. M. Udrea, D. N. Vizireanu, C. C. Oprea, and I. Pirnog, "A time-recursive adaptive algorithm for colored noise reduction in speech enhancement," Sixth Advanced International Conference on Telecommunications AICT 2010, pp.187-190, Barcelona, May 2010.

[2] S.F. Boll, "Suppression of acoustic noise in speech using spectral subtraction," IEEE Trans. Acoustic, Speech and Signal Processing, vol. 27, Apr. 1979, pp. 113-120.

[3] M. Berouti, R. Schwartz, and J. Makhoul, "Enhancement of speech corrupted by acoustic noise," Proc. IEEE Int. Conf. Acoust., Speech and Signal Proc., Apr. 1979, pp. 208-211.

[4] C. T. Lin, "Single-channel speech enhancement in variable noise-level environment," Systems, Man and Cybernetics, Part A, IEEE Trans. , Volume: 33 , Issue: 1, Jan. 2003, pp 137–143.

[5] S. Kamath and P. Loizou, "A multi-band spectral subtraction method for enhancing speech corrupted by colored noise," Proc. of ICASSP-2002, Orlando, FL, May 2002.

[6] R. M. Udrea and S. Ciochină, "Speech enhancement using spectral oversubtraction and residual noise reduction," Proc. of the Symposium "SCS 2003", Vol II, Iaşi, Romania, July 2003, pp. 165-169.

[7] R.M. Udrea, N. Vizireanu, S. Ciochina, and S. Halunga, "Nonlinear spectral subtraction method for colored noise reduction using multi-band Bark scale," Signal Processing, Vol. 88 Issue 5, ISSN: 0165-1684, May 2008, pp. 1299-1303.

[8] I. Cohen, "Noise spectrum estimation in adverse environments: Improved minima controlled recursive averaging," IEEE Trans. Speech Audio Processing, vol. 11, no 5, pp. 466-475, Sept. 2003.

[9] L. Lin, W.H. Holmes, and E. Ambikairajah, "Adaptive noise estimation algorithm for speech enhancement," Electronics Letters, vol. 39, no. 9, pp 754–755, May 2003.

[10] R. C. Hendriks, J. Jensen, and R. Heusdens, "Noise tracking using DFT domain subspace decompositions," IEEE Trans. Audio Speech and Language Processing, vol. 16, no. 3, pp. 541–553, March 2008.

[11] D.L. Wang and J.S. Lim, "The unimportance of phase in speech enhancement," IEEE Trans. On Acoustics, Speech, and Signal Processing, vol. 30, no.4, Aug. 1982, pp. 679-681.

[12] B. Moore, "An introduction to the psychology of hearing," 4th ed., London, Academic press,1997.

[13] E. Zwicker and H. Fastl, "Psychoacoustics," 1st ed., Berlin, Springer. 1990.

[14] H. G. Hirsch and C. Ehrlicher, "Noise estimation techniques for robust speech recognition," Proc. 20th IEEE Inter. Conf. Acoust. Speech Signal Process., ICASSP-95, Detroit, Michigan, pp. 153-156, 8-12 May 1995.

[15] A.P. Varga, H.J.M. Steeneken, M. Tomlinson, and D. Jones, "The NOISEX-92 Study on the Effect of Additive Noise on Automatic Speech Recognition," Tech. Rep., Speech Research Unit, Defense Research Agency, Malvern, U.K., 1992.

[16] ITU-T, Perceptual evaluation of speech quality PESQ, an objective method for end-to-end speech quality assessment of narrowband telephone networks and speech codecs, ITU-T Recommendation P.862, 2000.

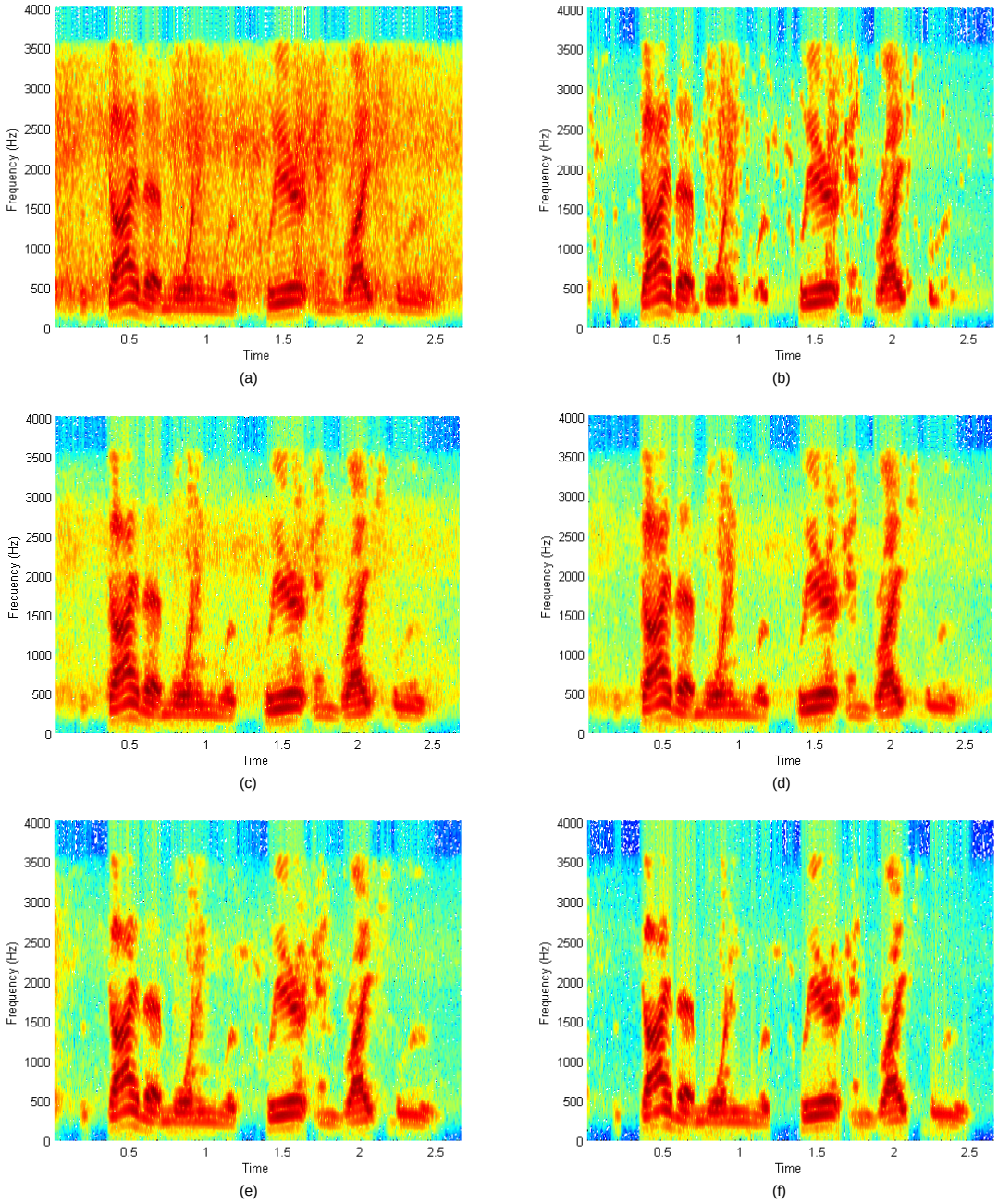

Figure 8. Spectrograms of speech affected by train noise at 10dB SNR (a) and of the enhanced speech obtained with:
standard spectral subtraction (b),
spectral over-subtraction using single-band subtraction factor (c),
multi-band spectral over-subtraction using four linearly-spaced bands (d),
multi-band spectral over-subtraction using four non-linear Bark spaced bands (e),
multi-band spectral subtraction using the time-recursive estimation of the noise PSD (f).

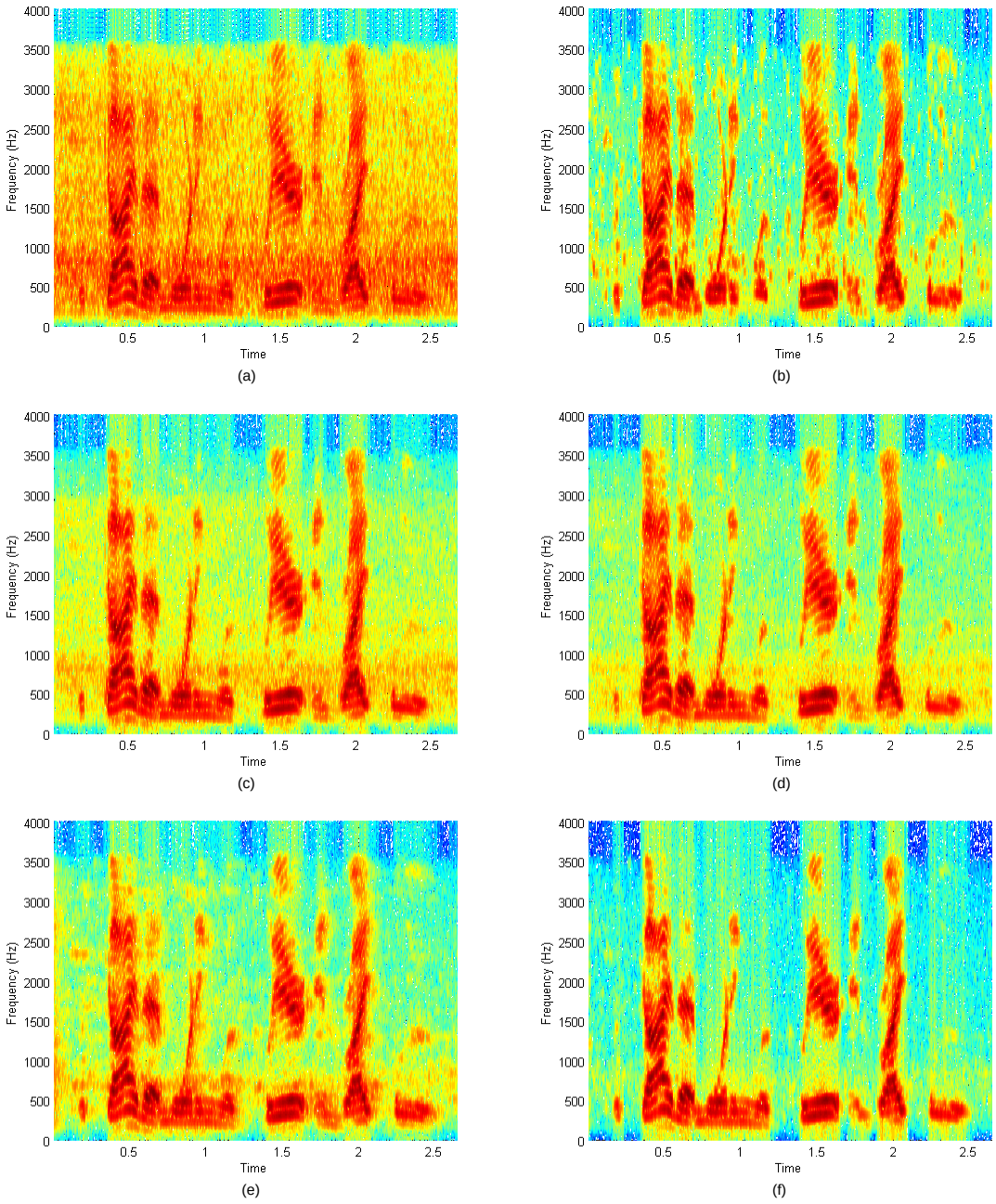

Figure 9. Spectrograms of speech affected by car noise at 10dB SNR (a) and of the enhanced speech obtained with:
standard spectral subtraction (b),
spectral over-subtraction using single-band subtraction factor (c),
multi-band spectral over-subtraction using four linearly-spaced bands (d),
multi-band spectral over-subtraction using four non-linear Bark spaced bands (e),
multi-band spectral subtraction using the time-recursive estimation of the noise PSD (f).

Performance Analysis of Multiuser DS-UWB system with Orthogonal and Non-orthogonal code under synchronous and Asynchronous transmission with UWB channel models

Prof. Himanshu B. Soni
Professor
GCET
V.V.Nagar, India
sony_himanshu@iitb.ac.in

Prof. U. B. desai
Director
IIT- Hyderabad
Hyderabad, India
ubdesai@iith.ac.in

Prof. S. N. Merchant
Professor
IIT- Bombay
Mumbai, India
merchant@ee.iitb.ac.in

***Abstract*—In this paper we have considered the downlink multimedia transmission with Direct Sequence-Ultra wideband (DS-UWB) [1] communication system. We have evaluated performance of DS-UWB system under multiuser scenario. We have investigated performance of the system under synchronous and asynchronous transmission. We have discussed the effect of orthogonal and non-orthogonal code selection with effect of different UWB pulse selection. Also the performance of DS-UWB with non-orthogonal code is compared with TH-PAM UWB [2]. We have considered AWGN and UWB channel model for simulation.**

***Keywords*-UWB; Synchronous-Asynchronous transmission; UWB channel model.**

I. INTRODUCTION

Ultra wideband (UWB) was known as Impulse radio [3], [4] as in principle, it uses the extremely short pulses for high speed data transmission. UWB promises to provide effective high speed data transmission in wireless personal area networks (WPAN) [5], [6]. In future WPAN networks (IEEE 802.15.3a, IEEE 802.15.4a), UWB will be the candidate at physical layer for enabling several Mbps data rate, which is quite higher than Bluetooth's data rate.

FCC assigned unlicensed spectrum of 3.1 GHz -10.6 GHz for UWB communication [7]. Signal with the fractional bandwidth (B_f) of more than 20 % at -10 dB emission points is considered as a UWB signal. Where fractional bandwidth is defined as a ratio of signal bandwidth to its centre frequency. New industrial definition for UWB signal is the signal which occupies bandwidth of more than 500 MHz in assigned frequency range, is considered as UWB signal [7]. For multiple access in UWB literatures [3], [8] suggest method based on Time Hopping (TH) technique. This access technique can be used with Pulse Position Modulation (PPM) or Pulse Amplitude Modulation (PAM) technique. Depending upon modulation scheme TH UWB signal is known as TH-PPM UWB [9], [10] or TH-PAM UWB [2]. Also Direct Sequence UWB (DS-UWB) approach proposed in [1] is same as TH-PAM UWB except minor difference. In all TH-UWB method single bit duration (T_b) is divided into number of frames (N_f) each with equal duration of (T_f). Further each frame duration (T_f) is divided into number of chips (N_c) of duration (T_c). During each chip period (T_c) UWB radio signal, which is Gaussian pulse or its derivative is transmitted depending upon unique TH code. UWB signal comprised of sub-nano second duration pulses. A sequence of pulses (N_f) are used to encode a transmitted symbol. In TH-PPM, UWB pulse will take additional delay of δ at the beginning of chip duration when data bit $'1'$ is transmitted. In TH-PAM instead of using shift of δ, antipodal signal is used for data bit $'1'$ and $'0'$.

In this paper, we have considered DS-UWB [1] method as a multiple access technique for multimedia transmission. We have considered downlink communication under multiuser environment. In this situation each user signal is identified with unique Pseudo random (PN) code. Here we investigated the performance of multiuser UWB system with DS-UWB under synchronous and asynchronous transmission. Also the effect of selection of orthogonal and non-orthogonal code is discussed with both the transmission schemes. Effect of selection of UWB pulse shape is discussed. Finally we have compared performance of DS-UWB multiuser system with TH-PAM UWB multiuser system with non-orthogonal codes.

Paper is organized as follows, In Section II, we have discuss the general scenario for downlink communication with multimedia transmission under multiuser environment. In section III the system model for DS-UWB is discussed. In section IV we have described the system model for TH-PAM UWB. Section V discusses different UWB channel model. In section VI we showed simulation results with AWGN and UWB channel for synchronous and asynchronous transmission. Also effect of selection of code is discussed in detail. Performance comparison with TH-PAM UWB has been discussed in section VI. Finally in Section VII, we conclude our work and discuss future scope in Section VIII. This work is an extension of our previously published paper [11].

II. Multimedia transmission scenario for UWB Communication

Figure 1 shows multimedia transmission scenario with UWB for multiuser environment. where different users (or Multimedia devices) data is transmitted by UWB device. Here, we have considered that this UWB device transmits data by, DS-UWB [1] or by other TH access technique [2], [9], [10]. We considered that this UWB device transmits data under two cases as synchronous and asynchronous transmission. This UWB device adds all users signal and transmits information together over downlink channel. Hence UWB device itself adds multiuser interference (MUI) in system.

To make uniformity throughout discussion we have considered all multimedia devices data as different users data and performance is discussed by considering multiuser environment for multimedia transmission.

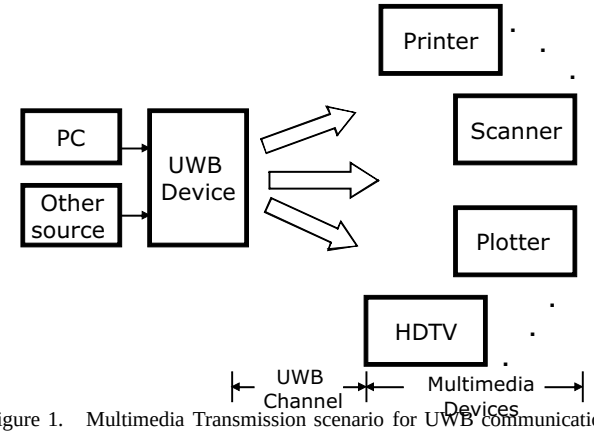

Figure 1. Multimedia Transmission scenario for UWB communication.

III. DS-UWB system

A. System Model DS-UWB

For Ultra wideband transmission, DS-UWB multiple access scheme is proposed in [1]. In DS-UWB one bit duration (T_b) is divided into number of frames (N_f) each with equal duration (T_f) such that T_b=N_f T_f. During each frame UWB pulse is transmitted which is Gaussian monocycle or Scholtz Monocycle. This pulse is a subnano second pulse. In Multiuser environment DS-UWB signal is represented as

$$s^{(k)}(t) = \sum_{i=-\infty}^{\infty} \sum_{j=0}^{N_f-1} d_{(i)}^{(k)} w(t - jT_f)$$

$s^{(k)}(.)$ is k^{th} user signal, $d_i^{(k)}$ is k^{th} user bipolar spreaded data, which is defined as $d_i^{(k)} = b_i^{(k)} c_i^{(k)}$. Where $b_i^{(k)}$ is k^{th} user raw data and $c_i^{(k)}$ is k^{th} user code. N_f is number of frames per bit, $w(.)$ is UWB pulse. Before transmission UWB device combines the entire users signal.

B. Receiver Configuration for DS-UWB

Received signal is contaminated by multipath fading and AWGN which is given as

$$r(t) = \int_0^{\infty} h(\tau, t) s(t - \tau)\, d\tau + n(t)$$

Where $h(\tau, t)$ is channel response, $n(t)$ is AWGN and $s(t)$ is

$$s(t) = \sum_{k=1}^{N} \sum_{i=-\infty}^{\infty} \sum_{j=0}^{N_f-1} d_i^{(k)} w(t - jT_f)$$

N is total number of users in the system. For synchronous transmission τ is zero. Here receiver is correlation based receiver as described in [1]. In which locally template $p(t)$ is generated and data is recovered by correlation receiver. Template $p(t)$ is defined as $p(t) = \sum_{j=0}^{N_f-1} w(t - jT_f)$. Correlation receiver output Z which is defined as $z = \int_0^{Tb} r(t)p(t)dt$. Using z decision is made in favour of transmitted data bit. After this particular user data is demodulated by code $c^{(k)}(.)$.

IV. TH-PAM UWB system

A. System Model for TH-PAM UWB system

In literature [2] TH-PAM UWB system is considered for Ultra wideband communication. In TH-PAM UWB single bit duration (T_b) is divided into N_f number of frames each with equal duration T_f, so $T_b = N_f T_f$. Further each frame is divided into N_c chips with chip duration of T_c such that $N_c T_c \leq T_f$. During each frame UWB pulse is transmitted which is either Gaussian monocycle or Scholtz Monocycle. UWB pulse occupy one chip slot depending on time hopping code c_j which can take value such that $0 \leq c_j \leq N_c - 1$. During each bit duration N_f UWB pulses are transmitted by TH-PAM transmitter. For modulation antipodal pulses are used. TH-PAM UWB signal is represented as

$$s^{(k)}(t) = \sum_{i=-\infty}^{\infty} \sum_{j=0}^{N_f-1} d_{(i)}^{(k)} w(t - jT_f - c_j^{(k)} T_c)$$

Where $S^{(k)}(.)$ is k^{th} user signal, $d_{(i)}^{(k)}$ is k^{th} user bipolar data, N_f is number of frames per bit and $w(.)$ is UWB pulse.

B. Receiver Configuration for TH-PAM UWB system

Received signal is contaminated by multipath fading and AWGN which is given as

$$r(t) = \int_0^{\infty} h(\tau, t) s(t - \tau)\, d\tau + n(t)$$

Where $h(\tau,t)$ is channel response, $n(t)$ is AWGN and $s(t)$ is

$$s(t)=\sum_{k=1}^{N}\sum_{i=-\infty}^{\infty}\sum_{j=0}^{N_f-1}d_{(i)}^{(k)}w(t-jT_f-c_j^{(k)}T_c)$$

N is total number of users in the system. Here receiver is correlation based receiver. In which locally template $p(t)$ is generated and data is recovered by correlation receiver. Correlation template $p(t)$ for k^{th} user is defined as,

$$p(t)=\sum_{j=0}^{N_f-1}w(t-jT_f-c_j^{(k)}T_c)$$

Correlation receiver generate output Z, which is given as $z=\int_0^{Tb}r(t)p(t)dt$. Using z decision is made in favour of transmitted data bit.

In DS-UWB and TH-PAM UWB, we have considered AWGN channel so for equiprobable binary symbols correlation receiver gives optimum results.

V. UWB CHANNEL MODEL

In wireless channel multipath fading [12] will take place due to scattering, reflection and refraction. This fading can be slow fading or fast fading, which will change parameter of received signal envelope and phase. This fading problem is more critical in indoor channel due to presence of many scatterers. So perfect channel modelling is required for improving performance of receiver.

By considering the assumption of static scatter the Channel impulse response(CIR) for time-invariant channel is given as,

$$h(t)=\sum_{n=0}^{N}\alpha_n\delta(t-\tau_n) \quad (1)$$

Here N is number of multipath components, α_n is attenuation for n^{th} path and τ_n is delay for n^{th} path. In UWB the channel model is based on Saleh-Valenzuela model [13].

A. UWB channel model recommendation by IEEE 802.15.3a working group

IEEE 802.15.3a working group has suggested channel model for indoor UWB communication. This model should be used for evaluating the performance of different physical layer proposal. This proposed model is based of input given by [13]–[21]. UWB channel model is cluster based model. In this model(SV model) the same pulses multipath components are grouped in to cluster. This cluster arrival is modelled as a Possion process with arrival rate of λ as,

$$P(T_n|T_{n-1})=\lambda e^{-\lambda(T_n-T_{n-1})} \quad (2)$$

Here, T_n is time of arrival for n^{th} cluster and T_{n-1} is time arrival of $(n-1)^{th}$ cluster. In each cluster the multipath components of same pulse is also model as a Possion process with arrival rate of Δ as,

$$P(\tau_{ni}|\tau_{(n-1)i})=\Delta e^{-\Delta(\tau_{ni}-\tau_{(n-1)i})} \quad (3)$$

Here,τ_{ni} is time of arrival of the n^{th} pulse in the i^{th} cluster and $\tau_{(n-1)i}$ is time of arrival of the $(n-1)^{th}$ pulse in the i^{th} cluster. The gain of the n^{th} pulse in i^{th} cluster is complex random variable as

$$A_{ni}\angle\Theta_{ni} \quad (4)$$

with,

$$p(A_{ni})=\frac{2A_{ni}}{E\left[|A_{ni}|^2\right]}e^{-\frac{A_{ni}^2}{E\left[|A_{ni}|^2\right]}} \quad (5)$$

and

$$p(\Theta_{ni})=\frac{1}{2\pi}with 0\le\Theta_{ni}\le 2\pi \quad (6)$$

Here,

$$E\left[|A_{ni}|^2\right]=E\left[|A_{00}|^2\right]e^{-\frac{T_n}{\Gamma}}e^{-\frac{\tau ni}{\gamma}} \quad (7)$$

A_{00} is the energy of the first path of the first cluster, Γ and γ power decay profile for cluster and components within cluster respectively. IEEE working group has suggested some variation in this SV model to make it more realistic channel model for UWB as, multipath gain amplitudes are considers as log-normal distributed. The UWB channel model is described as,

$$h(t)=X\sum_{n=1}^{N}\sum_{k=1}^{K(n)}\alpha_{nk}\delta(t-T_n-\tau_{nk}) \quad (8)$$

X is log-normal distributed which represent the gain of channel.N is number of clusters, $K(n)$ is the number of multipath components of same UWB pulse within the N^{th} cluster. α_{nk} is magnitude of component in N^{th} cluster. τ_{nk} is delay of component in N^{th} cluster. The channel coefficient $\alpha_{nk}=\pm(1)_{nk}\beta_{nk}$, whereβ_{nk} is the log-normal distributed channel coefficient of multi-path components k for cluster n. β_{nk} is defined as $\beta_{nk}=10^{\frac{x_{nk}}{20}}$ Where x_{nk} is assumed to be a Gaussian random variable with μ_{nk} mean and σ_{nk}^2 variance. The random variable x_{nk} is further decomposed as,

$$x_{nk}=\mu_{nk}+\xi_n+\zeta_{nk} \quad (9)$$

Where ξ_n andζ_{nk} are two Gaussian random variables which represent the variation of the channel coefficient on each cluster and in each path within cluster respectively.

Finally channel model of UWB channel is described by,

$$h(t) = X \sum_{n=1}^{N} \sum_{k=1}^{K(n)} \alpha_{nk} \delta(t - T_n - \tau_{nk}) \quad (10)$$

With following parameters,

The cluster arrival rate of λ

UWB pulse arrival rate with in cluster is Δ

Power decay profile of cluster and pulse with cluster is Γ and γ

The variance of σ_ξ^2 and σ_ζ^2 for variation of fluctuations of channel coefficient for cluster and pulse within cluster respectively.

This parameters are defined for different four cases of UWB communication as mentioned in table I below,

Table I
PARAMETERS FOR UBW CHANNEL MODEL

Case	Λ	λ	Γ	γ	σ_ξ	σ_ζ
Case A	0.0233	2.5	7.1	4.3	3.3941	3.3941
Case B	0.4	0.5	5.5	6.7	3.3941	3.3941
Case C	0.0667	2.1	14	7.9	3.3941	3.3941
Case D	0.0667	2.1	24	12	3.3941	3.3941

Here Case A is Line of sight(LOS) communication between transmitter and receiver with maximum separation between them is 2 meter, Case B is Non line of sight(NLOS) communication between transmitter and receiver with maximum separation between them is 2 meter, Case C is NLOS with 8 meter of maximum TR separation. Case D is Extreme NLOS multipath channel with maximum TR separation of 8 meter. Based on IEEE 802.15.3a channel model recommendation, figure 2, 3, 4, 5 illustrate the four typical power delay profile (PDP) of UWB channel model. From this PDP it is clear that in channel model case A the first received component has highest energy compared to subsequent component. So in this case if we use partial RAKE with lower fingers then we can expect good result. From figure 3 it can be seen that near to several strongest peak smaller peaks are surrounded. This indicates that channel response is combinations of the several overlapping clusters. Also the strongest peak is not first one but is can occur at any position in sequence due to reflections from scatterer. So here partial RAKE will not give expected result but we have to select the strongest component in cluster hence SRAKE is required to use. From channel model C figure 4, it can be seen that here channel is more time dispersive. Components are available up to around 70 nsec, while in case A and B it is available up to around 40 nsec. This indicate that here we have to use selective RAKE to achieve desired result. From figure 5 it can be seen that channel in this case is more time dispersive and components are available till 150nsec. So here the effective data rate goes down to achieve the ISI free communication. In this case more fingers required to consider for achieving good SNR at receiver.

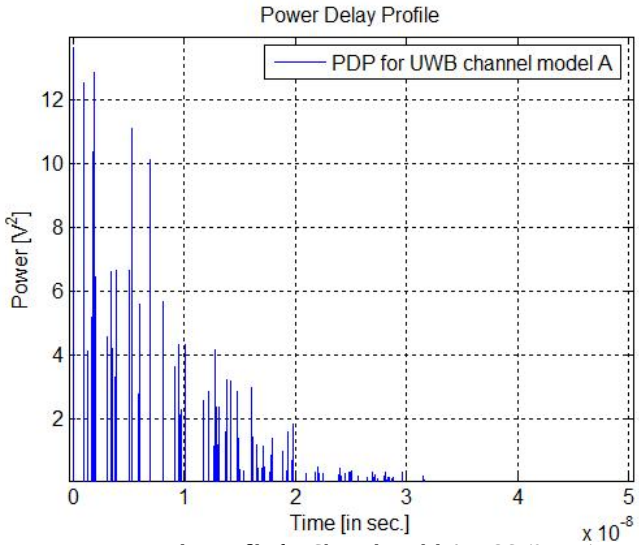

Figure 2. Power Delay Profile for Channel model A, LOS (0-4 mt).

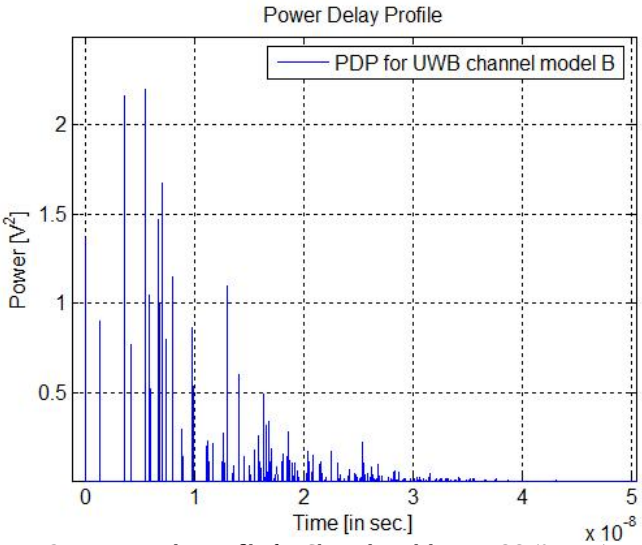

Figure 3. Power Delay Profile for Channel model B, NLOS (0-4, mt).

VI. SIMULATION RESULTS

Here we have investigated performance of DS-UWB system under synchronous and asynchronous transmission with orthogonal and non-orthogonal code. We investigated performance under AWGN channel. Bit error rate is used as performance comparison criterion. Also performance of DS-UWB is compared with TH-PAM UWB [2] with non-orthogonal code. For DS-UWB simulation parameters are shown in Table 1. For TH-PAM UWB simulation parameters are shown in Table 2. In both the cases performance is evaluated with Gaussian pulse shape and Scholtz monocycle as a UWB pulse.

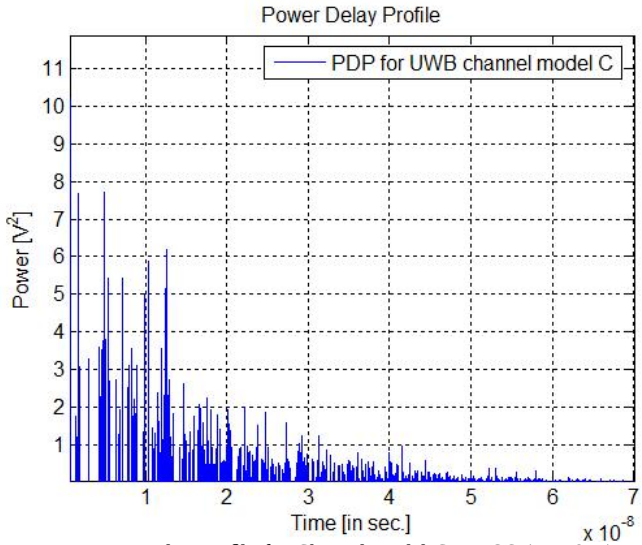

Figure 4. Power Delay Profile for Channel model C, NLOS (4 to 8mt).

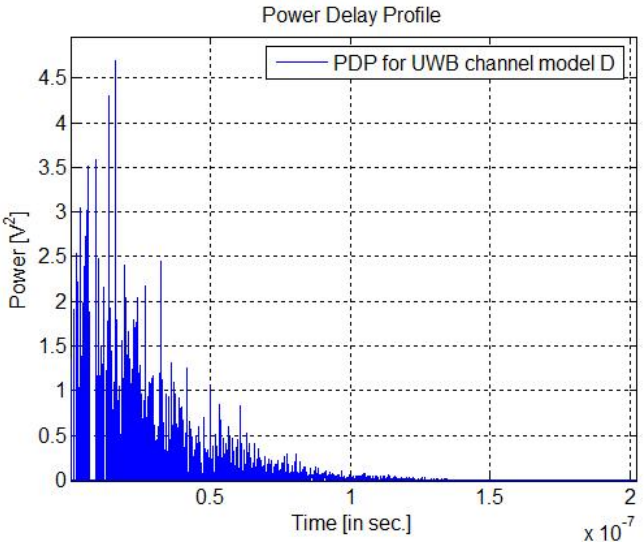

Figure 5. Power Delay Profile for Channel model D, extreme NLOS (up to 8 mt).

Table II
SIMULATION PARAMETERS FOR DS-UWB SYSTEM

DS-UWB Parameters	
Number of users	2 and 8
Data rate	62.5 Mbps
Number of frames (N_f)	8
Frame duration (T_f)	$2nsec$
UWB pulse duration (T_p)	$0.5nsec$
Pulse shape factor(τ)	$0.25nsec$
Async. transmission Delay	$< 2nsec$

Table III
SIMULATION PARAMETERS FOR TH-PAM UWB SYSTEM

TH-PAM UWB Parameters	
Number of users	2 and 8
Data rate	62.5 Mbps
Number of frames (N_f)	8
Frame duration (T_f)	$2nsec$
Number of chips (N_c)	3
Chip duration (T_c)	$0.67nsec$
UWB pulse duration (T_p)	$0.5nsec$
Pulse shape factor(τ)	$0.25nsec$
Async. transmission Delay	$< 2nsec$

Figure 6 shows performance of DS-UWB with orthogonal code under synchronous transmission. Here it can be seen that with compared to two user case almost 1 dB more power is required when number of users are eight in system with Gaussian pulse as a UWB signal. When Scholtz monocycle is considered as a UWB pulse almost same behaviour is observed. When Gaussian pulse shape is selected, under both the cases of two and eight users performance is better compared to Scholtz monocycle. This improvement factor is around 1 dB. Figure 7 shows the performance of DS-UWB with orthogonal code under asynchronous transmission. Here almost same performance is achieved with two and eight users under selection of Gaussian UWB pulse and Scholtz UWB pulse. From figure 6 and 7 we can see that almost same performance is achieved in DS-UWB with orthogonal code under synchronous and asynchronous transmission. If numbers of users are more than eight then system performance degrade as code would lose its orthogonality property as number of frames (N_f) are eight in DS-UWB. Under asynchronous transmission if the asynchronous transmission delay (τ) will more than frame duration (Here $2nsec$) then performance also degrade.

Figure 8 and 9 shows performance of DS-UWB with non-orthogonal code under synchronous and asynchronous transmission respectively. From figure 8 it can be seen that system performance degrades by large amount under synchronous transmission. From figure 8 it is clear that non-orthogonal code should not be selected under synchronous transmission. Also it can be seen that with Gaussian UWB pulse shape improvement factor is almost 1 dB compared to Scholtz monocycle as UWB pulse. In figure 9 performance under asynchronous transmission is shown with non-orthogonal code. Here almost 2dB improvement is achieved with two users compared to eight users case with both, Gaussian and Scholtz UWB signal. From figure 7 and 9 it can be seen that DS-UWB system performs better with orthogonal code under asynchronous transmission.

Also we have compared performance of DS-UWB with TH-PAM UWB [2] with non-orthogonal code. Here Gaussian pulse shape is considered as UWB pulse for comparison in both the cases. Here we evaluated the performance for non-orthogonal code. To accommodate large number of user under orthogonal code we need to select more chips/frames which actually puts limitation on effective data rate. In TH-PAM UWB number of chips (N_c) are three and to accommodate eight users with orthogonal code require eight

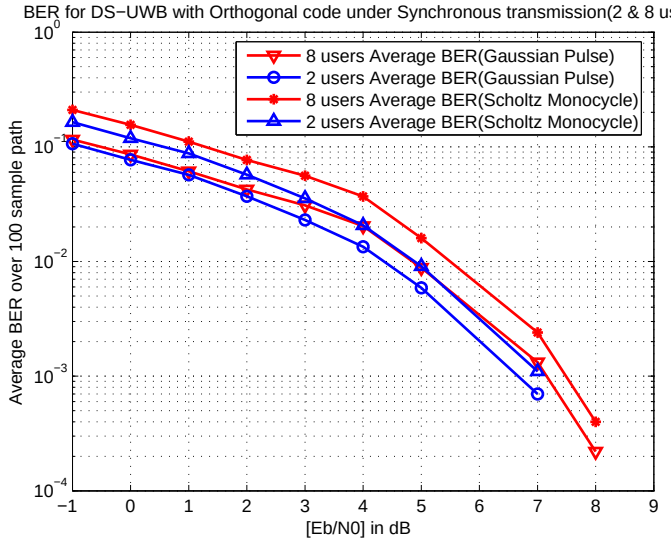

Figure 6. Avg. BER with orthogonal code and Synchronous transmission.

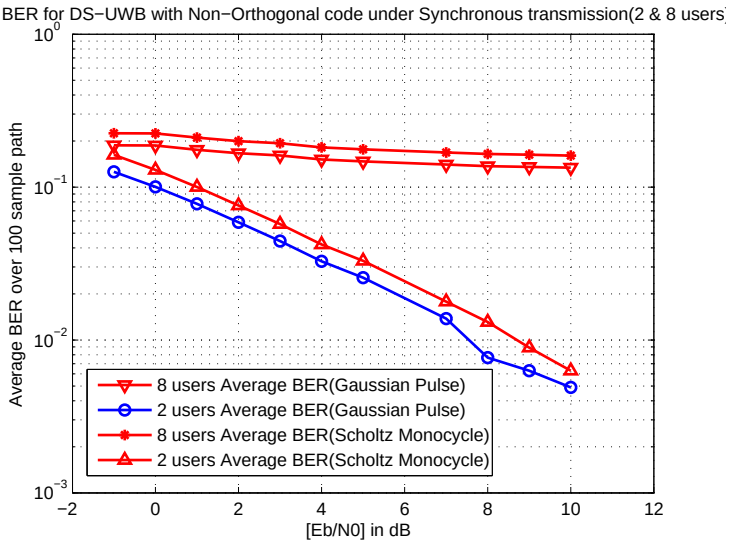

Figure 8. Avg. BER with Non-orthogonal code and Synchronous transmission.

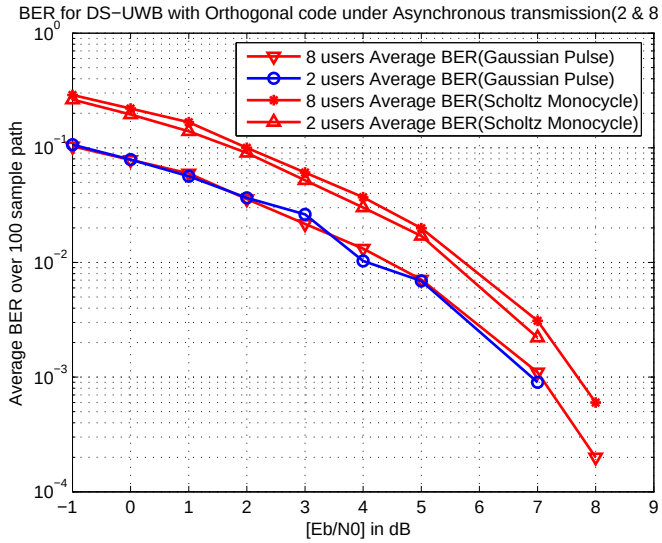

Figure 7. Avg. BER with orthogonal code and Asynchronous transmission.

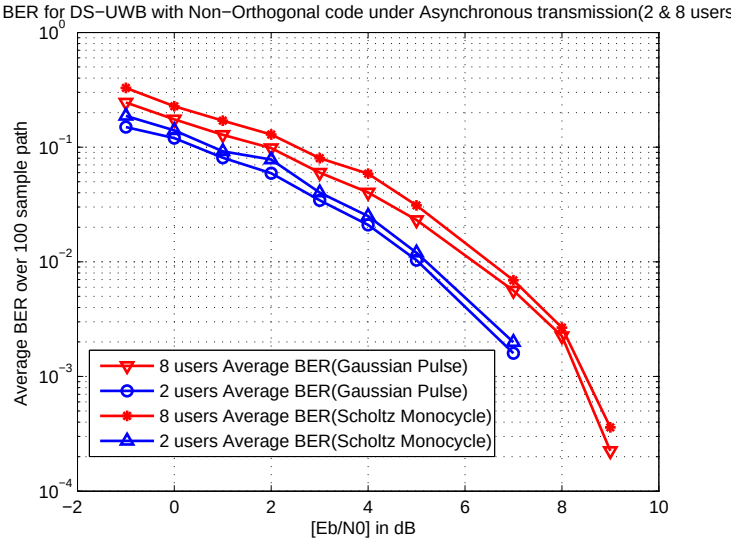

Figure 9. Avg. BER with Non-orthogonal code and Asynchronous transmission.

chips (N_c) which is not possible for the case which we have considered here in simulation. In TH-PAM UWB, selection of orthogonal code is possible if we select eight chips (N_c) by reducing data rate in system (parameter in Table 2). From figure 10 we can see that DS-UWB performs better compared to TH-PAM UWB under synchronous and asynchronous transmission. Under asynchronous transmission this improvement factor is of 1dB with eight users. For less interfering signals this improvement factor will be more. Figure 11 shows performance of DS-UWB under different users condition with orthogonal and non-orthogonal code with synchronous and asynchronous transmission.

Figure 12,13, 14 and 15 shown performance of DS-UWB with Different UWB channel model. Here in simulation we have consider perfect equalization of UWB channel. Figure 12 and 13 shows the performance of DS-UWB with UWB channel model A and B. Figure 12 shows the performance of UWB system with two and eight users under asynchronous transmission with non orthogonal code as a signature waveform. Except the synchronous transmission all parameters for simulation is same in Figure 13 as 12. From Figure 13 it is seen that under synchronous transmission for better performance orthogonal codes are required.

Figure 14 and 15 shows the performance of DS-UWB system with UWB channel model C and D. Same observation as channel model A and B is seen here.

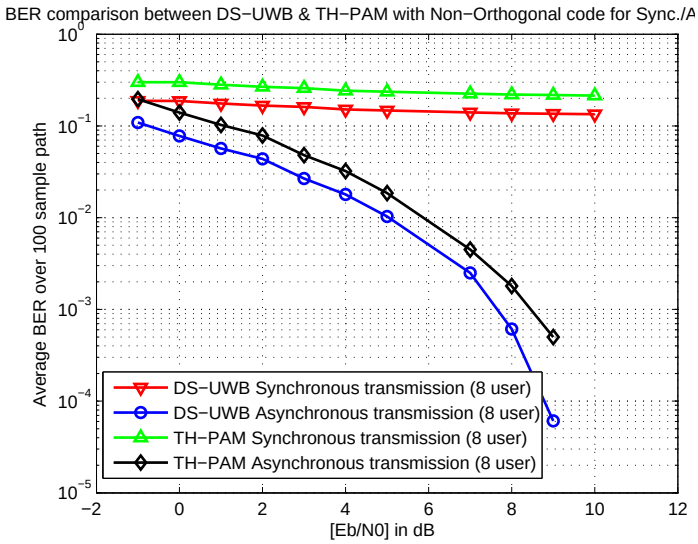

Figure 10. Avg. BER comparison with TH-PAM and DS-UWB with sync. and Async. transmission(8 users).

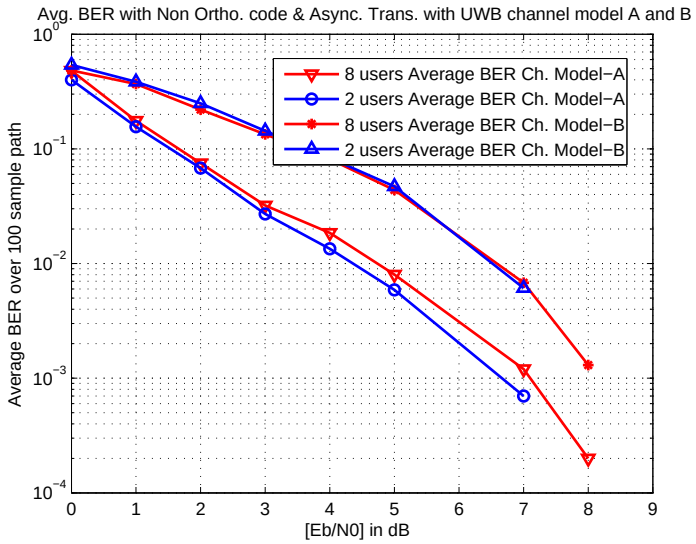

Figure 12. BER Performance with different users under Non Ortho. code with Async. Transmission (UWB ch. Model A B).

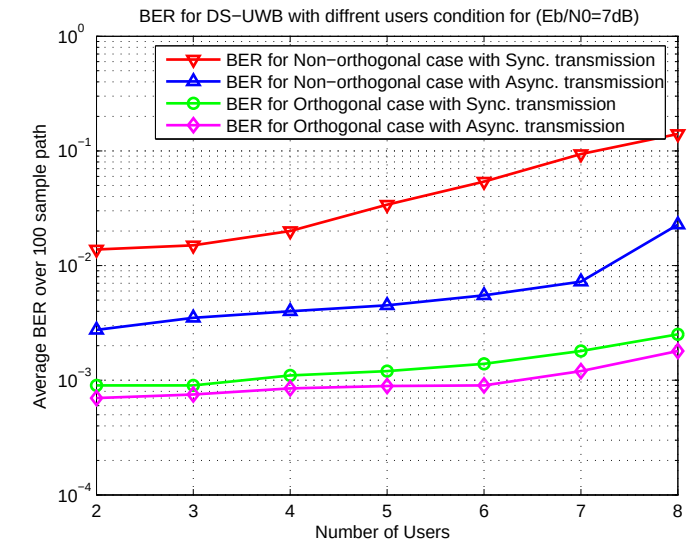

Figure 11. BER Performance with different users under different code with Sync and Async. transmission.

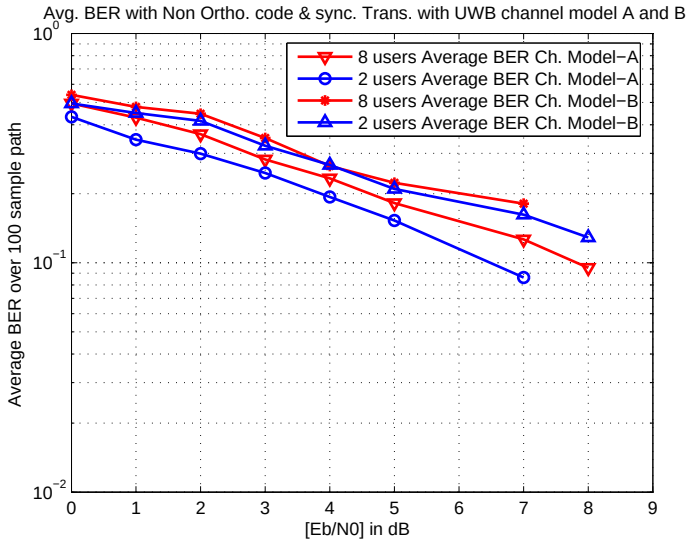

Figure 13. BER Performance with different users under Non Ortho. code with Sync. Transmission (UWB ch. Model A B).

VII. Conclusion

Here we have investigated performance of multiuser DS-UWB system with orthogonal and non-orthogonal code under synchronous and asynchronous transmission. BER is evaluated for each case with AWGN channel. Here it is seen that DS-UWB system performs equally with orthogonal code under synchronous and asynchronous transmission. When asynchronous transmission is considered in DS-UWB with non-orthogonal code, almost 2dB improvement is achieved with two users compared to eight users case. System performance degrade drastically when non-orthogonal codes are used under synchronous transmission. Under same situation system performs little better with asynchronous transmission. Also DS-UWB system perform better compared to TH-PAM UWB in multiuser environment. Non-orthogonal code with higher spreading factor can be selected in multiuser DS-UWB system when all users transmit data under asynchronous transmission. In multiuser environment asynchronous transmission is the more general case so in multiuser DS-UWB system non-orthogonal code can be chosen for increasing the capacity. Gaussian pulse shape gives better performance compared to Scholtz mono cycle as UWB pulse. For synchronous transmission orthogonal code

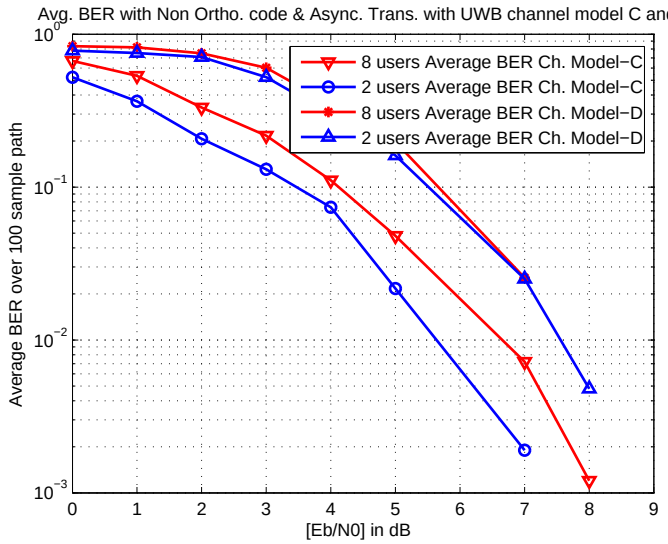

Figure 14. BER Performance with different users under Non Ortho. code with Async. Transmission (UWB ch. Model C D).

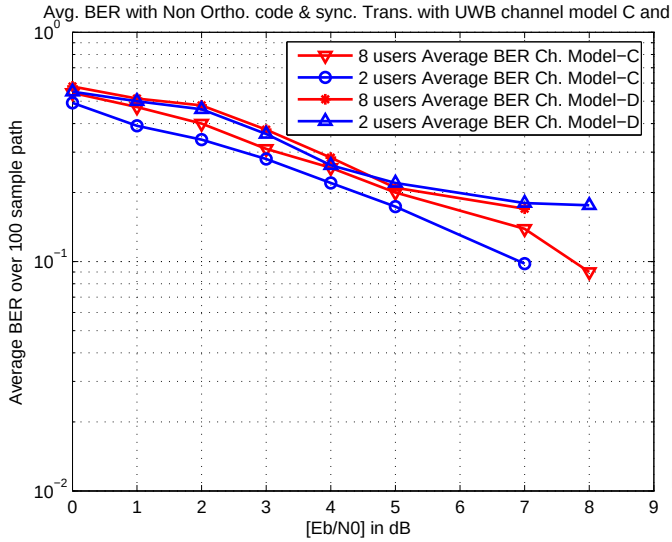

Figure 15. BER Performance with different users under Non Ortho. code with Sync. Transmission (UWB ch. Model C D).

is required with multiuser DS-UWB system.

VIII. Future Work

In this paper the system performance is evaluated with correlation based receiver. We will extend our work and ensure the performance of DS-UWB and other types of UWB system under multiuser environment with adaptive multiuser detection techniques [22].

References

[1] B. R. Vojcic and R. L. Pickholtz, "Direct-Sequence Code Division Muliple Access for Ultra-Wide Bandwidth Impulse Radio," *Proc. of MILCOM2003*, pp. 898–902, October 2003.

[2] Z. Bai and Kyungsup, "Performance Analysis of TH-PAM of UWB System and Coded Scheme," *Proceedings of International conference on Wireless communications, Networking and Mobile Computing*, pp. 296–299, September 2005.

[3] Maria-Gabreilla, D. Benedetto, and B. R.Vojcic, "Ultra Wideband Wireless Communication: A tutorial," *Journal of communications and networks*, vol. 5, pp. 290–302, December 2003.

[4] M. Z. Win and R. A. Scholtz, "Impulse radio -How it Works," *IEEE Communications letter*, vol. 2, pp. 10–12, January 1998.

[5] H. Jin and M. J. Kim, "Ultra-Wideband Communications Systems for Home Entertainment Network," *IEEE Transaction on consumer Electronics*, vol. 49, pp. 302–311, May 2003.

[6] H. Zhang, T. Udagawa, T. Arita, and M. Nakagawa, "Home Entertainment Network: Combination of IEEE 1394 and Ultra Wideband Solutions," *IEEE Conference on Ultra Wideband Systems and Technologies*, pp. 141–145, October 2002.

[7] L. Yang and G. B. Giannakis, "Ultra-Wideband Communications -An idea whose time has come," *IEEE Signal Processing Magazine*, pp. 26–58, November 2004.

[8] M. Z. Win and R. A. Scholtz, "Ultra-Wide Bandwidth Time-Hopping Spread-Spectrum Impulse Radio for Wireless Multiple-Access Communications," *IEEE Transactions on communications*, vol. 48, pp. 679–691, April 2000.

[9] B. Hu and N. Beaulieu, "Accurate Evaluation of Multiple-Access Performance in TH-PPM and TH-BPSK UWB Systems," *IEEE Transactions on communications*, vol. 52, pp. 1758–1765, October 2004.

[10] G.Durisi and S.Benedetto, "Performance Evaluation of TH-PPM UWB Systems in the Presence of Multiuser Interference," *IEEE Communications Letter*, vol. 7, pp. 224–226, May 2003.

[11] H.B.Soni, U.B.Desai, and S.N.Merchant, "Performance analysis of multiuser ds-uwb system with orthogonal and non-orthogonal code under synchronous and asynchronous transmission," *The Fourth International Conference on Wireless and Mobile Communications (ICWMC08)*, pp. 247–252, Oct 2008.

[12] W. C. Y. Lee, "Mobile communications engineering, theory and applications," *McGraw-Hill*, 1997.

[13] A. Saleh and R.A.Valenzuela, "A statistical model for indoor multipath propagation," *Journal on selected Area in communications*, vol. 5, pp. 128–137, February 1987.

[14] S. S. Ghassemzadeh and V. Tarokh, "Uwb path loss characterization in residential environments," *IEEE Radio frequency Integrated circuits symposium*, pp. 501–504, June 2003.

[15] M. Pendergrass and W.C.Beelar, "Empirically based statistically ultra-wideband(uwb) channel model," *available at http://grouper.ieee.org/groups/802/15/pubs/2002/jul02/02294rlp802-15$_S$G3a$-Empirically_b$ased$_U$W B$_c$hannel$_m$odel.ppt, July*

[16] J. Foerster and Q. Li, "Uwb channel modelling contribution from intel," *available at http://grouper.ieee.org/groups/802/15/pubs/2002/jul02/ 02279r0P802-15$_S$G3a $-$ $Channel$ $-$ $model$ $-$ $cont$ $-$ $intel.doc, June$2002.

[17] V. Hovinen, M. Hamalainen, and T. Patsi, "Ultra wideband indoor radio channel models: Preliminary results," *IEEE conference on Ultra wideband systems and technologies*, pp. 75–79, May 2002.

[18] J. Kunisch and J. Pamp, "Measurement results and modelling aspects for the uwb radio channel," *IEEE conference on Ultra wideband systems and technologies*, pp. 19–23, May 2002.

[19] S. Ghassemzadeh and V. Tarokh, "The ultra-wideband indoor path loss model," *available at http://grouper.ieee.org/groups/802/15/pubs/2002/jul02/ 02277rlP802-15$_S$G3a* $-$ 802.15 $-$ $UWB - propagation - path$

[20] A. Molisch, M. Z. Win, and D. Cassioli, "The ultra- wide bandwidth indoor channel: from statistical model to simulations," *available at http://grouper.ieee.org/groups/802/15/pubs/2002/jul02/ 02284r0P802-15$_S$G3a* $-$ $The - Ultra - Wide - Bandwidth - Indoor - Channel - from - statistical - model - to - simulatons.pdf, June$2002.

[21] R. Cramer, R. A. Scholtz, and M.Z.Win, "Evaluation of an indoor ultra-wideband propagation channel," *available at http://grouper.ieee.org/groups/802/15/pubs/2002/jul02/ 02286r0P802-15$_S$G3a* $-$ $Evaluation - of - an - indoor - Ultra - wideband - propagation - channel.doc, July$2002.

[22] S. Verdu′, "Multiuser Detection," *Cambridge University Press*, pp. 166–204, 1998.

A Semantic-oriented Framework for System Diagnosis

Manuela Popescu
University of Besançon
France
manuela.popescu@univ-fcomte.fr

Pascal Lorenz
University of Haute Alsace
France
lorenz@ieee.org

Jean Marc Nicod
University of Besançon
France
jean-marc.nicod@lifc.univ-fcomte.fr

Abstract - **In the field of system and network diagnosis, there is a variety of modeling and inference methods reported in literature. However, very few are focusing on the validation and knowledge transfer in case of similar symptoms. Many researchers targeted the use of a generic diagnosis framework, semantic-oriented solutions, and temporal aspects related to diagnosis validation. Event correlation and action triggering are essential for an accurate diagnosis decision. However, no industry-wide solution was considered so far. In this article, we are proposing an adaptive framework for diagnosis validation and transfer of information from successful outcomes for future use and optimization of the diagnostic activity. It is shown that this mechanism allows a post-validation of successful diagnosis actions, optimizing the diagnosis process and increasing its accuracy. We are presenting a series of ontology-driven mechanisms for system diagnosis. Mainly, we introduce event ontology and concepts related to semantic tag clouds and show how to manage the activities to build an ontology-based diagnosis. Additionally, we consider temporal aspects related to diagnosis validation. Event correlation and action triggering are essential for an accurate diagnosis decision. There are several time-related challenges referring to event timestamps, timely event correlations, and timely corrective actions, in both absolute time (precise moment), or relative time (between events, actions, and events and actions). We consider a series of temporal operators defining the event relative temporal position that allows a more fine grain interpretation of the system behavior. A combination of proposed mechanisms is used to complete the main functions of a diagnosis engine.**

Keywords - system diagnosis, diagnosis validation, knowledge transfer; ontology-based diagnosis; semantic tag clouds; progressive ontology; temporal features.

I. INTRODUCTION

System and network diagnosis is vital if network infrastructures are to function efficiently and maintain reliable delivery of service to customers. There are various management and control mechanisms acting on a system to monitor security, performance, optimization and so on. In case of faulty or unexpected behavior, diagnosis is usually the main activity triggered by the symptoms of the system under supervision.

Figure 1 depicts a very high level view of the diagnosis process. Collectors have been developed to assemble systems health data parameters. These parameters can fall within normal value ranges (accepted, desired, expected, etc.), or they can reflect an unhealthy situation (value not recognized, out of range, denied by policy, inconsistent or out of context). A formalized set of this data constitutes the symptoms of the network under consideration. System problems can thus be identified and the most suitable solution for healing is computed and implemented. A validation step is then necessary to assess the success of the repair. Validation is also performed to prevent illness, following small parameters variation from accepted range, or after a calm period.

We can identify two loops of the diagnosis process: (a) one loop deals with measuring the system parameters (system state, events, i.e., pre-conditions) and taking the most suitable actions; this is referred to as the *diagnosis loop* and (b) a second loop deals with validating that the corrective actions were indeed successful; this is referred to as the *validation loop*. The validation loop has two main goals: (a) to establish the new state of the system, i.e., post-conditions and (b) to gather knowledge on how to solve future similar situations, in case the actions taken were considered successful. In general, there is little or no cross-interaction between these two loops.

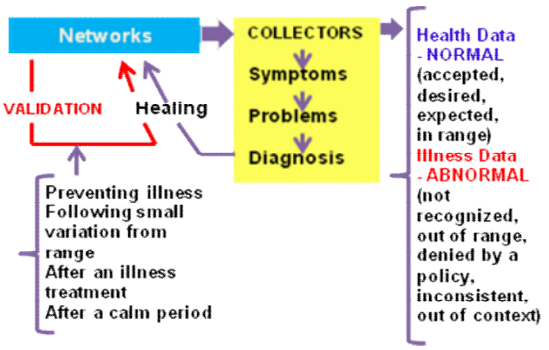

Figure 1. Diagnosis Theory [17, 25]

In addition, we introduce the concept of *Quality of Diagnosis (QoD)* into the validation loop to help make accurate decisions, based on past successful actions applied to similar situations.

However, there are too many actions in a system generating an unmanageably large number of events. It is estimated that a maximum of 8% of these events are considered by diagnosis systems; the rest of them are being discarded. Additionally, there is a diversity of technology domains driven by special diagnosis mechanisms. Mapping those mechanisms in a heterogeneous environment and correlating the diagnosis actions overwhelm the operators in NOCs (Network Operation Centers), leading to unsatisfactory solutions.

Towards an automated diagnosis, we introduce a progressive ontology (leading to progressive diagnosis) and therefore "progressive validation" of successful actions. This is intended to solve potential conflicts of the post-conditions of the actions already validated as "successful" and to evaluate the accuracy of the diagnosis actions (preciseness versus permanent damage). The basis is the definition of event ontology, followed by several concepts identifying the cause of a symptom and potential diagnosis actions.

The complexity of networks and distributed systems gives rise to management challenges when unexpected situations occur. There is an overwhelming number of feedback events coming from the system in the form of status reports towards the monitoring and management applications and human operators. Actually, very few of these events, less than 10%, can be considered for potential status understanding and remedy. Given the numbers, it is inevitable that many relevant events are dropped. The remedy actions can come too late (and sometimes be useless). There are numerous management applications in commercial use. However, the variety of the systems to be managed, their complexity, and the fact that most of the successful decisions are rarely recorded, rise serious challenges in the ability to accurately handle unexpected situations.

Some of the multiple causes leading to the current state are (i) lack of successful validation of corrective actions, (ii) heterogeneity of the events to be handled, and (iii) incomplete correlation and time synchronization between status reports, decision processing and corrective actions.

A step towards automated diagnosis was introduced in [23], where an event ontology and a progressive diagnosis ontology were proposed. Event dependencies captured by ontology and specific event relations were formalized. Probable cause and recommended actions were associated with events. Additionally, an augmented specification for actions was proposed to help the validation loop. Both proposals had as a target the reuse of knowledge for problem fixing, identification of recommended diagnosis actions, and validation of successful actions.

The third identified challenge is time-related; this refers to event timestamps, timely event correlations, and timely corrective actions, in both absolute time (precise moment), or relative time (between events, actions, and events and actions). This aspect is more difficult, as many events issued at different timestamps might be processed for event compression/aggregation. The correct adoption of temporal aspects can solve potential conflicts among the post-conditions of the actions already validated as "successful" and helps evaluate the accuracy of the diagnosis actions (preciseness versus permanent damage).

In this paper, we introduce a generic framework, propose an event ontology, highlight the relevance of temporal aspects, identify the challenging issues, and propose a new timestamp approach. We consider a series of temporal operators defining event relative temporal position that allows a more fine grain interpretation of the system behavior. A combination of proposed mechanisms is used to complete the main functions of a diagnosis engine.

II. RELATED WORKS

There is a variety of approaches dealing with the collection and actions-taking loop of the diagnosis process. However, very few solutions are focusing on the validation and knowledge transfer in case of similar symptoms.

2.1 Diagnosis Approaches

There are many modeling and inference methods of diagnosis, deriving from different areas of computer

science, including artificial intelligence, graph theory, neural networks, information theory and automata theory [1]. The most widely used diagnosis techniques are expert or knowledge-based systems [2] (rule-, model- and case-based systems, decision trees and neural networks). *Rule-based* techniques provide a powerful tool for eliminating the least likely hypotheses in small systems [3]. However, deep knowledge regarding the relationships among system entities was included [5, 6, 7] to address shortcomings related to the inability to learn from experience, inability to deal with new problems and difficulty in updating the system knowledge [4]. Model traversing techniques [8, 9] use formal representation of a system with clearly defined relationships among network entities. Model traversing techniques reported in literature use object-oriented representation of the system [10]. They are usually *event-driven* and naturally enable the design of distributed fault localization algorithms. Graph-theoretic techniques employ a Fault Propagation Model (FPM) [9], which is a graphical representation of all faults and symptoms occurring in the system and commonly take the form of causality or dependency graphs. Some graph-theoretic techniques include divide and conquer algorithm [11], context-free grammar [12], codebook technique [13], belief-network approach, and bipartite causality graphs [14].

Despite a vast research effort, there are open problems regarding diagnosis in complex systems, such as multi-layer fault diagnosis, distributed diagnosis, temporal correlation fault diagnosis in mobile ad hoc networks and root-cause analysis in a service-oriented environment.

2.2 Validation and Knowledge Transfer

Two challenging post diagnosis and repair actions are (1) validation and (2) knowledge acquisition and transfer.

For validation, an audit must be performed on the system status to assess the success of the repair actions. Knowledge acquisition and transfer regarding successful repair actions require a formal representation of the system, specification of the symptoms and the actions taken in particular cases, as well as a methodology to have this information available to facilitate later diagnosis of similar situations.

The main prior knowledge needed for diagnosis is the set of system failures and the relationship between the observed symptoms and the failures. Previous knowledge may be explicit, such as a table lookup, or may be deducted from some domain knowledge. This represents deep, model-based knowledge. Alternatively, or in addition to this knowledge, information may come from past experience with the system. This type of knowledge is known as shallow, compiled, evidential or process history-based knowledge [15].

To understand the system behavior expressed by issued events, we need to see how to instruct the diagnosis engine to trigger appropriate actions. A primary condition is to understand the information carried out by an event. Despite more than 3 decades of efforts, no common event syntax and semantic were achieved. Most of the existing solutions target a special area and it is rarely normalized; therefore, diagnosing heterogeneous systems is a challenge.

Log files represent the most used information source. Parsing the log files is the only way to extract the event information. Some log files have minimal event information, whereas others contain a variety of unstructured information. Since the amount of log file event is very large, the event processing should handle the file index of events already processed, especially whether the system is rebooted. Several log files may contain event information, e.g., Syslog log files, system console log files, application message files, etc. While log files are the most difficult source of events, Syslog files have a certain degree of structure. However, all log files require more normalization to help parsing and automate event processing.

Syslog messages (associated with Unix environments) are tailored as a free-form text message together with some defined fields, such as severity, facility, timestamp, etc. [17].

The structure of *SNMP* (Simple Network Management Protocols) *messages* is based on SNMP MIB (Management Information Base) Model, which is quite complex to be handled &&3]. However, this structure facilitates the normalization of these messages into a common format. An SNMP agent can asynchronously send SNMP messages to *a trap* receiver (SNMPv2). The mechanism called *informs* is provided by SNMPv2c that adds a reply message to a trap, as an acknowledgement. However, notification is not ensured to reach the destination. Since both SNMPv2c and SNMPv3 can deliver SNMP notifications via traps or informs method, the sending agent can select the mechanism to be used. This raises coordination challenge concerning message structure and information contained in it. A management process can poll with a given frequency various state parameters and built complex event structure based on the collected information. There is no validation of a successful action after a diagnosis action is performed.

The *RMON* (Remote Monitoring) mechanism defines a generalized threshold-based alarm, which generates in turn an RMON event that eventually causes a SNMP notification [20].

Other devices can use a Syslog to trap converter, as a unified mechanism to send traps or informs. However, most of details contained in the message text must be parsed for further processing, as for Syslog events.

Events can be generated at any level; the network management system itself can generate events using any of the mechanisms identified above.

Event formats were proposed for specialized domains, such as intrusion detection reports and vulnerability reports, but no event dependency or instruction on how to manage them were proposed. A proposal to direct event management was proposed in [25], where the event itself carries the processing instructions. The instructions were derived from the event source point of view, with no correlation with other events.

Most of the current attempts failed because of the complexity of target systems, leading to huge event models, practically describing unmanageable situations.

It appears that ontology per domain is more suitable; the initial condition is to have an event ontology. Definitively, inter-domains ontology matching is a challenge; however, it allows tackling the problem step-by-step.

2.3 Temporal Aspects

Temporal features are related to several generic aspects concerning (i) inaccurate (wrong, un-synchronized, or missing) clocks, (ii) loss of events, and (iii) hierarchical event processing at layers exposing different clocks. These are somehow related to event propagation skew but also to different syntactic and semantic implementation decisions of the timestamps (including time zones). One approach in dealing with real-time measurements of propagation skew uses a statistical evaluation to update the timer values [27].

Some diagnostic constraints might be temporal. In [23], temporal constraints are used for event tags to define the event ontology and to detect the relative temporal constraints. Walzer *et al.* [28] use specific operators for time-intervals with quantitative constraints in rule-based systems to trigger certain actions. In the following sections, we present the main approaches used to specify temporal aspects on events and actions.

2.3.1 Temporal aspects for events

Timestamps are usually carried by the events themselves; basic events possess special timestamp fields that are instantiated when an event instance occurs. Timestamps are storing time in the native format of the platform in which the event processing runs. There are two standard ways to represent the time: (i) using the universal time, or (ii) using time zones. Since one still needs to preserve the zone indication for a device for hourly performance reports, the representation in the universal time is only for the computational point of view. Another standard way to represent the time is the UNIX-format time as a four-byte integer that represents the seconds elapsed since January 1, 1970. For the same reasons, the time zone of the source device should be stored.

An event might have multiple timestamps; the source timestamp (not always present), the logging host timestamp, the console timestamp, and the processing timestamp. Temporal correlation and event aggregation should consider all these timestamps.

Event processing and correlation need a time-based logic to express the relative position of start / end /duration of the events [24]. While attempts were identified for classifying the relative position of the events, no particular commercial solutions are known where a full range of temporal situations is used.

2.3.2 Temporal Aspects for Actions

An enhanced action model was proposed in [23]. One temporal aspect is related to the triggering condition (guard). Others temporal aspects are related to the temporal dependencies between actions, *i.e.*, some action must start at a given period after one action was triggered or was deemed successfully finished.

A diagnosis-oriented augmented action definition was introduced in [23], as follows.

action::= <<guard><ID><post-conditions>
<mode><conflicting>,

where

ID::= READ | *WRITE* | *DELETE* | *CHANGE* | *, etc.*

mode ::= <potential | *recommended* | *successful <context>>,*

with
potential: any diagnosis action that is designated as being related to a potential domain

recommended: any potential action that is perceived as solving a given problem, eventually based on a diagnoses history
successful: when post-conditions were validated as true

context: <d:D, c:C>

d:D is d instance of Domain
c:C is c instance of Cloud

Also in [23], we associated the notion of "conflicting" with a given *action*, which designates the actions a potential action is in conflict with, in a given domain:

conflicting ::= <a_1, a_2,… a_k | a_i:A>

A <guard> is acting as pre-conditions and igniter (initial timestamp), and the <post-conditions> are expected to be true (after the action is considered successfully performed). In general, actions are applied following a simple rule:

IF <pre-conditions>

THEN <action> WITH <post-conditions>

Post-conditions are assumed to hold. A composition of actions, a plan, is a set of related actions and it is used to specify dependencies between actions. This is schematically represented in Figure 2. The model can be summarized as follows, where a plan is introduced as a temporal combination of atomic actions (see ID above) [29].

policy::= IF <pre-cond> THEN {<> 1<action> 1<plan>}

[ELSE {<> 1<action> 1<plan>} <action> 1<plan>}] <post-cond>]

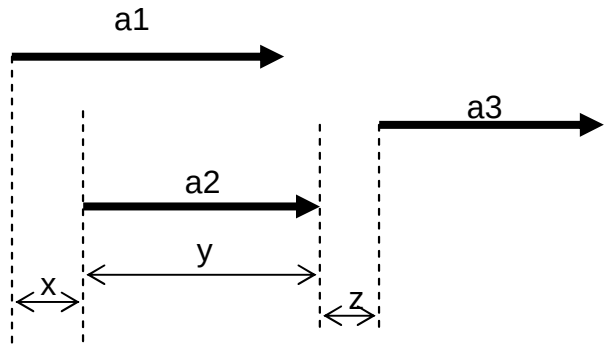

Figure 2. A plan ─ actions: a_1, a_2, a_3; time durations: x, y, z

Based on the analysis of the state of the art, we conclude that there is a need for a unified timestamps approach and a set of operators that must be used in synchronism to express the dependency between events, between actions, or between events and actions [25, 26].

In this article, we propose a representation of temporal features allowing various semantics used to correlate the events and the actions.

III. A SITUATION-BASED DIAGNOSIS SYSTEM

Let us first introduce the basic concepts used to formalize the system used here for validation, knowledge acquisition and transfer.

(1) *Symptoms* are external manifestations of failures. They can be observed as alarms, which alert of a potential failure. The alarms can originate from management agents via management protocol messages (SNMP traps, CMIP EVENT-REPORT etc.) from management systems monitoring the network status (*ping*) system log-files or character stream sent by external equipment [1].
(2) We introduce the concept of *situation* as representing the symptoms and the failure state of the system in consideration.
(3) A *problem* represents the failure state of the system and possible causes. This concept allows us to deal with events which might not be directly observable. Many types of events might not be directly observable due to (i) their intrinsically unobservable nature, (ii) local connective mechanisms built into a management system that destroy evidence of fault occurrence or (iii) lack of management functionality needed to provide evidence that a fault occurred. The state of the system implicitly represents these kind of un-observable events.
(4) A *context* represents a subset of states (including system topology, dependencies, configuration, etc.), services and their users, at a given time.
(5) We also introduce the use of *Quality of Diagnosis (QoD)* into the validation loop mentioned in Figure 1. This concept will drive more accurate decisions, based on past successful actions applied to similar situations.

We classify the states of a system in 3 types, associated with symptoms and probable causes, as shown in Figure 3.

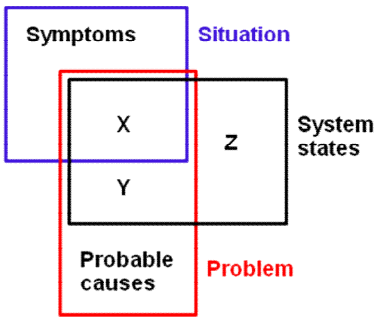

Figure 3. Basic concepts relationship

The system states of type X are states producing observable symptoms that indicate failures, the system states of type Y are states producing non-observable events of failure and the system states of type Z are behaviorally expected states that are not associated with failures.

3.1 Approach on Diagnosis Loop

As shown in on Figure 1, three related concepts are needed for a successful repair: (i) symptoms, as defined above, (ii) problems, as a set of potential causes based on the situations and (iii) diagnosis actions (most suitable) in a given situation. These concepts are applied in successive steps.

Let S, P, D, E, and A be the set of Symptoms, Problems, Diagnosis, Events, and Actions respectively. The diagnosis process can be summarized by (1).

$$(E)S \rightarrow P \rightarrow D(A) \quad (1)$$

Let $\mathbf{s_i}$, $\mathbf{p_i}$, $\mathbf{d_i}$, $\mathbf{e_i}$ and $\mathbf{a_i}$ represent a given instance of a symptom, problem, diagnosis, event and action respectively.

We introduce three types of symptoms, based on the completeness of the information coming from the system.

(1) *Reactive* - A set of events may reflect a set of problems that can be repaired by a set of diagnosis actions. In particular, the set of events may be received is a certain time window. In the case of reactive symptoms, most of the events occur spontaneously, i.e., SNMP traps, informs [16].

(i) Time-agnostic diagnosis:

$$\mathbf{[e_1, e_2, e_3 \ldots e_n] \rightarrow \{p_i\} \rightarrow \{d_i\}}$$

(ii) Time-oriented diagnosis (temporal context)

$$\mathbf{[e_1, e_2, e_3 \ldots e_n]t_1 \rightarrow \{p_i\}t_1 \rightarrow \{d_i\}t_1}$$

(2) *Proactive* - A set of events may be missing just one extra event before being able to infer a set of problems associated with the system. Depending on the nature of the event still to come, a different set of problems can be inferred. For proactive symptoms, new information can be solicited, for example, using polling mechanisms via specialized queries. In SNMP, GET state or the value of a parameter, is a solution. The decision of triggering such queries belongs to the diagnosis engine that might identify a potential symptom.

$$\mathbf{[e_1, e_2, e_3 \ldots e_{n-1}] + [e_n] \rightarrow \{p_i\}}$$
$$\mathbf{[e_1, e_2, e_3 \ldots e_{n-1}] + [e'_n] \rightarrow \{p'_i\}}$$

It is important to notice that the nature of the expected event might lead to different classes of problems.

(3) *Pre-emptive* - When a symptom is not complete, a threshold might be set on an expected set of events. This threshold depends on the type of events (Boolean, Integer, etc.). When the expected events are crossing the threshold (1) will take place. A simplified representation is shown below.

$$\mathbf{[e_1, e_2, e_3 \ldots e_{n-1}] + [threshold\ on\ \{e_i\}] \rightarrow \{p_i\},}$$

where "threshold" is used in a general sense, e.g., belonging to a class of events, occurring in a temporal vicinity (ε) of $\mathbf{e_{n-1}}$, or at least of delay of (δ) from $\mathbf{e_{n-1}}$.

All three types of symptoms described above are context-independent. When the context is taken into consideration, the relationship (1) becomes:

$$(E)S \rightarrow [P, C] \rightarrow D\mathbf{(A)} \quad (2)$$

where **C** is the set of possible contexts.

Most of the time, systems experience different problems in different contexts, leading to different diagnosis, i.e.,

$$\mathbf{[e_1, e_2, e_3 \ldots e_n]t_1 + [context_1] \rightarrow \{p_i\} \rightarrow \{d_i\}}$$
$$\mathbf{[e_1, e_2, e_3 \ldots e_n]t_2 + [context_2] \rightarrow \{p'_i\} \rightarrow \{d'_i\}}$$

The main manifestation of the diagnosis is the set of actions and their results (post-conditions of the respective actions). Generally, it is assumed that the post-conditions are true. However, potentially conflicting repair actions might leave the system in a questionable (or unknown) state, even when the post-conditions of each action hold.

In the next section, we propose and analyze a validation loop based on QoD.

3.2 Approach on Validation Loop

In general, diagnosis consists of a set of potential actions intended to fix a situation in a given context. Only some of them might be successful for a given problem in a given context.

The goal of the validation loop is to determine the successful diagnosis actions in the given situation, and to transfer this knowledge to the diagnosis engine for use in future similar situations.

We are introducing the QoD into the validation loop, as shown in Figure 4.

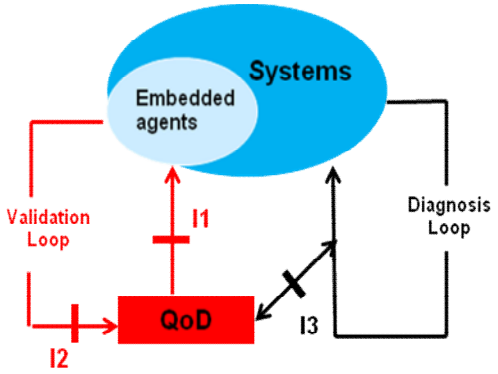

Figure 4. QoD

The QoD module is a dedicated validation engine, which interacts through three specialized interfaces with the system and the diagnosis loop. In particular, it receives diagnosis feedback from specialized system agents via the Interface I2 and asks for additional information (i.e., for audits) via the Interface I1. QoD communicates the diagnosis results to the Diagnosis Loop via the Interface I3. I3 can also be used by the diagnosis loop to ask the QoD for auditing information related to a given situation.

A diagnosis action has a set or pre-conditions and guarantees a set of post-conditions. QoD deals with validation (or evaluation) of post-conditions. Therefore, the QoD engine acts only during-diagnosis or post-diagnosis.

<pre-conditions>
<action-id> (3)
<post-conditions>

Based on the framework presented here, in the following section we propose the QoD mechanism.

3.3 QoD Mechanism

We identify two behavioral modes of the QoD engine: (i) listening mode and (ii) audit mode. In the listening mode, the QoD is waiting for input from the embedded agents or from the diagnosis loop. The audit mode can be triggered (i) by the diagnosis loop following the application of a set of repair actions to resolve a situation (ii) for a given time period or (iii) can be scheduled periodically/frequently.

At the end of the audit process, QoD returns to the diagnosis loop the subset of successful actions from all possible actions taken to repair a certain situation, in a certain context.

[S, C, {successful actions}] (4)
→ Diagnosis Loop

By request from the diagnosis loop, QoD can monitor: (a) a given action, (b) a set of given actions, or (c) all potential actions. The diagnosis loop provides the set of actions to be monitored, QoD being solely a validation engine.

The diagnosing actions are taken as part of the diagnosis loop. The successful actions, determined by the validation loop, will be the ones that make the system pass from a state of type X to a state of type Z.

Definition of a successful action

if
$\{state_i\} \rightarrow \{action_i\} \rightarrow \{state_j\}$
where
$\{state_i\} \in X \wedge$
$\{statej\} \in Z$
then
$\{action_i\}$ is successful

Note: An action can be successful in one context and failure in another context.

The validation loop will transfer the information regarding successful actions to the diagnosis loop for optimizing the diagnosis loop activity. The format of the information returned to the diagnosis loop can have 2 forms:

(1) The successful action, composed of pre-conditions, id and post-conditions as well as the symptom, problem and context.

[<pre-cond><id><post-cond> | <S,P,C>]

(2) The successful action, composed of pre-conditions, id and post-conditions as well as

a pointer. The pointer indicates the list of <S,P,C> in which the action in consideration was successful. The validation engine is responsible for keeping and updating this list.

[<pre-cond><id><post-cond> | <pointer>]
where
<pointer> = {…<S,P,C>$_i$, <S,P,C>$_j$…}

We present below an algorithm summarizing the QoD mechanism.

Algorithm

input:
System states, X, Y, Z
S, P, C
a_i
pre-condition a_i = state$_i$
post-condition a_i = state$_j$
update type [one action, pointer]
if state$_i \in X \ \wedge \ state_j \in Z$
then
forward <a_i> <S,P,C>
or
update <a_i><pointer>
where
<pointer> =
{…<S,P,C>$_i$, <S,P,C>$_j$…}

In summary, the QoD engines takes as input the possible system states and their type (X , Y or Z), the symptom, problem, context, the action to validate, the initial system state (pre-condition), the final system state (post-condition) and the update type. If the initial system state is of type X and the final system state is of type Z, then (1) forward to the diagnosis loop the action and the set <S,P,C> or (2) update the pointer, where the pointer represents the list of all possible <S,P,C> combinations known so far in which the action under consideration is successful.

To tackle the problem, we propose an ontology for diagnosis composed of (i) an event ontology, (ii) tag and semantic diagnosis tag clouds, and diagnosis clouds matching.

3.4 Event Ontology

To address the issues described in the previous sections, we propose here an event ontology.

The three main concepts of the ontology are: (1) *Event*, (2) *Domain* and (3) *Event Manager*.

An *Event* is a software message that indicates something of importance has happened. A *Domain* is defined as a technological area, such as VPN or VoIP, a sub-network or specific management area, such as fault, security. An *Event Manager* provides real-time information for immediate use and logs events for summary reporting used to analyze network performance.

The main relations between these concepts are depicted in Figure 5. The Events are owned by the Event Manager. Also, an Event refers to a Domain.

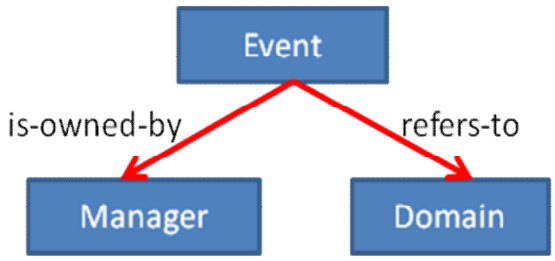

Figure 5. Event Ontology Main Concepts

In addition to the main relationships between an Event, Manager and Domain, an Event is defined by explicitly-declared event ID, source, version, timestamp, priority, and free-text (see Figure 2). An event can be stored at an URL, Library-ID, Repository or Log Server. These locations can be explicitly-declared or found as a result of a search. An Event can be referred to by another Event or can refer to another Event. Also, an Event can be similar to another Event. The ontology identifies the relationship between events (example “is-similar-to<event>”,”refers-to <domain>” etc.) and the management properties of a given event (e.g., “can-be-accessed-by <application>”, “can-be-modified-by <application/human>” etc.).

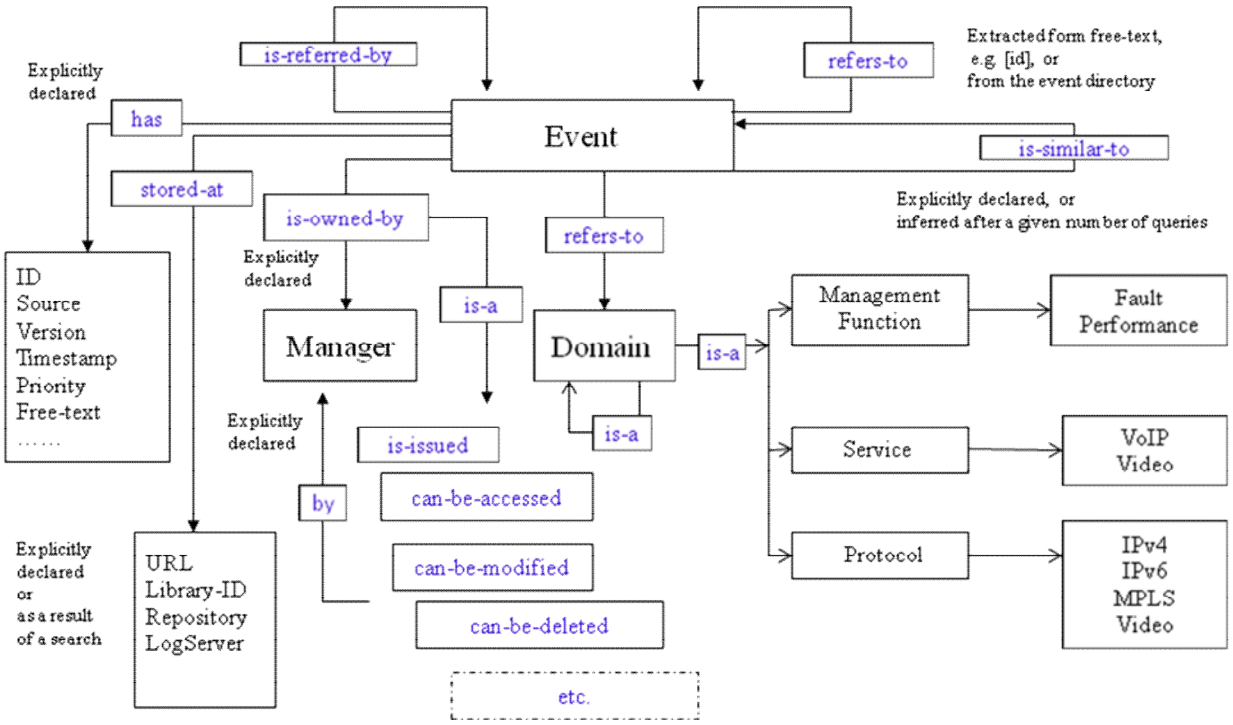

Figure 6. Details of the Event Ontology

In Figure 6, an Event depends on a Manager by <is-owned-by> relation that can be refined in a few inheriting relations such as <can-be-accessed-by>, <can-be-modified-by>, or <can-be-deleted-by>. As an example, the last relation defines what managers have rights to delete a particular event. If we combine with the proposal from [25], the manager is also instructed how to proceed.

Expanding the ontology from Figure 5, we illustrate in Figure 7 the main concepts and the core relations. Apart the dependency relations, we also consider the aggregation relation, where events are aggregated during the processing. The main relation <is-owned-by> is specialized in a few relations, as managers can be specialized too.

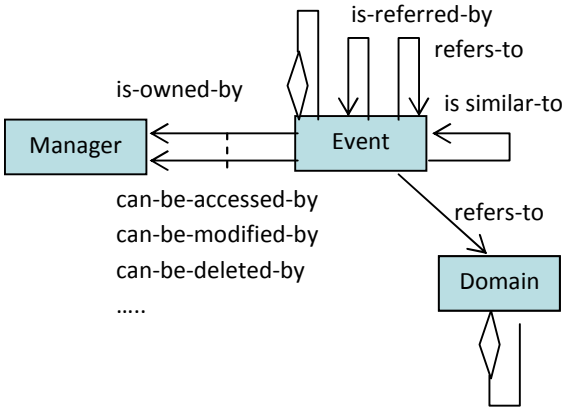

Figure 7. Adding relations to the main concepts (UML notation)

A domain instance can be one of the specialties that have been illustrated in Figure 6.

3.5 Semantic Tag Clouds

The first challenge in deriving semantic clouds is the complexity, when considering all the expansions of the diagnosis domains. As an example, let us consider the following tag subdivisions targeting fault diagnosis (List 1). We have a coarse grain tag embedded hierarchy, while a fine grain tag list can be progressively developed. As a note, each time a tag expansion is made, a validation is required.

- TAGS
  - IPv6, IPTV
    - fault in IPv6
      - fault in IPTV
        - security IPv6
        - security sensors
        - IPTV with IPv6
        - IPTV management
- Refined /TAG list/
  - latent fault, authentication, M5, IPSec, link-Syslog, CLI-Z

List 1. Example of Tag List

Two concepts are considered in defining (identifying) tags, as expressed in Figure 8.

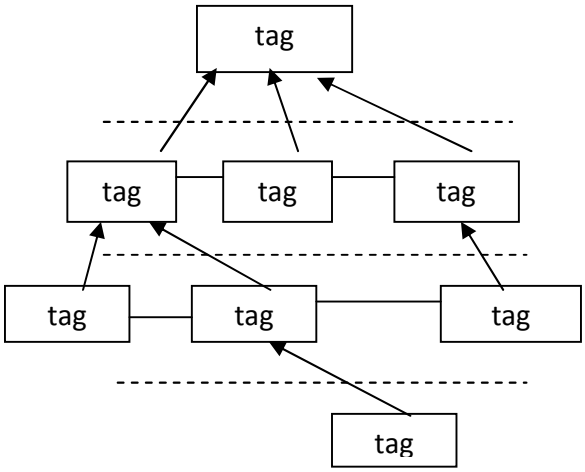

Figure 8. Hierarchical tags and their relations

As suggested by List 1, tags have a *hierarchy* within each domain; this defines a special dependency relation between tags. Also, at each layer, tags may embed different associations (e.g., *port-85* and *SNMP traps*).

During the diagnosis activities, tags are relevant, but without the tag relationships, no much progress can be achieved. One step ahead is to form tag clouds; a tag cloud refers to a tag list focusing on a particular domain (see Figure 9).

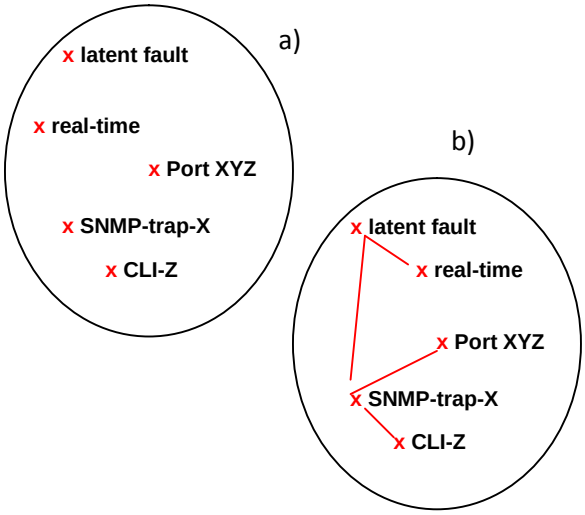

Figure 9. Tag Clouds and Semantic Tag Clouds

As an example, we localize in Figure 9 (a) a tag cloud concerning real-time fault diagnosis. We identify a series of relationships between a given CLI (Command Line Interface), a SNMP-trap that refers to a given port, on one side, and between latent fault and real-time tags, on the other side (Figure 9 (b)).

3.6 Mapping Semantic Clouds in a Context

Let us assume that there are two semantic clouds, as shown in Figure 10. Semantic cloud#1 defines the tags and their relationships for a fault related to a power supply issue, while Semantic cloud #2 relates to a potentially real-time and latent fault.

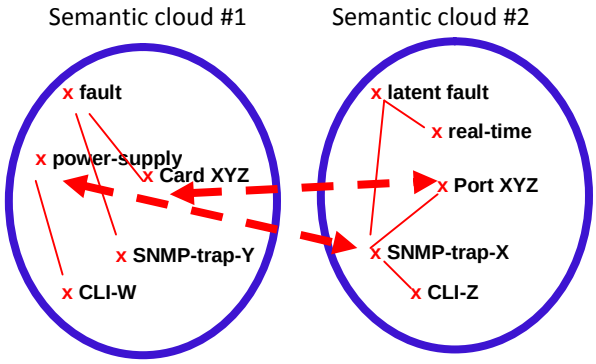

Figure 10. Cross-semantics of Semantic Tag Clouds

An appropriate diagnosis is triggered by linking the port ID and the card ID, then identifying the SNMP trap defined for power-supply behaviors. With these cross-semantic connections, one can identify the potential CLI leading to the situation, or a particular fault on power supply.

As mentioned before, the number of events produced by a system exceeds by far the capacity of processing them. An accurate selection of those events 'of interest' reduces the burden of monitoring and diagnosing and leads to a more adapted solution.

On the other side, the event mediation is less process consuming as both the diagnosis engine and the validation engine [17] refer to the same event ontology.

3.7 Progressive Ontology

A diagnosis engine is validating successful diagnosis actions based on a given set of semantic tag clouds. As expected, since the technology evolves, new devices and applications are developed. We adopt a series of heuristics on validating new semantic tags and new semantic tag clouds.

3.7.1 New Semantic Tags

For the purpose of ontology control, the following heuristic was experimented:

START
New tag TAG
1. Temporary accept a 'tag'
2. Set a threshold of its use for a time window
3. If the diagnosis engine uses it in that time window, then insert it as *permanent* in the 'tag cloud'
4. Then consider tag relations based on the diagnosis-context (situation)
5. If the diagnosis engine do not use the new tag in the given time window, add it to the *list* of *potential tags* to be considered in the future, but avoid definitive insertion
END

Heuristic #1. Inserting a New Semantic Tag

The tag inventory process keeps a few records concerning a specific tag, e,g., the cloud it belongs to, if it is on a potential tag list, or whether it was declined for a list of clouds.

3.7.2 Semantic Tag Cloud State

As the technology evolves, building new tag clouds and maintaining the created and validated ones are current cloud management activities. To accurately communicate to a diagnosis engine what clouds can be used, we introduced the cloud state. Cloud state belongs to *{progressive, in_test, validated, obsolete}*.

The state *progressive* denotes a cloud that it is in a building phase; it can be updated, but not used in a diagnosis process. *In_test* represents a cloud that achieved a certain degree of completeness; in this state, different diagnosis are tested and mapped against the cloud semantic relations to validate them. The state *validated* is declared by the diagnosis engines; it allows a semantic tag cloud to be used in the diagnosis decisions. *Obsolete* is declared when none of the components of a cloud is in use any more.

3.7.3 Inter-clouds Relations

The main achievements with ontology are building small models and link them via relations. Therefore, building inter-clouds relations are crucial for diagnosis. The procedure is captured by the following heuristic:

START
1. Identify the clouds potentially related
2. Identify the intra-cloud relationships
3. Validate the cloud status
4. Build inter-clouds relationships and validate them
5. Identify for each semantic tag cloud:
   a. "one-hop" related clouds
   b. type of relationship
      /start/cloud1<->end/cloud2/
END

Heuristic #2. Steps for building inter-cloud relations

3.7.4 Specific Aspects in Defining Tags

Tags are context-driven; they are defined without a global view, by different teams. Building inter- and intra-cloud relations is conditioned by a full understanding of the semantic of a tag and its relations with other tags. The following aspects are considered: (i) *temporary tags*, (ii) *synonymous tags*, and (iii) *ambiguous tags*. Some of the tags are originally embedded into a given cloud; until at least one relation with the existing tags is identified, it is labeled as 'temporary'. Synonymous tags are more difficult to be identified; tag definition is usually human-driven, if there is no formal semantic behind tag definitions. Ambiguous tags can be identified inter- and intra-clouds. Disambiguation is achieved by either duplicating a given tag in two tags with dissimilar identifications, or by reducing the semantic of a considered tag.

3.7.5 Diagnosis Actions Associated with Tag Clouds

In the proposed progressive ontology, each semantic tag cloud has attached a list of suggested potentially successful diagnosis actions.

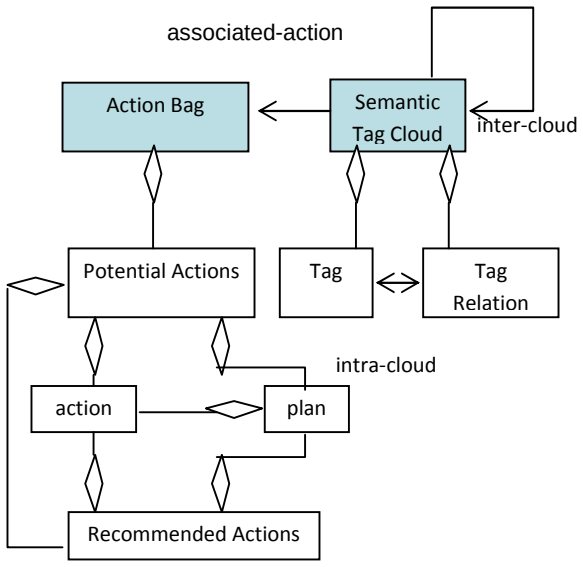

Figure 11. Semantic tag clouds and associate actions (UML notation)

We depict in Figure 11 the diagnosis counter-part of event ontology modeling, i.e., the required actions. There are a number of diagnosis *potential* actions associated with a

semantic cloud. A subset of them is *recommended*, based on the successful diagnosis history. In triggering a diagnosis decision, we consider two potential solutions: an *action*, or a *plan*. A plan is a predefined combination of some actions, implying parallelism, serialization, and temporal relations between actions.

There are some aspects when associating many tag semantic clouds and the actions belonging to them. Within a semantic tag cloud, some actions are defined with special *guards* (for validating the triggering), or explicitly specify *conflicting* actions (in given conditions). When two or more semantic tag clouds are mapped some conflicts might disappear, while *emerging* conflicts may occur, too. To deal with all these aspect a better formalism is needed to express structures, relationships, actions, and constraints during the diagnosis activity (and its validation). The following section deals with some of these aspects.

3.8 Timestamps

This section describes aspects related to timestamps, event correlation with temporal operators and gives an example of use of temporal operators.

In a hierarchical model, an event model should allow multiple timestamps, depending on the event hosting and processing. In an XML-like specification, we introduce for the device (source), host (server), and processing application (management application or console), the timestamp and the time zone a source, host or processing application belongs to.

TABLE I: Timestamp specification

<time>
<device_time> device_time></device_time>
<device_zone> device_time_zone</device_zone>
<server_time> server_time</server_time>
<server_zone> server_time_zone</server_zone>
< processor_time> event_processor_time</ processor_time>
<processor_zone> processor_time_zone</processor_zone>
</time>

The timestamp of the event is best set by the event producer (*device_time*). The timestamp representing the moment of event registration on the server, *server_time* is of relevance for correlation. Finally, the timestamp of the entity performing correlation or event processing is relevant for synchronization among multiple such event processing systems.

Any of these three entities can belong to different time zones that should be considered when temporal priorities count.

The values of these parameters are set by various entities. Some protocols provide the capability to supply the time in the occurred event, or the time when the event producer sent the event. With the Network Time Protocol (NTP) the time from event producers will be the most accurate. Alternatively, the time registered by the event processing system might be considered.

We advocate the following representation, similar to Syslog protocol, *e.g., device_time: Jan 1 14:22:45* represents the local time on the device at the time the message is signed. For devices with no clocks, *device_time: Jan 1 00:00:00* should be the representation.

3.8.1 Event Correlation with Temporal Operators

Temporal relations are used to build time-dependent event correlations between events. For instance, we may correlate the alarms that happened within the same 10-minutes period, which means the correlation window is 10 minutes. We abstract an event and consider only the temporal aspects.

Let ***e1*** and ***e2*** be two events defined on a time interval:

$T_1 = [t_1, t_1']$
$T_2 = [t_2, t_2']$
and e_1 within T_1
e_2 within T_2

two events occurring within the time intervals T_1 and T_2, respectively.

The following temporal relations R(t) or R are identified:

R(t):: = {**after**(t), **follows**(t), **before**(t), **precedes(**t)}

R ::= {**during**, **starts**, **finishes**, **coincides**, **overlaps**}

The following deductions hold:

after: e_2 ***after(t)*** $e_1 \Leftrightarrow t_2 > t_1 + t$

follows: e_2 ***follows(t)*** $e_1 \Leftrightarrow t_2 \geq t_1' + t$

before: e_2 ***before(t)*** $e_1 \Leftrightarrow t_1' \geq t_2' + t$

precedes: e_2 ***precedes(t)*** $e_1 \Leftrightarrow t_1 \geq t_2' + t$

during: e_2 ***during*** $e_1 \Leftrightarrow t_2 \geq t_1$ *and* $t_1' \geq t_2''$

starts: e_1 ***starts*** $e_2 \Leftrightarrow t_1 = t_2$

finishes: e_1 ***finishes*** $e_2 \Leftrightarrow t_1' = t_2'$

coincides : e_2 ***coincides*** *with* $e_1 \Leftrightarrow t_2 = t_1$ *and* $t_1' = t_2'$

overlaps: e_1 ***overlaps(ε)*** $e_2 \Leftrightarrow t_2' \geq t_1' \pm \varepsilon > t_2 \geq t_1 \pm \varepsilon$
where ε is the accepted threshold for measurement variation.

With respect to the algebraic properties of the temporal relations,

- all are transitive, except **overlaps**,
- **starts**, **finishes**, **conincides** are also symmetric relations.

3.8.2 Example of Using Temporal Operators

In [22], time-oriented diagnosis was defined as

$$[e_1, e_2, e_3 \ldots e_n]t_1 \rightarrow \{p_i\}t_1 \rightarrow \{d_i\}t_1,$$

where

p_i, d_i, and e_i represent a given instance of a problem, diagnosis, and event, respectively.

As an example, let us consider the instantiation:

$$[e_1, e_2, e_3] \mid e_2 \textbf{\textit{follows}}(x)\ e_1\ \&\ e_2 \textbf{\textit{overlaps}}(\varepsilon)\ e_3\} \rightarrow p_{123} \rightarrow d_{123}$$

where x is the time duration between e_1 and e_2.

As a note,

$$[e_1, e_2, e_3] \mid e_2 \textbf{\textit{precedes}}(x)\ e_1\ \&\ e_2 \textbf{\textit{overlaps}}(\varepsilon)\ e_3\} \rightarrow p'_{123} \rightarrow d'_{123}$$

represents a different problem and therefore, a different diagnosis.

In the case that the above specification designates a given diagnosis and it is determined that e_1 did not follow e_2 after time x, a diagnosis engine issues an anomaly (no concrete diagnosis is derived).

An event has a series of event attributes, which we represent as:

$e = (f_1, f_2, f_3 \ldots, f_n)$
where f: $(value:V)$,
where V is the type of the attribute

Examples of event attributes that we consider are:

f_1: *ID*
f_2: *source*
f_3: *timestamp*
f_4: *timezone*
f_5: *English text defining the potential cause*
etc.

$e.f_3$ represents the value of attribute f_3 in event e.

The operators on relative event position (**follows**, **overlaps**, etc.) are related to the attributes f_3 and f_4.

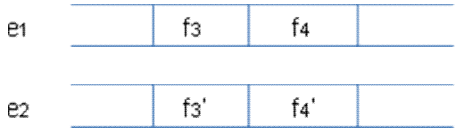

Figure 12.Timestamp and timezone event fields

In this example, $e_1.f_4$ and $e_2.f_4$' are known, since they represent the timezones of the sources of the two events. Only $e_1.f_3$ and $e_2.f_3$' need to be set by the local clocks. Let us assume that:

clk_1 sets $e_1.f_3$ and clk_2 sets $e_2.f_3$',
where *clk* is the local clock of the event source.

$|clk_1 - clk_2| \leq \varepsilon_{12}$,
where ε_{12} is the clock skew between the two local clocks for two domains represented by two semantic clouds [23].

e_2 ***follows***(x) e_1 is computed as follows:
$(e_1.f_3 + \varepsilon_{12}) + x < e_2.f_3$ (for the same time zone)

For different time zones, this becomes:
$[(e_1.f_3 + \varepsilon_{12}) \blacksquare Abs(e_1.f_4)] + x < (e_2.f_3) \blacksquare Abs(e_2.f_4)$,
where $\blacksquare$ $Abs(e.f_4)$ represents the operator for normalizing the time between timezones.

Following the same logic, e_2 ***overlaps***(ε) e_3 for different time zones is computed as follows:
$|(e_2.f_3) \blacksquare Abs(e_2.f_4) - (e_3.f_3) \blacksquare Abs(e_3.f_4)| < \varepsilon_{23}$
where
|x| is the absolute value of x
and
ε_{23} represents an acceptable error.

These event-based computations are performed each time a diagnosis is triggered and validated.

In the next section we will use this example in the diagnosis scenario.

3.9 Using Temporal Features for Diagnosis

This section presents a formal specification of the ontology-based diagnosis, considering temporal relations. Let us assume that the diagnosis engine and the Quality of Diagnosis (QoD) engine introduced in [22] have to trigger the following operations: INTERPRET, APPLY, VALIDATE and MARK.

- Diagnosis engine: INTERPRET events from the system.
- Diagnosis engine: APPLY the diagnosis actions.
- Quality of Diagnosis engine:
  VALIDATE the diagnosis actions.
  and
  MARK successful actions.

The APPLY, VALIDATE and MARK functions were shown in [23]. We reconsider the example with INTERPRET functionality as well.

As discussed in [23], there is a semantic tag hierarchy within each domain, with special dependency relations between semantic tags. Within a domain, semantic tags and their relations form a semantic tag cloud; a domain might have multiple semantic tag clouds associated with it. Let us assume that a system is represented by two semantic tag clouds (Figure 13). Semantic cloud #1 defines the tags and their relationships for a fault related to a power supply while Semantic cloud #2 relates to a potentially real-time and latent fault.

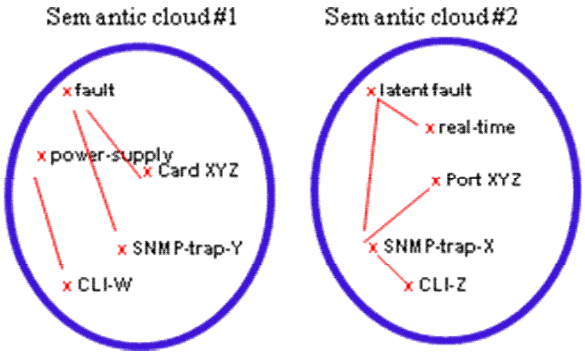

Figure 13. Two Semantic Tag Clouds [23]

When some event patterns occur and diagnosis actions must be triggered (and validated), the Diagnosis Engine interprets the events from the system and applies the diagnosis actions. Next, the Quality of Diagnosis engine validates the actions and marks the successful actions.

The following algorithm is used by the engines to perform the required actions for a given occurrence of combinations of events. A particular series of events occurs as shown in the INTERPRET part of the following algorithm (we use the '.' Notation, i.e., *a.b* means the property '*b*' of the instance '*a*'). When the conditions (2) and (3) explained in Section III hold, the necessary condition to enter the rest of the algorithm is met.

START

INTERPRET
IF {[e_1, e_2, e_3] | e_2 precedes(x) e_1 & e_2 overlaps e_3}
CLOCK = t_0

Legend (for details, see [18]):
r_C: R_C | r_C ::= <c_1: C, c_2: C>, cloud to cloud relation
r_T: R_T | r_t ::= <t_1: T, t_2: T>, tag to tag relation
r_{CA}: R_{CA} | r_{CA} ::= <c :C, {a_i : A | p_i: P}>, cloud to action relation
r_{dto}: R_{Dto} | r_{dto} ::= <e:E, d:D>, event to domain relation.

AND e_1 belongs to $cloud_1$
AND e_2 belongs to $cloud_2$
AND e_3 belongs to $cloud_2$
AND $x < t_0$
THEN
ERROR
ELSE
ASSUME
e_2 precedes(x) e_1 & e_2 overlaps e_3 = = TRUE
AND
IF there is exist r_c < $cloud_1$, $cloud_2$>
AND $cloud_1$.state = active
AND $cloud_2$.state = active
AND
IF there is r_{dto} <e_1, $domain_1$>
AND tag_1 belongs to $domain_1$
AND tag_1 belongs to $cloud_1$
AND tag_2 belongs to $domain_2$
AND there is r_T <tag_1, tag_2>
AND there is r_{CA1} <$cloud_1$, {$action_1$}>
AND there is r_{CA2} <$cloud_2$, {$action_1$}>
WITH
$action_1$ = {a_1, a_3, a_6}
AND
$action_2$ = {a_1, a_5, a_7}
THEN

APPLY {{a_1, a_3, a_5, a_6, a_7} – {
a_1.conflicting ∪
a_3.conflicting ∪
a_5.conflicting ∪
a_6.conflicting ∪
a_7.conflicting}
VALIDATE
a_1.post-conditions = TRUE
a_3.post-conditions = TRUE
a_5.post-conditions = TRUE
a_6.post-conditions = TRUE
a_7.post-conditions = TRUE
MARK
a_1.mode = successful
a_3.mode = successful
a_5.mode = successful
a_6.mode = successful
a_7.mode = successful
END

IV. CASE STUDY

The concepts proposed in this paper are implementable, at-large, but considerations must be taken when designing new systems to follow the formal approach. In this section, we highlight the main challenges of a full implementation of the proposed diagnosis solutions. While fixing legacy systems

remains a complex problem, avoiding the same errors for newly designed systems seems be to the most appropriate approach. We illustrate partial solutions for different concepts introduced via a case study simulation. The case study is conducted in connection with Cisco DFM (Device Fault Manager).

4.1 Challenges in Implementing the New Approach

Two main complementary contributions were proposed in this paper, namely: (i) a new mechanism for validating diagnosing actions, while promoting the reuse of diagnosis actions in similar situations, and (ii) a new approach on events and actions. While the usefullenss of each new concept and mechanism was highlighted when they were introduced, developping a large scale system using these concepts requires substantial effort and time.

There are several "de facto" constraints in developping a totally new diagnosis approach. In the following sections, we consider the most important challenges, based on our experience in validating our approach.

4.1.1 Customized Event Model used by Different Systems

One difficulty in validating our approach is related to the customized model used by different system/network devices/software to construct and send an event. To complicate the task further, even subsequent releases of the same entity might expose different event models. For this reason, any previous diagnosis algorithms and diagnostic systems become obsolete. Since designing and implementing a new event is relatively easy, there are thounsands of useless events (not easily captured by any diagnosis algorithm or system) and, consequenlty, thousands of "exception handling" cases; the latter are usually sent to a human operator in NOCs (Network Operating Centers).

Even in cases when a standard is available, the recommendations are too generic . For example, in ITU recommendation X.745 [81], the parameter status can be "mandatory", "optional", "conditional" or "not applicable". Aditionally, an 'implementstion status" ("implemented" or "not-implemented") needs to be considered (Figure 14).

<parameter>
<parameter status>:: = *mandatory* | *optional* | *conditional* | *not applicable or out of scope*
<implementation status> ::= *implemented* | *not implemented*
<parameter/>

Figure 14. Recommendations for Event Parameters

In this case, even if an event model is enforced, the value of *parameter status* and *implementation status* are not helpful, since, for the same event definition, some features might not be mandatory or implemented.

In other cases, the implementaiton of the events is very customized and leaves little opportunity for syntax harmonization, yet alone consideration for the semantic aspects. For example, Figure 15 presents a Syslog event issued by Cisco's GSR (Gigabit Switch Router) [30].

%EE48-3-ALPHAERR: [chars] error: cpu int [hex] mask [hex]\n addr [hex] data hi [hex] data lo [hex] parity [hex]\n fs [hex],pf [hex], prep [hex] (pc [hex]), pc1 [hex]\n plu int [hex] int en [hex] err en [hex] err [hex] ecc [hex]\n tlu int [hex] err [hex] ecc [hex], mip [hex] (pc [hex]), pc2 [hex]\n pst [hex], cam [hex], nf [hex], pop [hex] (pc [hex]), ssram adr [hex] err [hex]\n pipe ctl [hex] avl [hex] end [hex] fatal [hex], gather [hex]\n xmb read [hex] rclw1 [hex] rclw2 [hex] rclr [hex]\n tailw1 [hex] tailw2 [hex] tail [hex]\n sts1 [hex] sts2 [hex]\n pcr regs: fs [hex] prep [hex] plu [hex] pc1 [hex] tlu [hex] dummy [hex] mip [hex] pc2 [hex] mtch [hex] post [hex] pop [hex] gthr [hex]

Figure 15. Example of a Syslog Event issued by GSR (Cisco)

We see that there are many different types of formats for the events. Automating extraction of useful information from event text message is close to impossible. To extract a useful piece of information, or *token*, a diagnosis tool has to know the format apriori and write "*rules*" to parse messages into tokens, when the messages are generated from various sources. Currently, Syslog messages are generated by numerous sources: various IOS protocol code modules, device driver code module, etc. Updating all these sources implies changing tens of millions of lines of code, a task close to impossible.

We note here that SNMP traps have a standard format, using ASN1 (Abstract Syntax Notation One) [30]. An example of an SNMP trap notification is shown in Figure 16.

4.1.2 Events are Issued in Isolation

The second challenging aspect consists in the fact that change reports (events) are issued in isolation, with an implicit semantic on their potentially related events. This is due to the fact that the events are designed by the entity designers; they do not have a full picture of where the entity will be used, its interactions, etc.

Most of the diagnosis decisions are human-held heuristics. In many cases, intuition plays a major role. Some diagnosis decisions are experience-based, and

very rarely based on rigourous knowledge processing. As a drawback, accuracy and correctness migth lead to a late diagnosis.

To illustate the difficulty in dealing with legacy systems for a correct diagnosis, we consider two examples.

First, let us consider the example of a SNMP trap notification as shown in Figure 16. SNMP MIBs define these kind of messages in a standard way by NOTIFICATION-TYPE. The varbind will indicate neighbor = xxx.yy.zzz.mm; status = Down. Despite the more formalized strauctures of SNMP traps, a tool cannot syntactically "tokenize" the message following the same approach, unless the message is somehow recognized. This means that a tool user or developer has to know the message format, write a "rule" to recognize the format, then, when the message arrives with the prefix "%BGP-5-ADJCHANGE", that relevant "rule" can be triggered to tokenize the text content.

```
Nov 11 11:52:40.735: %BGP-5-ADJCHANGE: neighbor xxx.yy.zzz.mm Down - Peer closed the session
```

Figure 16. Example of a SNMP Trap Notification

Writing such rules is a cumbersome activity, especially since a rule needs to be written for each event. Additioanlly, having millions of rules is not scalable, raises conflicts, and diagnosis decisions come too late.

```
VSEC-6-VLANACCESSLOGNP: vlan [dec] (port [dec]/[dec]) denied ip protocol = [dec] [int] -> [int], [dec] packet(s)
```

Figure 17. A Report Syslog Event

Next, let us consider the example presented in Figure 17. To understand the explanation of the Syslog message shown here, a special rule must be written. The rule should capture that this message indicates that an IP packet from the identified VLAN and physical port that matches the VACL log criteria was detected. The first [dec] is the VLAN number, the second [dec]/[dec] is the module/port number, the third [dec] is the L4 protocol type, and the fourth [dec] is the number of packets received during the last logging interval. The first [int] is the source IP address, and the second [int] is the destination IP address.

As a conclusion, the huge volume of events issued by a system, the large variation in both synatax and semantic, gives little chance to have a general diagnosis approach that covers all the cases, for all system entities. While fixing legacy systems remains a complex problem, avoiding the same errors for newly designed systems seems be to the most appropriate approach.

4.2 Validation of the Paper Proposal

We can summarize that the paper presents a step-by-step system diagnosis approach by proposing a way to define events (with a well defined syntax and semantic), and their links with potentially related events. Instead of a "unique format", we proposed an ontology-based approach, per small domains.

While writing rules has proven to be a tedious activity, if not almost impossible, discovering event patterns, associating a potential list of recommended diagnosis actions for each pattern, and keeping track of succesfull actions (via diagnosis validation engine) seems to be a feasable approach.

4.2.1 Industrial Connection of the Solution – Cisco Device Fault Manager (DFM)

We recall that the status on the network elements is captured via notifications, polling, etc., and a behavioral deviation may be identified. The simulations were performed in connection with Cisco DFM (Device Fault Manager) [30], which will be briefly presented below.

Cisco's Device Fault Manager (DFM) is a specialized software offering real-time assistance for system diagnosis. The main activities it performs are:
(i) Monitors and displays the operational network health data;
(ii) Analyzes the events triggered in the network and determines when a possible fault has occurred, and
(iii) Sends notifications to pre-determined users through Graphical User Interface display or through a series of configurable notifications.

Figure 18 [30] shows the tasks performed by DFM and the relations with other components. The software constantly gathers information from system elements, analyzes and prioritizes the data, and sends the appropriate notifications.

DFM can send three types of notifications:
(i) SNMP Trap Notifications – DFM processes the traps and events it receives, and generates its own traps with the format defined in CISCO-EPM-NOTIFICATION-MIB [30].
(ii) E-mail Notification - DFM sends e-mail messages with the information about the event and the alert that caused it.
(iii) Syslog Notification - DFM generates Syslog messages that can be forwarded to Syslog daemons on remote systems.

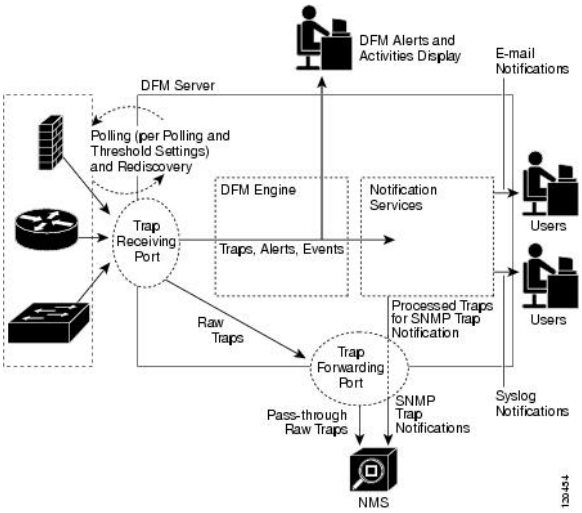

Figure 18. DFM Architecture [30]

DFM uses the concept of *subscriptions* to allow the specification of the elements needed for its activity. SNMP Trap Notification subscriptions, or E-mail subscriptions, have the following elements in common:
(i) Devices, representing the devices of interest;
(ii) Alert Severity and Status;
(iii) Event Severity and Status (the names of the events can also be customized);
(iv) Recipients, representing one or more hosts to receive the SNMP traps or uses to received the e-mails, and
(v) Name, needed to uniquely identify the subscription.

DFM analyzes the events as they arrive, or polls the elements regularly. When an event or alert occurs that matches a subscription, a notification is sent. An event trigger can be either normal polling, a threshold that was exceeded, or a trap that was received.

A category of traps are generated by system elements, but are not processed by DFM; these re referred to as *pass-through traps.* They appear in the Alerts and Activities Display of the software, if they were generated by a device managed by DFM. The software can be configured to forward pass-through traps from managed or unmanaged devices to other elements. If DFM does not know which device generated the trap, it ignores the trap.

DFM perform system elements polling via two mechanisms:
(i) Using a high-performance, asynchronous ICMP poller with two threads.
(ii) Using the SNMP poller, which has ten synchronous threads running in parallel.

The two polling mechanisms are coordinated for optimal results.

4.2.2 Event Definition

In the previous sections, we presented a way to define an event; we applied this approach for a limited number of events, as a proof of concept for the proposal. The progressive approach we adopted for the validation was to develop the event features, represented in fields, in a context, as shown in Figure 19.

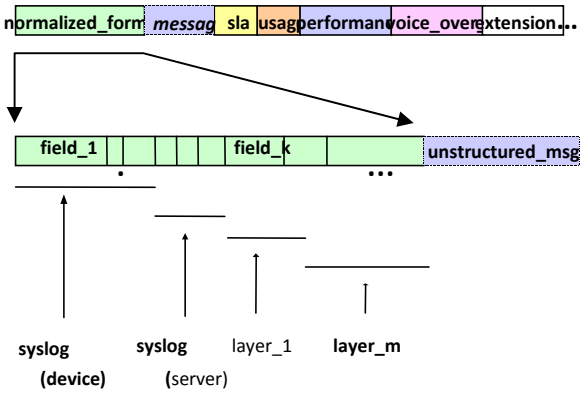

Figure 19. A Progressive, Context-oriented, Event Definition

We started with a basic set of fields (features), with a precise syntax and semantic. Then, we considered extended features in a domain. This helped control the diagnosis rules in a particlar context. For example, there are specific rules in SLA domain, such as SLA violations, SLA penalties, etc. In our simulation, the *SLA domain* and *performance domain* were considered. This approach was facilitated by the fact that, for each domain, there are well defined and accepted concepts, i.e., semantic tags. For each such domain, we built a semantic tag cloud. Therefore, bridging between a semantic tag cloud belonging to the *performance domain* and another one belonging to the *SLA domain* was easier.

4.2.3 Symptoms-Problems-Diagnosis Rules

Based on the trio S-P-D (symptoms-problems-diagnosis), a diagnosis process was triggered, performed by the "diagnosis engine" and based on the framework presented in Figure 20.

In Figure 20, the "management console", the "management system (mgmt)", and the "device fault manager" are existing components. Since we were not focusing on gathering network events and status, a DFM-like input was used for the simulation. As the current network entities do not issue events in the required form to apply our strategy, we rather used transformation processes to get the information as needed.

The selected events were normalized first ("1" in Figure 20) following the general process pictured in Figure 19. The QoD engine ("2" in Figure 27) took as input the status of monitored parameters (counters, CPU, memory, ports, etc.), while ("3" in Figure 27) processed the coming events to identify patterns, and, hence, correlate them, and sent the recommended actions associated with a given pattern to the mgmt (DFM) (actually, to the operator console). It also stored the situation (set of the watched states) when a set of the recommended actions are issued. In a real environment, it also stores the status of the system after one or more selected actions are declared "successful". This allows the finding of a more rapid solution when the same situation occurs.

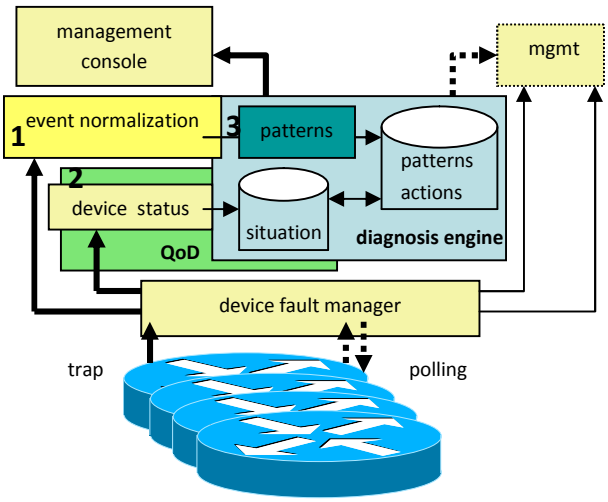

Figure 20. Simulation Architecture Considering DFM features

It is expected that a validation takes place, either preventively (for preventive diagnosis), following a small variation in the normal behavior, after a diagnosis, or a stable period.

Implementation of the diagnosis decisions is based on the same symptom-problem-diagnostic trio paradigm. Based on symptoms sent by NEs (Network Elements) to the monitoring and diagnosis applications, or polled by these applications themselves, a set of problems (or only one single problem) become candidates for leading to a diagnostic. Upon the confidence degree of the diagnosis engine, more information may be polled from the NEs to complete, make more accurate, or re-validate a status with the final goal of triggering the most suitable action on the managed system, or providing the most accurate diagnosis (best-practices, recommended actions, reports) to the network operator or managing systems.

S-P-D may be executed on different engines, as they may be distributed; in our case, we used one single diagnosis engine.

Recursive receiving/polling actions may be performed at any stage of processing, within S, P, and D processes.

4.2.4 Events Processing

The first step in the simulation process was to normalize the input events, as shown in Figure 21. The main achievement of the normalization was that the same property represented by the field value of an event, will always be on the same position in the normalized event, regardless of its initial position in the non-normalized input event. Obviously, there are empty fields in the normalized event for use when new event types arrive, with new fields/features. Following an ontology model previously described, the normalized events also included pointers to other event types that an event has relations to.

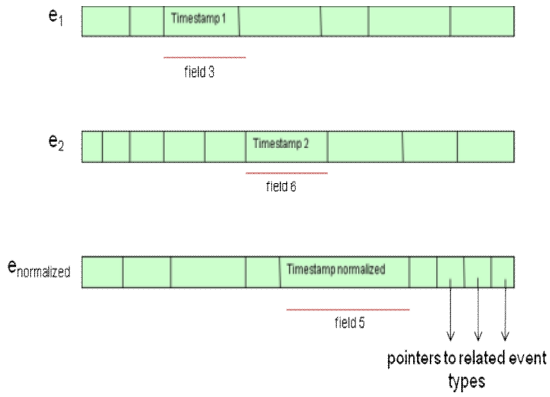

Figure 21. Event Normalization

Post-event normalization, several operations were needed to process the events in terms of their number and referring to the problems they report. The events falling within a specified time window were considered. We recall that a group of events that are correlated form what we refer to as *a pattern*. We used the following *operators* to identify the patterns in our simulation:

(i) Compression [a, a,...,a] ➔ *a*

Compression is done when *identical alarms* are produced by the same network element and they have the same message contents except timestamps. Compression is the task of reducing multiple occurrences of identical alarms into a single representative of the alarm.

(ii) Filtering [a , p(a)< H] ➔ *Ø*

Filtering is the most widely used operation to reduce the number of alarms presented to the operator. If some parameters *p(a)* of alarm *a*, e.g., priority, type, location of the network element, timestamp, severity, etc., do

not fall into the set of predefined legitimate values *H*, then alarm *a* is simply discarded or sent into a log file.

(iii) Suppression [a , C] ➔ *Ø*

Suppression is a context-sensitive process in which an event *a* is temporarily inhibited depending on the dynamic operational context *C* of the network management process. Temporary suppression of multiple alarms and control of the order of their exhibition is a basis for dynamic focus monitoring of the network management process.

(iv) Count [n a]* ➔ *b*

Count results from counting the number of repeated arrivals of identical alarms. When a pre-defined threshold is met, the specified number of alarms are substituted by a new alarm.

(v) Escalation [n a, p(a)]* ➔ *a, p'(a), p'>p*

Escalation assigns a higher value to some parameter *p'(a)* of alarm *a*, usually the severity, depending on the operational context, for example, the number of occurrences of the event.

(vi) Generalization [a, a⊂b] ➔ *b*

Alarm *a* is replaced by its super class *b*. Alarm generalization has a potentially high utility for network management. It allows one to deviate from a low-level perspective of network events and view the situations from a higher level.

(vii) Specialization [a, a⊃b] ➔ *b*

Specialization is the opposite procedure of alarm generalization. It substitutes an alarm with a more specific subclass of this alarm.

(viii) Temporal relation [a T b] ➔ *c*

Temporal relation T between *a* and *b* allows them to be correlated depending on the order and time of their arrival.

(ix) Clustering [a, b, ..T,∧,∨,¬,] ➔ *c*

Clustering allows the creation of complex correlation patterns using logical operators ∧*(and)*, ∨(*or)*, and ¬(*not)* over component terms. The terms in the pattern could be primary network alarms, or previously defined correlations (following the event ontology).

These operators were applied to the normalized events to identify several patterns in our time window. Each event contains information on the source of the event. The "state" of all event sources in a pattern was gathered by polling the sources themselves. These states acted as "pre-conditions" to the diagnosis process. An example of a pattern format is presented below:

{(e_1, $source_1$, $status_1$), (e_2, $source_2$, $status_2$)} ::= $pattern_1$

The sources of the events in a pattern are part of a semantic tag cloud, which is associated with a set of recommended actions. For each pattern, if all the sources belong to the same semantic tag cloud, the recommended actions associated with that cloud are forwarded to the management console. If the sources in a pattern belong to multiple semantic clouds, a union of the recommended actions of all these semantic clouds is forwarded to the management console.

4.2.5 Actions Triggering

When the diagnosis P-D rule identifies specific actions to be triggered, different rules may be in place with respect to triggering rights, such as:

(i) Only the network operator may be allowed to perform the suggested actions. In this case, the diagnosis must be human-understandable, accurate, unambiguous, and feasible. This is mainly related to the event format and specification of the diagnosis actions. DFM uses appropriate Tcl_Tk (Tool Command Language Toolkit) scripts to determine if a message needs to be sent to a human operator of to other management applications for processing.

(ii) The diagnosis engine itself is automatically triggering the diagnosis actions. This was not yet experimented.

(iii) Other management applications are in charge of the diagnosis actions and their results.

In one of these manners, the recommended actions are applied and the diagnosis engine is notified to poll the new states of the event sources determine the "post-conditions". If the post-conditions hold, the action is marked as "successful" for use in future similar situations.

4.2.6 Points to Consider for Implementation

There are several points to consider when implementing the system proposed in this paper. We briefly mention some of them in this section.

(i) Console information is crucial in detecting severe crashes allowing a key message to describe the probable cause. In some situations, the device is not longer able to send the message to some server, or any other device. Commonly, Cisco routers are configured to send console events as Syslog messages. However, even in the case of crashes, the messages printer just before can help diagnose the nature of the problem.

(ii) Cisco IOS devices (IOS 11.2 and above) can be configured to send Syslog messages to a Syslog message-trap converter. Several SNMP notifications have been pre-configured, while others are enabled. Certain are mandatory (coldStart, warmStart, authenticationFailure, linkDown, linkUp, egpNeighborLoss). Since authenticationFailure and LinkUp/LinkDown may trigger a lot of events, one can apply some selective thresholds. Alternatively, a polling procedure may be started on those parameters causing these events. Equally, link state notification should be

enabled only for some objects, devices, and especially for LinkDown.

(iii) For those entities that require event configuration, one can use an approach where the device checks the trigger point and generates the events according to the threshold type (no need to collect and filter data). The risk of this method is that events can be lost for many reasons other than non-crossing threshold points. Threshold on devices are called *agent-based threshold*. SNMP MIB and RMON MIB allow setting thresholds on devices. Alternatively, data can be collected at a management station and analyzed against the appropriate threshold. This kind of setting is called *network management system-based triggering*.

V. CONCLUSION AND FUTURE WORK

The concepts proposed in this paper are implementable, at-large, but considerations must be taken when designing new systems for follow the formal approach. In this section, we highlighted the main challenges of a full implementation of the proposed diagnosis solutions. While fixing legacy systems remains a complex problem, avoiding the same errors for newly designed systems seems be to the most appropriate approach. We illustrated partial solutions for different concepts introduced via a case study simulation.

As a result, the successfully marked actions can be re-used as recommended actions when similar event patterns occur. When an event pattern inventory exists, a similar algorithm is associated with each pattern. In this case, the Diagnosis Engine behavior is a combination of all these algorithms.

We presented an adaptive framework for diagnosis validation and transfer of information from successful outcomes for future use and optimization of the diagnostic activity. It was shown that the current diagnosis techniques needs validation of successful actions and a process for knowledge transfer. We introduced the QoD, an engine that validates the successful actions and transfer knowledge for use in similar situations. This new approach pave the way to adaptive diagnosis, where only those previously classified as “successful actions” are deemed to be applied in similar situations.

Towards automation, a few open issues are in our plans for future exploration and solutions. Criteria for symptom similarly must de defined and experimented in different contexts. Metrics for measuring accuracy of the QoD evaluation should be derived per technology domain and domain context. We intend to explore a progressive ontology (leading to progressive diagnosis) and therefore “progressive validation” of successful actions. This is intended to solve potential conflicts of the post-conditions of the actions already validated as “successful” and to evaluate the accuracy of the diagnosis actions (preciseness versus permanent damage). A specific target is to propose a flow engine, as an instantiation of the QoD that identifies context-based temporal patterns of successful or failure diagnosis actions.

VI. REFERENCES

[1] M. Steinder and A. S. Sethi, A survey of fault localization techniques in computer networks, Science of Computer programming 53 (2004) 165-194

[2] A. Patel, G. McDermott, and C. Mulvihill, Integrating network management and artificial intelligence, in: B.Meandzija, J.Westcott (Eds.), Integrated Network Management I, North-Holland, Amsterdam, 1989, pp. 647–660

[3] I. Katzela, Fault diagnosis in telecommunications networks, Ph.D. Thesis, School of Arts and Sciences, Columbia University, New York, 1996

[4] L. Lewis, A case-based reasoning approach to the resolution of faults in communications networks, in: H.G. Hegering, Y. Yemini (Eds.), Integrated Network Management III, North-Holland, Amsterdam, 1993, pp. 671–681

[5] M. Frontini, J. Griffin, and S. Towers, A knowledge-based system for fault localization in wide area network, in: I. Krishnan, W. Zimmer (Eds.), Integrated Network Management II, North-Holland, Amsterdam, 1991, pp. 519–530

[6] J. Goldman, P. Hong, C. Jeromnion, G. Louit, J. Min, and P. Sen, Integrated fault management in interconnected networks, in: B. Meandzija, J. Westcott (Eds.), Integrated Network Management I, North-Holland, Amsterdam, 1989, pp. 333–344

[7] C. Joseph, J. Kindrick, K. Muralidhar, and T. Toth-Fejel, MAP fault management expert system, in: B.Meandzija, J.Westcott (Eds.), Integrated Network Management I, North-Holland, Amsterdam, 1989, pp. 627–636

[8] B. Gruschke, Integrated event management: Event correlation using dependency graphs, in: A.S. Sethi (Ed.), Ninth Internet. Workshop on Distributed Systems: Operations and Management, University of Delaware, Newark, DE, October 1998, pp. 130–141

[9] S. Kätker and K. Geihs, A generic model for fault isolation in integrated management systems, Journal of Network and Systems Management 5 (2) (1997) 109–130

[10] K. Houck, S. Calo, and A. Finkel, Towards a practical alarm correlation system, in: A.S. Sethi, F. Faure-Vincent, Y. Raynaud (Eds.), Integrated Network Management IV, Chapman and Hall, London, 1995, pp. 226–237

[11] I. Katzela and M. Schwartz, Schemes for fault identification in communication networks, IEEE/ACM Transactions on Networking 3 (6) (1995) 733–764

[12] A.T. Bouloutas, S. Calo, and A. Finkel, Alarm correlation and fault identification in communication networks, IEEE Transactions on Communications 42 (2–4) (1994) 523–533

[13] S. Kliger, S. Yemini, Y. Yemini, D. Ohsie, and S. Stolfo, A coding approach to event correlation, in: A.S. Sethi, F. Faure-Vincent, Y. Raynaud (Eds.), Integrated Network Management IV, Chapman and Hall, London, 1995, pp. 266–277

[14] M. Steinder and A. S. Sethi, End-to-end service failure diagnosis using belief networks, in: R. Stadler, M. Ulema (Eds.), Proc. Network Operation and Management Symposium, Florence, Italy, April 2002, pp. 375–390

[15] V. Venkatasubramanian, R. Rengaswamy, K. Yin, and S. N. Kavuri, "A review of process fault detection and diagnosis, Part I: Quantitative model-based methods," Computer and Chemical Engineering, vol.27, pp.293–311, 2003.

[16] W. Stallings, SNMP, SNMPv2, and CMIP: The Practical Guide to Network-Management Standards, Addison-Wesley Publishing Company, 1993, ISBN 0-201-63331-0

[17] M. Popescu, P. Lorenz, and J.M. Nicod, An adaptive Framework for Diagnosis Validation, The Proceedings of The Third International Conference on Advanced Engineering Computing and Applications in Sciences (ADVCOMP) 2009. IEEE Press, pp. x-y

[18] Cisco IOS Network Management Configuration Guide, 2008 http://www.cisco.com/en/US/docs/ios/netmgmt/configuration/guide/nm_esm_syslog_ps6441_TSD_Products_Configuration_Guide_Chapter.html (last accessed December 2009)

[19] W. Stallings, SNMP, SNMPv2, and CMIP: The Practical Guide to Network-Management Standards, Addison-Wesley Publishing Company, 1993, ISBN 0-201-63331-0

[20] Network Management System: Best practices White Paper, 2008 http://www.cisco.com/en/US/tech/tk869/tk769/technologies_white_paper09186a00800aea9c.shtml (last accessed December 2009)

[21] Augmented Bachus-Naur form http://web.mit.edu/macdev/mit/doc/www/devdoc/Augmented%20BNF.html

[22] M. Popescu, P. Lorenz, and J.M. Nicod, An Adaptive Framework for Diagnosis Validation, The Proceedings of The Third International Conference on Advanced Engineering Computing and Applications in Sciences, ADVCOMP 2009, Sliema, Malta, pp. 123-129, IEEE Press

[23] M. Popescu, P. Lorenz, M. Gilg, and J.M. Nicod, Event Management Ontology: Mechanisms and Semantic-driven Ontology, The Proceedigns of The Sixth International confernces on Networking and Servcies, ICNS 2010, Cancun, Mexico, pp. 129 - 136, IEEE Press

[24] W. Stallings, SNMP, SNMPv2, and CMIP: The Practical Guide to Network-Management Standards, Addison-Wesley Publishing Company, 1993, ISBN 0-201-63331-0

[25] M. Popescu et al., US Patent 7275017, Method and apparatus for generating diagnoses of network problems

[26] L. Lamport, TLA: Temporal logic of Actions, http://research.microsoft.com/enus/um/people/lamport/tla/tla.html (last accessed August 12, 2010)

[27] R. Griffith, J.L. Helelrstein, G. Kaiser, and Y. Diao, Dynamic Adaptation of Temporal Event Correlation for QoS Management in Distributed Systems, 2006 www.cs.columbia.edu/techreports/cucs-055-05.pdf (last accessed August 2, 2010)

[28] K. Walzer, T. Breddin, and M. Groch, Relative temporal constraints in the RETE algorithm for complex event detection, Proceedigns of the Second International Conference on Distributed Event-based Systems, 2008, pp. 147-155

[29] M. Popescu, Temporal-oriented policy-driven network management, Master Thesis, Mcgill University, Canada 2000, p. 140

[30] M. Popescu, Semantic Mechanisms for Cross-Domain System Diagnosis Mécanismes Sémantiques pour le Diagnostic des Systèmes, PhD Thesis, University of Besançon, France, 2010

ICI Reduction Through Shaped OFDM in Coded MIMO-OFDM Systems

Wei Xiang, Julian Russell
Faculty of Engineering and Surveying
University of Southern Queensland
Toowoomba, QLD 4350
E-mail: xiangwei@usq.edu.au

Yafeng Wang
Wireless Theories & Technologies Laboratory
Beijing University of Posts and Telecommunications
Beijing 1000876, China
E-mail: wangyf@bupt.edu.cn

***Abstract*—The default pulse shaping filter in the conventional multiple-input and multiple-output (MIMO) based orthogonal frequency division multiplexing (OFDM) system is a rectangular function, which unfortunately is highly sensitive to frequency synchronization errors and the Doppler spread. Shaped OFDM is able to considerably alleviate the effect of inter-carrier interference (ICI) as well as reduce the out-of-band frequency leak. In this paper, we study various pulse shaping functions and investigate their efficacy for reducing the ICI in the space-time block coded MIMO-OFDM system. We compare a new shaping pulse termed harris-Moerder pulse with several other popular Nyquist pulses such as the raised-cosine pulse and better than raised-cosine pulse. Our simulation results confirm that pulse shaping using a suitable shaping function other than the default rectangular one can alleviate ICI and thus achieve better bit error rate (BER) performance. Furthermore, it is demonstrated that the harris-Moerder shaping pulse is the most successful one in suppressing ICI.**

***Index Terms*—Pulse shaping, inter-carrier interference (ICI) reduction, orthogonal frequency-division multiplexing (OFDM), multiple-input and multiple-output (MIMO), space-time coding, Rayleigh fading channel.**

I. Introduction

Orthogonal frequency-division multiplexing (OFDM) [1], [2] has become an attractive modulation technology with wide employment in a variety of current telecommunications standards such as asymmetric digital subscribe line (ADSL) for high-speed wired Internet access, digital audio broadcasting (DAB), and digital terrestrial TV broadcasting (DVB). More recently, OFDM has made remarkable inroads into current and future wireless standards, e.g., WLAN (IEEE 802.11a/g/n), WiMAX (IEEE 802.16), 3GPP long term evolution (LTE), and IMT-Advanced.

OFDM is essentially a block modulation technique, which converts a wideband frequency selective fading channel into a number of parallel narrowband orthogonal sub-carriers that experience only flat fading. The primary advantages of OFDM lies in its ability to cope with severe frequency-selective fading due to multi-path without complex equalization filters. OFDM is able to attain high frequency efficiency as opposed to conventional frequency-division multiplexing techniques by overlapping the orthogonal sub-carriers. However, this advantage comes at the expense of the sensitivity to frequency offset leading to inter-channel interference and hence performance degradation.

Meanwhile, multiple-antenna technology, also dubbed multiple-input and multiple-output (MIMO), is emerging as an enabling technique to achieve high data rate and spectral efficiency by simultaneously transmitting parallel data streams over multiple antennas [3], [4]. The essential idea behind MIMO technology is space-time signal processing in which both the time and spatial dimensions are exploited through the use of multiple spatially distributed antennas. As such, a MIMO system effectively transforms multi-path propagation, traditionally treated as a nemesis for wireless communications, into user benefits.

The inaugural concept of MIMO was pioneered in Bell Labs in middle 1990s. Telatar studied MIMO system capacity under Gaussian channels in 1995 [5], while Foschini invented the layered space-time architecture in 1996 [6]. To realise the enormous capacity of MIMO systems, Wolniansky established the world's first MIMO testbed based upon the vertical Bell Laboratories layered space-time (V-BLAST) algorithm in 1997 [8], which achieved unprecedented spectral efficiency of 20-40 bit/s/Hz in indoor rich scattering propagation environments. V-BLAST breaks input data into parallel sub-streams that are transmitted through multiple antennas [6], [7], [9]. The astonishingly high spectral efficiency stem from parallel signal transmission resulting in remarkable spatial multiplexing gains. Another important category of MIMO techniques that strive to maximize diversity gains in lieu of rate increase is termed space-time coding, including space-time block codes (STBCs) [10], [11] and space-time trellis codes (STTCs) [12]. The third type of MIMO technology exploits channel state knowledge at the transmitter side through decomposing the channel coefficient matrix using singular value decomposition (SVD). The decomposed unitary matrices via SVD can be used to configure pre- and post-filters at the transmitter and receiver to achieve near optimum MIMO capacity [4].

MIMO and OFDM technologies can be used in conjunction to provide broadband wireless services for future fourth-generation (4G) wireless communications systems [13]. For a wideband MIMO channel whose fading is frequency selective, the complexity of optimum maximum likelihood (ML) MIMO detection grows exponentially with the product of the bandwidth and the delay spread of the channel. To this end,

MIMO-OFDM is preferred over MIMO-SC (single-carrier) in that OFDM modulation is employed to overlay on MIMO so as to convert a frequency-selective MIMO channel into multiple flat fading subchannels. MIMO-OFDM can be implemented as space-time coded OFDM (ST-OFDM), space-frequency coded OFDM (SF-OFDM), or space-time-frequency coded OFDM (STF-OFDM) [14]. In this paper, we restrict our system model to ST-OFDM as the focus of the paper is on reducing inter-carrier interference (ICI) using pulse shaping in MIMO-OFDM.

In a MIMO-OFDM system, inter-symbol interference (ISI) caused by multi-path propagation (time dispersion) can be eliminated by adding a frequency guard interval dubbed the cyclic prefix (CP) between adjacent OFDM symbols. However, the CP offer no resilience against frequency dispersion, where carrier frequency offset is introduced due to the Doppler spread. This causes a loss of orthogonality between the sub-carriers, and thus results in ICI. The frequency-localization of the pulse shaping filter in the MIMO-OFDM system plays a critical role in alleviating the sensitivity to frequency offset and thus reducing ICI caused by the loss of orthogonality. Another important benefit of pulse shaping is to reduce out-of-band frequency leak and hence increase spectral efficiency. For conventional MIMO-OFDM systems, the pulse shaping filter is a rectangular function, which exhibits a poor frequency decay property, and is thus highly sensitive to frequency synchronization errors and Doppler spread. This observation has motivated recent studies on the design of better pulse shaping functions for OFDM.

Shaped OFDM can reduce the effect of single tone interference such as produced by an in-band jammer. If an interfering signal has an integer number of cycles per OFDM frame interval, it will interfere only with one sub-carrier. However, if the interfering signal has a non-integer number of cycles, it will contribute a component to every OFDM sub-carrier. Therefore, a jammer within the OFDM band could project into all OFDM sub-carriers due to the side lobes of the $sinc(x)$ frequency response. However, using pulse shaping the interference could be isolated to a few OFDM channels by suppressing the side lobes with an appropriate window to filter the basis signal set [15].

Pulse shaping in MIMO-OFDM aims to replace the basic rectangular pulse which performs poorly in dispersive channels. Unfortunately, while the majority of work on MIMO-OFDM has been focused on the system design, and channel estimation and synchronization, limited research to date has been dedicated to this important niche area of research for MIMO-OFDM. Several approaches to pulse shaping for OFDM systems have been tried including Hermite waveforms [16] and Weyl-Heisenberg (or Gabor) frames [17]. In [18], the authors examined the use of pulse shaping to reduce the sensitivity of OFDM to carrier frequency offset. Several pulse shaping filters such as the rectangular pulse, raised-cosine pulse and the so-called "better than" raised-cosine pulse [19] were compared in [20]. The authors advocated that the "better than" raised-cosine pulse gave the best performance in the reduction of ICI. The effects on ICI reduction of several widely used Nyquist pulses including the Franks pulse, the raised-cosine pulse, and the "better than" raised-cosine pulse were compared in [24]. The Franks pulse [25] was reported to give the best performance. In [21], a new pulse shape was proposed and compared against Nyquist-I pulses [22]. Improved performance results for the proposed pulse shape were reported. Most recently, another new pulse termed the sinc with modified phase was proposed to reduce ICI in OFDM systems in [23].

In this paper, we investigate the effect of impulse shaping on ICI reduction for the space-time block coded MIMO-OFDM communications system. Although the above studies have reported results on the performance of various shaping pulses on the resistance to carrier frequency offset in OFDM systems, to the best of our knowledge, we are unable to find any published work on pulse shaping for MIMO-OFDM systems in the literature to date. More importantly, we will investigate the performance of a new shaping pulse dubbed the harris-Moerder pulse [26] on ICI reduction in coded MIMO-OFDM systems. We will present simulation results using various OFDM pulse shapes in different time-varying wireless fading channels, showing, among other things, how the channel model used has a significant effect on the final bit error rate (BER). Our comparative studies demonstrate that the harris-Moerder pulse outperforms other popular Nyquist pulses.

The remainder of this paper is organized as follows. Section II describes the software defined modules of the transceiver. Section III describes the various channel models used. Section IV describes the pulse shapes transmitted. Section V presents the bit error rate results obtained in the simulation, while in Section VI conclusions are presented for further research.

II. MIMO-OFDM Transceiver Model

A. System Model

In this paper, we consider the space-time block coded MIMO-OFDM communications systems. The transceiver architecture of the system is illustrated in Fig. 1. As can be observed from the figure, the MIMO-OFDM transceiver is comprised of the quadrature phase shift keying (QPSK) modulator, the space-time block coding component over OFDM with a cyclic prefix, the interleaver and block coding transmitting through various terrestrial Rayleigh fading channels. The system is able to achieve diversity gains in the space, time and frequency domains as well as coding gains from the interleaving and block coding. SBTC is implemented using the well-known *Alamouti* scheme [10] with two transmit and two receive antennas.

For the MIMO-OFDM transceiver model depicted in Fig. 1, denote by N_T, N_R, and N the number of transmit and receive antennas, and the number of sub-carriers, respectively. For the Alamouti scheme, we have $N_T = N_R = 2$.

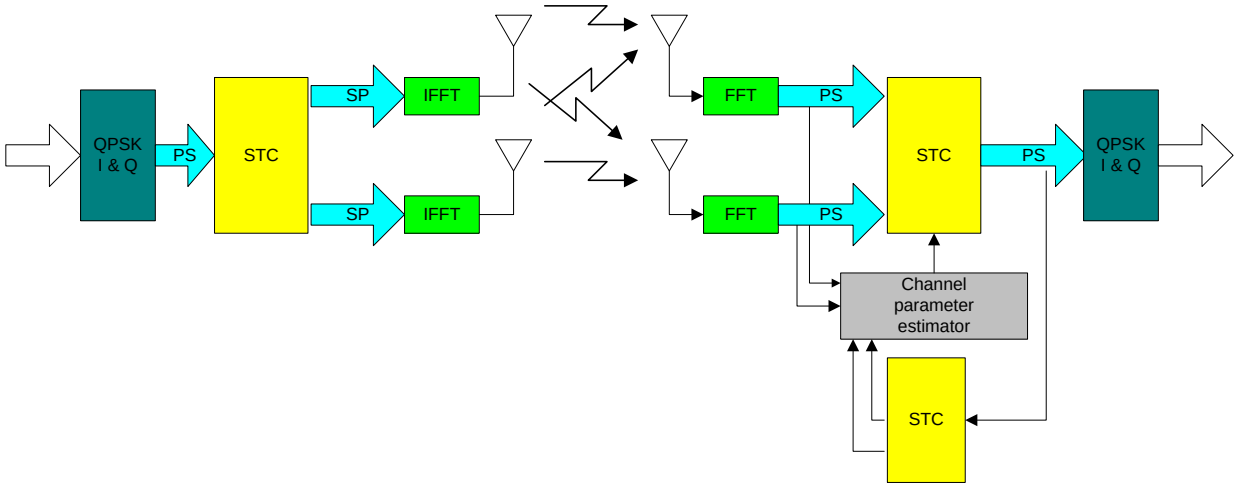

Fig. 1. Transceiver block diagram for the space-time block coded MIMO-OFDM communications system.

B. ICI Analysis

For the system model shown in Fig. 1, the complex envelope of the N-subcarrier OFDM block with pulse shaping sent through the ith transmit antenna can be expressed as

$$x_i(t) = e^{j2\pi f_c t} \sum_{k=0}^{N-1} d_{i,k} p(t) e^{2\pi f_k t} \tag{1}$$

where j is the imaginary unit, f_c is the carrier frequency, f_k is the sub-carrier frequency of the kth sub-carrier, $p(t)$ is the time-limited pulse shaping function, and $d_{i,k}$ is the data symbol sent through the kth sub-carrier of the ith transmit antenna, where $i = 1, 2, \cdots, N_T$, and $k = 0, 1, \cdots, N$. The data symbol $d_{i,k}$ is assumed uncorrelated with zero mean and normalized average symbol energy

$$E[d_{i,k} d_{i,m}^*] = \begin{cases} 1, & k = m \\ 0, & k \neq m \end{cases} \tag{2}$$

where * denotes the complex conjugate operator.

To ensure that the sub-carriers are mutually orthogonal, the following relationship must hold

$$\int_{-\infty}^{+\infty} p(t) e^{j2\pi f_k t} e^{-j2\pi f_m t} dt = \begin{cases} 1, & k = m \\ 0, & k \neq m. \end{cases} \tag{3}$$

Equation (3) implies that the Fourier transform of the pulse shaping function $p(t)$ must have spectral nulls to guarantee orthogonality at the frequencies of $f_k = \pm kW/N$, where W is the total available bandwidth, and $k = 1, 2, \cdots, N$.

It is well known that wireless fading channel distortion and the crystal oscillator frequency mismatch between the transmitter and receiver will introduce the carrier frequency offset $\triangle f$ and the phase error θ. Consequently, this introduces a multiplicative factor at the OFDM receiver. As a result, the received signal is expressed as [20]

$$r(t) = e^{(j2\pi \triangle f t + \theta)} \sum_{k=0}^{N-1} d_k p(t) e^{2\pi f_k t}. \tag{4}$$

Note that the transmit antenna index i is dropped in the above equation for ease of exposition.

The output from the mth sub-carrier correlation demodulator is given as

$$\begin{aligned} \hat{d}_m &= \int_{-\infty}^{+\infty} r(t) e^{-j2\pi f_m t} dt \\ &= d_m e^{j\theta} \int_{-\infty}^{+\infty} p(t) e^{j2\pi \triangle f t} dt \\ &\quad + e^{j\theta} \sum_{\substack{k=0 \\ k \neq m}}^{N-1} d_k \int_{-\infty}^{+\infty} p(t) e^{j2\pi (f_k - f_m + \triangle f) t} dt. \end{aligned} \tag{5}$$

With some further mathematical manipulation, the average ICI power for the mth data symbol can be shown as [20]

$$\bar{\sigma}_{\text{ICI}}^m = \sum_{\substack{k=0 \\ k \neq m}}^{N-1} \left| P\left(\frac{k-m}{T} + \triangle f \right) \right|^2 \tag{6}$$

where $P(f)$ is the Fourier transform of the pulse function $p(t)$. Denote by $\bar{\gamma}_{\text{SIR}}$ the ratio of the average signal power to average ICI power ratio, which can be obtained as

$$\bar{\gamma}_{\text{SIR}} = \frac{|P(\triangle f)|^2}{\sum_{\substack{k=0 \\ k \neq m}}^{N-1} \left| P\left(\frac{k-m}{T} + \triangle f \right) \right|^2}. \tag{7}$$

It is evident from (6) that the average ICI power for the mth symbol average across different sequences is contingent on the number of sub-carriers N and the spectral magnitudes of $P(f)$ at the frequencies of $((k-m)/T + \triangle f), k \neq m, k = 0, 1, \cdots, N-1$.

As indicated in (3), $P(f)$ is designed to have spectral nulls at the frequency points of $(k-m)/T$. Therefore, (6) is evaluated to zero providing $\triangle f = 0$. However, we have $\triangle f \neq 0$ under realistic channels. The focus of our research is to find a new pulse shaping function which is able to minimize (6).

III. Pulse Shapes

The data pulse input into the inverse fast Fourier transform (IFFT) modulator, and transmitted as a complete pulse on one sub-carrier, has a very large bandwidth due to the steep edges of the square pulse [2]. The data pulse can be shaped to reduce the side lobes, which then also reduces the amount of energy transmitted out of band and the resultant channel effects. This is termed *shaped* OFDM.

Shaped OFDM can reduce the effect of single tone interference such as produced by an in-band jammer. If an interfering signal has an integer number of cycles per OFDM frame interval it will interfere only with one subcarrier, however if the interfering signal has a non-integer number of cycles it will contribute a component to every OFDM sub-carrier. Therefore a jammer within the OFDM band could project into all OFDM sub-carriers due to the side lobes of the $sinc(x)$ frequency response, however using pulse shaping the interference could be isolated to a few OFDM channels by suppressing the side lobes with an appropriate window to filter the basis signal set.

One measure of success of a specific pulse shape is how much it reduces the spectral side lobes of the transmitted signal. The other main cause of degradation in OFDM is the ICI between sub-carriers, which can also be reduced with pulse shaping. The shaping also introduces controlled ISI at times other than the samples taken during the receiver decision times.

Another major advantage of shaping the OFDM signal is to reduce sensitivity to carrier frequency offset errors due to a time varying channel and Doppler effects, thereby destroying the orthogonality between channels. The most common rectangular pulse $p_{\text{rec}}(t)$, expressed as follows, does not offer robustness even to modest frequency offset.

$$p_{\text{rec}}(t) = \begin{cases} \frac{1}{T}, & -\frac{T}{2} \leq |t| \leq \frac{T}{2} \\ 0, & \text{otherwise.} \end{cases} \quad (8)$$

Some simulation work has showed that in an OFDM system even a simple Gaussian shaped pulse, with a spread width of 10% of the symbol time, will reduce the sensitivity of the system to a frequency offset by a factor of almost 6 dB [28].

An additional advantage of shaping is that an interfering tone in the frequency band of the OFDM sub-carriers may interfere with all the sub-carriers however the interference may be isolated to a few sub-carriers by replacing the square envelope with a shaped envelope. The envelope can be a standard window or the impulse response of a low pass filter applied to the basis signal set.

Pulse shaping can be then be done with polyphase filters. A window shaped envelope has high adjacent ICI and low ISI, while a filter shaped envelope has high ISI and low adjacent ICI, allowing a trade-off between the two by shaping the filter accordingly. Equalization can be added after the IFFT or polyphase filter to suppress the interference and decouple the adjacent channels and time frames

In this section, we compare five different shaping pulses. We start with the classic raised-cosine pulse, which although does reduce side lobes but is not the optimum pulse shape. A greater side lobe suppression can be obtained with a "better than raised-cosine pulse" as described in [20]. The third and fourth pulse shapes tested are the *duo-binary* pulse and the *triangular* pulse. The last shaping pulse introduced is the recently proposed *harris-Moerder* window [15], which is a modified square root Nyquist pulse using a *harris taper*. It will be demonstrated with simulation results present in Section V that the harris-Moerder pulse is the best performing shaping pulse in the sense of reducing ICI and achieving the best BER performance for the shaped MIMO-OFDM system.

A. Raised-Cosine Pulse

A commonly used pulse shape is the raised-cosine pulse, i.e., the frequency domain reciprocal of the time domain Nyquist pulse, which significantly suppresses spectral re-growth (side lobes) and ICI. When side lobes are suppressed the width of the pulse is increased.

The time domain expression of the raised-cosine pulse shaping function denoted as $p_{\text{rc}}(t)$ is given at the bottom of the next page, where α is the roll-off factor, and $0 \leq \alpha \leq 1$. As α approaches to zero, the pulse shape becomes closer to a rectangular.

Let $P_{\text{rc}}(f)$ represent the Fourier transform of the raised-cosine pulse. The time and frequency representations $p_{\text{rc}(t)}$ and $P_{\text{rc}}(f)$ of the raised-cosine pulse are shown in Fig. 2.

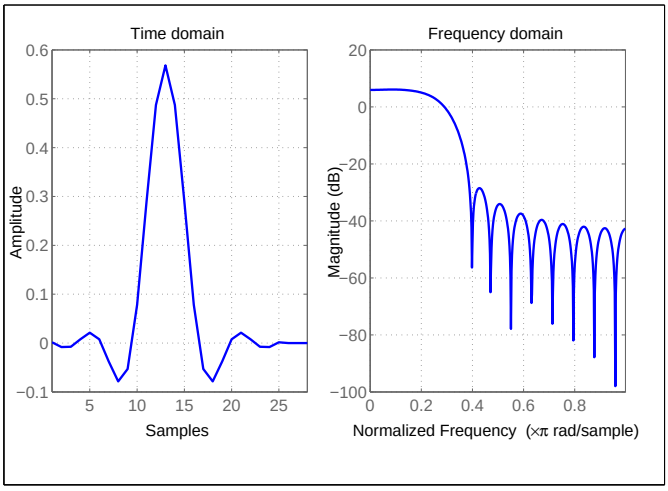

Fig. 2. Time and frequency domain representation of the raised-cosine pulse.

B. Better Than Raised Cosine Pulse

Recently, a new shape of pulse has been discovered that can increase the BER performance of the OFDM system [19], including reducing even further the ICI [20]. This pulse shape has been termed the *better than raised cosine* (BTRC) pulse. The mathematical expression for the time domain representation of the BTRC pulse is given at the bottom of the next page.

Fig. 3 shows the time domain representation of the pulse for three different values of α. At an α of 0.5, the BTRC

pulse samples are divided into three parts equally between the leading edge, the flat top and the trailing edge. At an α of 0m the BTRC pulse becomes a square wave. It can be observed that the BTRC pulse requires a large number of samples to achieve leading and trailing edges with detailed shape, and most of these samples are in the flat top. It is noted that both the raised-cosine and BTRC pulses collapse the rectangular pulse. The normalized frequency response of the BTRC pulse at $\alpha = 1$ is shown in Fig. 4.

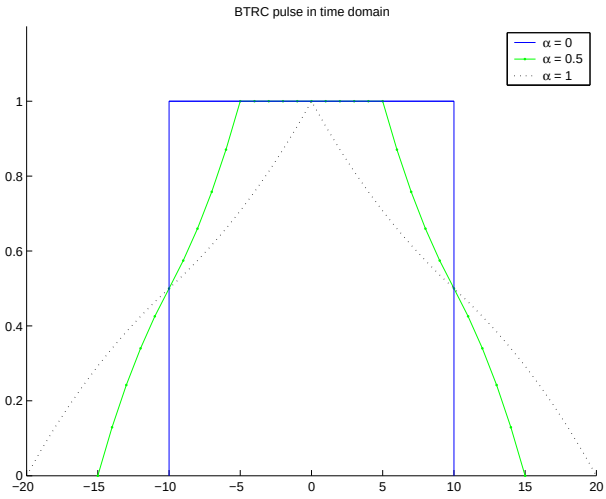

Fig. 3. Time domain representation of the better than raised-cosine pulse with three different α values.

Experimental and theoretical results indicate that $p_{\text{btrc}}(t)$ outperforms the rectangular and raised-cosine pulses in the reduction of the average ICI power. Calculations show that for a minimum average signal power to ICI ratio (SIR) of 25 dB, when using the raised-cosine pulse, the normalized frequency offset must be less than 0.1052. In contrast, the tolerable normalized frequency offset may be as large as 0.1844 when one uses the BTRC pulse.

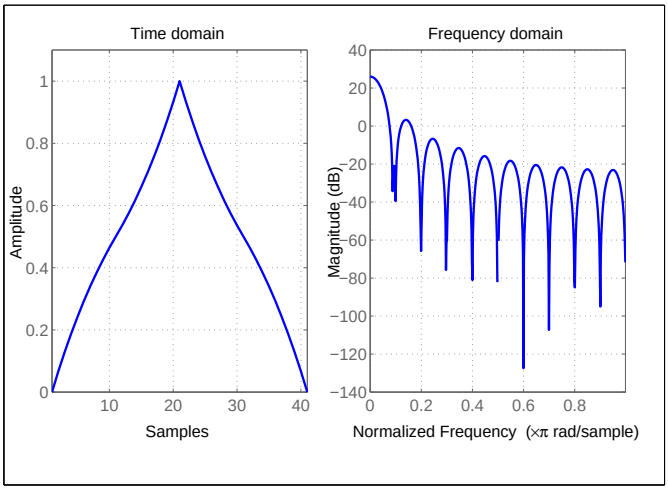

Fig. 4. Time and frequency domain representations of the better than raised-cosine pulse at $\alpha = 1$.

C. Duo-Binary

The duo-binary pulse is designed to minimize ISI in a band-limited channel (all real channels are band limited). This shape where controlled ISI is introduced is classified as a *partial response signal*. Its spectrum decays to zero smoothly [29].

The duo-binary pulse shape is given as follows

$$x(t) = sinc(2Wt) + sinc(2Wt - 1) \tag{11}$$

where W is the bandwidth and the $sinc$ function is defined as $\sin(x)/x$. A symbol rate of $2W$, being the Nyquist rate, is achieved thereby giving greater bandwidth efficiency compared to the raised cosine pulse.

The properties of this pulse can be further enhanced by precoding the signal using modulo two subtraction on the original data sequence to prevent error propagation during detection.

D. Triangular Pulse

Using an up-sampling rate of four samples on the BTRC pulse has the effect of reducing it to a triangular shape with

$$p_{\text{rc}}(t) = \begin{cases} \dfrac{1}{T}, & 0 \le |t| \le \frac{T(1-\alpha)}{2} \\ \dfrac{1}{2T}\left\{1 + \cos\left[\dfrac{\pi}{\alpha T}\left(|t| - \dfrac{T(1-\alpha)}{2}\right)\right]\right\}, & \frac{T(1-\alpha)}{2} \le |t| \le \frac{T(1+\alpha)}{2} \\ 0, & \text{otherwise.} \end{cases} \tag{9}$$

$$p_{\text{btrc}}(t) = \begin{cases} \dfrac{1}{T}, & 0 \le |t| \le \frac{T(1-\alpha)}{2} \\ \dfrac{1}{T} e^{\left(\frac{-2ln2}{\alpha T}\left(|t| - \frac{T(1-\alpha)}{2}\right)\right)}, & \frac{T(1-\alpha)}{2} \le |t| \le \frac{T}{2} \\ \dfrac{1}{T}\left\{1 - e^{\left(\frac{-2ln2}{\alpha T}\left(\frac{T(1+\alpha)}{2} - |t|\right)\right)}\right\}, & \frac{T}{2} \le |t| \le \frac{T(1+\alpha)}{2} \\ 0, & \text{otherwise.} \end{cases} \tag{10}$$

values of 0, 0.5, 1, 0.5, 0.

E. harris-Moerder Pulse

An improvement on the standard root raised-cosine (RRC) filter is the recently proposed harris-Moerder pulse [26]. This is an improved Nyquist pulse that reduces ISI by eliminating distortion associated with truncation of the standard RRC filter impulse response. The pulse is generated using the Parkes-McClelllan (or Remez) algorithm [26].

A comparison of the harris-Moerder pulse, using 20 symbols in the filter and specifying equi-ripple side lobes, with the standard root raised-cosine filter, is shown in Fig. 5.

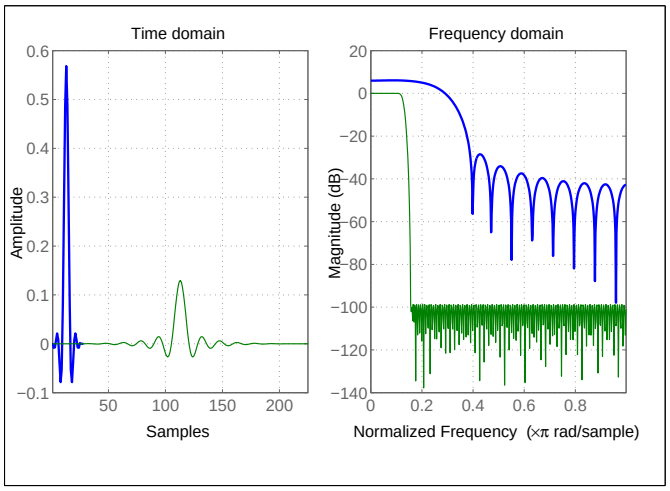

Fig. 5. Comparison of the harris-Moerder pulse (20 symbols, equiripple side lobes, green pulse on right) with a root raised cosine filter (left pulse in blue).

As will be shown in Section V, the harris-Moerder pulse will remarkably reduce ICI and thus improve the BER performance of the MIMO-OFDM system in comparison with other shaping pulses.

F. Equalization

ISI is caused by both channel distortion, which varies with time, and the overlapping raised cosine signal pulses after the receiver filter, which is a fixed amount set by the transmitter and receiver filters. The signal can be therefore be described by three components as follows

$$y_k = a_k + \sum_{\substack{n=0 \\ n \neq k}}^{\infty} a_n x_{k-n} + n_k \qquad (12)$$

where a_k represents the desired information symbol at the kth sampling instant, and n_k is the noise at the kth sampling instant. The middle term on the right hand side of (12) is the ISI term.

The fixed ISI renders the signal virtually unintelligible and needs to be removed. The simplest method to remove this fixed ISI is with a standard zero-forcing equalizer (ZFE). However, a ZFE equalizer has the serious disadvantage of amplifying noise. A minimum mean square error (MMSE) equalizer that tolerates a specified amount of ISI is used in the simulations as will be presented in Section V.

IV. Terrestrial Fading Channel Models

As aforementioned, the wireless fading channel in conjunction with pulse shaping has a considerable influence on the performance of the MIMO-OFDM communications system. In this section, we look into various terrestrial air channel models.

Terrestrial radio reception normally suffers degradation by fading due to multi-path reception of reflected signals that result in statistical cancelation or addition of the received signal. For simplicity, a radio channel is often modeled as a flat fading channel with independent identically distributed (i.i.d.) complex Gaussian coefficients. However, real channels are not so simple and the un-modeled parameters can have significant positive or negative effects depending upon the characteristics of the signal transmitted.

In a wireless fading channel with additive white Gaussian noise (AWGN), signals that do not include a direct path component follow a Rayleigh distribution, which means the square of the path gains are exponentially distributed. A Rayleigh distribution is therefore a more realistic air channel model than a basic Gaussian model.

The Rayleigh distribution is a specific case of the two parameter Weibull distribution [30]

$$f(T) = \beta/\eta \, (T/\eta)^{\beta-1} \, e^{-(T/\eta)^{\beta}} \qquad (13)$$

where the shape or slope parameter β equals two, and the scale parameter η is variable. As the ratio of the LOS signal power over the multi-path signal power increases (called the K factor), the Rician distribution tends to an AWGN distribution. As the ratio decreases, the Rician tends towards the Rayleigh distribution.

When the bandwidth of the transmitted signal is narrow enough to be within the coherence bandwidth, where all spectral components of the transmitted signal are subject to the same fading attenuation, then this ideal case is described as a flat fading channel. A channel is *slow fading* if the symbol period is much smaller than the coherence time, and *quasi-static* if the coherence time is in the order of a "block interval".[1]

It is obviously easier to compensate for fading in a flat channel than the one where fading is non-linear. Diversity techniques over fading channels non correlated in time, frequency and space are used to reduce the effects of fading and therefore improve the spectral efficiency of the air channel.

The following wireless fading channel models are used in our simulations.

A. Jakes Model

Practical models for mobile communications assume there are many multi-path components and all have the same Doppler spectrum with each multi-path component being itself

[1]It is noted, however, that different authors use considerably different definitions of a "block", some mean no fading over one whole transmitted frame while others mean over either one or even two sampled symbol periods. The simulation results in this work assume constant fading over one symbol period.

the sum of multiple rays. The first model to take into account both Doppler effects and amplitude fading effects was devised by Jakes in 1974 [31].

The Doppler effect of a moving receiver is described by the classical Jakes spectrum, which gives a "bathtub" shape of signal power against velocity, with singularities at the minimum and maximum Doppler frequencies. The basic Jakes channel fading model incorporating this Doppler shift simulates time correlated Rayleigh fading waveforms.

The model assumes that N equal strength waves arrive at a moving receiver with uniformly distributed angles, coming from 360° around the receiver antenna, as illustrated in Fig. 6. The fading waveforms can therefore be modeled with $N+1$ complex oscillators. This method, however, still creates unwanted correlation between waveform pairs.

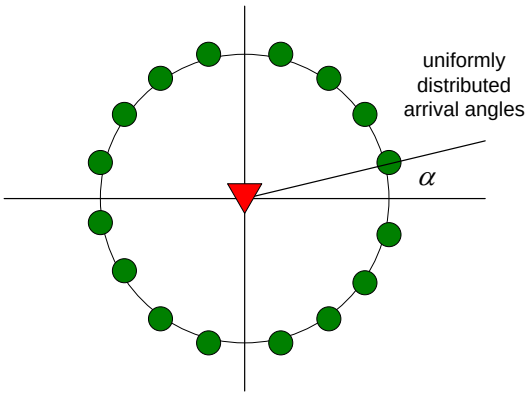

Fig. 6. Jakes model of multi-path interference.

B. Dent's Model

The unwanted correlation of Jake's model is removed in a modification by Dent *et al*. The unwanted correlation can be corrected by using orthogonal functions generated by Walsh-Hadamard codewords to weigh the oscillator values before summing so that each wave has equal power [32]. The weighting is achieved by adjusting the Jake's model so that the incoming waves have slightly different arrival angles α_n.

The modified Jakes model is given by

$$T(t) = \sqrt{\left(\frac{2}{N_0}\right)} \sum_{n=1}^{N_0} \left[\cos(\beta_n) + i\sin(\beta_n)\right] \cos(\omega_n t + \theta_n) \tag{14}$$

where the normalization factor $\sqrt{(2/N_0)}$ gives rise to $E\{T(t)T^*(t)\} = 1$, $N_0 = N/4$, $i = \sqrt{(-1)}$, $\beta_n = \pi * n/N_0$ is phase, θ is initial phase that can be randomized to provide different waveform realisations, and $\omega_n = \omega_M \cos(\alpha_n)$ is the Doppler shift.

Dent's model successfully generates uncorrelated fading waveforms thereby simulating a Rayleigh multi-path air channel. The "bathtub" shaped power spectrum distribution (PSD) of Rayleigh fading based on Dent's model is estimated by the periodogram as shown in Fig. 7. For an input data stream $x(n)$ that is a zero-mean, stationary random process and its discrete Fourier transform (DFT) denoted by $X(w)$, the periodogram is defined as $I(w) = |X(w)|^2/N$, where N is the data length.

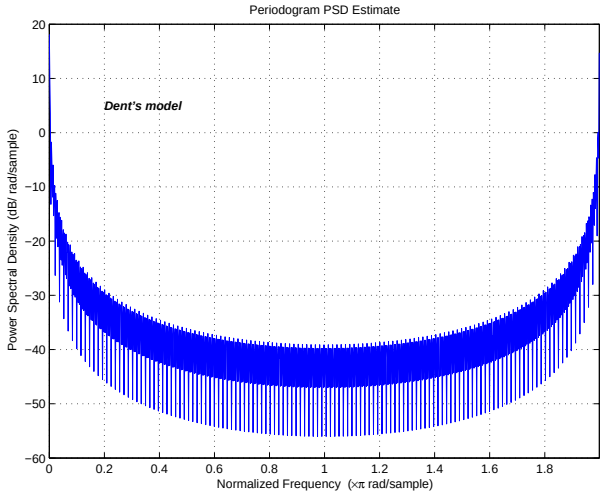

Fig. 7. Power spectrum distribution of Rayleigh fading using Dent's model.

C. Auto-regressive Model

Most fading models assume Rayleigh fading in an isotropic channel. However, this assumption is not always valid. In an attempt to add directional fading to the model, an autoregressive approach has been successfully developed in [33]. Furthermore, it has been proved that the classical Jakes model introduces fading signals that are not wide sense stationary, and the auto-regressive model remedies this shortcoming.

The periodogram of the autoregressive model, shown in Fig. 8, is still a "bath tub" shape, albeit with a narrower cut-off than Dent's model.

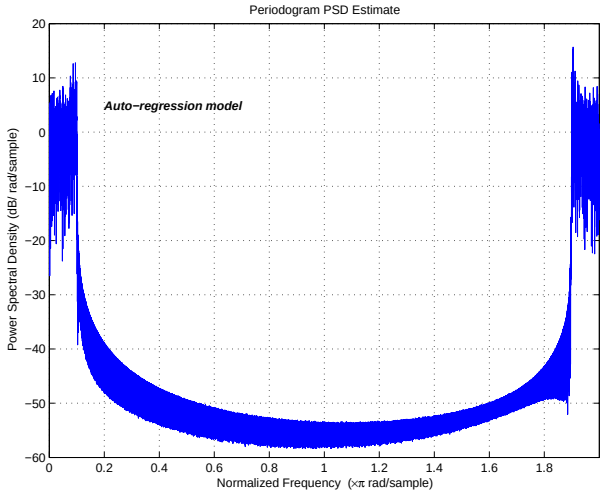

Fig. 8. Power spectrum distribution of Rayleigh fading using the auto-regressive model.

D. Stanford University Interim Models

For the purposes of the IEEE 802.16 standard on LAN/MAN air interfaces, the IEEE have adopted and modified a series of models called the Stanford University Interim (SUI) models [34]. These channel models for fixed wireless applications cover six scenarios of terrain and environment for the 1-4 GHz band.

The SUI models are different from the previous models since they assume time-variant (frequency-selective) channels. As a result, they need to be modeled with a *tapped delay line* in lieu of a more simple transfer function. Each tap represents the path of a different delayed frequency. Although there are theoretically an infinite number of frequencies, it has been found that modeling with three taps is accurate enough.

The SUI model differs from the simpler Rayleigh fading distribution in that it does not exhibit the typical Rayleigh PSD of the previous two models. The difference is most noticeable in the PSD estimate where the power spectral density at the high end of the spectrum does not increase asymptotically but instead tapers to zero forming a "half bathtub" shape, as shown in the periodogram Fig. 9.

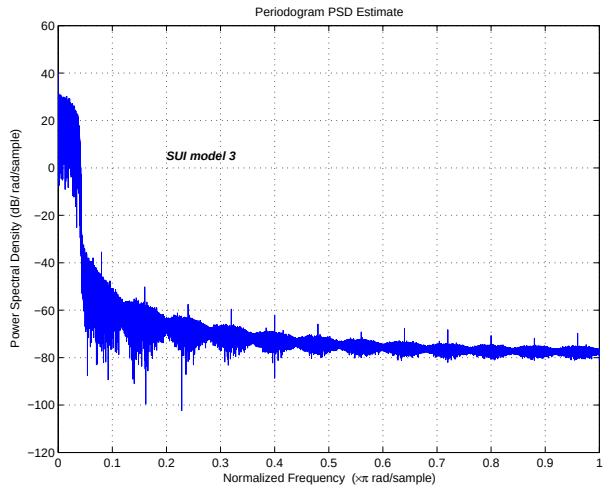

Fig. 9. SUI-3 PSD showing tapering at high frequency.

E. Tropospheric Model

The tropospheric (non-ionospheric) communications in the VHF (30 to 300 MHz) and UHF (300 MHz to 3 GHz) bands can cover several hundred kilometers. In these bands oxygen and water vapor absorb RF energy with the loss being dependent on frequency and atmospheric conditions such as humidity. The previous models would not be suitable for this environment. The frequency selective absorption characteristics can be modeled by a transfer function of the following form

$$H(f) = He^{j0.02096f[10^6+N(f)]l} \tag{15}$$

where $N(f)$ is the complex refractivity of the atmosphere in parts per million. The resulting channel model can be simulated using finite impulse response filtering techniques [35].

An example of a tropospheric model for microwave communication between fixed antenna towers is *Rummler's model*. This is a line of sight model with a very small number of multi-path components resulting in very slow fading [35].

The channel model becomes especially important in the case of designing MIMO algorithms since these are especially sensitive to the channel matrix properties. Some authors [36] caution that since results for realistic channels are still unknown the predicted gains of MIMO systems may be premature.

V. Simulation Results

In this section, we present experimental simulation results to demonstrate the performance improvements of shaping the coded MIMO-OFDM system using the various time-limited pulse shaping functions discussed in Section III. We will first show the the frequency responses of shaped OFDM sub-carriers using these shaping pulses, followed by the presentation of the BER curves to demonstrate the error performance of the MIMO-OFDM system over wireless fading channels.

A. System Configuration Parameters

The OFDM signals are generated with a 64-point IFFT, thereby givingv 64 sub-carriers conforming to the IEEE 802.11 standard. The baseband frequencies therefore range from 512 KHz to 32.8 MHz. Assuming a typical bandwidth of 16.56 MHz (as in 802.11a), the channel separation is $16.56/64 = 258.74$ KHz and the OFDM frame duration is 3.86 μs. To counter ISI, the cyclic prefix added is set at 25% of the OFDM block, thereby adding another 0.96 μs to the transmitted frame. The data bit frame length is 131072 bits, while the IQ symbol frame length is 524288.

Error detection and correction is performed by using a linear block coder of codeword length of 4 and parity length of 2. Optimum results for the MMSE equalizer are obtained experimentally by varying firstly the roll-off factor, a value of 0.495 is found optimum, and secondly varying the symbol noise power, a value of 6 is optimum. The optimum parameters are found by empirical try and error methods.

B. Frequency Spectrum of Shaped OFDM Signal

The frequency response of the OFDM sub-carrier signals at the transmitter after the IDFT modulation and shaping using a standard root raised-cosine filter is shown in Fig. 10. The filtered signal shows a sidelobe suppression of about 30 dB. At the receiver the signal was passed through a second root raised cosine pulse prior to input to the DFT demodulator. The resulting frequency response of a subcarrier is shown in Fig. 11.

The frequency response of the OFDM demodulated output, without shaping and with shaping using the raised-cosine pulse filter at the receiver *after* demodulation is shown in Figs. 12 and 13. With the shaped OFDM the 64 sub-carriers can clearly be seen approximately 20 dB above the noise, while in the unshaped signal, the subcarriers cannot be seen amongst the noise.

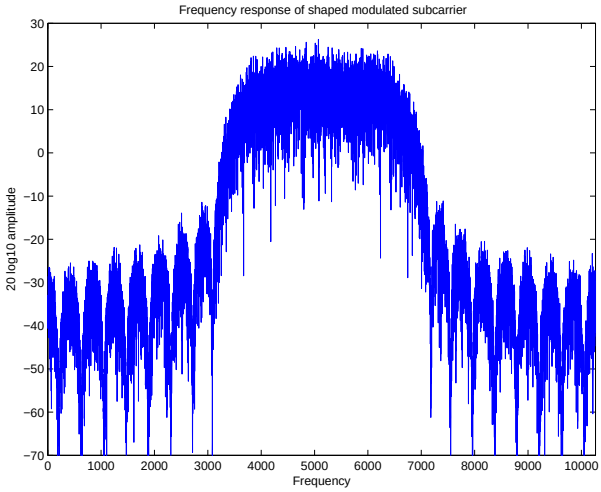

Fig. 10. Frequency response of the shaped OFDM signal at the transmitter using the root raised-cosine filter.

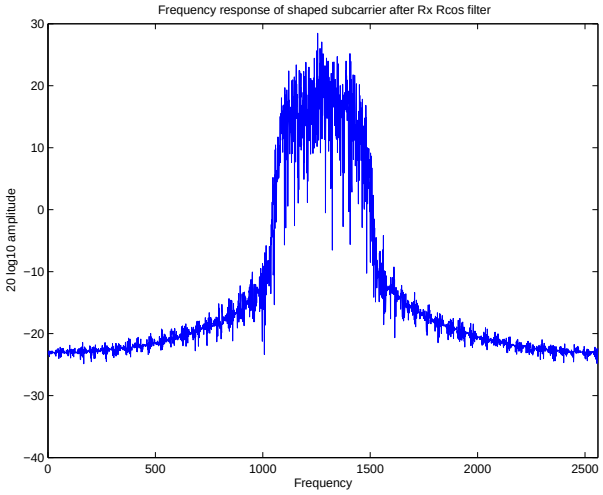

Fig. 11. Frequency response of the shaped OFDM signal after passing through the receiver root raised-cosine filter and before the the DFT.

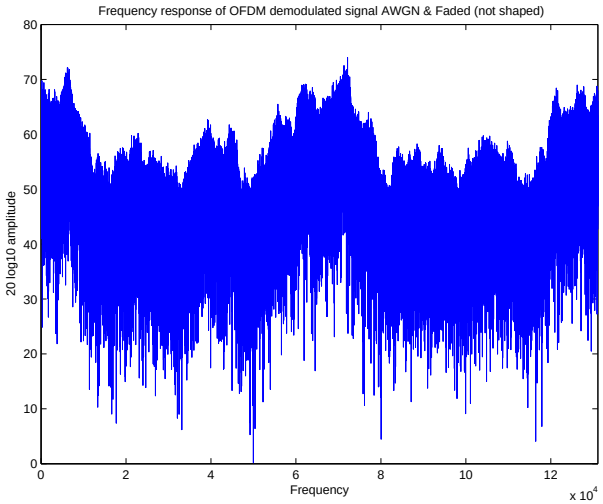

Fig. 12. Frequency response of demodulated (not-shaped) OFDM.

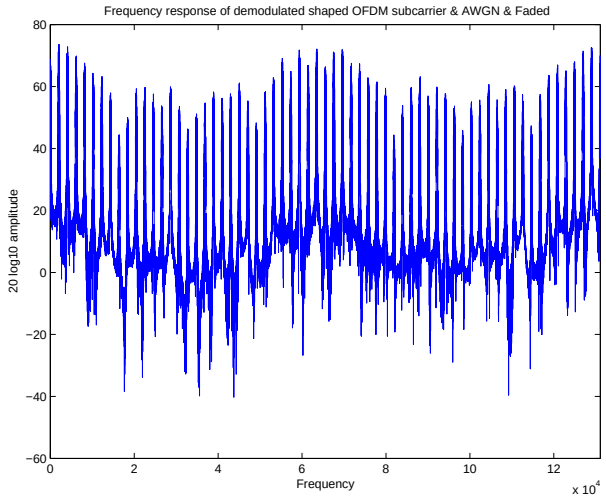

Fig. 13. Frequency response of demodulated shaped OFDM showing the sub-carriers.

The frequency response of an OFDM sub-carrier through a raised-cosine pulse is shown in Fig. 14, whereas the same pulse after equalization with five coefficients is shown in Fig. 15. The axes of the two plots are the same for comparison purposes. It can be observed how the MMSE equalization, using only five coefficients, suppresses the out of band sidelobes by about 40 dB.

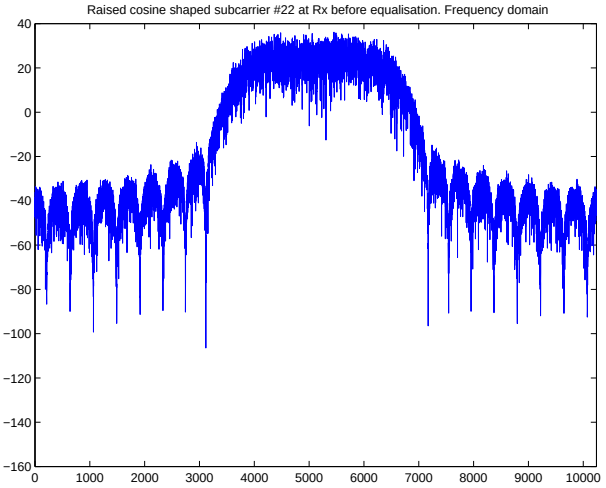

Fig. 14. Frequency response of raised-cosine shaped OFDM sub-carriers before equalization.

Figs. 16 and 17 show an OFDM sub-carrier shaped using the harris-Moerder pulse before equalization, and after equalization using seven equalization coefficients. The graphs have the same axis scales for comparison. The equalization can be seen to be very effective even though the MMSE equalizer uses less than half the number of coefficients as there are samples in the harrise-Moerder shaping pulse.

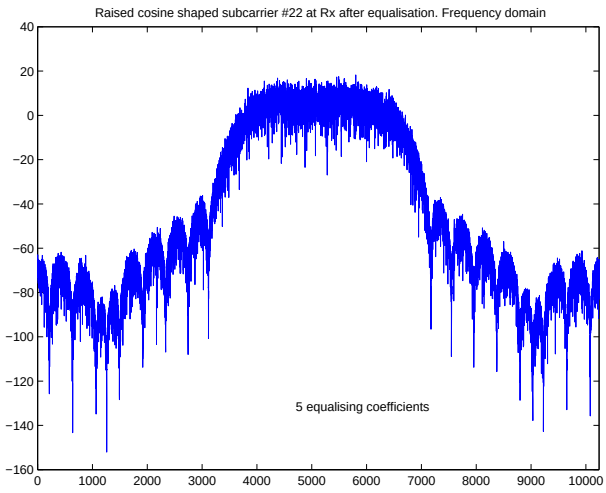

Fig. 15. Frequency response of raised-cosine shaped OFDM sub-carriers after equalization.

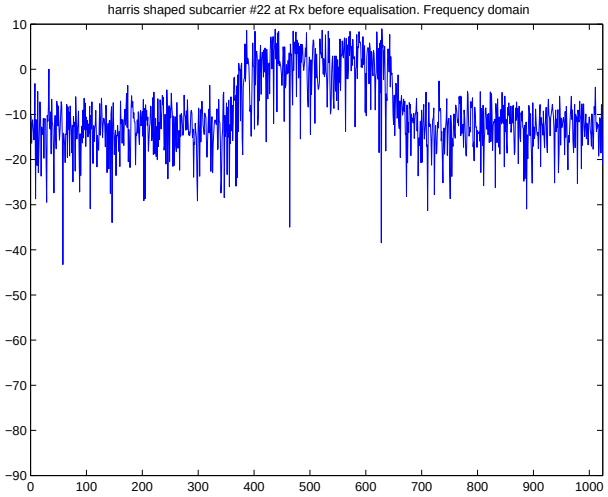

Fig. 16. OFDM sub-carrier no. 22 with `harris-Moerder` pulse (20 symbols, equi-ripple side lobes) before equalization.

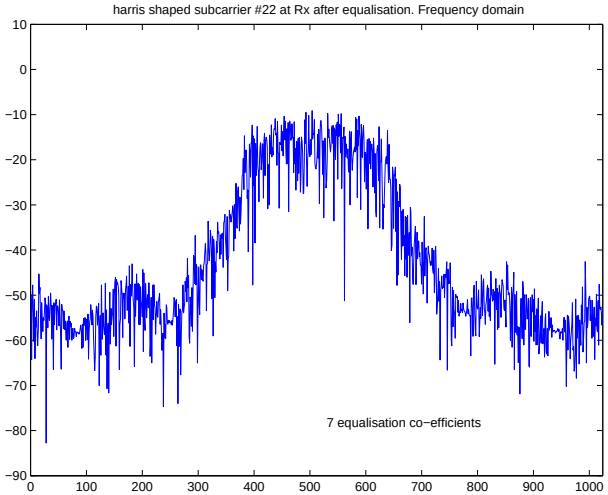

Fig. 17. `harris-Moerder` pulse equalized with seven coefficients (20 symbols, equiripple side lobes).

C. BER Performance Results

First of all, we plot several basic performance curves in Fig. 18 for the baseline MIMO-OFDM system using the Alamouti STBC scheme without pulse shaping.

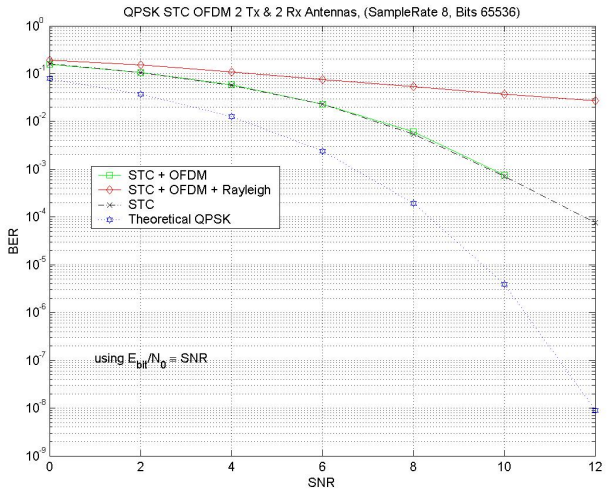

Fig. 18. Comparisons of the BER performance curves for STC, STC OFDM and STC OFDM under Rayleigh fading.

1) Raised Cosine and harris-Moerder Pulse Shaped OFDM: Shaping the OFDM pulse significantly improves the BER. As shown in Fig. 19, a Matlab designed raised cosine pulse, divided between the transmitter and receiver as root raised cosine filters, achieves about a 3 dB improvement over non shaped MIMO-OFDM. it can be seen that shaping with the harris-Moerder pulse at the transmitter increases the BER by more than 2 dB over raised cosine shaped MIMO-OFDM. The Rayleigh fading in these cases uses the auto-regressive model.

2) DuoBinary Pulse Shaped OFDM: The standard DuoBinary pulse, 61 samples long and equalised with the maximum number of coefficients (61) could not successfully be overlapped in the time domain when up-sampled by a factor of four. Fig. 20 shows the best results obtained, leveling out at an error rate of about 12% at an SNR around 6 dB.

Increasing the upsampling rate by double, to eight samples, gives better results, as shown in Fig. 21. However, curiously the BER curve for an AWGN channel follows the shape of a Rayleigh fading channel.

3) BTRC Pulse Shaped OFDM: The least successful pulse shape is the BTRC pulse. Equalisation is unsatisfactory, a greater upsampling rate is required than for other pulses meaning that it would be less practical to implement than other pulse shapes since sampling hardware would have to work at much higher speeds. Although this pulse shape was previously used successfully in OFDM to reduce the effects of unwanted frequency offset [37], the authors used an OFDM pulse length of the same length as the the BTRC pulse shaping filter. Additionally, since there was no time domain overlap there was no need to implement equalisation in their simulation.

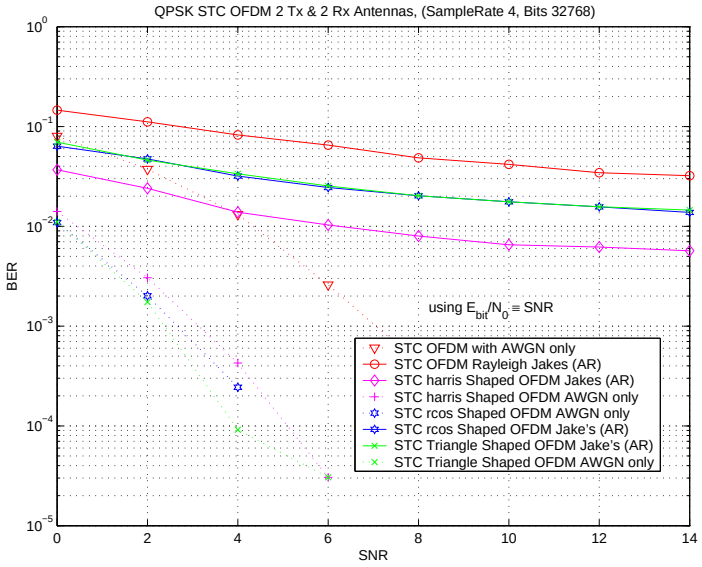

Fig. 19. Comparison of STC OFDM with AWGN only (not faded) with STC OFDM, STC Shaped OFDM (raised cosine), STC Shaped OFDM (harris-moerder) filter, equalized with 5 and 7 coefficients respectively, using the auto-regressive model of Rayleigh fading.

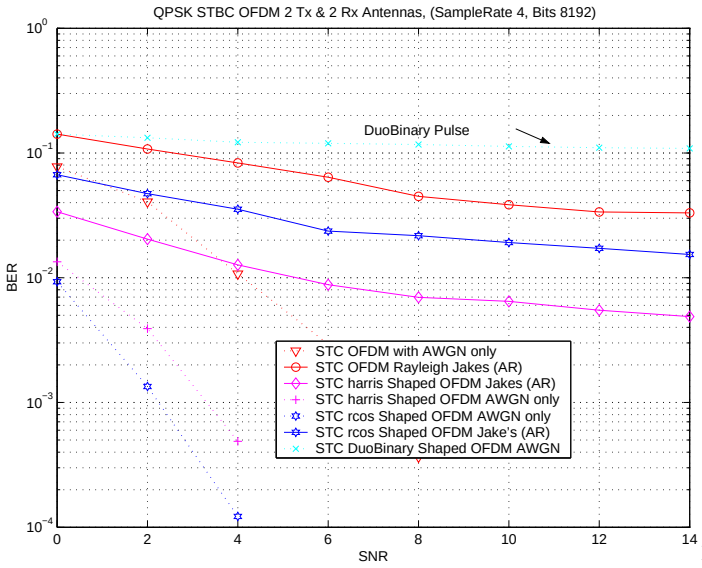

Fig. 20. DuoBinary pulse shaped OFDM with very high BER.

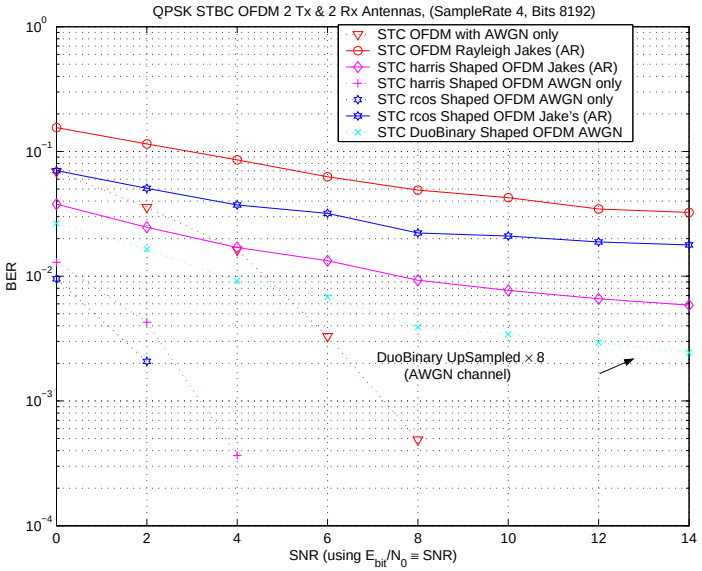

Fig. 21. DuoBinary pulse shaped OFDM upsampled by eight.

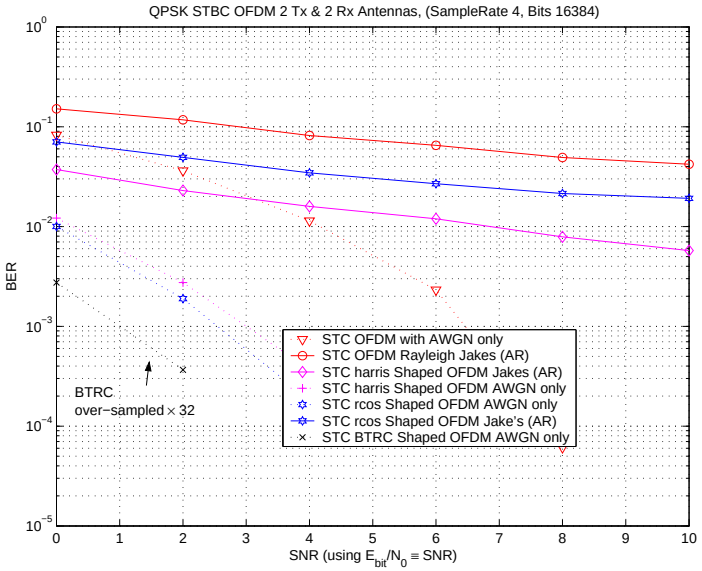

Fig. 22. Comparison of STC BTRC shaped OFDM (black line, alpha = 0.5 and upsampling by 32) with STC OFDM with AWGN only (not faded) with STC OFDM, STC shaped OFDM (raised cosine).

For an over-sampling of 8 and an α of 0.1 the BER curve still is not as good as unshaped STC OFDM in an AWGN channel. For the extreme case of an over sampling rate greater than the pulse width (therefore no time domain overlap) the BTRC gives the best results for an AWGN channel, as shown in Fig. 22. It should be noted that using the BTRC pulse in this manner is not a comparison under like conditions with the other modulation techniques.

4) Triangular Pulse Shaped OFDM: Modifying the BTRC pulse by truncating the long flat top of the pulse, and up-sampling at a rate four, inadvertently produced a triangular wave with values [0 0.5 1 0.5]. The BER of the triangular pulse were very similar to the raised cosine pulse at this sample rate, as shown in Fig. 23.

Not all possible variations of pulse shapes and equalisation parameters under different fading environments have been tested here. There may be versions that are optimised under some circumstances and not under others.

VI. Conclusions

In this paper, we investigate the efficacy of impulse shaping in reducing the ICI for the space-time block coded MIMO-OFDM communications system. Little existing work is known about the influence of pulse shaping for space-time coded

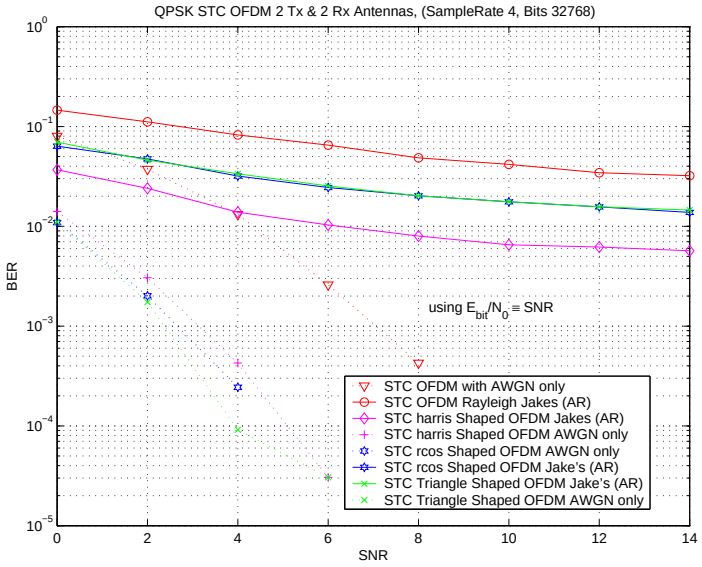

Fig. 23. Comparison of STC OFDM, STC shaped OFDM (raised cosine), STC Triangular shaped OFDM, STC shaped OFDM (harris-moerder), (under both AWGN and Jake's auto-regressive model of Rayleigh fading.

MIMO-OFDM systems. This work studies various shaping pulses and reports on their effect on alleviating the ICI for the MIMO-OFDM system. More importantly, we investigate the shaping performance of the new harris-Moerder pulse.

Simulation results are presented to demonstrate that shaping the OFDM pulse significantly improves on the system BER performance. Our results clearly indicate that the new harris-Moerder pulse outperforms other popular Nyquist pulses in the sense of improve the BER of the OFDM system. Moreover, the underlying channel model used has a significant effect on the BER.

The system could most likely be improved by adding further features, albeit at a cost of increasing the computational complexity. The optimum number of equalisation coefficients for each shape still needs to be determined. Adaptive pulse shaping by varying the parameters of the pulse shapes could also be explored for optimum performance in a time variant channel.

ACKNOWLEDGEMENT

We are grateful to Professor fred harris (sic) at San Diego State University for his assistance with the *harris-Moerder* pulse shape in this work.

This work is partly supported by the *International Science Linkages* established under the Australian Government's innovation statement *Backing Australia's Ability*.

REFERENCES

[1] J. Russell and W. Xiang, "Pulse shaping in MIMO COFDM over Rayleigh fading channels," in *Proc. International Conference on Wireless and Mobile Communications (ICWMC'09)*, Cannes, France, Aug. 2009, pp. 174-178.

[2] R. Prasad, *OFDM for Wireless Communications Systems*, Boston, M.A., Artech House, 2004.

[3] D. Gesbert, M. Shafi, D-S. Shiu, P. J. Smith, and A. Naguib, "From theory to practice: An overview of MIMO space-time coded wireless systems," *IEEE J. Sel. Areas Commun.*, vol. 21, no. 3, pp. 281-302, Apr. 2003.

[4] A. J. Paulraj, D. A. Gore, R. U. Nabar, and H. Bolcskei, "An overview of MIMO communications - a key to gigabit wireless," *Proc. IEEE*, vol. 92, no. 2, pp. 198-218, Feb. 2004.

[5] E. Telatar, "Capacity of multi-antenna Gaussian channels," *European Transactions on Telecommunications*, vol. 10, no. 6, pp. 585-595, Nov./Dec. 1999.

[6] G. J. Foschini, "Layered space-time architecture for wireless communication in a fading environment when using multi-element antennas," *Bell Labs Tech. J.*, vol. 1, no. 2, pp. 41-59, Autumn 1996.

[7] G. D. Golden, G. J. Foschini, and R. A. Valenzuela, "Detection algorithm and initial laboratory results using V-BLAST space-time communication architecture," *Electronics Letters*, vol. 35, no. 1, pp. 14-16, Jan. 1999.

[8] P. W. Wolniansky, G. J. Foschini, G. D. Golden, and R. A. Valenzuela, "V-BLAST: an architecture for realizing very high data rates over the rich-scattering wireless channel," *Proc. IEEE International Symposium on Signals, Systems, and Electronics (ISSSE'98)*, Pisa, Italy, Sep.-Oct. 1998, pp. 295-300.

[9] A. Benjebbour, H. Murata, and S. Yoshida, "Comparison of ordered successive receivers for space-time transmission," in *Proc. IEEE 54th Vehicular Technology Conference (VTC'01 Fall)*, Atlantic City, NJ, Oct. 2001, pp. 2053-2057.

[10] S. Alamouti, "A simple transmit diversity technique for wireless comminications," *IEEE J. Sel. Areas Commun.*, vol. 16, no. 8, pp. 1451-1458, Oct. 1998.

[11] V. Tarokh, H. Jafarkhani, and A. R. Calderbank, "Space-time block codes from orthogonal designs," *IEEE Trans. Inform. Theory*, vol. 45, no. 5, pp. 1456-1467, Jul. 1999.

[12] V. Tarokh, N. Seshadri, and A. R. Calderbank, "Space-time codes for high data rate wireless communication: Performance criterion and code construction," *IEEE Trans. Inform. Theory*, vol. 44, no. 2, pp. 744-765, Mar. 1998.

[13] G. L. Stüber, J. R. Barry, S. W. Mclaughlin, Y. Li, M. A. Ingram, and Thomas and G. Pratt, "Broadband MIMO-OFDM wireless communications," *Proc. IEEE*, vol. 92, no. 2, pp. 271-294, Feb. 2004.

[14] G. B. Giannakis, Z. Liu, X. Ma, and S. Zhou, *Space-Time Coding for Broadband Wireless Communications*, Hoboken, NJ, Wiley-Interscience, 2003.

[15] D. Vuletic, W. Lowdermilk, and f. harris, "Advantage and implementation considerations of shaped OFDM signals," in *Proc. 37th Asilomar Conference on Signals, Systems and Computers*, Pacific Grove, CA, Nov. 2003, pp. 683-687.

[16] I. Trigui, M. Siala, S. Affes, A. Stéphenne, and H. Boujemâa, "Optimum pulse shaping for OFDM/BFDM systems operating in time varying multi-path channels," in *Proc. IEEE Globecom'07*, Washington, DC, Nov. 2007, pp. 3817-3821.

[17] H. Bölcskei, "Efficient design of pulse shaping filters for OFDM systems," in *Proc. SPIE on Wavelet Applications in Signal and Image Processing VII*, Denver, CO, USA, Jul. 1999, pp. 625-636.

[18] J. Armstrong, "Analysis of new and existing methods of reducing intercarrier interference due to carrier frequency offset in OFDM," *IEEE Trans. Commun.*, vol. 47, pp. 365-369, Mar. 1999.

[19] N. C. Beaulieu, C. C. Tan, and M. O. Damen, "A 'better than' Nyquist pulse," *IEEE Commun. Lett.*, vol. 5, vol. 9, pp. 367-368, Sep. 2001.

[20] P. Tan and N. C. Beaulieu, "Reduced ICI in OFDM systems using the "better than" raised-cosine pulse," *IEEE Commun. Lett.*, vol. 8, vol. 3, pp. 135-137, Mar. 2004.

[21] H-A M. Mourad, "Reducing ICI in OFDM Systems using a proposed pulse shape," *Wireless Person. Commun.*, vol. 40, pp. 41-48, 2006.

[22] A. Assalini and A. M. Tonello, "Improved Nyquist pulses," *IEEE Commun. Lett.*, vol. 8, vol. 2, pp. 87-89, Feb. 2004.

[23] N. D. Alexandru and A. L. Onofrei, "ICI reduction in OFDM systems using phase modified sinc pulse," *Wireless Person. Commun.*, vol. 53, pp. 141-151, 2010.

[24] P. Tan and N. C. Beaulieu, "Analysis of the effects of Nyquist pulse-shaping on the performance of OFDM systems with carrier frequency offset," *European Transactions on Telecommunications*, vol. 20, pp. 9-22, 2009.

[25] L. E. Franks, "Further results on Nyquist's problem in pulse transmission," *IEEE Transactions Communications Technology*, vol. 16, no. 4, pp. 337-340, 1968.

[26] f. harris, C. Dick, S. Seshagiri, and K. Moerder, "An improved square-root Nyquist shaping filter," in *Proc. Software Defined Radio Technical Conference and Product Exposition*, Orange County, CA, Nov. 2005.

[27] T. Pollet, M. V. Bladel, and M. Moeneclaey, "BER sensitivity of OFDM systems to carrier frequency offset and Wiener phase noise," *IEEE Trans. Commun.*, vol. 43, no. 2/3/4, pp. 191-193, Feb./Mar./Apr. 1995.

[28] H. Nikookar and B. G. Negash, "Frequency offset sensitivity reduction of multicarrier transmission waveshaping," in *Proc. IEEE Conference on Personal Wireless Communications*, Hyderabad, India, Dec. 2000, pp. 444-448.

[29] J. Proakis and M. Salehi, *Digital Communications*, New York, McGraw-Hill, 2007.

[30] W. Weibull, "A statistical distribution function of wide applicability," *J. Appl. Mech.-Trans. ASME*, vol. 18, no. 3, pp. 293-297, 1951.

[31] W. C. Jakes, *Microwave Mobile Communications*, New York, John Wiley & Sons, 1976.

[32] P. Dent, G. E. Bottomley, and T. Croft, "Jakes fading model revisited," *Electron. Lett.*, vol. 29, vol. 13, pp. 1162-1163, Jun. 1993.

[33] K. E. Baddour and N. C. Beaulieu, "Autoregressive modeling for fading channel simulation," *IEEE Wireless Commun.*, vol. 4, no. 4, pp. 1650-1662, Jul. 2005.

[34] IEEE 802.16.3c-01/29r4, "Channel models for fixed wireless applications," *IEEE 802.16 Broadband Wireless Access Working Group*, Jul. 2001.

[35] W. Tranter, K. Shanmugan T. Rappaport, and K. Kosbar, *Communications Systems Simulation with Wireless Applications*, Upper Saddle River, NJ, Prentice Hall, 2004.

[36] M. Debbah and R. Müller, "MIMO channel modeling and the principle of maximim entropy," *IEEE Inf. Theory*, vol. 51, no. 5, pp. 1667-1690, May 2005.

[37] P. Tan and N. C. Beaulieu, "Improved BER performance in OFDM systems with frequency offset by novel pulse-shaping," in *Proc. IEEE Globecom'04*, Dallas, TX, Nov.-Dec. 2004, pp. 230-236.

Performance Comparative Study of eXtended Satellite Transport Protocol over Traditional Satellites Networks and Nanosatellite Constellations

Maria-Mihaela BURLACU
Dept. MIPS/GRTC, University of Haute Alsace
Colmar, France
e-mail: maria-mihaela.burlacu@uha.fr

Pascal LORENZ
Dept. MIPS/GRTC, University of Haute Alsace
Colmar, France
e-mail: lorenz@ieee.com

Joséphine KOHLENBERG
Dept. RST, IT/Télécom SudParis
Evry, France
e-mail: Josephine.Kohlenberg@it-sudparis.eu

Abstract*—The design of efficient communication mechanisms for small satellite networks is a challenging task, requiring the definition and implementations of specific protocols and architectures appropriate to space's critical conditions. In this paper, we have proposed a specific nanosatellite mission and we have evaluated various nanosatellite constellations, using SaVi simulator, in order to identify the best constellation which satisfies mission requirements in terms of coverage and minimal number of nanosatellites. Next, XSTP (eXtended Satellite Transport Protocol) has been identified as candidate protocol for nanosatellite networks. Foremost, we implement XSTP in NS-2 simulator. The simulations were done for LEO traditional satellite network and nanosatellite constellation respectively. Finally, through analysis and simulations in NS2, we evaluated the performance of XSTP over traditional satellite networks and nanosatellite networks. Also, we were interested to compare XSTP performance to some TCP clones, in case of a high BER environment. The specific scenarios, implementations aspects and simulation approaches are presented in detail along with the respective results.

Keywords - transport protocol; nanosatellite; constellation; STP; XSTP; simulation.

I. INTRODUCTION

Traditional satellite missions are extremely expensive to design, build, launch and operate. Consequently, both the space industry and the research community have started directing their attention to missions involving many, small, distributed and inexpensive satellites. Furthermore, many space projects in universities laboratories are focused on the development of micro-, nano- and pico-satellites for both scientific and educational purposes.

New concepts arise as small satellite domain imposes itself as a particular field. Therefore, the concept of constellation became popular because of its potential to perform coordinated measurements for remote control missions and its capacity of long-term mission. A satellite constellation is a group of similar satellites, with coordinated ground coverage, that are synchronized to orbit the Earth in some optimal way. Also, formation flying mission aims to replace a large satellite with a "virtual satellite" – a cluster of smaller satellites, flying in very precise relative positions.

Making small satellites more cost-effective demands new technologies that must be certified for spaceflight. Certainly, there is a higher risk associated with uncertified technology. Thus, a small satellite mission is the best way to perform a first flight verification.

The small satellite technology has opened a new era of satellite engineering by decreasing space mission cost, without reducing the performance. However, the biggest long-term challenge for the small satellite community is to develop a robust commercial market capable of industrializing the process of building small satellites.

The proliferation of low-cost, "micro-", "nano-" and "pico-satellite" missions in low-earth orbit has presented new challenges to the research community.

The unique challenges imposed by nanosatellite networks (e.g., onboard resources, limited communications opportunities, limited bandwidth, scalability, redundancy, power availability, high-speed node mobility, the type of communication among satellites, assigning or not a separate communication channel for positioning, timing and synchronization issues) requires us to revise communication protocol design, network management, and to consider novel routing mechanisms to accomplish "more with less".

In order to identify candidate protocols that can be used or adapted for small satellite networks, we conducted a study of routing mechanisms in traditional satellite network, Ad Hoc network and sensor networks. This study is part of PERSEUS (*Projet Etudiant de Recherche Spatiale Européen*

Universitaire et Scientifique) program, launched by CNES (*Centre National d'Etudes Spatiales*) in June 2005 [1, 2]. Based on this study, XSTP (eXtended Satellite Transport Protocol) has been identified as transport protocol targeted for small satellite constellations.

The main objective of this paper is to propose a dedicated nanosatellite constellation mission and a nanosatellite constellation model. Various nanosatellite constellation configurations have been evaluated in order to identify the optimal constellation which satisfies the mission objectives. Secondly, the performance of XSTP-probing mechanism, proposed by Maged E. Elaasar in paper [3] is evaluated, through NS2 simulations, in satellite network and nanosatellite network scenarios respectively.

The reminder of the paper is organized as follows. Section II describes the mission that we envisaged for our nanosatellite constellation. Then, Section III presents the nanosatellite network model that we proposed in order to accomplish our mission. Section IV briefly explains STP and XSTP protocols, with a point on XSTP-probing mechanism. The simulation configuration, the performance metrics and the implementation solution are described in Section V. Simulation results in terms of nanosatellite constellation configurations and XSTP performance are discussed in Section VI and Section VII. Finally, Section VIII concludes the paper.

II. MISSION DESCRIPTION

Worldwide, there are a lot of unexploited regions in terms of mineral resources. Indeed, the Simpson Desert (in Australia) is rich in uranium, the Sahara Desert is rich in iron ore and salt, the Atacama Desert (Chile) is rich in iron and copper ore. Therefore, it is highly likely that in the near future, industrial companies will exploit those areas for their precious wealth.

As mentioned in paper [1], the global demand for lithium, the lightweight metal used to make high-powered batteries for cell phones, laptops, and hybrid cars, is expected to triple in the next 15 years. Fifty to 70 percent of the world's supply of this critical mineral is contained in just one place – Bolivia's Uyuni salt flats, shown in Fig. 1.

The United States Geological Survey [5] says that 5.4 million tons of lithium could potentially be extracted in Bolivia, compared with 3 million in Chile, 1.1 million in China and just 410,000 in the United States.

Therefore, we focus on the Salar de Uyuni, the world's largest salt flat desert of 10,582 square kilometers. It is located in the southwest Bolivia (Fig. 1), near the crest of the Andes, and is elevated 3,656 meters above the mean sea level.

At present, the reserves of lithium are at the centre of the attentions of several multinationals, as well as the government. The latter intends to build its own pilot plant with a modest annual production of 1,200 tons of lithium and to increase it to 30,000 tons by 2012. [6]

Comibol, the state agency that oversees mining projects, is investing about $6 million in a small plant near the village of Río Grande on the edge of Salar de Uyuni, where it hopes to begin Bolivia's first industrial-scale effort to mine lithium from the white, moonlike landscape and process it into carbonate for batteries. [17]

Figure 1. Salar de Uyuni viewed from space, with Salar de Coipasa in the top left corner.

Considering this context, we propose to deploy a nanosatellite operator that provides communications services (voice, SMS and images) for an industrial company in charge of lithium resources exploitation in Salar de Uyuni desert. It is important to mention that this small satellites system can be applied to any similar remote area. Unless stated differently, in this paper, the term "nanosatellite" means any satellite with a mass of 50 kg.

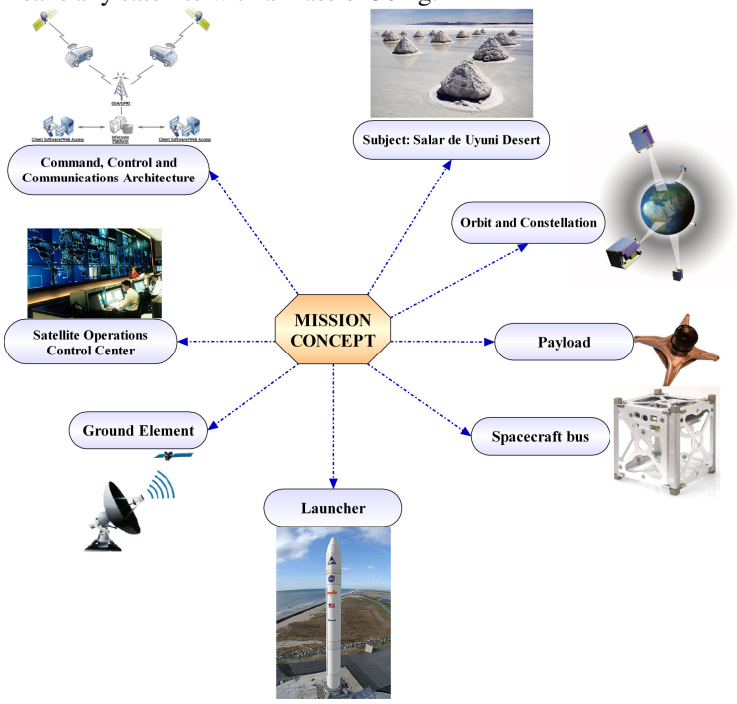

Figure 2. Mission concept basic elements.

Figure 2 presents all the elements of our mission, which implies high-level processes from mission analysis and design to cost estimation models.

Firstly, we have investigated the existing Bolivian mobile operators and theirs coverage areas. There are 3 mobile operators:

- Telefonica Celular De Bolivia S.A. (TELECEL BOLIVIA), operating within GSM850 band;
- Entel SA, operating within GSM1900 band;
- Nuevatel PCS De Bolivia SA, operating within GSM1900 band.

As seen in Fig. 3, 4 and 5, none of the operators have coverage over or close to the Salar de Uyuni desert.

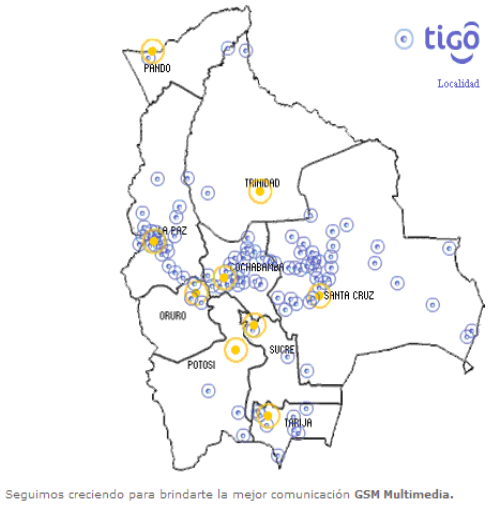

Figure 3. TELECEL BOLIVIA coverage map.

Figure 4. Entel SA coverage map (Credits : 2009 GSM Association; Europa Technologies Ltd.).

Figure 5. Nuevatel PCS De Bolivia SA coverage map (Credits : 2009 GSM Association; Europa Technologies Ltd.).

Secondly, an analysis of possible needs of the industrial company personnel yields the following requirements:

1. Continuous coverage of the target area (24h/24).
2. Mobile terminals with voice and data capabilities (e.g., voice, SMS, imaging).
3. Group Voice communications among on-site personnel.

The network architecture should be 'flexible' in that it is able to provide direct coverage to the area without having to go through a hierarchical command center.

Our system architecture is divided into three segments:

- Space segment is represented by the nanosatellite constellation;
- Ground segment is represented by Mobile Ground Station (or MGS). Based on the same principle as the i-c@r, used to provide WiFi Internet over a certain area via satellite, we can consider a similar, modified MGS, with an S-band transceiver to ensure the satellite link via a 3m wide satellite dish.
- User segment is represented by Mobile User Terminals (or MUT) with voice and data capabilities.

III. NANOSATELLITE CONSTELLATION MODEL

The design of a satellite constellation is very complex due to all the factors that need to be considered, from orbit elements to perturbations that act on each satellite.

Specifying all orbit elements for each satellite of the constellation is inconvenient and overwhelming. A reasonable approach is to begin with satellite constellation in circular orbits and at common inclination angle and altitude. In this case, the period, velocity and node rotation rate will be the same for all satellites.

The constellation size and structure has a strong impact on the system's cost and performance, so it is necessary to evaluate various constellation designs and to explain the reasons for final choice.

In paper [7], James R. Wertz states that if the regions of interest do not include the poles, then an equatorial constellation may provide all the coverage with a single orbital plane, which leads to flexibility, multiple performance plateaus and graceful degradation.

Thus, Salar de Uyuni desert is placed on 20º S latitude so, a constellation having several equatorial nanosatellites with enough altitude to provide the appropriate coverage at the smallest elevation angle (ε) is the best solution for our mission.

The formal mathematical problem definition could be written as:

Objectives: min *Ns* and max *Cov*

Constraints: Subject to

$$\textbf{Altitude } 500 \text{ Km} \leq h \leq 2000 \text{ Km}$$

$$\textbf{Minimum elevation angle } 5^{o} \leq \varepsilon_{min} \leq 30^{o}$$

Given: Latitude L = 20º S

Sun-synchronous, equatorial orbit

The purpose is to find the best constellation design which satisfies simultaneously the two mission objectives:

1. the number of nanosatellites has to be minimized;
2. the coverage of the desert has to be maximized (the nanosatellite has to stay as long as possible over the target area so, time in view need to be maximized).

We model our problem as a box with inputs and outputs. Therefore, some parameters are defined as input data for a constellation module (box) that will delivers output data. Fig. 6 illustrates key inputs and outputs of the constellation module.

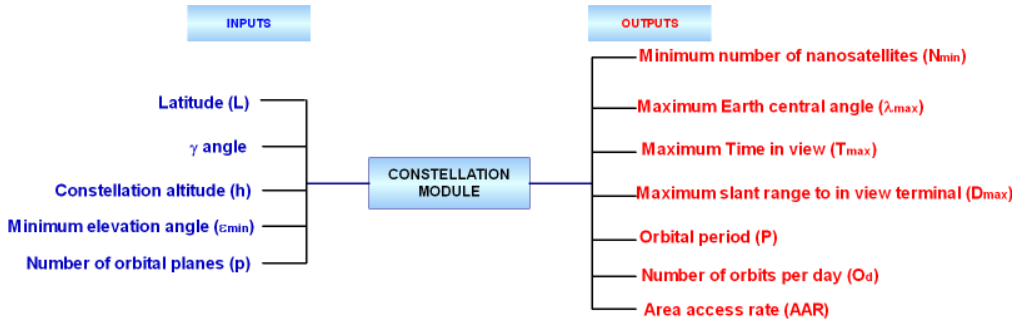

Figure 6. Inputs and outputs of constellation module.

Two vectors were defined: design vector and constants vector. The first one contains the attributes that will distinguish and differentiate alternative nanosatellite constellations. The latter contains attributes that will not differentiate alternative system architectures. For example, the latitude of Salar de Uyuni dessert is a constant value of 20º regardless of the other attributes of the architecture.

Six variables – minimum number of nanosatellites, constellation altitude, minimum elevation angle, number of satellites per orbital plane, number of orbital planes in the constellation, and maximum Time in view – make up the design vector.

Latitude (***L***), inclination angle (***i***) and ***γ*** angle are variables of constant vector.

Our nanosatellite constellation model includes some assumptions that simplify numerical calculations. We assumed that nanosatellites are placed on an equatorial, sun-synchronous LEO type orbit and it is passing near a target represented by a ground station. Also, we assume that Earth is a perfect sphere, an adequate assumption for most mission geometry applications. For precise calculation, a correction for oblateness must be applied. In our calculations, we neglected the Earth's rotation in the short period for which the nanosatellite passes over the interested area.

Figure 7 illustrates computational geometry of satellite.

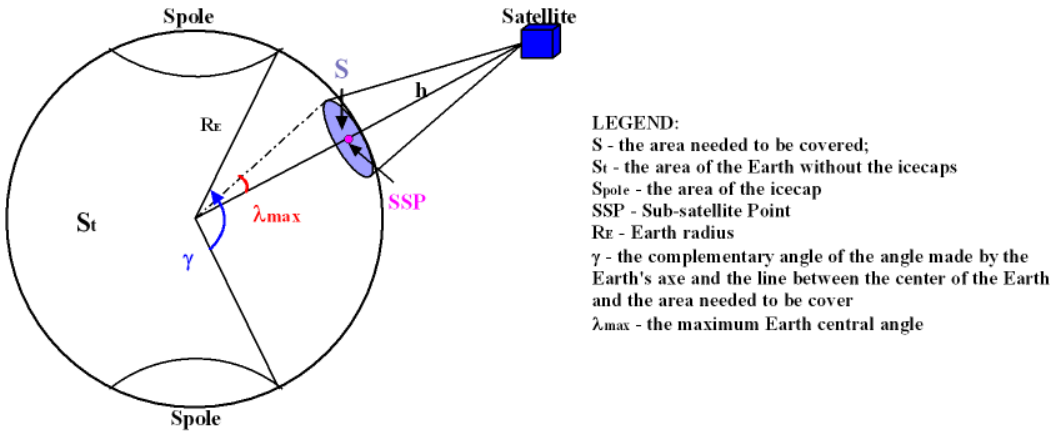

Figure 7. Computational geometry of satellite parameters.

According to Fig. 7, the area of the Earth, excluding icecaps is calculated as:

$$S_t = S_{Earth} - 2 \times S_{pole} \quad (1)$$

The Earth area is:

$$S_{Earth} = 4\pi R_E^2 \quad (2)$$

The area of every icecap is:

$$S_{pole} = 2\pi R_E^2 \times (1 - \cos\gamma) \quad (3)$$

By replacing Eq. 2 and Eq.3 in Eq. 1, we obtain:

$$S_t = 4\pi R_E^2 \times \cos\gamma \quad (4)$$

The area that needs to be covered is:

$$S = 2\pi R_E^2 \times (1 - \cos\lambda_{max}) \quad (5)$$

We estimated the minimum number of nanosatellites needed to cover the surface S as:

$$N_s = \frac{S_t}{S} \quad (6)$$

By replacing Eq. 4 and Eq. 5 in Eq. 6:

$$N_s = \frac{2\cos\gamma}{1-\cos\lambda_{max}} \quad (7)$$

As James R. Wertz states in paper [7], for communications, the satellite must be more than 5° above the horizon. In practice, we select a specific value of ε_{min} and we use this value. This parameter has a major influence on other computed parameters.

Given minimum elevation angle ε_{min}, we define the maximum Earth central angle λ_{max}, the maximum nadir angle η_{max}, measured at the satellite from nadir to the ground station and the maximum slant range D_{max} at which the satellite will still be in view. All these parameters are calculating using formulas presented in paper [15]:

$$\sin\eta_{max} = \sin\rho\cos\varepsilon_{min} \quad (8)$$

$$\lambda_{max} = arccos\left(\frac{R_E}{R_E+h}\cos\varepsilon_{min}\right) - \varepsilon_{min} \quad (9)$$

$$\eta_{max} = arcsin\left(\frac{R_E}{R_E+h}\cos\varepsilon_{min}\right) \quad (10)$$

$$\lambda_{max} = 90° - \varepsilon_{min} - \eta_{max} \quad (11)$$

$$D_{max} = R_E\frac{\sin\lambda_{max}}{\sin\eta_{max}} \quad (12)$$

The maximum time in view T_{max} for any point P on the surface of the Earth occurs when the satellite passes overhead:

$$T_{max} = P\frac{\lambda_{max}}{180°} \quad (13)$$

The orbit period P of each satellite may be calculated as a function of the constellation altitude h:

$$P = 1.658669 \times 10^{-4} \times (R_E + h)^{3/2} \quad (14)$$

The area access rate as the satellite sweeps over the ground for the target region is:

$$AAR = \frac{2K_A\times\sin\lambda}{P} \quad (15)$$

where K_A=2.55604187*10^8.

According to Eq. (7), (9) and (13), we observe some interesting variations useful for space segment dimensioning:

- the minimum number of nanosatellites is increasing as the minimum elevation angle is increasing, for the same altitude;
- for the same elevation angle, the minimum number of nanosatellites is decreasing as the altitude is increasing;
- the maximum time in view of any given point on Earth is increasing as the altitude is increasing, for the same elevation angle.

We have validated our nanosatellite network model with small satellites constellations currently in orbit. Two examples are important to be mentioned here: RapidEye constellation [15] and Disaster Monitoring Constellation (DMC) [16].

IV. STP AND XSTP OVERVIEW

This section discusses the Satellite Transport Protocol (STP) and explains the general design of XSTP protocol. There is a particular focus on XSTP-probing mechanism as it is most relevant to this paper.

A. Satellite Transport Protocol

The Satellite Transport Protocol (STP), proposed by Katz and Henderson [8, 9] is a transport protocol, which is specifically optimized for the unique constraints of satellite network environment. STP is found to outperform TCP in environments characterized by high BER, severe asymmetry and varying RTTs, typically characteristics of LEO satellite links.

Based on paper [4], the main features of STP can be summarized as follows:

- Enforcing the separation between data and control information in order to minimize the control overhead in smaller data segments;
- Mechanism that adapts to the amount of rate control required in the network, ranging from no rate control to explicit rate control. Unlike TCP, which uses a self-clocking property, STP depends on a delayed send timer to pace transmissions uniformly over the estimated RTT. The main benefit of the pacing mechanism is the reduction of the risk of introducing large bursts to the network.
- Segment type overloading for supporting a fast connection start mechanism.
- Efficient acknowledgement strategy
  STP employs an automatic repeat request (ARQ) mechanism that uses selective negative acknowledgements (NACK). By using this mechanism, only segments reported missing by receivers are retransmitted. The advantage is lower reverse link traffic when the loss is negligible and a speedy recovery when the loss is severe. In contrast with TCP, there is no RTO mechanism in STP, which makes it more resilient to RTT variations.

Finally, it is important to mention that even if STP includes many of the basic principles found in TCP, it is only functionally but not semantically equivalent to it. Unfortunately, the STP protocol inherits the congestion control bias from its ancestor protocols (i.e., TCP, SSCOP [10]). Although the protocol can efficiently recover from multiple losses in the same round trip, its error recovery tactics can negatively affect its overall performance.

B. eXtended Satellite Transport Protocol

XSTP is a software implementation of the STP protocol in the PIX (Protocol Implementation Framework for Linux) framework. [11] The protocol is used to host a new error control strategy, called XSTP-probing. Typically, XSTP protocol can be deployed on top of a network protocol (e.g., IP). The protocol provides a reliable connection-oriented byte streaming service to application protocols (e.g., FTP).

An XSTP session is composed of one lower and one upper session. Fig. 8 depicts a typical configuration for a

communication suite including XSTP. As Maged E. Elaasar explains in paper [3], when such a suite is initialized, an instance of the XSTP protocol is created, configured and then installed in the appropriate location in the protocol hierarchy. Once there, application level protocols can use the service of the protocol to manipulate XSTP sessions.

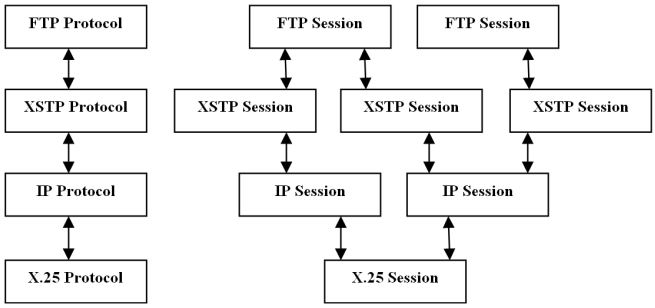

Figure 8. PIX protocol and session configurations including XSTP. [3]

An XSTP session plays double role (sender and receiver), which implies defining two new classes: an XSTP sender and an XSTP receiver. An instance of each of those classes is created in the private state of the session's object. As depicted in Fig. 9, these two instances play the sending and receiving roles of the session.

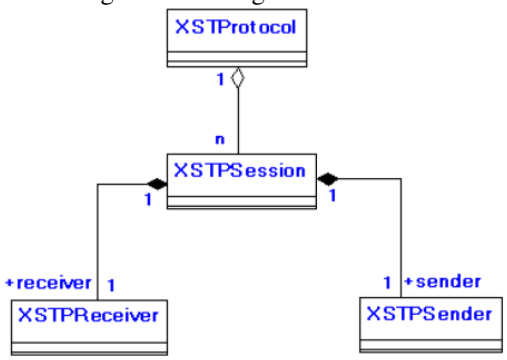

Figure 9. XSTP class diagram. [3]

C. XSTP-probing mechanism

The aim of developing the XSTP-probing mechanism was to stretch the STP protocol's ability to adapt to the different types of error found in LEO satellite networks.

According to papers [3, 4], the goal of any error control strategy is to adapt the sender's transmission rate to the varying error conditions in the network. This goal is usually accomplished by taking an aggressive attitude when the error is detected to be transient and a conservative one, when it is persistent. The XSTP-probing mechanism makes no exception to this principle.

The mechanism is triggered upon detecting a segment loss to assess the level of congestion in the network. If congestion is detected, the mechanism responds by invoking congestion control; otherwise, it resumes with *Immediate Recovery* (restoring congestion window to the same level as before probing).

Additionally, this mechanism evaluates the connection for possible error free conditions and only transmitting in those windows. As described in paper [4], it suspends new data transmission upon detecting a loss and initiates a probing cycle to collect RTT statistics on the connection. Then, it compares these RTT statistics to the RTT estimate available when the loss was discovered. It is interesting to observe that the duration of that probing cycle is proportional to the level of error in the network, which helps the connection sit out the error conditions. After the cycle is finished and if congestion is detected by proliferating RTTs, congestion control is immediately invoked. Otherwise, transmission levels are restored without taking any action. Finally, the missing segments are immediately retransmitted. Fig. 10 presents the basic algorithm of XSTP-probing mechanism.

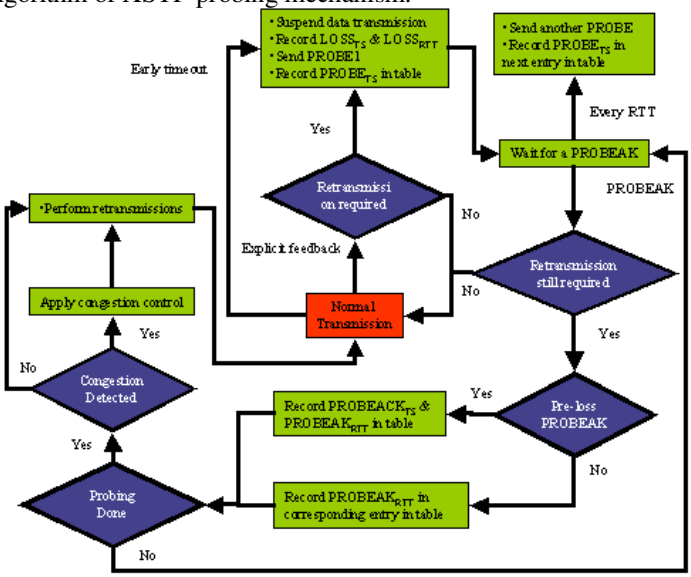

Figure 10. XSTP-probing mechanism.[3]

The XSTP–probing mechanism is implemented as a configurable option on the XSTP session. The mechanism is modeled as a class called XSTPProbing. For a more comprehensive overview of STP, XSTP and its probing mechanism, the interested reader is directed to papers [3] and [4].

V. SIMULATION CONFIGURATION

The performance of a protocol for varying network conditions and settings can effectively be evaluated using simulations. This section describes simulation environment, performance metrics and test scenarios.

A. Simulation environment

To analyze the performance of XSTP protocol, we have implemented the proposed protocol in the discrete-event network simulator NS-2 [12]. We used TCP modules corresponding to common variants of TCP (e.g., New Reno, Reno, SACK, Tahoe, Vegas), and wrote two new simulation modules for STP and XSTP.

We used SaVi simulator [13] for evaluating various nanosatellite constellations in terms of coverage area. SaVi

allows satellite orbits and coverage simulations, in two and three dimensions and is particularly useful for simulating satellite constellations.

B. Simulation scenarios

Using NS2 simulations, XSTP-probing mechanism is tested in various error conditions and performance is quantified.

We defined two scenarios – one-way communication, aiming to meet symmetric channels, and bidirectional communication for considering asymmetric channels. Each time, we quantify the performance metrics defined in Section V.E.

C. XSTP implementation solution

XSTP protocol is a derived class from STP class, the latter being derived from transport Agent class. Firstly, TCP like congestion mechanism is implemented. Then, we extended STP to XSTP by implementing the probing mechanism, described in Section IV.C, with 3 configuration parameters:

- Maximum number of trackable probe exchanges (MAX_PROB);
- Number of requested probe exchanges (REQ_PROB);
- RTT tolerance ratio (RTT_TOL).

The simulation configuration consists of 2 network nodes: source node and destination node. In the first scenario, the destination node is considered as a well of data, while in the second one, both endpoints are going to play the role of transmitter / receiver at the same time.

As Fig. 11 illustrates, we attach an XSTP agent to the source node and a STPSink agent to the destination node. Because an XSTP agent does not generate application data, we connected it to a FTP traffic generator so that we can send large data packets.

By using a background HTTP traffic generator, HTTP traffic is added for emulating the current use of WWW. The purpose was not to block the network, but to add a variability component to simulation.

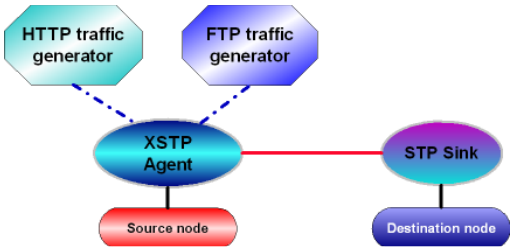

Figure 11. Nodes configuration.

The size of packages sent by the source node is 1000 bytes. The size of receiver's window is fixed to 200 and the initial size of transmitter's congestion window is 1. The maximum number of trackable probes is set to 4, and the number of consecutive RTT measurements sufficient to finish the probing cycle is set to 2. The polling frequency is set to 3 per RTT, and when the probing mechanism is triggered, the polling rate becomes 1 per RTT. The duration of every simulation is 60 seconds. The BER varies between 10^{-8} and 10^{-3}.

Due to the random behavior of the Web traffic, every simulation is repeated four times and the final results are calculated by making the average between the intermediate simulation results.

Table 1 presents the simulation parameters.

TABLE I. SIMULATION PARAMETERS

Parameter	*Value*
Sender buffer size	64 Kb
Receiver buffer size	64 Kb
MSS (maximum segment size)	1000 bytes
Maximum window size	64 segments
Sender's initial congestion window	1 segment
Maximum burst size	8 segments
Initial RTT	0.08 s

D. Simulation network topologies

For all the envisaged scenarios, we have used two network topologies:

- a satellite network (Fig. 12) based upon the LEO satellite constellation proposed by Teledesic [14];
- a nanosatellite network (Fig. 13) based on SaVi simulations and numerical results presented in Section VI.

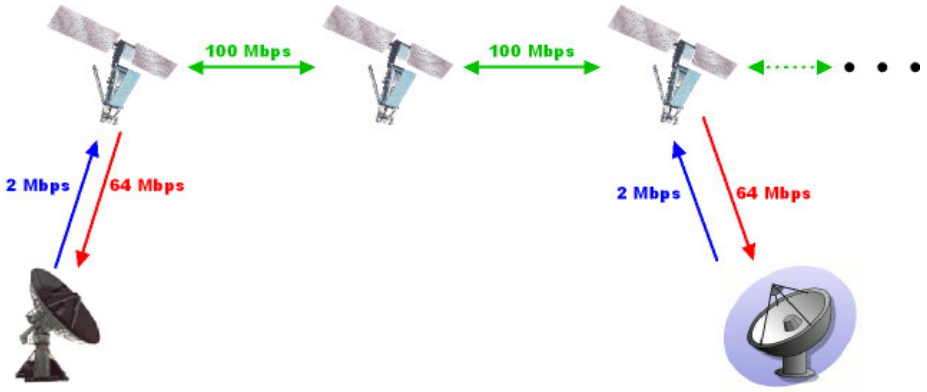

Figure 12. Satellite network model.

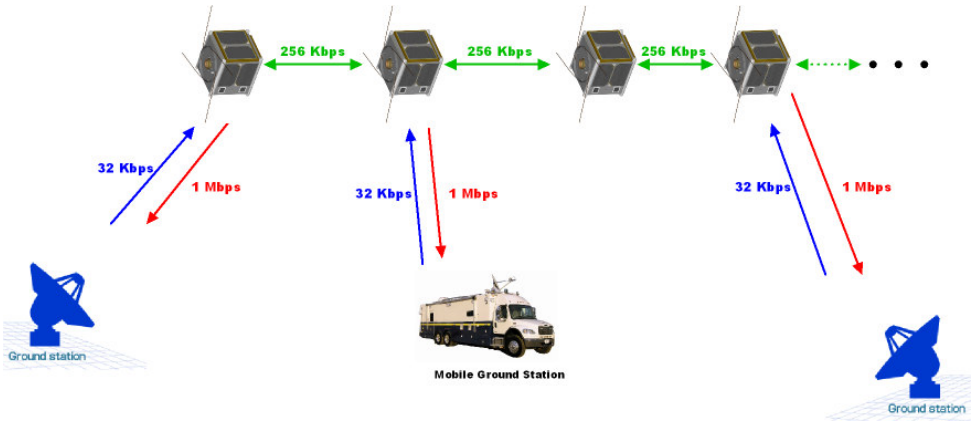

Figure 13. Nanosatellite network model

Table 2 presents the main constellations parameters, while table 3 summarizes data link parameters.

TABLE II. CONSTELLATION PARAMETERS

Parameter	*Satellite constellation*	*Nanosatellite constellation*
Nominal altitude	1375 km	1500 km
No. of planes	12	1
No. of satellites/plane	24	9
Planes separation distance in altitude	2 km	-
Nominal inclination	84.7 °	0º
Minimum Earth elevation angle	40º	15º
Orbital period	113.23 min	115.98 min

TABLE III. DATA LINK PARAMETERS

Parameter	*Satellite constellation*	*Nanosatellite constellation*
Uplink frequency	28.6 - 29.1 GHz	VHF, UHF
Downlink frequency	18.8- 19.3 GHz	S band (2-4GHz)
Uplink data rate	2 Mbps	32 Kbps
Downlink data rate	64Mbps	1 Mbps
Inter-satellite link (ISL) rate	100 Mbps	256 Kbps
ISL propagation delay	10 ms	50 ms
Ground-to-satellite link propagation delay	5 ms	15 ms

E. Performance metrics

The relevant performance metrics defined for NS2 simulations are based on paper [4]:

1) Effective throughput is defined as the average data rate (bps) as seen by the data link session and it is calculated using the following formula:

$$Effective\ throughput = \frac{original\ size}{simulation\ time} \quad (16)$$

2) Transmission overhead is defined as the percentage of extra bytes expended in the reliable transmission of the original data bytes. The transmission overhead is calculated, in %, using the following formula:

$$Transmission\ overhead = \frac{total\ size - original\ size}{original\ size} \times 100 \quad (17)$$

3) Efficiency describes the channel utilization. It is defined as the ratio between the packet original size and the total size of transmitted data:

$$Channel\ efficiency = \frac{original\ size}{total\ size} \quad (18)$$

4) Reverse channel utilization describes the backwards channel utilization. It shows the protocol efficiency on asymmetric links where the bandwidth is not the same in both directions. It is calculated using the following formula:

$$Reverse\ channel\ utilization = \frac{backward\ original\ size}{simulation\ time} \quad (19)$$

VI. SAVI SIMULATION RESULTS

This section presents SaVi simulation results in terms of coverage. Table 4 describes the parameters for four types of nanosatellite constellations simulated in our study. The numerical calculations of these parameters were made based on equations defined in Section III.

According to Table 4, we observe that constellation C_4 satisfies our mission objectives because:

- it has a minimum number of nanosatellites (9 nanosatellites);
- it offers a coverage band between 0º and 22º S latitude, thus assuring a total coverage of Salar de Uyuni Desert;
- the time in view of every nanosatellite is maximized.

Therefore, constellation C_4 has been implemented in NS2 for studying the XSTP performance over nanosatellite networks.

TABLE IV. CONSTELLATION CANDIDATES

Constellation	C_1	C_2	C_3	C_4
Minimum number of nanosatellites within the constellation (N_{min})	**18**	**14**	**14**	**9**
Coverage latitude	**0º - 18º**	**0º - 19º**	**0º - 20º**	**0º - 22º**
Maximum Time in view (T_{max})	**8.9 min**	**10.62 min**	**10.73 min**	**15.17 min**
Minimum elevation angle (ε_{min})	**15º**	**10º**	**15º**	**15º**
Number of orbital planes (N_p)	1	1	1	1
Constellation altitude (h)	800 km	800 km	1000 km	1500 km
Orbital period (P)	100.87min	100.87 min	105.11 min	115.98 min
Number of orbits per day (O_d)	14.23	14.23	13.66	12.38
Maximum slant range (D_{max})	2032 km	2367 km	2408.38 km	3258.45 km
Maximum Earth central angle (λ_{max})	15.87º	18.95º	18.38º	23.55º
Area Access Rate (AAR)	$1.38*10^6$ km^2/min	$1.645*10^6$ km^2/min	$1.53*10^6$ km^2/min	$1.76*10^6$ km^2/min
Nanosatellite velocity (v)	7.4561 m/s	7.4561 m/s	7.3507 m/s	7.1136 m/s

For Fig. 14 to 17, satellite coverage, represented in yellow/red, is intended to give an idea of the number of nanosatellites visible from a point on Earth. The higher the number of nanosatellites covering a point, the deeper the shade of red is. Also, coverage decay, illustrated in shades of blue, gives an idea of where a satellite footprint has been and is going, even when you look at a still map snapshot.

Constellation C_1 is constituted of 18 nanosatellites placed on an equatorial orbit at 800 km of altitude and having a minimum elevation angle of 15°. As seen in Fig 14, the coverage area will be between 0 and 18 ° of latitude S, but our target region is situated at 20° S latitude. Thus, this configuration does not satisfy our mission goal in terms of coverage.

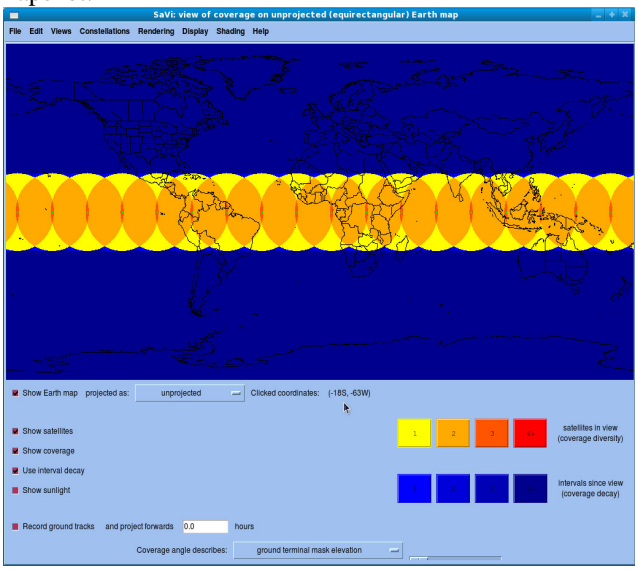

Figure 14. Coverage of nanosatellite constellation including 18 nanosatellites placed on a LEO, equatorial orbit at an altitude of 800 Km and minimum elevation angle of 15º

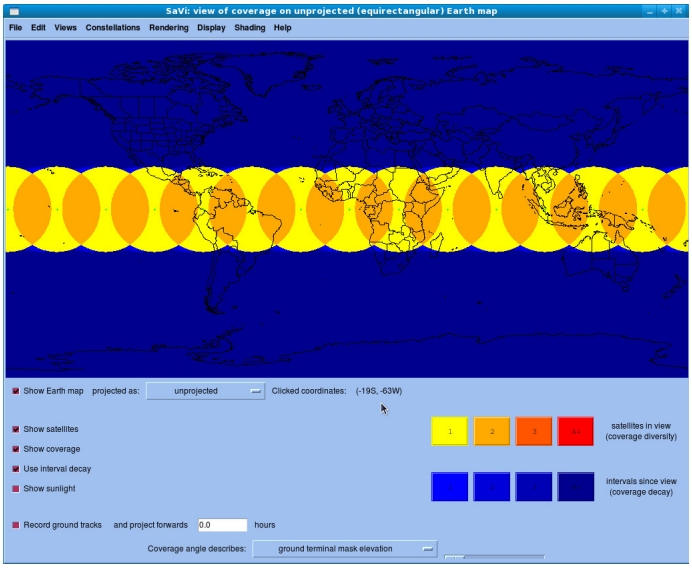

Figure 15. Coverage of nanosatellite constellation including 14 nanosatellites placed on a LEO, equatorial orbit at an altitude of 800 Km and minimum elevation angle of 10º

With the purpose of obtaining the desired coverage, we modified the minimum elevation angle of 10º and we obtained constellation C_2 of 14 nanosatellites placed at 800 km of altitude. Unfortunately, the coverage area (Fig. 15) will be between 0º and 19º S latitude, solution that still not corresponds to our mission. Additionally, this constellation might suffer of bad visibility, given the natural and manmade obstacles that would block nanosatellites at lower elevation angles out of view.

Knowing that Salar de Uyuni desert has a flat surface, we thought that a minimum elevation angle of 15º is sufficient to have visibility at any given point on the desert. Thus, a possible solution to our coverage problem seems to be constellation altitude increasing. By increasing altitude at 1000 km and for ε_{min}=15º, we obtain constellation C_3 of 14 nanosatellites (Fig. 16). This constellation defines a coverage band between 0º and 20º S latitude, solution that satisfy the second mission objective (the coverage), but not the first one (minimizing the number of nanosatellites within the constellation).

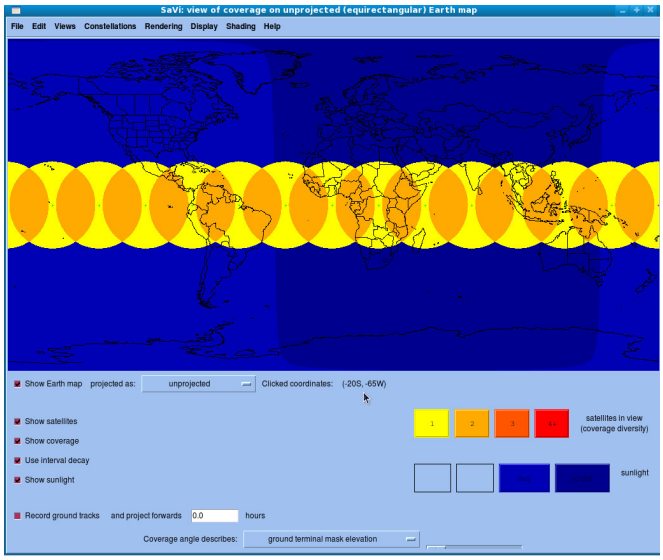

Figure 16. Coverage of nanosatellite constellation including 14 nanosatellites placed on a LEO, equatorial orbit at an altitude of 1000 Km and minimum elevation angle of 15°

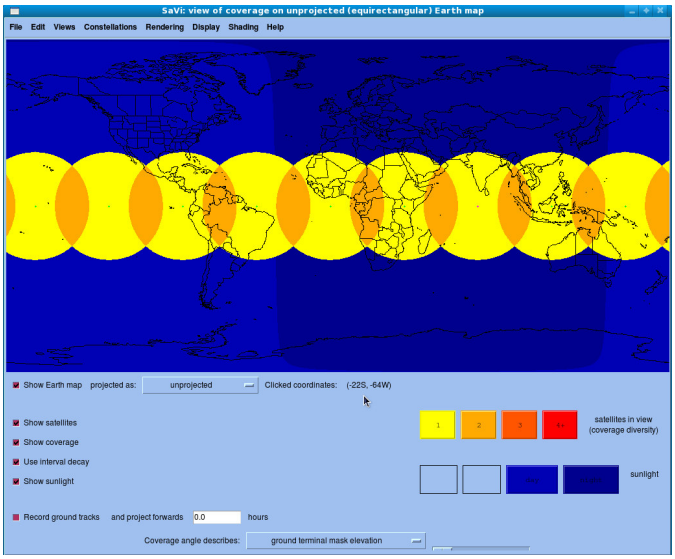

Figure 17. Coverage of nanosatellite constellation including 9 nanosatellites placed on a LEO, equatorial orbit at an altitude of 1500 Km and minimum elevation angle of 15°

Our numerical calculations have showed that the number of nanosatellites is decreasing with altitude increasing. Considering this type of variation and for minimizing the number of nanosatellites, a solution might be to increase constellation altitude to a value that satisfies our requirements. Thus, for an altitude of 1500 Km and ε_{min}=15°, we obtain constellation C_4 of 9 nanosatellites (Fig. 17), which is the best architecture that satisfy our two mission goals.

VII. NS2 SIMULATION RESULTS

In this section, NS2 simulation results for satellite network and nanosatellite network scenarios are reported and discussed. Also, we were interested to compare XSTP performance to some TCP clones, in case of a high BER environment.One-way transmission scenario

In this scenario we consider symmetric channels.

Fig. 18a and Fig. 18b illustrate effective throughput variation with respect to BER for satellite network and nanosatellite network respectively. For both networks, XSTP outperforms all TCP clones for high BER conditions (10^{-3}), mainly due to its probing mechanism. Unlike XSTP, STP and TCP clones reduce their transmission rate at every error detection.

In satellite network scenario, TCP Sack has a comparative throughput to STP and XSTP (roughly, 1400 Kbps) for low BER, but a significant difference is observed as BER increases.

Compared to satellite network case, in nanosatellite scenario, TCP Sack outperforms XSTP only for low BER environment. For high BER rates, XSTP assures 2 times more effective throughput than TCP clones. Also, TCP Vegas has the best performance among TCP clones due to its robust detection mechanism that minimize packet losses. We have also noticed that effective throughput of TCP clones is significantly reduced. The reason is that the latter make a processing operation after congestion detection, which is not the case of XSTP that makes the difference between an error due to congestion and an error due to transmission.

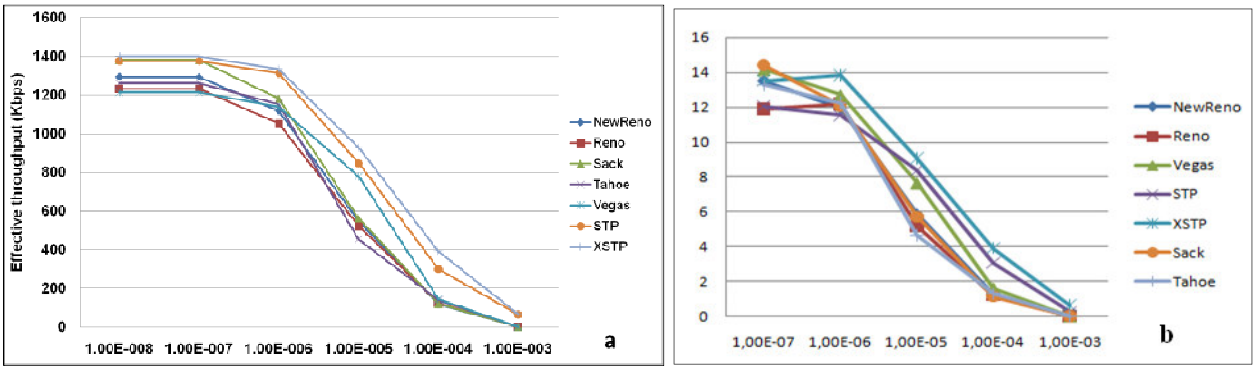

Figure 18. Effective throughput variation (one-way scenario): a) satellite network; b) nanosatellite network.

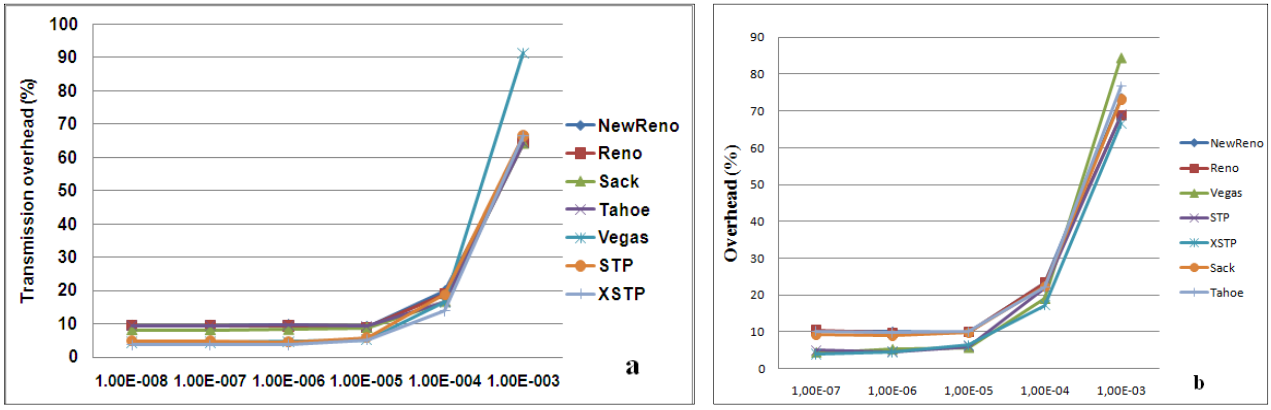

Figure 19. Transmission overhead variation (one-way scenario): a) satellite network; b) nanosatellite network.

Fig. 19a and Fig. 19b illustrates overhead variation as a function of BER for satellite network and nanosatellite network respectively.

Overhead packets are supplementary packets transmitted over the network. More the protocol is powerful less overhead packets are transmitted. Protocol designers have always tried to minimize the overhead. In the satellite networks domain, reducing overhead means minimizing the energy spent uselessly by the satellite, knowing that the energy used for overhead transmission is because the energy spent during overhead transmission is considered as lost energy. Considering this, our simulations shows that XSTP protocol consumes less energy than TCP clones for overhead transmission thus, it has more energy for data transmission.

According to Eq. (17) and Eq. (18), overhead test is complement to efficiency test. Unlike efficiency, the overhead increases with BER increasing.

During probing cycle, receiver sends one POLL per RTT and stops data transmission in order to avoid data losses, reducing this way the number of control packets. At the end of this cycle and if there is no congestion, sender doesn't reduce its congestion window; thus, it gives user the possibility to send much more data over the network.

Contrary, STP maintains 3 POLL per RTT and because it doesn't stop data transmission during polling cycle, the number of control packets increases due to successive losses. This is the raison why STP has much more overhead than XSTP.

As seen in Fig. 19a and Fig. 19b, XSTP has the lowest overhead, offering two times less than NewReno, Reno, Tahoe and Sack, in case of low BER conditions (10^{-8}–10^{-6}). We have also noticed that among TCP clones, TCP Vegas has the biggest overhead for high BER conditions and the lowest value for low BER. This means that its congestion control mechanism is better than other TCP mechanisms in a low BER environment.

One of the most important aspects in satellite networks is energy consumption. Researchers have always tried to minimize the energy spend by satellites for data transmission. Channel efficiency shows channel utilization. In case of significant amount of data user, efficiency is closed to 1, which means that channel is well used. Contrary, if efficiency is closed to 0, the channel is not well exploited.

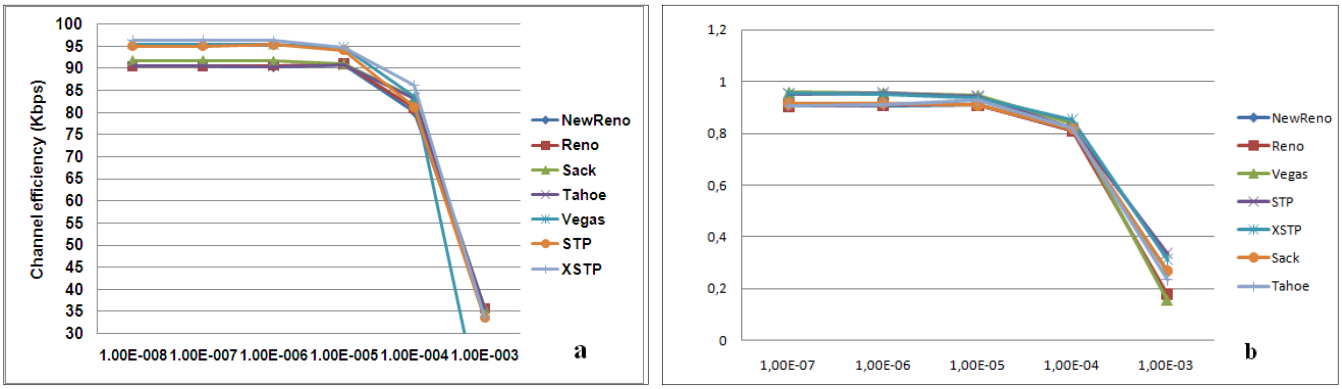

Figure 20. Channel efficiency (one-way scenario): a) satellite network; b) nanosatellite network.

According to Fig. 20a and Fig. 20b, STP and XSTP have a slightly higher performance than TCP clones for low BER conditions, thus exploiting better the communication channel. For both networks (i.e., satellite and nanosatellite), for high BER conditions (10^{-3}), TCP Vegas attains the lowest channel efficiency, which is four

times less than the other protocols. In other words, in high BER conditions, Vegas lose a lot of data packets.

Generally, reverse channel is used for ACKs transmission. Reverse channel bandwidth varies as a function of the number of ACKs transmitted over the channel, their type and size. It is important to mention that reverse channel bandwidth has to be minimized at the very most due to satellite link asymmetry.

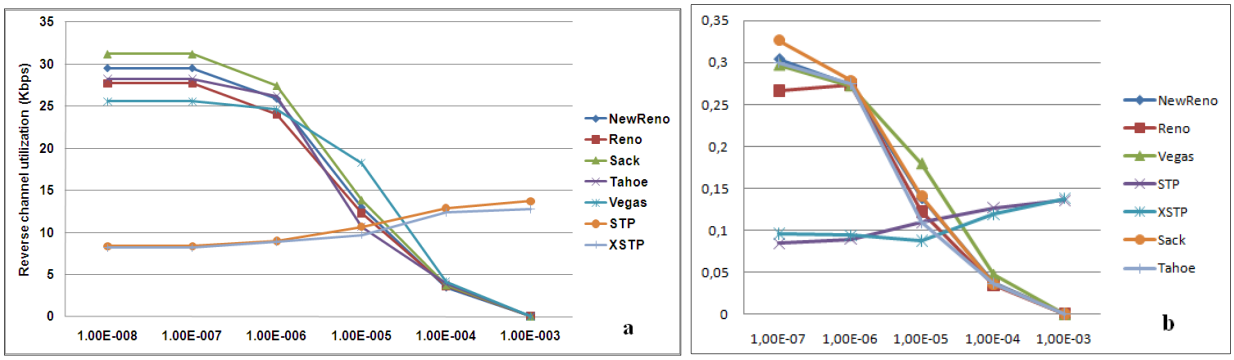

Figure 21. Reverse channel utilization (one-way scenario): a) satellite network; b) nanosatellite network.

Fig. 21a and Fig. 21b illustrates reverse channel variation with respect to BER for satellite and nanosatellite scenarios respectively. We have noticed that XSTP and STP bandwidth for reverse channel increases with BER increasing; this means that XSTP needs a low bandwidth for reverse channel. Instead, reverse channel bandwidth for TCP clones decreases with BER increasing. The explanation of these variations lies directly on every protocol's principle of using bandwidth.

In fact, TCP clones use reverse channel for acknowledgements transmission. Thus, the ACKs are sent when data packets are received, which explains why TCP clones use a lot of bandwidth in low BER conditions. In other words, if there are no losses, the reverse channel bandwidth is increasing as many packets are received. Contrary, in high BER conditions, receiver doesn't transmit many ACKs; therefore, reverse channel bandwidth decreases.

Unlike TCP clones, STP and XSTP send STAT and USTAT messages over the reverse channel. When BER is low, receiver sends many small size STAT messages that demand a low reverse channel bandwidth. For high BER, reverse channel utilization is significant due to large size USTAT messages that demand a lot of bandwidth.

An important remark is that XSTP needs a lower reverse channel bandwidth than STP because the number of STAT messages transmitted during probing cycle is decreasing as the number of POLL per RTT decreases (1 STAT message per POLL).

In case of STP, the number of POLL per RTT remains unchanged (i.e., 3 POLL per RTT) during Polling cycle. Because STP doesn't suspend transmission, it sends many USTAT messages even when BER is high.

A. *Bidirectional transmission scenario*

In this scenario, data transmission is made in both ways (a node is sender and receiver too). As compare to one-way communication case, data rate of all protocols decreases because of reverse path transmission.

XSTP effective throughput has a smoothness decrease as compare to one-way scenario.

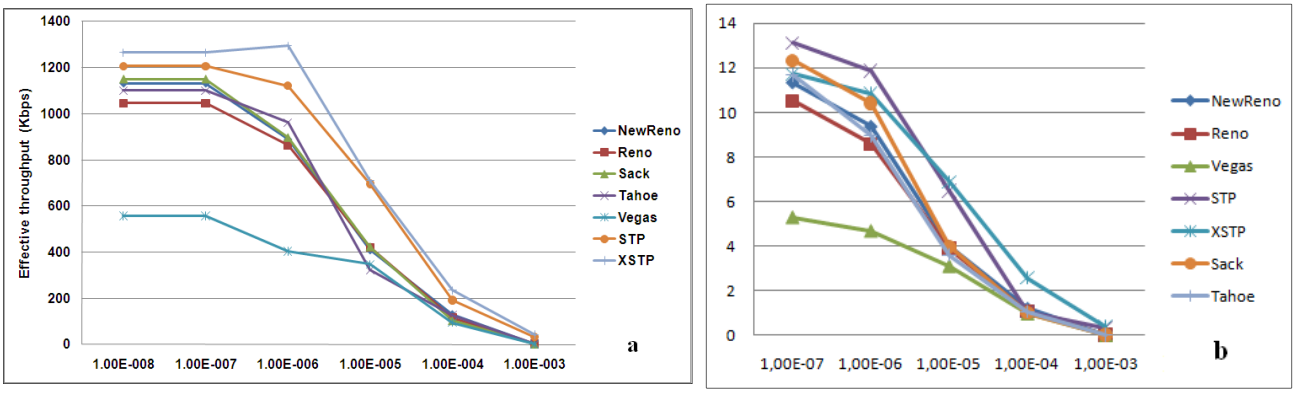

Figure 22. Effective throughput variation (bidirectional scenario): a) satellite network; b) nanosatellite network.

As seen in Fig. 22a, XSTP has a comparative performance with STP and TCP clones for low BER conditions. Instead, XSTP outperforms all TCP clones in case of high BER (10^{-3}), by offering an effective throughput almost 30 times more than TCP clones.

In nanosatellite scenario (Fig. 22b), STP attains the best performance for low BER environment (10^{-7}). For example, the effective throughput of STP is better than TCP Sack because STP doesn't use a timeout for ACKs reception.

For both network types considered in our simulations, we have also observed that TCP Vegas is strongly influenced by reverse path transmission, having, even in low BER conditions, a data rate 3 times less than the other protocols.

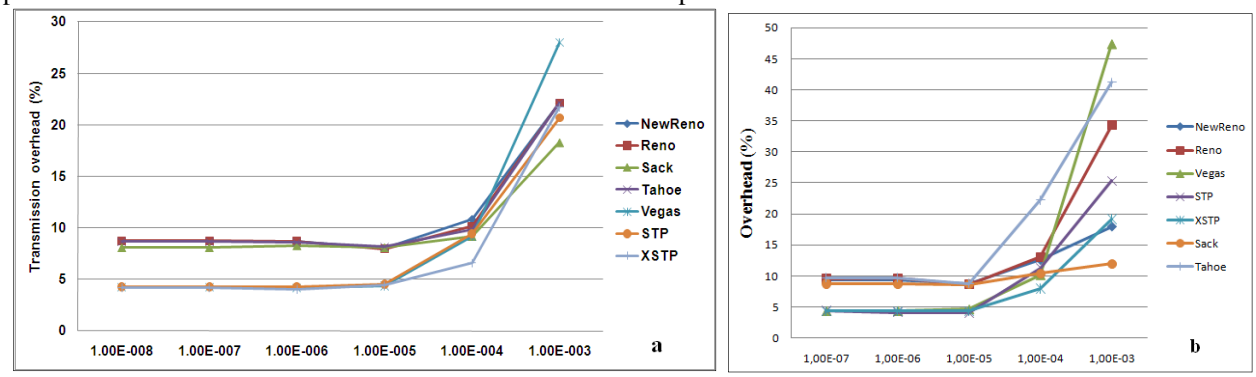

Figure 23. Transmission overhead variation (bidirectional scenario): a) satellite network; b) nanosatellite network.

In case of satellite network, by comparing Fig. 19a and Fig. 23a, we observed that XSTP offers 3 times less overhead than in one-way scenario, for high BER conditions. Also, all protocols have almost the same performance for high bit error rates, except for Vegas which still has the worst performance.

For nanosatellite scenario (Fig. 23b), STP, XSTP and Vegas attain an overhead two times less than the other protocols for low BER (10^{-7} – 10^{-5}). Instead, for high BER (10^{-3}), TCP Sack offers the lowest overhead, which is 2 times less than STP and 0.6 times less than XSTP.

The main difference is that the overhead does not increase as much as in one-way transmission when the BER is very high. This is due to the fact that all protocols decrease their transmission rate when there are other transmissions on the reverse channel.

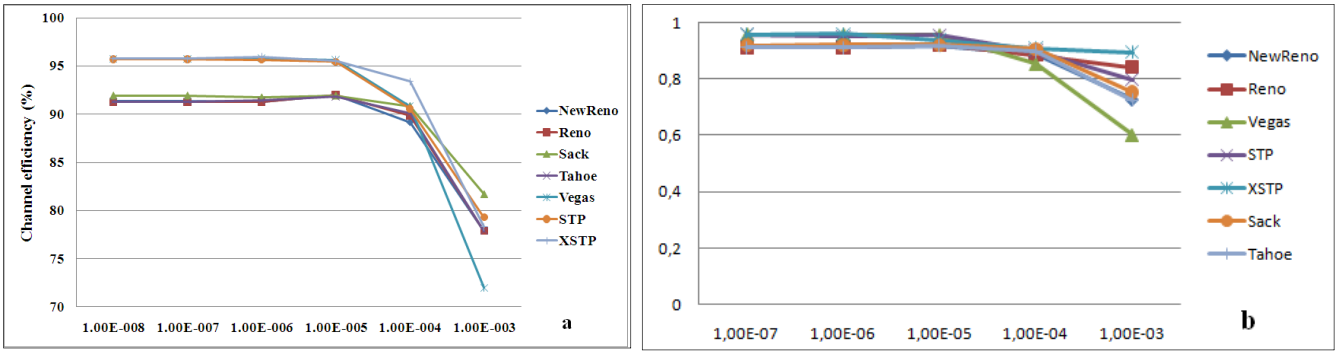

Figure 24. Channel efficiency (bidirectional scenario): a) satellite network; b) nanosatellite network.

Figure 24 presents channel efficiency variation with respect to BER for satellite network and nanosatellite network respectively. XSTP remains the best protocol with regard to STP and TCP clones.

Considering satellite network case (Fig. 20a and Fig. 24a), we observe a significant improvement of XSTP efficiency with respect to the first scenario (78% versus 33%), for high BER conditions (10^{-3}). Same trend is seen for nanosatellite network scenario (Fig. 20b and Fig. 24b), where XSTP efficiency is 3 times more in bidirectional transmission for BER=10^{-3}.

Our simulations have shown that, in high BER environment, XSTP efficiency for nanosatellite network is better than in case of conventional satellite network (90% versus 78%).

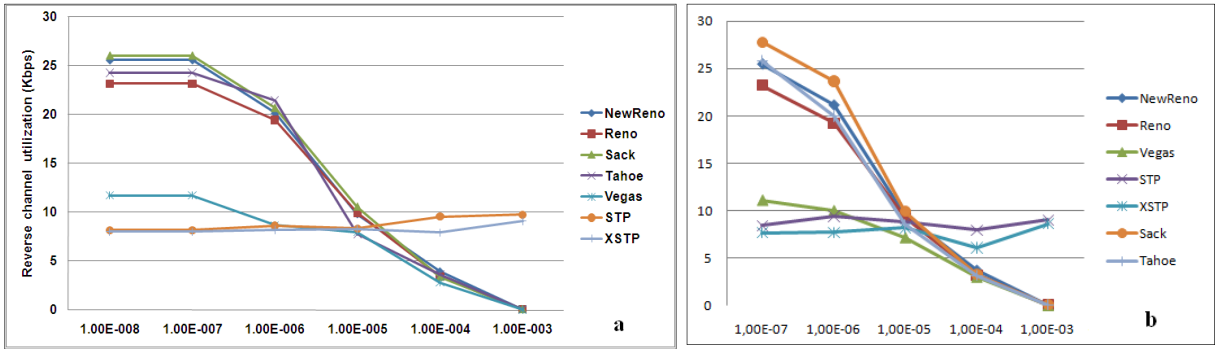

Figure 25. Reverse channel utilization (bidirectional scenario): a) satellite network; b) nanosatellite network.

Generally, all the explanations given for one-way scenario remains valid. We have noticed that the curves follow the same shape as in the one-way transmission, by regarding Fig. 21 and Fig. 25. TCP Sack uses a lot of bandwidth for reverse channel. Interestingly, TCP Vegas uses a low reverse channel bandwidth (2.83 Kbps), for high BER conditions, performing much better than STP and XSTP (Fig. 13a).

VIII. CONCLUSION AND FUTURE WORK

In this paper, we have proposed a small satellite mission intended to deploy a nanosatellite network over a specific desert region (Salar de Uyuni Desert). Also, a nanosatellite constellation model is proposed for the envisaged mission. Several nanosatellite constellations are simulated and analyzed in order to find the best nanosatellite configuration which responds to our mission objectives.

After STP and XSTP protocol description, we presented simulation results of XSTP implementation for a conventional satellite network and nanosatellite network respectively. According to our simulations, XSTP has shown its efficiency by proving that it is useless to continue data transmission during loss detection and to invoke directly congestion control procedure, which induces a degradation of effective bandwidth. Also, XSTP attained higher effective throughput, much lower overhead, and better channel efficiency as compare to TCP clones. In spite of all these performances, XSTP protocol for satellite networks is not perfect. We propose here some future research guidelines concerning XSTP protocol. We observed that transmission overhead on the return channel is significant in high BER conditions (10^{-3}) and this need to be reduced. Also, at the probing-mechanism level, the decision principle needs to be improved in order to discriminate between congestion and other types of errors that might be found in satellite networks. Another important aspect is the energy level spent during probing cycle. An interesting research will be to find how can we measure and quantify this energy. Other future studies could be directed towards XSTP performance over other types of topologies (i.e., Flower constellation, clusters, hybrid constellation – conventional satellites and nanosatellites). Another proposal is a comparison study between XSTP probing and TCP probing mechanisms, considering that both protocols can be configured with similar set of parameters as in our survey. This comparison might show the most effective mechanism in terms of adaptation to various satellite links errors. Finally, probing mechanism could be studied in wireless communication context or in a similar domain characterized by various types of communications errors.

REFERENCES

[1] http://www.perseus.fr/presentation.php; March 30th, 2010

[2] http://www.cnes.fr/web/CNES-fr/6115-communiques-de-presse.php?item=1313; March 30th, 2010

[3] Maged E. Elaasar – "XSTP: eXtended Satellite Transport Protocol", Master Thesis, Ottawa-Carleton Institute for Computer Science, Carleton University, Ottawa, Canada, January 8th, 2003

[4] Maged E. Elaasar, Zheyin Li, Michel Barbeau, and Evangelos Kranakis – "The eXtended Satellite Transport Protocol: Its Design and Evaluation", 17th Annual AIAA/USU Conference on Small Satellites

[5] http://www.nytimes.com/2009/02/03/world/americas/03lithium.html; September 5th, 2010

[6] http://en.wikipedia.org/wiki/Salar_de_Uyuni; July 8th, 2010

[7] James R. Wertz, Wiley J. Larson - "Space Mission Analysis and Design", 3rd edition, 2007, Space Technology Library, Microcosm Press and Springer

[8] Thomas R. Henderson and Randy H. Katz - "Transport Protocols for Internet-Compatible Satellite Networks", IEEE Journal on Selected Areas of Communications, 1999

[9] R. Katz – "Satellite Transport Protocol", PhD thesis, Dec. 1999

[10] T. Henderson and R. Katz – "Satellite transport protocol (STP): An SSCOP-based transport protocol for datagram satellite networks", Proceedings of 2nd Workshop on Satellite-Based Information Systems, 1997

[11] M. Barbeau – "Protocol implementation framework for Linux (PIX), Technical report, 2002

[12] http://www.isi.edu/nsnam/ns/; February 5th, 2010

[13] http://savi.sourceforge.net/; September 8th, 2010

[14] http://web.archive.org/web/19981206074614/www.teledesic.com/tech/details.html; September 7th, 2010

[15] http://www.rapideye.de/; September 8th, 2010

[16] http://www.dmcii.com/; September 8th, 2010

[17] http://www.landcoalition.org/cpl-blog/?p=1387; September 8th, 2010

www.iariajournals.org

International Journal On Advances in Intelligent Systems
ICAS, ACHI, ICCGI, UBICOMM, ADVCOMP, CENTRIC, GEOProcessing, SEMAPRO, BIOSYSCOM, BIOINFO, BIOTECHNO, FUTURE COMPUTING, SERVICE COMPUTATION, COGNITIVE, ADAPTIVE, CONTENT, PATTERNS, CLOUD COMPUTING, COMPUTATION TOOLS
issn: 1942-2679

International Journal On Advances in Internet Technology
ICDS, ICIW, CTRQ, UBICOMM, ICSNC, AFIN, INTERNET, AP2PS, EMERGING
issn: 1942-2652

International Journal On Advances in Life Sciences
eTELEMED, eKNOW, eL&mL, BIODIV, BIOENVIRONMENT, BIOGREEN, BIOSYSCOM, BIOINFO, BIOTECHNO
issn: 1942-2660

International Journal On Advances in Networks and Services
ICN, ICNS, ICIW, ICWMC, SENSORCOMM, MESH, CENTRIC, MMEDIA, SERVICE COMPUTATION
issn: 1942-2644

International Journal On Advances in Security
ICQNM, SECURWARE, MESH, DEPEND, INTERNET, CYBERLAWS
issn: 1942-2636

International Journal On Advances in Software
ICSEA, ICCGI, ADVCOMP, GEOProcessing, DBKDA, INTENSIVE, VALID, SIMUL, FUTURE COMPUTING, SERVICE COMPUTATION, COGNITIVE, ADAPTIVE, CONTENT, PATTERNS, CLOUD COMPUTING, COMPUTATION TOOLS
issn: 1942-2628

International Journal On Advances in Systems and Measurements
ICQNM, ICONS, ICIMP, SENSORCOMM, CENICS, VALID, SIMUL
issn: 1942-261x

International Journal On Advances in Telecommunications
AICT, ICDT, ICWMC, ICSNC, CTRQ, SPACOMM, MMEDIA
issn: 1942-2601